AD-770 084

INVESTIGATION OF FACTORS AFFECTING CORROSION RATE DETERMINATION BY RESISTANCE POLARIZATION

Robert L. Kuhnle

Air Force Institute of Technology
Wright-Patterson Air Force Base, Ohio

May 1973

DISTRIBUTED BY:

NTIS
National Technical Information Service
U. S. DEPARTMENT OF COMMERCE
5285 Port Royal Road, Springfield Va. 22151

AD-770084

(1)

Reproduced from best available copy.

DDC
RECEIVED
NOV 27 1973
B

INVESTIGATION OF FACTORS AFFECTING CORROSION RATE DETERMINATION BY RESISTANCE POLARIZATION

GAM/MC/73-8

ROBERT L. KUHNLE
LCDR USCG

Reproduced by
NATIONAL TECHNICAL
INFORMATION SERVICE
U S Department of Commerce
Springfield VA 22151

Approved for public release; distribution unlimited

378

UNCLASSIFIED

Security Classification

DOCUMENT CONTROL DATA - R & D

(Security classification of title, body of abstract and indexing annotation must be entered when the overall report is classified).

1. ORIGINATING ACTIVITY *(Corporate author)* AIR FORCE INSTITUTE OF TECHNOLOGY (AFIT/EN) WRIGHT-PATTERSON AIR FORCE BASE, OHIO 45433	2a. REPORT SECURITY CLASSIFICATION UNCLASSIFIED 2b. GROUP

3. REPORT TITLE

INVESTIGATION OF VARIOUS FACTORS AFFECTING CORROSION RATE DETERMINATION BY (GALVANOSTATIC) RESISTANCE POLARIZATION

4. DESCRIPTIVE NOTES *(Type of report and inclusive dates)*

AFIT THESIS - MAY 1973

5. AUTHOR(S) *(First name, middle initial, last name)*

ROBERT L. KUHNLE
LCDR USCG

6. REPORT DATE MAY 1973	7a. TOTAL NO. OF PAGES ~~374~~ 378	7b. NO. OF REFS 66
8a. CONTRACT OR GRANT NO. b. PROJECT NO. c. d.	9a. ORIGINATOR'S REPORT NUMBER(S) GAM/MC/73-8 9b. OTHER REPORT NO(S) *(Any other numbers that may be assigned this report)*	

10. DISTRIBUTION STATEMENT

Approved for public release, distribution unlimited.

11. Approved for public release; IAW AFR 190-17 JERRY C. HIX, Captain, USAF Director of Information	12. SPONSORING MILITARY ACTIVITY Aerospace Research Laboratories Wright-Patterson AFB, Ohio 45433

13. ABSTRACT

Controlled laboratory tests using galvanostatic resistance polarization techniques have provided generally reliable, reproducible, and accurate indications of the instantaneous rate of metal surface dissolution. This investigation sought to design and test an apparatus for use in operating environments to reliably and accurately indicate, by galvanostatic resistance polarization techniques, the metal surface corrosion rate. Cathodic and anodic resistance polarization data were obtained within ±10 millivolts of the steady-state corrosion potential in both a laboratory and the experimentally designed test cells at 24 hour intervals during the 120 test hours. Using two high purity iron specimens with different impurity content, tests were conducted in hydrogen saturated and aerated environments of 1N and 0.1N sulfuric acid and 3% sodium chloride/0.5N potassium sulfate. In the experimental test cell, resistance polarization data were obtained at various cathode-to-anode surface area ratios. Both graphical and computerized linear regression techniques were used to determine specific run and average polarization resistance values. Indicated corrosion rates were calculated using the Stern-Geary relationship and Faraday's law. Weight-loss tests were conducted simultaneously with resistance polarization tests to provide comparative "actual" corrosion rate information. In addition, actual corrosion penetration measurements were made and photomicrographs taken to show the extent of localized attack. In both laboratory and experimental test cells, both cathodic and anodic resistance polarization techniques appeared to accurately indicate the metal surface dissolution rate. Corrosion rates determined from weight-loss tests were consistently higher than those determined by resistance

(SEE ATTACHED SHEET)

DD FORM 1 NOV 65 1473

UNCLASSIFIED

Security Classification

polarization techniques. Similarly, actual penetration was much greater than indicated by either resistance polarization or weight-loss tests. Localized attack - intergranular, pitting, and crevice attack - could not be eliminated from either corrosion rate indicating system. Actual corrosion damage was found most dependent upon grain orientation, electrolyte agitation, and the specific impurity content. A correlation was observed between the variation of steady-state corrosion potential and instantaneous indicated corrosion rate with time.

INVESTIGATION OF FACTORS AFFECTING CORROSION RATE DETERMINATION BY RESISTANCE POLARIZATION

THESIS

Presented to the Faculty of the School of Engineering
of the Air Force Institute of Technology

Air University

in Partial Fulfillment of the
Requirements for the Degree of
Master of Science

by

ROBERT L. KUHNLE, B.S.A.E.
LCDR USCG

Graduate Aerospace-Mechanical Engineering

May 1973

Approved for public release; distribution unlimited.

Preface

I have chosen to investigate corrosion as a result of my experience in U. S. Coast Guard aviation where a great majority of recurring and time-consuming maintenance effort is directed toward corrosion control. If I am more able to contribute to the successful control of future Coast Guard corrosion problems as a result of my research efforts, I will consider such efforts worthwhile. In addition, I hope that the data accummulated, the analysis offered, and the conclusions drawn may be useful to future corrosion researchers.

This research effort is my first within the corrosion field and represents many hours of successful and, more often than not, unsuccessful laboratory experimentation to support the learning acquired from many hours of library research. Although much experimentation has been done by others and much literature published which could have served to guide my efforts, this investigation could not have been completed without the guidance and encouragement of Dr. James R. Myers. To him I am especially grateful. In addition, I am indebted to Mr. Sylvester G. Lee for his technical assistance and supply support; Mr. Jim Ray of the Aerospace Research Laboratories for providing the necessary glasswork; the AFIT School Shops personnel for their technical suggestions and assistance in fabrication of the experimental apparatus; and Mr. Joseph Cain for his data treatment and analysis assistance. Finally, to my wife and family should go much of the credit for any degree of success which I may have achieved.

Contents

	Page
Preface	ii
List of Figures	vi
List of Tables	xi
Abstract	xiii
I. Introduction	1
Statement of the Problem	1
Research Objectives	4
Preliminary Assumptions	5
II. Background, Theory, and Current Thought	7
The Corrosion Cell	7
Electrochemical Corrosion Theory	9
Variables Affecting Corrosion Rate	13
Electrochemical Factors	13
Metallurgical Factors	16
Environmental Factors	17
Methods of Determining Corrosion Rate	20
Weight-Loss Testing	20
Tafel Extrapolation Method	23
Resistance Polarization Method	26
III. Experimental Apparatus	32
Electrical Circuitry	32
Laboratory Polarization Test Cell	34
Laboratory Electrode Assemblies	36
Working Electrode Assembly	36
Auxiliary Electrode Assembly	36
Reference Electrode Assembly	38
Salt Bridge Assembly	38
Purging Gas Assembly	39
Experimental Polarization Test Cell	39
Experimental Electrode Assembly	40
Electrolyte	40
Specimen Selection and Fabrication	43
Specimen Selection	43
Annealing	43
Specimen Fabrication	43
IV. Data Collection, Treatment, and Analysis Procedures	45

Page

Preparation 45
Electrical Apparatus 45
Component Cleanliness 45
Electrolyte 46
Specimens 46
Laboratory Test Cell 47
Experimental Test Cell 48
Data Collection Procedures 50
Equilibrium Corrosion Potential 50
pH Determination 50
Preliminary Electrical Set-up 51
Resistance Polarization Testing 51
Data Treatment Procedures 53
Resistance Polarization Data Preparation . . . 54
Polarization Resistance Determination 54
Daily Corrosion Rate Determination 55
Steady-State Corrosion Rate Determination . . 55
Weight-Loss Test Results 56
Data Analysis Procedures 57

V. Analysis of Results 58

Electrolyte pH 58
Steady-State Corrosion Potentials 58
Resistance Polarization Data 60
Polarization Resistance Determination 67
Daily Corrosion Rate Determination 68
Laboratory Test Cell 69
Experimental Test Cell 70
Indicated Steady-State Corrosion Rate 71
C/A Ratio Effects 71
Laboratory and Experimental Test Cell Results. 73
Observed vs. Indicated Results 77
Iron Purity Effects 85

VI. Results and Conclusions 89

Results 89
Conclusions 92

Bibliography 94

Appendix A: pH Determinations for Hydrogen Saturated Electrolytes in the Laboratory Test Cell . 99

Appendix B: Effect of Time on Steady-State Corrosion Potential 100

Appendix C: The Effect of Time on Galvanostatic Polarization Resistance of High Purity Iron I Using a Laboratory Probe 108

Page

Appendix D: The Effect of Time on Galvanostatic Polarization Resistance of High Purity Iron I Using an Experimental Probe 133

Appendix E: Supplementary Investigation - Effect of Time on Polarization Resistance and Corrosion Rate in Deaerated 0.01N Sulfuric Acid 264

Appendix F: Effect of Time on the Instantaneous Corrosion Rate of High Purity Iron I as Indicated Using Resistance Polarization Techniques and a Laboratory Probe 271

Appendix G: The Effect of Time on the Instantaneous Corrosion Rate of High Purity Iron I as Indicated Using Resistance Polarization Techniques and an Experimental Probe . . . 284

Appendix H: Indicated Steady-State Corrosion Rates of High Purity Iron I in a Laboratory Test Cell 309

Appendix I: The Effect of Experimental Probe C/A Ratio on the Indicated Steady-State Corrosion Rate of High Purity Iron I . . . 311

Appendix J: The Effect of Time on Polarization Resistance and Instantaneous Corrosion Rate of High Purity Iron II 321

Appendix K: Weight-Loss Testing Results 332

Appendix L: Photomicrographs of Specimens From Various Test Configurations and Environments . . . 335

Appendix M: Linear Regression Program Instructions . . 349

Appendix N: Data Treatment Computer Program 351

Vita 360

List of Figures

Figure		Page
1	Simplified Corrosion Cell - Open External Circuit.	7
2	Simplified Corrosion Cell - Closed External Circuit.	7
3	Simplified Polarization Diagram.	9
4	Polarization Diagram - Hydrogen Partial Reactions.	11
5	Polarization Diagram - Metal Partial Reactions	11
6	Total Polarization Diagram - Zinc in Deaerated Acidic Solution	12
7	Polarization Curve - Activation and Concentration Polarization	14
8	Generalized Anodic and Cathodic Polarization Curve	15
9	Effect of Velocity on Corrosion Rate	18
10	Effect of Temperature on Corrosion Rate.	18
11	Effects of pH on Corrosion Rate of Iron.	19
12	Effect of Time on Corrosion Rate	21
13	Polarization Diagram - Cathodic Polarization	27
14	Electrical Circuitry for Galvanostatic Resistance Polarization	33
15	Laboratory Test Cell	35
16	Laboratory Working Electrode Assembly	37
17	Experimental Test Cell	41
18	Experimental Electrode Assembly	42
19	Comparison of Data Providing Equivalent Polarization Resistance Indications Using Linear Regression Techniques	68
20	Effect of Time on the Steady-State Corrosion Potential of High Purity Iron I in Hydrogen Saturated 0.1N Sulfuric Acid	102

Figure		Page
21-32	Effect of Time on Galvanostatic Polarization Resistance of High Purity Iron Determined Using a Laboratory Probe	110
33-97	Effect of Time on Galvanostatic Polarization Resistance of High Purity Iron Determined Using an Experimental Probe	134
98	Effect of Time on Galvanostatic Anodic Polarization Resistance of High Purity Iron in Hydrogen Saturated 0.01N Sulfuric Acid Determined Using a Laboratory Probe	266
99	Effect of Time on Galvanostatic Cathodic Polarization Resistance of High Purity Iron with C/A Ratio = 1 in Hydrogen Saturated .01N Sulfuric Acid Determined Using an Experimental Probe	268
100	Effect of Time on the Instantaneous Corrosion Rate of High Purity Iron I in Hydrogen Saturated 0.01N Sulfuric Acid	270
101-112	Effect of Time on the Corrosion Rate of High Purity Iron Determined Using a Laboratory Probe	272
113-124	Effect of Time on the Corrosion Rate of High Purity Iron Determined Using an Experimental Probe	285
125-130	Effect of C/A Ratio on the Steady-State Corrosion Rate of High Purity Iron Determined Using an Experimental Probe	312
131	Effect of Time on Galvanostatic Cathodic Polarization Resistance of High Purity Iron II in Hydrogen Saturated 1N Sulfuric Acid Determined Using a Laboratory Probe	324
132	Effect of Time on Galvanostatic Cathodic Polarization Resistance of High Purity Iron II with C/A Ratio = 3 in Hydrogen Saturated 1N Sulfuric Acid Using an Experimental Probe	326
133	Effect of Time on Galvanostatic Cathodic Polarization Resistance of High Purity Iron II with C/A Ratio = 2 in Hydrogen Saturated 1N Sulfuric Acid Using an Experimental Probe	328
134	Effect of Time on the Corrosion Rate of High Purity Iron II in Hydrogen Saturated 1N Sulfuric Acid Determined by Cathodic Polarization Using a Laboratory Probe	330

Figure		Page
135	Effect of Time on the Corrosion Rate of High Purity Iron II at Various C/A Ratios in Hydrogen Saturated 1N Sulfuric Acid Determined by Cathodic Polarization Using an Experimental Probe	331
136	Approximate Center of the Exposed Surface of a 1 cm^2 Laboratory Specimen of High Purity Iron I After 120 Hour Immersion in Aerated 1N Sulfuric Acid (20X)	336
137	Approximate Center of the Exposed Surface of a 1 cm^2 Laboratory Specimen of High Purity Iron I After 120 Hour Immersion in Aerated 1N Sulfuric Acid (100X)	336
138	Approximate Center of the Exposed Surface of a 1 cm^2 Laboratory Specimen of High Purity Iron I After 120 Hour Immersion in Aerated 1N Sulfuric Acid (1000X)	337
139	Approximate Center to Circumference of Exposed Surface and Unexposed Surface of 1 cm^2 Laboratory Specimen of High Purity Iron I After 120 Hour Immersion in Deaerated 0.1N Sulfuric Acid (20X)	337
140	Circumference of Exposed Surface Area of 1 cm^2 Laboratory Specimen (Figure 139) of High Purity Iron I After 120 Hour Immersion in Deaerated 0.1N Sulfuric Acid (100X)	338
141	Area Approximately 0.3 cm Toward Center From Exposed Surface Circumference of 1 cm^2 Laboratory Specimen (Figure 140) of High Purity Iron I After 120 Hour Immersion in Deaerated 0.1N Sulfuric Acid (500X)	338
142	Approximate Center of Exposed Surface Area of 1 cm^2 Laboratory Specimen (Figure 139) of High Purity Iron I After 120 Hour Immersion in Deaerated 0.1N Sulfuric Acid (200X)	339
143	Approximate Center to Circumference of Exposed Surface and Unexposed Surface of 1 cm^2 Laboratory Specimen of High Purity Iron II After 120 Hour Immersion in Deaerated 1N Sulfuric Acid (20X)	339
144	Approximate Center of Exposed Surface of 1 cm^2 Laboratory Specimen (Figure 143) of High Purity Iron II After 120 Hour Immersion in Deaerated 1N Sulfuric Acid (200X)	340

Figure		Page
145	Approximate Center of Exposed Surface of 1 cm^2 Laboratory Specimen (Figure 143) of High Purity Iron II After 120 Hour Immersion in Deaerated 0.1N Sulfuric Acid (500X)	340
146	Approximate Center of Exposed Surface of 1 cm^2 Laboratory Specimen of High Purity Iron I After 120 Hour Immersion in Aerated 3% Sodium Chloride/ 0.5N Potassium Sulfate (500X)	341
147	Approximate Center of Exposed Surface of 1 cm^2 Laboratory Specimen of High Purity Iron I After 120 Hour Immersion in Aerated 3% Sodium Chloride/ 0.5N Potassium Sulfate (1000X)	341
148	Unexposed (bottom) Surface of 10 cm^2 Experimental Specimen of High Purity Iron I After 120 Hour Immersion in 1N Deaerated Sulfuric Acid (20X)	342
149	Increased Magnification of Unexposed Surface (Figure 148) of High Purity Iron I After 120 Hour Immersion in 1N Deaerated Sulfuric Acid (100X)	342
150	Further Increased Magnification of Unexposed Surface (Figure 148) of High Purity Iron I After 120 Hour Immersion in 1N Deaerated Sulfuric Acid (200X)	343
151	Unexposed Surface of 10 cm^2 Experimental Specimen of High Purity Iron I After 120 Hour Immersion in 1N Deaerated Sulfuric Acid (200X)	343
152	Exposed Circumferential Surface of 5 cm^2 Experimental Specimen of High Purity Iron I After 120 Hour Immersion in Deaerated 3% Sodium Chloride/ 0.5N Potassium Sulfate (20X)	344
153	Pitted Area on Exposed Circumferential Surface of 5 cm^2 Experimental Specimen (Figure 152) of High Purity Iron I After 120 Hour Immersion in Deaerated 3% Sodium Chloride/0.5N Potassium Sulfate (500X)	344
154	Exposed End of 2 cm^2 Experimental Specimen of High Purity Iron II After 120 Hour Immersion in Deaerated 1N Sulfuric Acid (20X)	345
155	Exposed End of 2 cm^2 Experimental Specimen of High Purity Iron II After 120 Hour Immersion in Deaerated 1N Sulfuric Acid (100X)	345

Figure		Page
156	Grain Structure of Polished and Etched High Purity Iron II Specimen (2000X)	346
157	Polished Surface of a Laboratory Specimen (Figure 136) After 120 Hour Immersion in Aerated 1N Sulfuric Acid	346
158	Polished Surface of a Laboratory Specimen (Figure 136) After 120 Hour Immersion In Aerated 1N Sulfuric Acid (180X)	347
159	Polished Surface of a Laboratory Specimen (Figure 136) After 120 Hour Immersion in Aerated 1N Sulfuric Acid (200X)	347
160	Polished Surface of a Laboratory Specimen (Figure 136) After 120 Hour Immersion in Aerated 1N Sulfuric Acid (1000X)	348

List of Tables

Table		Page
I	Chemical Composition of High Purity Iron Specimens	44
II	Experimental Electrode Activation Cycle	49
III	Indicated Steady-State Corrosion Rates in the Experimental Test Cell	74
IV	Effect of Time on the Steady-State Corrosion Potential of High Purity Iron I in Hydrogen Saturated 1N Sulfuric Acid	101
V	Effect of Time on the Steady-State Corrosion Potential of High Purity Iron I in Aerated 1N Sulfuric Acid	103
VI	Effect of Time on the Steady-State Corrosion Potential of High Purity Iron I in Hydrogen Saturated 0.1N Sulfuric Acid	104
VII	Effect of Time on the Steady-State Corrosion Potential of High Purity Iron I in Aerated 0.1N Sulfuric Acid	105
VIII	Effect of Time on the Steady-State Corrosion Potential of High Purity Iron I in Hydrogen Saturated 3% Sodium Chloride	106
IX	Effect of Time on the Steady-State Corrosion Potential of High Purity Iron I in Aerated 3% Sodium Chloride	107
X	Electrolyte pH Data for 0.01N Sulfuric Acid	265
XI	Effect of Time on High Purity Iron I Steady-State Corrosion Potential in 0.01N Sulfuric Acid	265
XII	Laboratory Test Cell Indicated Steady-State Corrosi Rate Range	310
XIII	Computed Steady-State Corrosion Rates in 1N Sulfuric Acid Using an Experimental Probe	318
XIV	Computed Steady-State Corrosion Rates in 0.1N Sulfuric Acid Using an Experimental Probe	319
XV	Computed Steady-State Corrosion Rates in 3% Sodium Chloride Using an Experimental Probe	320

Table		Page
XVI	Electrolyte pH Data for 1N Sulfuric Acid	322
XVII	Effect of Time on Steady-State Corrosion Potential of High Purity Iron II in Deaerated 1N Sulfuric Acid	322
XVIII	Weight-Loss Test Results for High Purity Iron II	323
XIX	Test Cell Configuration Classifications	333
XX	Corrosion Rates Determined from Weight-Loss Tests.	334

Abstract

Controlled laboratory tests using galvanostatic resistance polarization techniques have provided generally reliable, reproducible, and accurate indications of the instantaneous rate of metal surface dissolution. This investigation sought to design and test an apparatus for use in operating environments to reliably and accurately indicate, by galvanostatic resistance polarization techniques, the metal surface corrosion rate. Cathodic and anodic resistance polarization data were obtained within ±10 millivolts of the steady-state corrosion potential in both a laboratory and the experimentally designed test cells at 24 hour intervals during the 120 test hours. Using two high purity iron specimens with different impurity content, tests were conducted in hydrogen saturated and aerated environments of 1N and 0.1N sulfuric acid and 3% sodium chloride/0.5N potassium sulfate. In the experimental test cell, resistance polarization data were obtained at various cathode-to-anode surface area ratios. Both graphical and computerized linear regression techniques were used to determine specific run and average polarization resistance values. Indicated corrosion rates were calculated using the Stern-Geary relationship and Faraday's law. Weight-loss tests were conducted simultaneously with resistance polarization tests to provide comparative "actual" corrosion rate information. In addition, actual corrosion penetration measurements were made and photomicrographs taken to show the extent of localized attack. In both laboratory and experimental test

cells, both cathodic and anodic resistance polarization techniques appeared to accurately indicate the metal surface dissolution rate. Corrosion rates determined from weight-loss tests were consistently higher than those determined by resistance polarization techniques. Similarly, actual penetration was much greater than indicated by either resistance polarization or weight-loss tests. Localized attack - intergranular, pitting, and crevice attack - could not be eliminated from either corrosion rate indicating system. Actual corrosion damage was found most dependent upon grain orientation, electrolyte agitation, and the specific impurity content. A correlation was observed between the variation of steady-state corrosion potential and instantaneous indicated corrosion rate with time.

INVESTIGATION OF FACTORS AFFECTING CORROSION RATE DETERMINATIONS BY RESISTANCE POLARIZATION

I. Introduction

Statement of the Problem

Corrosion can be defined as destruction or deterioration of a metal surface as the result of some reaction, normally electrochemical, with the local environment[1, 62]. Not all corrosion is undesirable, e.g. the formation of protective aluminum oxide on the surface of aluminum; however, most corrosion is undesirable. Although damage may be limited to marring the appearance of a metal surface, corrosion may (1) cause contamination of a system, (2) cause increased operating and maintenance costs, (3) impair safety, or (4) ultimately lead to work stoppages and equipment shutdown.

One corrosion mechanism, general corrosion or uniform attack, is considered responsible for more tonnage of metal deterioration than any other form of corrosion[1]. Because of the material loss attributed to uniform attack, this form of corrosion has been a topic of great concern in recent years. However, with the advancement of corrosion knowledge and the development of new alloys, the problem of equipment failure due to general corrosion has somewhat diminished.

By designing a structure of different material, a desired equipment life can be assured and uniform attack problems minimized. However, economic considerations, cost and material availability, and operating restrictions such as weight and balance may limit application of such a procedure.

In addition, economic circumstances can and do change. More effective corrosion control may become necessary to increase operating life beyond that for which equipment was originally designed. Similarly, economic considerations may necessitate an equipment life which is beyond that for which the equipment can be designed unless effective corrosion control techniques are continuously developed and used. Finally, with technological advances and new products, steps may be necessary to minimize or alter the corrosion processes within existing systems to prevent contamination of the new product or alteration of its properties (e.g. JP-7 thermal stability may be reduced by the presence of certain metallic ions).

The most desirable method of guaranteeing longer equipment life would be to eliminate undesirable corrosion damage completely; but, at present, there is no known, all-inclusive "cure" for corrosion. As a result, and until suitable preventive measures are found, efforts will continue to be directed at the control and minimization of corrosion.

Corrosion control, like other optimization efforts where economic considerations play an important role, involves the minimization of some selected undesirable quantity,

subject to certain identifiable constraints. Before optimization efforts can begin, certain preliminary requirements must be satisfied. First, the form or forms of corrosion involved must be identified. Because of the tonnage of material loss attributed to uniform attack and because of the continuing need to provide effective control against uniform attack, this form of corrosion was chosen for investigation.

Next, an adequate measure of the existence of corrosion, specifically uniform attack, must be available. Because uniform attack is seldom absent, a qualitative indication of the presence or absence of corrosion is considered insufficient; an effective quantitative measure is needed. Corrosion rate (e.g. mils/year or microns/year) has been accepted and widely used to indicate the extent of uniform attack.

Another important prerequisite of efforts to minimize uniform attack is that suitable techniques must be available by which to measure corrosion rate. The technique or techniques chosen should provide accurate, reliable, and reproducible data during appropriate real time or accelerated tests. One electrochemical technique, the resistance polarization method, has been used to provide instantaneous corrosion rate information; however, the success realized has been only partial. Closely controlled laboratory tests using resistance polarization techniques have achieved adequate levels of reliability, reproducibility, and accuracy.

However, attempts to achieve acceptable results under actual operating conditions have been much less successful. It is these corrosion rates, occurring during actual operations, in which a user is concerned. Determining the availability of and providing reliable, reproducible, and accurate instantaneous corrosion rate information economically and in a useable form is the essence of the problem toward which this investigation was directed.

Research Objectives

The ultimate goal of this research was to determine if and how, under normal operating conditions, resistance polarization methods could be used to provide accurate, reliable, and reproducible indications of the instantaneous rate of uniform attack upon metal surfaces immersed in aqueous environments. Achievement of such a goal was considered beyond the scope of this investigation due to time and data availability limitations. As a result, this research effort was limited to:

1. Attempted design of an apparatus which would indicate the instantaneous rate of uniform attack of iron immersed in selected aqueous environments for use outside the laboratory.

2. The investigation of the effects of specimen size and composition on the indicated corrosion rates compared with laboratory-determined corrosion rates.

3. The investigation of the effects of aqueous environment concentration on indicated corrosion rates compared with laboratory-determined corrosion rates.

4. The investigation of the effects of environment aeration upon indicated corrosion rate compared with laboratory-determined corrosion rates in similarly aerated environments.

5. The investigation of the corrosion rates indicated by both anodic and cathodic resistance polarization techniques.

Preliminary Assumptions

This research effort was begun based upon certain initial assumptions. An additional research goal was to determine the validity of these assumptions. For this study, it was assumed that:

1. Electrochemical methods could be used to predict the rate at which uniform attack of a metal surface proceeds.

2. Results of weight loss tests were an accurate baseline upon which to evaluate the rates of uniform attack determined by other methods.

3. Resistance polarization provided an accurate and reliable method to measure the instantaneous rate of uniform attack in laboratory tests.

4. Techniques based upon resistance polarization methods could be used to achieve some measure of instantaneous corrosion rates under operating conditions, although the usefulness of the determined rate information was not known initially.

5. The results of corrosion rate tests obtained for a given material were representative of the results which would be obtained for similar materials under similar environmental conditions.

6. Triplicate results were sufficient to establish meaningful reproducibility.

7. During resistance polarization tests, the entire specimen surface was either primarily anodic or cathodic.

8. The initial exposed specimen surface area remained essentially unchanged and could be used for corrosion current density calculations for the entire test duration.

9. For the materials and environments used in this investigation, 120 hours was considered sufficient to achieve steady-state corrosion rates.

10. The actual corrosion process was not significantly altered by the resistance polarization techniques used to obtain laboratory data.

II. Background, Theory, and Current Thought

The Corrosion Cell

A corrosion cell requires the presence of four constituents: (1) an anodic surface, (2) a cathodic surface, (3) an environment capable of conducting direct current, and (4) a current path between anode and cathode external to that environment[2]. Consider the basic corrosion cell (Fig. 1) in which two metal surfaces, A and C, are completely immersed within an aqueous environment. These surfaces may be of different metals or different areas on the same metal surface. Each surface has an open circuit potential, E_a or E_c, relative to some standard reference electrode. If the potentials are not equal ($E_a \neq E_c$), a current will tend to flow from the more negative potential (E_a) of the anodic surface through the aqueous environment, the electrolyte, to the more positive potential (E_c) of the cathodic surface when the external circuit is closed (Fig. 2).

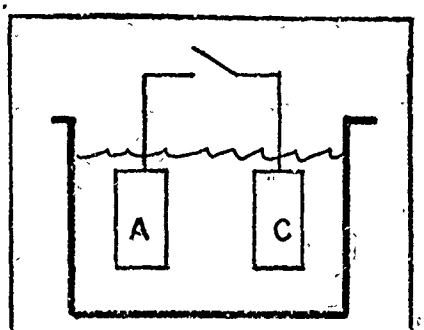

Figure 1: Simplified Corrosion Cell - Open External Circuit

This current flow corresponds to the flow of electrons from the anodic surface to the cathodic surface through the external current path. Associated with this electron flow is the occurrence of anodic and cathodic reactions. The anodic

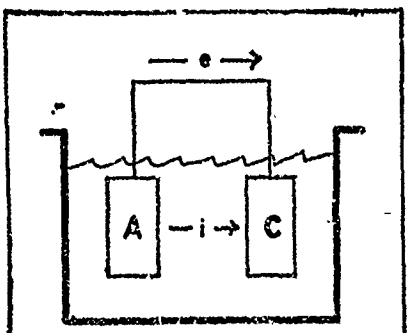

Figure 2: Simplified Corrosion Cell - Closed External Circuit

reaction, shown in Eq (1), involves the oxidation of the anode surface. It is by this reaction that metal ions are provided to the electrolyte at the anodic surface.

$$M \longrightarrow M^{+n} + ne^- \tag{1}$$

The cathodic reaction is not as simply defined. In general, the cathodic reaction is a reduction reaction during which electrons are gained. Depending upon environmental conditions, this reaction commonly involves hydrogen ion or oxygen reduction. Hydrogen ion reduction (Eq (2)) commonly occurs when acidic aqueous environments are involved. In neutral or alkaline environments, a common cathodic reaction is the reduction of oxygen (Eq (3))[1].

$$2H^+ + 2e^- \longrightarrow 2H \longrightarrow H_2 \tag{2}$$

$$2H_2O + O_2 + 4e^- \longrightarrow 4OH^- \tag{3}$$

It should be noted that more than one oxidation or reduction reaction may occur on the anodic or cathodic surface, respectively. Such multiple reactions may serve to increase or decrease the corrosion rate, but the basic corrosion mechanism remains unchanged. The effects of multiple oxidation and reduction reactions on corrosion rate are discussed in a subsequent section.

With the external circuit closed, the potential difference between anodic and cathodic regions will decrease (i.e., the cathodic potential becomes more negative, while the anodic potential becomes less negative). This potential shift away from equilibrium resulting in a current flow

is called "polarization." Polarization continues until a steady-state condition is reached. At this point the cell has achieved an "equilibrium corrosion potential", E_{corr}, and corrosion current density, i_{corr}. Figure 3 is a simplified representation of the polarization process and suggests the electrochemical nature of uniform attack.

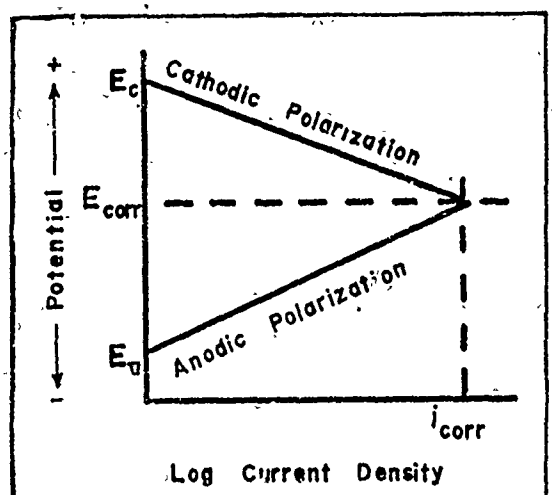

Figure 3: Simplified Polarization Diagram (Ref. 3)

Electrochemical Corrosion Theory

The correlation between electrochemical data and metal surface corrosion rate was first discussed by Whitney[4] in 1903. In 1932, Evans and Hoar[5] suggested a relationship between the amount of metal dissolution and corrosion cell current flow. In 1938, Wagner and Traud[6] discussed the mixed potential theory which forms the basis for much of today's corrosion theory. The mixed potential theory is based upon th hypotheses (1) that an electrochemical reaction is the sum of two or more partial oxidation and reduction reactions, and (2) that during an equilibrium corrosion process

on an immersed isolated metal surface the rate of oxidation equals the rate of reduction[1].

According to the second hypothesis, an isolated immersed metal surface in equilibrium with its metal ions will have a characteristic potential compared to some known reference. At this equilibrium potential, the rates of oxidation (r_o) and reduction (r_r) occurring on that metal surface will be equal and no net current flow exists. By using Faraday's law,

$$r_o = r_r = i_o/nF, \tag{4}$$

where n is the number of electrons per transfer and F is Faraday's constant, the exchange current density, i_o, can be determined. Although no current actually flows, the exchange current density is a measure of the "equilibrium" reaction rate on the metal surface and is characteristic of the material and the environment, i.e. the oxidation and reduction reactions involved. It should remain nearly constant until the cell environment is altered sufficiently to cause changes in the oxidation and reduction reaction rates.

If two metal surfaces are placed in a "corrosion cell", one surface will tend to be anodic and will involve a reaction between metal and metal ions. The other surface will tend to be cathodic and some element, commonly hydrogen ions or oxygen, will be reduced. By the first hypothesis of the mixed potential theory, each surface has an equilibrium potential, E_a or E_c, and a corresponding exchange current density, i_{oa} or i_{oc}. At the anodic surface, metal and metal ions will be in

equilibrium, for example

$$Zn \rightleftharpoons Zn^{++} + 2e^{-} \tag{5}$$

while at the cathodic surface, assuming a deaerated acid environment for example, hydrogen ions and hydrogen will be in equilibrium.

$$2H^{+} + 2e^{-} \rightleftharpoons 2H \rightleftharpoons H_2 \tag{6}$$

By considering the first hypothesis of the mixed potential theory, these partial oxidation and reduction reactions may be summed to form the resulting corrosion cell reaction. Typical partial reactions [Figs. 4 and 5] for the surfaces on which metal and hydrogen reactions occur may be summed to form the total cell reaction (Fig. 6). The point at which oxidation and reduction reaction rates are equal determines the characteristic E_{corr} and i_{corr}. This "equilibrium" can only occur when the reduction reaction occurs at the cathodic surface and the oxidation reaction at the anodic surface. This corresponds to the E_{corr} and i_{corr} intersection. The resulting corrosion current density, i_{corr}, is a measure of the rate of metal ion dissolution, i.e. the general corrosion rate.

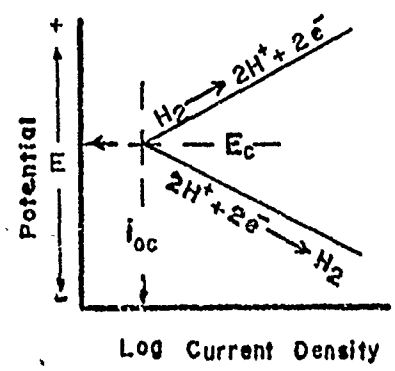

Figure 4: Polarization Diagram - Hydrogen Partial Reactions

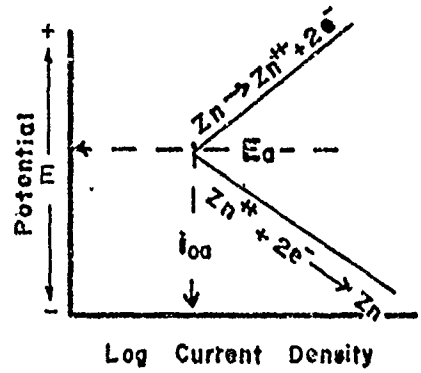

Figure 5: Polarization Diagram - Metal Partial Reactions

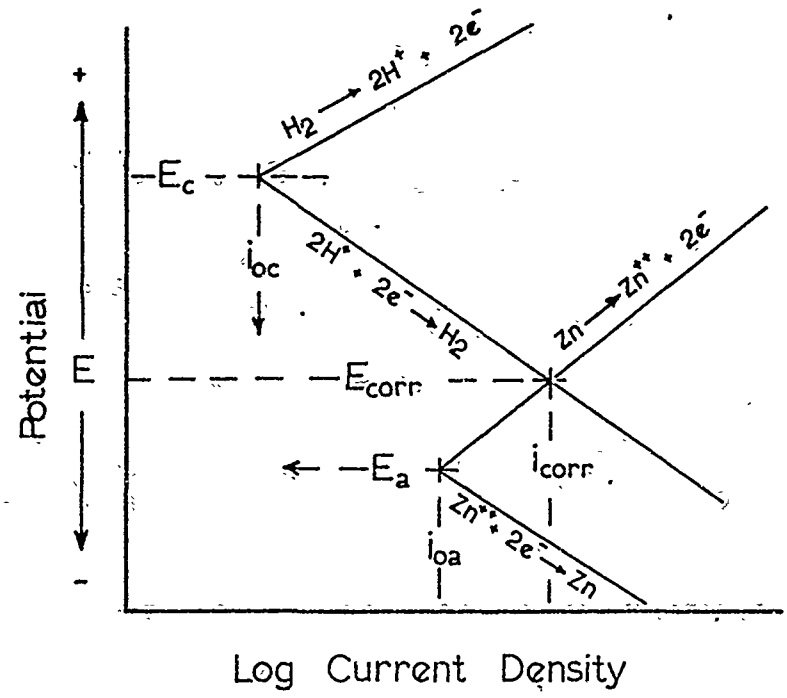

Figure 6: Total Polarization Diagram – Zinc in Deaerated Acidic Solution (1)

This discussion has described the corrosion process in terms of the hypotheses of the mixed potential theory. As with many theoretical models, actual experimentation may be influenced by several variable factors. The corrosion process is no exception. Numerous variable factors affect the actual rate of metal surface uniform attack. The influence of certain variables may cause actual corrosion rates to vary widely from theoretically predicted results.

Variables Affecting Corrosion Rate

The actual rate of uniform attack may vary considerably due to changing electrochemical, metallurgical, or environmental factors. In addition, indicated corrosion rates may vary due to undesirable variables introduced by the corrosion rate observation techniques. As a result, indicated corrosion rates may vary considerably. Because this study was directed at investigating several variable factors and their effect upon indicated corrosion rate, a discussion of variable factors is included.

Electrochemical Factors. The rate at which reactions can occur within a corrosion cell may be limited by numerous factors. The limitation of the rate at which a reaction can proceed is called polarization, either activation or concentration polarization. An electrochemical reaction which is limited only by how fast the reaction sequence can occur is subject to activation polarization, while a reaction which could proceed faster but is limited by the rate at which the constituents can diffuse to or away from the reaction surface is subject to concentration or diffusion polarization.

The importance of the distinction should not be overlooked. The effects produced by environmental variables such as electrolyte velocity and concentration may depend largely upon the type of controlling polarization[1]. For example, a reaction rate controlled by the rate of constituent diffusion may be significantly altered by changes in electrolyte velocity or hydrogen ion concentration. In contrast, a

reaction controlled by activation polarization may be relatively insensitive to changes in these variables.

Concentration polarization effects may also be significant during electrochemical testing when high cathodic currents are applied. Figure 7 shows typical characteristics of reaction rate as cathodic overvoltage (η) is applied. As the overvoltage is increased, the reaction rate, converted into current density using Faraday's law, increases until a limiting value is reached. At this point the reaction is controlled by concentration polarization.

Two currently-used electrochemical methods for corrosion rate determination, the Tafel extrapolation method and the resistance polarization method, assume that the corrosion process is controlled by activation polarization. However, the Tafel extrapolation method may require sufficiently large applied current densities for concentration polarization to become a controlling factor. This susceptibility to concentration polarization provides one disadvantage to use of the Tafel technique.

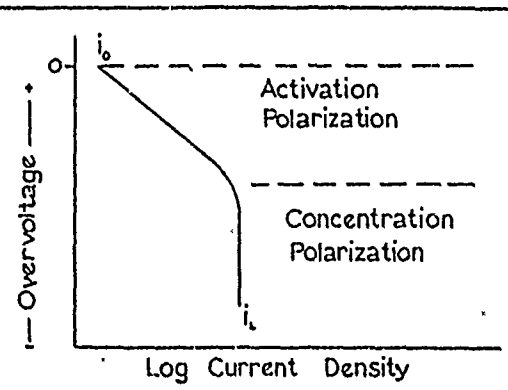

Figure 7: Polarization Curve - Activation and Concentration Polarization (1)

A second electrochemical factor is passivity. Passivity is the loss of chemical reactivity, i.e., the decrease of corrosion rate experienced by certain metal surfaces under particular environmental conditions[1]. When passivity occurs, the anodic surface tends to display a more noble behavior, the corrosion potential increases, and the corrosion current density decreases to a nearly constant value which is independent of the overvoltage (Fig. 8).

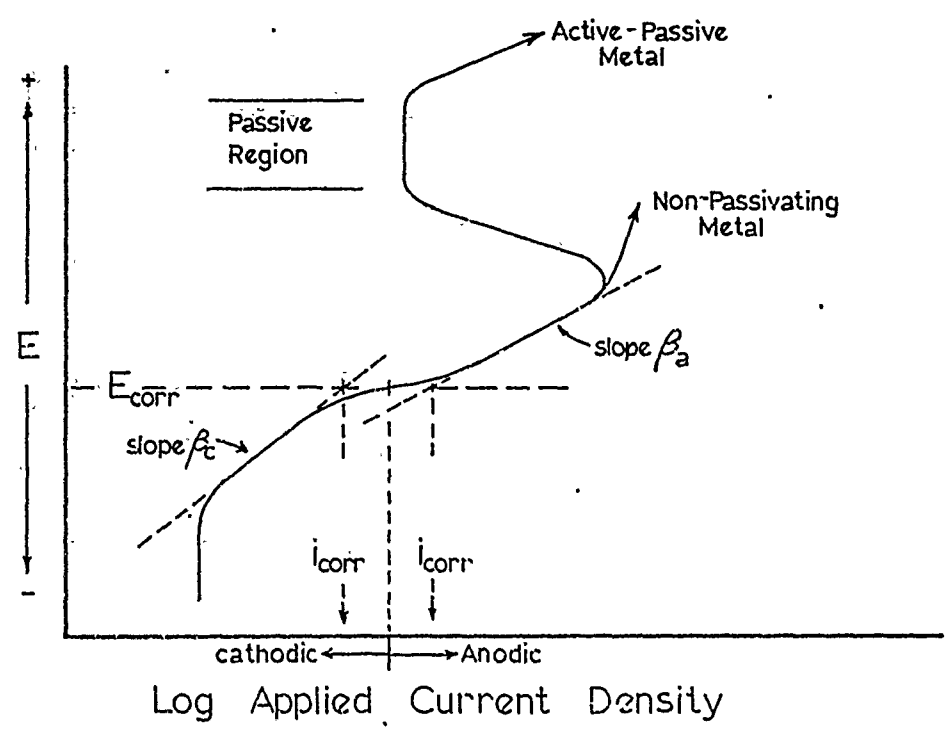

Figure 8: Generalized Anodic and Cathodic Polarization Curve (3)

A passive metal surface is generally much more corrosion resistant than an active metal surface. The higher and more variable corrosion rate of an active metal surface may be the reason that active metals have been studied

more thoroughly. Because corrosion of an active surface can be a greater problem than corrosion of a passive surface, only active iron surfaces were considered in this investigation.

Metallurgical Variables. The grain orientation, grain size, purity, heat treatment, and amount of cold work in a metal can influence corrosion rate. Because areas of high energy tend to be more active or anodic with respect to lower energy areas[1], grain boundaries tend to be anodic compared to the bulk grain. Metal surfaces with small grains tend to have more grain boundary area and thus should tend to have corrosion rates higher than surfaces which have been heat treated to a larger grain size. This difference may be small. In general, the ratio of bulk grain area to grain boundary area is large regardless of grain size[9].

The presence of impurity atoms within the crystalline lattice structure may tend to affect corrosion rate, although investigations as to the effects of such impurities have produced varied and conflicting results. Fontana[1] reported that the corrosion rate of aluminum increases by a factor of 30,000 when the purity is lowered from 99.998 to 99.2%. This contradicts the views of Stern[8, 10], who found that the presence of impurities may have little overall effects on the corrosion rate, and Greene and Saltzman[9], who found no correlation between chemical composition of the metal under observation and corrosion rate. Greene and Clary[49] have provided the most thorough investigation encountered. By

investigating 53 high-purity iron and steel alloys, and utilizing statistical linear regression techniques, the effects of adding various small quantities of impurity (alloying) elements were determined with results ranging from impurities producing little or no change to the basic corrosion rate to impurities producing very significant change in the corrosion rate.

Because no direct correlation exists between metallurgical properties and indicated or actual corrosion rate, and because of the varied opinions as to the effects of metallurgical properties on corrosion rate, all tests conducted in this investigation were done using high purity iron with as identical metallurgical properties as possible so as to minimize the variations in corrosion rate which might be caused by differences in metallurgical variables.

Environmental Factors. The environmental factors of greatest concern in this investigation were velocity, temperature, electrolyte composition and concentration, degree of aeration, and the area relationships of the metal surfaces under investigation.

The effects of velocity upon corrosion rate are complex and are largely dependent upon electrochemical, metallurgical and other environmental factors. Figure 9 depicts the typical relationships between velocity and corrosion rate Curve A shows a reaction controlled by cathodic diffusion polarization; curve B shows a corrosion process controlled by

activation polarization; and curve C shows the effects of high velocity upon corrosion rate. Velocity effects were minimized in this investigation by using environments previously reported as controlled by activation polarization. In addition, the velocity of the electrolyte was limited to that random motion produced by aeration or deaeration.

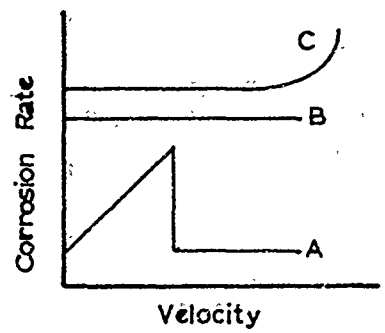

Figure 9: Effect of Velocity on Corrosion Rate (1)

In most chemical processes, the reaction rate increases with increases in temperature. The corrosion process is no exception, as shown in Fig. 10. The effects of temperature variation were minimized throughout this investigation by operating at room temperature (22°C). This practice also minimized the temperature dependence of the reference electrode potential. Significant potential variations could be encountered if temperature fluctuations over a wide range were permitted.

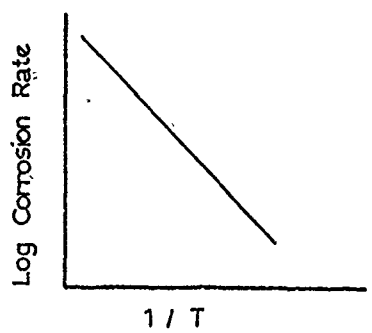

Figure 10: Effect of Temperature on Corrosion Rate (1)

Associated with the electrolyte in which the corrosion process occurs are two variables which must also be considered. These variables are the composition and concentration of the electrolytes. Figure 11 depicts the effects of

pH upon the corrosion rate of iron. During this investigation the effects of pH were observed by varying the electrolyte concentration.

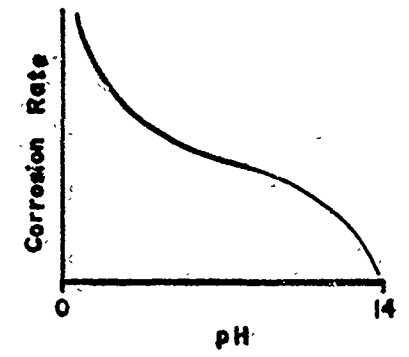

Figure 11: Effects of pH on Corrosion Rate of Iron

The degree of electrolyte aeration may also cause the corrosion rate to vary by changing the primary reduction reaction. In an acidic, deaerated environment the cathodic reaction is normally the reduction of hydrogen ions. At equilibrium a film of hydrogen tends to cover the cathode, increasing the resistance to current flow and decreasing the corrosion current density. If the cell is then aerated, oxygen will tend to remove the hydrogen layer according to a reaction similar to Eq (7). Thus, the closed circuit resistance of the cell is lowered and the corrosion current density increases. The indicated corrosion rate should reflect this change in the degree of aeration.

$$2H_2 + O_2 \longrightarrow 2H_2O \qquad (7)$$

The size and composition of the metal surfaces used to electrochemically predict corrosion rates were studied. During many laboratory determinations of corrosion rate, a noble metal (e.g., platinum) is used as the cathodic surface and a standard half cell (e.g., the saturated calomel

electrode) is used as a reference electrode. This investigation examined the possibility of using identical metals as anodic, cathodic, and reference-electrode surfaces. In addition, varying the cathode-to-anode surface area ratio may also vary the actual and/or the indicated corrosion rate. Many investigators[3, 8, 10, 11] believed that accurate indications of corrosion rate were not possible unless the cathodic surface was much larger than the anodic surface. This investigation attempted to determine if the corrosion rate indicated by the corrosion cell with electrodes of identical composition was affected by the cathodic-to-anodic surface area ratio.

The effect of electrode configuration upon the indicated corrosion rate is unreported. Phelps[2] did report the need to maintain the reference and anodic surfaces as close as possible to avoid any losses associated with the electrolyte conductivity (e.g., IR drop). This investigation attempted to determine a configuration which would provide accurate, reliable, and reproducible indications of corrosion rate using similar materials as anode, cathode, and reference-electrode surfaces.

Methods of Determining Corrosion Rate

Weight-Loss Testing. Long before methods were available for determining corrosion rate from electrochemical data, the need for metal surface corrosion rate information existed. One of the oldest and most widely-accepted methods for determining the rate of uniform corrosion is weight-loss testing,

which allows determination of an average rate of uniform surface corrosion upon test completion. Although such information may be of value, it can be misleading.

Several investigators[1, 3, 10] have demonstrated that the corrosion rate of a metal surface is not constant, but rather demonstrates a time dependence (Fig. 12). This relationship appears to be of the general exponential form

$$A = A_o \, e^{k/t} \tag{8}$$

where A is the instantaneous corrosion rate at time, t; A_o is the steady-state corrosion rate; and k is a factor which determines the rate at which the steady-state rate is approached. Because A_o and k may vary considerably, the shape of the corrosion rate vs. time plot may also vary considerably.

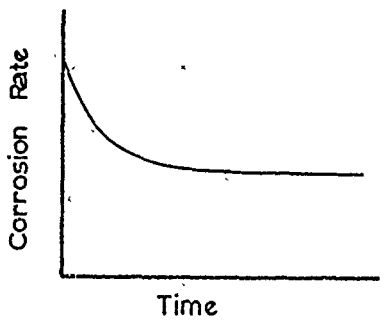

Figure 12: Effect of Time on Corrosion Rate

The weight lost by a test specimen during time, t, is a function of the area beneath the plot of corrosion rate versus time. If the steady-state corrosion rate is achieved rapidly and the test is of sufficient length, the results of weight loss and electrochemical tests should be comparable with weight loss test results being slightly higher. However, if the initial rate is high and the rate of decay

to steady state conditions slow, the results of weight loss tests could be considerably higher than the electrochemically determined instantaneous steady state value.

Thus, weight-loss techniques provide accurate corrosion rate information only after very lengthy tests. Depending upon the corrosion rate of the metal under investigation, these tests could require a year or more to complete. Only for rapidly corroding metals can accurate rate information be obtained in relatively-short-time, weight-loss tests.

However, there is no guarantee that an accurate measure of uniform corrosion attack will be provided even after lengthy weight-loss tests. Localized forms of corrosion, such as pitting and crevice corrosion, may also contribute significantly to the total corrosive damage. If the rate of uniform corrosion is sufficiently small and the specimen is subjected to considerable localized attack, the results of weight-loss tests may provide greatly distorted information about the rate of uniform attack.

In addition, weight-loss tests provide no indication of the corrosion rate until after test completion. An entire system might be damaged beyond repair due to an unexpected and excessively high corrosion rate before any such damage is indicated by weight-loss tests. Finally, if the corrosion rate is subject to extreme fluctuations or oscillations as the result of some change within the "corrosion cell", the results of weight-loss tests will be unable to detect such fluctuations or oscillations.

For these reasons, a measure of instantaneous corrosion rate is desirable. With such a measure, an accurate determination of the corrosion rate of even the most slowly corroding metals can be made in a relatively short time period. In addition, a corroding system can be monitored continuously to detect changes or fluctuations in the corrosion rate and steps may be taken to reduce the rate during periods when it could otherwise be unusually and unacceptably high.

Two of the methods available for predicting the instantaneous corrosion rate of a metal surface, the Tafel extrapolation and resistance polarization methods, utilize electrochemical data obtained during relatively short duration tests to predict the steady-state corrosion rate for a particular test material in a test environment with a steady-state corrosion rate being achieved within 72 to 96 hours for most materials[12]. Both methods can be used to predict extremely low corrosion rates and to continuously monitor corrosion rate. However, the Tafel extrapolation method does have some definite disadvantages which are not encountered when using resistance polarization techniques. A brief discussion of the Tafel extrapolation method is included to identify and discuss these disadvantages.

Tafel Extrapolation Method. A metal surface is said to exhibit Tafel behavior if a plot of overvoltage (η) versus the logarithm of applied polarization current density takes a shape similar to that of Fig. 8. The apparently linear

region beginning at approximately 50mv of overvoltage is called the Tafel region and is described by the relationship

$$\eta = \pm\beta \log \frac{i}{i_o} \tag{9}$$

which is the Tafel equation. The slope parameter β is referred to as the Tafel slope. If the linear portion of the polarization curve is extrapolated to the equilibrium corrosion potential, the corrosion current density, i_{corr}, is obtained. Since the corrosion current density is fixed, equivalent results should be obtained using either anodic or cathodic polarization.

There are several problems which arise when using the Tafel extrapolation method. First, the derivation of the Tafel equation is based upon the equilibrium reactions occurring at a single electrode where, upon polarization, the entire surface becomes either anodic or cathodic. In a corrosion cell, both anodic and cathodic surfaces exist. Phelps[2] reported that the Tafel prediction of corrosion rate may be twice the actual value if anodic and cathodic surface areas are in a 1:1 ratio. Thus, the value of corrosion rate predicted by the Tafel extrapolation method may be greater than the actual corrosion rate. In addition, the predicted rate may be great y influenced by the cathode-to-anode surface area ratio.

The polarization curve Tafel region is not generally reached until sufficient current is applied to produce approximately 50mv overvoltage. To achieve this overvoltage, current

of approximately ten times the corrosion current must be applied[13]. In addition, one to two decades (orders of magnitude) of current density should be spanned to insure accurate Tafel region prediction. Application of such a large current may disturb the actual corrosion process which is occurring, causing the validity of corrosion rate information obtained by the Tafel extrapolation method to be questionable[14, 15]. This is particularly true of anodic polarization where the applied current tends to increase the rate of metal dissolution.

Another problem is created by the magnitude of the current density which must be applied. The polarization curve (Fig. 8) is constructed assuming that the entire process is controlled by activation polarization. However, concentration effects may make it impossible to apply sufficient current to accurately determine the slopes of the Tafel regions. Finally, the values of the Tafel slopes, β_a and β_c, are determined based upon the assumption that single oxidation and reduction reactions occur in the corrosion cell. This may not be a valid assumption. More than one reaction may occur simultaneously or the predominant reaction on a cathodic or anodic surface may change[13]. If either occurs, the Tafel region may become distorted, rendering the results of Tafel extrapolation less than meaningful.

For these reasons, the results of Tafel extrapolation tests may be of questionable relevance and some other method must be used which utilizes the advantages of electrochemical

methods while eliminating the disadvantages associated with the Tafel extrapolation method.

Resistance Polarization Method. The resistance polarization method was developed by Stern and Geary[13] in 1957 after other investigators[16, 17] had reported a linear applied voltage, current-density relationship in the vicinity of the equilibrium corrosion potential, E_{corr}, and a correlation between the slope of this relationship ($\Delta E/\Delta I$) and the instantaneous corrosion rate of the material. The name resistance polarization arose from the units of the slope of the linear potential versus applied current density relationship, i.e., $\Delta E/\Delta I$ = volts/amp/cm^2 or ohms/cm^2. This method has been called the "linear polarization method" but recent literature has used the term resistance-polarization method. This change in terminology may be due, in part, to recent articles questioning the linearity of this potential - applied current relationship[18, 19, 20, 21]. Because of the recent articles and because resistance polarization is the method upon which electrochemical data are used to determine the rate of uniform corrosion within this investigation, a thorough discussion of resistance polarization is included.

The Stern-Geary equation is derived based upon the assumptions that the current density is low enough to ensure activation polarization and that the resulting overvoltages are small. The reasons for these assumptions will become apparent during the following discussion of the Stern-Geary equation derivation. During cathodic polarization from the

cell equilibrium point (E_{corr}, i_{corr}) an applied current of

$$i_{applied} = i_c - i_a \tag{10}$$

will flow (Fig. 13) and produce an overvoltage, i.e. will

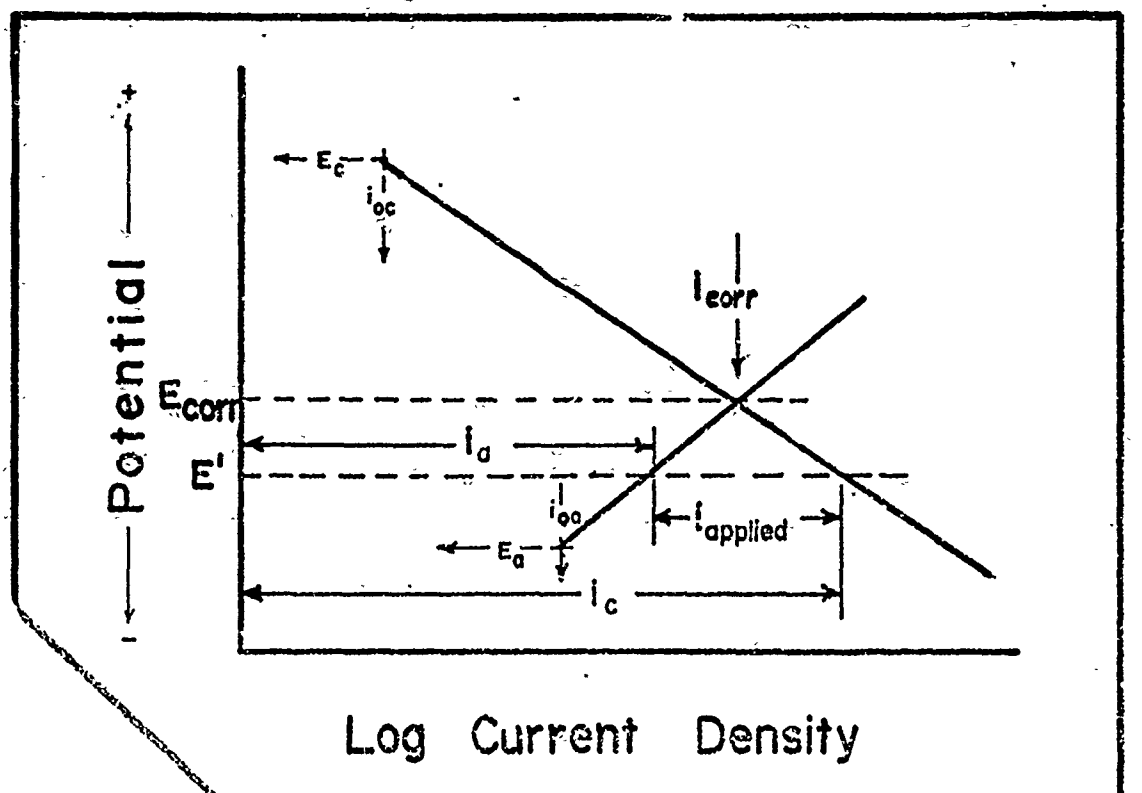

Polarization Diagram - Cathodic Polarization (Ref 22)

polarize the cell to E'. From the Tafel equation, an expression for the overvoltage can be written as

$$|E_{corr}-E'| = \Delta E = \beta_c \log (i_c/i_{corr}) = \frac{\beta_c}{2.3} \ln(i_c/i_{corr}) \tag{11}$$

In a similar manner, the expression for the identical anodic overvoltage can be formulated as

$$\Delta E = -\beta_a \log (i_a/i_{corr}) = -\frac{\beta_a}{2.3} \ln(i_a/i_{corr}) \tag{12}$$

Solving these expressions for i_c and i_a and substituting them into Eq (10) yields

$$i_{applied} = 2.3\, i_{corr}[e^{\Delta E/\beta_c} - e^{-\Delta E/\beta_a}] \tag{13}$$

By utilizing the assumption that the overvoltage is much smaller than unity, the exponential term may be expanded as

$$e^x = 1 + x + x^2/2! + x^3/3! + \ldots, \text{where } x = \Delta E/\beta_i$$

and Eq (12) written as

$$i_{applied} \doteq 2.3\ i_{corr} \Delta E(1/\beta_c + 1/\beta_a) \tag{14}$$

where the higher order terms ($x^2/2!$, $x^3/3!$,. . .) are neglected. This expression can be written as

$$i_{corr} = \frac{\beta_a \beta_c}{2.3\ (\Delta E/i_{applied})(\beta_a + \beta_c)} \tag{15}$$

which is the normal form of the Stern-Geary equation[13]. In a subsequent article Stern[8] demonstrated that even with concentration polarization the predicted corrosion rates are in error by less than 40% (a factor considered excellent by corrosion scientists and engineers).

Mansfeld and Oldham[20] have questioned the Stern-Geary derivation because it assumes that each metal surface is completely anodic or cathodic. With extremely small applied current densities and resulting overvoltages, the possibility of having both oxidation and reduction reactions on the same metal surface does exist. This may occur when the equilibrium corrosion potential of a cell is close to either of the individual metal surface reversible potentials, E_a or E_c. The result presented is as follows:

$$\left(\frac{\partial I}{\partial E}\right)_{E_{corr}} = i_{corr} \left[\frac{1}{b_a} + \frac{1}{b_c} + \frac{1}{\Delta\varphi_a} + \frac{1}{\Delta\varphi_c}\right] \tag{16}$$

where b_a and b_c are equivalent to $2.3/\beta_a$ and $2.3/\beta_c$ respectively from the Stern-Geary equation. The terms $\Delta\varphi_i$ represent the potential differences between the reversible potential of the anodic (or cathodic) surface and the corrosion potential, E_{corr}, e.g. $\Delta\varphi_a = |E_{corr}-E_a|$. These terms are insignificant and may be neglected as long as the corrosion potential is far removed from the reversible potentials. If neglected, the resulting equation is the Stern-Geary equation.

In a subsequent article[21], Mansfeld and Oldham point out that if $\eta = |E - E_{corr}|$ is the polarization overvoltage and if $i = f(\eta)$ is the shape of the polarization curve, the equation for current density, i, can be written as a McLaurian expansion such that

$$i = f_{(o)} + \eta f'_{(o)} + \frac{\eta^2}{2!} f''_{(o)} + \frac{\eta^3}{3!} f'''_{(o)} + \ldots \tag{17}$$

By considering the physical problem, several conditions become apparent. First, since without an overvoltage no applied current can exist, $f_{(o)} = 0$. Then, because of continuity requirements, f', f'', . . . cannot be infinite. Therefore,

$$i = C\eta + D\eta^2 + E\eta^3 + \ldots \tag{18}$$

where C, D, E, . . . are finite constants. Again, if η is small as it is during resistance polarization tests,

$$i \approx C\eta \tag{19}$$

which is a linear function as predicted by Stern and Geary. Mansfeld and Oldham[21] reiterate that their purpose in writing was not to discredit the Stern-Geary equation, but rather to provide an explanation for situations where a linear relationship of the form of Eq (15) is not encountered.

If it can be assumed that the overvoltage is small and that the Stern-Geary equation is an accurate representation of the linear behavior of the overvoltage versus applied current relationship in the vicinity of the equilibrium corrosion potential, the question arises as to whether there is any difference between the corrosion rates determined from anodic and cathodic polarization. Similarly, there is question as to whether either of the polarization methods is advantageous to the other. Theoretically, both the cathodic and anodic polarization methods should provide indentical results[8]. However, several reasons have been proposed as to why cathodic polarization is advantageous to anodic polarization. First, cathodic polarization does not interfere with the actual corrosion process where anodic polarization may provide interference[2]. Second, cathodic polarization may provide a greater linear region[8]. Finally, previous investigators [8, 20] agree that, in general, the slope of the cathodic region is less than the anodic region. Thus, a given overvoltage requires a greater applied cathodic current density. As a result, more data points can be obtained and, in general, greater accuracy can be realized in determining the corrosion rate using cathodic polarization during laboratory tests. No quantitative data were found which demonstrate the magnitude of the differences between the indicated corrosion rates obtained by these methods. As a result, both anodic and cathodic data were obtained in the present study in order to evaluate the differences in the indicated corrosion rates obtained by each method.

Two techniques may be used to obtain polarization data. The potentiostatic technique involves the application of a controlled, constant potential between the anodic and cathodic surfaces and observing the resulting current flow. The galvanostatic technique involves the application of a controlled, constant current between anodic and cathodic surfaces and observing the resulting overvoltage. The potentiostatic technique permits investigation of the passive region; however, it is relatively insensitive to current density changes at small values of applied potential (i.e., in the range where a linear relationship should exist). The galvanostatic method does not permit investigation of the passive region, but it is highly sensitive at small applied currents. Because resistance polarization involves small applied currents and overvoltage near the equilibrium corrosion potential, i.e., within the active region, the galvanostatic technique was considered to be much better suited for this investigation.

In summary, of the methods currently available to determine the rate of uniform surface attack, the galvanostatic resistance polarization method is considered most desirable. This method can provide large quantities of corrosion rate data in a reasonably short time, can be used to measure very small corrosion rates, and can be used to continuously monitor the rate of uniform attack for a corroding system. For these reasons, the galvanostatic resistance polarization method was selected for use in this investigation.

III. Experimental Apparatus

To determine corrosion rates using galvanostatic resistance polarization, the basic apparatus used by Haugen[3] and modified by Coburn[10] was chosen. This apparatus was considered most suitable for several reasons. First, the apparatus had provided accurate and reliable corrosion rate information during these earlier investigations. Second, the procedures for use of the apparatus were well documented. Thus, a metal used in previous investigations could be rerun to develop consistent operator technique. This practice was considered important because Stern[8] reported that corrosion rate determination is subject to investigator technique.

Electrical Circuitry

The electrical circuitry is given schematically in Fig. 14. It is identical to that used by Coburn[10] with the exception that an additional power source was added for use when indications of extremely small corrosion rates were sought. The regulated DC power source produced sufficient current fluctuations to interfere with the experimental results at very low applied current densities.

A constant current was provided by the power source, either the regulated DC power supply (Heathkit Model PS-4) or the battery pack, the decade-resistance bank, R-12, the rotary selector switch, S-1, and the double-pole, double-throw selector switch, S-2. With the appropriate power supply selected, the rotary switch, S-1, allowed selection

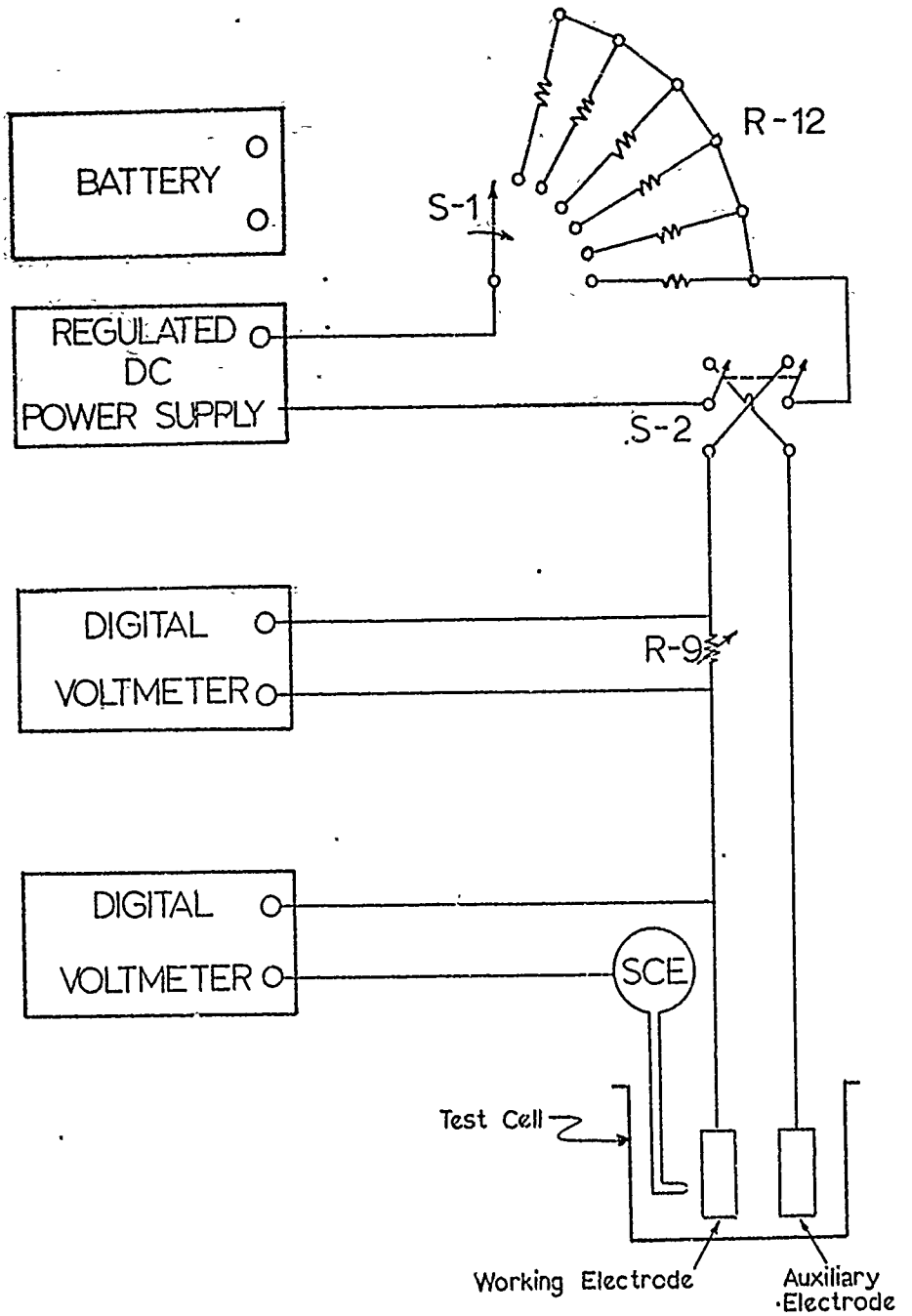

Figure 14: Electrical Circuitry for Galvanostatic Resistance Polarization

of one of the twelve resistors of the resistance bank, R-12. An appropriate resistance was selected so that a suitable current range was available for the entire experiment. The switch, S-2, allowed the direction of current flow to be reversed so that cathodic or anodic resistance polarization data could be obtained.

The two high-impedence (10^{10} ohms) Hewlett-Packard Model 3400A digital voltmeters were used to obtain polarization overvoltage and applied current data. One voltmeter was used to indicate the potential difference between the reference and working electrodes to ±0.1mv. The other indicated the current within the circuit by measuring the potential drop across resistor R-9 (a decade bank of ±1% precision resistors) which provided control of the voltmeter decimal point. Thus, a high degree of accuracy could be achieved and, over wide current ranges, scales could be shifted without introducing greater than 1% indicated current fluctuations.

Laboratory Polarization Test Cell

The laboratory polarization test cell described by Smulczeński[23] and modified by Haugen[3] was used. This cell consists of a specially-constructed two-liter beaker and a fluorocarbon cover designed to provide a gas tight seal. The cover contains five fittings, two ground glass fittings for the thermometer and the purging gas assembly and three O-ring fittings for the working-electrode, auxiliary electrode, and salt bridge assemblies. The cell, shown in Fig. 15, is designed so that all components are visible during testing.

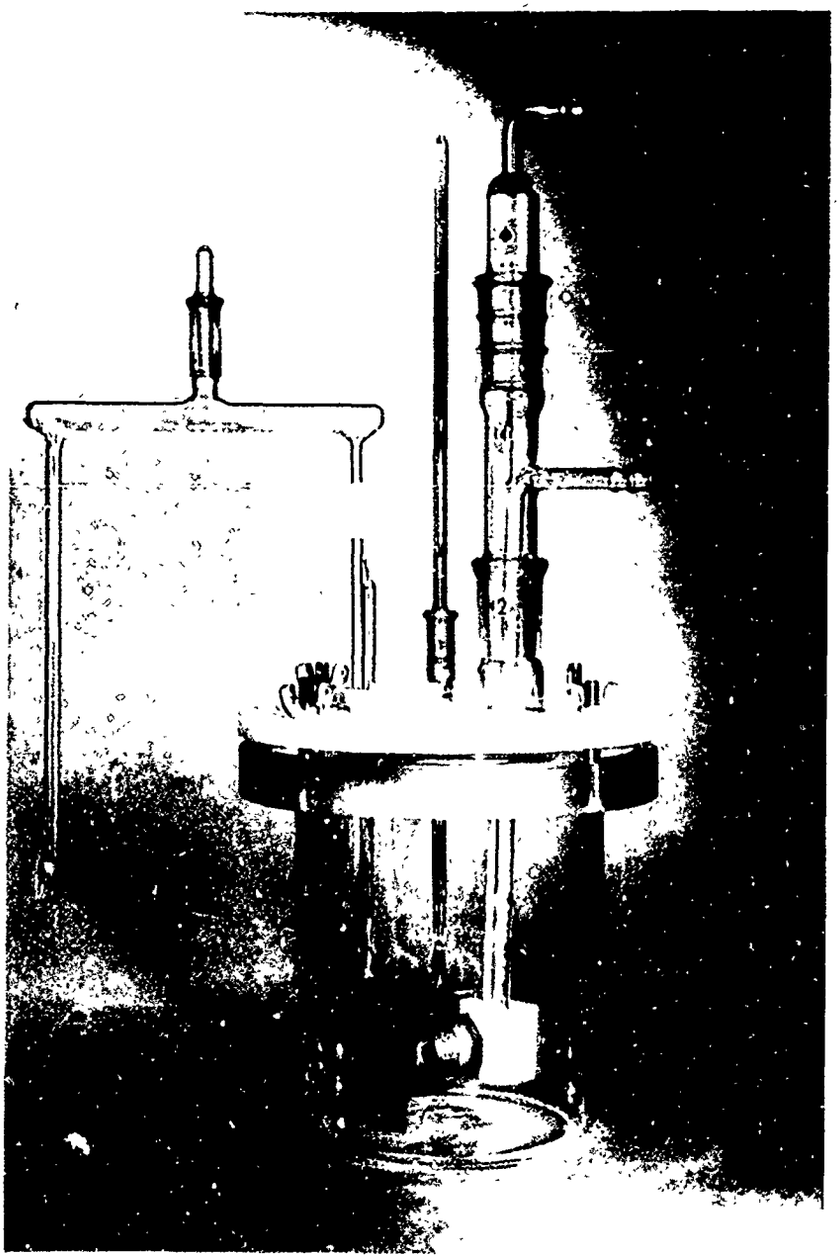

Figure 17: Laboratory Test Cell[3]

Laboratory Electrode Assemblies

The laboratory determination of corrosion rate by the resistance polarization method utilized three electrode assemblies, the working, auxiliary, and reference-electrode assemblies and a salt bridge assembly. These assemblies were not modified from those used by Haugen[3] and Coburn[10].

Working Electrode Assembly. The working electrode assembly used was described by Myers[24] and is shown in Fig. 16. The purpose of this assembly was to suitably hold a metal specimen which has been machined into a right circular cylinder of diameter 1.27 ±0.02cm and of thickness 0.8 ±0.5cm. The exposed surface area design attempted to minimize crevice effects and the accumulation of gas bubbles on the specimen surface. The one square centimeter surface area simplified current density calculations. The importance of avoiding crevice effects has been reported by several investigators[24, 25, 26] because of the accelerating effect which a crevice can have upon the actual corrosion rate.

The fluorocarbon washer inserted into the specimen holder before the specimen served two purposes. First, it provided the one square centimeter of surface area. Second, it provided a sealing surface for the metal specimen so that crevice effects could be minimized.

Auxiliary Electrode Assembly. The auxiliary electrode was a 25 square centimeter platinum gauze spot welded to a 17 centimeter long platinum wire which was supported by

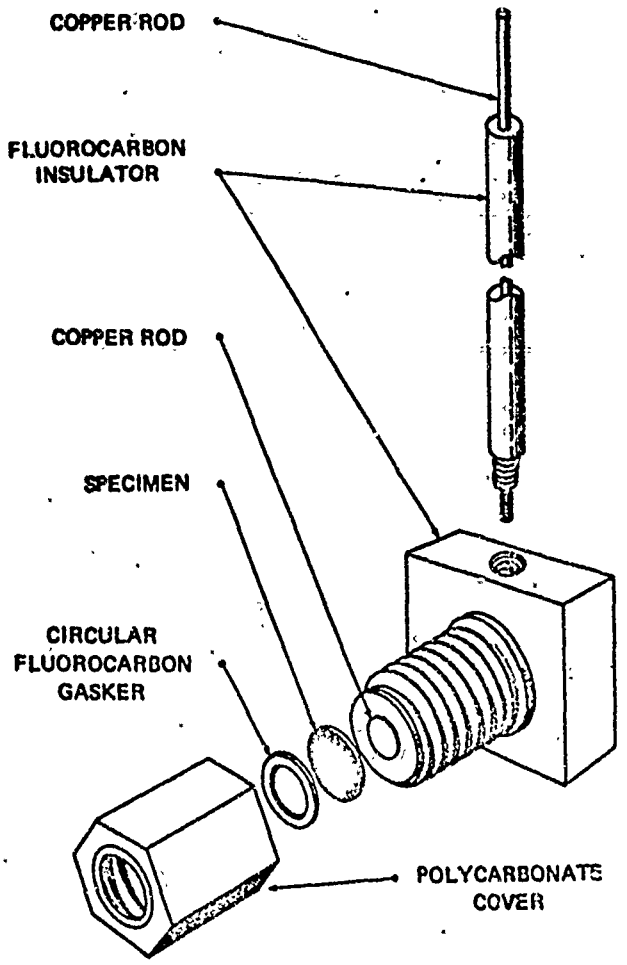

Figure 16: Laboratory Working Electrode Assembly (Ref 24)

sealed glass tubing. This design allowed the maintenance of a gas-tight seal at the cell lid. Platinum was used because it is inert in the electrolytes chosen and the cathodic reaction could occur readily on its surface[1]. When hydrogen was chosen as the gas with which to purge the cell, this electrode became equivalent to a standard hydrogen electrode (SHE). Under these conditions, calculation of the electrolyte pH was facilitated.

Reference Electrode Assembly. A saturated calomel electrode (SCE), Leeds and Northrup Standard 1199-3, was used as the reference electrode because its potential remains stable in a wide range of electrolytes. By operating the test cell at a constant temperature (22 ±1°C), variations due to the dependence of potential indications upon temperature were avoided. The reference electrode was placed in a 150 ml beaker containing 60-100 ml of the test cell electrolyte. The controlled-leak reference electrode was placed external to the test cell to avoid contamination of the test cell electrolyte.

Salt Bridge Assembly

The two-part salt bridge assembly, consisting of a Luggin probe and a salt bridge joined by a fluorocarbon seal, was used to complete the electrical circuit between the reference and working electrodes and to minimize the potential losses associated with the measurement of this potential difference. The Luggin probe, having a one millimeter diameter tip, was mounted through one of the O-ring fittings in the test cell cover.

The salt bridge was designed with a Haber capillary tip at the bottom of the vertical tube section[27]. This tip allowed one drop of electrolyte to gravity flow in approximately thirty minutes[10]. A ground glass joint and stopper were also provided so that the salt bridge assembly could be easily filled with electrolyte. By using a small syringe, electrolyte was drawn from the test cell to fill the salt bridge assembly. A backside capillary was not necessary because the electrolyte concentration remained unchanged during testing and electrolyte flow was not a problem[28].

Purging Gas Assembly

The purging gas assembly allowed filtered gas to enter the test cell and be bubbled through the electrolyte. The gas entered the electrolyte approximately 10cm below the surface through a fritted plug and was vented to a laboratory exhaust hood through the purging gas assembly at the top of the test cell. This exhaust procedure was followed as a safety precaution for tests when hydrogen gas was used.

Experimental Polarization Test Cell

Although the laboratory polarization test cell has provided relatively reliable, reproducible, and accurate data by which to determine the rate of uniform attack, test cell complexity has resulted in restriction of cell use to a laboratory environment. In an attempt to make use of the basic design and experimental techniques of the laboratory cell

while eliminating unnecessary complexity, the experimental polarization test cell was constructed by modifying the laboratory cell. The experimental test cell, shown in Fig. 17, required minor modification of the laboratory test cell cover and extensive modification of the laboratory electrode assemblies.

Experimental Electrode Assembly. The experimental electrode assembly, shown in Fig. 18, incorporated the working, auxiliary, and reference electrode into one assembly and eliminated the need for the platinum auxiliary electrode, standard calomel reference electrode, and salt bridge assemblies. The electrode centers were evenly spaced 2.54 ±0.20cm apart. By using electrodes of different sizes, the cathode-to-anode surface area ratio could be varied. Fluorocarbon washers were provided so that crevice effects were minimized and contamination of the system was avoided. The electrode posts were made of steel for two reasons: first, to provide a strong post which would withstand application of sufficient electrode installation torque to ensure sealing of the electrode base and, second, to minimize cell contamination in the event that minor leakage did result and could not be eliminated.

Electrolyte

The electrolytes used were 1N and 0.1N sulfuric acid, and 3% sodium chloride containing 0.5N potassium sulfate. Reagent grade sulfuric acid (99.5 to 96.5% H_2SO_4) was used in preparing the acid solutions. All solutions were prepared using triple-distilled water.

Reproduced from best available copy.

Figure 17: Experimental Test Cell

Figure 18: Experimental Electrode Assembly

Specimen Selection and Fabrication

Specimen Selection. High-purity iron was selected as the test material because iron-base materials are commonly-used materials of construction and because considerable data are available with which to compare the results of this investigation. Table I gives the analyses of the materials studied.

Annealing. The iron was annealed at 870°C for 24 hours and furnace cooled to room temperature. Disposable heat treatment bags were used to minimize surface oxidation during the annealing process.

Specimen Fabrication. Because of the nature of the experimentation conducted, two specimen types were required. The first was used in the laboratory apparatus; the second was used in the experimental apparatus. The specimens used in the laboratory apparatus were machined right circular cylinders of 1.27 ±0.02cm diameter and 0.7 to 1cm thick. The specimens used in the experimental apparatus were machined right circular cylinders of various lengths so that the surface area ratio effects could be investigated.

Table I

Chemical Composition of
High Purity Iron Specimens*

Element	Composition by Weight Percent	
	I	II
Silicon	<.01	<.01
Manganese	.04	.02
Phosphorous	<.005	<.005
Sulfur	.015	.010
Carbon	.03	.02
Nickel	.04	.01
Chromium	.02	.01
Molybdenum	.01	.005
Copper	.05	.01
Aluminum	<.002	<.002
Vanadium	<.002	<.002
Tin	.005	.005
Iron	Remainder	Remainder

*Analysis performed by Bowser-Morner Testing Laboratories, Dayton, Ohio.

IV. Data Collection, Treatment, and Analysis Procedures

Data were collected using procedures similar to those of previous investigators[3, 10, 29]. The minor changes made are pointed out in the following discussion. Comparison of experimental results obtained using materials similar to those of previous investigators[10, 11] indicated that results were not noticeably affected by the changes made.

Preparation

Electrical Apparatus. The power supply was placed on standby and the digital voltmeters were turned on at least one hour prior to use to insure stabilization of component operations. The digital voltmeter sample rate selector was set to maximum during this period.

Component Cleanliness. With the exception of the auxiliary and reference electrodes, all components were washed thoroughly with detergent, rinsed with distilled and triple-distilled water, and air dried. The auxiliary electrode was cleaned in boiling aqua regia for one minute or until foaming stopped and rinsed thoroughly with triple-distilled water. (Future investigators are cautioned against allowing the glass tube to enter the boiling liquid. Allowing this to happen may increase the glass's susceptibility to breakage). The reference electrodes were kept submerged in distilled water and rinsed with triple-distilled water before use.

Electrolyte. The test cell beaker was filled with approximately 1250-1500 ml of the selected electrolyte and covered with a fluorocarbon lid containing only a purging gas fitting. Either filtered air or hydrogen was bubbled through the electrolyte for a minimum of one hour depending upon the environment (aerated or deaerated) desired. This was a departure from previous procedures. Early investigators[30, 31] reported that from one to eighteen hours were required to achieve deaeration. Recent investigators[3, 10] have reported stable hydrogen electrode potentials in times as short as twenty minutes. Therefore, one hour was considered sufficient to ensure adequate deaeration in the environments selected.

Specimens. Laboratory test specimens were machined and polished on one face through 4/0 emery paper. Experimental test specimens were machined and polished on the untapped face and circumferentially through 4/0 emery paper. After polishing, specimen diameter and height (or thickness) were measured and recorded. This allowed computation of experimental specimen surface areas and provided initial dimensions so that the attempts could be made to compare the results of weight loss tests with actual penetrations realized.

The specimens were washed and rinsed in triple-distilled water to remove residue left by the polishing process, boiled in benzene for three minutes to remove any grease accummulation, and rinsed again in triple-distilled water to remove any remaining residue. The cleaned samples were then placed

in a drying oven maintained at 90°C. After five to ten minutes of drying time, the specimens were removed and weighed on a Williams, Brown and Earle Model 220SP Analytical Balance.

Laboratory Test Cell. The working electrode assembly was readied by placing the cleaned and polished specimen and an unused washer into position in the specimen holder. Washer reuse was avoided because the grooving which occurred during use could have provided an environment suitable for crevice attack during subsequent tests. (Future investigators are cautioned against application of excessive torque to the knurled electrode head. Head cracking and washer deformation may result, significantly changing the exposed surface area and/or providing an environment by which crevice effects may develop and interfere with results.)

The working electrode assembly, the auxiliary electrode assembly, and the Luggin probe were fitted into the test cell cover with the tip of the Luggin probe positioned approximately 2mm from the face of the specimen to avoid shielding effects of the current distribution[32]. The auxiliary electrode assembly was aligned nearly parallel to the specimen face. All O-ring fittings were tightened to insure a gas tight seal.

At the completion of the initial gas purging process, the gas was stopped and the cover removed. Approximately 70 ml of electrolyte were removed and placed in a 150 ml beaker. The laboratory cell cover was installed and the

thermometer and purging gas assembly fitted into the cover. The purging gas assembly was immediately restarted.

The salt bridge was fitted to the Luggin probe with the fluorocarbon sleeve and filled using the small syringe at the ground glass joint. The Haber capillary leg of the salt bridge and the reference electrode were placed in the small beaker of electrolyte drawn from the test cell. By using appropriately-sized blocks, the beaker was positioned so that the vertical leg of the salt bridge was immersed in the electrolyte and the level of electrolyte in the small beaker was below that of the test cell. This was done to insure that electrolyte was not syphoned from the small beaker into the test cell causing test cell contamination.

Experimental Test Cell. The experimental electrode was assembled using three test specimens and three unused washers. In seating the electrodes on the fluorocarbon washer, care was exercised not to damage the electrode surface. (Pliers and a hollowed rubber stopper were used successfully.) With the electrode assembly readied, the purging gas was stopped, the test cell cover removed and replaced with the readied cover. The purging gas assembly and thermometer were fitted to the cover and the purging gas assembly immediately restarted.

Specimen Activation

1. Laboratory Specimen. The laboratory specimen was cathodically activated to remove any surface films which may have formed after specimen cleaning. Activation was accomplished using a 1.5 volt dry-cell battery. The negative

and positive terminals were connected to the working and auxiliary electrodes, respectively, for a period of one minute. The specimens evolved gas bubbles from the exposed surface during activation.

2. Experimental Specimens. The three electrodes of the experimental electrode assembly were each activated for approximately one minute using the 1.5 volt battery. When specimens of equal surface area were to be used, each electrode was labeled as either working, auxiliary or reference and used as indicated throughout the test for standardization purposes and to eliminate variations which might have been introduced by other techniques. During investigations of the effects of varying cathode-to-anode (C/A) surface area ratio, each electrode served as anode, cathode and reference during some portion of the test. A specific testing order was established when C/A ratio effects were investigated and the first test configuration served as the basis for the activation cycle. This activation cycle, shown in Table II, was used for both equal and variable surface area tests.

Table II
Experimental Electrodes Activation Cycle

Step	Working	Auxiliary	Reference
1	+		-
2		-	+
3	-	+	

Data Collection Procedures

Both anodic and cathodic polarization behavior were investigated. The procedures outlined applied to both experimental and laboratory test cells. All tests were conducted at 22 ±1°C and one atmosphere of pressure after sufficient time was allowed for establishment of a "steady-state" corrosion potential, i.e., a potential which varied less than one millivolt during a 15 minute period.

Equilibrium Corrosion Potential

1. Laboratory Test Cell. To determine the "steady-state" corrosion potential, E_{corr}, the digital voltmeter was connected between the working and reference electrode assemblies and the potential monitored until a steady-state value was achieved.

2. Experimental Test Cell. The design of the experimental test cell did not provide a means of determining the equilibrium corrosion potential. Potential differences between the working and auxiliary electrodes and the reference electrode were recorded to allow investigation of their relationship to the indicated corrosion rate.

pH Determination

1. Laboratory Test Cell. The pH of a hydrogen-saturated electrolyte was determined by using the Nernst equation

$$E = E_o - 0.059 \text{ pH} \tag{19}$$

where E is the auxiliary to reference electrode potential at equilibrium conditions and E_o is the potential of the reference electrode with respect to a standard hydrogen

electrode (SHE). The values of pH obtained were compared with those reported by other investigators[3, 10].

2. Experimental Test Cell. The experimental test cell design did not allow pH determination.

Preliminary Electrical Set-up

1. The leads from switch S-2 were connected to the auxiliary and working electrodes and switch S-2 positioned to permit cathodic polarization.

2. The remaining lead (ground) from the digital voltmeter was connected to the reference electrode. Thus, the digital voltmeter provided the working to reference-electrode potential difference.

3. The appropriate power source was connected to the circuit, the variable output knob rotated fully counter clockwise, switch S-1 positioned at a sufficiently high resistance to minimize current flow, and the power turned on.

Resistance Polarization Testing. These procedures were followed using both laboratory and experimental test cells.

1. Current was slowly increased until approximately one millivolt of potential change resulted. Based upon the magnitude of this current increase, an appropriate position of S-1 was selected so that the entire test run could be completed without additional variation of S-1. Similarly, R-9 was positioned so that suitable indicated current accuracy was obtained. The current was decreased to zero and the cathodic polarization test begun.

2. The current was increased slowly to produce approximately one millivolt of potential change and the potential and current recorded. This initial current increment became the "step" by which current was slowly increased to obtain successive data points. No appreciable "stabilization period" was utilized as had been reported by previous investigators[5, 10, 11]. Current was "stepped" a sufficient number of times to achieve a potential change of approximately ten millivolts.

NOTE: Potential values were randomly double checked with a Leeds and Northrup potentiometer (Catalog #8687) during all test runs and entire runs were randomly reproduced to ensure accuracy and reproducibility.

3. A table of corresponding applied current, ΔI, and potential change, ΔE, was constructed.

4. Upon completion of each cathodic polarization test, the applied current was adjusted to zero and switch S-2 positioned to permit an anodic polarization test. Steps 2 and 3 were subsequently repeated.

5. For tests using the experimental test cell, steps 2-4 were repeated for the various cathode-to-anode ratios selected.

6. Upon completion of each test run, all electrical connections to the test cell were removed, the power source turned off or to the standby position, and the digital voltmeters turned off or adjusted to a very low sample rate. As a

departure from the techniques of previous investigators[3,10], the purging gas assembly was not turned off. The purging gas was allowed to flow at a nearly constant rate for the duration of each test in hydrogen saturated environments.

7. The process was repeated at 24 hour intervals for 120 hours.

8. After completing each test, the test cell was disassembled and thoroughly cleaned.

9. Each specimen was washed and the exposed surface cleaned in accordance with weight-loss test procedures[33]. The specimens were dried and reweighed to determine the weight-lost during the test. After weighing, the dimensions of each test specimen were recorded to determine the extent of uniform attack penetration.

10. Where possible, on laboratory specimens, an actual depth of corrosion penetration was determined by carefully polishing the specimen surface until visible traces of corrosion damage were removed and remeasuring the thickness. The difference between initial and final thickness was used as an indication of the penetration of the corrosion attack.

Data Treatment Procedures

Corrosion rate calculations were made using the data obtained by galvanostatic resistance polarization testing and weight loss testing. To minimize mathematical errors and human bias, computerized techniques were used wherever possible.

Resistance Polarization Data Preparation. The data obtained during resistance polarization tests were coded by the experimental run and the day of each run. In general, three runs, each of six days, were used. Thus, in most situations, 18 sets of data were available for polarization resistance determination on a "by run, by day" basis for each configuration (i.e., combination of variables) used. In addition, for each configuration tested, the data for all runs were grouped on a "combined daily" basis to allow determination of an average polarization resistance for each of the six testing days.

Polarization Resistance Determination. To determine the values of polarization resistance, coded data were treated using standard linear regression techniques based upon least square estimation methods. The specific computer program used for this purpose is stored in the AFLC CREATE Computer System. The instructions for obtaining and/or using the program are contained in Appendix M.

The coded data were treated "by run, by day" and on a "combined daily" basis with the intercept suppression option selected. With applied current density, X, and the resulting potential, Y, known, the coefficient β of

$$Y = \beta X \tag{20}$$

was read directly as the appropriate polarization resistance. The statistical F-test, provided automatically by the computer program, served to indicate the agreement of the actual data with the estimated linear relationship of Eq (20).

Daily Corrosion Rate Determination. Daily corrosion rates were computed using the Stern-Geary equation, Eq (15), and Faraday's Law, Eq (4). Tafel slopes, β_a and β_c, used were determined by Ali[11]. Material density was laboratory determined for the material tested. No density difference was noted between the two specimens selected.

Actual computation was done using the computer program of Appendix N. This program was used to (1) tabulate resistance polarization data by run, by day, (2) tabulate polarization resistance values on by run, by day and combined daily bases, (3) compute and tabulate corrosion current density (ma/cm^2) data on by run, by day and combined daily bases, (4) compute and tabulate corrosion rate (microns/year) information on by run, by day and combined daily bases, and (5) compute and tabulate combined daily corrosion rate information in several units to permit more rapid comparison with data from other sources. All output is filed with the Department of Mechanics, School of Engineering, AFIT.

Steady-State Corrosion Rate Determination.

1. Graphical Techniques. To determine the indicated steady-state corrosion rate by graphical techniques, each figure in Appendices F and G was analyzed. In general, the limits of the converged and stabilized corrosion rate envelope, which existed during the final 48-72 test hours, were used as the indicated steady-state corrosion rate range. However, where stability was not observed (e.g., .1N sulfuric acid in the laboratory test cell) considerable judgment was involved.

The steady-state of uniform attack in these instances was considered to be the range of the minimum corrosion rate observed during the final 96 test hours.

2. Computer Techniques. The steady-state corrosion rate achieved by each test configuration was also determined by using regression techniques. All values of corrosion rate calculated on the by run, by day and combined daily bases were combined and used as input data. The combined daily data were included to provide a final steady-state corrosion rate which was somewhat weighted toward the average of the daily corrosion rate values.

A steady-state corrosion rate was found by attempting to fit actual data to a relationship of the general form

$$Y = \beta_0 + \frac{\beta_1}{X} \tag{21}$$

where Y is the corrosion rate at time X. By using this relationship, the coefficient β_0 indicated the steady-state value of corrosion rate directly, since as time, X, becomes very large, the term $\frac{\beta_1}{X}$ approaches zero. The relationship shown as Equation 21 was chosen to approximate Eq (8) for reasons similar to those used by Stern[13] in conjunction with approximating Eq (13) with Eq (14). A goal of the present study was to investigate the validity of this approximation.

Weight Loss Test Results. For each electrochemical test conducted, weight loss tests were performed. The resulting weight loss data were converted to units of corrosion rate (microns/year). Each rate was classified by the electrolyte

(and concentration), the degree of aeration (aerated or hydrogen saturated), and the type of electrode assembly (laboratory or experimental) used. For each class, a mean corrosion rate was calculated and the range of corrosion rates noted. These values, the mean and range, were tabled to allow comparison with electrochemically determined corrosion rates.

Data Analysis Procedures

Data analyses were specifically directed toward achieving the goals and verifying the various assumptions of this investigation. Wherever possible, both graphic and computer techniques were used. In general, computer results were used to supplement and support the results of graphical analyses. This procedure was considered necessary until sufficient experience was gained to determine the accuracy of computer techniques.

V. Analysis of Results

Electrolyte pH

Determination of pH for hydrogen saturated electrolytes in a laboratory test cell are given in Appendix A where maximum, minimum, and mean values are shown. The mean pH obtained for 1N sulfuric acid agrees with that reported by others[3,10]. Similarly, the pH of 0.1N sulfuric acid agrees with the 1.09-1.25 reported by others[40, 66]. The consistency of pH observations for sulfuric acid environments was considered adequate.

Values of pH for 3% sodium chloride/0.5N potassium sulfate were unreported; however, the mean pH was in agreement with the value reported by Prochko[65] for 3% sodium chloride. Due to the greatly reduced hydrogen ion concentration of this electrolyte, the range of pH observed was not unexpected. As shown in Figure 11, wide pH variation in this region (pH 5-7) may have had little effect upon corrosion rate.

Steady-State Corrosion Potentials

Steady-state corrosion potentials relative to a standard calomel electrode (SCE) were recorded daily for aerated and deaerated laboratory test cell environments. The potentials for high purity iron I are shown in Appendix B. Data accumulated for hydrogen saturated 1N and 0.1N sulfuric acid were in general agreement with those reported by Coburn[10] and Mottern[40], respectively. In 3% sodium chloride/0.5N potassium sulfate, potential variations were large; however, both magnitude and range generally agreed with data reported by LaQue and Cox[64].

The corrosion potentials observed in hydrogen saturated 1N sulfuric acid displayed a consistent behavior with time. This is in contradiction to the random behavior reported by Coburn[10]. In this environment, corrosion potentials tended to become more noble during the first 48 test hours, while, during the remaining 72 test hours, change in corrosion potential was small and appeared random. These tendencies are shown in Figure 20 of Appendix B.

Steady-state corrosion potentials observed in aerated 1N sulfuric acid and aerated and hydrogen saturated 3% sodium chloride/0.5N potassium sulfate displayed tendencies similar to those in hydrogen saturated 1N sulfuric acid. As with electrolyte pH, considerably more variation amongst runs was noted in the 3% sodium chloride than in the 1N sulfuric acid; however, corrosion potentials tended to stabilize after 48 hours for each run in these environments. A similar tendency was reported by Coburn[10] for aluminum in deaerated 1N sulfuric acid.

Steady-state corrosion potentials observed in aerated and hydrogen saturated 0.1N sulfuric acid did not show the same tendencies. As Tables VI and VII show, the corrosion potential in 0.1N sulfuric acid tended to become more active during the first 24 test hours; however, during the final 96 test hours, potential change was random. A general shift in the noble direction toward the initial corrosion potential was noted during the final 96 hours.

Although no relationship between corrosion potential and corrosion rate has been reported by previous investigators, the general shape of Figure 20 for hydrogen saturated 1N sulfuric

acid was similar to those of Figures 101 and 102 of Appendix F which show the effect of time on the indicated instantaneous corrosion rate of high purity iron I in hydrogen saturated 1N sulfuric acid. Comparison of the effect of time on the steady-state corrosion potential with the effect of time on the instantaneous corrosion rate for aerated 1N sulfuric acid and both aerated and hydrogen saturated 3% sodium chloride/0.5N potassium sulfate showed similar correlation.

Comparison of corrosion potential vs. time, Table VI, Appendix B and corrosion rate vs. time, Figures 105 and 106, Appendix F, for 0.1N sulfuric acid show an interesting correlation. Both corrosion rate and the absolute value of corrosion potential tended to reach minimum values after approximately 24 test hours. Both tended to increase during the final 96 test hours. Thus, for all data collected, similar variation of both corrosion potential and corrosion rate with time was observed.

Resistance Polarization Data

Data obtained using cathodic and anodic resistance polarization techniques are shown in Appendices C and D. Appendix C contains data obtained using the laboratory probe. Appendix D contains data obtained using the experimental probe. In general, similar results were obtained using both probes. Data accumulated for hydrogen saturated 1N sulfuric acid were compared with similar data reported by Coburn[10]; however, no data were reported in the literature surveyed with which to compare the remainder of the resistance polarization test results of this investigation.

The results of resistance polarization tests for the laboratory probe in 1N sulfuric acid are shown in Figures 21-24 of Appendix C. These figures show that (1) similar results were obtained using either cathodic or anodic resistance polarization techniques, (2) the maximum and minimum observed slopes generally converged and stabilized with time, although the data for a particular run may have moved randomly within the maximum-minimum slope envelope, and (3) data from each run were essentially linear. Individual data points agreed closely with computer provided solutions. Any deviation of individual data points from the computer solution appeared random.

Although in general agreement with data reported by Coburn[10], data accumulated for hydrogen saturated 1N sulfuric acid showed considerably greater slope variation amongst runs on a given day than had been previously reported. This variation was most noticeable during the first 24-48 test hours. However, because of the convergence of data during the final 72 test hours and the general agreement of the average slope in this region with that reported by Coburn[10], the results of resistance polarization tests using a laboratory probe in hydrogen saturated 1N sulfuric acid were considered acceptable. In addition, aerated 1N sulfuric acid data consistency was considered adequate to assure data reliability and reproducibility.

Data obtained using the laboratory probe in 0.1N sulfuric acid are shown in Figures 25 - 28 of Appendix C. Although

Reproduced from best available copy.

generally similar cathodic and anodic results were obtained, slope envelope convergence and stability with time were not apparent. In general, slope convergence occurred during the first 24-48 test hours; however, during the final 72-96 test hours, cathodic data tended to diverge widely. During the same period the anodic data slope envelope remained almost unchanged. For both cathodic and anodic data, slopes tended to increase during the first 24 test hours and decrease during the remainder of the test. Only in an aerated environment using cathodic techniques was 120 test hour data available. Rapid, random potential oscillations were observed at 120 test hours in all other 0.1N sulfuric acid, laboratory probe tests.

Individual data points obtained using anodic techniques closely followed a linear relationship. However, using cathodic techniques, at high applied current densities, evidence of deviation from linearity was noted (e.g. runs 1, 2, 5 at 48 hours and run 3 at 120 hours in Figure 27). This deviation was opposite that expected as the result of concentration effects which may occur during cathodic resistance polarization testing (See Figure 7).

In addition, concentration effects were also observed when aeration was accomplished. Using filtered airflow, rapid and random potential fluctuations over an excessive range were generally observed. If the airflow was stopped after initial aeration and a sufficient time allowed for electrolyte motion to be minimized, potential fluctuations were also minimized. Electrolyte random motion caused by the filtered airflow may

have been sufficient to produce varying diffusion rates at the corroding surface. The investigator technique of stopping the airflow may have changed the controlling polarization process from activation to concentration polarization. Resistance polarization data did not show the presence of concentration effects.

Using the laboratory probe in 3% sodium chloride/0.5N potassium sulfate, resistance polarization data shown in Figures 29-32 were obtained. Cathodic and anodic techniques provided almost identical results. The slope envelope observed remained generally stable; however, little, if any, slope convergence occurred. The number of data points which varied from a linear relationship and the magnitude of the random variations were consistently greater than for either 1N or 0.1N sulfuric acid. No evidence of concentration effects was noted; however, after initial aeration, airflow was stopped in aerated environments. Considering the range of observed pH, the variations shown amongst slopes for each run on a given day were not considered excessive. These data were considered to have provided adequate reliability and reproducibility.

Resistance polarization data obtained using the experimental probe for 1N sulfuric acid are shown in Figures 33 - 56 of Appendix D. Similar results were obtained using either cathodic or anodic techniques. Slope stability was established after 24-48 test hours in both aerated and hydrogen saturated environments for each C/A ratio investigated. Slope convergence was considered excellent except for C/A ratio = 0.2 and 2 (Figures 35, 38, 41, and 44). At these C/A ratios, little,

if any, convergence was noted after 24 test hours, however, the size of the slope envelope was not considered excessive. No concentration effects were noted; however, in aerated environments, airflow was stopped after initial aeration.

For the experimental probe in 0.1N sulfuric acid, resistance polarization data of Figures 57 - 77 were obtained. Cathodic and anodic techniques provided similar results. In contrast to laboratory probe results, slope stabilization was observed after 48-72 test hours. Slope trends during the first 24-48 hours were not as observed in 1N sulfuric acid. Where slopes for 1N sulfuric acid tests tended to increase steadily during the first 24-48 hours, the slope data produced from 0.1N sulfuric acid tests for C/A ratio $\leq$ 2 showed that slopes tended to decrease during the first 24 hours. During the remainder of the test time, a generally increasing slope tendency, similar to that observed for 1N sulfuric acid, was shown. Concentration effects were not observed; however, airflow was stopped in aerated environments.

Experimental probe, 3% sodium chloride (0.5N potassium sulfate) resistance polarization data are shown in Figures 78-97. Again, cathodic and anodic techniques produced similar results. In general, larger and more numerous deviations from linearity were observed in this environment. Computed t-test statistics verified this observation. The deviation from linearity was considered random during anodic tests.

Unlike the sulfuric acid environments investigated, considerably different results were observed for hydrogen

saturated and aerated 3% sodium chloride environments. In hydrogen saturated environments, data could be obtained throughout the 120 test hours with characteristics similar to those generally observed for sulfuric acid. In general, slopes increased during the first 24-48 test hours and stabilized thereafter. Slope convergence was considered excellent.

Aerated environment resistance polarization test results were less satisfactory. Zero and 24 test hour data were available on only one run. Although slopes were stable with time, no slope convergence was observed. Significant differences were observed between maximum and minimum slopes on a given day. Potential fluctuations were similar to those observed in aerated 0.1N sulfuric acid; therefore, airflow was stopped Concentration effects were observed (Figs.83-92).

Tests were conducted to determine the extent of the concentration effects in aerated 3% sodium chloride/0.5N potassium sulfate. The results of limited tests indicated that significant concentration effects may have been present. Weight loss tests were conducted on two high purity iron I laboratory specimens for which previously consistent corrosion rates had been observed. One specimen was tested in an aerated environment with no airflow; the other was tested with a continuous filtered airflow. After a 120 hour test, the electrolyte of the first specimen was clear and contained a slight reddish-brown residue. The electrolyte of the other specimen was reddish-brown and the specimen was not visible through the electrolyte. Weight loss tests showed

that the weight lost by the second specimen was approximately seven times that of the first. Converted to corrosion rate, the two specimens lost weight at rates of 93 and 651 microns/year, respectively. Although testing was limited, results do tend to show that concentration effects may be significant in aerated environments and that investigator technique (e.g. stopping the airflow) may have had a significant effect upon corrosion rate.

Because of the unexplained data non-linearity and slope divergence observed for aerated 0.1N sulfuric acid using cathodic techniques, supplementary tests were conducted using 0.01N sulfuric acid. Data could not be obtained in an aerated environment because of excessive potential fluctuations. The results of resistance polarization tests in hydrogen saturated 0.01N sulfuric acid are shown in Appendix E.

In a laboratory test cell, cathodic data could not be obtained. Using cathodic techniques, large current densities produced little, if any, overvoltage indication. In contrast, anodic techniques provided consistent resistance polarization data. Both techniques provided similar data for the experimental test cell; however, only cathodic data are reported.

Of particular interest in these tests was the behavior of the steady-state corrosion potential with time. Both corrosion rate and corrosion potential (absolute value) reached minimum values at approximately 72 test hours. Both increased during the remainder of the test, although the corrosion potential increase was small. (Table XI and Figure 100 of Appendix E).

In conclusion, the consistency of data obtained using the experimental probe in deaerated environments was considered adequate to assume data reliability and reproducibility. Although considerable consistent data were obtained for aerated sulfuric acid environments, effects observed in 0.1N and 0.01N sulfuric acid and 3% sodium chloride/ 0.5N potassium sulfate produced doubt as to the relevance of aerated environment data. In general, data consistency decreased as electrolyte pH increased.

Polarization Resistance Determination

Polarization resistance values were determined by using graphical and computer techniques. In general, regardless of environment or test technique, "by run, by day" data tended to verify the existence of a linear overvoltage vs. applied current density relationship in the immediate vicinity of the steady-state corrosion potential. Statistical t-test provided by the linear regression program confirmed this observation.

However, use of computer techniques alone to determine polarization resistence values and verify the linearity of potential vs. applied current density relationships was found unsatisfactory. For example, data shown in Figure 19 may produce equivalent computed slopes and acceptable t-test statistics; but, entirely different conclusions are drawn about data linearity and the presence of concentration effects when the data are examined graphically. Therefore, use of graphical techniques was considered essential.

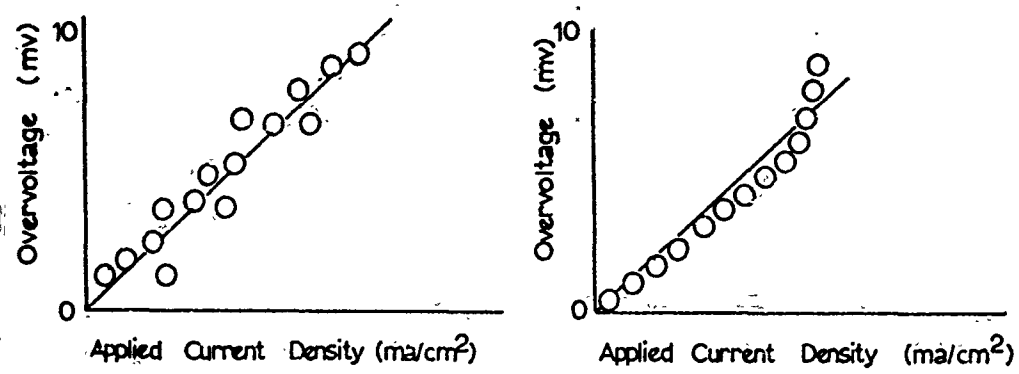

Figure 19: Comparison of Data Providing Equivalent Polarization Resistance Indications Using Linear Regression Techniques.

Determination of average daily polarization resistance values was also done using both graphical and computer techniques. The general tendency for slope convergence after 24-48 test hours was shown by computer results. Statistical t-tests showed that data correlation was generally excellent during the final 72-96 test hours. Similarly, the lack of correlation during the initial 24-48 hours was also indicated. Since in no instance were concentration effects similar to Figure 7 observed for data on a "combined daily" basis, the statistical t-test was considered an adequate indication of combined daily data correlation.

Daily Corrosion Rate Determination

Appropriate polarization resistance values for "by run, by day" and "combined daily" data were used as input data for the computer program of Appendix N. Appropriate polarization resistance values were considered those determined by graphical analyses; however, wherever possible, computer determined values were used. In general, only for a few randomly located cases

during the first 24 test hours were graphical and computer results different. These situations arose only when average polarization resistance was being determined and a large data envelope was observed.

The effect of time on computed instantaneous corrosion rate is shown in Appendices F and G for the laboratory and experimental test cells, respectively. Corrosion rate "envelopes" were drawn (1) to show approximate observed corrosion rate ranges and (2) to show corrosion rate convergence and stability tendencies. In general, the figures of Appendices F and G simplified and/or reinforced much of the resistance polarization data analysis.

Laboratory Test Cell. Figures 101-108 of Appendix F show that, generally, greater indicated corrosion rate convergence was observed using anodic techniques for sulfuric acid environments. This tendency was not observed for 3% sodium chloride/0.5N potassium sulfate. Therefore, no general conclusion could be drawn.

The expected decrease and stabilization of corrosion rate with time was observed using cathodic techniques for hydrogen saturated 1N sulfuric acid in a laboratory test cell (Figure 101). In the remainder of the sulfuric acid environment tests, the indicated instantaneous corrosion rate reached a minimum value after approximately 24 test hours and increased during the remainder of the test. The indicated corrosion rate increase during the final 96 test hours was most noticeable for cathodic observations in 0.1N sulfuric acid. Anodic

techniques may have produced similar results, however, 120 test hour data were not available due to excessive potential fluctuations. Laboratory test cell, 3% sodium chloride (0.5N potassium sulfate) test results, shown in Figures 109-112, were less convergent and more stable than sulfuric acid tests.

Experimental Test Cell. The instantaneous indicated corrosion rate of high purity iron I in 1N sulfuric acid as indicated in the experimental test cell is shown in Figures 113-116 of Appendix G. Data convergence was generally greatest at C/A ≥ 2.5. Only at 120 test hours in a hydrogen saturated environment using anodic techniques was data divergence noted. In general, the indicated corrosion rate decreased and stabilized after 24-48 test hours. Data convergence and stability during the final 72-96 test hours were considered adequate for each C/A ratio investigated.

Data for 0.1N sulfuric acid are shown in Figures 117-120. Adequate data convergence and stability were observed for each C/A ratio investigated in a deaerated environment, although widely varying characteristics were observed during the first 24 test hours. In aerated 0.1N sulfuric acid environments, similar variations in results for the first 24 hours were observed; however, the adequacy of data convergence was questionable. At C/A ≥ 2.5, indicated corrosion rates varied over a wide range. Little, if any, convergence was observed during the final 72 test hours. At C/A ≤ 2.0, convergence and stability of anodic and cathodic data during the final 96 test hours was considered excellent.

Deaerated 3% sodium chloride/0.5N potassium sulfate environments provided excellent data convergence and stability for each C/A ratio investigated (Figures 121-124). Although greatest convergence was noted at C/A =0.2, all data was considered excellent. Average aerated data was generally stable during the final 72 test hours; however, widely varying by run, by day results with little, if any, convergence were observed during this period.

Indicated Steady-State Corrosion Rate

Using graphical and computer techniques, the indicated steady-state corrosion rate data shown in Appendices H and I were obtained. Table XII of Appendix H shows the graphically determined, laboratory test cell, indicated steady-state corrosion rates. Figures 125-130 of Appendix I show the graphically determined indicated corrosion rates for experimental test cell configurations plotted as a function of cathode-to-anode surface area ratio. Computer regression techniques were used to determine whether or not observed instantaneous corrosion rate vs. time data obtained in the experimental test cell fit the relationship of Eq (21). The resulting data are shown in Tables XIII - VX of Appendix I.

C/A Ratio Effects. The effect of cathode-to-anode surface area ratio on the steady-state corrosion rate indicated in an experimental test cell was negligible for 1N sulfuric acid, hydrogen saturated 0.1N sulfuric acid, and aerated 3% sodium chloride/0.5N potassium sulfate. Although the indicated corrosion rate ranges varied considerably amongst the

various C/A ratios investigated in these environments, corrosion rate did not tend to increase or decrease as C/A ratio was increased. Cathodic and anodic polarization techniques provided similar results.

In the remaining environments, aerated 0.1N sulfuric acid and hydrogen saturated 3% sodium chloride/0.5N potassium sulfate, C/A ratio effects may have been observed. In aerated 0.1N sulfuric acid, the upper limit of the corrosion rate range increased as C/A ratio increased. The increase was particularly noticeable for C/A $\geq$ 2.5 (Figure 128); however, these results were considered inconclusive for two reasons. First, not enough C/A ratios were investigated to provide conclusive results; and, second, the region in which C/A $\geq$ 2.5 was also the region in which anode size was reduced from $5cm^2$ to $2cm^2$.

In 0.1N sulfuric acid, especially in aerated conditions, considerable pitting attack was observed (Figure 142 of Appendix L). Although this photomicrograph was taken of a laboratory specimen, similar pitting attack to a lesser degree was observed on the exposed end (i.e., the end grains) of experimental specimens after 0.1N sulfuric acid tests. Very little, if any, localized attack was observed on the circumferential exposed area.

Experimental specimens were machined to a constant diameter and surface area changed by varying specimen length. As surface area was decreased, the end of the experimental specimen comprised a larger percentage of the surface area. Thus, a greater percentage of the surface area was subjected

to pitting attack and the exposed surface area was most noticeably changed in size and shape. This change in surface area size and shape as a result of pitting attack may have been more responsible for the increased corrosion rate range than the increased C/A ratio.

Hydrogen saturated 3% sodium chloride environments produced results shown in Figure 120 of Appendix I. Test results indicated that the upper and lower steady-state corrosion rate limits increased by approximately 10 microns/year over the range of C/A ratios investigated. This represented approximately a 50% corrosion rate increase which was considered insignificant when compared to the seven fold increase observed by varying electrolyte agitation.

Thus, tests conducted using the experimental test cell do show that, over the range of cathode-to-anode ratios investigated and using the techniques described in Chapter IV, cathode-to-anode surface area ratio had little effect upon indicated corrosion rate. Similarly, pitting attack on end grain areas of experimental specimens of various lengths may have been responsible for the significant increase of the upper limit of the indicated steady-state corrosion rate range. The indicated steady-state corrosion rate ranges from the experimental test cell tests of this investigation are shown in Table III.

Laboratory and Experimental Test Cell Results. Comparison of steady-state corrosion rates indicated in laboratory and experimental test cells was completed using Table III and

Table III

Indicated Steady-State Corrosion Rates in the Experimental Test Cell

Test Cell Configuration*	Polarization Technique	Corrosion Rate Ranges (microns/year)		
		Minimum	Maximum	Range
2	Cathodic	340	525	185
	Anodic	340	560	220
4	Cathodic	360	550	190
	Anodic	360	570	210
6	Cathodic	170	330	160
	Anodic	190	360	170
8	Cathodic	160	350	190
	Anodic	210	370	160
12	Cathodic	20	32	12
	Anodic	20	38	18
14	Cathodic	60	135	75
	Anodic	70	150	80

*See Table XIX, Appendix K for explanation of configuration numbering.

Table XIII, Appendix H. In the hydrogen saturated envi[illegible]nts tested, laboratory and experimental test cell results w[illegible] consider[illegible] equivalent. In deaerated sulfuric acid envi[illegible]ments, the indicated corrosion rate ranges were smaller [illegible] the labor[illegible]ory test cell than in the experimental test [illegible]. Consideri[illegible] the cost, accuracy, and sensitivity of labo[illegible]y equipment, this was as expected. In deaerated 3% sodi[illegible] chlorid[illegible]/0.5N potassium sulfate, both test cells produ[illegible] im-ilar re[illegible]s. Considering the wide pH range observed [illegible] laborat[illegible] test cell, the magnitude of the laboratory [illegible] cell co[illegible]ion rate range was not unexpected.

Res[illegible]s obtained for aerated sulfuric acid enviro[illegible] did not [illegible]w the degree of correlation shown in hydrog[illegible] saturat[illegible]nvironments. Steady-state corrosion rates [illegible]cated in[illegible]e experimental test cell were not greatly a[illegible]d by chan[illegible] the degree of aeration (i.e. both aerated [illegible] hydroge[illegible]turated environments provided similar resu[illegible] In contr[illegible], laboratory test cell results showed that [illegible]tion di[illegible]bstantially increase the indicated steady-[illegible] corrosi[illegible]rate range. For 1N sulfuric acid, both low[illegible] upper c[illegible]sion rate limits were increased by approxi[illegible] a facto[illegible] two. For 0.1N sulfuric acid, aeration of [illegible] laborat[illegible] test cell increased the upper corrosion r[illegible]it by 50-1[illegible]ercent, while the lower limit increased o[illegible] slightl[illegible].

Ex[illegible]mental test cell results for aerated 3% so[illegible] chlorid[illegible].5N potassium sulfate tended to verify prev[illegible]

discussed results concerning the sensitivity of this test cell configuration to increased aeration and electrolyte agitation. For each C/A ratio investigated, lower and upper rate limits increased by approximately factors of 3 and 4, respectively, upon aeration. In contrast, laboratory test cell results increased by less than a factor of two upon aeration. The significantly different hydrogen ion concentrations of sulfuric acid and sodium chloride may explain the different aeration effects observed in these environments.

Computer Techniques. Regression analyses of experimental test cell data to determine whether or not actual data fit the relationship of Eq (21) were considered insufficient to draw general conclusions. However, some problems were found in interpreting computer output.

The computed steady-state corrosion rate, β_0, was given as a single value without variance. The coefficient, β_1, was given as an estimated coefficient with a variance. This variance was computed as if constant for the entire length of the estimated line (Eq (21)). However, from practical experience, the variance was not constant, but rather decreased rapidly during the first 24-48 test hours to a more constant value. Thus, standard deviation information shown in Tables XIII-XV of Appendix I may be considerably higher than actually present in the region where the steady-state corrosion rate was indicated.

The computed t-test and F statistics provided by the program should have indicated the general agreement of actual

data with the estimated relationship. Because of the wide variation in actual data during the first 24 test hours, use of these statistics was considered unreliable. Although data generally fit the estimated relationship, especially during the final 96 test hours, no conclusion to this fact could be drawn from the computer results alone.

Observed vs. Indicated Results

Up to this point, the discussion has focused on data obtained during this investigation using resistance polarization techniques. Thus, the discussion has not approached the question of the accuracy of indicated corrosion rate data.

The results obtained using galvanostatic resistance polarization techniques for hydrogen saturated 1N sulfuric acid were compared with the results of Coburn[10]. The indicated corrosion rate ranges (270-480 microns/year and 340-570 microns/year using the laboratory and experimental test cells, respectively) were slightly less than the 642 microns/year which was reported by Coburn[10]; however, this was as expected. By allowing the hydrogen to flow throughout the test, the long periods of aeration previously encountered between daily resistance polarization tests were avoided.

Weight-loss tests performed simultaneously with resistance polarization tests provided a corrosion rate range of 648-1223 microns/year or a mean of 989 microns/year from six tests (Table XX, Appendix K) in the laboratory test cell. Experimental test cell results were 674-1122 microns/year or a mean of 859 microns/year for eight tests. The consistency

of these results indicated that actual weight losses in the two test cells were comparable. These results were slightly higher than indicated by resistance polarization techniques; however, weight-loss test results agreed more closely with the rates reported by McKay and Worthington[17] (835 microns/year), Plumb[48] (1170 microns/year), Greene and Saltzman[9] (1580 microns/year), and Mottern[40] (1[illegible] microns/year). Actual penetrations of 10-15 mils were observed after 120 hour tests in laboratory test cells.

In aerated 1N sulfuric acid, actual penetrations of 14-22 mils were noted in laboratory specimens after the 120 hour tests. Again, actual penetration was greater than indication by resistance polarization techniques or as observed from weight-loss tests; however, the consistency of weight-loss and resistance polarization data should be noted. For the laboratory specimens, the indicated corrosion rate range was 500-960 microns/year. This was approximately twice the rate observed in hydrogen saturated environments. Correspondingly, the results of weight-loss tests showed a similar increase (1019-2150 microns/year or a mean rate was 1342 microns/year for six tests). Thus, for laboratory specimens, resistance polarization and weight-loss test results varied similarly; however, corrosion rates were not comparable.

The experimental test cell indicated a corrosion rate range of 360-580 microns/year. A mean corrosion rate of 787 microns/year was found from weight-loss tests. This correlation was better than observed for the laboratory

probe. Since laboratory specimen exposed surface was completely endgrain material and since endgrain areas appeared most susceptible to accelerated attack (i.e. little accelerated attack was noted on the circumferential surface of the experimental probes), the increased experimental specimen corrosion rate correlation may have been due to the reduced percentage of exposed endgrains.

The severity of actual corrosion damage is shown in Figures 136-138 of Appendix L. Comparison of these photomicrographs with Figures 157-160 suggests the susceptibility of the laboratory specimens to intergranular attack. Similar attack to a much lesser extent was noted on the exposed end of the experimental specimens. For either specimen type, hydrogen saturated environments produced considerably less actual damage; however, the same corrosion mechanism was apparently present.

Thus, in 1N sulfuric acid resistance polarization techniques may have adequately indicated the rate of metal surface dissolution. Weight-loss test results and photomicrographs (Figs. 137, 158, and 159) indicated that actual metal loss may have been primarily intergranular and that intergranular attack may have proceeded completely around bulk grains. Resistance polarization techniques generally produced corrosion rate indications somewhat less than weight-loss tests. Neither accurately indicated the severity of the actual penetration damage occurring at the metal surface.

In 0.1N sulfuric acid, localized endgrain corrosion was also evidenced; however, this accelerated attack appeared

to be crevice and pitting attack. In addition, these localized forms of attack appeared to be present regardless of the degree of aeration.

In the laboratory test cell, resistance polarization techniques may have indicated that some form of localized attack was present. The rapid increase in indicated corrosion rate after 24 test hours indicated by Figs. 105-108 may have provided this indication. Similarly, the variation of steady-state corrosion potential (Tables VII and VIII, Appendix B) may also have signaled the presence of localized attack.

Laboratory specimen weight-loss test results verified that localized attack was present. Six tests provided a corrosion rate range of 1175-1858 microns/year with a mean of 1556 microns/year in deaerated environments. In aerated environments, the mean and range were 1564 microns/year and 1015/1958 microns/year, respectively. These results tended to show that the pitting and crevice attack which occurred were independent of the degree of aeration.

Photomicrographs further confirmed the presence of severe pitting and crevice attack (Figs. 139-142, Appendix L). These photomicrographs may also have shown why weight-loss test results were considerably higher than could have been predicted from the area beneath the indicated corrosion rate vs. time graphs. In Figures 139 and 140, severe localized damage (i.e. crevice attack) is visible. This crevice attack occurred in the region where the fluorocarbon seal contacted the metal surface. Various amounts of applied electrode assembly head torque could not eliminate the presence of this crevice.

Examination of Figure 140 shows that at two points within the crevice, the attack has apparently proceeded intergranularly around metal particles. If this occurred often within the crevice, a considerable amount of metal could be lost from the surface. Similarly, if resistance polarization methods indicated the metal dissolution rate, these particle losses may have gone undetected. In addition, due to the pitting attack shown in Figure 142, the metal surface shape and area have been significantly altered. These combined factors may account for the difference between the indicated corrosion rate and actual weight-loss realized.

As in 1N sulfuric acid, neither weight-loss nor resistance polarization techniques accurately indicated the actual penetration to which corrosion damage proceeded. Actual penetrations of 16-27 mils were observed in laboratory specimens. Thus, for 0.1N sulfuric acid in the laboratory test cell, the presence of localized attack may have been indicated by both resistance polarization and weight-loss techniques; however, the actual damage was not adequately indicated.

For the experimental specimens, resistance polarization techniques indicated that aeration had little effect upon corrosion rate. Weight-loss tests showed that aeration did affect corrosion rate. Resistance polarization techniques indicated corrosion rate ranges of 170-360 and 160-370 microns/year for deaerated and aerated environments, respectively. Weight-loss tests produced a mean corrosion rate of 537 microns/year from twelve tests with a range of 434-633

microns/year in deaerated environments. In aerated environments, a mean of 732 microns/year for nine tests and a range of 550-945 microns/year were observed.

Endgrain corrosion may have accounted for the differences noted between resistance polarization and weight-loss test results. Weight-loss-determined corrosion rates were generally larger for small samples. The percentage of the total surface which was endgrain material also increased as specimen size decreased. As was noted for laboratory specimens, endgrain attack was localized and relatively independent of the degree of aeration. As specimen size decreased, the average surface area weight loss could have been expected to increase. Thus, the size of the weight-loss test specimens and grain orientation may have been more of a determining factor than the degree of aeration. No method was found by which weight-loss data could be used to identify and quantify portions of the attack as general or localized.

In both 1N and 0.1N sulfuric acid, crevice attack was observed on the base of the experimental specimens. Typical damage is shown in Figures 148-151 of Appendix L. Various sealing surfaces and applied installation torque combinations were used; however, no technique was found to eliminate the crevice effects which occurred. Similar damage occurred on all experimental specimens in both aerated and deaerated environments. This further supported the observations that crevice attack was independent of the degree of aeration.

These photomicrographs also indicated that localized attack began at some distance from the specimen circumference.

Variation in applied installation torque appeared to change the radial distance of the observed crevice (i.e. the greater the torque, the closer the crevice to the circumference of the specimen base); however, the crevice could not be eliminated. For crevices close to the specimen circumference, attack similar to Figure 151 was observed with the eventual destruction or loss of material between the crevice and the specimen circumference. This loss or destruction may have contributed significantly to the weight lost during the test period and, thus, the larger weight-loss determined corrosion rate of experimental specimens.

In hydrogen saturated 3% sodium chloride/0.5N potassium sulfate the indicated laboratory specimen corrosion rate of approximately 19-55 microns/year by resistance polarization techniques was consistent with the average of 59 microns/year observed from three weight-loss tests. Very little accelerated attack was observed. At the circumference of the exposed surface area, an area of slight intergranular attack was present; however, actual penetration was found to be less than 2-3 mils. Actual penetration may have been less than micrometer accuracy.

Experimental specimen results in deaerated 3% sodium chloride were not as comparative. The resistance polarization indicated corrosion rate range of 20-38 microns/year was considerably less than the 83-93 microns/year observed from six weight-loss tests. The unusually high weight-loss corrosion rates may have been due to localized attack. Figures 152-153

of Appendix L show typical pitting attack which occurred on the circumferential exposed surface of the experimental specimens. This attack was greater than that observed on experimental specimens in sulfuric acid environments. Thus, because of the very low corrosion rate reported for iron in environments with pH = 5-7 (e.g. McKay and Worthington[17] report 45-90 microns/year), any localized attack may have been a large portion of the total weight-loss observed.

In addition, small amounts of face pitting and base crevice attack similar to that observed in 0.1N sulfuric acid were observed. Again, because of the low indicated corrosion rate, forms of localized attack may have contributed significantly to the total weight lost. If the weight lost by localized attack was by a bulk intergranular mechanism as indicated for 0.1N and 1N sulfuric acid environments, then the theory that resistance polarization techniques indicated the rate of metal dissolution could be further supported. Pit surface roughness (Fig. 153) may indicate the intergranular nature of localized attack; however, no conclusive evidence was found.

In aerated 3% sodium chloride environments, the difference amongst laboratory and experimental test cell and weight-loss test results was greater than in deaerated environments. The laboratory test cell indicated corrosion rate range of 38-62 microns/year was considerably less than the range of 60-150 microns/year observed in the experimental test cell. Both of these ranges were considerably lower than corresponding weight-

loss test ranges. Weight-loss tests showed that laboratory and experimental specimens had corrosion rate ranges of 111-185 and 167-342 microns/year, respectively.

The intergranular attack occurring on laboratory specimen surfaces is shown in Figures 146 and 147 of Appendix L. Although the variation between resistance polarization and weight loss results is not explained, the photomicrographs do show that actual penetration (3-7 mils) was considerably greater than either resistance polarization or weight loss techniques indicated.

In summary, resistance polarization techniques generally provided an accurate indication of the rate of metal dissolution by electrochemical processes. Weight-loss tests provided a more accurate indication of the total material weight loss. However, because of observed localized endgrain corrosion, neither technique accurately described the actual corrosion penetration. In addition, it is doubtful that resistance polarization specimens could be used effectively over extended periods because of the observed susceptibility of these specimens to localized forms of attack. Finally, although the corrosive attack on the test specimen may be accurately indicated, the correlation of this attack to that occurring in an operating system has yet to be shown.

Iron Purity Effects

Because of the effect of iron purity on corrosion rate reported by Greene and Clary[49], high purity iron specimen II (Table I) was tested to determine (1) if corrosion rate was

sensitive to changes in iron purity and (2) if this sensitivity could be detected using resistance polarization techniques. Test results are shown in Appendix J. Due to time constraints, only limited testing was completed. Hydrogen saturated 1N sulfuric acid was chosen for the tests because of the correlation achieved between laboratory and experimental test cells in this environment.

The effects of time on instantaneous indicated corrosion rate for laboratory and experimental test cells are shown in Figures 134 and 135, respectively. The indicated steady-state corrosion rate of a laboratory specimen was approximately 9,000 microns/year. The experimental specimen steady-state corrosion rates were similar for the C/A ratios selected. Corrosion rates of 6500-9500 and 4500-7000 microns/year were indicated for C/A ratios of two and three, respectively.

Weight-loss tests were conducted during the two laboratory test cell runs. The results are shown in Table XIX, Appendix J. As expected, the actual metal loss was greater than the resistance polarization corrosion rate range; however, the magnitude of the difference was not expected. Although only limited testing was done, no correlation was found between resistance polarization and weight-loss corrosion rates.

Photomicrographs of both laboratory and experimental test cell specimens were taken. The laboratory specimen is shown in Figures 143-145, Appendix L. The experimental specimen is shown in Figures 154-155. Both specimens

incurred considerable corrosion attack. Because of the magnitude of the damage, the mechanism by which the damage occurred was not visible at low magnification. However, at higher magnification (Figs. 144 and 145) an indication of the corrosion mechanism may have been visible.

In these photomicrographs, a surface film, which appeared to be iron oxide, could be seen. However, the film was not continuous. The surface film pattern may have marked the location of grain boundaries. If so, the theory that metal dissolution occurred at the more active grain boundaries may be further supported. The grain structure of specimen II is shown in Figure 156.

The corrosion process which occurred on the surface of an iron II specimen was violent. Evidence of this violence was visible during corrosion rate tests. Gaseous bubbles were continuously evolved from the surface. If the reaction was as violent as indicated, the protective hydrogen film may have broken down almost as fast as it was formed. If this occurred and left a more anodic unprotected grain and a more noble (cathodic) protected grain boundary, a metal oxide coating may have tended to form slowly on the bulk grain surface. If for some reason the oxide coating at the grain boundary tended to breakdown, a situation similar to Figure 145 might result. At this point, rapid and severe intergranular attack may have begun. No reason can be offered as to why the grain boundary oxide would tend to be less stable and cohesive than the oxide formed on the bulk grain unless the speed of oxide formation

affected its stability and cohesiveness (i.e. the slower the oxide forms, the more cohesive the oxide coating).

Using the results of Greene and Clary[49] and the laboratory analyses of the composition of the two specimens used during this investigation, the corrosion rate of specimen II could have been predicted as greater than specimen I; however, the magnitude of the difference between indicated and/or observed corrosion rates of the two specimens could not have been predicted. No explanation could be found for the magnitude of the difference in corrosion rates; however, this limited testing did indicate that knowing the corrosion rate of "pure iron" in an operating environment may be of little or no value. The synergistic effects produced by the various impurity (alloying) elements may be far more important. Thus, unless tests are conducted using an anodic surface which is a sample of the material for which corrosion rate information is desired, the results may be less than meaningful. For the particular specimens tested in hydrogen saturated 1N sulfuric acid, polarization resistance indicated corrosion rates were considered accurate measures of the rate of metal surface dissolution; however, these indicated rates were not considered accurate measures of the actual damage (i.e. the penetration of corrosion damage).

VI. Results and Conclusions

Results

1. An experimental probe with anode, cathode, and reference electrodes of the same material was designed and tested using resistance polarization techniques.

2. Experimental test cell resistance polarization data displayed sufficient slope convergence and stability after a 120 hour test period to permit determination of steady-state corrosion rates.

3. Experimental test cell resistance polarization data displayed sufficient reproducibility during the final 72-96 test hours to permit steady-state corrosion rate determination within a factor of two.

4. From resistance polarization tests, steady-state corrosion rate ranges determined using cathodic and anodic techniques were in general agreement. In 1N sulfuric acid and 3% sodium chloride/0.5N potassium sulfate, corrosion rate ranges agreed within 20%. In 0.1N sulfuric acid agreement was within 25%.

5. Corrosion rates determined from weight-loss tests were 2-3 times higher than corresponding rates indicated using resistance polarization techniques.

6. Actual corrosion penetrations due to localized attack were 30-70 times greater than penetrations indicated by resistance polarization.

7. Photomicrographs showed the presence of considerable localized attack - intergranular, crevice, and pitting attack - on the endgrain surfaces of both laboratory and experimental

specimens. With time, localized attack caused considerable increase of the exposed surface area.

8. From the laboratory specimen, weight-loss tests and penetration measurements, intergranular attack increased with electrolyte aeration, while pitting and crevice attack were independent of the degree of aeration.

9. From photomicrographs, some weight loss appeared to result from complete intergranular grain boundary destruction and the loss of grains from the original crystalline structure.

10. With time, resistance polarization data could not be obtained due to excessive potential fluctuations; however, the general behavior of steady-state corrosion potential could be determined throughout the 120 test hours.

11. In the laboratory test cell, instantaneous corrosion rate vs. time curves did not consistently display the expected corrosion rate decrease and stabilization with time. Especially in 0.1N sulfuric acid, corrosion rate and corrosion rate range increase were observed during the final 72-96 test hours.

12. In the laboratory test cell, using high purity iron I, steady-state or "equilibrium" corrosion potential (E_{corr}) and instantaneous rate data displayed similar trends with time.

13. Varying the experimental probe cathode-to-anode surface area ratio did not affect the indicated steady-state corrosion rate range.

14. Daily anodic resistance polarization data were linear within $\pm$ 10 millivolts of the steady-state corrosion potential for each test environment.

15. In 3% sodium chloride/0.5N potassium sulfate, cathodic resistance polarization data displayed evidence of concentration polarization.

16. In aerated 0.1N sulfuric acid, cathodic resistance polarization data deviated from linearity opposite that which would have been expected due to concentration polarization. In additional tests using deaerated 0.1N sulfuric acid, similar deviations were observed. Applied cathodic current densities produced little overvoltage. In both 0.1 and 0.01N sulfuric acid, anodic data could be obtained.

17. Electrolyte motion and agitation from filtered airflow in 3% sodium chloride/0.5N potassium sulfate caused a seven fold increase in the corrosion rate as determined from weight-loss tests.

18. Resistance polarization data could not be obtained with filtered airflow in 0.1N sulfuric acid or 3% sodium chloride due to excessive, random overvoltage fluctuations. After stopping the airflow and allowing electrolyte stabilization, resistance polarization data could be obtained.

19. In some instances, during the first 24 test hours, average polarization resistance values could not be obtained by computer techniques due to a wide variation among resistance polarization data for the test runs. Where wide corrosion rate variation during the first 24 test hours and/or corrosion rate increase during the final 72-96 hours were observed, computer determined steady-state corrosion rates were not within the graphically determined steady-state corrosion rate range.

20. The corrosion rate of iron specimen II was approximately 10-20 times that of iron specimen I in deaerated 1N sulfuric acid.

Conclusions

1. Resistance polarization techniques appear to provide reliable, reproducible, and accurate indication of the instantaneous rate of general metal surface dissolution.

2. Bulk material loss, undetected by resistance polarization tests, may occur as the result of localized attack. Thus, weight-loss tests may provide a more accurate measure of the actual metal surface destruction than resistance polarization techniques.

3. Neither resistance polarization nor weight-loss techniques may be able to accurately indicate actual corrosion penetration when forms of localized attack are present.

4. Computer techniques used to determine average polarization resistance and steady-state corrosion rate were considered unsatisfactory without accompanying graphical analyses.

5. Based upon the tests of this investigation, corrosion damage to high purity iron may be most dependent upon grain orientation, electrolyte agitation (and velocity), and the specific impurity composition. Exposed endgrains may be subject to considerable localized attack. Over the pH range 1-7, diffusion or concentration polarization may occur and any electrolyte velocity or agitation may cause considerable increase in the corrosion damage. The effects of impurity content upon corrosion rate may be synergistic. Knowing the

effect of each individual constituent on the corrosion rate may be of little value in predicting corrosion rate.

6. Investigator techniques during corrosion rate testing (e.g., the method used to provide electrolyte aeration) may significantly affect the corrosion rates determined.

7. Cathodic and anodic resistance polarization may indicate similar corrosion rates; however, at reduced electrolyte concentrations, significantly more information may be obtained from cathodic polarization data.

8. When localized attack is present, use of the initial exposed surface area for corrosion rate calculations may be unsatisfactory.

9. Steady-state corrosion potential may vary with time as does indicated corrosion rate. Either may indicate the presence of localized attack. Neither may indicate the severity of the actual damage when localized attack is present.

10. Elimination of localized attack from a corroding system or from a corrosion rate indicating system may be impossible. As a result, corrosion rate indicating systems may not adequately indicate the extent of the damage done to an operational system. Similarly, the forms of corrosion acting in a corrosion rate indicating system may not represent the types of corrosion present in the operational system. A correlation between operating system and indicating system corrosion damage has yet to be shown.

11. Considerable work remains before adequate corrosion rate indicating systems can be developed for operating use.

Bibliography

1. Fontana, M. G. and N. D. Greene. Corrosion Engineering. New York: McGraw-Hill Book Co., 1967.

2. Phelps, E. H. "Electrochemical Techniques for Measurement and Interpretation of Corrosion." Corrosion, 18: 239t-246t (1962).

3. Haugen, W. J. An Evaluation of Corrosion Characteristics Utilizing the Linear-Polarization Technique. Unpublished thesis, Wright-Patterson Air Force Base, Ohio, Air Force Institute of Technology, June 1970.

4. Whitney, W. R. "The Corrosion of Iron." Journal of the American Chemical Society, 25: 394-406 (1903).

5. Evans, V. R. and T. P. Hoar "The Velocity of Corrosion From the Electrochemical Standpoint. Part II." Proceedings of the Royal Society, A137: 343-365 (1932).

6. Wagner, C. and N. Traud. "Uber die Deutung von Korrosionsvorgangien usw." Zeitschrift fur Elektrochemie, 44: 391-402 (1938).

7. Komp, M. E. and H. E. Trout, Jr. "Effects of Microstructure on Anodic Polarization of Carbon Steel in Sulfuric Acid." Corrosion, 24: 11-16 (1968).

8. Stern, M. "A Method for Determining Corrosion Rates from Linear-Polarization Data." Corrosion, 14: 440t-444t (1958).

9. Greene, N. D. and G. A. Saltzman. "Effect of Plastic Deformation on the Corrosion of Iron and Steel." Corrosion, 20: 293t-298t (1964).

10. Coburn, W. M. Investigation of the Effect of Alloying Elements on the Corrosion Resistance of Iron and Aluminum in Sulfuric Acid. Unpublished thesis, Wright-Patterson Air Force Base, Ohio, Air Force Institute of Technology, March 1972.

11. Ali, S. T. Effect of Selected Alloying Elements on the Anodic Polarization Behavior of Iron and Aluminum. Unpublished thesis, Wright-Patterson Air Force Base, Ohio, Air Force Institute of Technology, March 1972.

12. Wagner, A. H. and J. R. Myers. "Effect of Time on Corrosion Rates in Sulfuric Acid Predicted from Electrochemical Data." Corrosion, 26: 79-85 (1970).

13. Stern, M. and A. L. Geary. "Electrochemical Polarization, I. A Theoretical Analysis of the Shape of Polarization Curves." Journal of the Electrochemical Society, 104: 56-63 (1957).

14. Evans, S. and E. L. Koehler. "Use of Polarization Methods in the Determination of the Rate of Corrosion of Aluminum Alloys in Anaerobic Media." Journal of the Electrochemical Society, 108: 509-514 (1961).

15. Legault, R. A. and M. S. Walker. "Linear Polarization Measurements in the Study of Corrosion Inhibition." Corrosion, 19: 222t-226t (1963).

16. Skold, R. V. and T. E. Larson. "Measurement of Instantaneous Corrosion Rate by Means of Polarization Data." Corrosion, 13: 139t-142t (1957).

17. McKay, R. J. and R. Worthington. "Iron and Steel" Corrosion Resistance of Metals and Alloys. New York: Reinhold Publishing Corp., 1948.

18. Mansfeld, F. and K. B. Oldham. "Some Limitations of the Linear Polarization Technique in Evaluating Corrosion Behavior." Corrosion, 26: 207-208 (1970).

19. Mansfeld, F. and K. B. Oldham. "Technical Note: On the So-Called Linear Polarization Method for Measurement of Corrosion Rate." Corrosion, 27: 434-435 (1971).

20. Mansfeld, F. and K. B. Oldham. "A Modification of the Stern-Geary Linear Polarization Equation." Corrosion Science, 11: 787-796 (1971).

21. Jones, D. A. "Discussion on the So-Called Linear Polarization Method for Measurement of Corrosion Rates." Corrosion, 27: 434-(1971).

22. Uhlig, H. H. Corrosion and Corrosion Control. New York: John Wiley and Sons, Inc., 1963.

23. Smulczenski, L. A. Polarization Behavior of Ni-Cr-Al and Ni-Cr-Ti Alloys in Sulfuric Acid. Unpublished thesis, Wright-Patterson Air Force Base, Ohio: Air Force Institute of Technology, June 1968.

24. Myers, J. R., E. G. Gruenler, and L. A. Smulczenski. "Improved Working Electrode Assembly for Electrochemical Measurements." Corrosion, 24: 352-353 (1968).

25. France, W. D. Jr., "A Specimen Holder for Precise Electrochemical Polarization Measurements on Metal Sheets and Foils." Journal of the Electrochemical Society, 114: 818-819 (1967).

26. Greene, N. D., et al. "Electrode Mounting for Potentiostatic Anodic Polarization Studies." Corrosion, 21: 275 (1965).

27. Kortum, G. and J. O. M. Bockris. Textbook of Electrochemistry, Amsterdam: Elsevier Publishing Co., 1951.

28. Eisenberg, M., C. W. Tobias, and C. R. Wilke. "Application of Backside Capillaries in the Measurement of Non-Uniform Polarization." Journal of the Electrochemical Society, 102: 415-419 (1955).

29. Rickard, T. J. An Investigation of the Corrosion Characteristics of Dental Alloys. Unpublished thesis, Wright-Patterson Air Force Base, Ohio: Air Force Institute of Technology, June 1971.

30. Haynie, F. H. and S. Ketchem. "Electrochemical Behavior of Aluminum Alloys Susceptible to Intergranular Corrosion. II. Electrode Kinetics of Oxide Covered Aluminum." Corrosion, 19: 403t-407t (1963).

31. Sayano, R. R. and K. Nobe. "Continuous and Pulse Polarization of Ni in H_2SO_4." Corrosion, 32: 81-87 (1966).

32. Barnatt, S. "Magnitude of IR-Drop Corrections in Electrode Polarization Measurements Made With A Lugging-Haber Capillary." Journal of the Electrochemical Society, 108: 102-104 (1961).

33. ASTM Standards, Part 4. Philadelphia, Pa.: American Society for Testing and Materials, 1969.

34. Kaesche, H. and N. Hackerman. "Corrosion Inhibition by Organic Amines." Journal of the Electrochemical Society, 105: 191-198 (1958).

35. Stern, M. and E. D. Weisert. "Experimental Observations on the Relation Between Polarization Resistance and the Corrosion Rate." Proceedings of the American Society for Testing and Materials, 59: 1280-1291 (1959).

36. Jones, D. A. and N. D. Greene. "Electrochemical Measurement of Low Corrosion Rates." Corrosion, 22: 198-205 (1966).

37. Wilde, B. E. "Adaptation of Linear-Polarization Techniques for In-Situ Corrosion Measurements in Water Cooled Nuclear Reactor Environments." Corrosion, 23: 379-384 (1967).

38. Greene, N. D. and D. A. Jones. Corrosion of Surgical Implants, presented at ASTM-ASM Medical Materials Symposium, Detroit, Michigan, October 19, 1965.

39. Collangelo, V. J., et al. Corrosion Rate Measurements in Vivo, presented at the National Association of Corrosion Engineers meeting, Los Angeles, California, 1967.

40. Mottern, M. M. and J. R. Myers. "Polarization Behavior of Iron-Cobalt Alloys in Sulfuric Acid Solutions." Corrosion, 24: 197-205 (1968).

41. Seaman, G. T., J. R. Myers, and R. K. Saxer. "Anodic Polarization Behavior of Cobalt-Chromium Alloys in Sulfuric Acid Solutions." Electrochemical Aeta, 12: 855-871 (1967).

42. Donahue, F. M. and K. Nobe. "Aqueous Oxygen Corrosion of Iron. Transient and Steady-State Galvanostatic Phenomena in Sulfuric Acid." Proceedings of the Second International Congress on Metallic Corrosion. New York: National Association of Corrosion Engineers, 1964.

43. Hansen, M. Constitution of Binary Alloys. New York: McGraw-Hill Book Co., 1958.

44. Milam, E. E. Anodic and Cathodic Polarization of Iron-Aluminum Alloys in Sulfuric Acid Solutions. Unpublished thesis, Wright-Patterson Air Force Base, Ohio: Air Force Institute of Technology, June 1968.

45. Petrocelli, J. V. "Anodic Behavior of Aluminum at Low Potentials." Journal of the Electrochemical Society, 106: 566-570 (1959).

46. Jeffreys, J. V. Anodic and Cathodic Polarization of Ferrosilicon Alloys in Sulfuric Acid Solutions. Unpublished thesis, Wright-Patterson Air Force Base, Ohio: Air Force Institute of Technology, June 1967.

47. Poubaix, M. Atlas of Electrochemical Equilibria in Aqueous Solutions. Oxford, England: Pergamon Press, 1966.

48. Plumb, G. L. Polarization Characteristics of Iron-Manganese Alloys in Sulfuric Acid Solutions. Unpublished thesis, Wright-Patterson Air Force Base, Ohio: Air Force Institute of Technology, June 1969.

49. Cleary, H. J. and N. D. Greene. "Corrosion Properties of Iron and Steel." Corrosion Science, 2: 821-831 (1967).

50. Rabald, E. Corrosion Guide (First Edition). New York: Elsevier Publishing Co., 1951.

51. Rabald, E. Corrosion Guide (Second Edition). New York: Elsevier Publishing Co., 1968.

52. Makrides, A. C. "Dissolution of Iron in Sulfuric Acid and Ferric Salt Solutions." Journal of the Electrochemical Society, 107: 869 (1970).

53. Greene, N. D. "Predicting Behavior of Corrosion Resistant Alloys by Potentiostatic Polarization Methods." Corrosion, 18: 136t-142t (1962).

54. LaQue, F. L. "Theoretical Studies and Laboratory Techniques in Sea Water Corrosion Testing Evaluation." Corrosion, 13: 303t-314t (1957).

55. Stern, M. "Surface Area Relationships in Polarization and Corrosion." Corrosion, 14: 329t-332t (1958).

56. Steigerwald, R. F. "Electrochemistry of Corrosion." Corrosion, 24: 1-11 (1968).

57. McKay, R. J. and R. Worthington. Corrosion Resistance of Metals and Alloys. New York: Reinhold Publishing Co., 1936.

58. Beveridge, W. I. B. The Art of Scientific Investigation. New York: W. W. Norton & Co. Inc., 1957.

59. Brinkworth, B. J. An Introduction to Experimentation. New York: American Elsevier Publishing Co. Inc., 1968.

60. Bunge, M. Scientific Research II: The Search for Truth. Heidelberg, Germany: Springer-Verlag, 1967.

61. Lloyd, L. E. Techniques for Efficient Research. New York: Chemical Publishing Co. Inc., 1966.

62. Webster's New Collegiate Dictionary. Springfield, Mass.: G&C Merriam Company, 1970.

63. Wilson, E. B. Introduction to Scientific Research. New York: McGraw-Hill Book Co. Inc., 1952.

64. LaQue, F. L. and G. L. Cox. "Some Observations of the Potentials of Metals and Alloys in Sea Water." American Society of Testing Materials Proceedings, 40: 673 (1940).

65. Prochko, R. J. Corrosion of Beryllium Sheet by Total Immersion in Natural Sea Water. Unpublished thesis, Wright-Patterson Air Force Base, Ohio: Air Force Institute of Technology, June 1964.

66. Crow, W. B., J. R. Myers, and J. V. Jeffreys. "Anodic Polarization of Fe-Si Alloys in Sulfuric Acid Solutions." Corrosion, 28: 78 (1972).

Appendix A

pH Determinations for Hydrogen Saturated Electrolytes in the Laboratory Test Cell

Electrolyte	Observations	pH		
		maximum	minimum	mean
1N H_2SO_4	8	.42	.39	.40
.1N H_2SO_4	4	1.27	1.19	1.26
3% NaCl	3	6.7	5.9	6.3

Appendix B

Effect of Time on Steady-State Corrosion Potential

The effect of time on the observed steady-state corrosion potential of high purity iron I in aerated and deaerated (hydrogen saturated) 1N and 0.1N sulfuric acid and 3% sodium chloride, 0.5N potassium sulfate environments are shown in Tables IV-IX of this appendix. In addition, the effect of time on the observed steady-state corrosion potential in deaerated 1N sulfuric acid is also shown in Figure 20. Note that the absolute value of corrosion potential is shown as the ordinate. All potentials are relative to a standard calomel electrode (SCE).

Table IV

Effect of Time on the Steady-State Corrosion Potential of High Purity Iron I in Hydrogen Saturated 1N Sulfuric Acid

	CORROSION POTENTIAL (V) VS. S.C.E.					
RUN \ HOURS	00	24	48	72	96	120
1	-0.4921	-0.4860	-0.4827	-0.4820	-0.4810	-0.4815
2	-0.5044	-0.4929	-0.4845	-0.4796	-0.4788	-0.4790
3	-0.5040	-0.4825	-0.4830	-0.4862	-0.4888	-0.4877
4	-0.4920	-0.4797	-0.4836	-0.4822	-0.4822	-0.4824
5	-0.5100	-0.4817	-0.4813	-0.4786	-0.4811	-0.4807
6	-0.4800	-0.4756	-0.4759	-0.4765	-0.4780	-0.4776
7	-0.4983	-0.4847	-0.4890	-0.4898	-0.4885	-0.4872
8	-0.4813	-0.4802	-0.4796	-0.4798	-0.4801	-0.4797

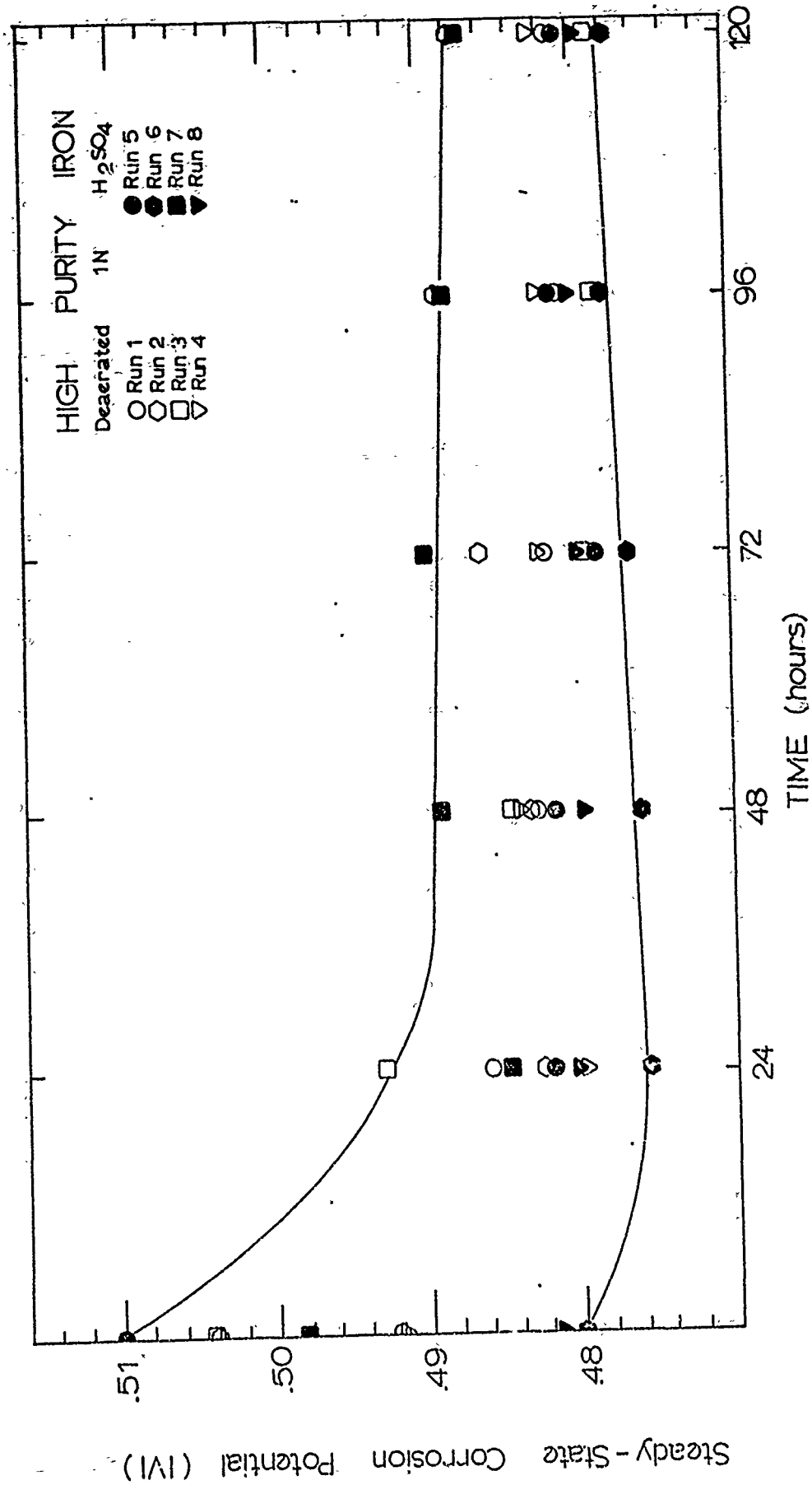

Figure 20: Effect of Time on the Steady-State Corrosion Potential of High Purity Iron I in Hydrogen Saturated 1N Sulfuric Acid.

Table V

Effect of Time on the Steady-State Corrosion Potential of High Purity Iron I in Aerated 1N Sulfuric Acid

RUN \ HOURS	CORROSION POTENTIAL (V) VS. S.C.E.					
	00	24	48	72	96	120
1	-0.4901	-0.4808	-0.4820	-0.4839	-0.4786	-0.4742
2	-0.4976	-0.4944	-0.4930	-0.4878	-0.4897	-0.4870
3	-0.5010	-0.4863	-0.4820	-0.4870	-0.4858	-0.4859
4	-0.5033	-0.4913	-0.4908	-0.4890	-0.4886	-0.4880
5	-0.5102	-0.4956	-0.4929	-0.4902	-0.4891	-0.4883
6	-0.5120	-0.4952	-0.4922	-0.4902	-0.4892	-0.4880
7	-0.5072	-0.4910	-0.4911	-0.4886	-0.4872	-0.4878
8	-0.5142	-0.4947	-0.4926	-0.4901	-0.4889	-0.4885

Table VI

Effect of Time on the Steady-State Corrosion Potential of High Purity Iron I in Hydrogen Saturated 0.1N Sulfuric Acid

RUN \ HOURS	CORROSION POTENTIAL (V) VS. S.C.E.					
	00	24	48	72	96	120
1	-.5301	-.5441	-.5600	-.5556	-.5490	-.5426
2	-.5355	-.5323	-.5478	-.5490	-.5498	-.5475
3	-.5385	-.5338	-.5553	-.5660	-.5655	-.5620
4	-.542	-.534	-.5418	-.5473	-.5460	-.5425

Table VII

Effect of Time on the Steady-State Corrosion Potential of High Purity Iron I in Aerated 0.1N Sulfuric Acid

	CORROSION POTENTIAL (V) VS. S.C.E.					
RUN \ HOURS	00	24	48	72	96	120
1	-.5294	-.531	-.5237	-.534	-.5404	-.5514
2	-.5137	-.5158	-.5233	-.5266	-.5325	-.536
3	-.5188	-.5229	-.5201	-.5193	-.5213	-.5235
4	-.5458	-.5262	-.5484	-.5553	-.5546	-.55
5	-.5458	-.531	-.5384	-.5397	-.5468	-.548

Table VIII

Effect of Time on the Steady-State Corrosion Potential of High Purity Iron I in Hydrogen Saturated 3% Sodium Chloride

RUN \ HOURS	CORROSION POTENTIAL (V) VS. S.C.E.					
	00	24	48	72	96	120
1	-.8038	-.787	-.7865	-.785	-.786	-.7835
2	-.8821	-.8516	-.8501	-.851	-.8492	-.85
3	-.8102	-.7926	-.7909	-.7891	-.7924	-.793

Table IX

Effect of Time on the Steady-State Corrosion Potential of High Purity Iron I in Aerated 3% Sodium Chloride

RUN \ HOURS	CORROSION POTENTIAL (V) VS. S.C.E.					
	00	24	48	72	96	120
1	-.7336	-.7102	-.7115	-.7092	-.7138	-.7100
2	-.8123	-.8006	-.7984	-.7992	-.7764	-.7859
3	-.7642	-.7596	-.7550	-.7580	-.7600	-.7628

Appendix C

The Effect of Time on Galvanostatic Polarization Resistance of High Purity Iron I Using a Laboratory Probe

The effect of time on the galvanostatic cathodic and anodic polarization resistance of high purity iron specimen I in aerated and deaerated (hydrogen saturated) 1N and 0.1N sulfuric acids and 3% sodium chloride environments as determined using the laboratory probe described in Chapter III are shown in this appendix. In addition, the linear regression analyses determined maximum, minimum, and "combined daily" data values of polarization resistance are also shown. (See "Polarization Resistance Determination" in Chapter IV for terminology definitions). Maximum and minimum computed polarization resistance values for a given time on a by run, by day basis are shown as broken lines. The value of polarization resistance determined from "combined daily" data is shown as a solid line. Note that at a given test time, if the values of polarization resistance from each run are not significantly different, either the maximum and minimum or "combined" data polarization resistance values have been omitted for clarity purposes. Also, note that the abscissa scale may vary considerably from graph to graph and amongst figures.

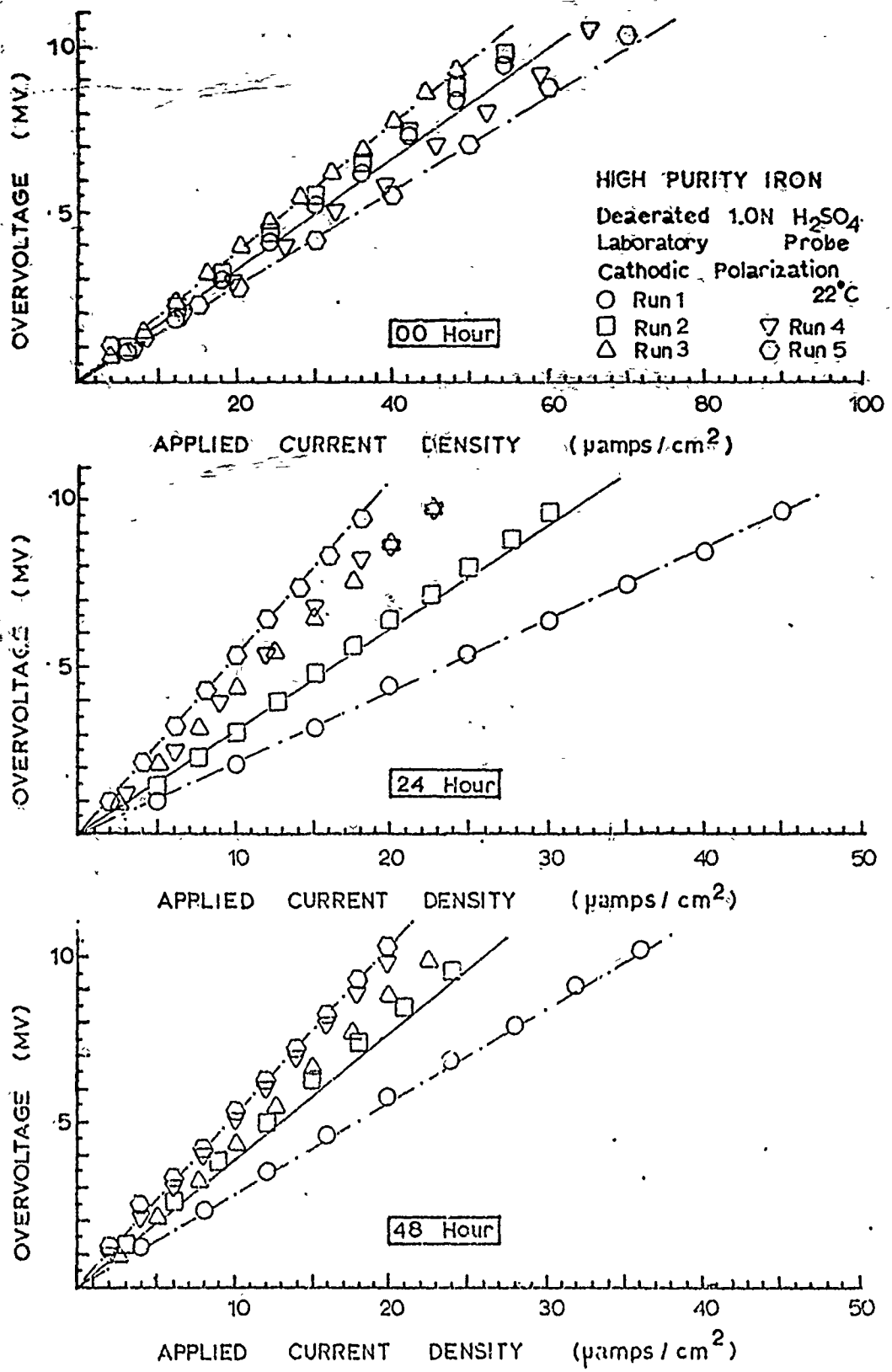

Figure 21: Effect of Time on Galvanostatic Cathodic Polarization Resistance of High Purity Iron in Hydrogen Saturated 1N Sulfuric Acid Determined Using a Laboratory Probe. (Cont)

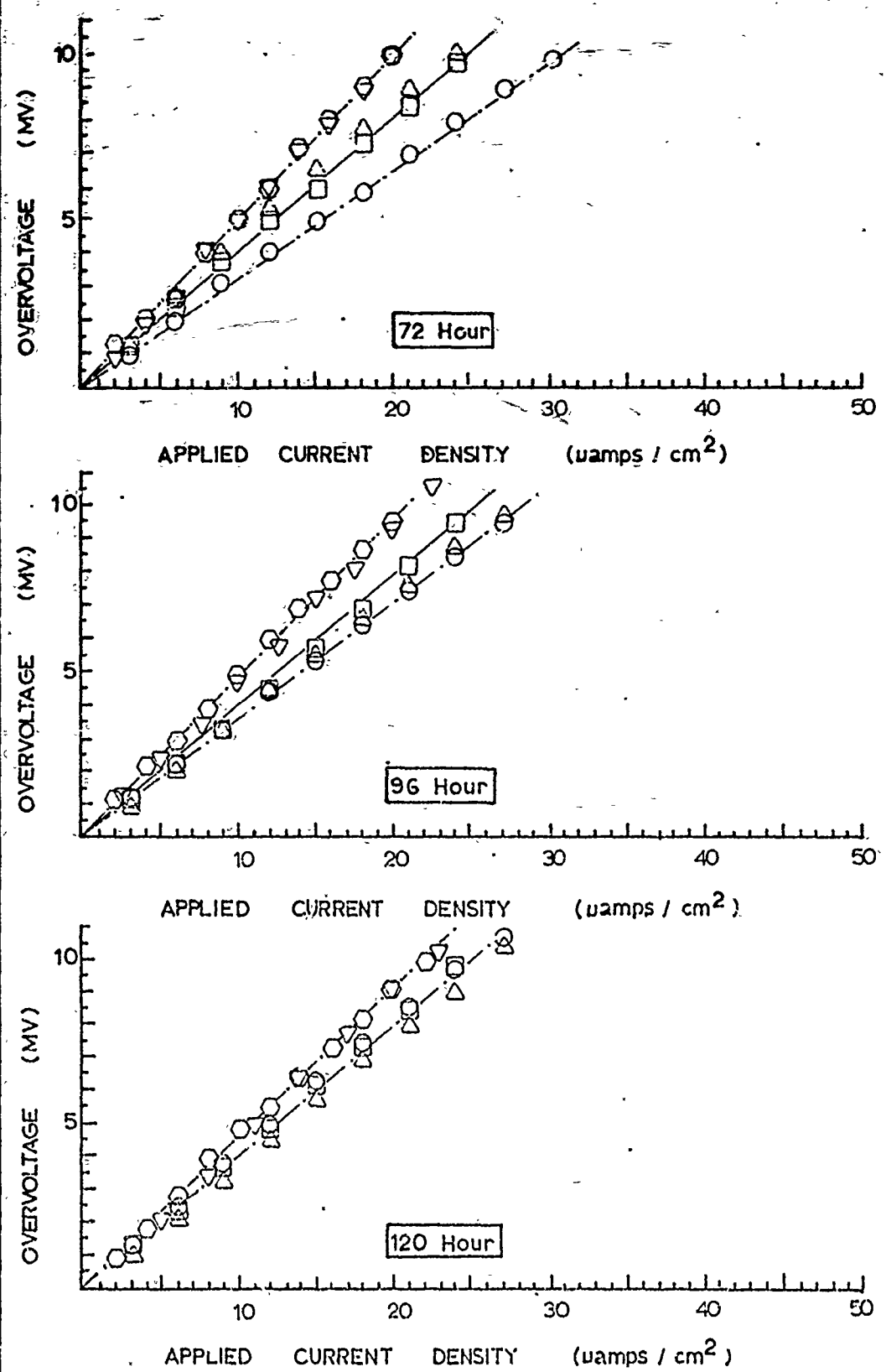

Figure 21: (Cont) Effect of Time on Galvanostatic Cathodic Polarization Resistance of High Purity Iron in Hydrogen Saturated 1N Sulfuric Acid Determined Using a Laboratory Probe.

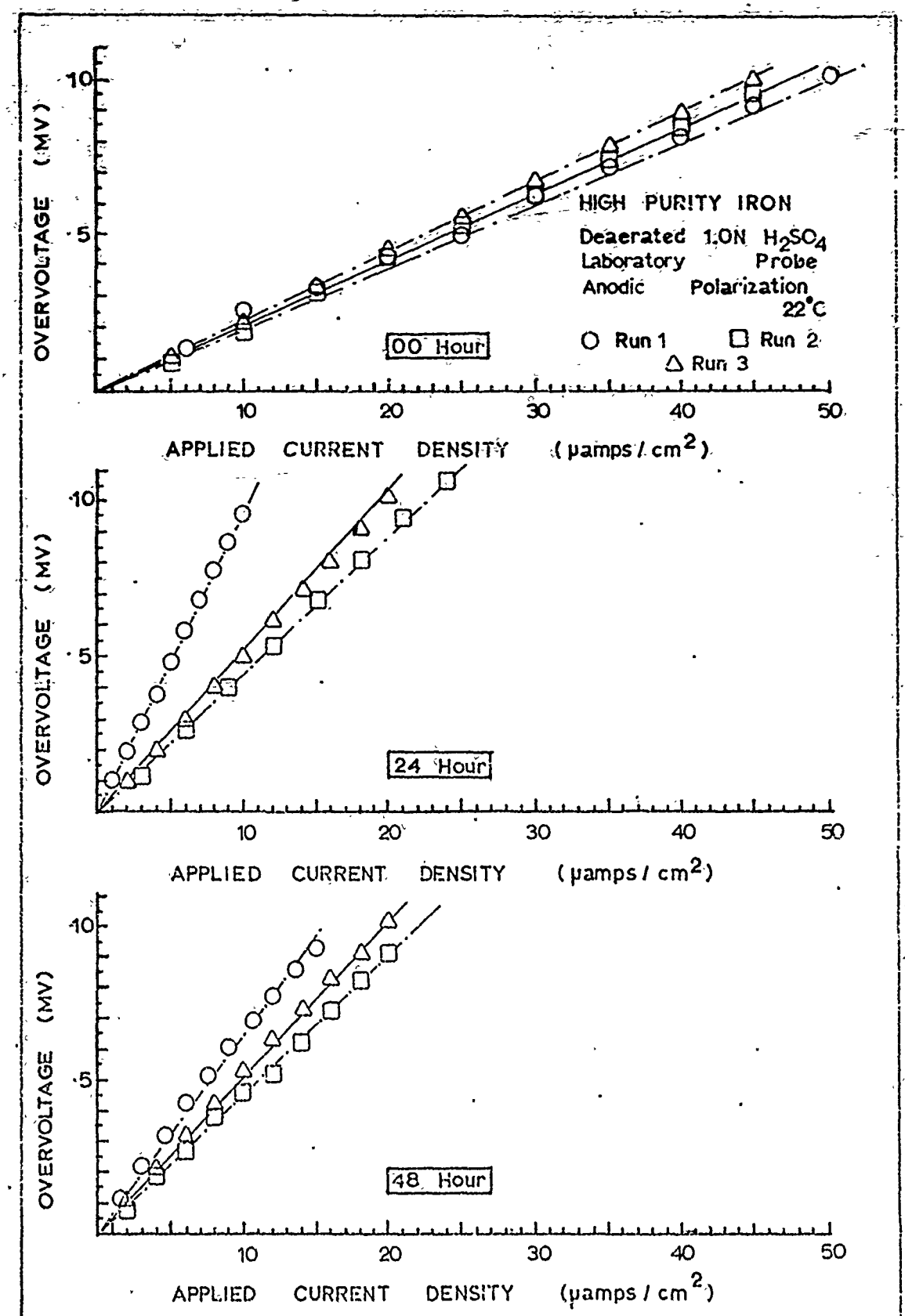

Figure 22 : Effect of Time on Galvanostatic Anodic Polarization Resistance of High Purity Iron on Hydrogen Saturated 1N Sulfuric Acid Determined Using a Laboratory Probe. (Cont)

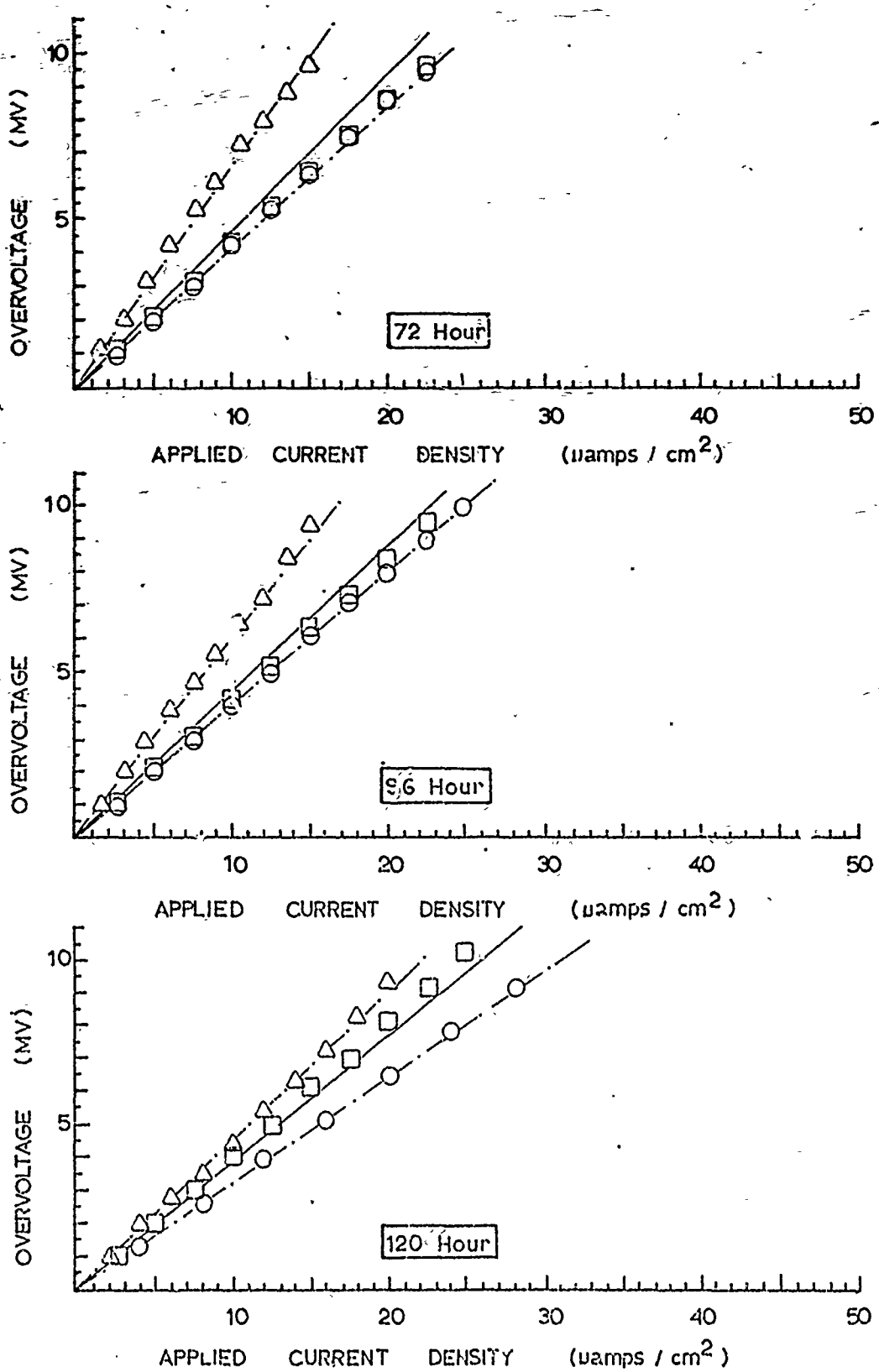

Figure 22: (Cont) Effect of Time on Galvanostatic Anodic Polarization Resistance of High Purity Iron on Hydrogen Saturated 1N Sulfuric Acid Determined Using a Laboratory Probe.

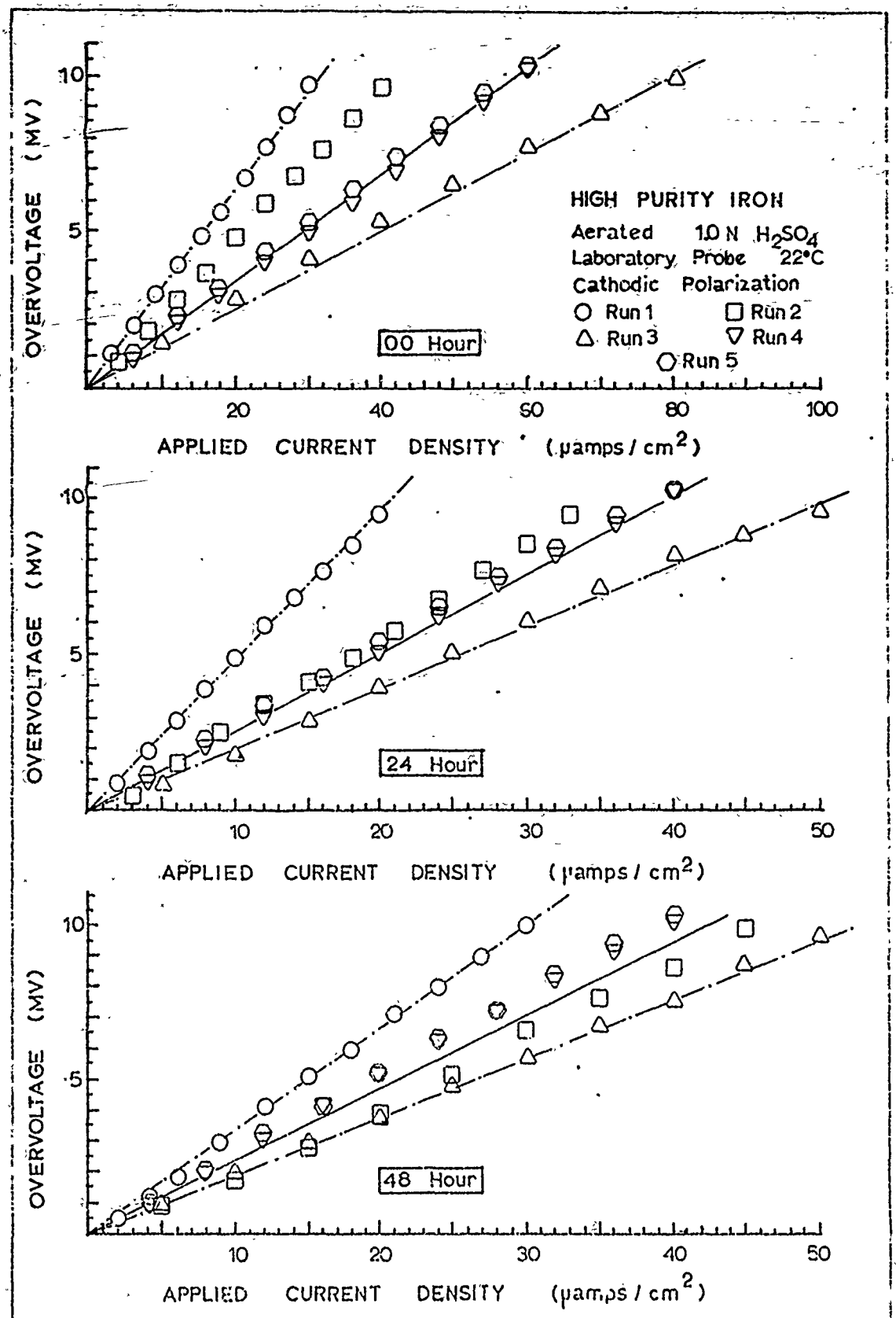

Figure 23 : Effect of Time on Galvanostatic Cathodic Polarization Resistance of High Purity Iron in Aerated 1N Sulfuric Acid Determined Using a Laboratory Probe. (Cont)

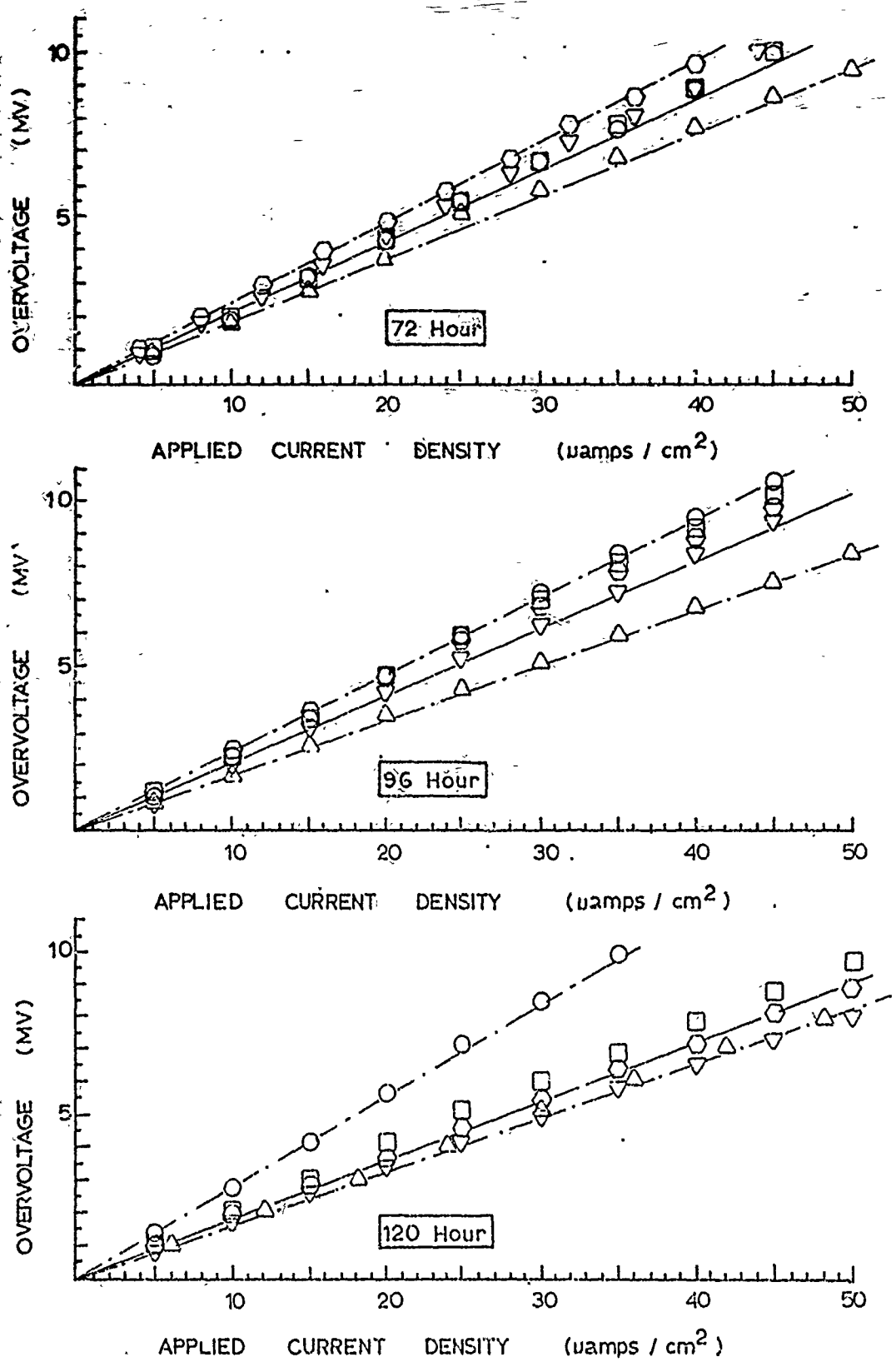

Figure 23 : (Cont) Effect of Time on Galvanostatic Cathodic Polarization Resistance of High Purity Iron in Aerated 1N Sulfuric Acid Determined Using a Laboratory Probe.

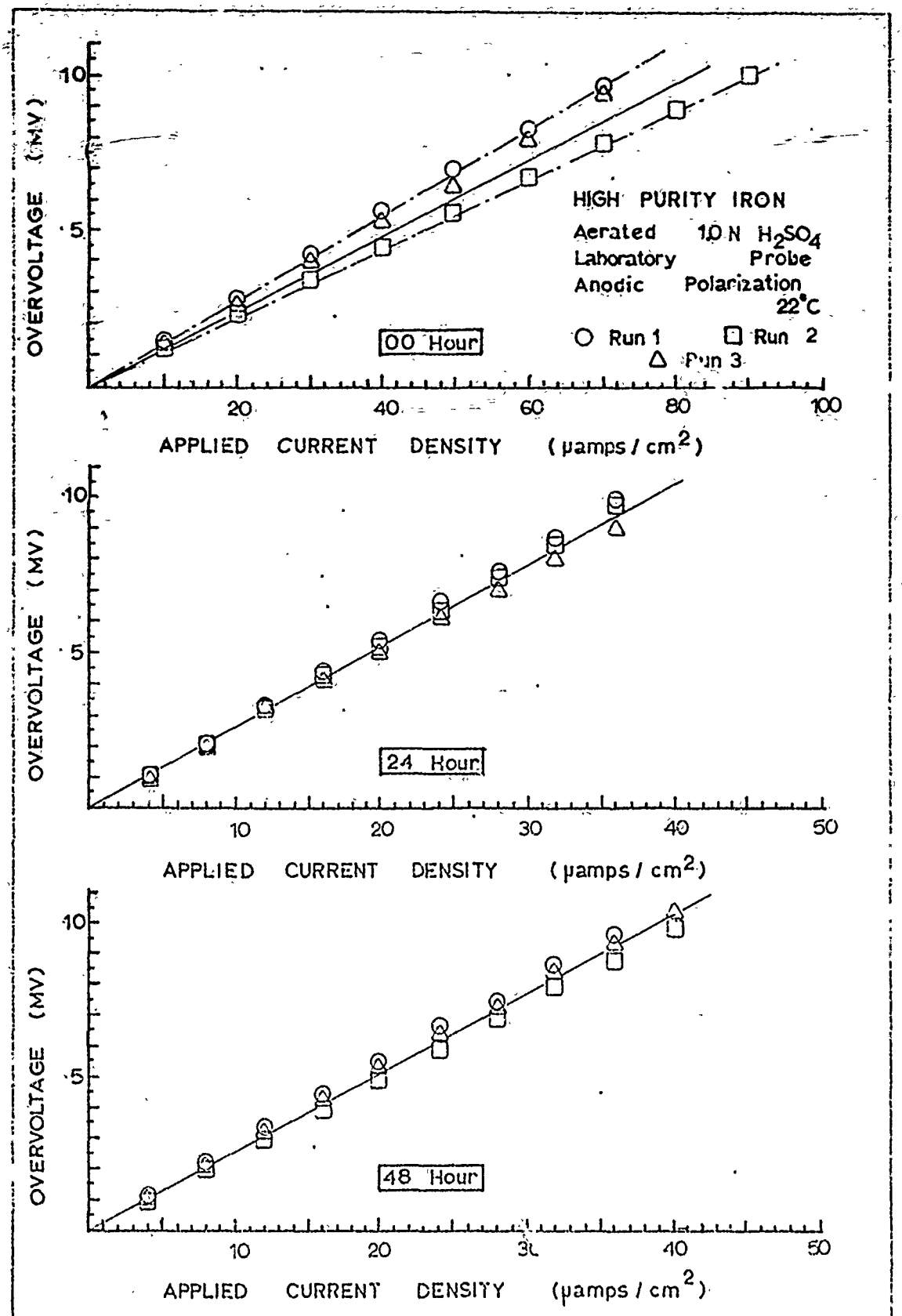

Figure 24 : Effect of Time on Galvanostatic Anodic Polarization Resistance of High Purity Iron in Aerated 1N Sulfuric Acid Determined Using a Laboratory Probe. (Cont)

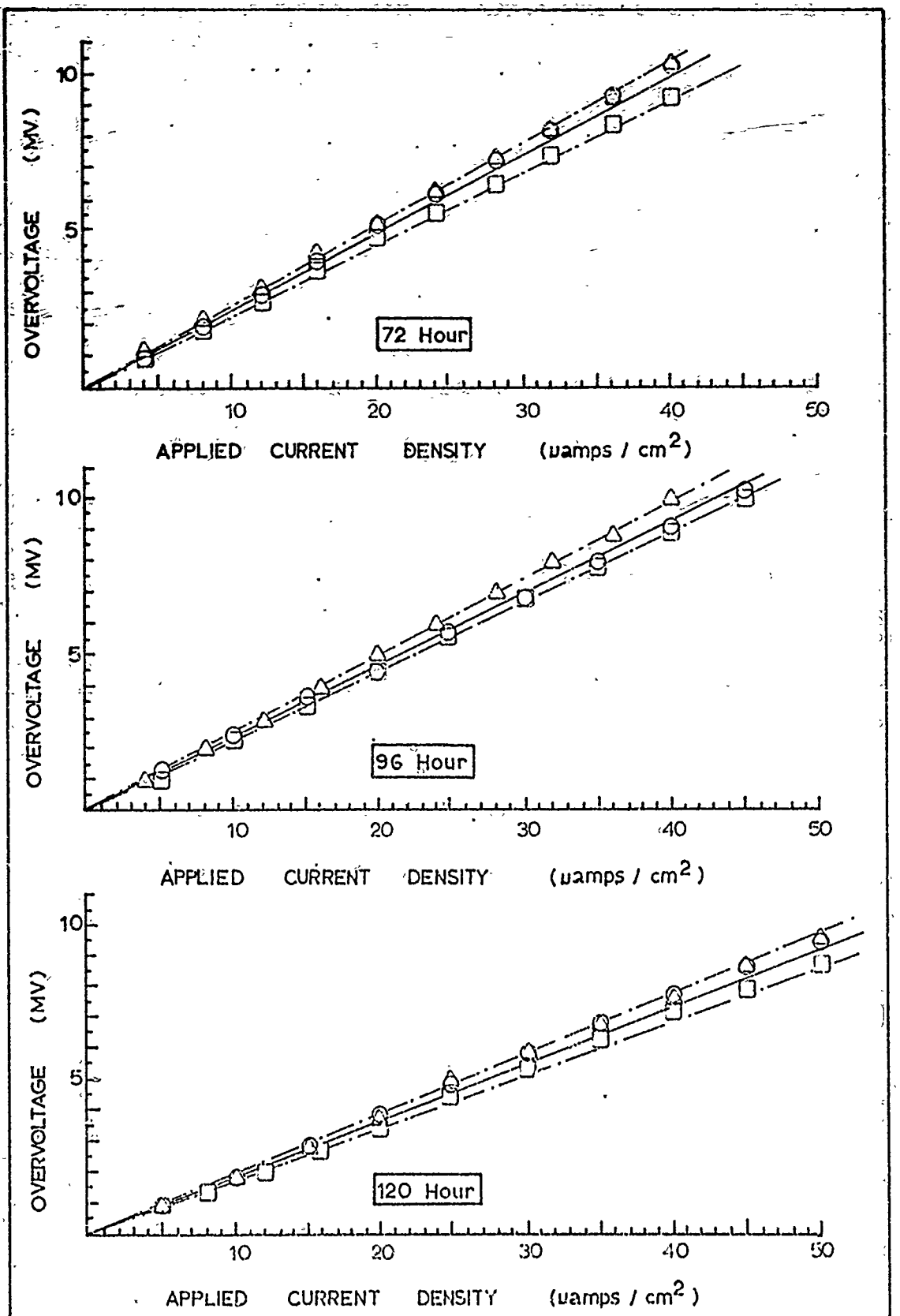

Figure 24 : (Cont) Effect of Time on Galvanostatic Anodic Polarization Resistance of High Purity Iron in Aerated 1N Sulfuric Acid Determined Using a Laboratory Probe.

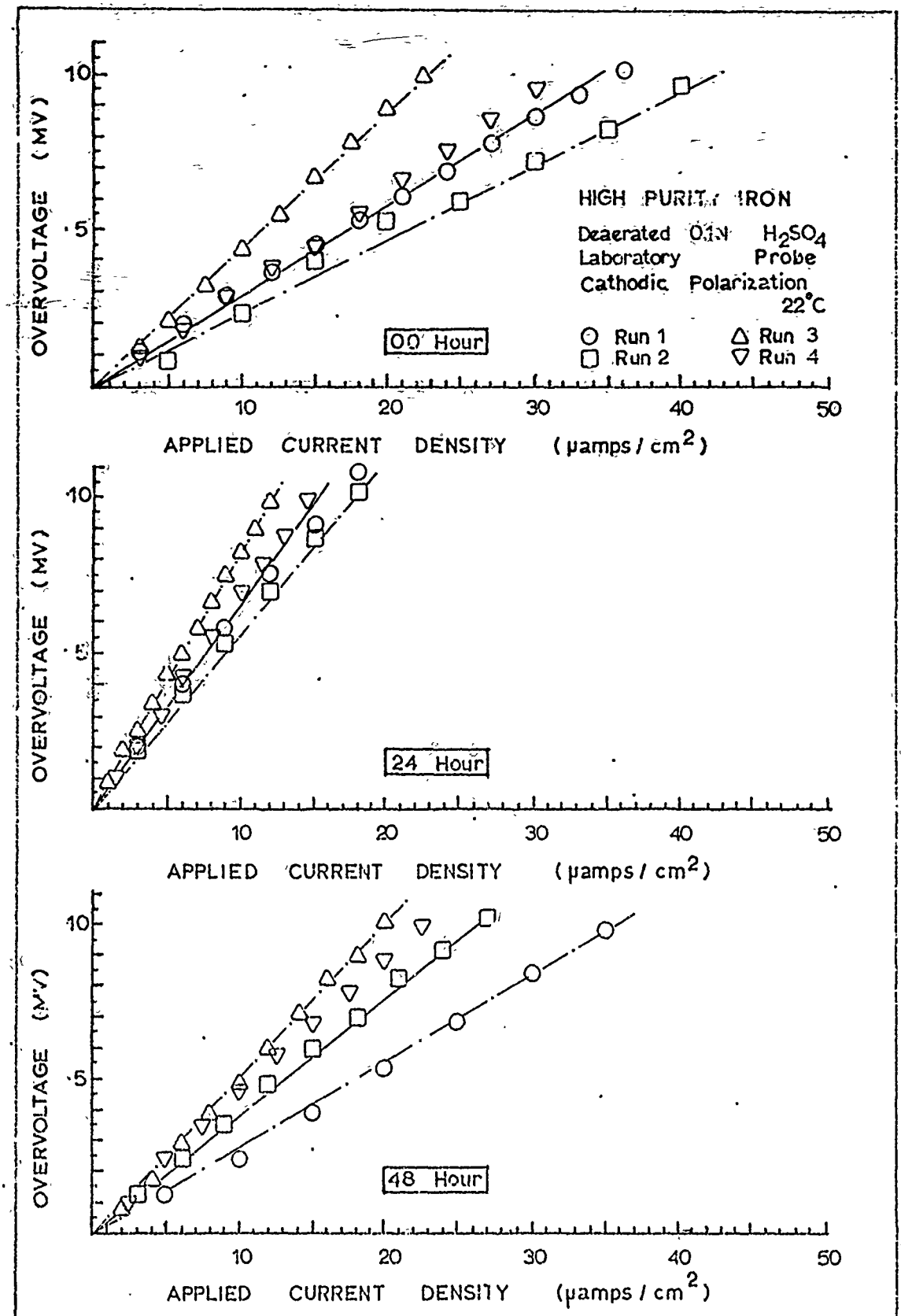

Figure 25: Effect of Time on Galvanostatic Cathodic Polarization Resistance of High Purity Iron in Hydrogen Saturated .1N Sulfuric Acid Determined Using a Laboratory Probe. (Cont)

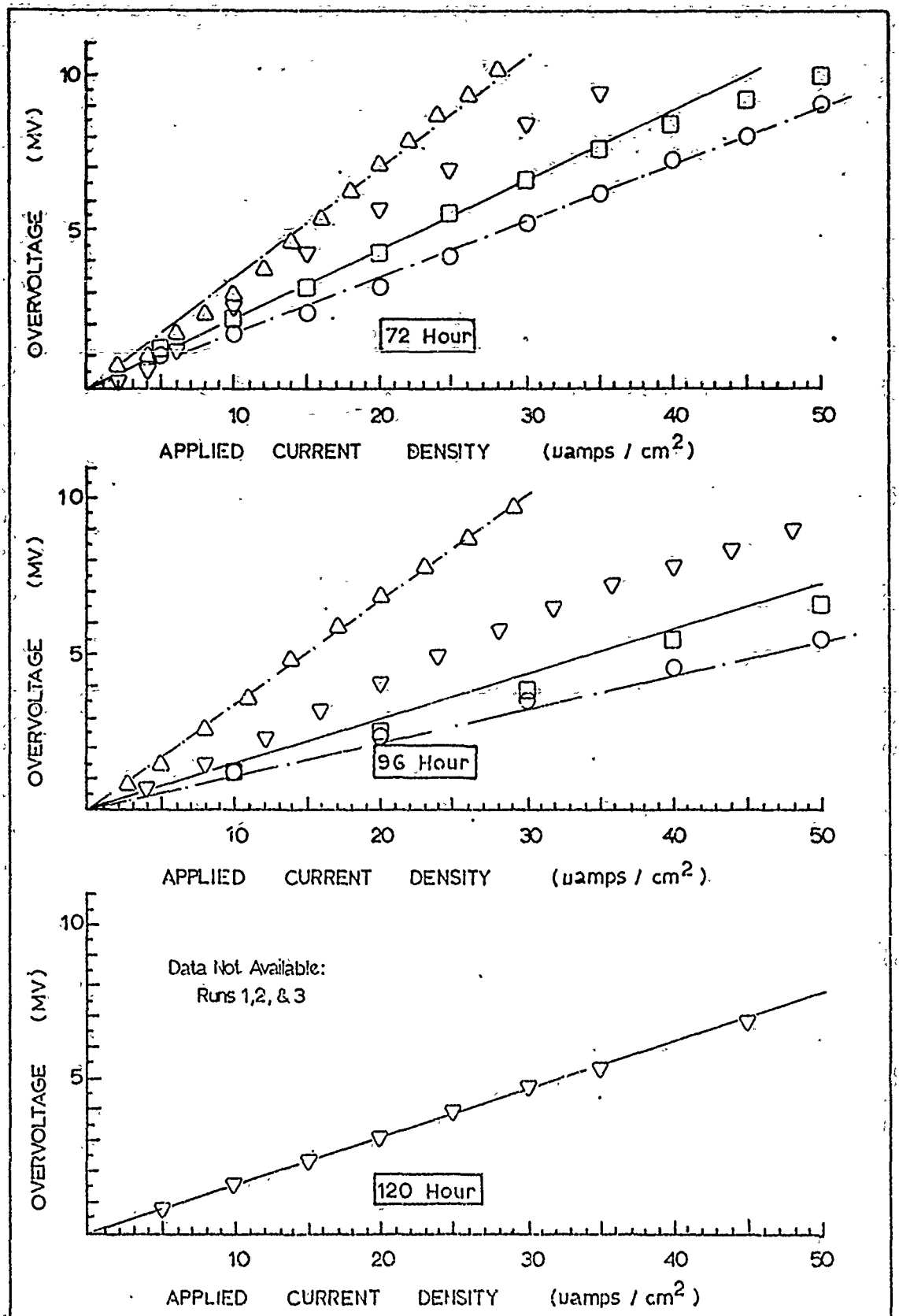

Figure 25: (Cont) Effect of Time on Galvanostatic Cathodic Polarization Resistance of High Purity Iron in Hydrogen Saturated .1N Sulfuric Acid Determined Using a Laboratory Probe.

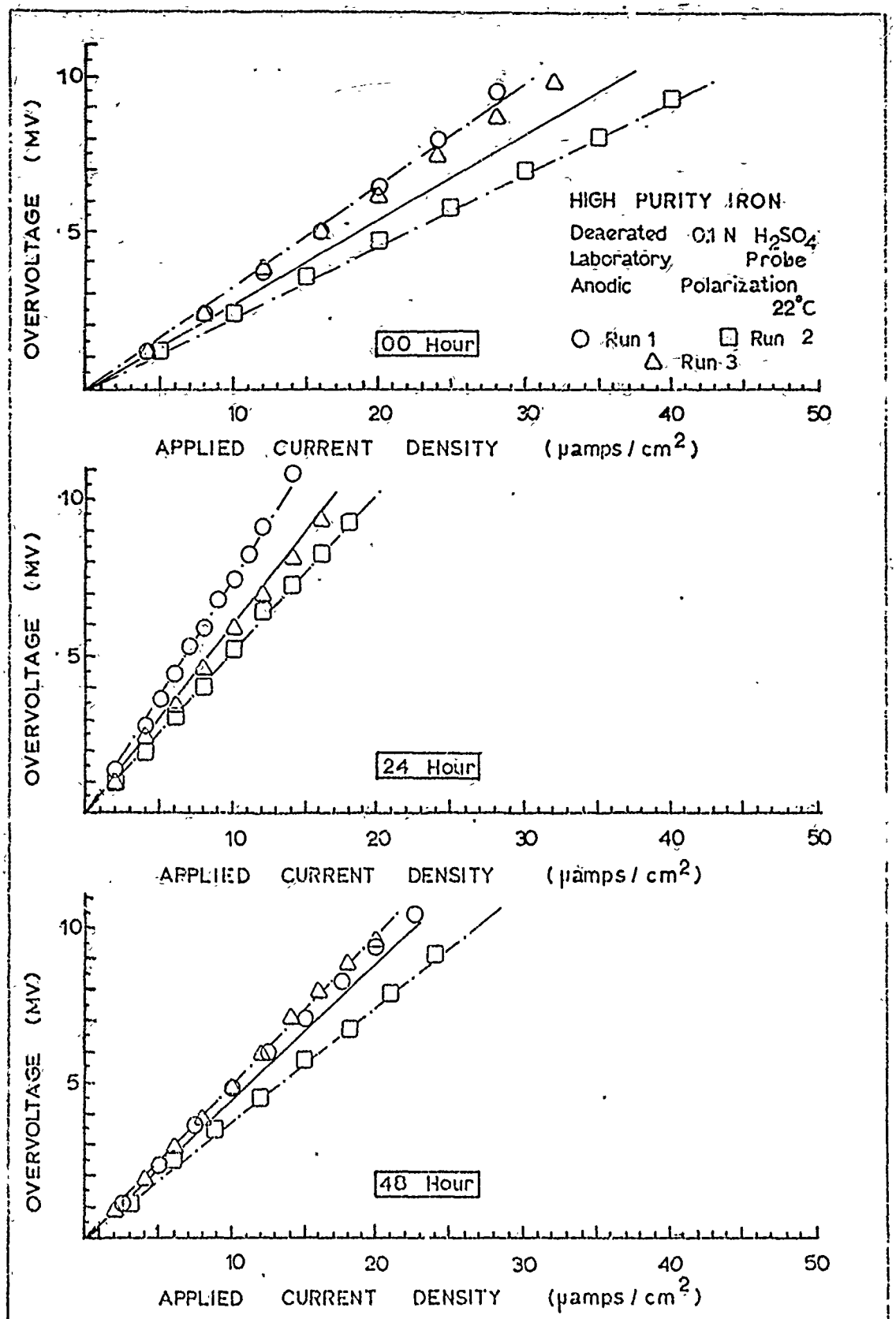

Figure 26: Effect of Time on Galvanostatic Anodic Polarization Resistance of High Purity Iron in Hydrogen Saturated .1N Sulfuric Acid Determined Using a Laboratory Probe. (Cont)

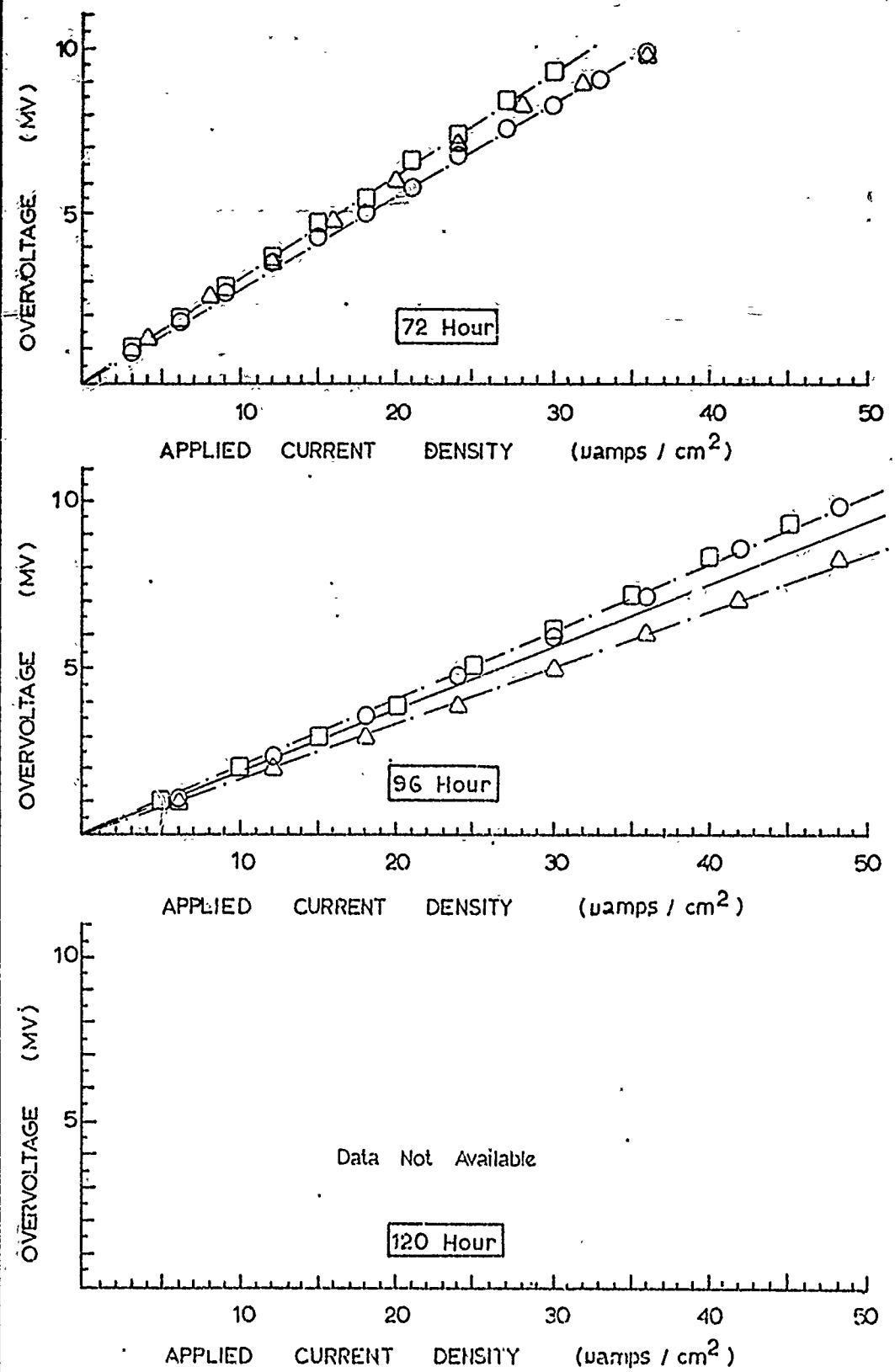

Figure 26: (Cont) Effect of Time on Galvanostatic Anodic Polarization Resistance of High Purity Iron in Hydrogen Saturated .1N Sulfuric Acid Determined Using a Laboratory Probe.

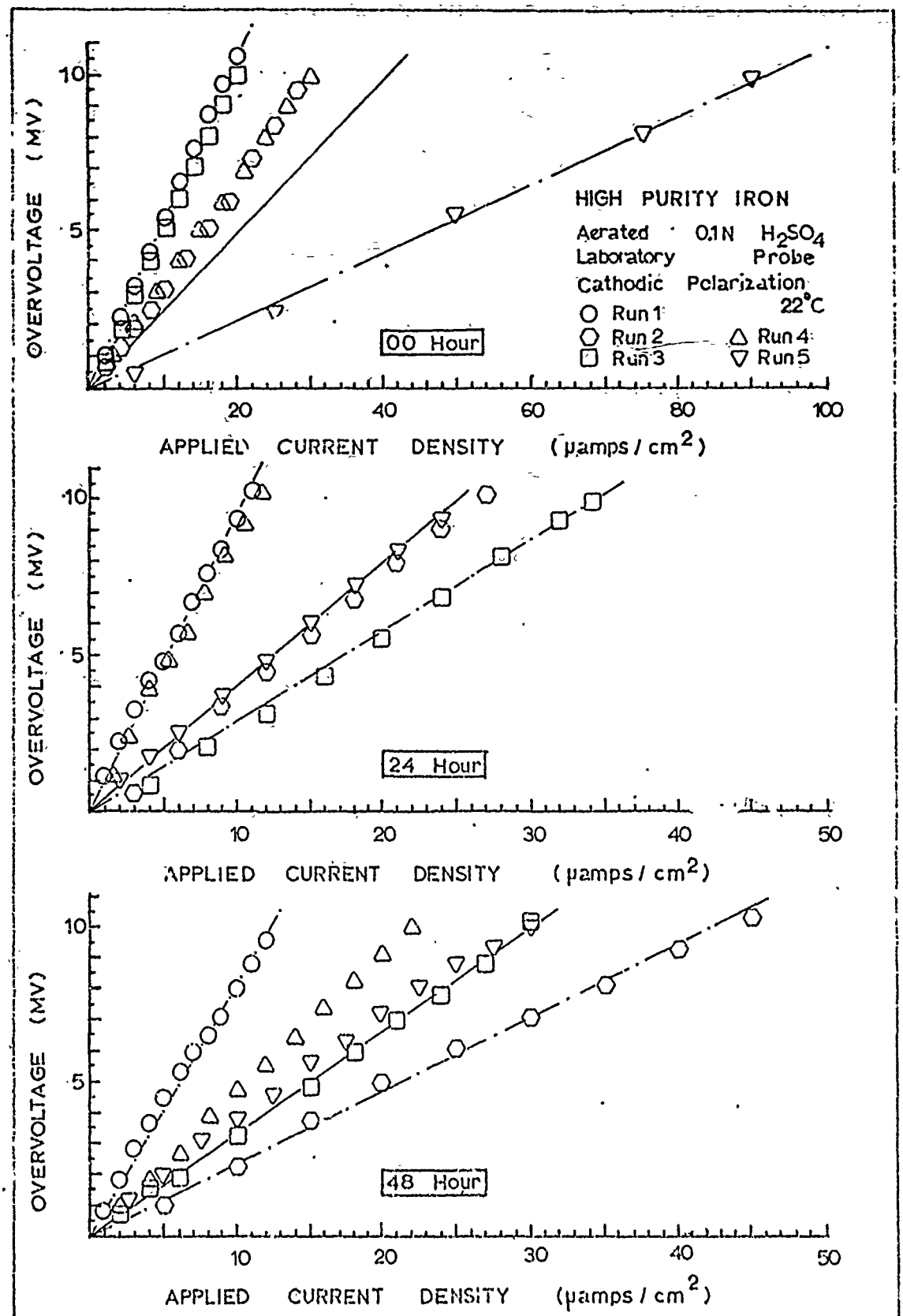

Figure 27: Effect of Time on Galvanostatic Cathodic Polarization Resistance of High Purity Iron in Aerated .1N Sulfuric Acid Determined Using a Laboratory Probe (Cont)

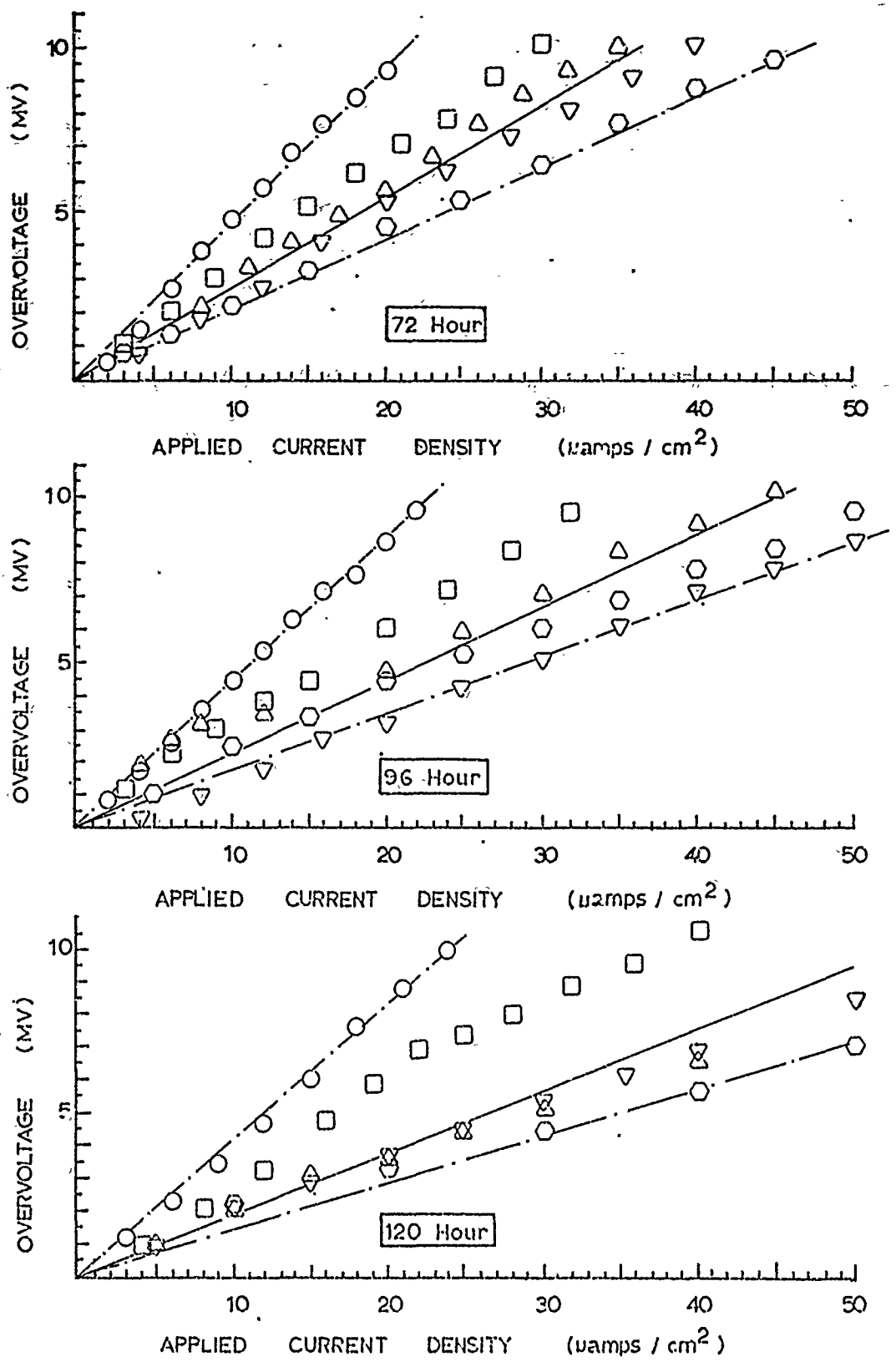

Figur 27: (Cont) Effect of Time on Galvanostatic Cathodic Polarization Resistance of High Purity Iron in Aerated .1N Sulfuric Acid Determined Using a Laboratory Probe.

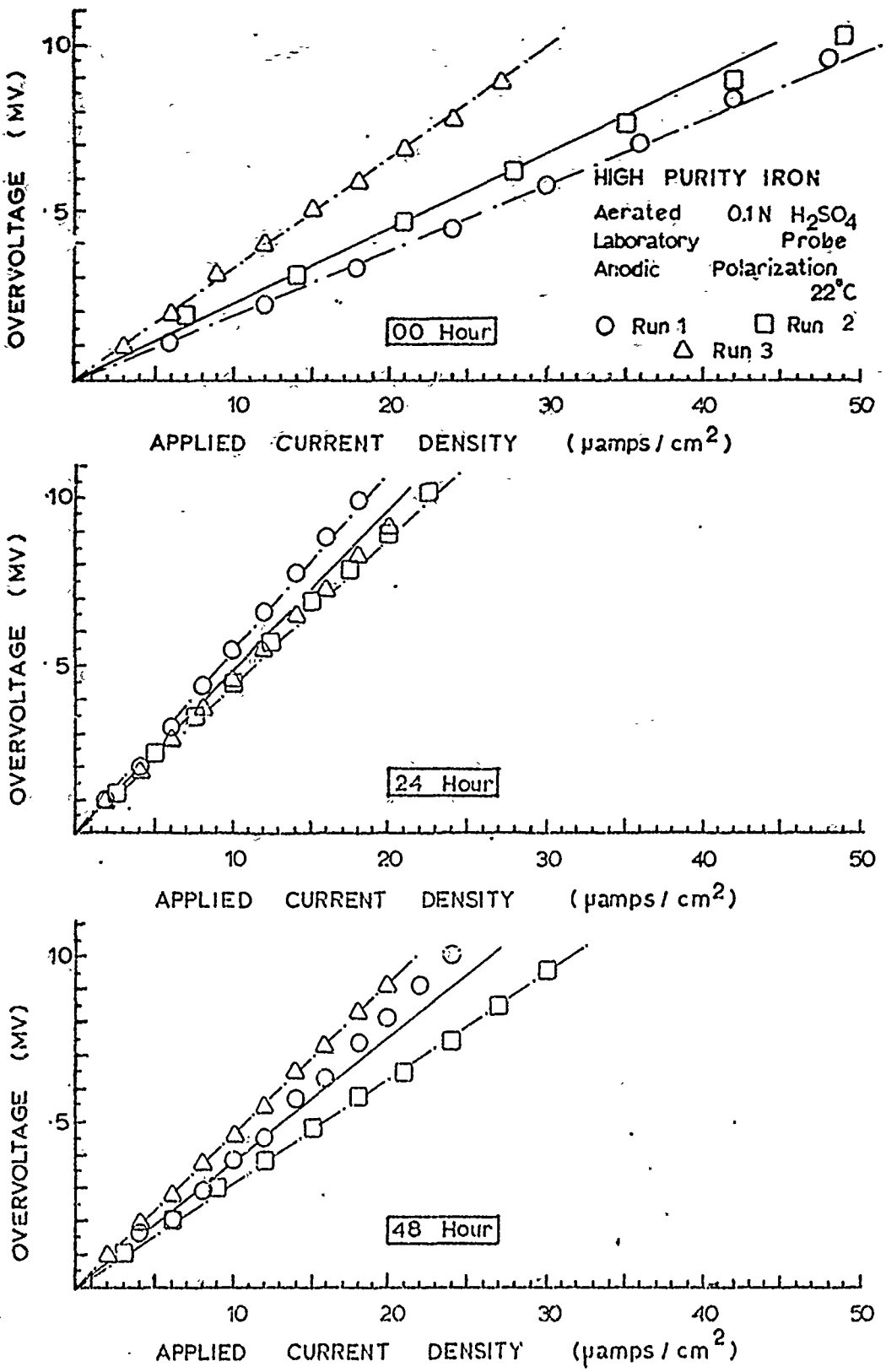

Figure 28: Effect of Time on Galvanostatic Anodic Polarization Resistance of High Purity Iron in Aerated .1N Sulfuric Acid Determined Using a Laboratory Probe. (Cont)

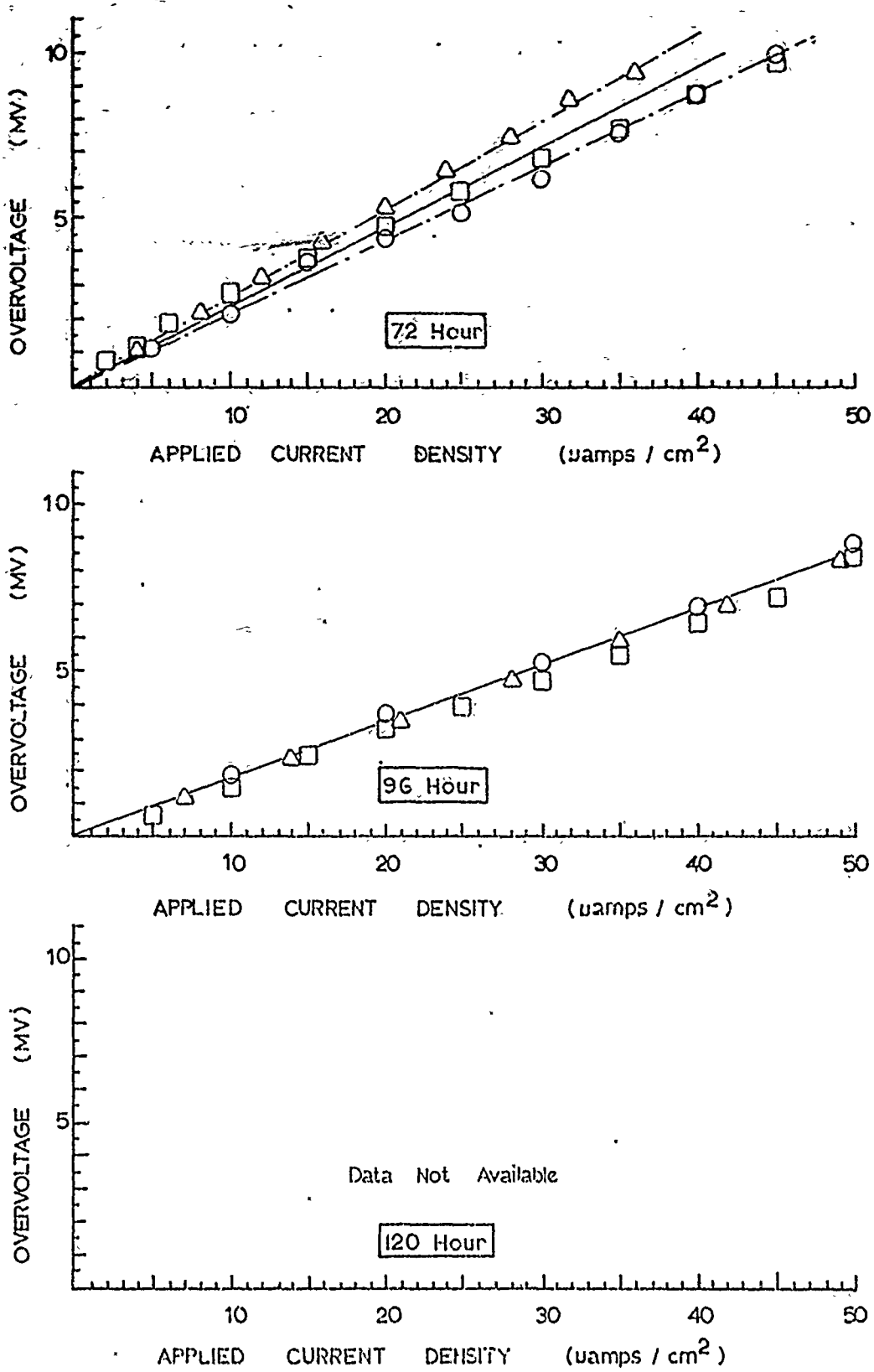

Figure 28: (Cont) Effect of Time on Galvanostatic Anodic Polarization Resistance of High Purity Iron in Aerated .1N Sulfuric Acid Determined Using a Laboratory Probe.

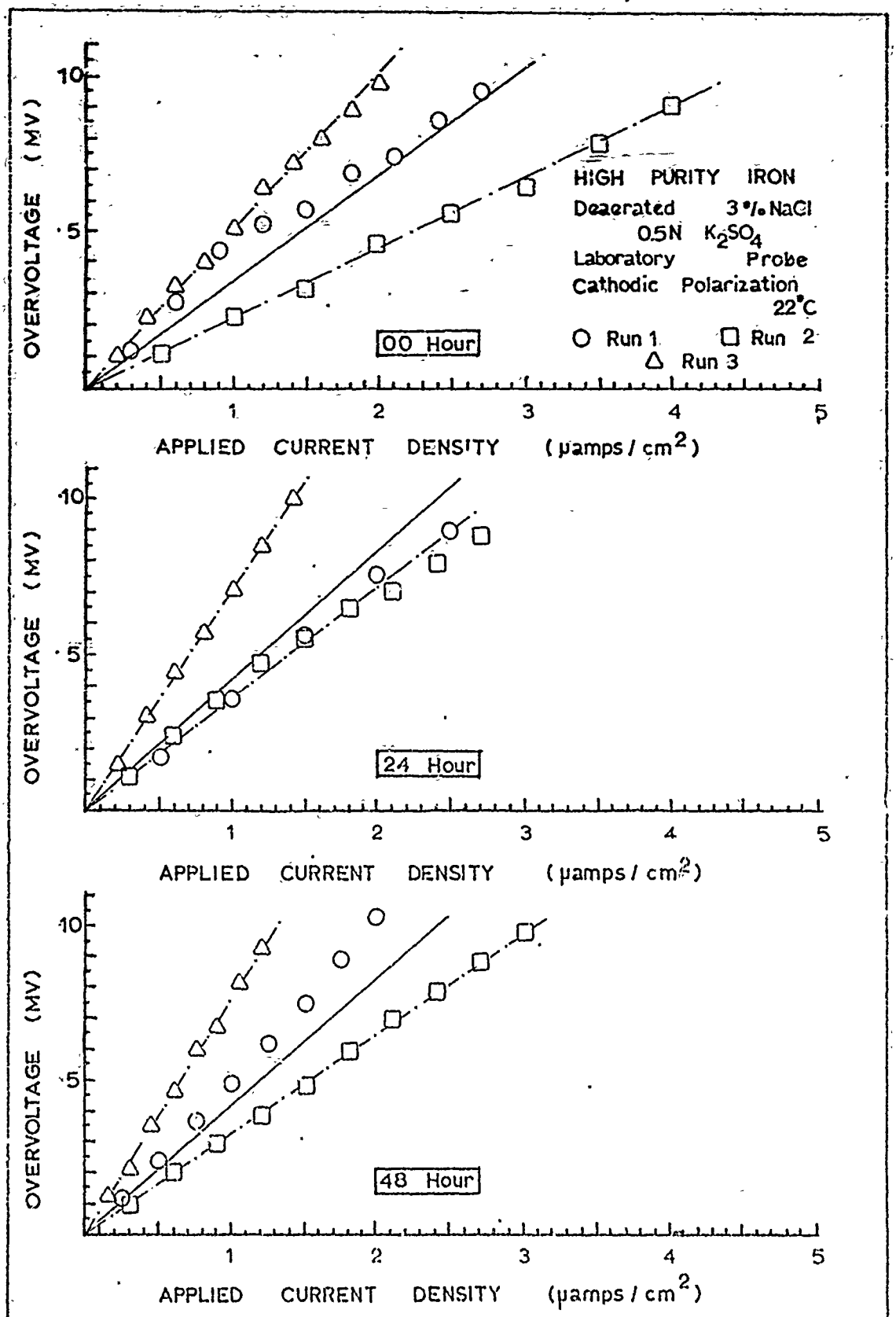

Figure 29: Effect of Time on Galvanostatic Cathodic Polarization Resistance of High Purity Iron in Hydrogen Saturated .5N Sulfuric Acid Determined Using a Laboratory Probe. (Cont)

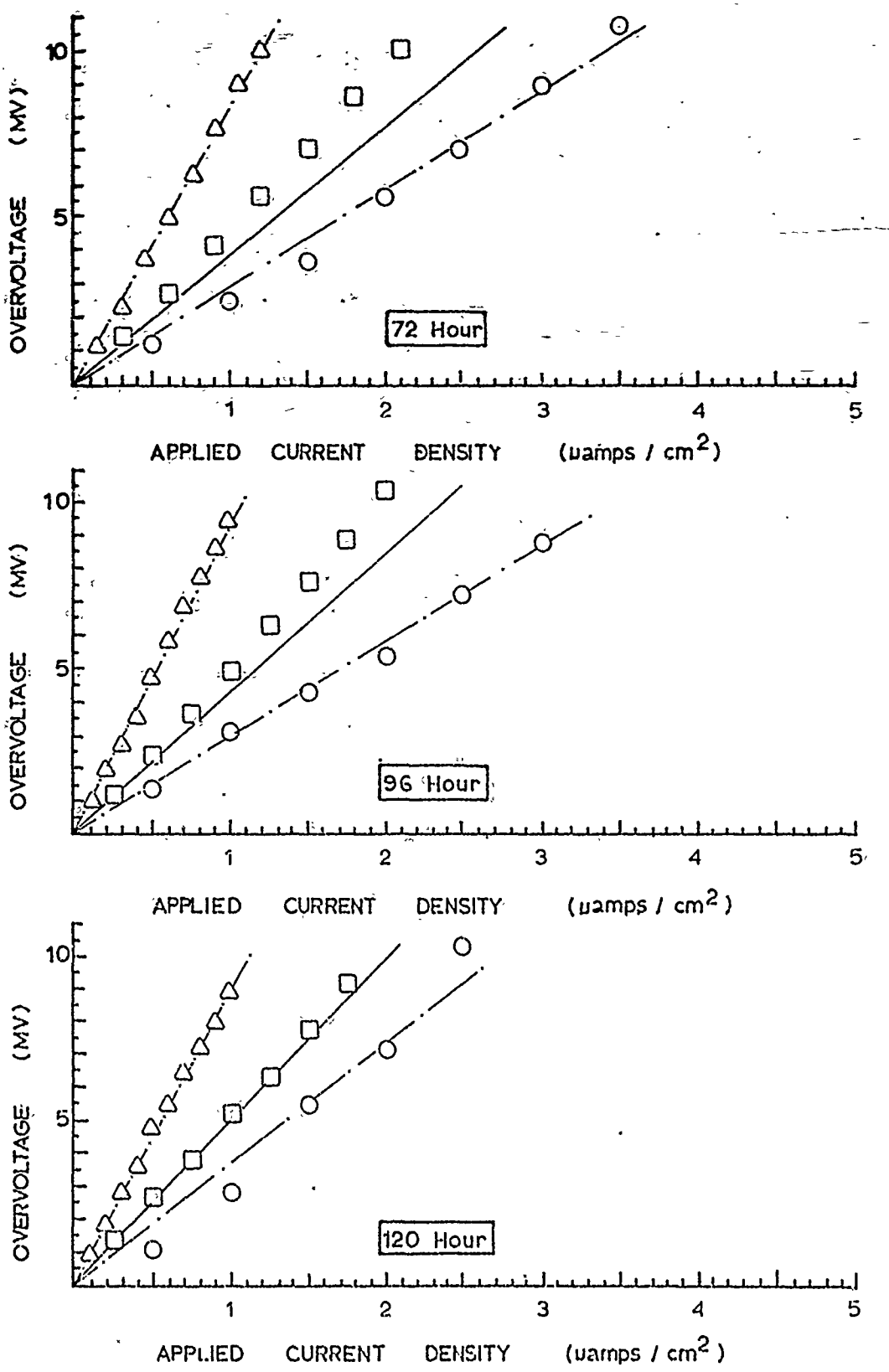

Figure 29: (Cont) Effect of Time on Galvanostatic Cathodic Polarization Resistance of High Purity Iron in Hydrogen Saturated .5N Sulfuric Acid Determined Using a Laboratory Probe.

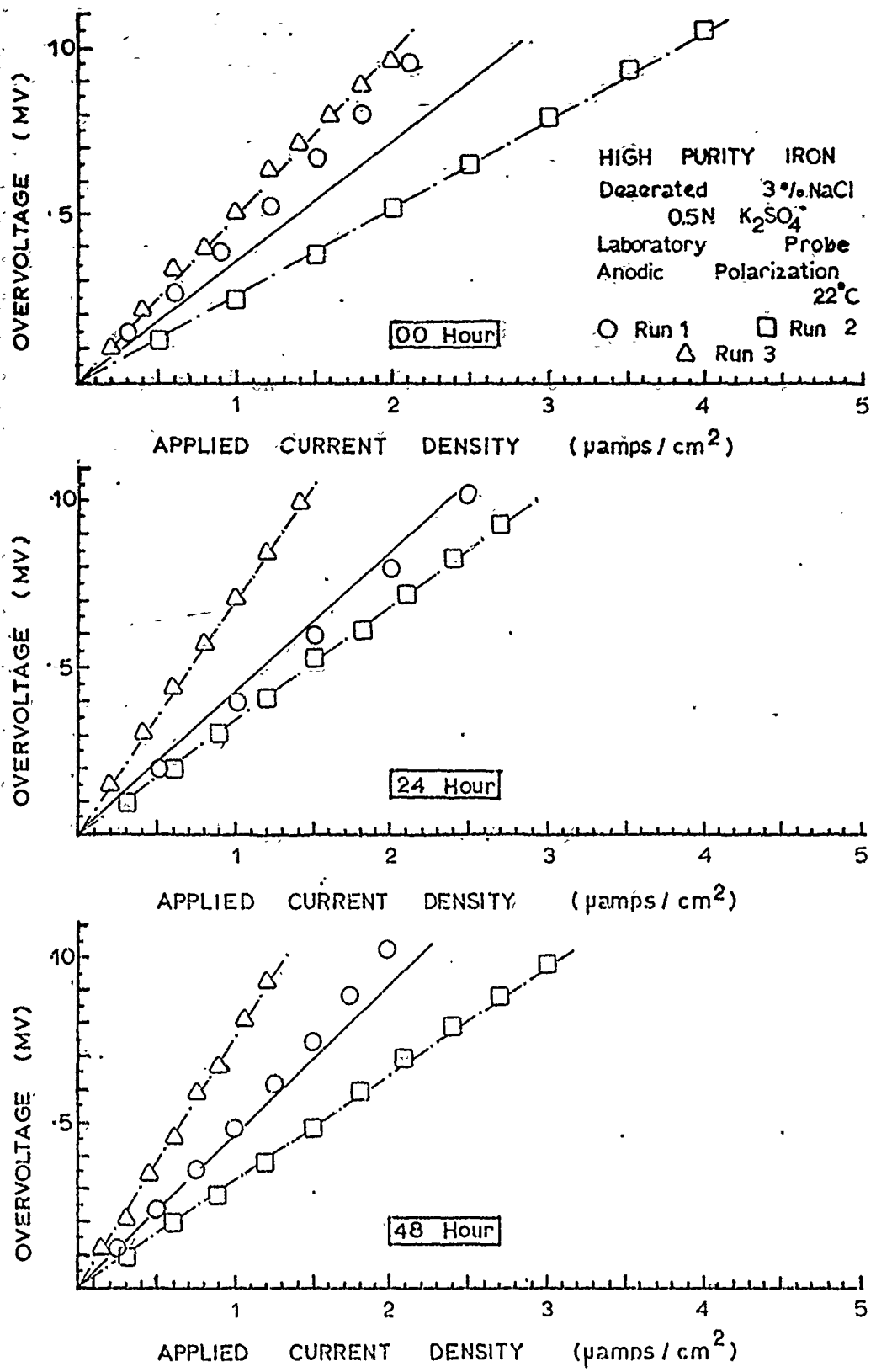

Figure 30: Effect of Time on Galvanostatic Anodic Polarization Resistance of High Purity Iron in Hydrogen Saturated .5N Sulfuric Acid Determined Using a Laboratory Probe. (Cont)

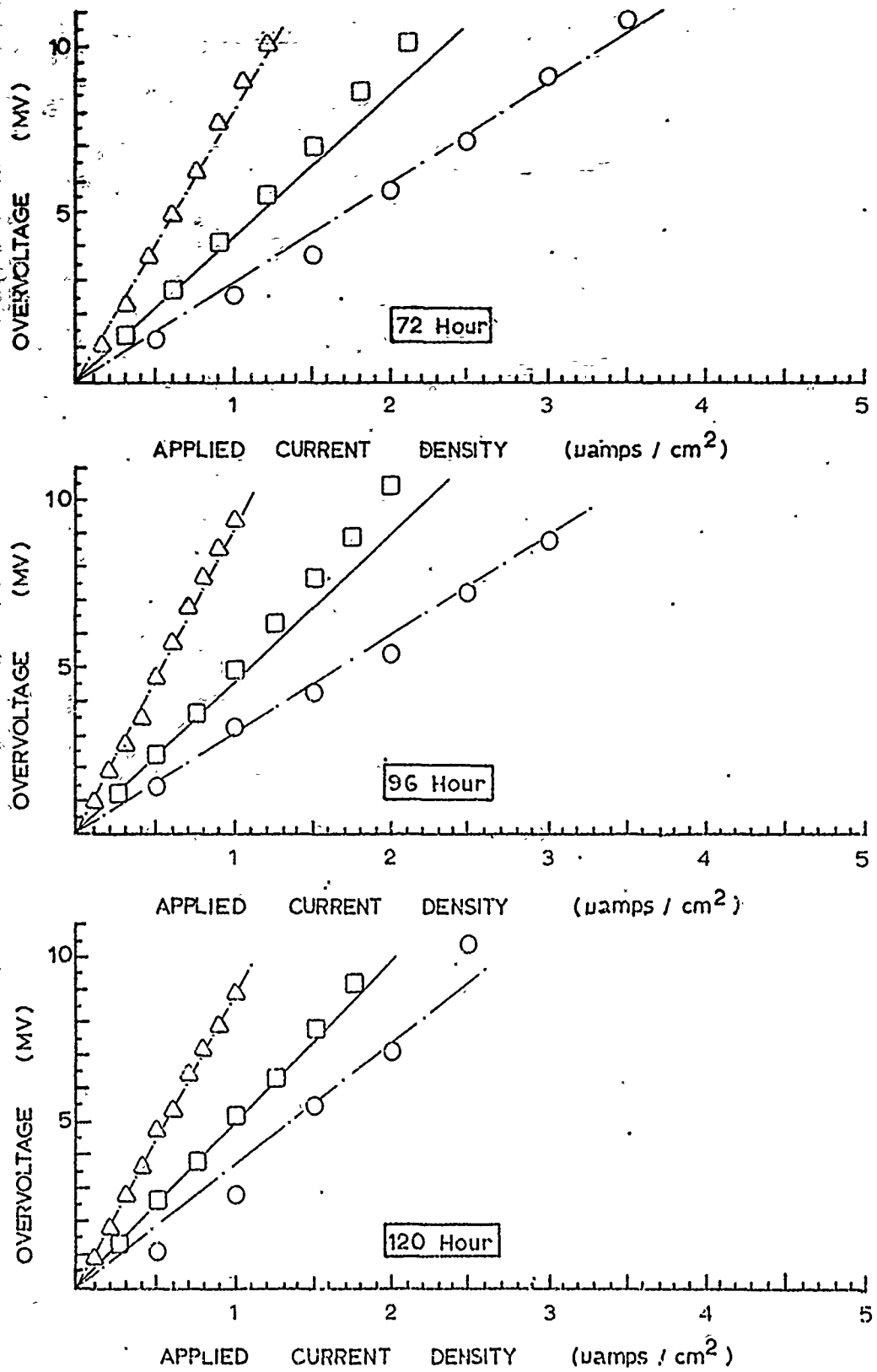

Figure 30: (Cont) Effect of Time on Galvanostatic Anodic Polarization Resistance of High Purity Iron in Hydrogen Saturated .5N Sulfuric Acid Determined Using a Laboratory Probe.

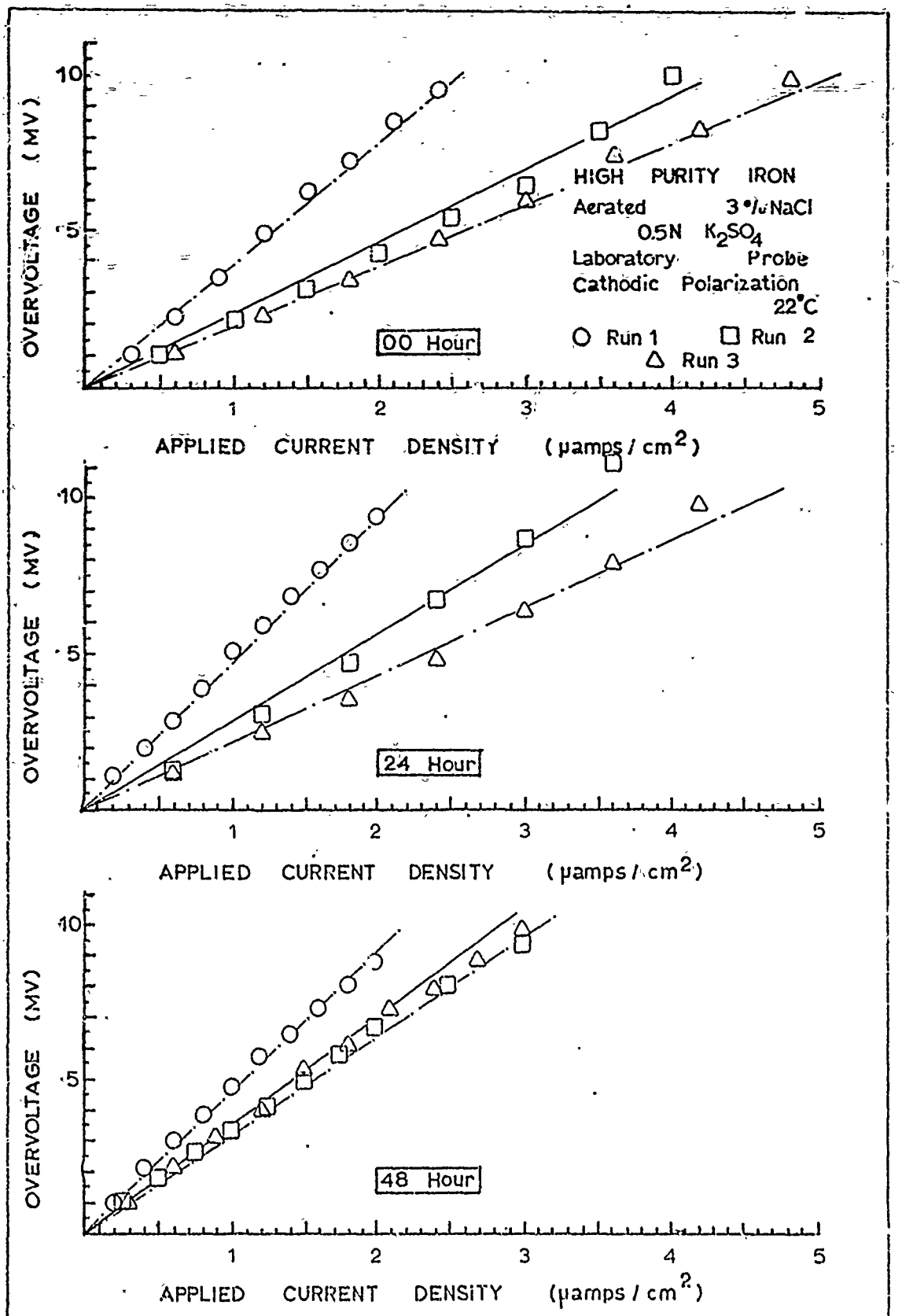

Figure 31: Effect of Time on Galvanostatic Cathodic Polarization Resistance of High Purity Iron in Aerated .5N Sulfuric Acid Determined Using a Laboratory Probe. (Cont)

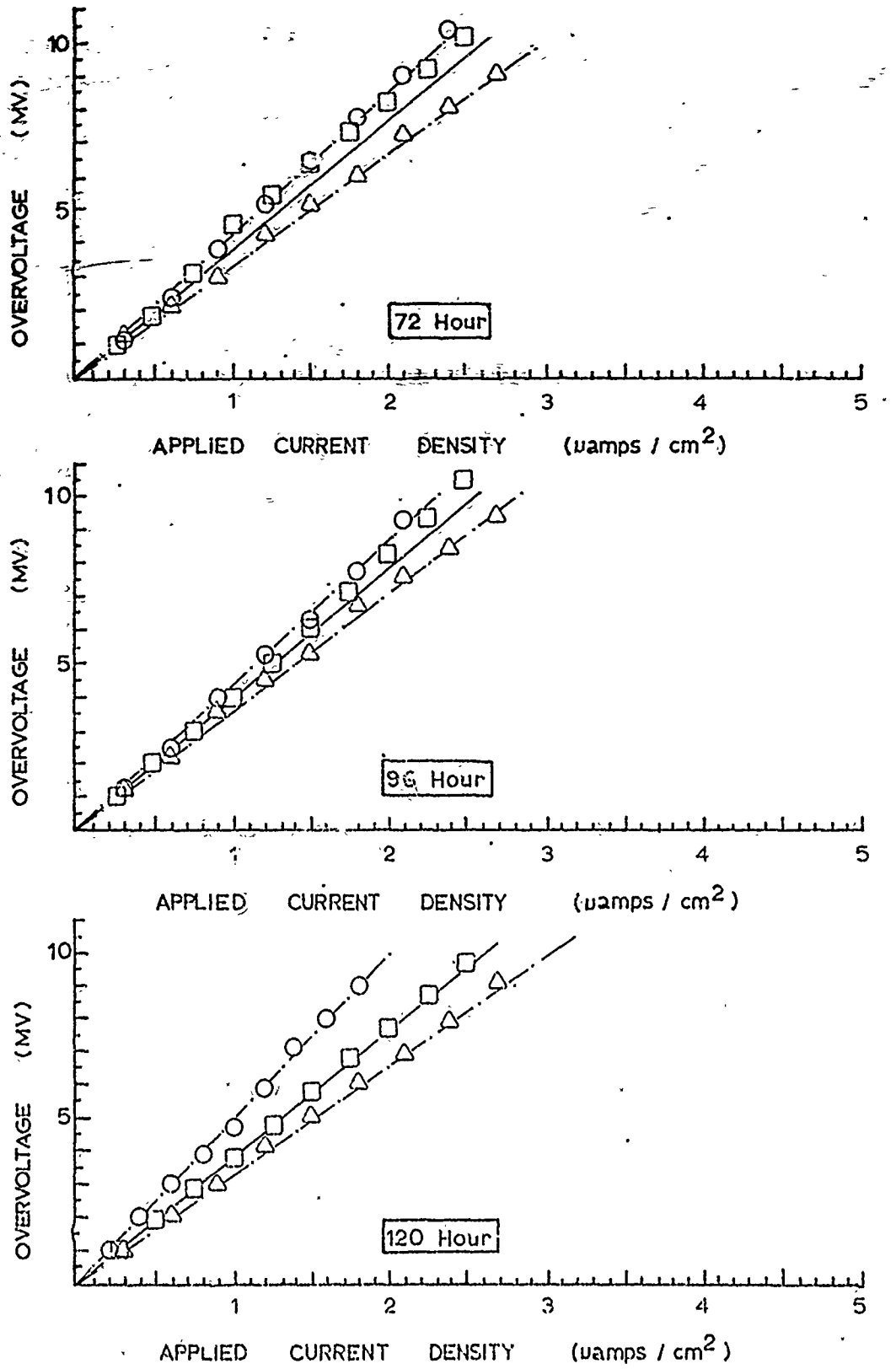

Figure 31: (Cont) Effect of Time on Galvanostatic Cathodic Polarization Resistance of High Purity Iron in Aerated .5N Sulfuric Acid Determined Using a Laboratory Probe.

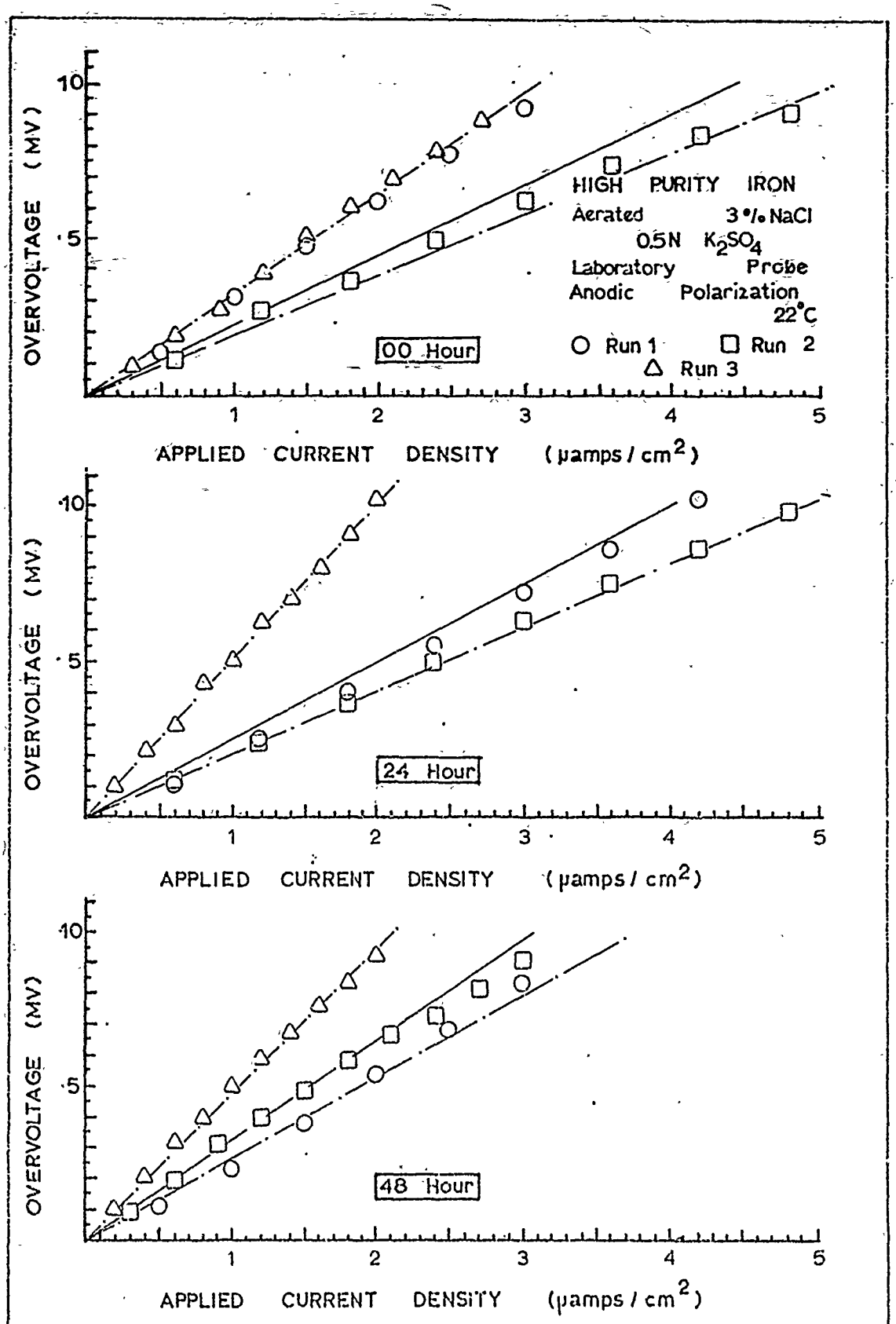

Figure 32: Effect of Time on Galvanostatic Anodic Polarization Resistance of High Purity Iron in Aerated .5N Sulfuric Acid Determined Using a Laboratory Probe. (Cont)

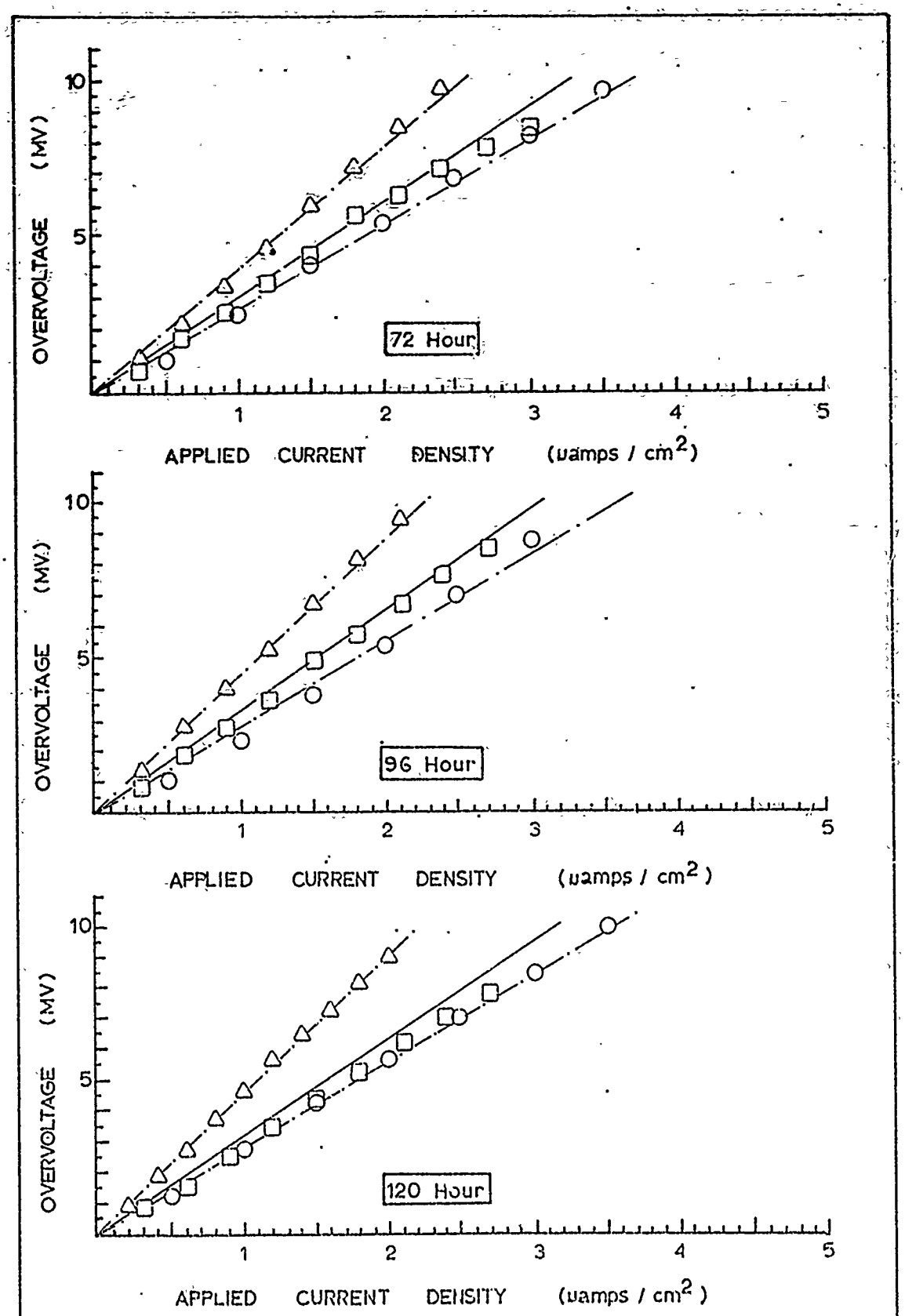

Figure 32: (Cont) Effect of Time on Galvanostatic Anodic Polarization Resistance of High Purity Iron in Aerated .5N Sulfuric Acid Determined Using a Laboratory Probe.

Appendix D

The Effect of Time on Galvanostatic Polarization Resistance of High Purity Iron I Using an Experimental Probe

The effect of time on the galvanostatic cathodic and anodic polarization resistance of high purity iron (specimen I) in aerated and deaerated (hydrogen saturated) 1N and 0.1N sulfuric acids and 3% sodium chloride environments as determined by using the experimental probe described in Chapter III are shown in this appendix. In addition, the linear regression analyses determined maximum, minimum, and "combined daily" data values of polarization resistance are also shown. (See "Polarization Resistance Determination" in Chapter III for terminology definitions). Maximum and minimum computed polarization resistance values for a given time on a by run, by day basis are shown graphically as broken lines. The values of polarization resistance determined from "combined daily" data are shown as a solid line. Note that at a given test time, if the values of polarizaiton resistance from each run are not significantly different, either the maximum or minimum or "combined" data polarization resistance values have been omitted for clarity purposes. Also, note that the abscissa scale may vary considerably from graph to graph and amongst figures.

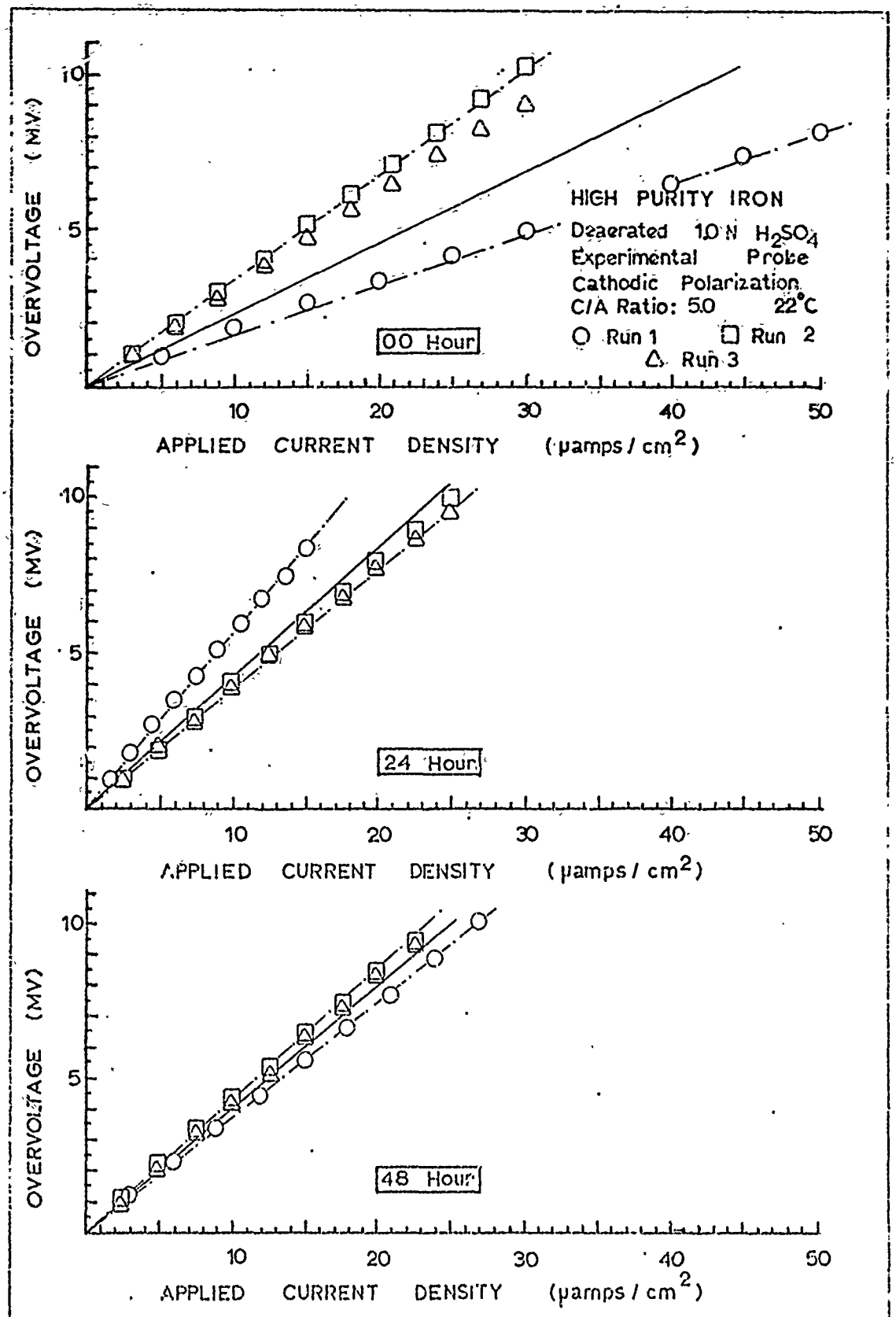

Figure 33 : Effect of Time on Galvanostatic Cathodic Polarization Resistance of High Purity Iron with C/A Ratio = 5 in Hydrogen Saturated 1N Sulfuric Acid Determined Using an Experimental Probe. (Cont)

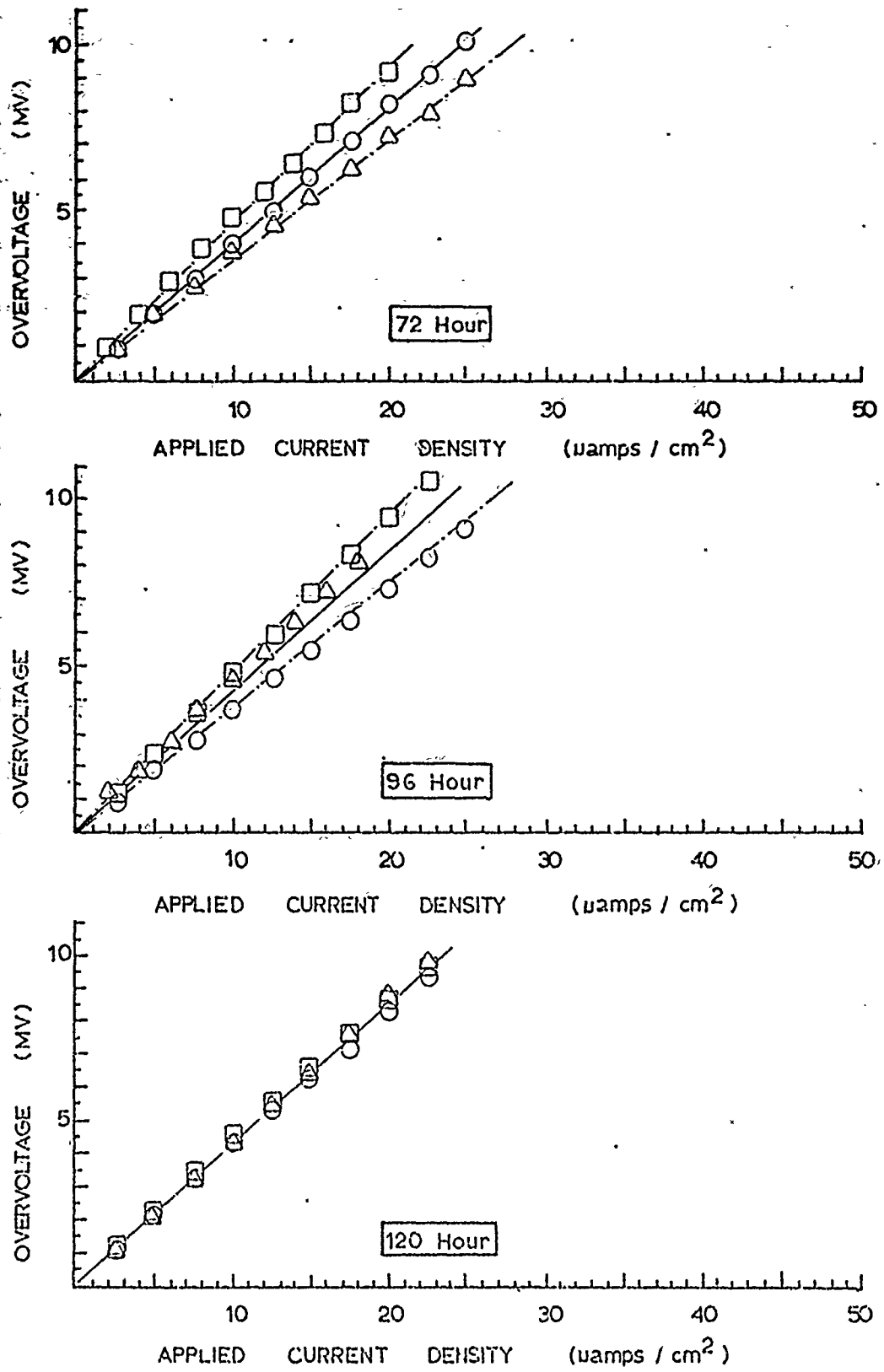

Figure 33: (Cont) Effect of Time on Galvanostatic Cathodic Polarization Resistance of High Purity Iron with C/A Ratio = 5 in Hydrogen Saturated 1N Sulfuric Acid Determined Using an Experimental Probe.

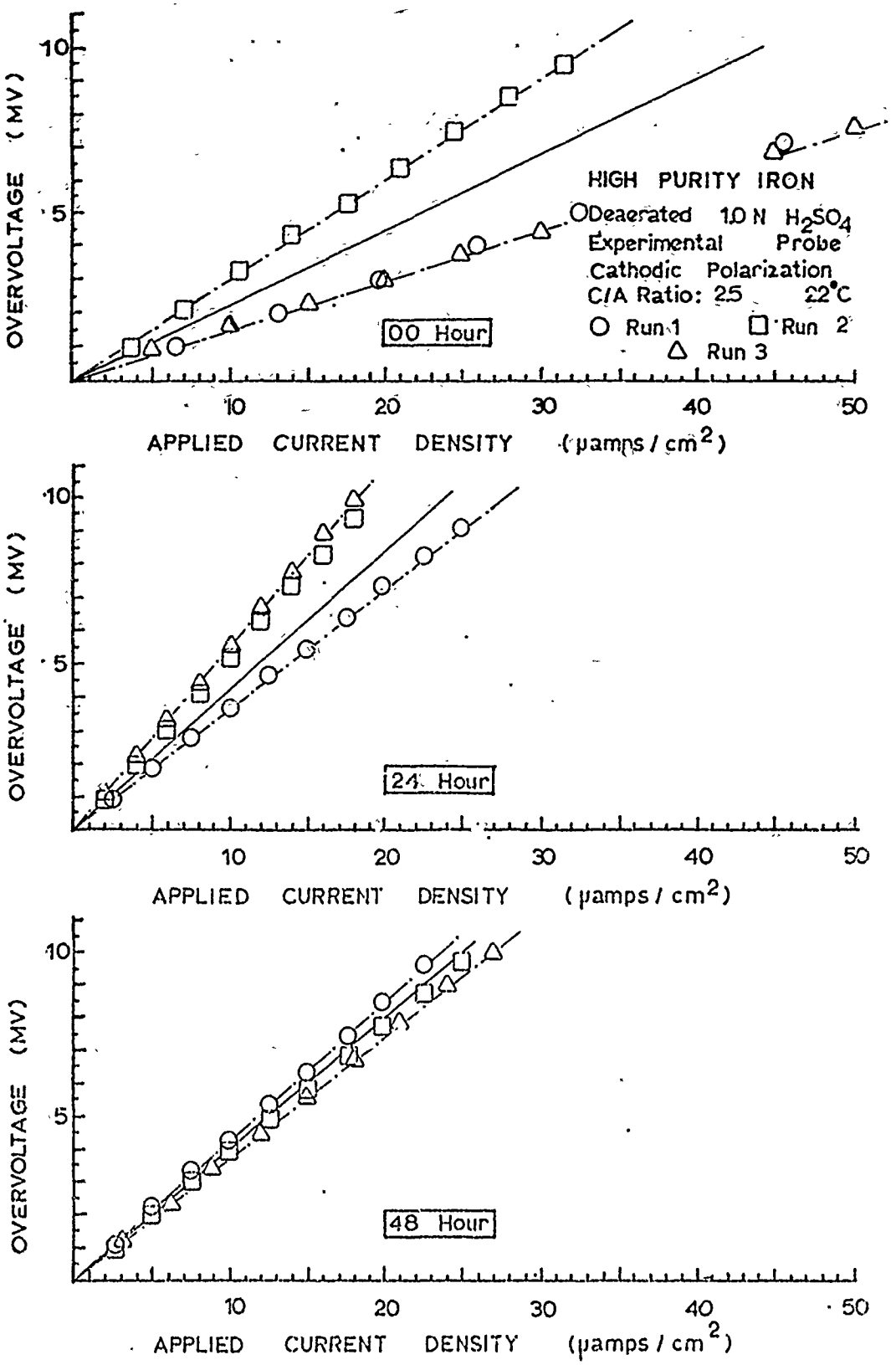

Figure 34 : Effect of Time on Galvanostatic Cathodic Polarization Resistance of High Purity Iron with C/A Ratio = 2.5 in Hydrogen Saturated 1N Sulfuric Ac Determined Using an Experimental Probe. (Cont)

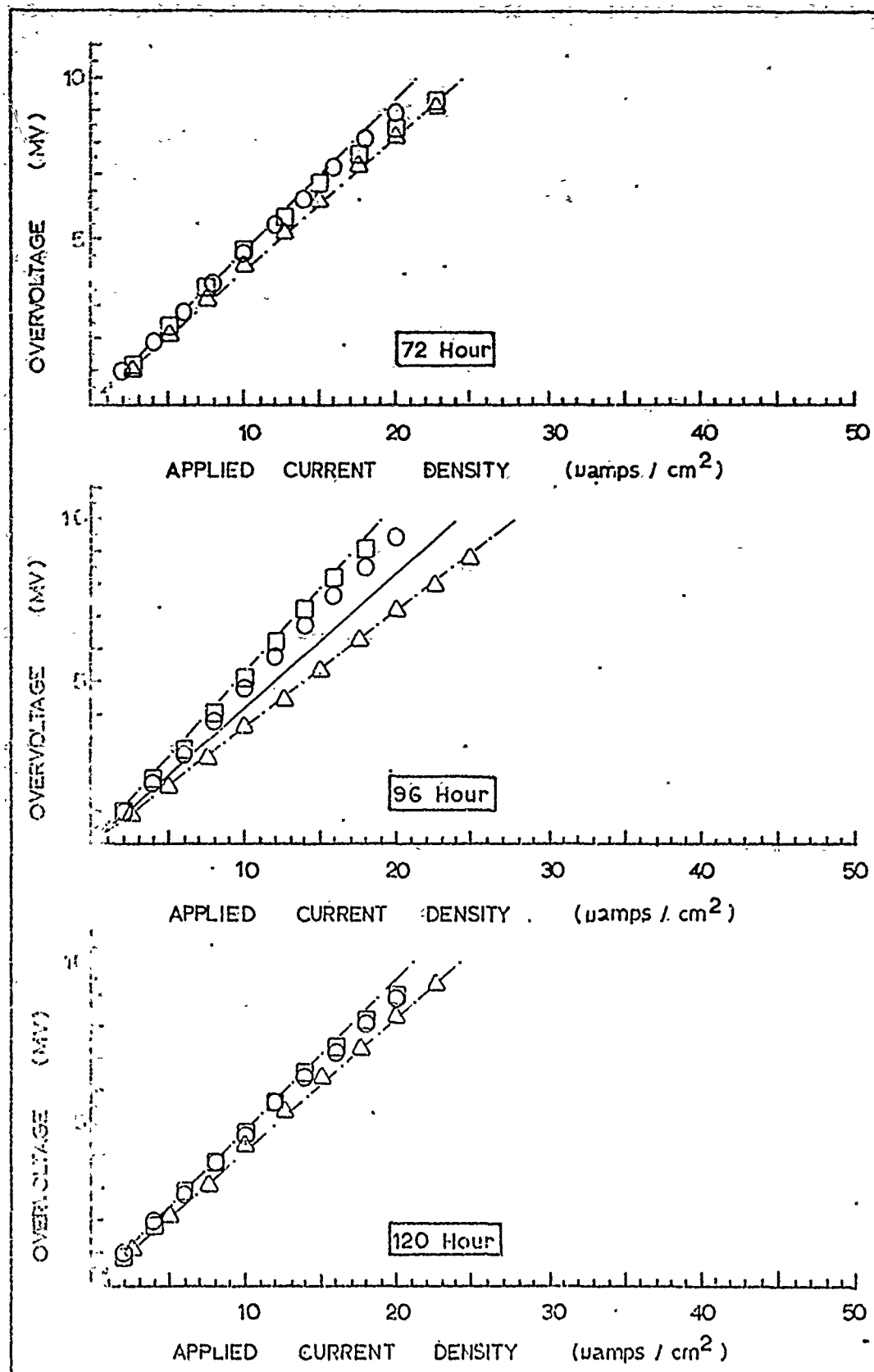

Figure 34 : (Cont) Effect of Time on Galvanostatic Cathodic Polarization Resistance of High Purity Iron with C/A Ratio = 2.5 in Hydrogen Saturated 1N Sulfuric Acid Determined Using an Experimental Probe.

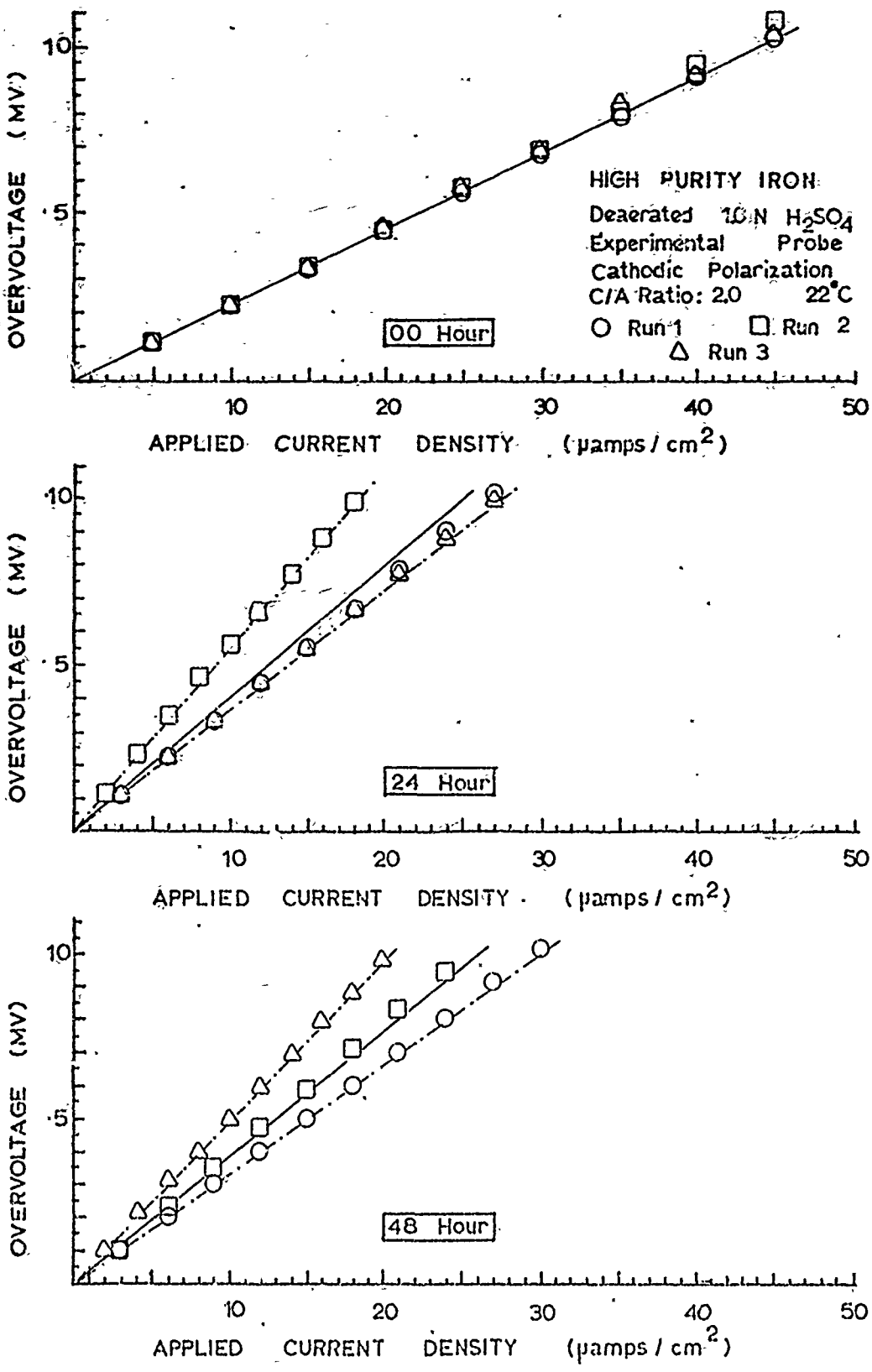

Figure 35 : Effect of Time on Galvanostatic Cathodic Polarization Resistance of High Purity Iron with C/A Ratio = 2 in Hydrogen Saturated 1N Sulfuric Acid Determined Using an Experimental Probe. *(Cont)*

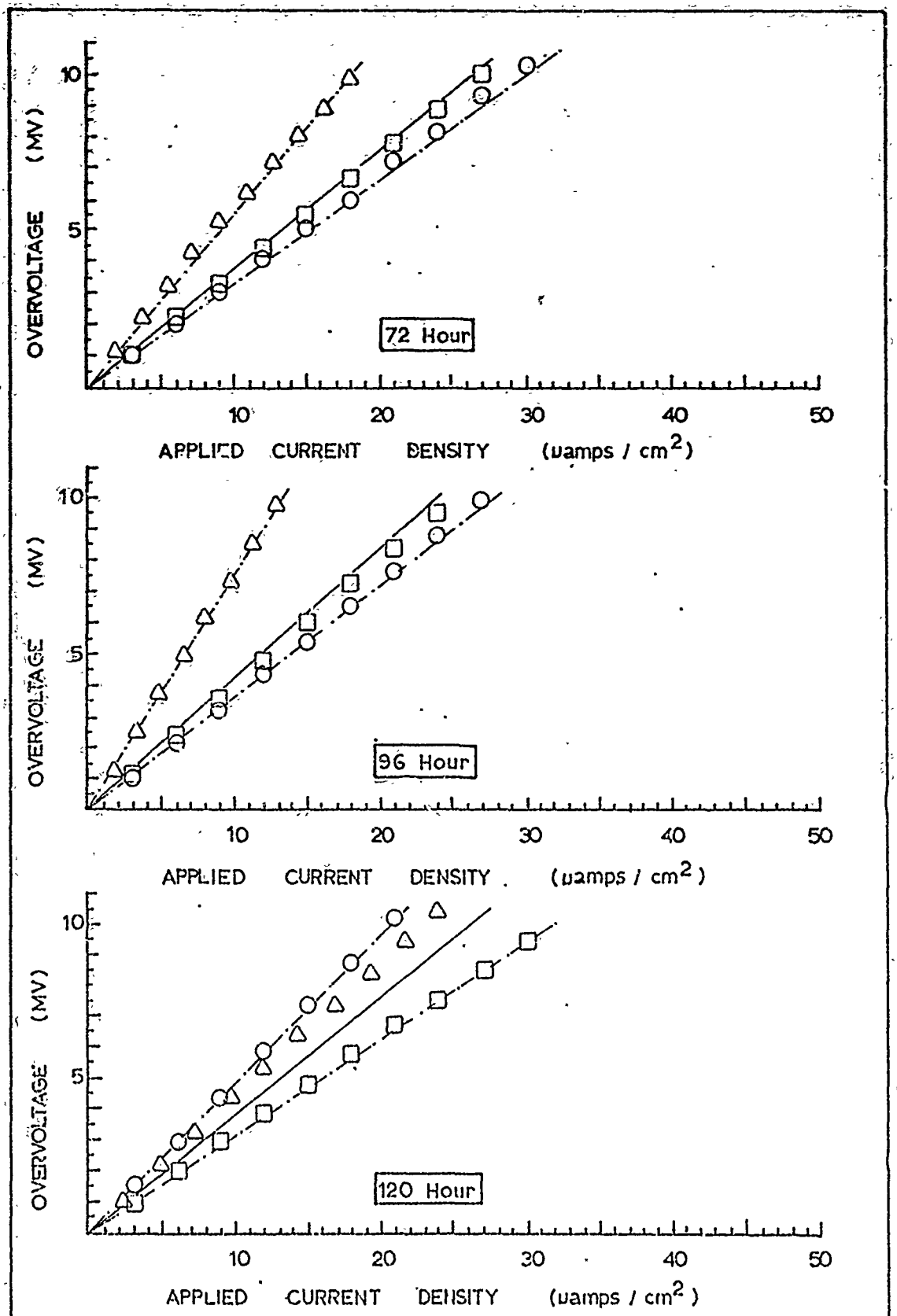

Figure 35 : (Cont) Effect of Time on Galvanostatic Cathodic Polarization Resistance of High Purity Iron with C/A Ratio = 2 in Hydrogen Saturated 1N Sulfuric Acid Determined Using an Experimental Probe.

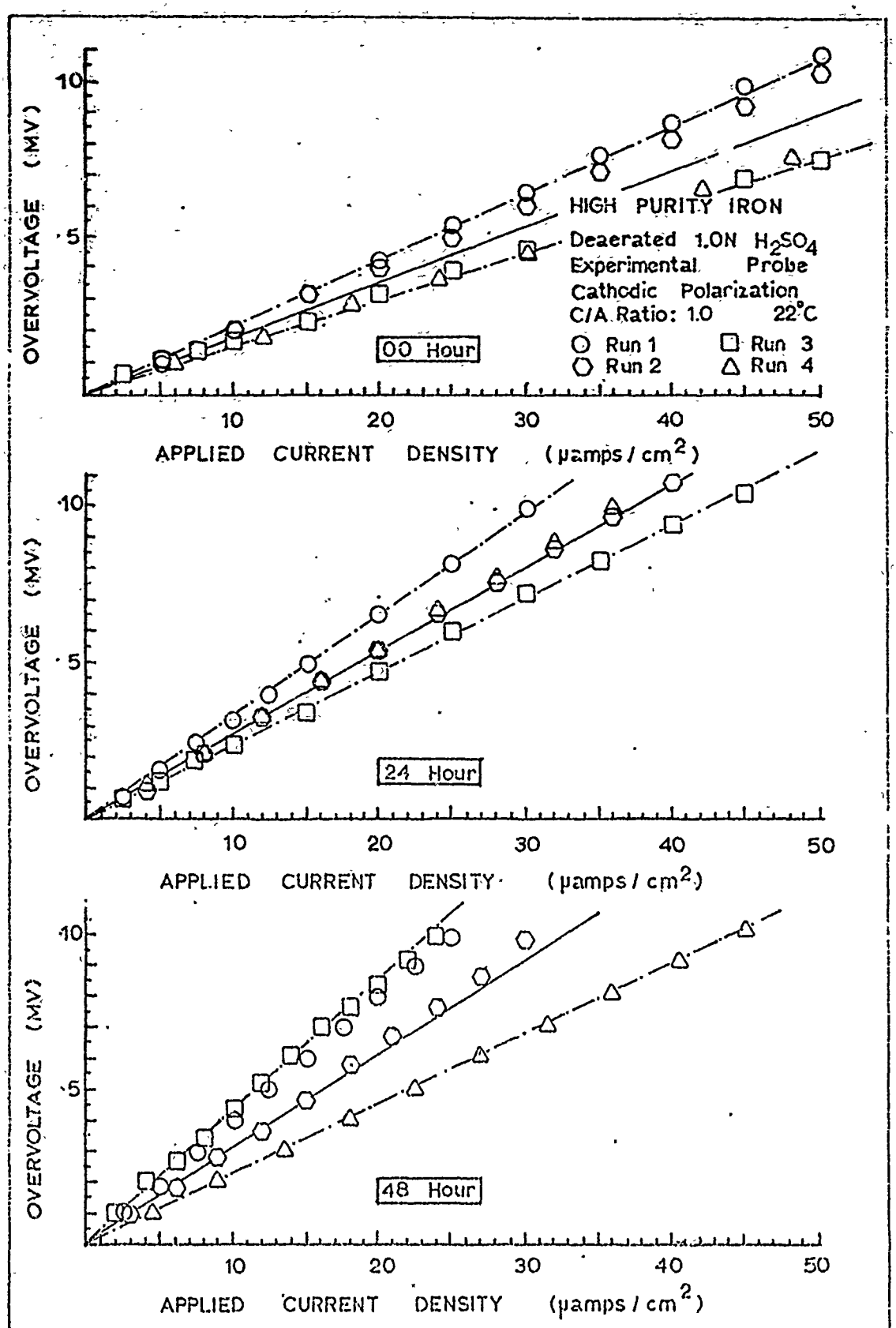

Figure 36: Effect of Time on Galvanostatic Cathodic Polarization Resistance of High Purity Iron with C/A Ratio = 1 in Hydrogen Saturated 1N Sulfuric Acid Determined Using an Experimental Probe. (Cont)

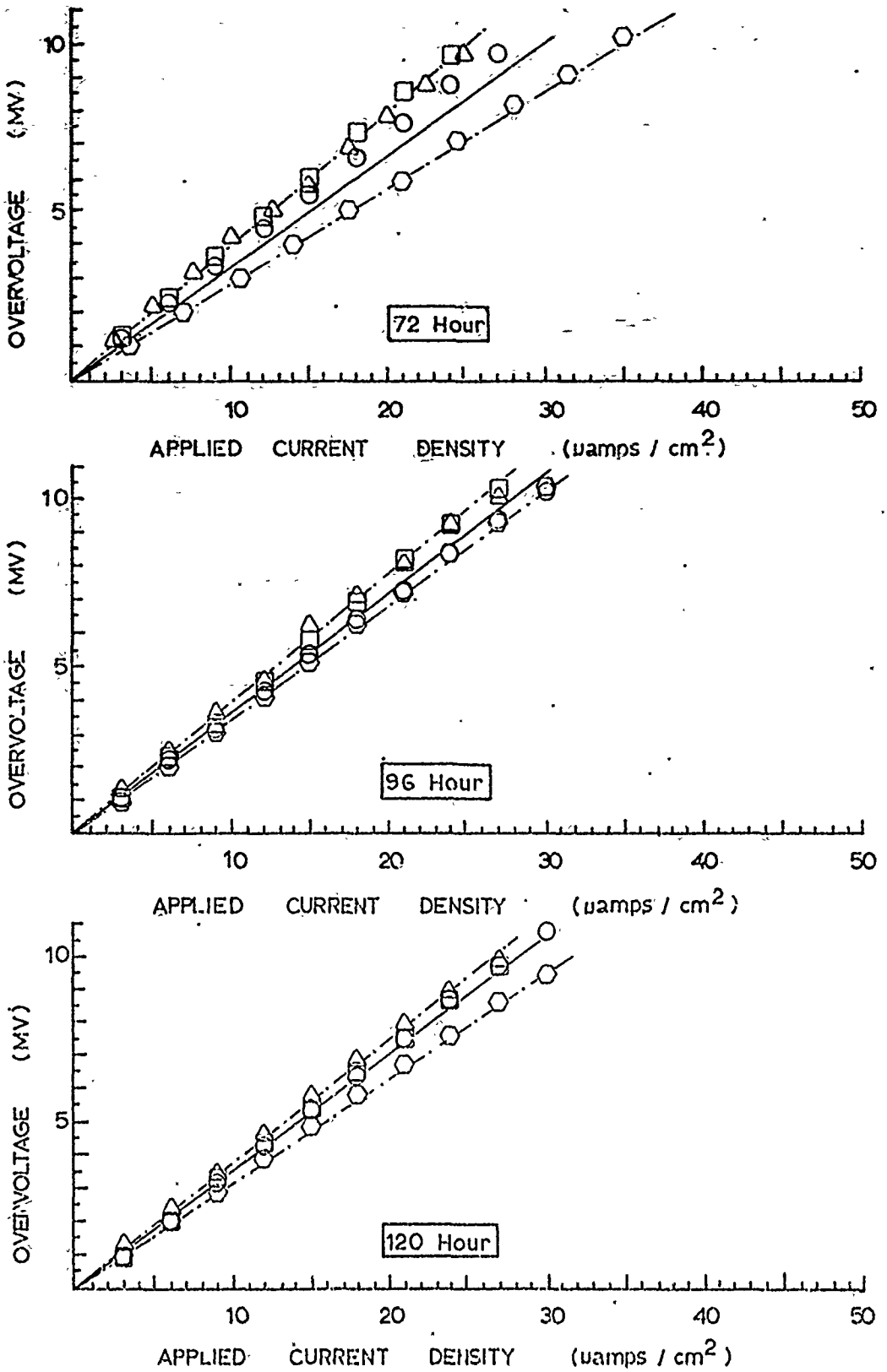

Figure 36 : (Cont) Effect of Time on Galvanostatic Cathodic Polarization Resistance of High Purity Iron with C/A Ratio = 1 in Hydrogen Saturated 1N Sulfuric Acid Determined Using an Experimental Probe.

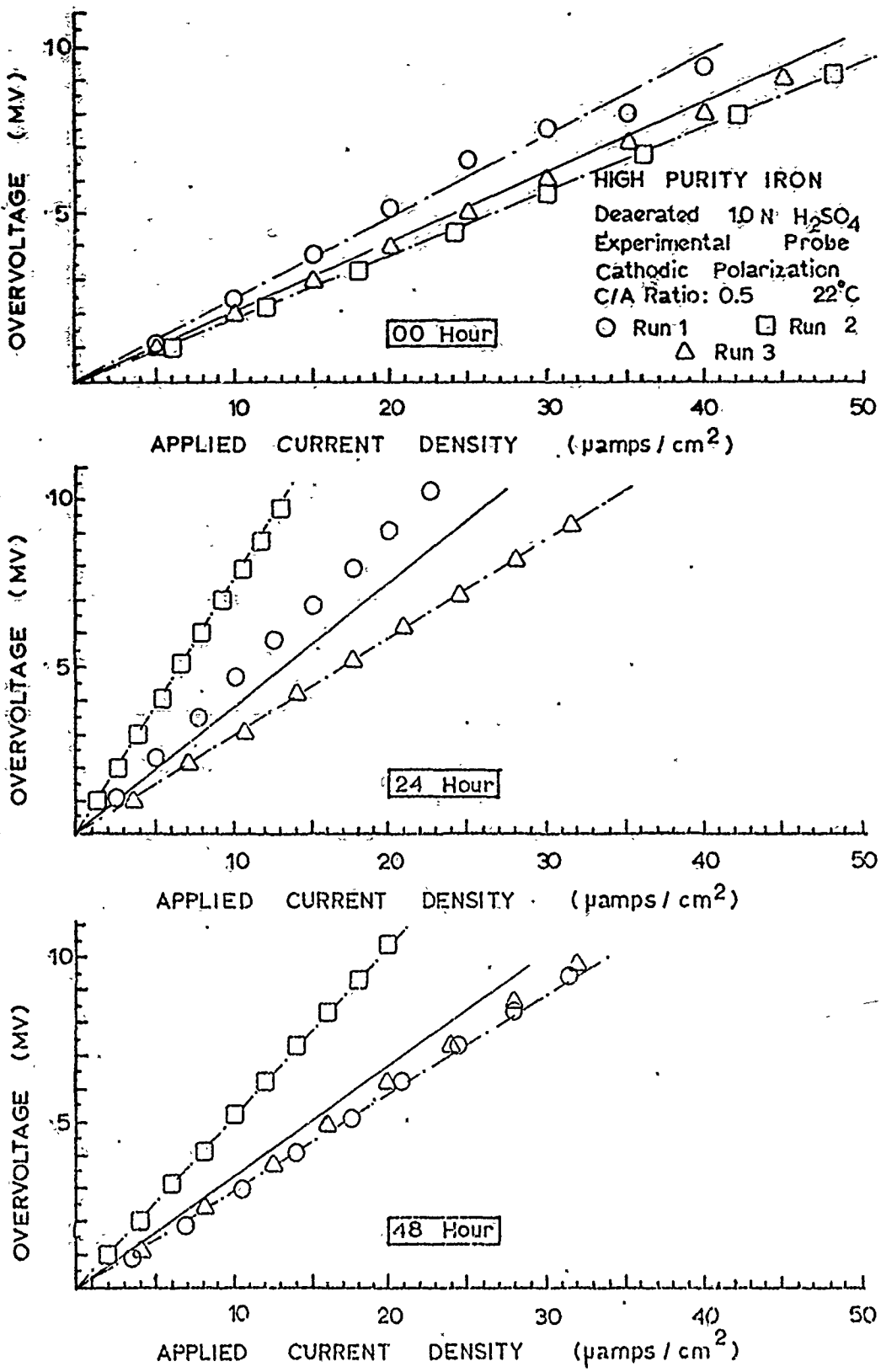

Figure 37 : Effect of Time on Galvanostatic Cathodic Polarization Resistance of High Purity Iron with C/A Ratio = .5 in Hydrogen Saturated 1N Sulfuric Acid Determined Using an Experimental Probe. (Cont)

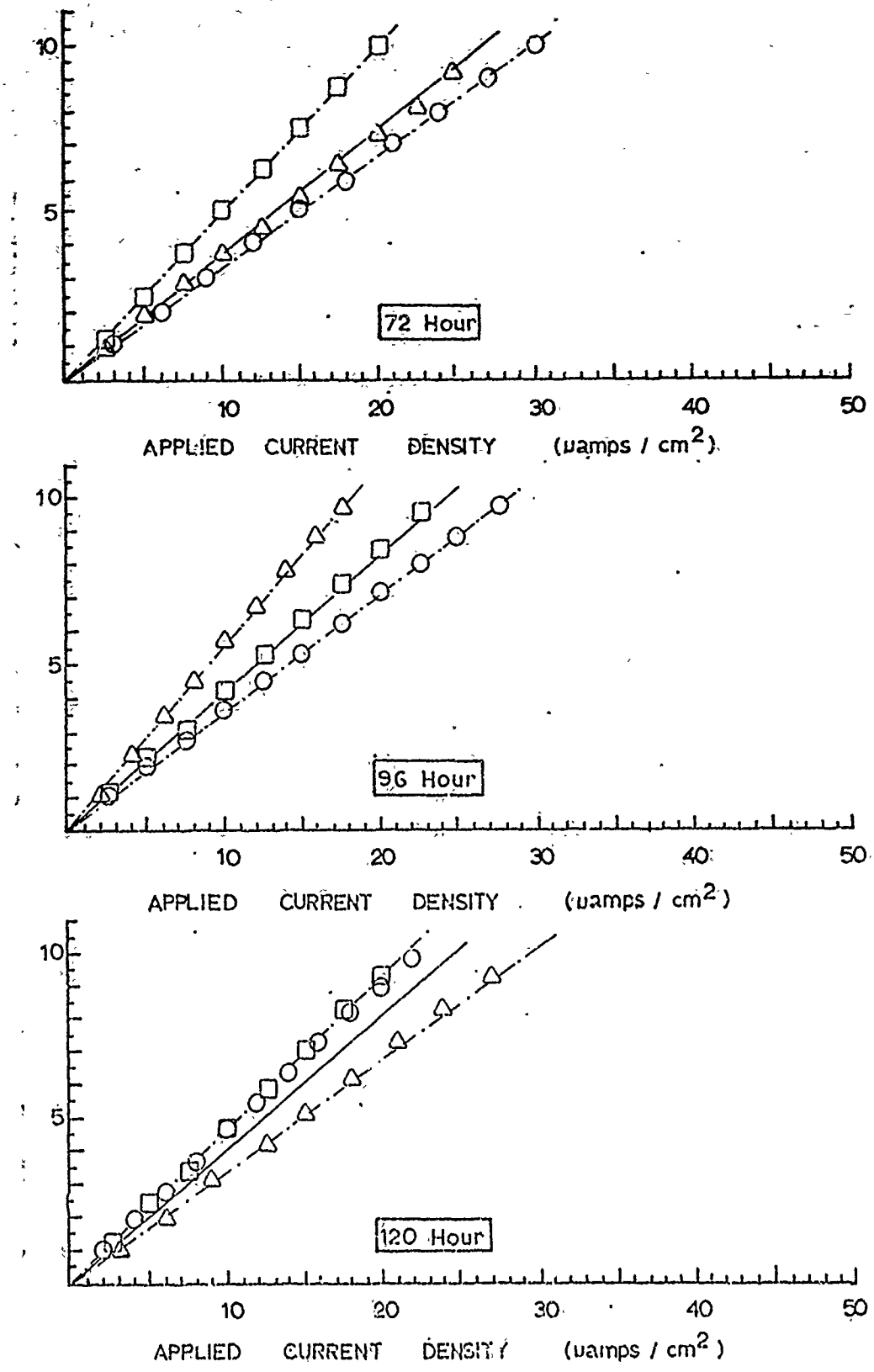

Figure 37 : (Cont) Effect of Time on Galvanostatic Cathodic Polarization Resistance of High Purity Iron with C/A Ratio = .5 in Hydrogen Saturated 1N Sulfuric Acid Determined Using an Experimental Probe.

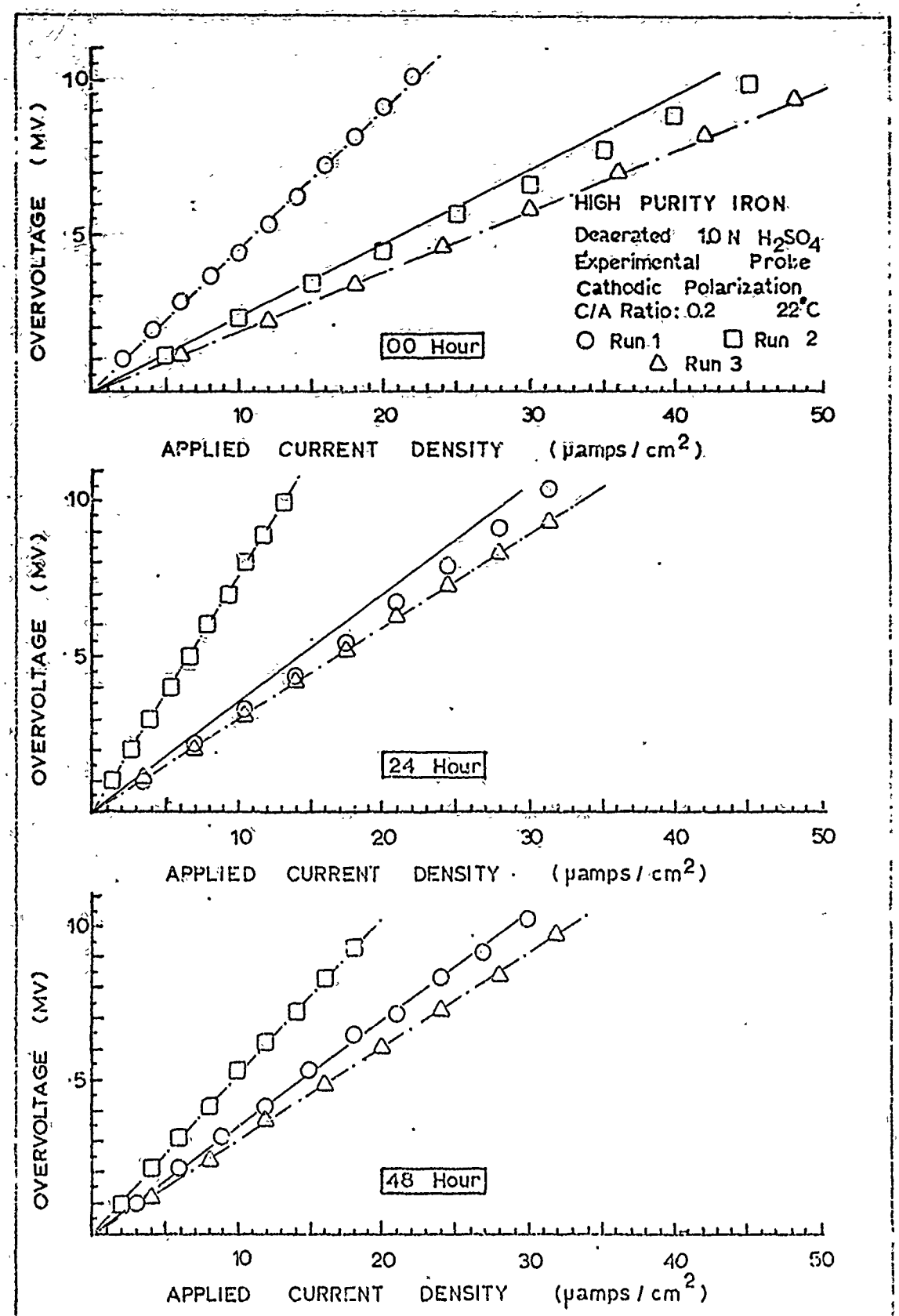

Figure 38 : Effect of Time on Galvanostatic Cathodic Polarization Resistance of High Purity Iron with C/A Ratio = .2 in Hydrogen Saturated 1N Sulfuric Acid Determined Using an Experimental Probe. (Cont)

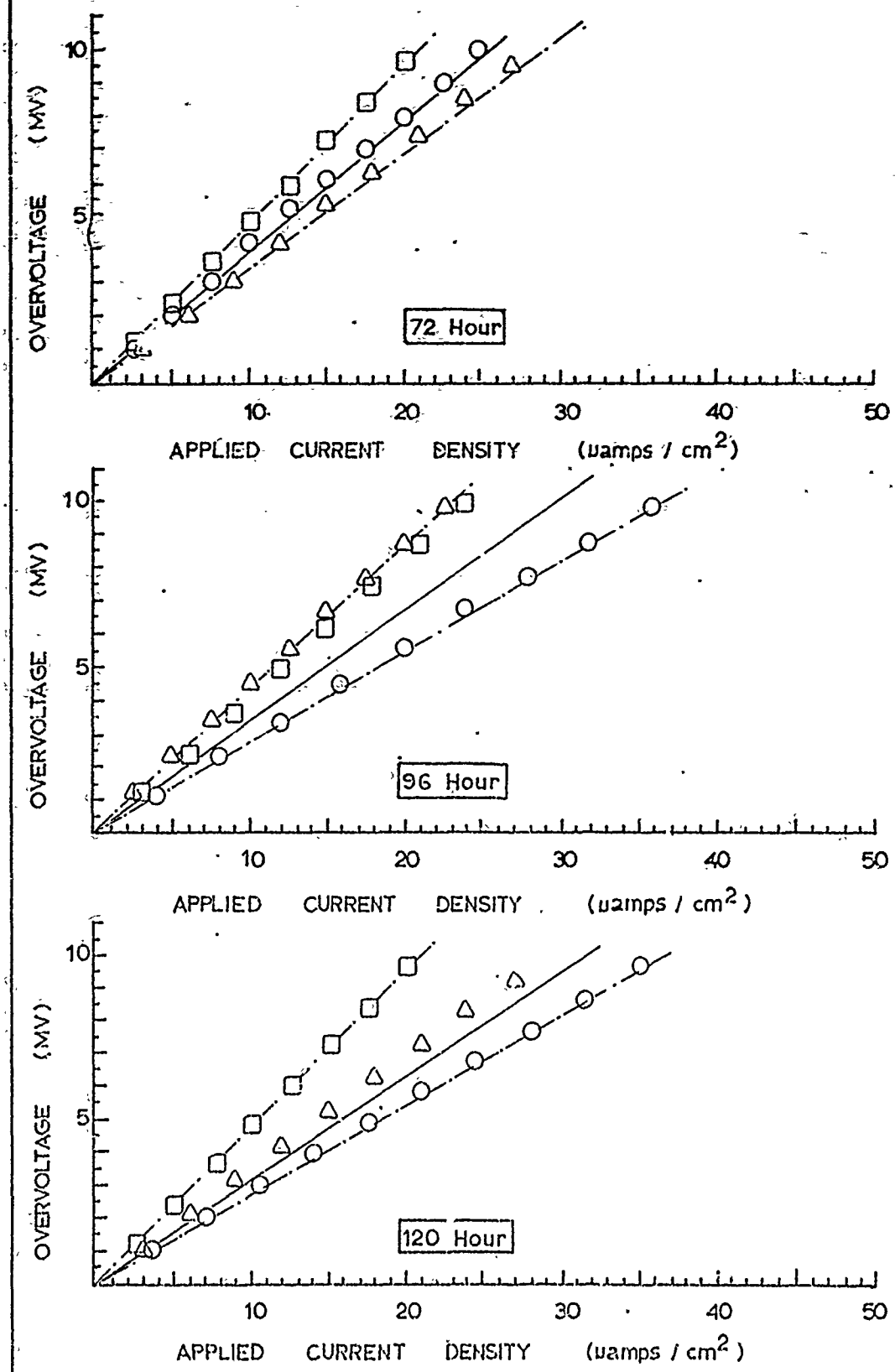

Figure 38 : (Cont) Effect of Time on Galvanostatic Cathodic Polarization Resistance of High Purity Iron with C/A Ratio = .2 in Hydrogen Saturated 1N Sulfuric Acid Determined Using an Experimental Probe.

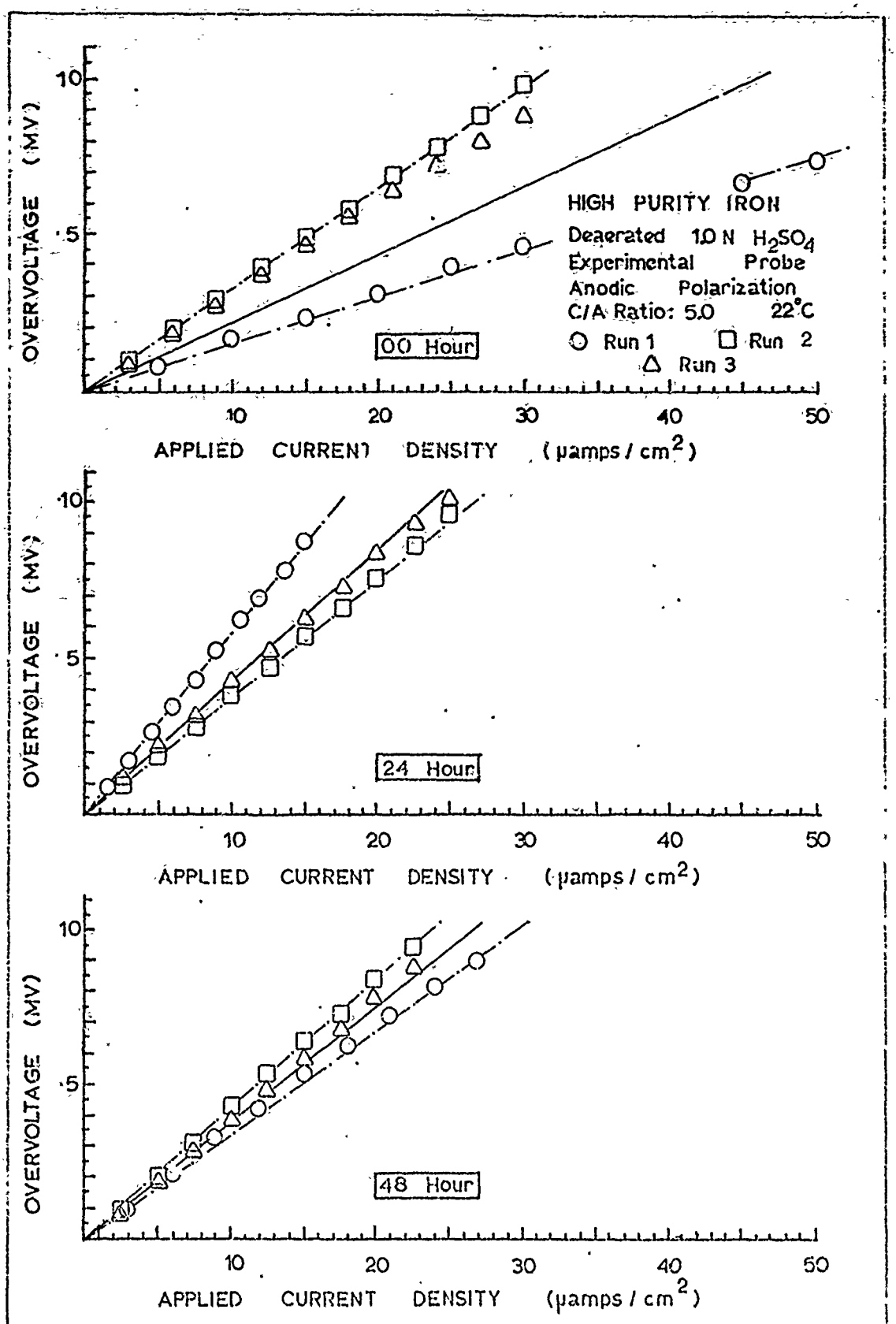

Figure 39 : Effect of Time on Galvanostatic Anodic Polarization Resistance of High Purity Iron with C/A Ratio = 5 in Hydrogen Saturated 1N Sulfuric Acid Determined Using an Experimental Probe. (Cont)

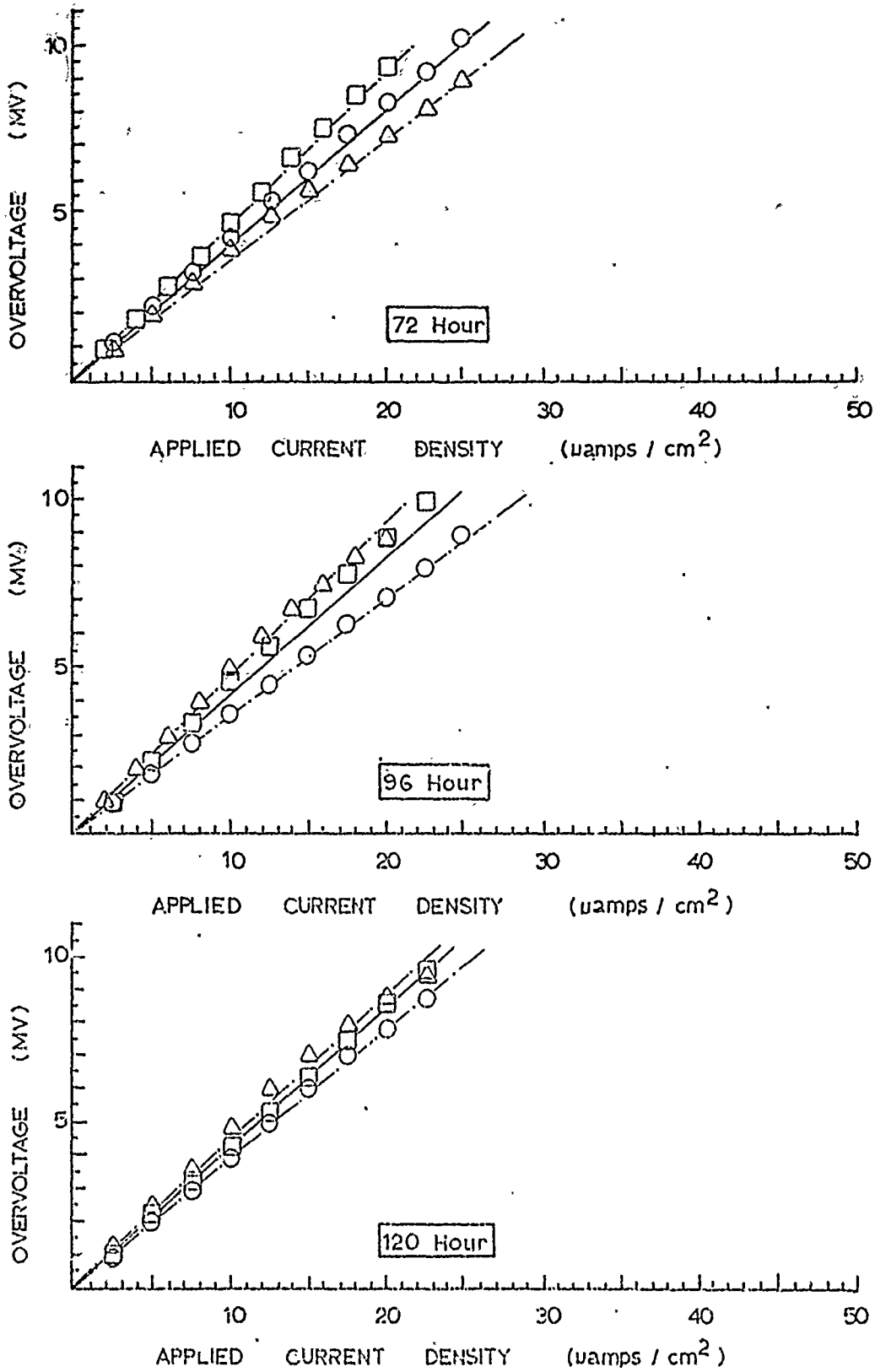

Figure 39 : (Cont) Effect of Time on Galvanostatic Anodic Polarization Resistance of High Purity Iron with C/A Ratio = 5 in Hydrogen Saturated 1N Sulfuric Acid Determined Using an Experimental Probe.

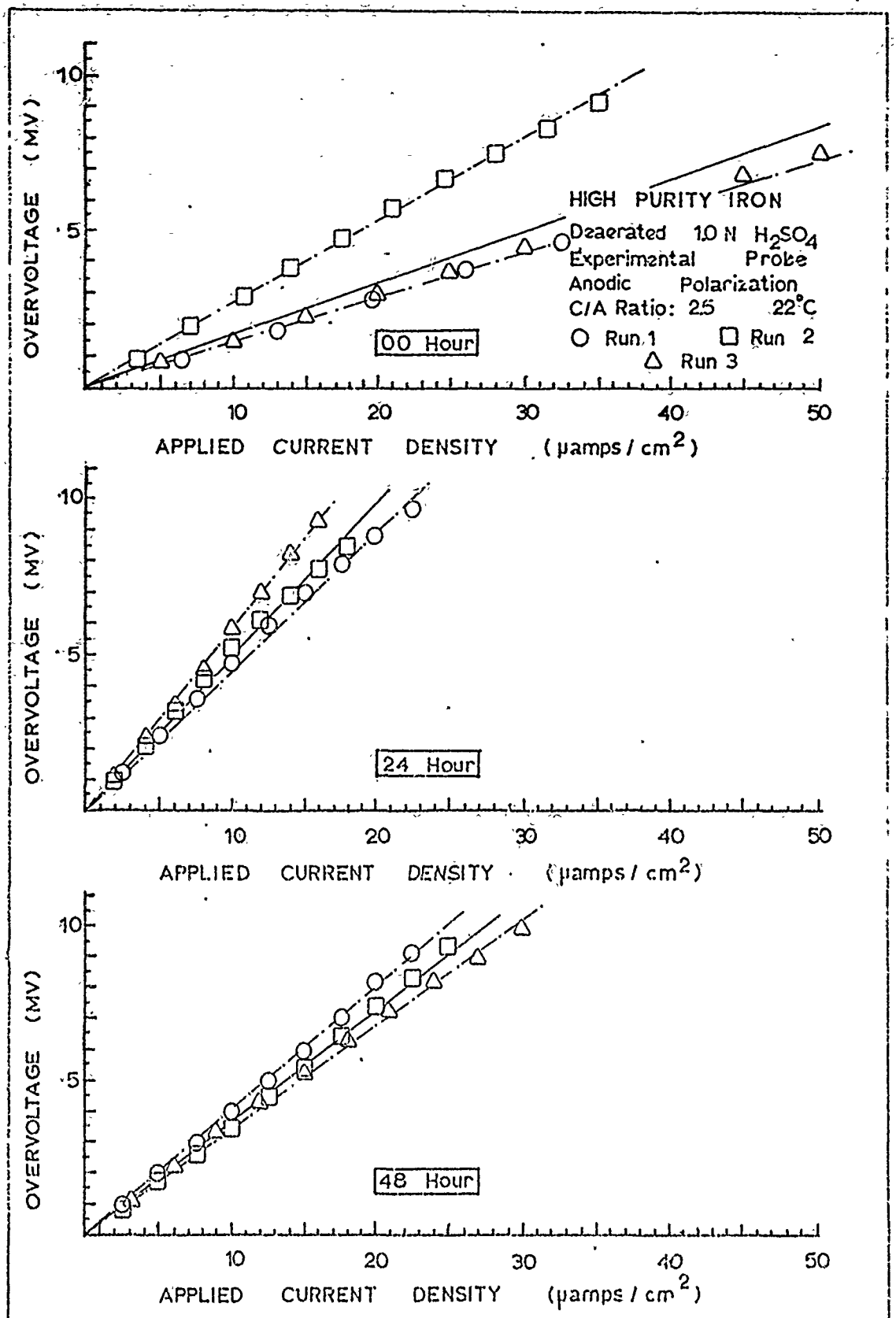

Figure 40 : Effect of Time on Galvanostatic Anodic Polarization Resistance of High Purity Iron with C/A Ratio = 2.5 in Hydrogen Saturated 1N Sulfuric Acid Determined Using an Experimental Probe. (Cont)

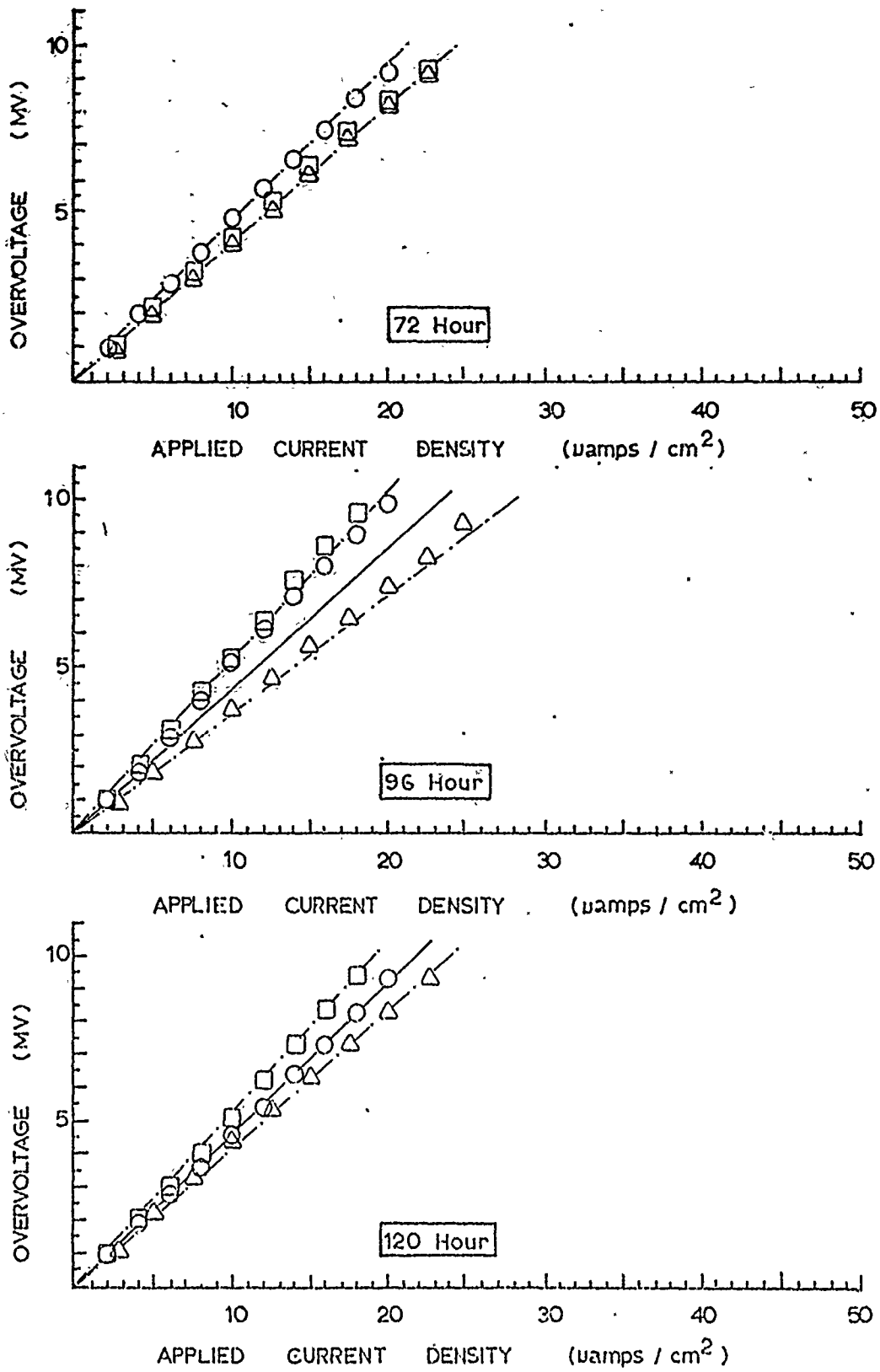

Figure 40 : (Cont) Effect of Time on Galvanostatic Anodic Polarization Resistance of High Purity Iron with C/A Ratio = 2.5 in Hydrogen Saturated 1N Sulfuric Acid Determined Using an Experimental Probe.

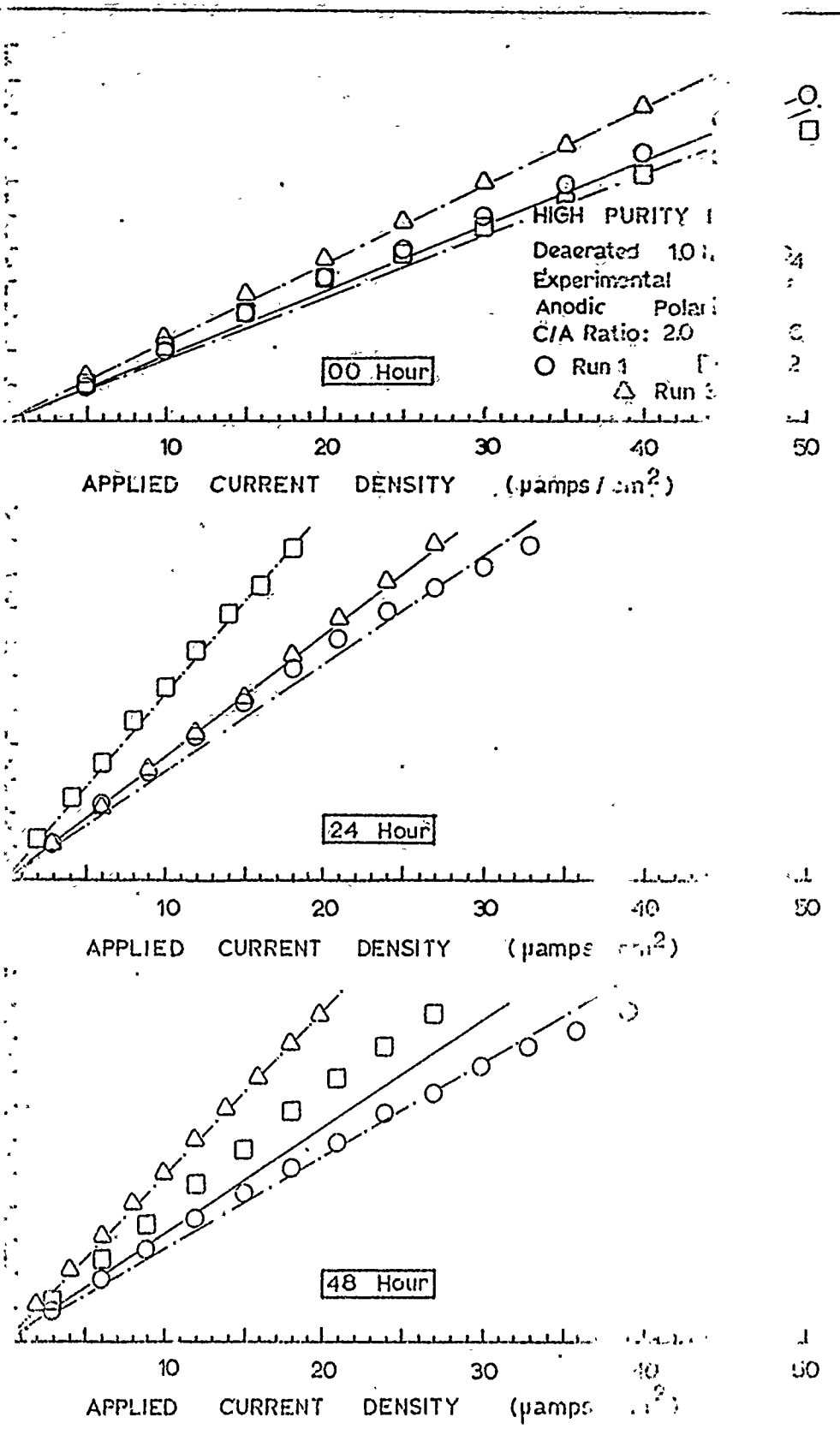

gure 41 : Effect of Time on Galvanostatic Anodic Polariza
Purity Iron with C/A Ratio = 2 in Hydrogen S
Determined Using an Experimental Probe. (Cont)

Reproduced from best available copy.

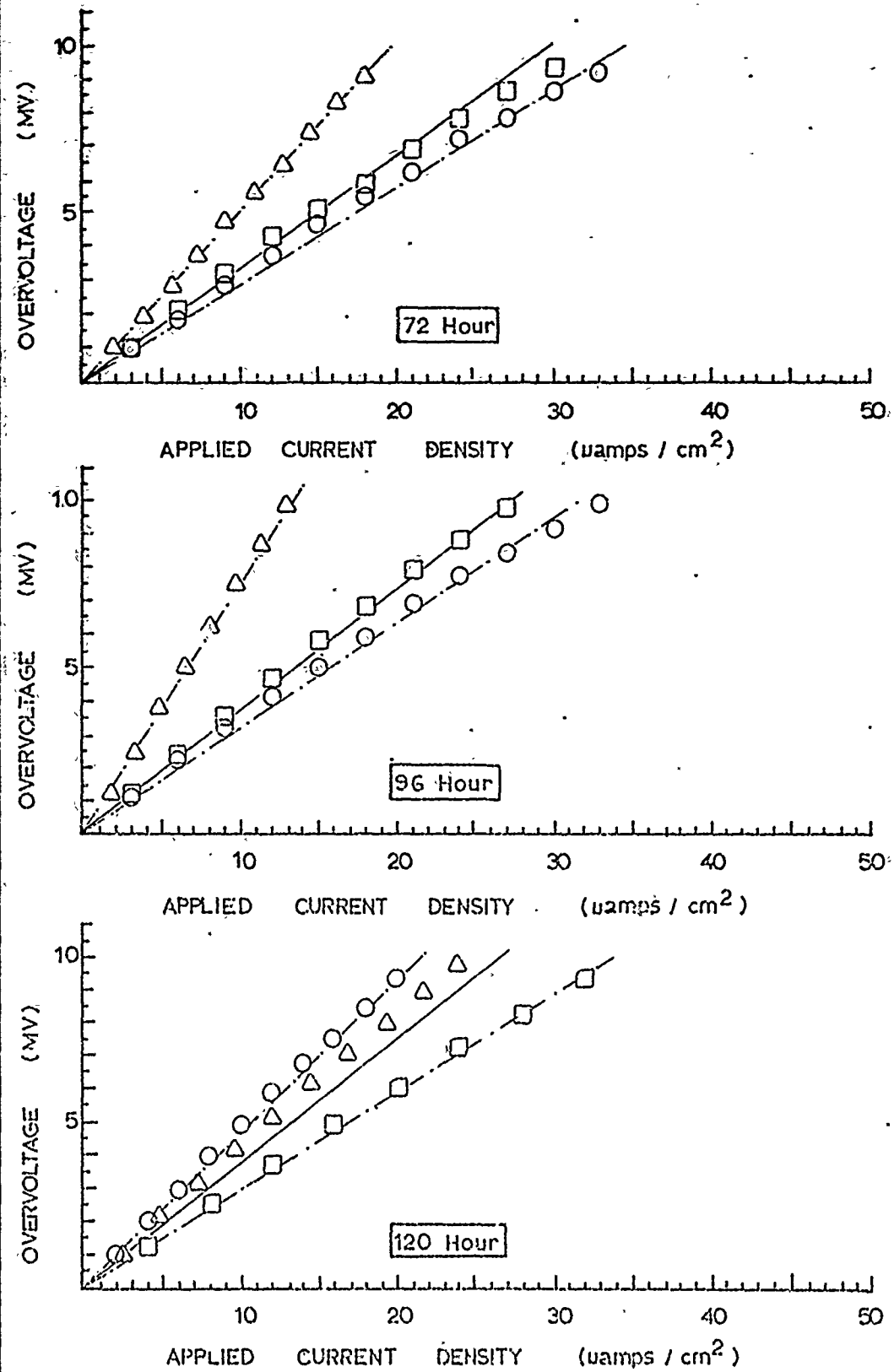

Figure 41: (Cont) Effect of Time on Galvanostatic Anodic Polarization Resistance of High Purity Iron with C/A Ratio = 2 in Hydrogen Saturated 1N Sulfuric Acid Determined Using an Experimental Probe.

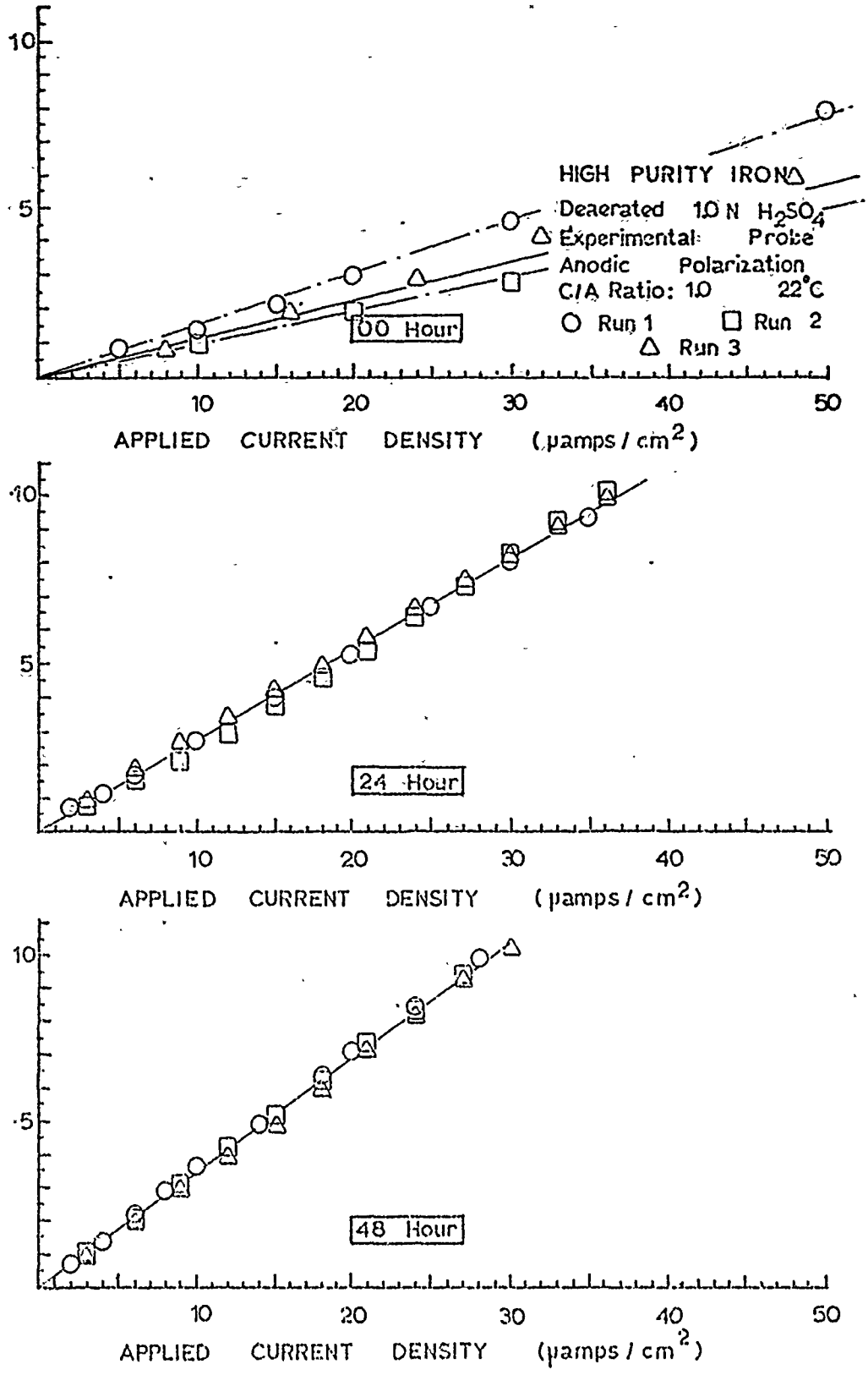

Figure 42 : Effect of Time on Galvanostatic Anodic Polarization Resistance of High Purity Iron with C/A Ratio = 1 in Hydrogen Saturated 1N Sulfuric Acid Determined Using an Experimental Probe. (Cont)

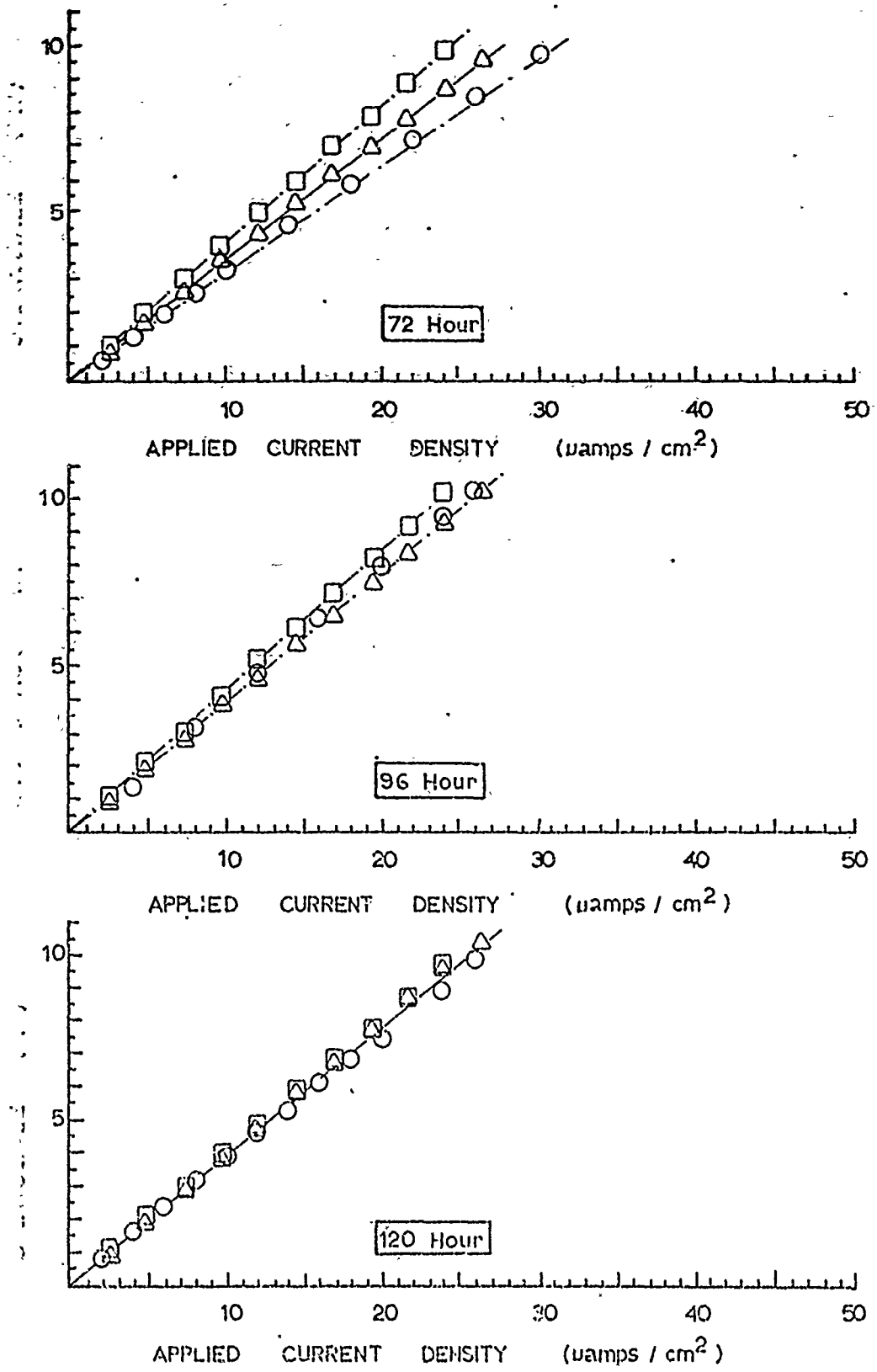

Figure 42 : (Cont) Effect of Time on Galvanostatic Anodic Polarization Resistance of High Purity Iron with C/A Ratio = 1 in Hydrogen Saturated 1N Sulfuric Acid Determined Using an Experimental Probe.

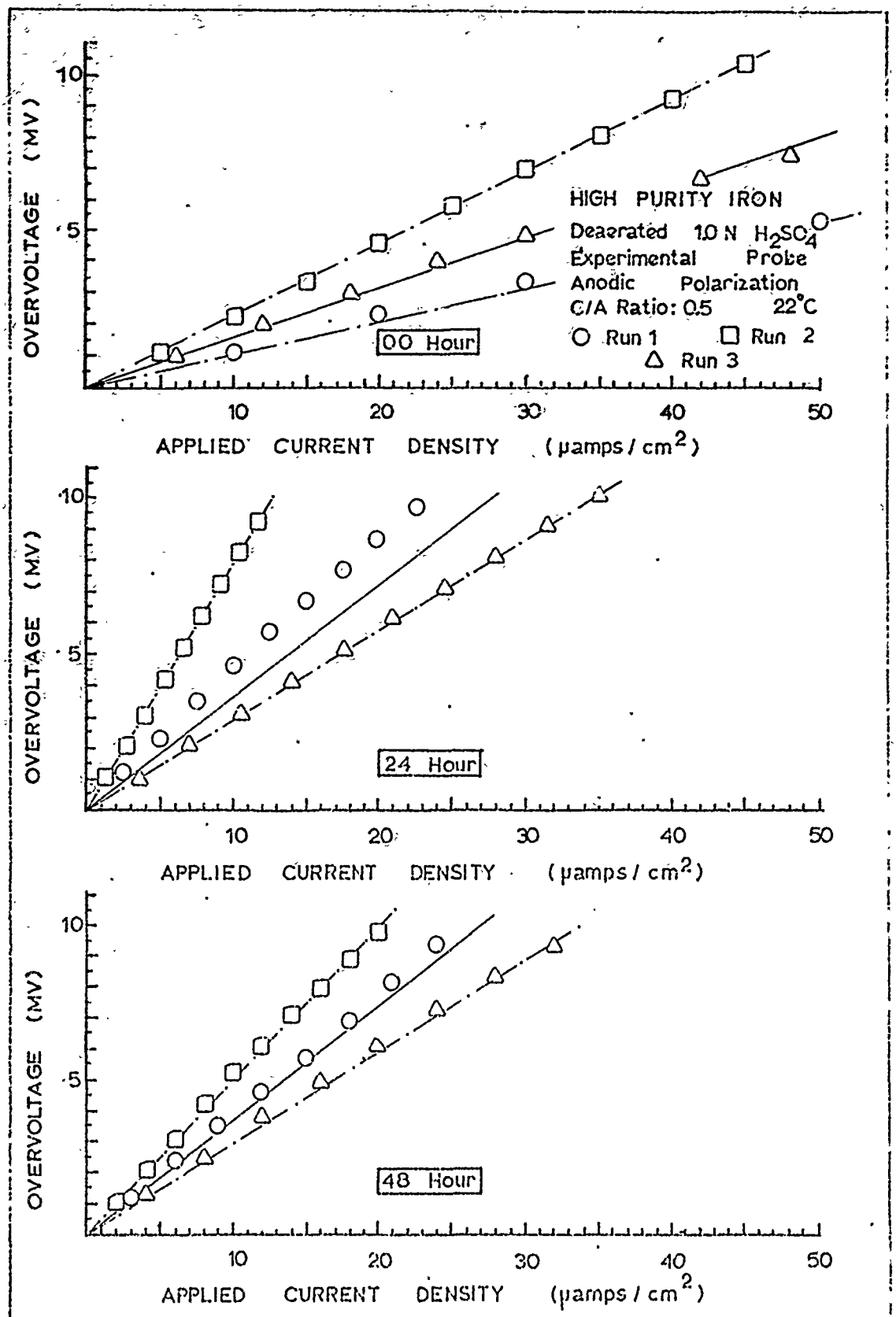

Figure 43 : Effect of Time on Galvanostatic Anodic Polarization Resistance of High Purity Iron with C/A Ratio = .5 in Hydrogen Saturated 1N Sulfuric Acid Determined Using an Experimental Probe. (Cont)

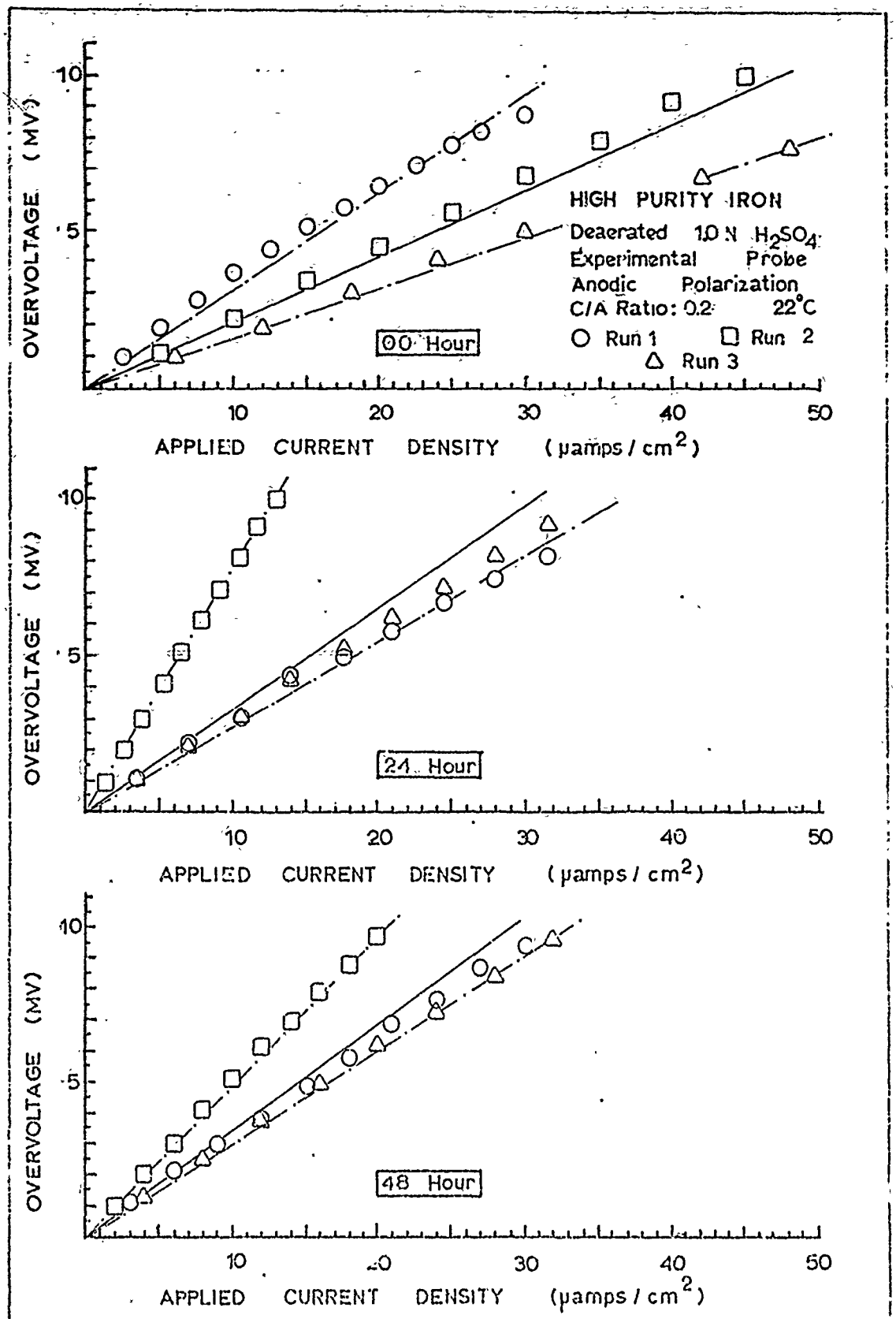

Figure 44 : Effect of Time on Galvanostatic Anodic Polarization Resistance of High Purity Iron with C/A Ratio = .2 in Hydrogen Saturated 1N Sulfuric Acid Determined Using an Experimental Probe. (Cont)

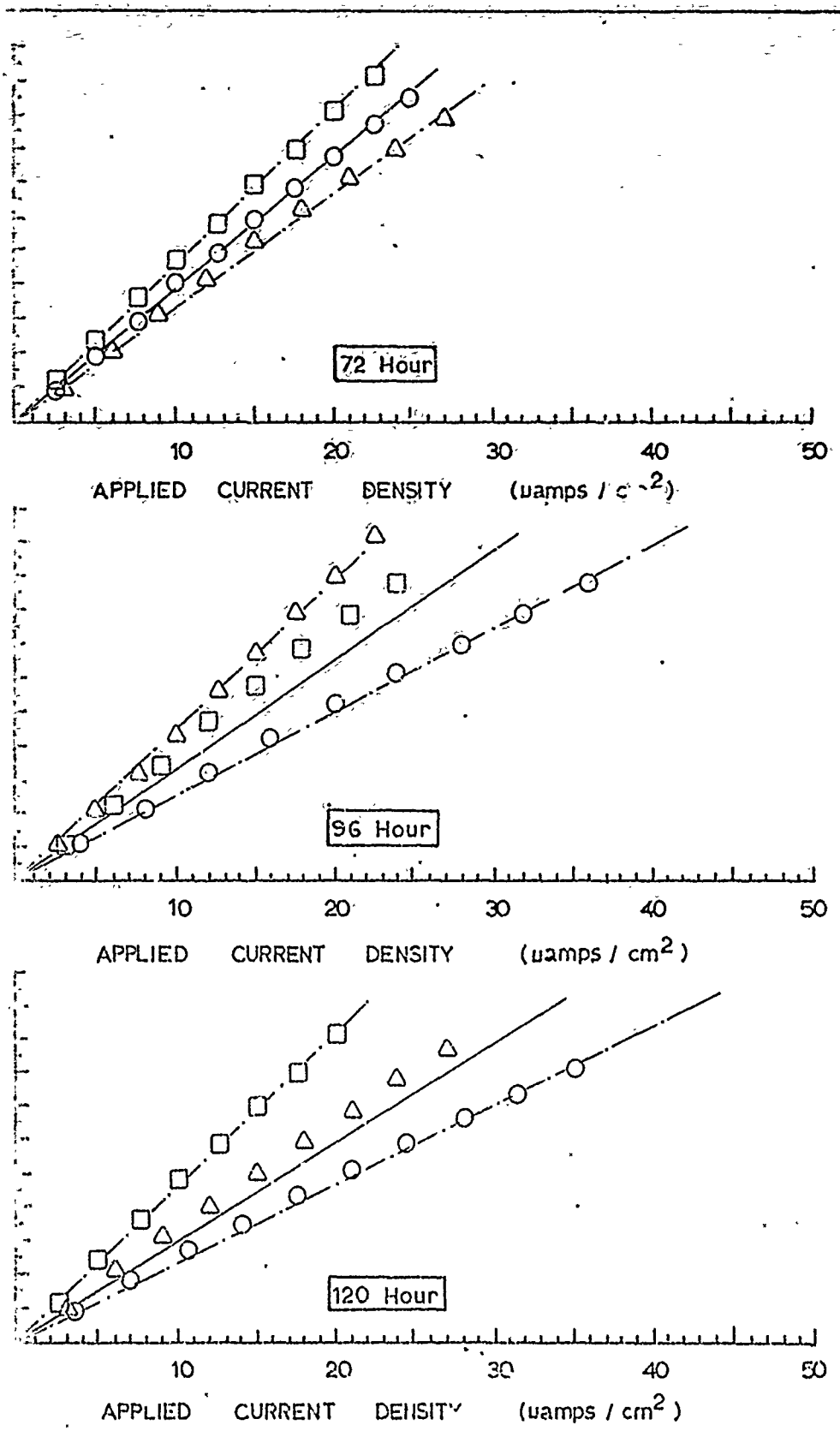

igure 44 : (Cont) Effect of Time on Galvanostatic Anodic Polarization Resistance of High Purity Iron with C/A Ratio = .2 in Hydrogen Saturated 1N Sulfuric Acid Determined Using an Experimental Probe.

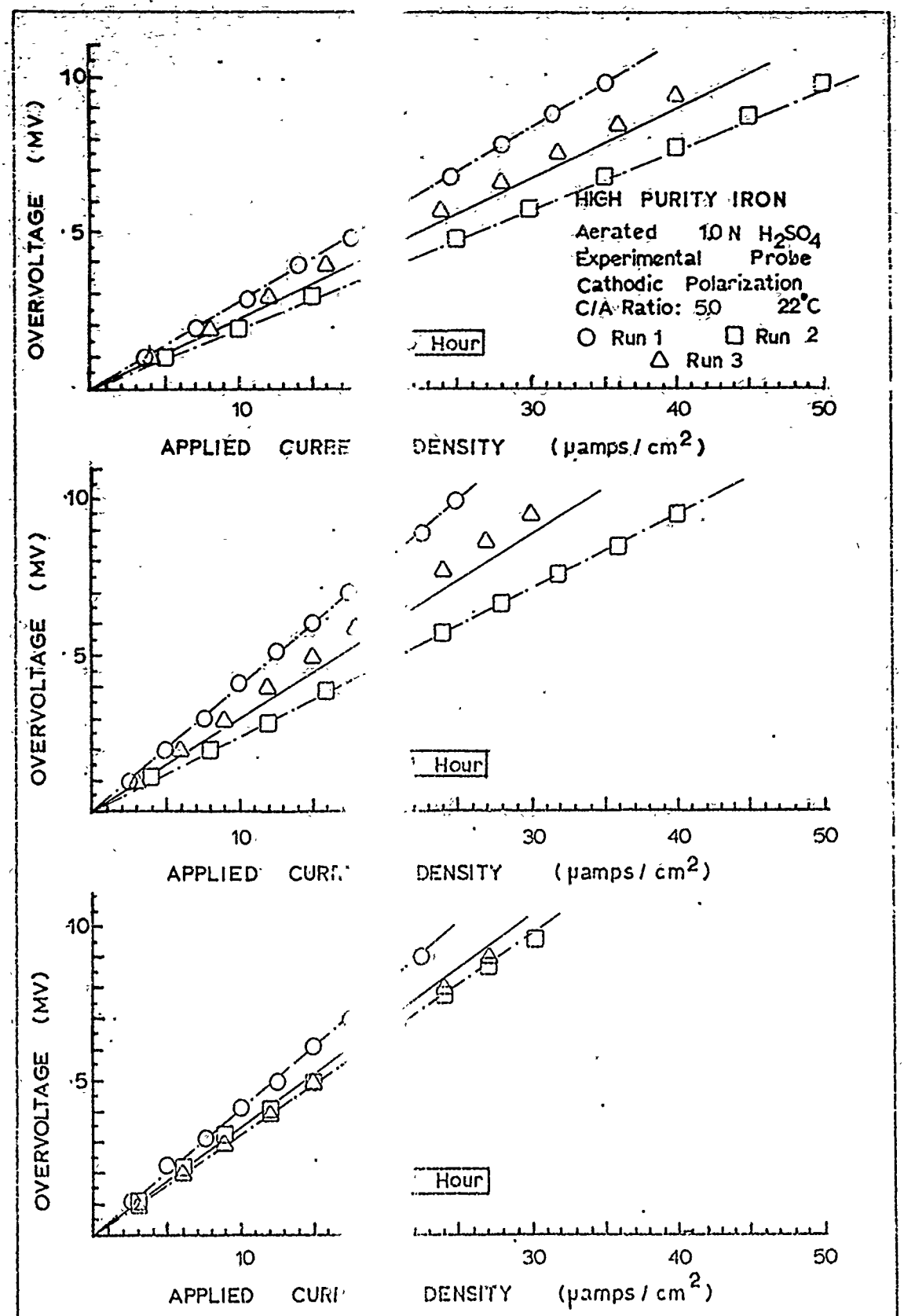

Figure 45 : Effect of Time ·nostatic Cathodic Polarization Resistance of High Purity Iron with ·tio = 5 in Aerated 1N Sulfuric Acid Determined Using an Experi ·rc ·e. (Cont)

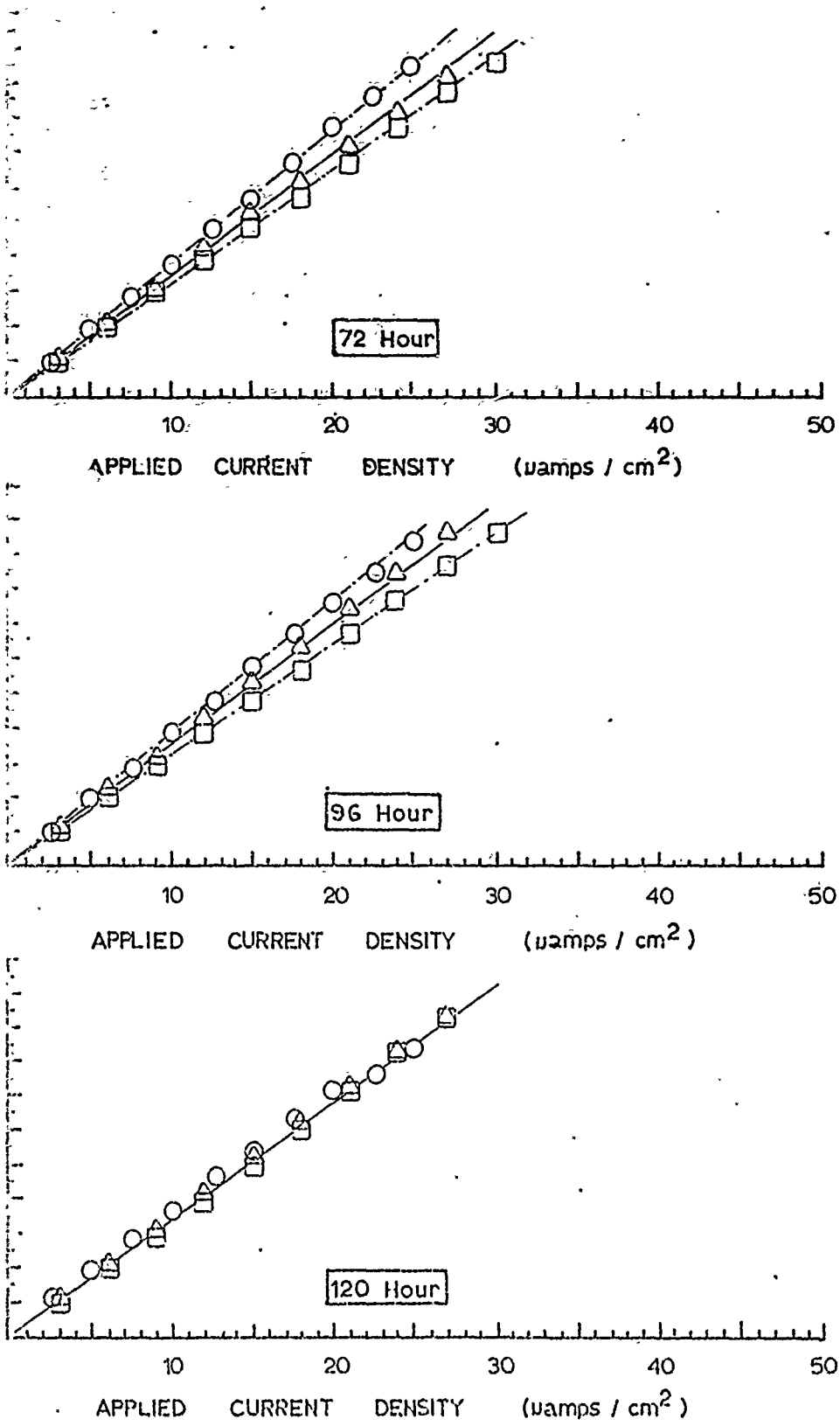

Figure 45 : (Cont) Effect of Time on Galvanostatic Cathodic Polarization Resistance of High Purity Iron with C/A Ratio = 5 in Aerated 1N Sulfuric Acid Determined Using an Experimental Probe.

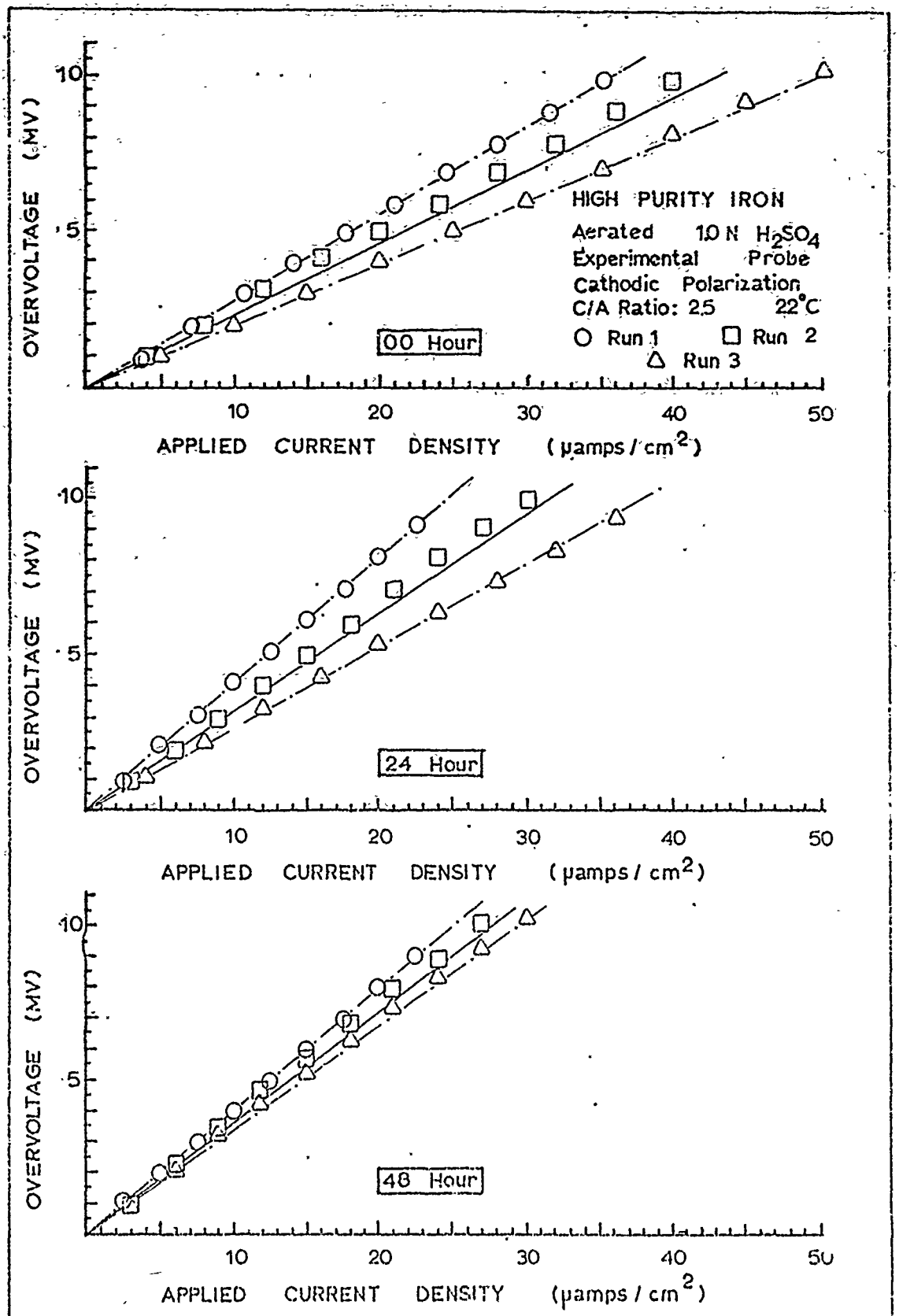

Figure 46 : Effect of Time on Galvanostatic Cathodic Polarization Resistance of High Purity Iron with C/A Ratio = 2.5 in Aerated 1N Sulfuric Acid Determined Using an Experimental Probe. (Cont)

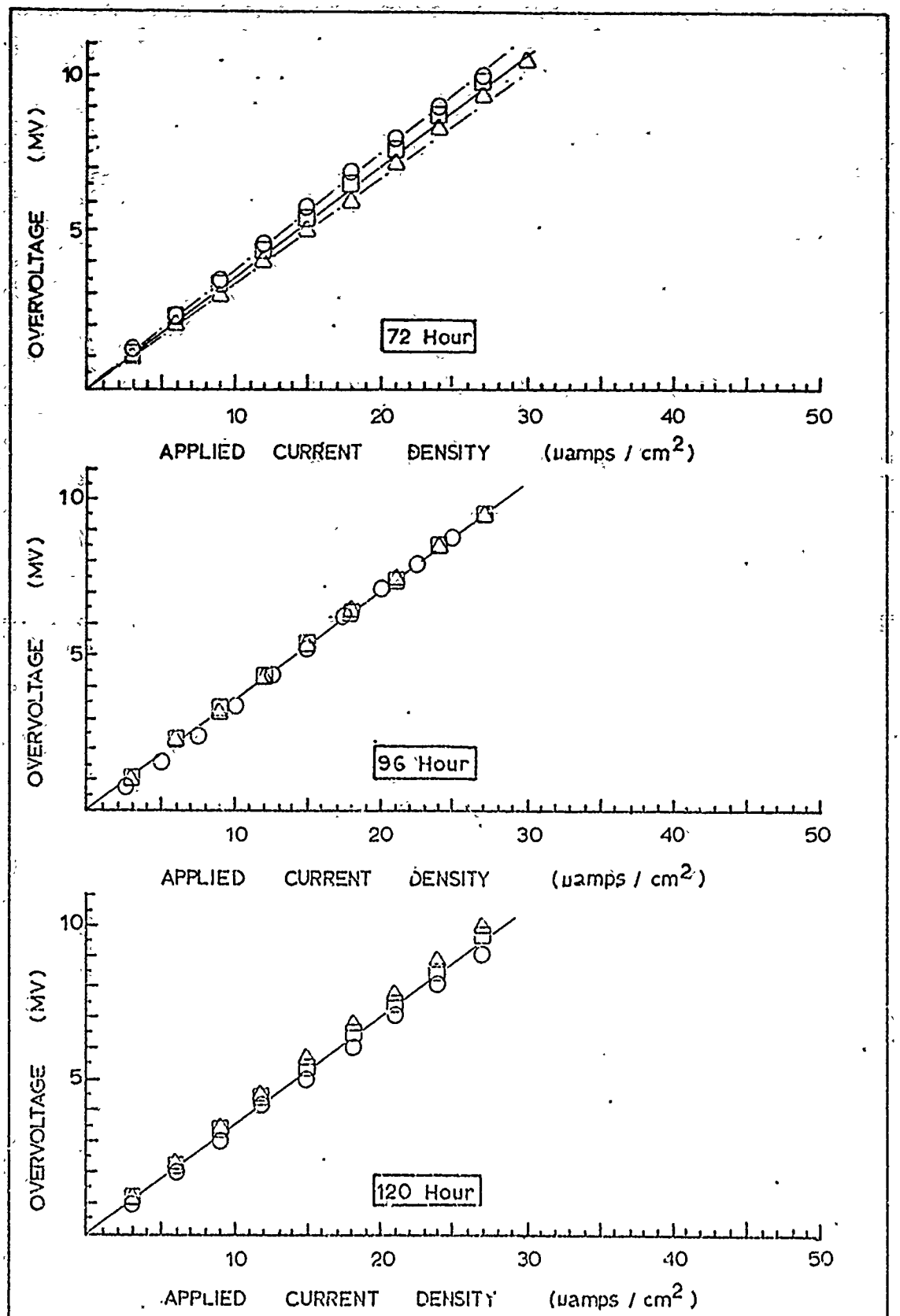

Figure 46 : (Cont) Effect of Time on Galvanostatic Cathodic Polarization Resistance of High Purity Iron with C/A Ratio = 2.5 in Aerated 1N Sulfuric Acid Determined Using an Experimental Probe.

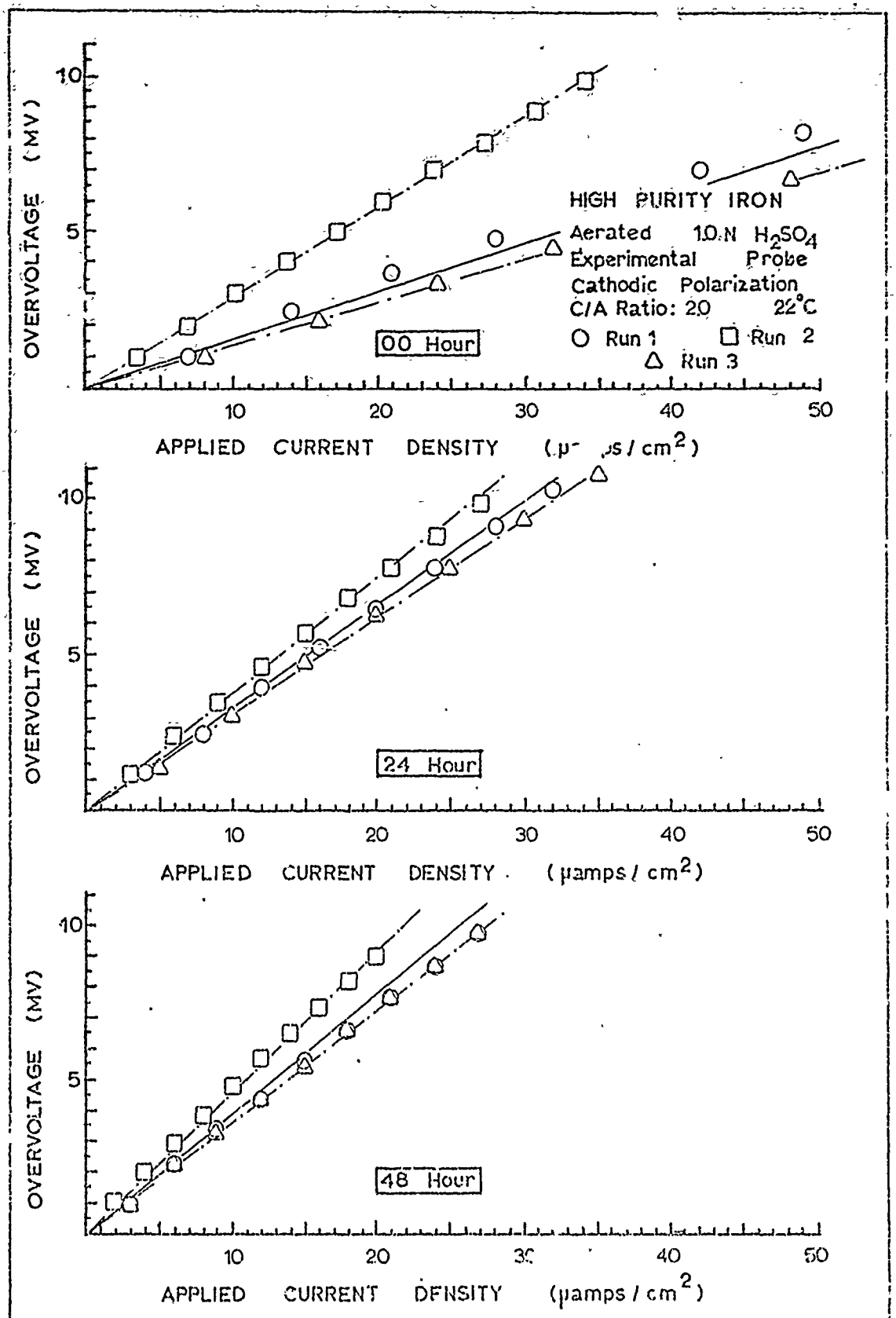

Figure 47 : Effect of Time on Galvanostatic Cathodic Polarization Resistance of High Purity Iron with C/A Ratio = 2 in Aerated 1N Sulfuric Acid Determined Using an Experimental Probe. (Cont)

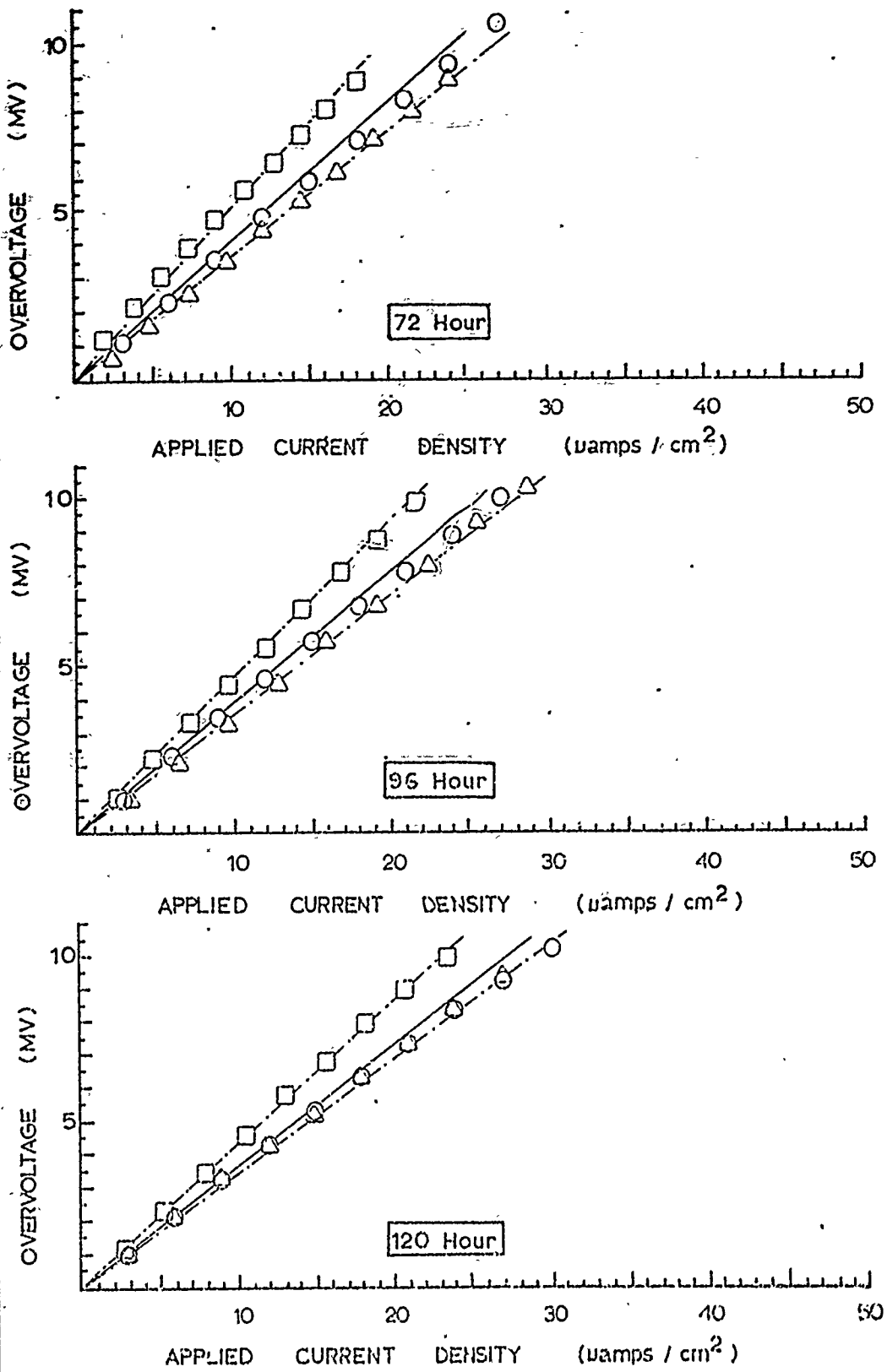

Figure 47 : (Cont) Effect of Time on Galvanostatic Cathodic Polarization Resistance of High Purity Iron with C/A Ratio = 2 in Aerated 1N Sulfuric Acid Determined Using an Experimental Probe.

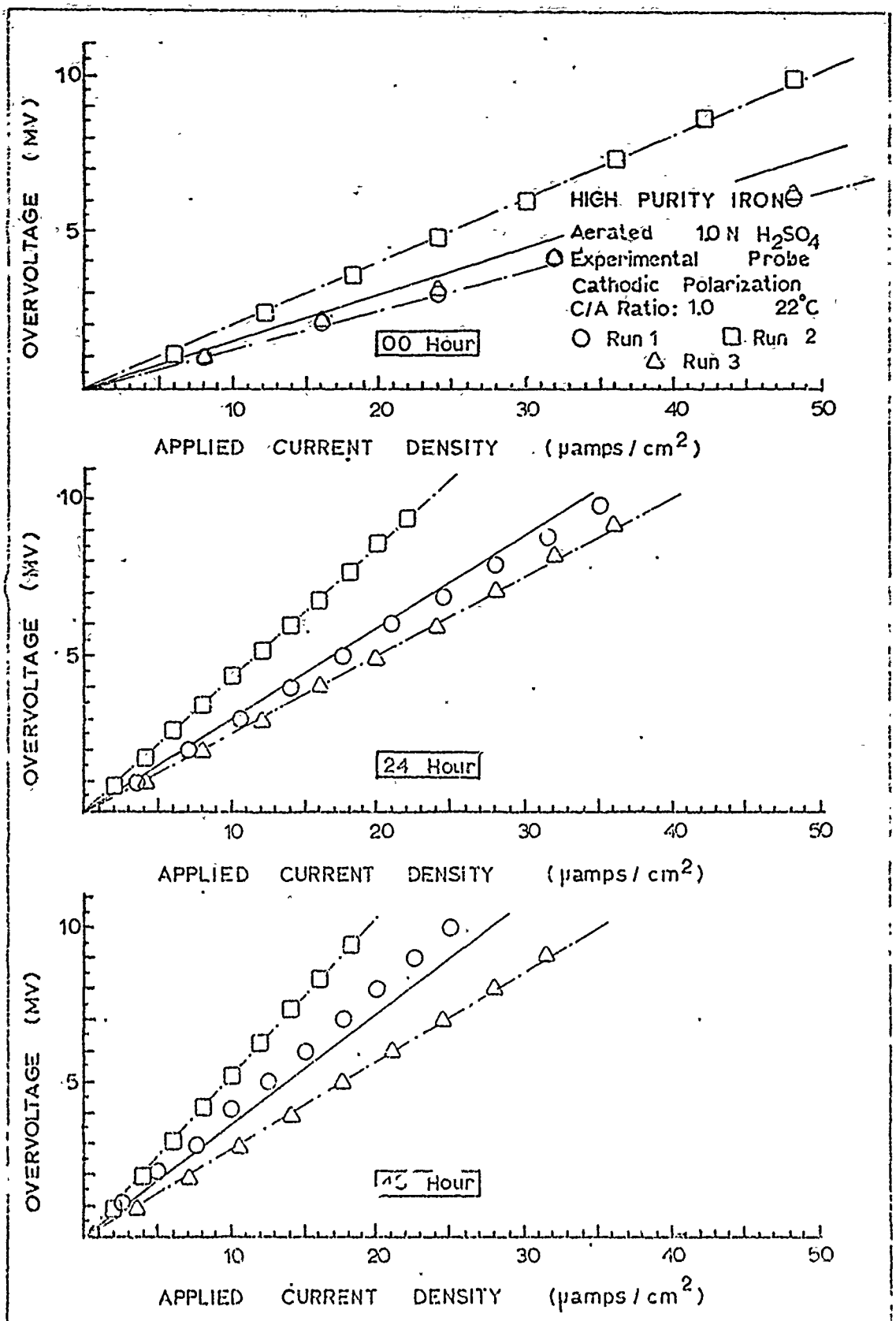

Figure 48 : Effect of Time on Galvanostatic Cathodic Polarization Resistance of High Purity Iron with C/A Ratio = 1 in Aerated 1N Sulfuric Acid Determined Using an Experimental Probe. (Cont)

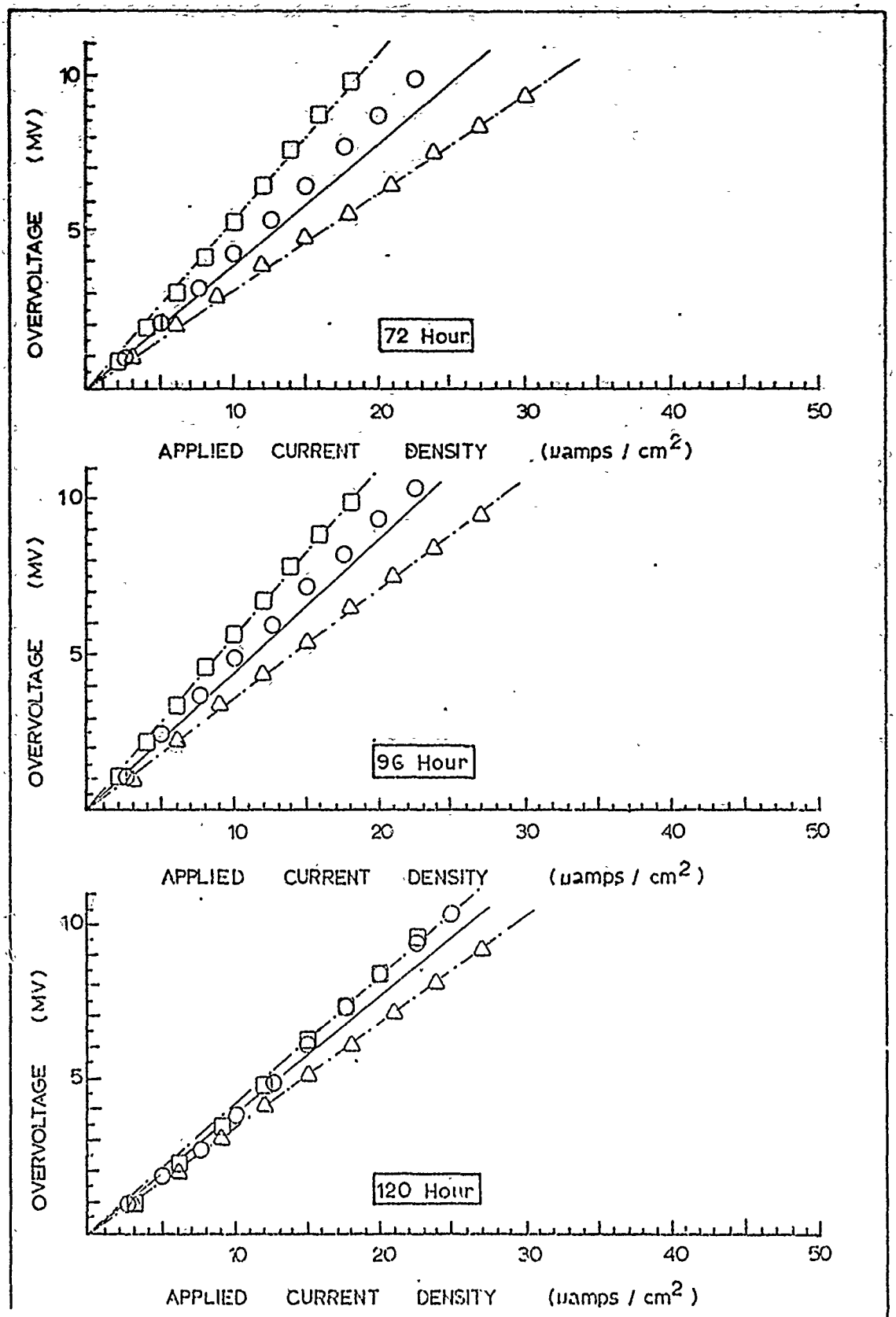

Figure 48 : (Cont) Effect of Time on Galvanostatic Cathodic Polarization Resistance of High Purity Iron with C/A Ratio = 1 in Aerated 1N Sulfuric Acid Determined Using an Experimental Probe.

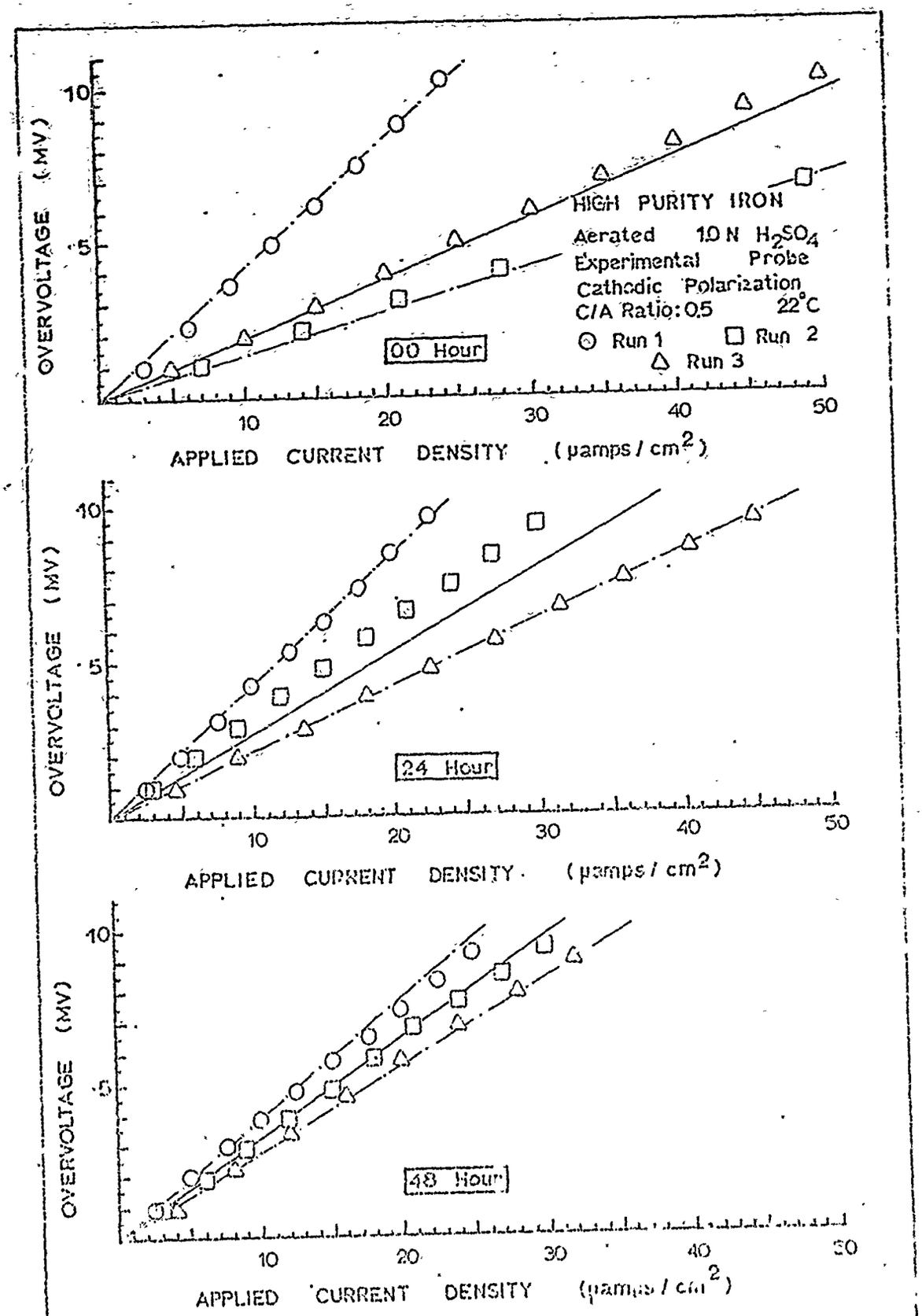

Figure 49 : Effect of Time on Galvanostatic Cathodic Polarization Resistance of High Purity Iron with C/A Ratio = .5 in Aerated 1.0 N Sulfuric Acid Determined Using an Experimental Probe. (Cont)

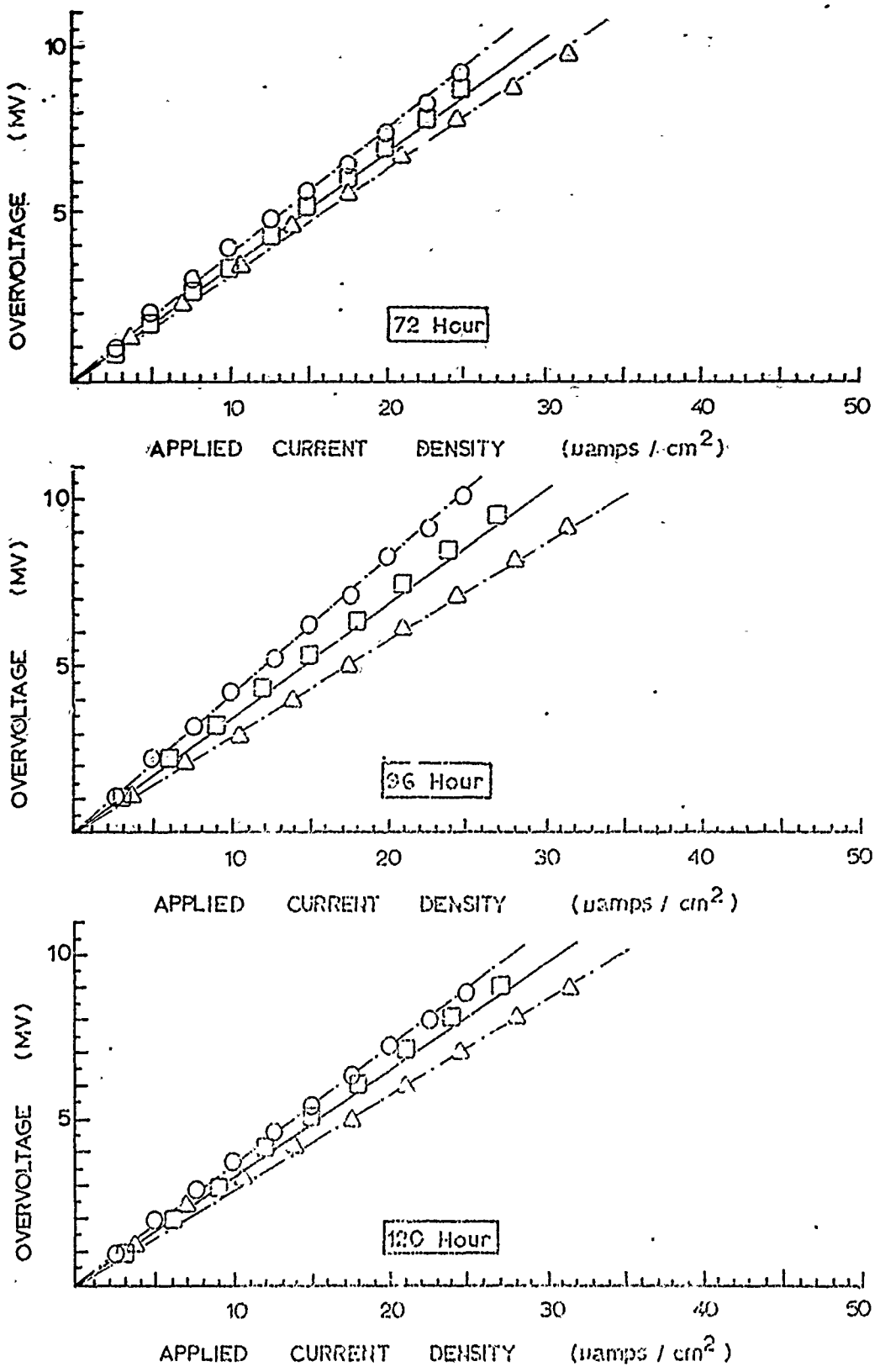

Figure 49 : (Cont) Effect of Time on Galvanostatic Cathodic Polarization Resistance of High Purity Iron with C/A Ratio - .5 in Aerated 1N Sulfuric Acid Determined Using an Experimental Probe.

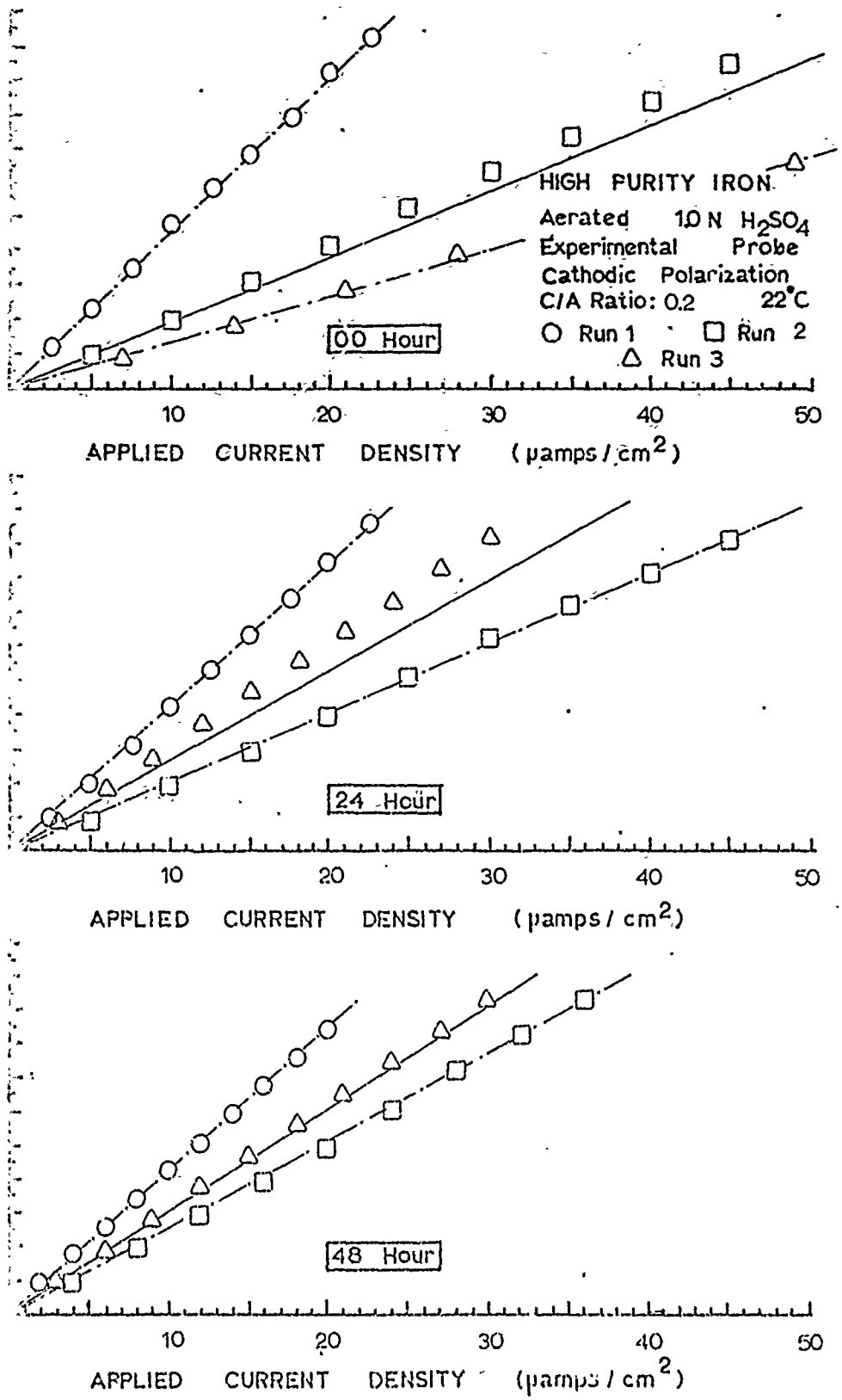

Figure 50 : Effect of Time on Galvanostatic Cathodic Polarization Resistance of High Purity Iron with C/A Ratio = .2 in Aerated 1N Sulfuric Acid Determined Using an Experimental Probe. (Cont)

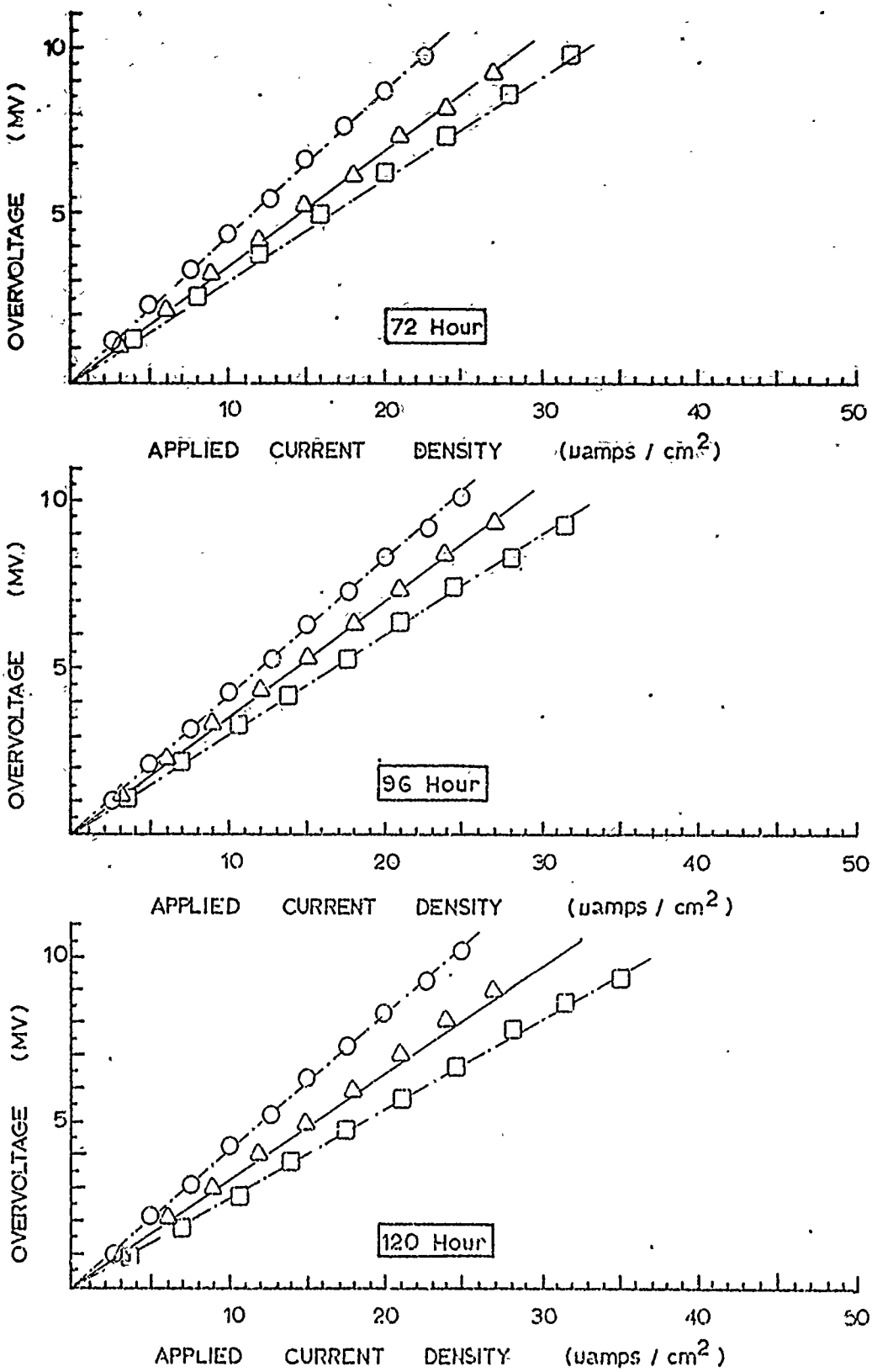

Figure 50 : (Cont) Effect of Time on Galvanostatic Cathodic Polarization Resistance of High Purity Iron with C/A Ratio = .2 in Aerated 1N Sulfuric Acid Determined Using an Experimental Probe.

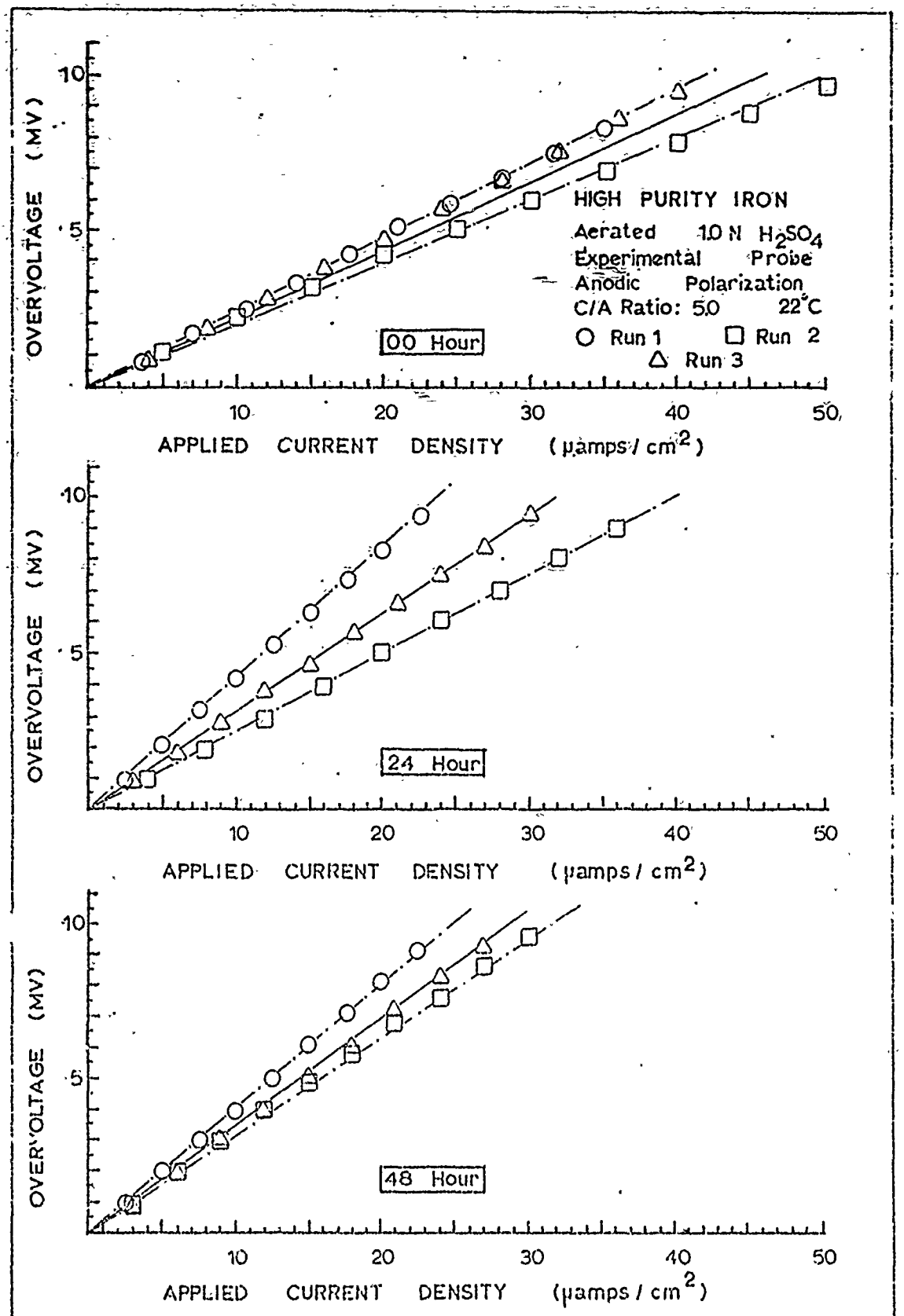

Figure 51 : Effect of Time on Galvanostatic Anodic Polarization Resistance of High Purity Iron with C/A Ratio = 5 in Aerated 1N Sulfuric Acid Determined Using an Experimental Probe. (Cont)

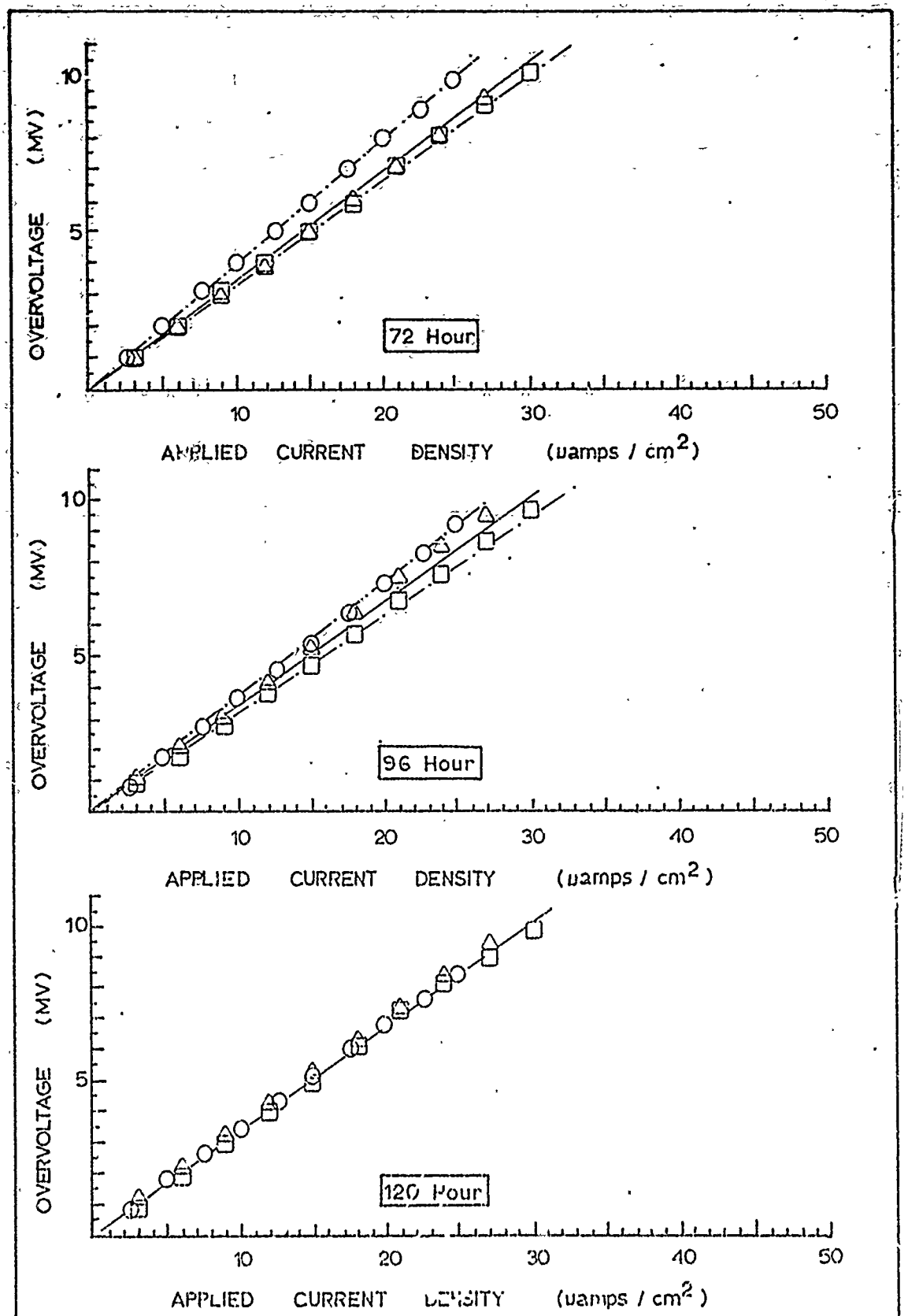

Figure 51 : (Cont) Effect of Time on Galvanostatic Anodic Polarization Resistance of High Purity Iron with C/A Ratio = 5 in Aerated 1N Sulfuric Acid Determined Using an Experimental Probe.

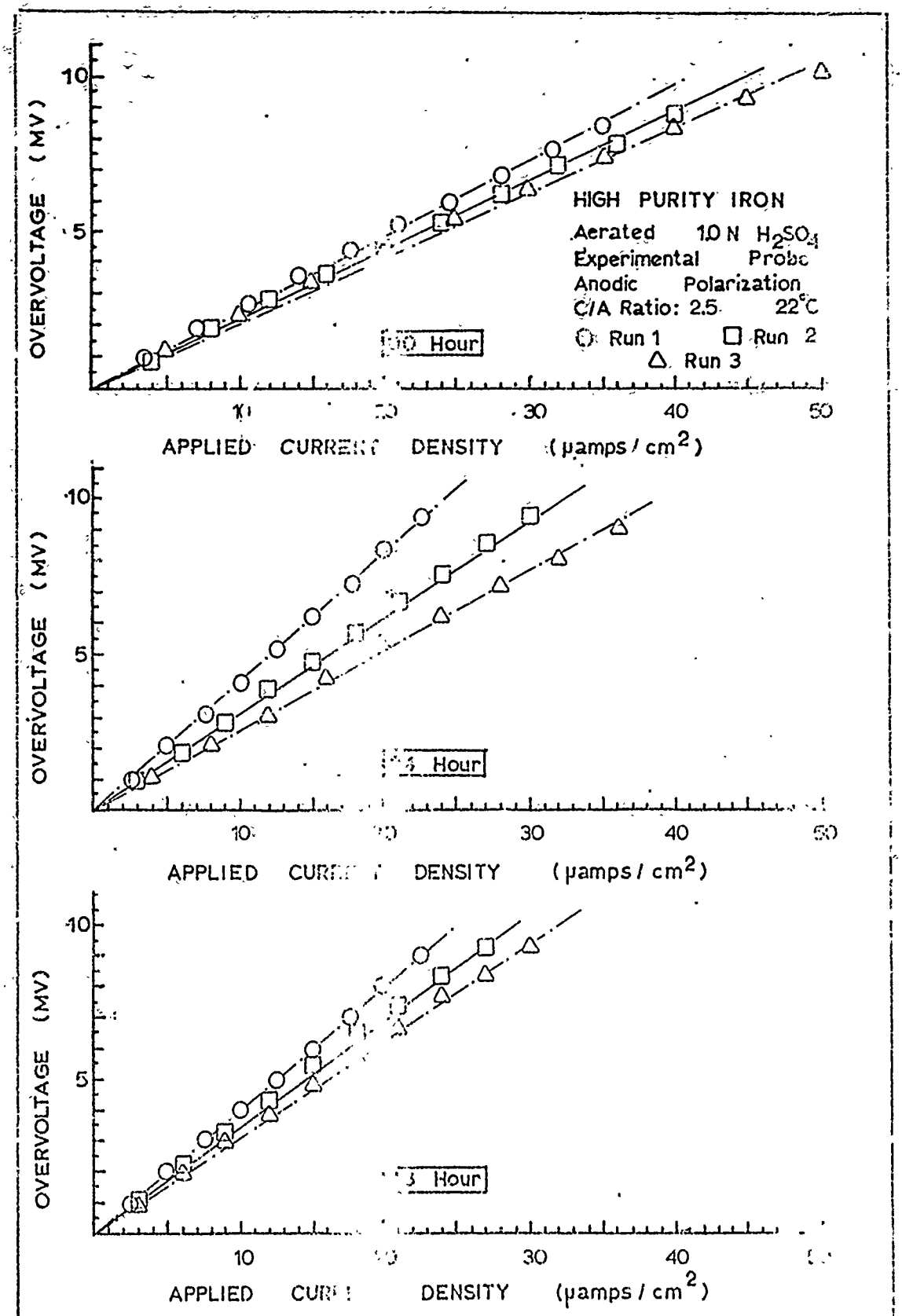

Figure 52 : Effect of Tim... ...nostatic Anodic Polarization Resistance of ... Purity Iron wit... ...atio = 2.5 in Aerated 1N Sulfuric Acid D... mined Using an... ...mental Probe. (Cont)

Reproduced from best available copy.

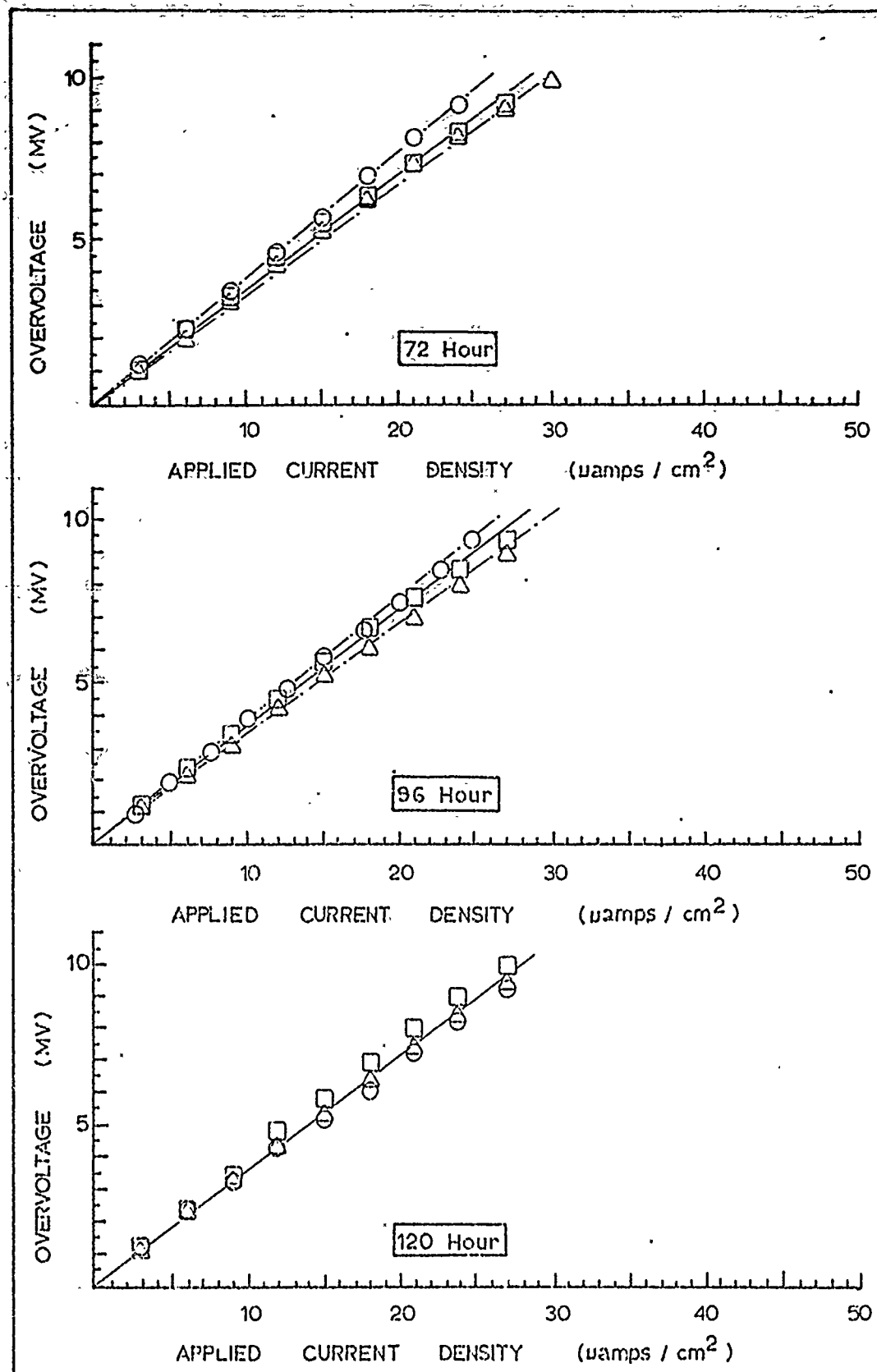

Figure 52 : (Cont) Effect of Time on Galvanostatic Anodic Polarization Resistance of High Purity Iron with C/A Ratio = 2.5 in Aerated 1N Sulfuric Acid Determined Using an Experimental Probe

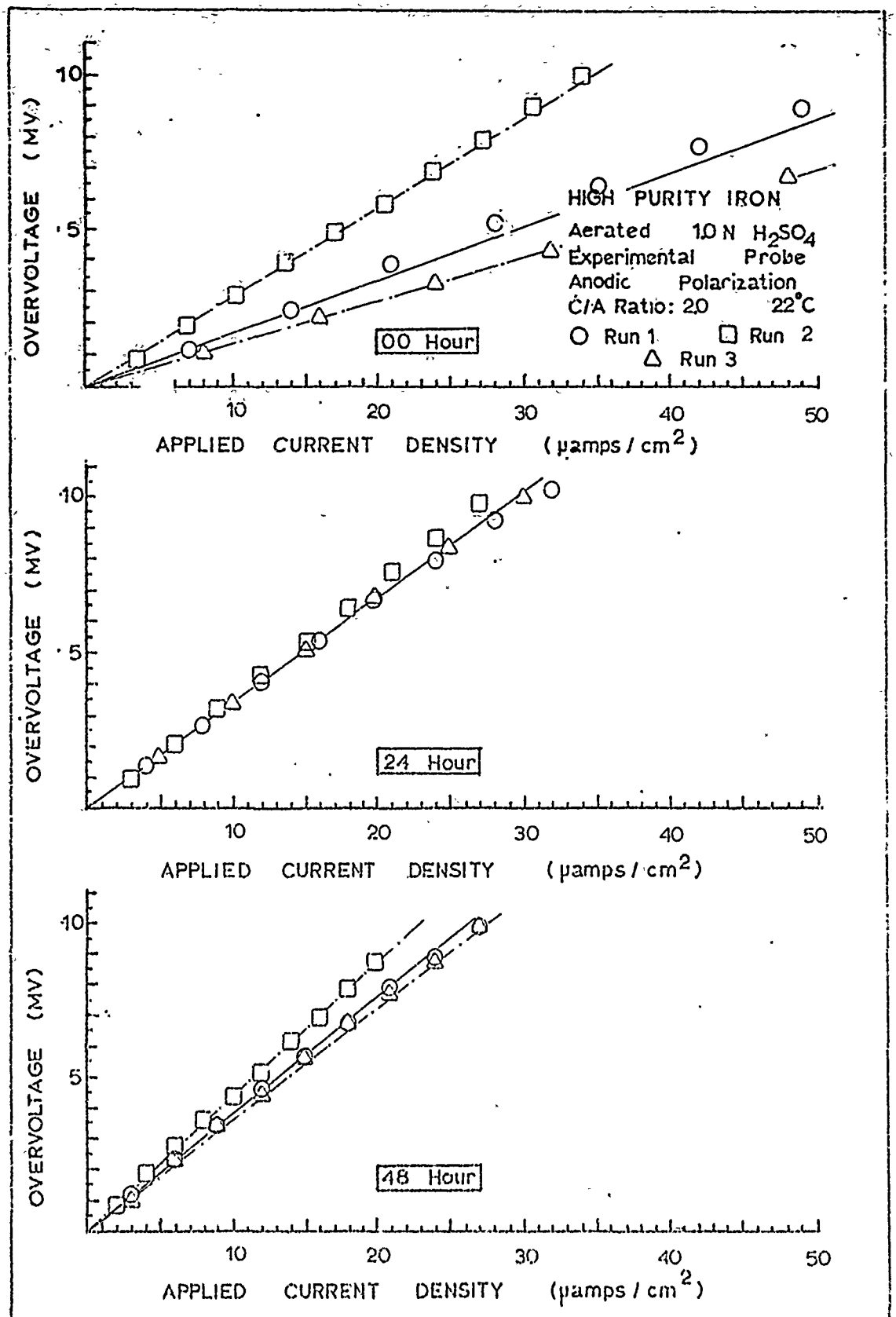

Figure 53 : Effect of Time on Galvanostatic Anodic Polarization Resistance of High Purity Iron with C/A Ratio = 2 in Aerated 1N Sulfuric Acid Determined Using an Experimental Probe. (Cont)

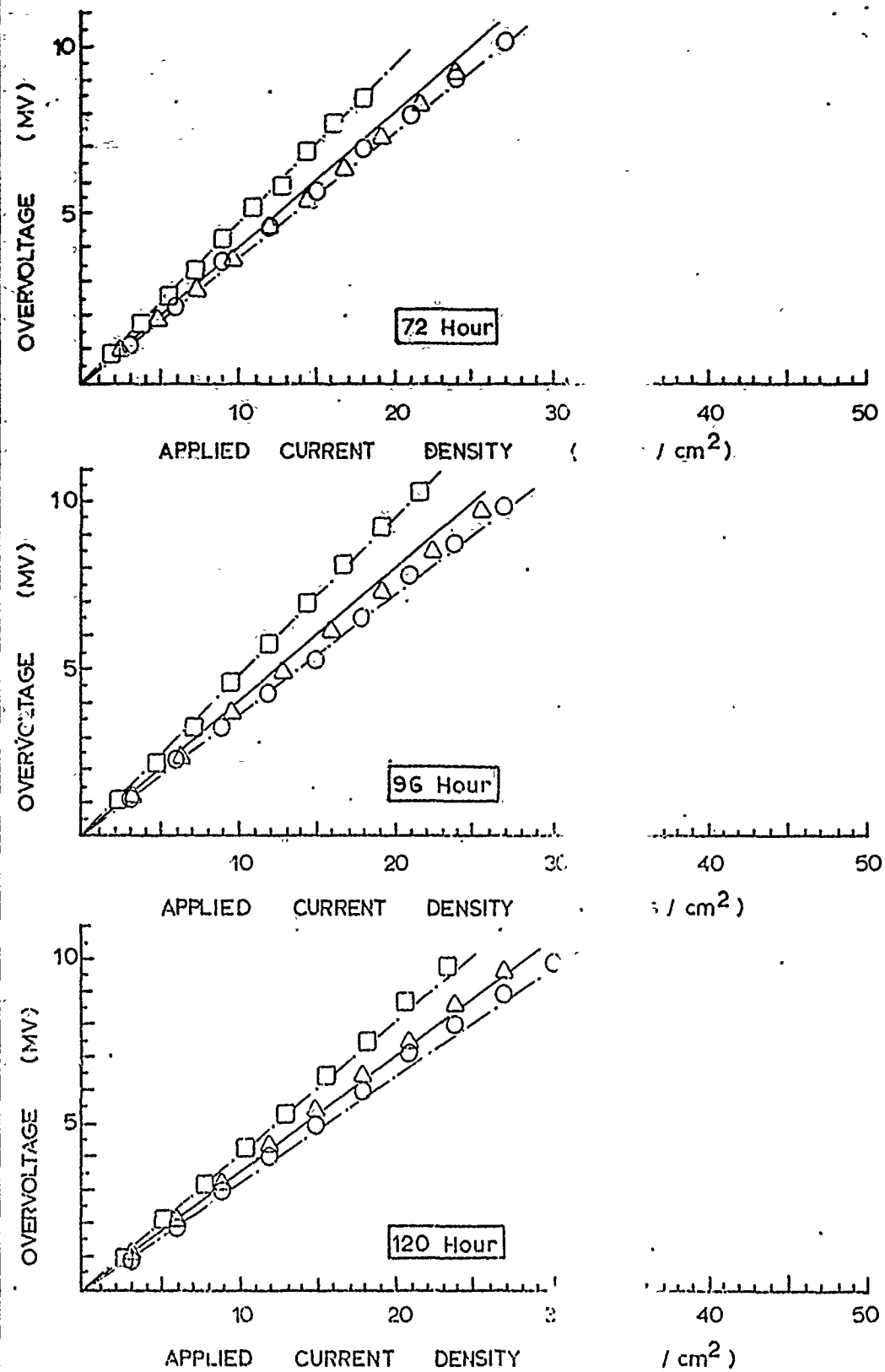

Figure 53 : (Cont) Effect of Time on Galvanost[illegible] Polarization Resistance of High Purity Iron with C/A Ratio [illegible]ted 1N Sulfuric Acid Determined Using an Experimental P[illegible]

Reproduced from best available copy.

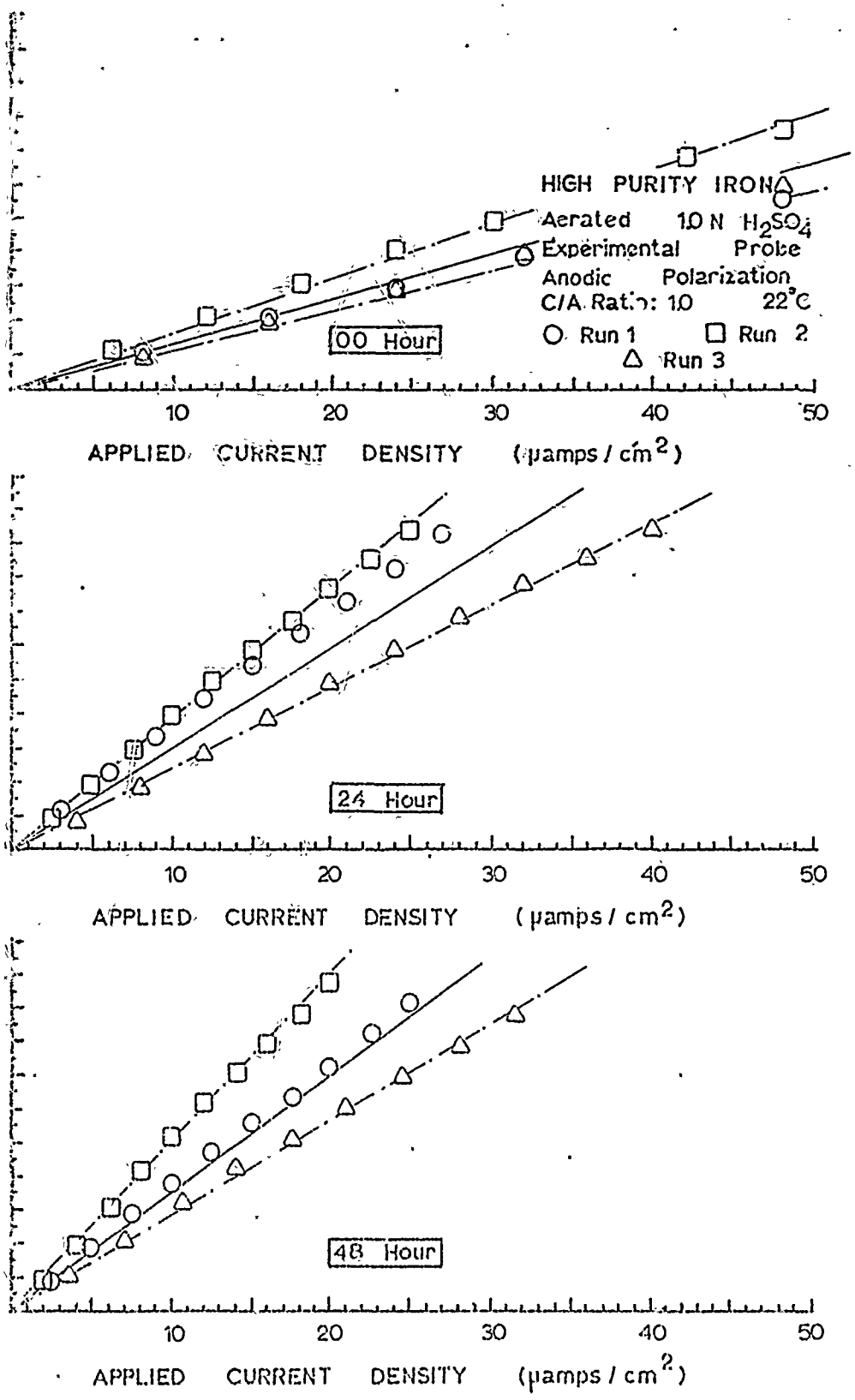

Figure 54 : Effect of Time on Galvanostatic Anodic Polarization Resistance of High Purity Iron with C/A Ratio = 1 in Aerated 1N Sulfuric Acid Determined Using an Experimental Probe. (Cont)

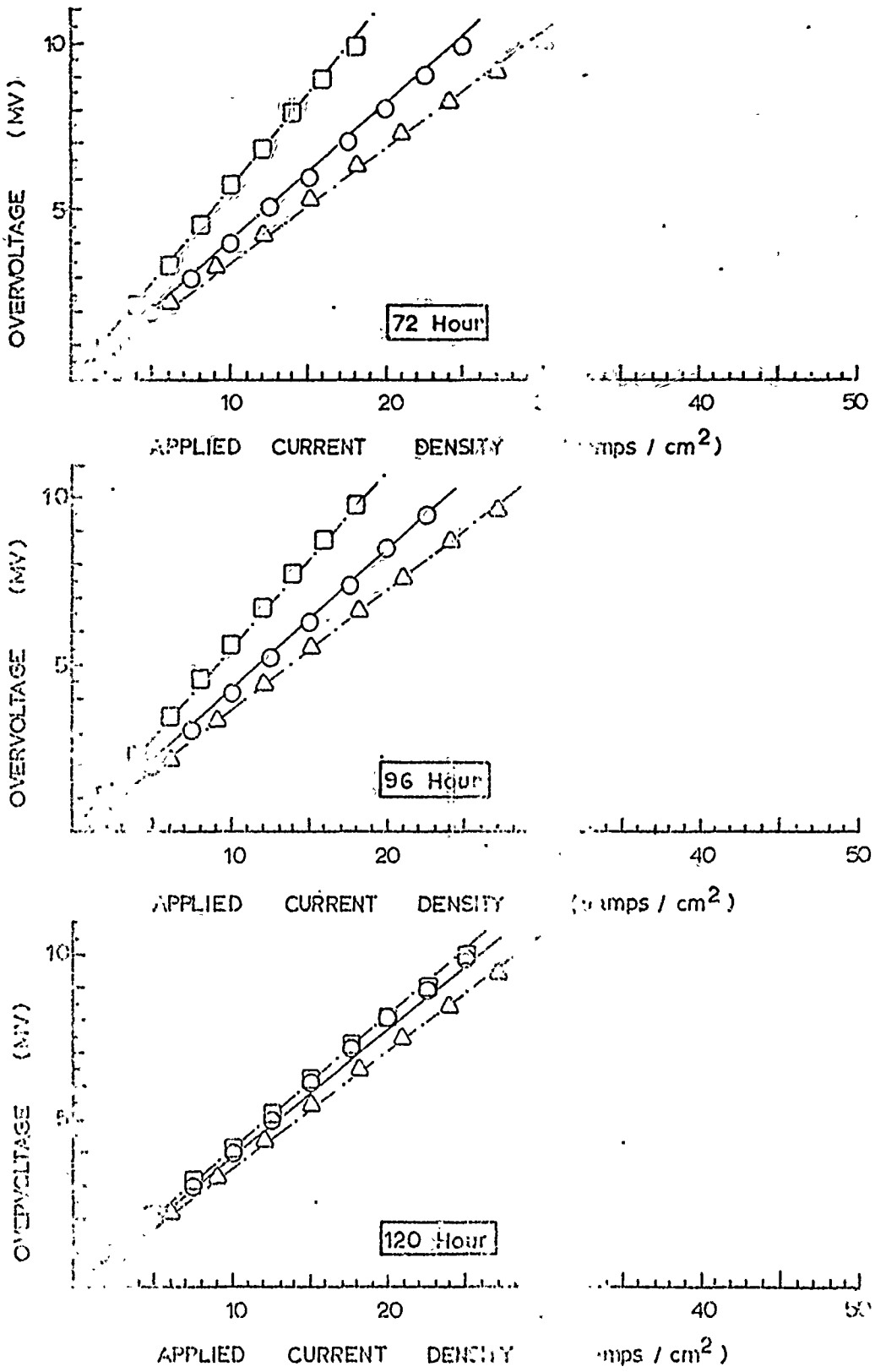

F... (Cont) Effect of Time on Gal... odic Polarization Resistance of High Purity Iron with C/A ... Aerated 1N Sulfuric Acid Determined Using an Experim...

produced from best available copy.

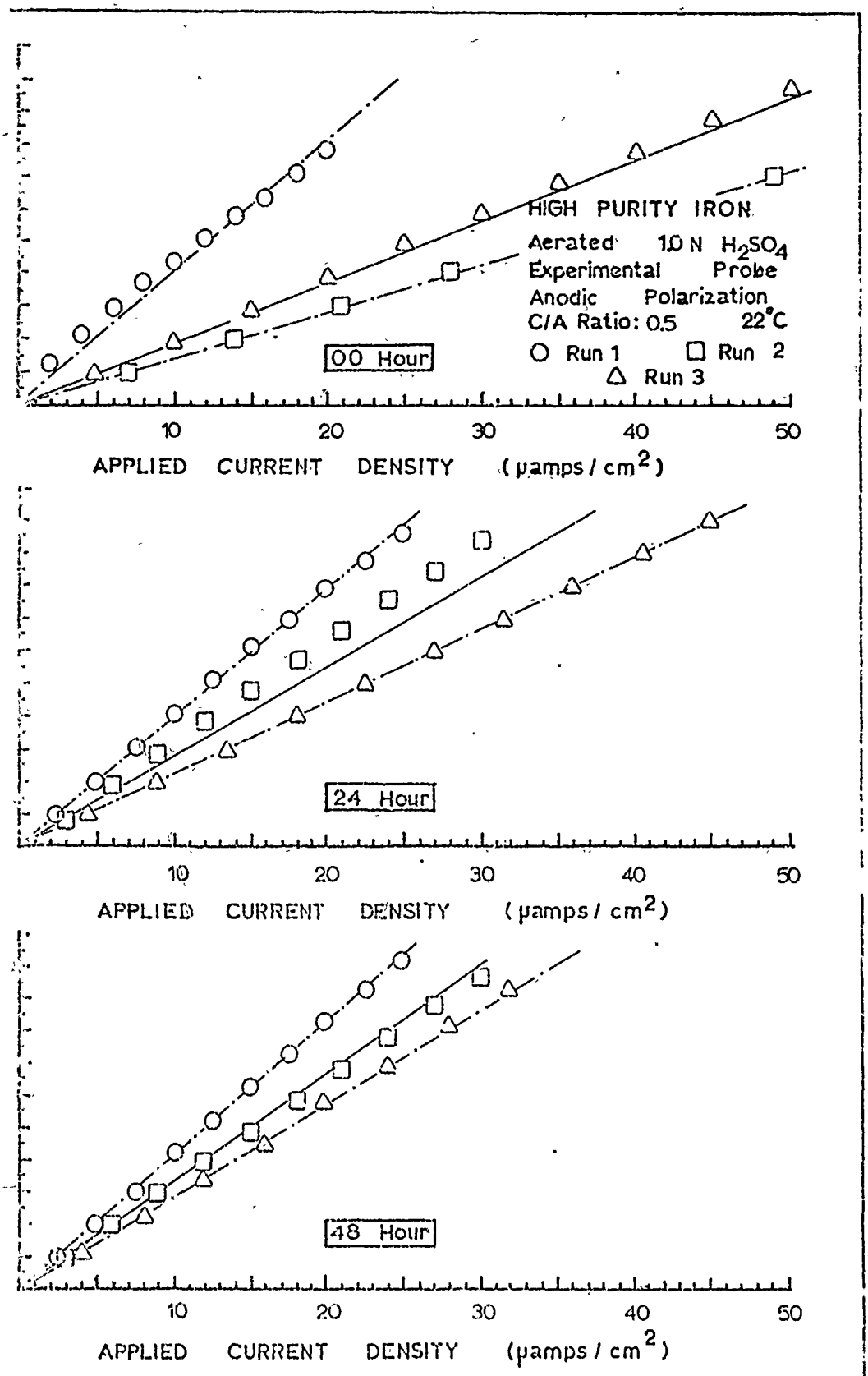

Figure 55 : Effect of Time on Galvanostatic Anodic Polarization Resistance of High Purity Iron with C/A Ratio = .5 in Aerated 1N Sulfuric Acid Determined Using an Experimental Probe. (Cont)

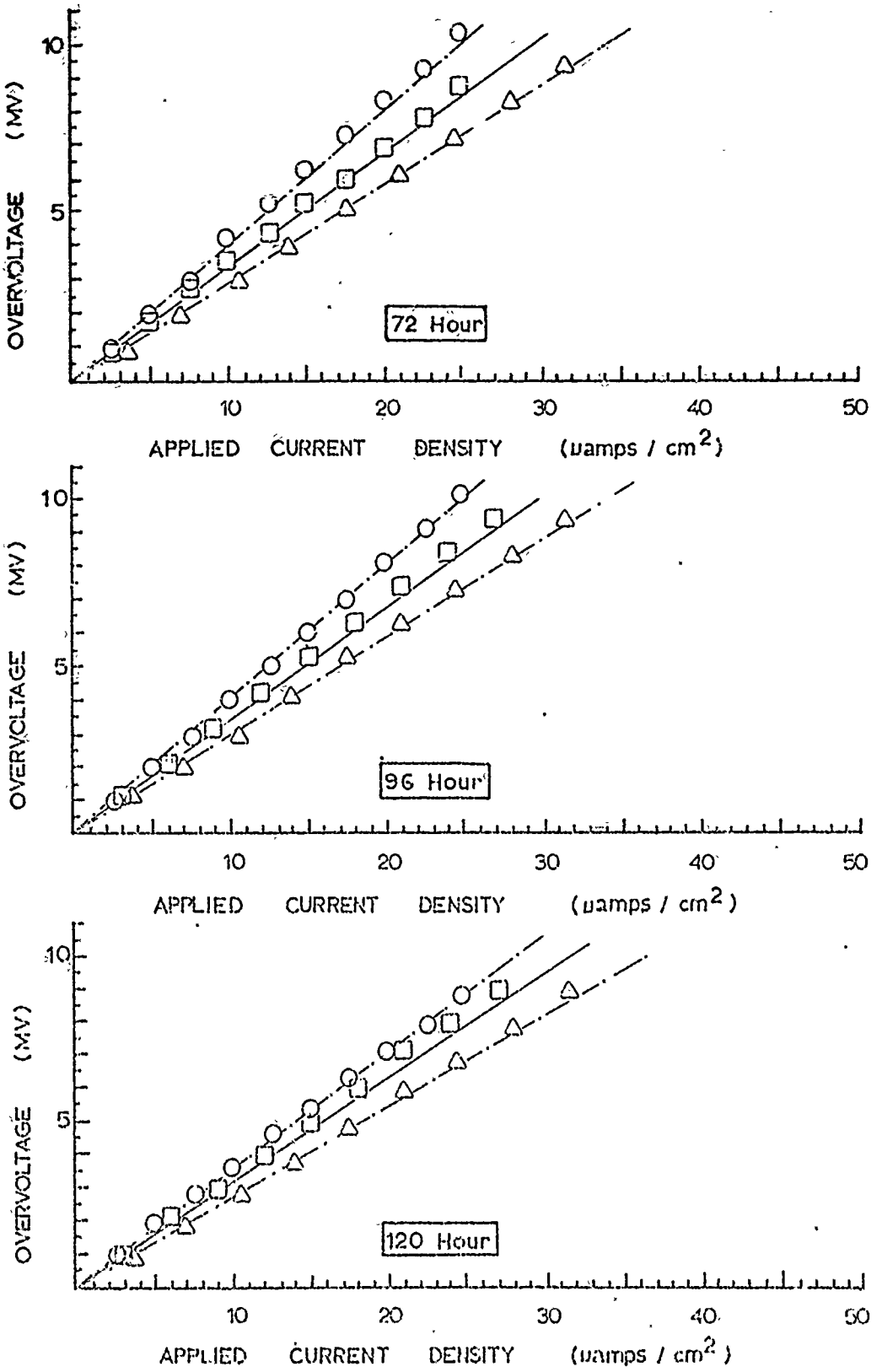

Figure 55 : (Cont) Effect of Time on Galvanostatic Anodic Polarization Resistance of High Purity Iron with C/A Ratio = .5 in Aerated 1% Sulfuric Acid Determined Using an Experimental Probe.

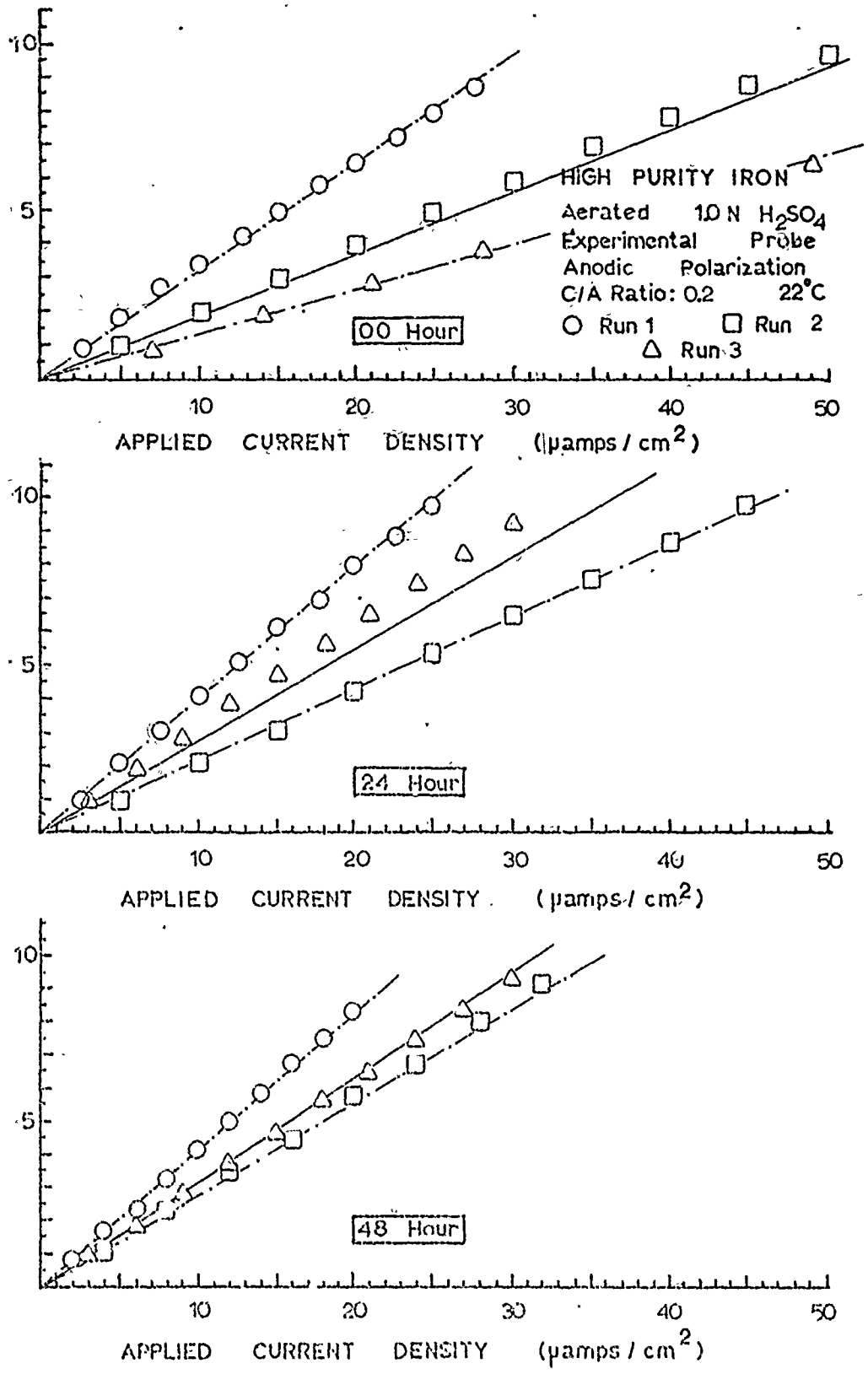

Figure 56 : Effect of Time on Galvanostatic Anodic Polarization Resistance of High Purity Iron with C/A Ratio = .2 in Aerated 1N Sulfuric Acid Determined Using an Experimental Probe. (Cont)

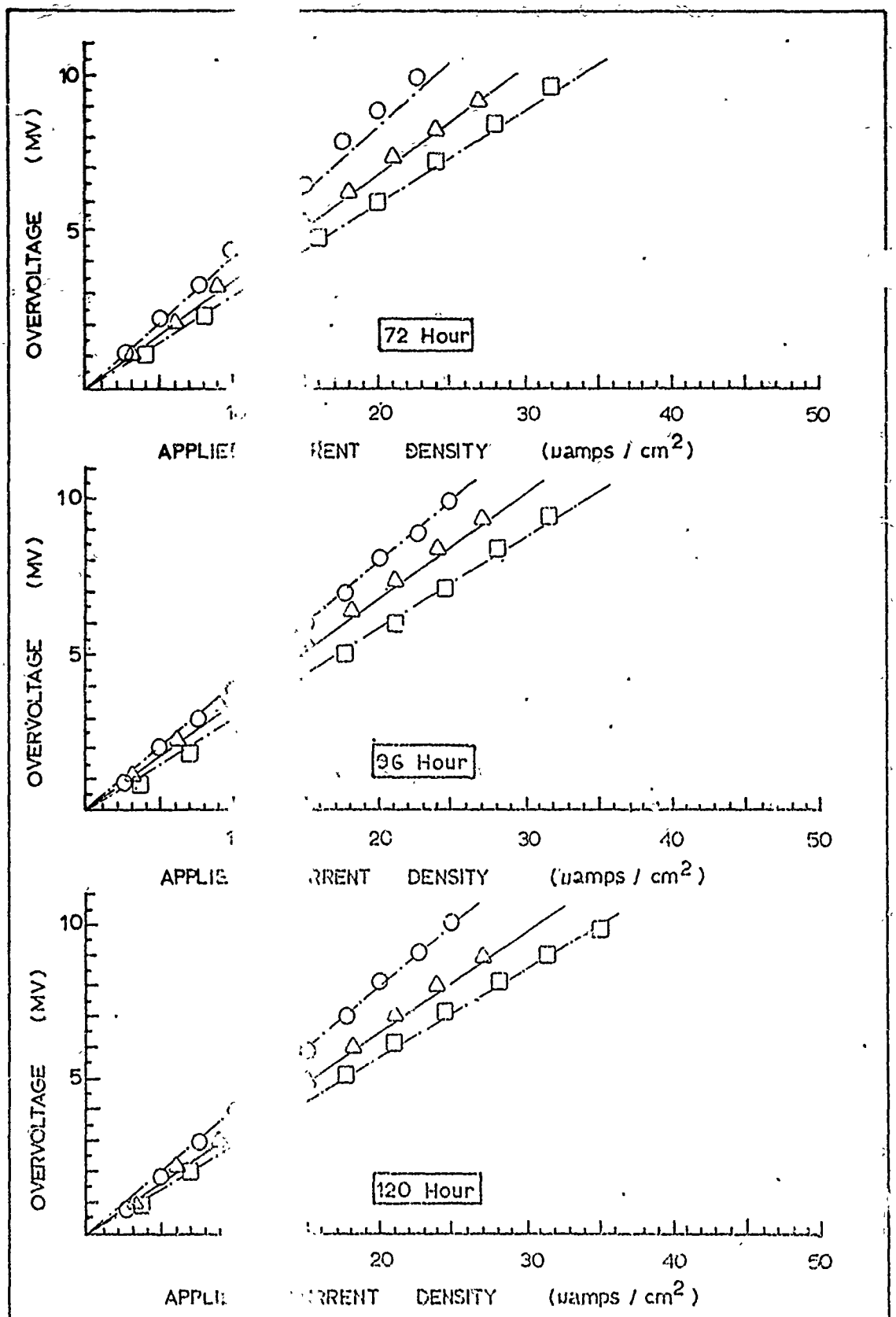

Figure 56 : (C[illegible] of Time on Galvanostatic Anodic Polarization Resistance of [illegible] iron with C/A Ratio = .2 in Aerated 1N Sulfuric Acid D[illegible] ing an Experimental Probe.

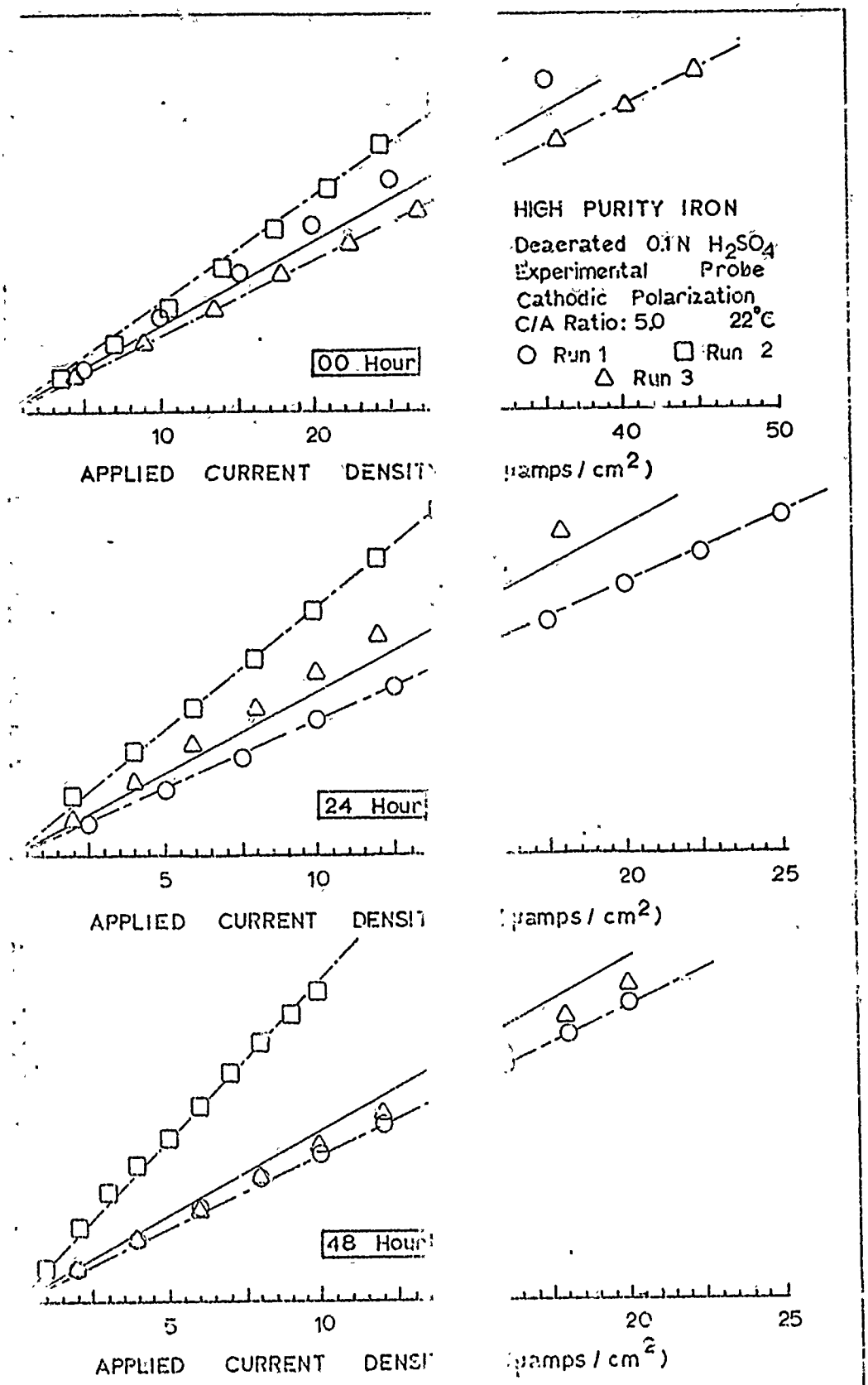

ure 57 : Effect of Time on Galvanostati
Purity Iron with C/A Ratio =
Determined Using an Experimen

Polarization Resistance of High
en Saturated .1N Sulfuric Acid
(Cont)

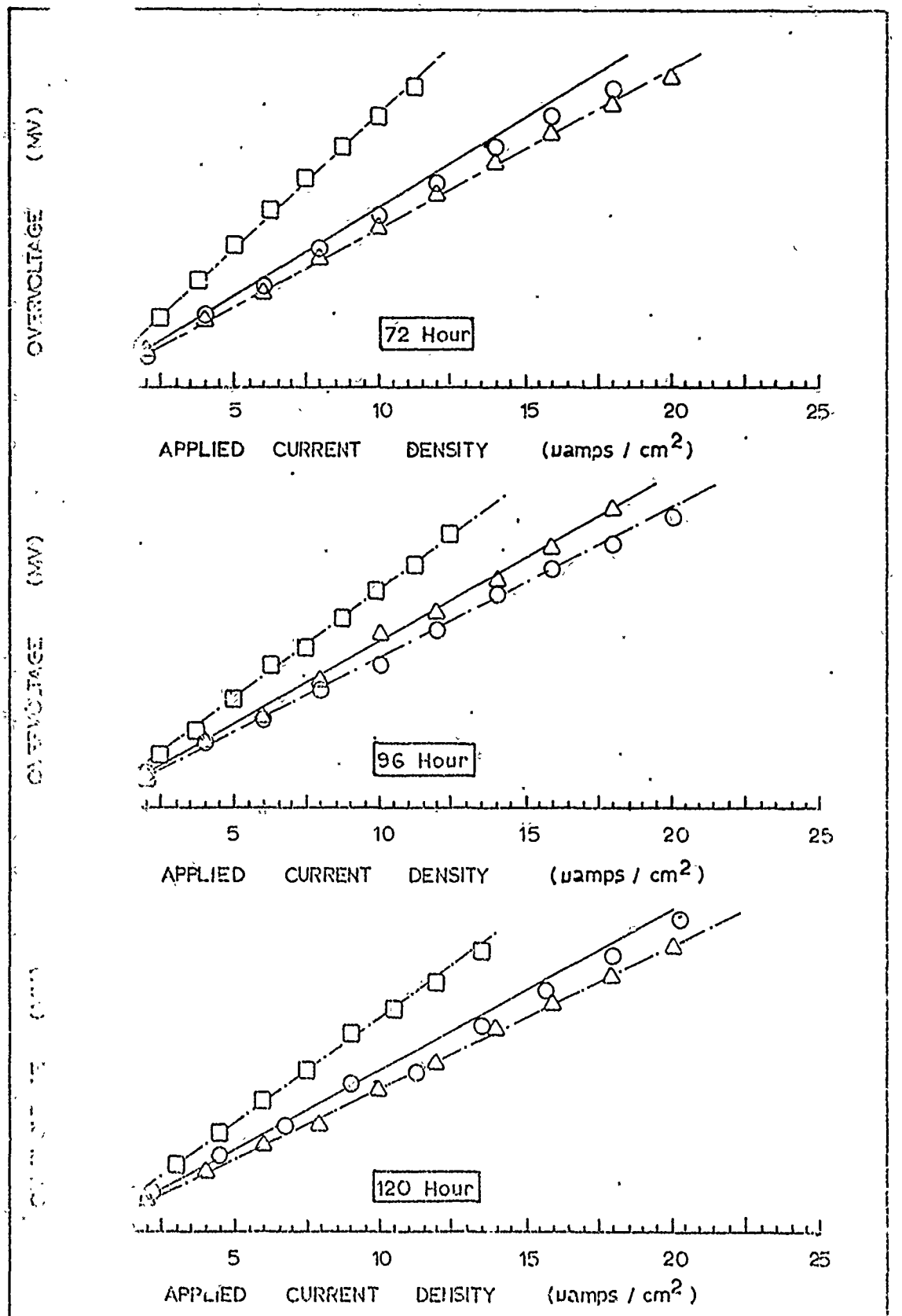

57 : (Cont) Effect of Time on Galvanostatic Cathodic Polarization Resistance of High Purity Iron with C/A Ratio = 5 in Hydrogen Saturated .1N Sulfuric Acid Determined Using an Experimental Probe.

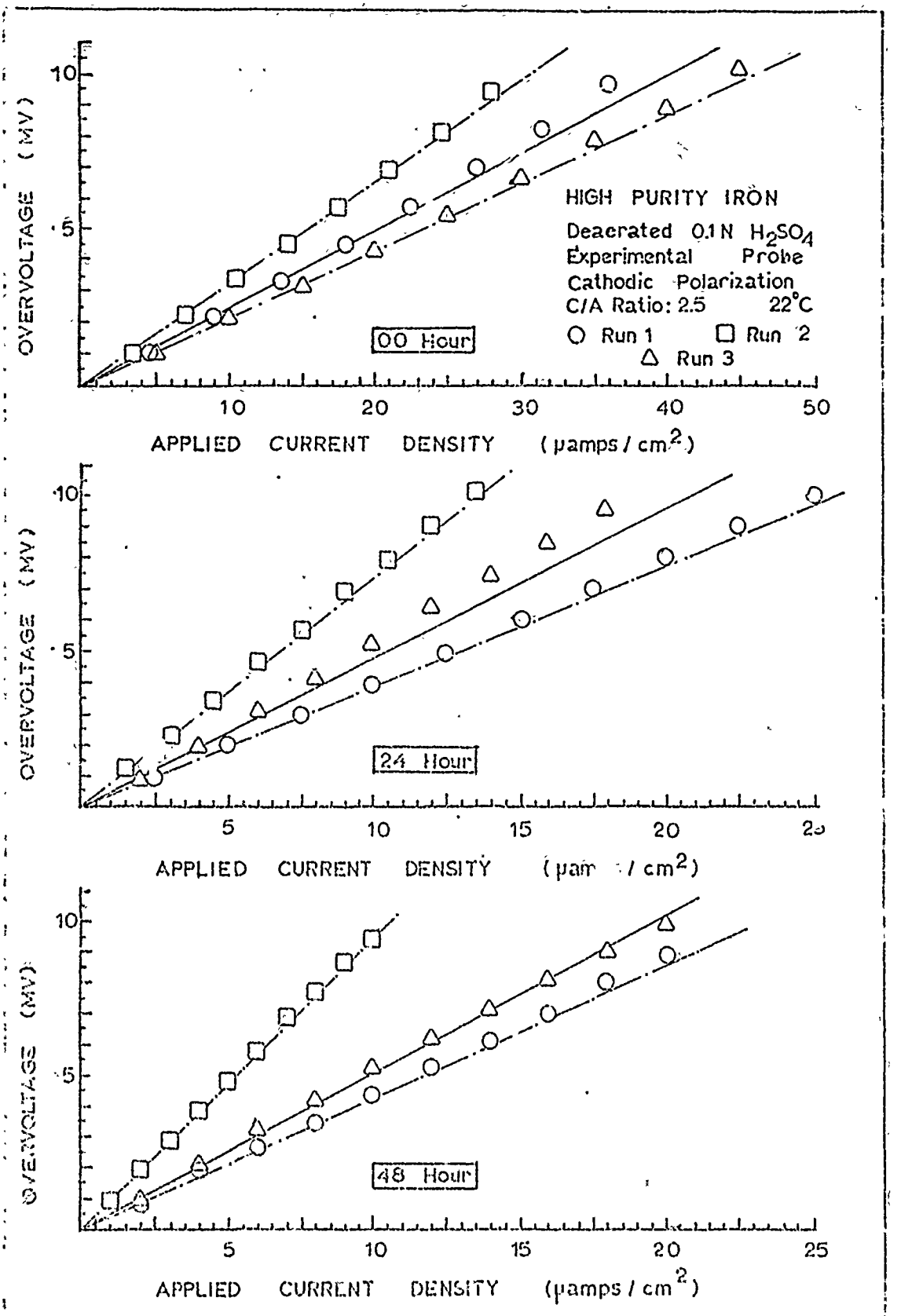

Figure 59 : Effect of Time on Galvanostatic Cathodic Polarization Resistance of High Purity Iron with C/A Ratio = 2.5 in Hydrogen Saturated .1N Sulfuric Acid Determined Using an Experimental Probe. (Cont)

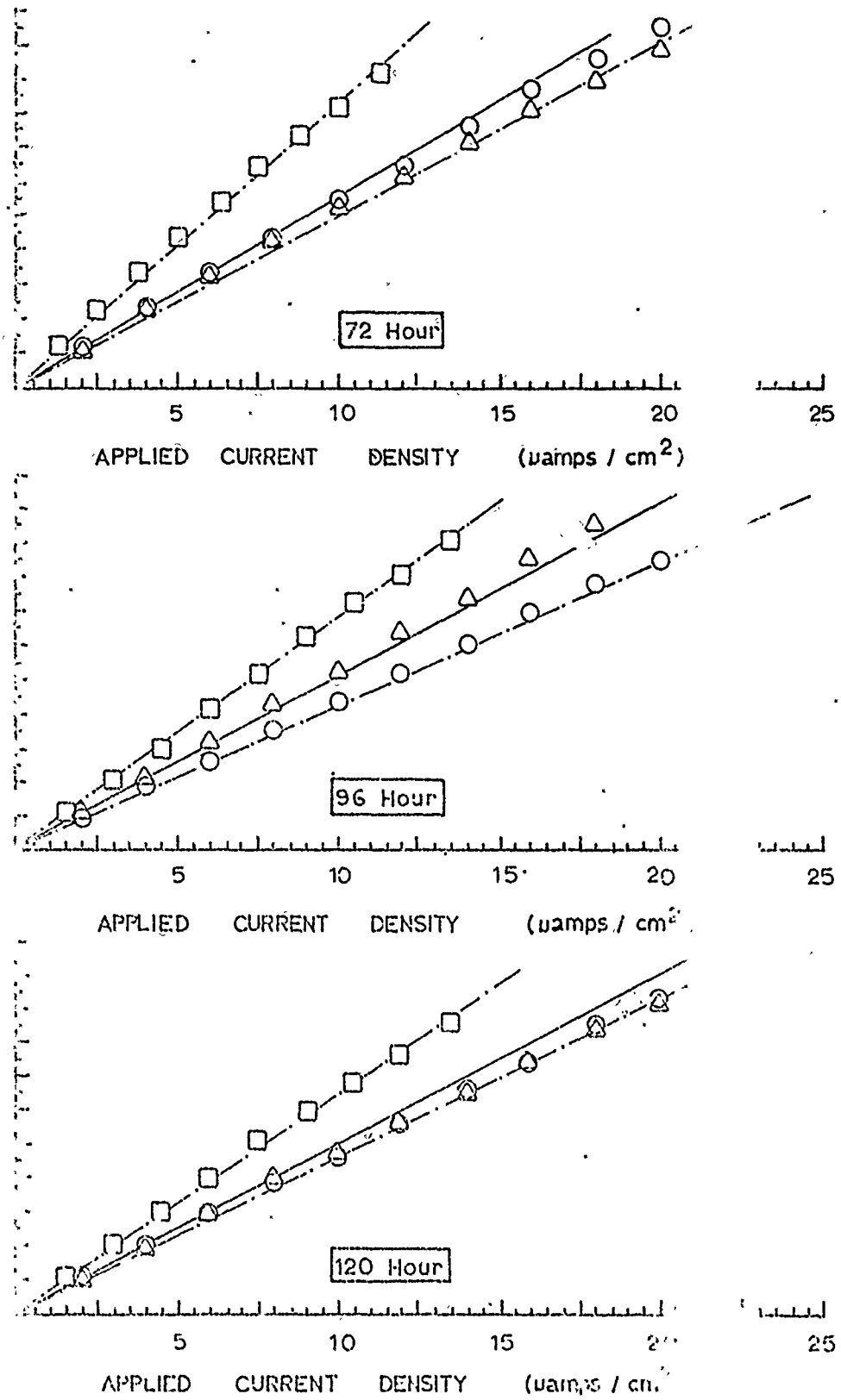

Figure 58 : (Cont) Effect of Time on Galvanostatic Cathodic Pola ... Resistance of High Purity Iron with C/A Ratio = 2.5 in Hydro... ...d .1N Sulfuric Acid Determined Using an Experimental Prob...

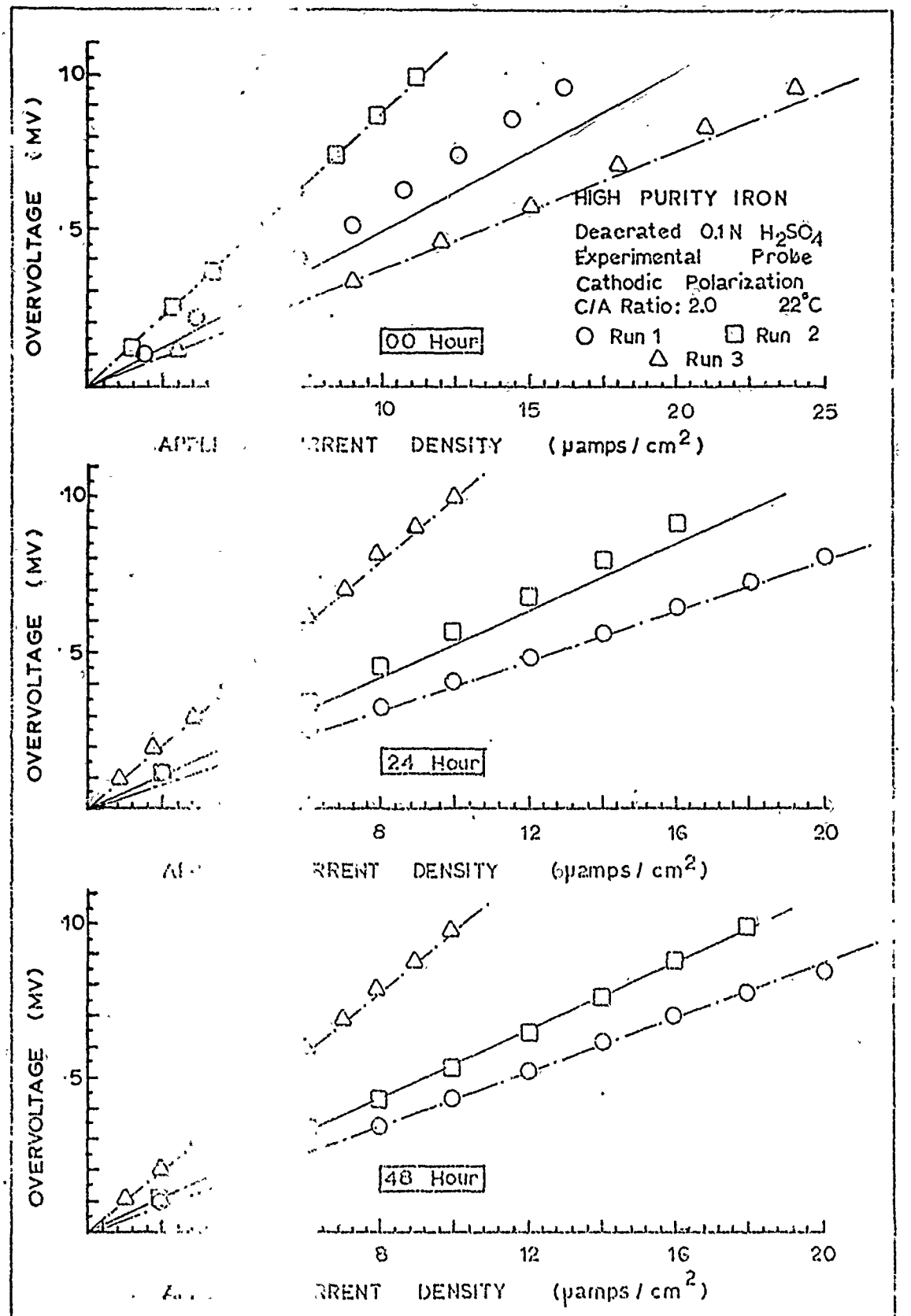

Figure 59 · on Galvanostatic Cathodic Polarization Resistance of High th C/A Ratio = 2 in Hydrogen Saturated .1N Sulfuric Acid ng an Experimental Probe. (Cont)

Reproduced from best available copy.

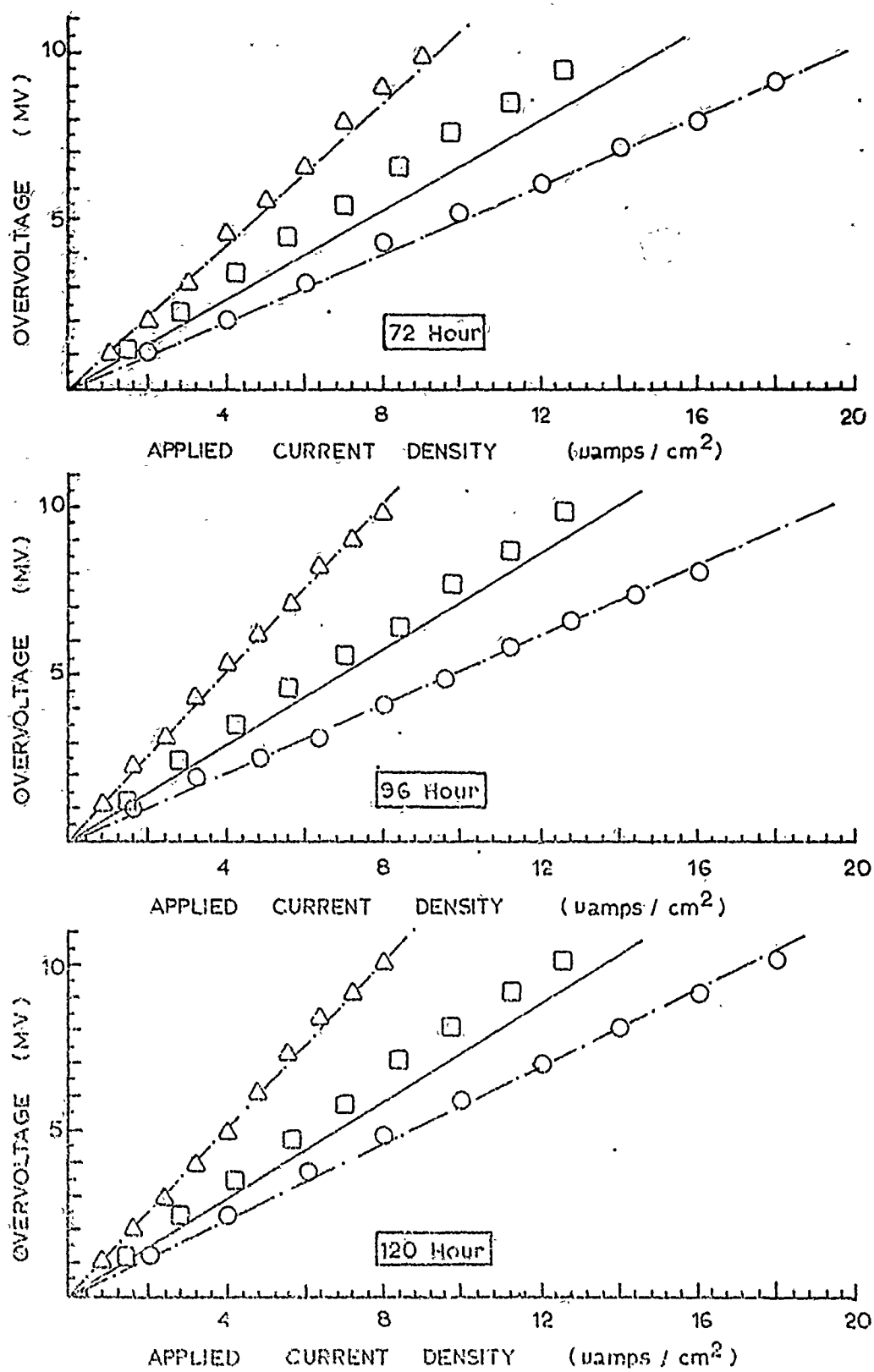

Figure 59 : (Cont) Effect of Time on Galvanostatic Cathodic Polarization Resistance of High Purity Iron with C/A Ratio = 2 in Hydrogen Saturated .1N Sulfuric Acid Determined Using an Experimental Probe.

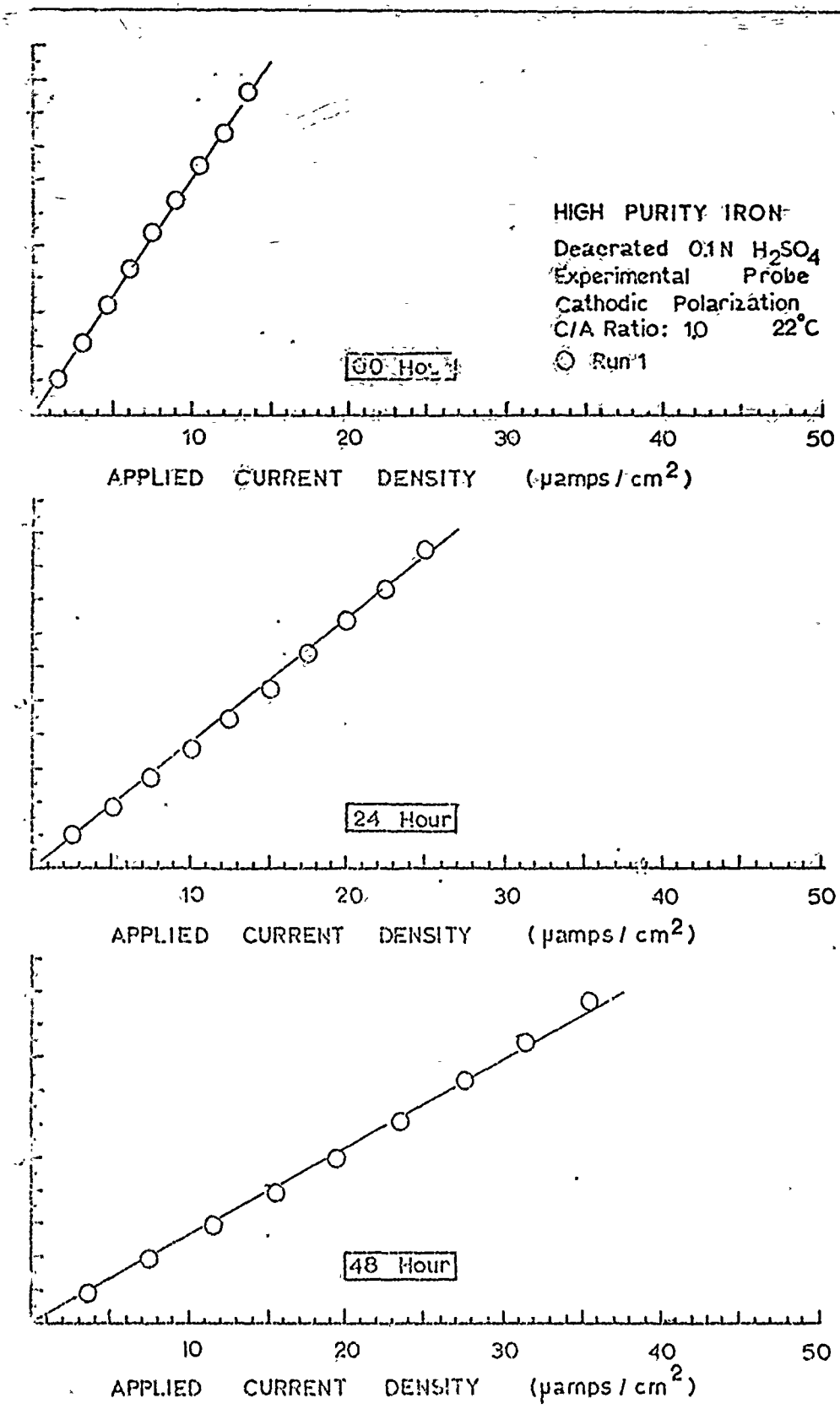

Figure 69 : Effect of Time on Galvanostatic Cathodic Polarization Resistance of High Purity Iron with C/A Ratio = 1 in Hydrogen Saturated .1N Sulfuric Acid Determined Using an Experimental Probe. (Cont)

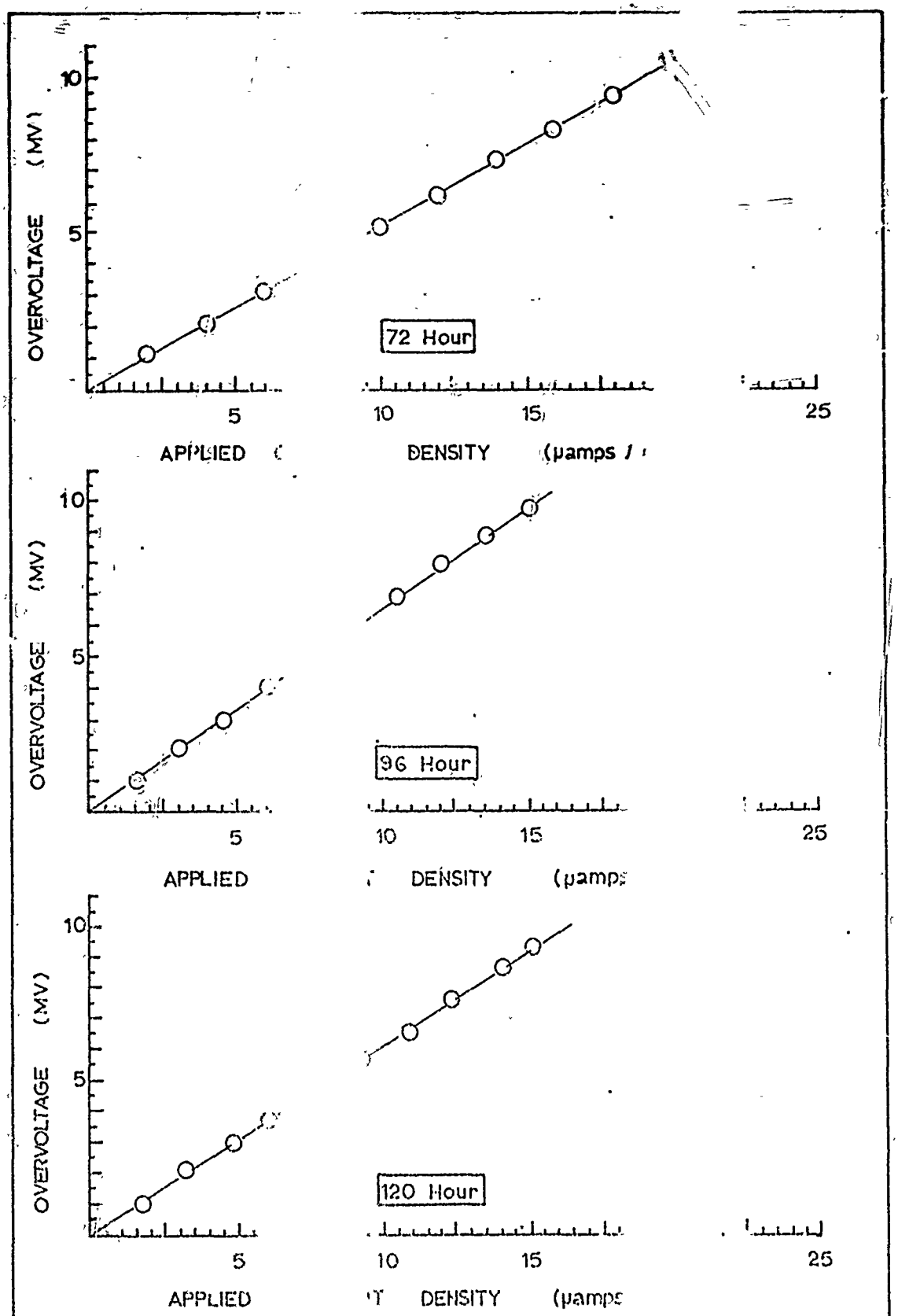

Figure 60 : (Cont) ... ine on Galvanostatic Cathod ... Resistance of He ... with C/A Ratio = 1 in H ... d ,1N Sulfu ... mined Using an Experiment

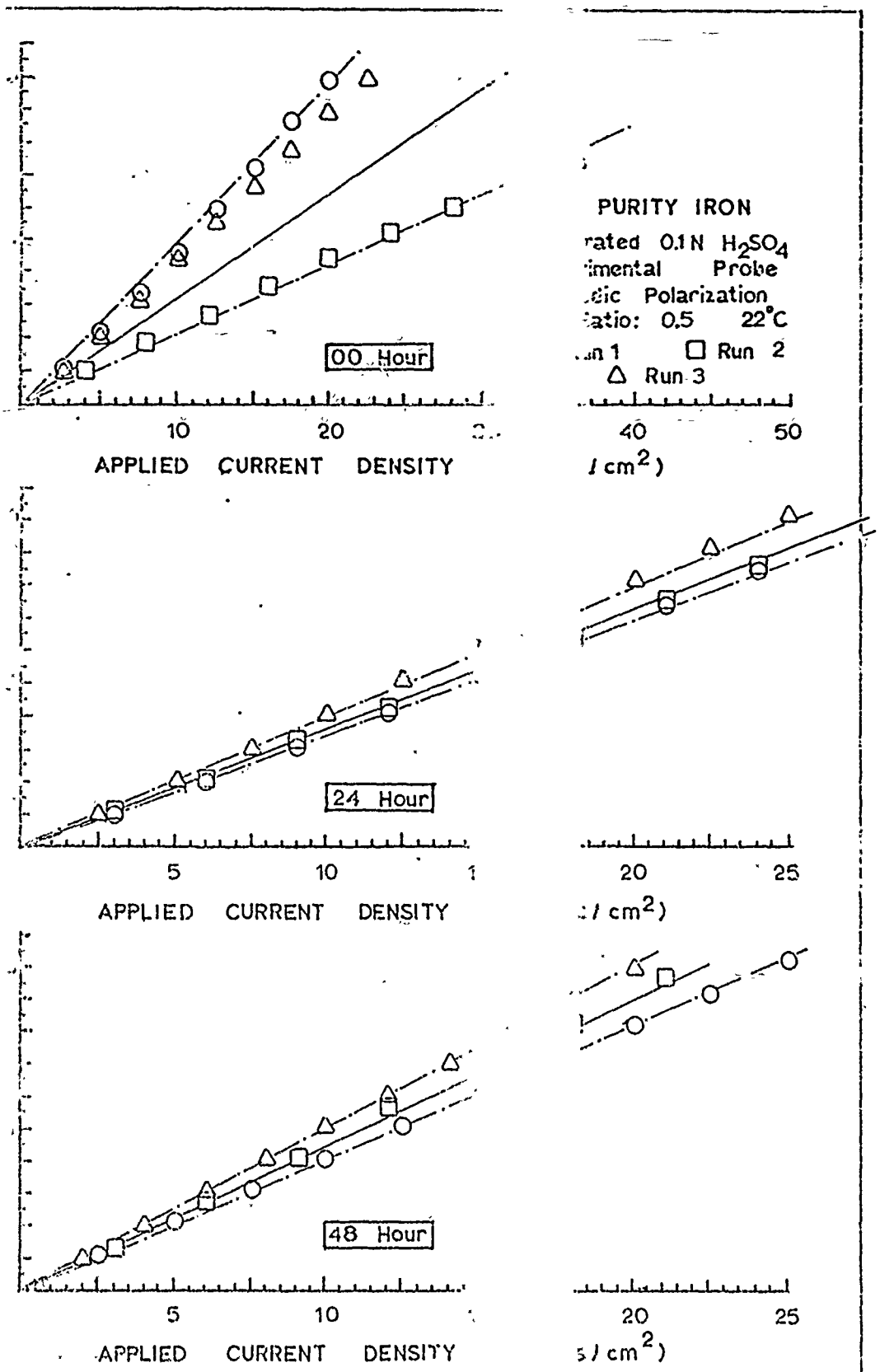

Figure 61 : Effect of Time on Galvanostatic Cat ation Resistance of High Purity Iron with C/A Ratio = .5 in turated .1N Sulfuric Acid Determined Using an Experimental P

Reproduced from best available copy.

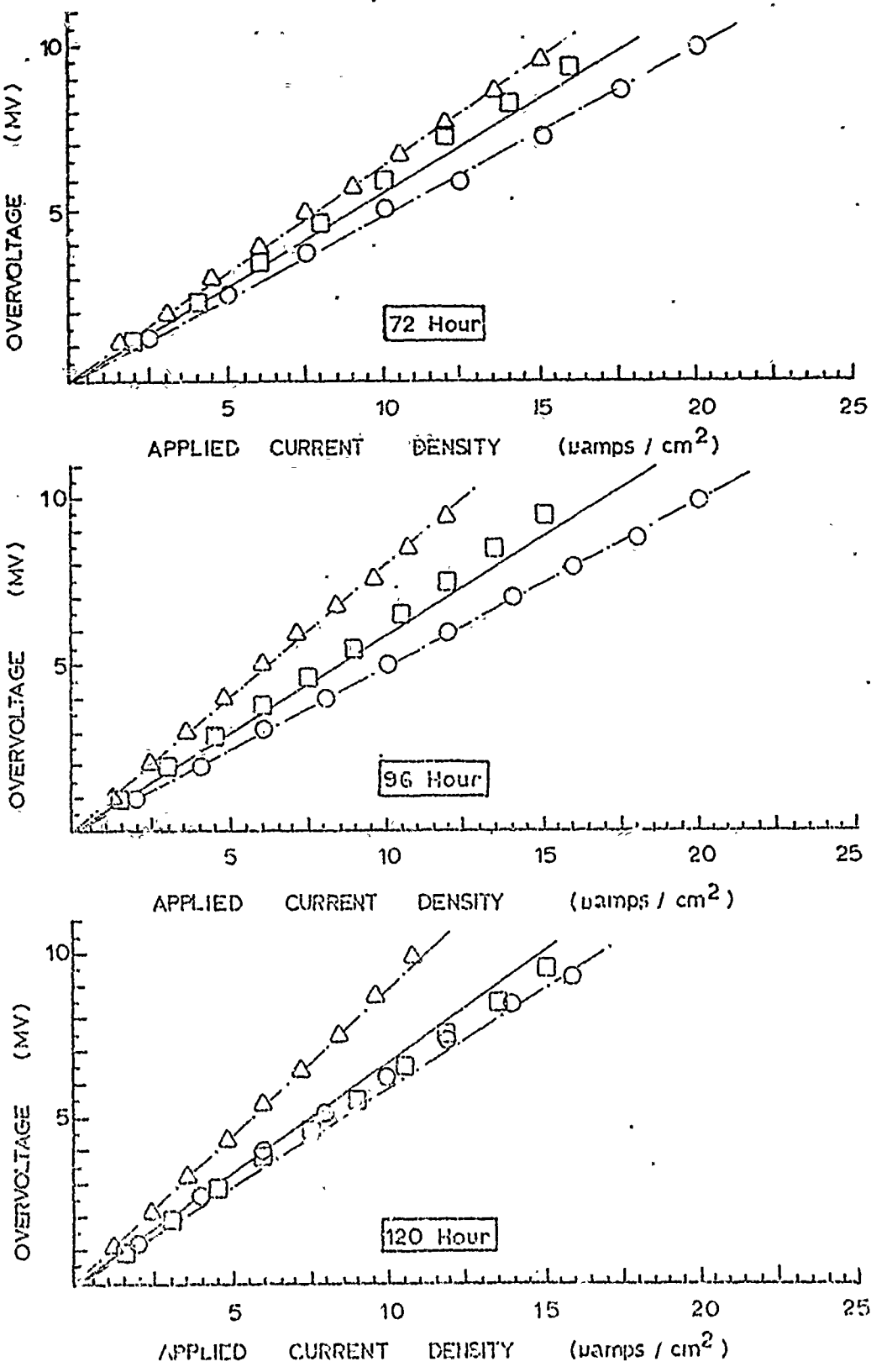

Figure 61 : (Cont) Effect of Time on Galvanostatic Cathodic Polarization Resistance of High Purity Iron with C/A Ratio = .5 in Hydrogen Saturated .1N Sulfuric Acid Determined Using an Experimental Probe.

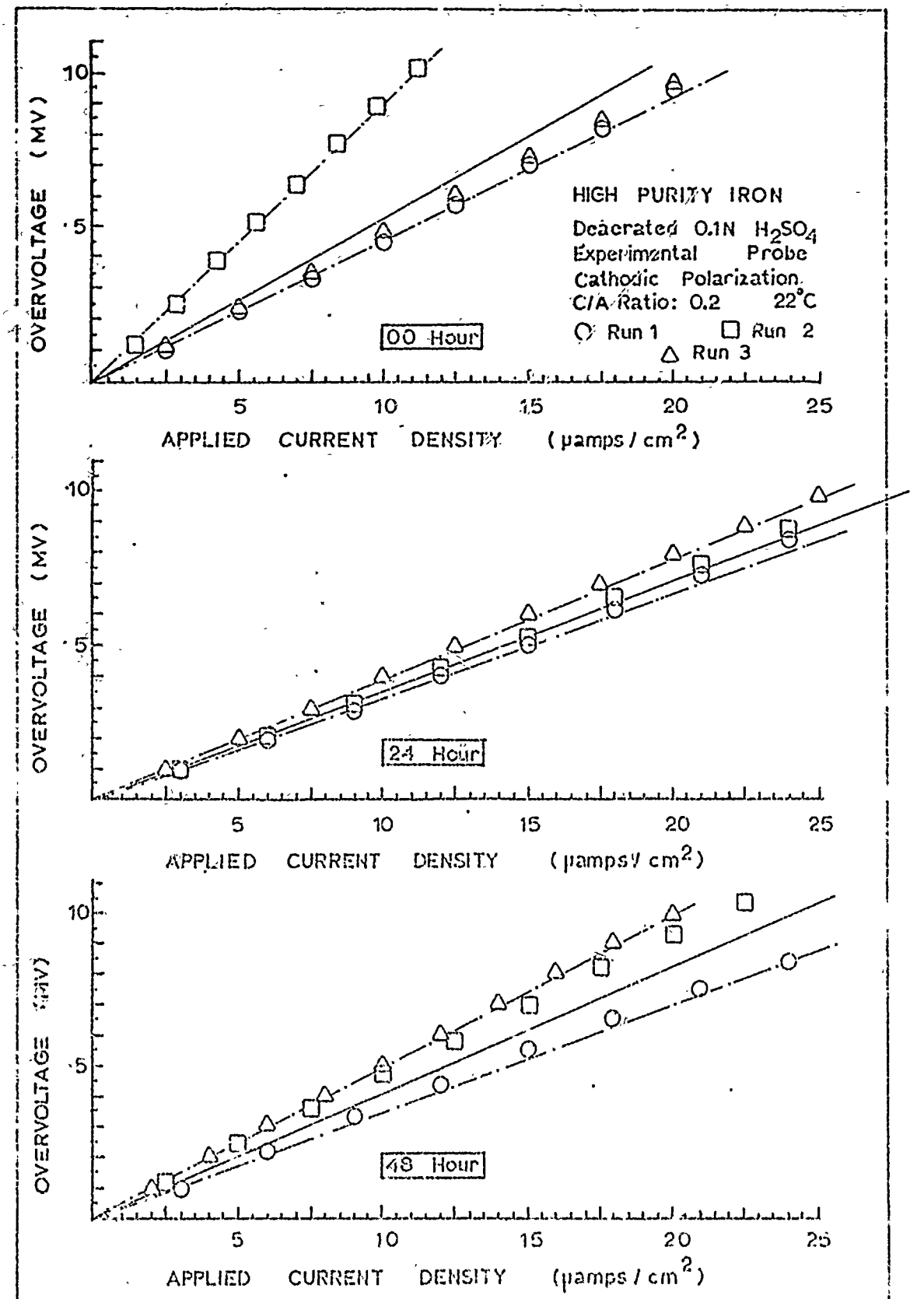

Figure 62: Effect of Time on Galvanostatic Cathodic Polarization Resistance of High Purity Iron with C/A Ratio = 2 in Hydrogen Saturated .1N Sulfuric Acid Determined Using an Experimental Probe. (Cont)

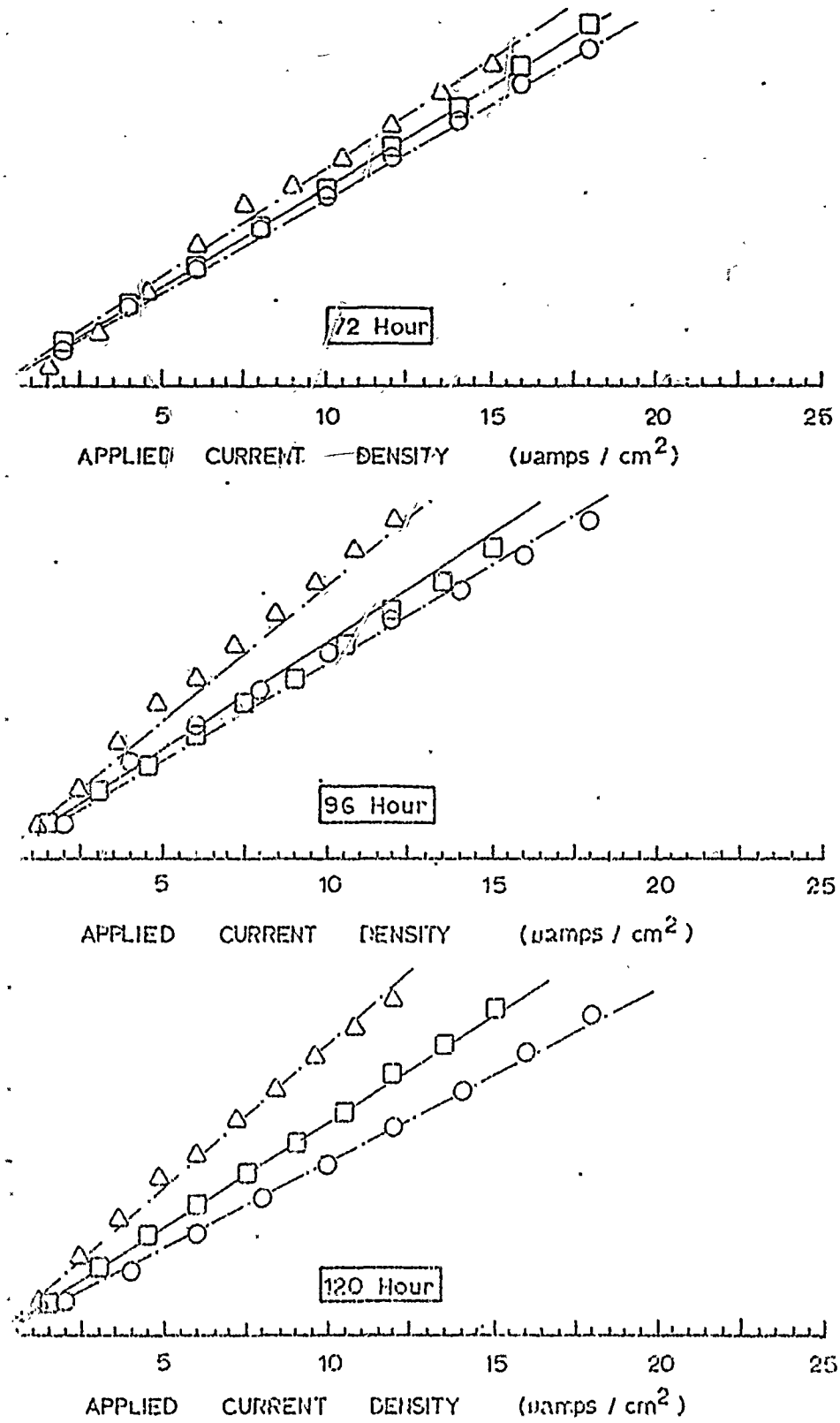

ure 62 : (Cont) Effect of Time on Galvanostatic Cathodic Polarization Resistance of High Purity Iron with C/A Ratio = .2 in Hydrogen Saturated .1N Sulfuric Acid Determined Using an Experimental Probe.

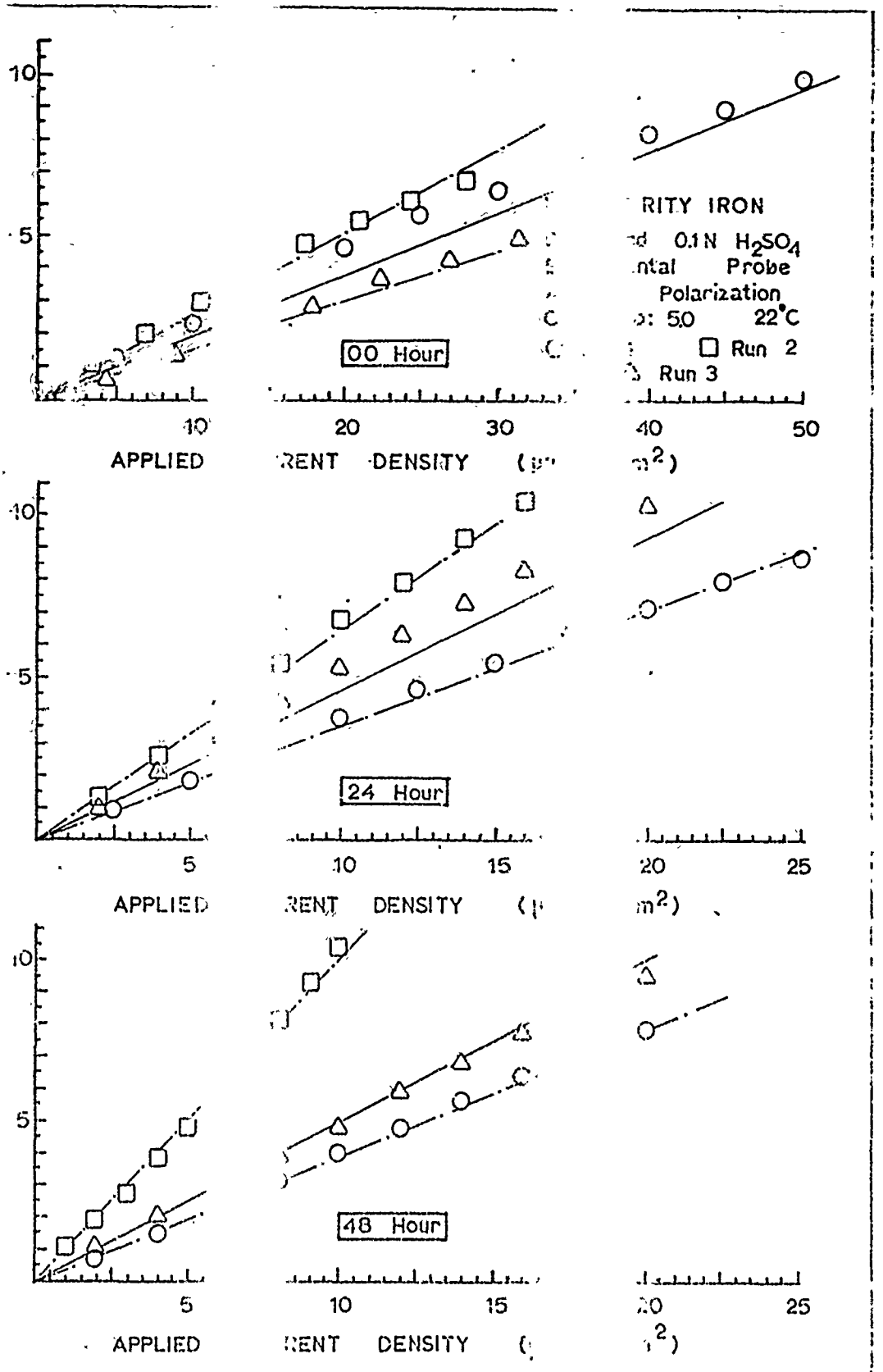

Figure 63: Effe... on Galvanostatic Anodic ... istance of High Pu... th C/A Ratio = 5 in Hyd... .1N Sulfuric Aci... ned Using an Experimenta...

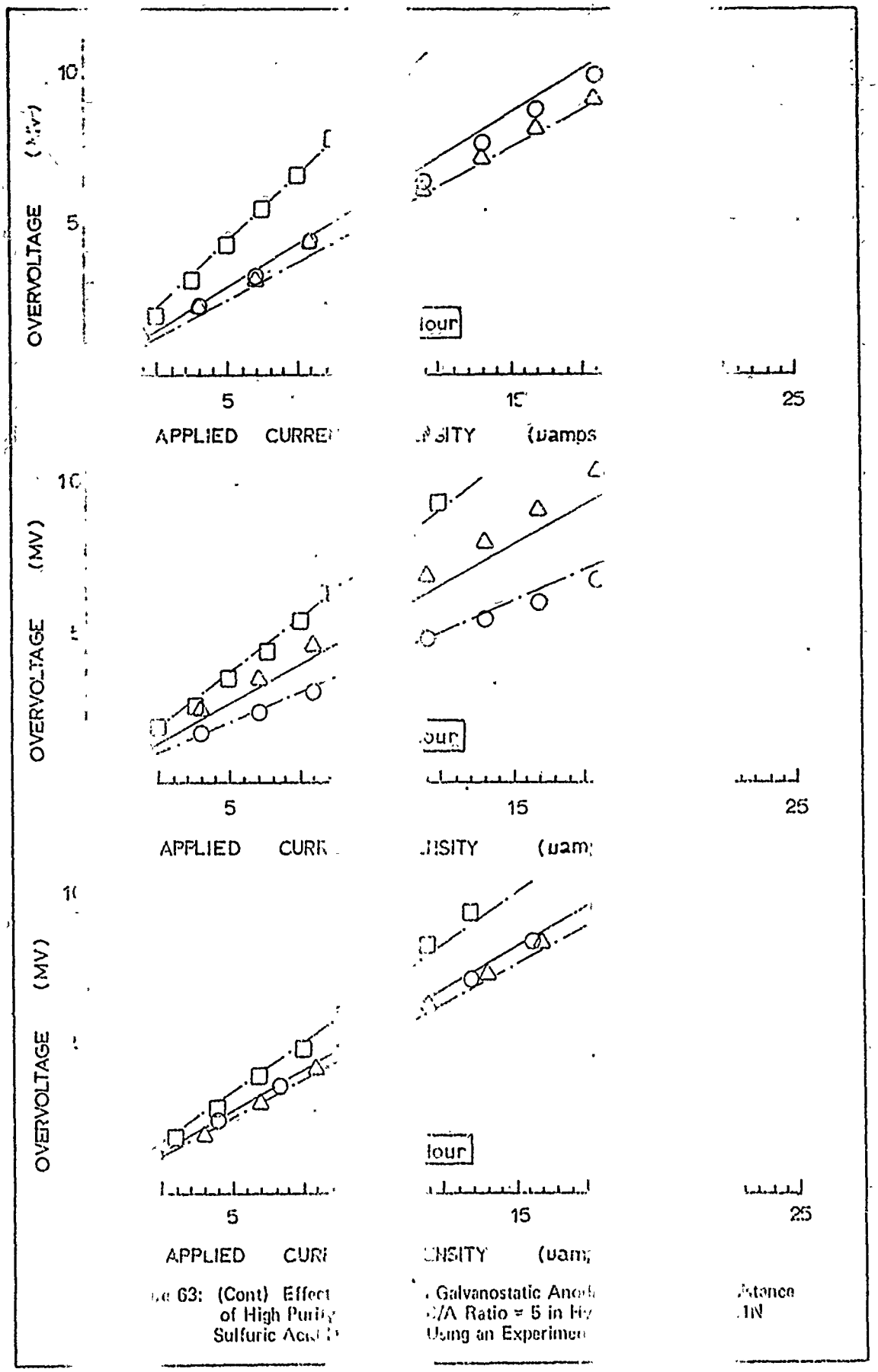

e 63: (Cont) Effect . Galvanostatic Anod stance
of High Purity C/A Ratio = 5 in Hy .1N
Sulfuric Acid Using an Experimen

Reproduced from best available copy.

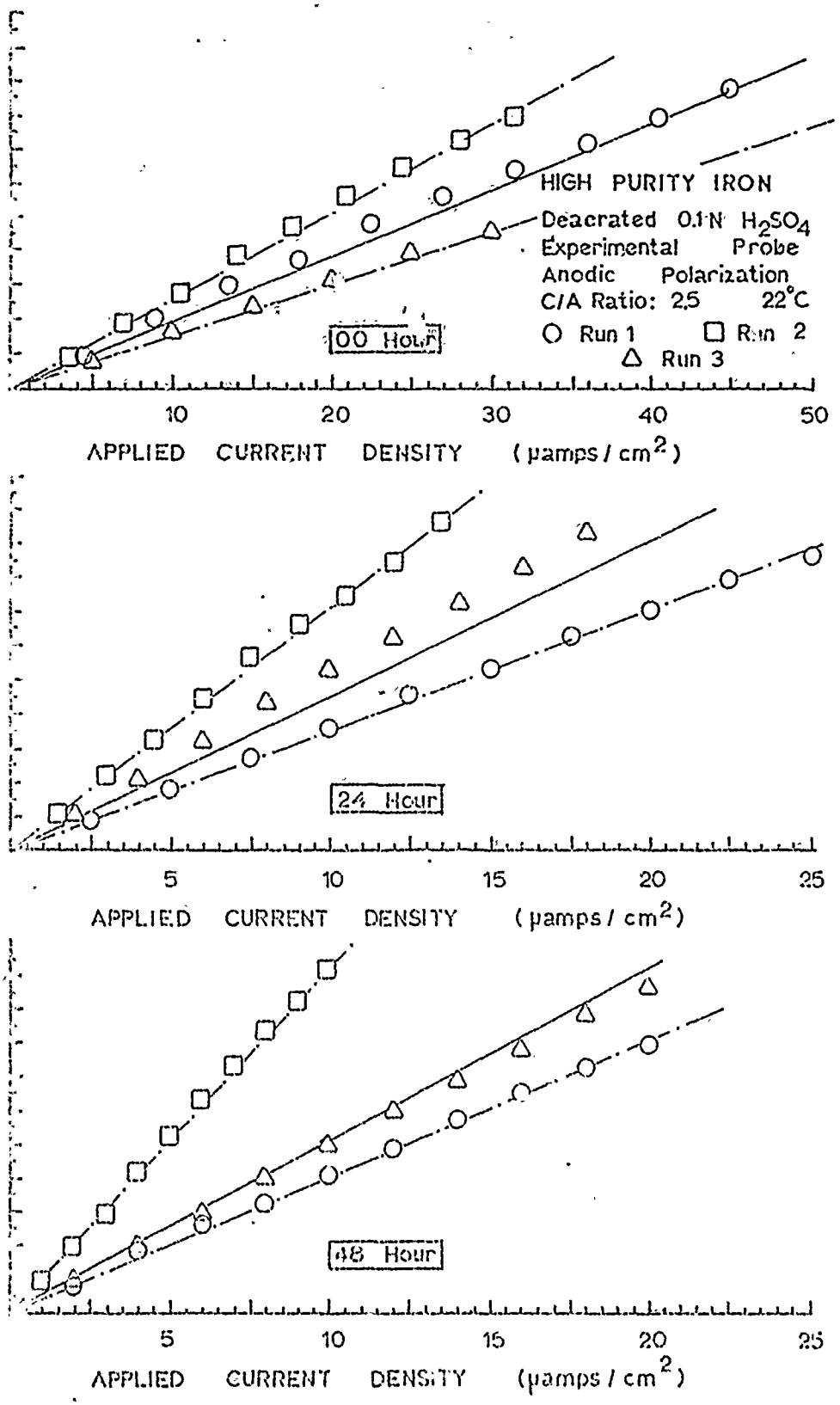

Figure G4: Effect of Time on Galvanostatic Anodic Polarization Resistance of High Purity Iron with C/A Ratio 2.5 in Hydrogen Saturated .1N Sulfuric Acid Determined Using an Experimental Probe. (Cont)

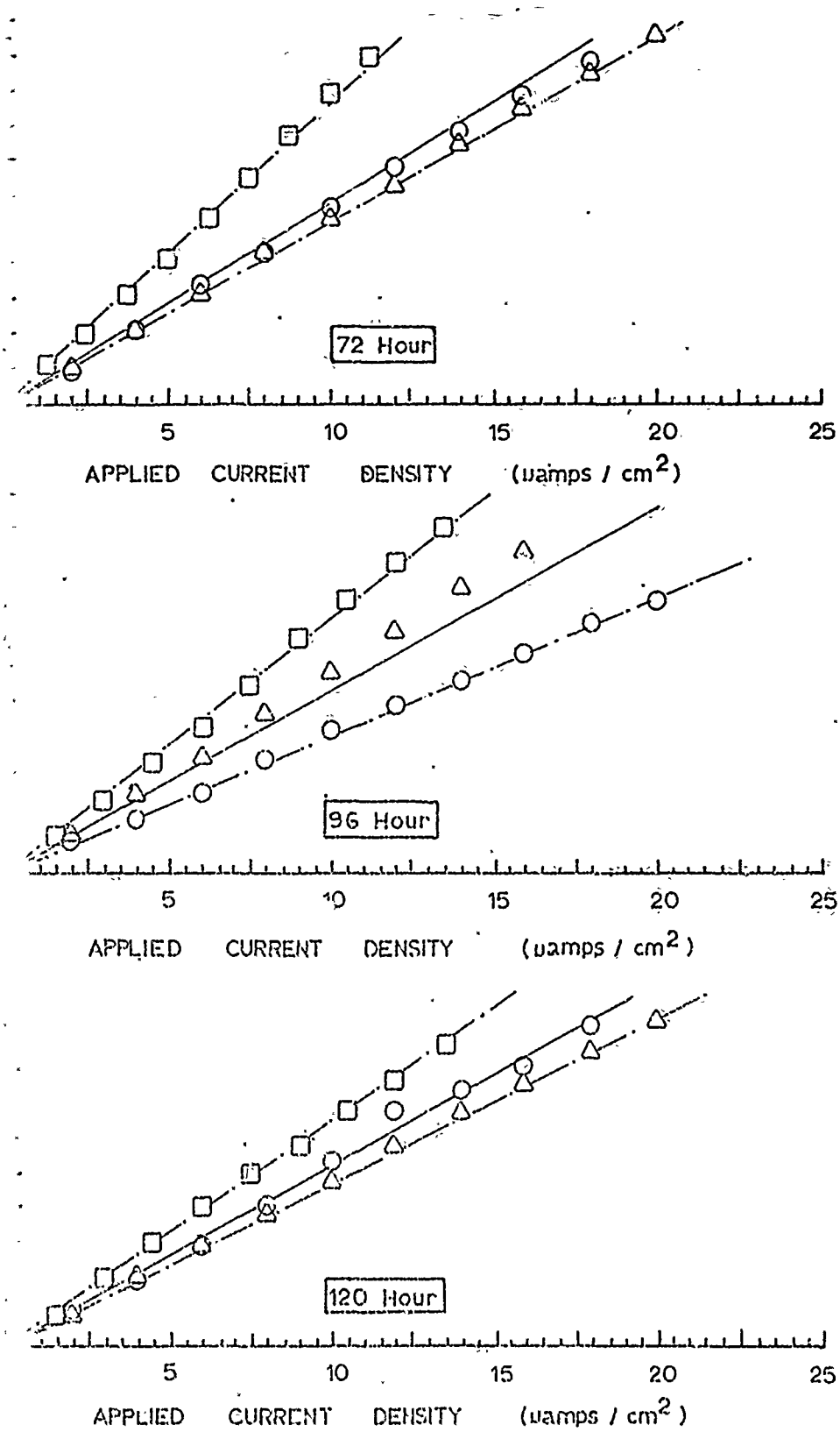

Figure G4: (Cont) Effect of Time on Galvanostatic Anodic Polarization Resistance of High Purity Iron with C/A Ratio - 2.5 in Hydrogen Saturated .1N Sulfuric Acid Determined Using an Experimental Probe.

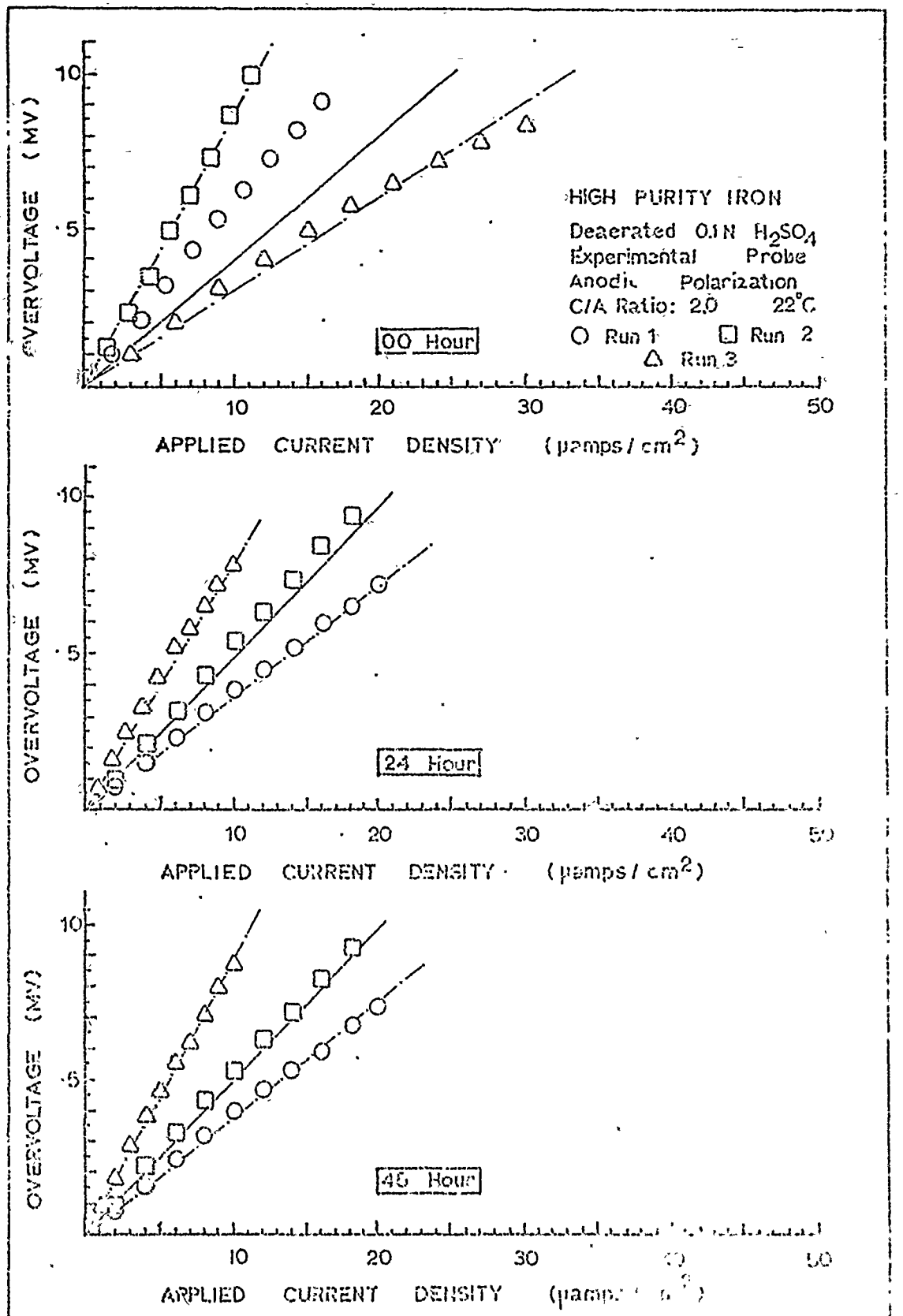

Figure 65: Effect of Time on Galvanostatic Anode Polari[illegible] of High Purity Iron with C/A Ratio = 2 in Hydrogen [illegible] Sulfuric Acid Determined using an Experimental Probe, (Cell)

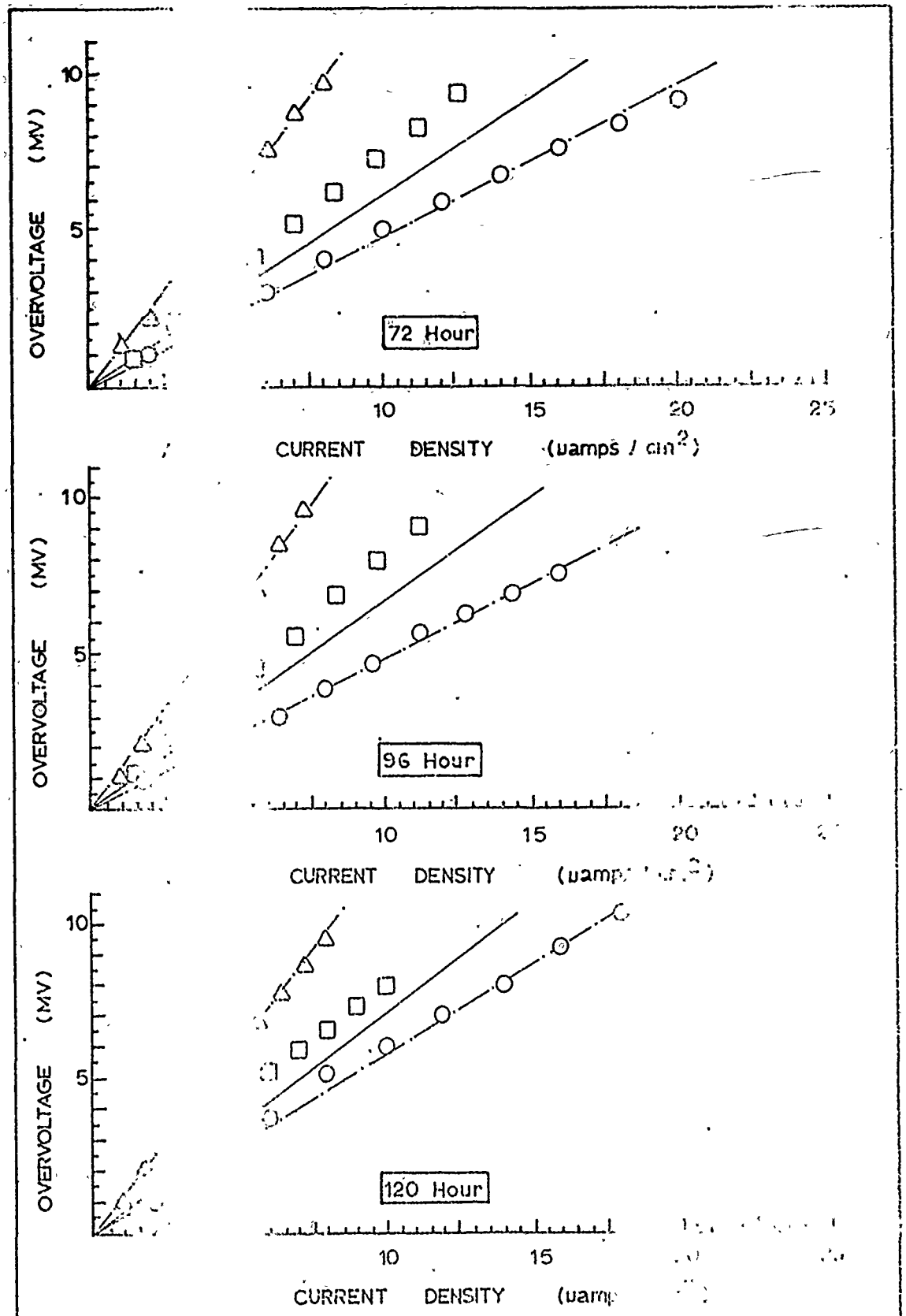

Fi... ...t) Effect of Time on Galvanostatic Anod... ...igh Purity Iron with C/A Ratio = 2 in Hy... ...ric Acid Determined Using an Experimen...

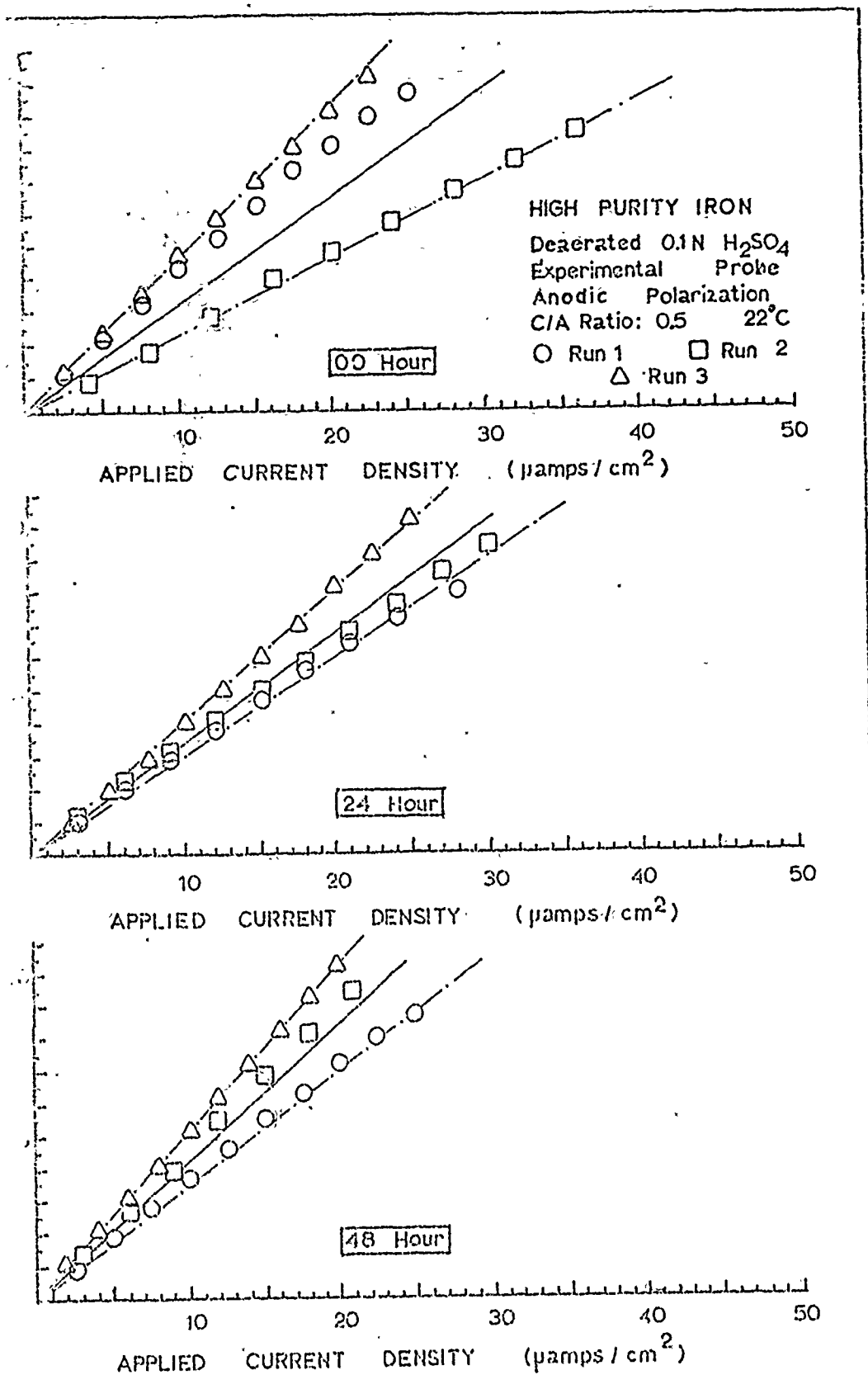

Figure 66: Effect of Time on Galvanostatic Anodic Polarization Resistance of High Purity Iron with C/A Ratio = .5 in Hydrogen Saturated .1N Sulfuric Acid Determined Using an Experimental Probe. (Cont)

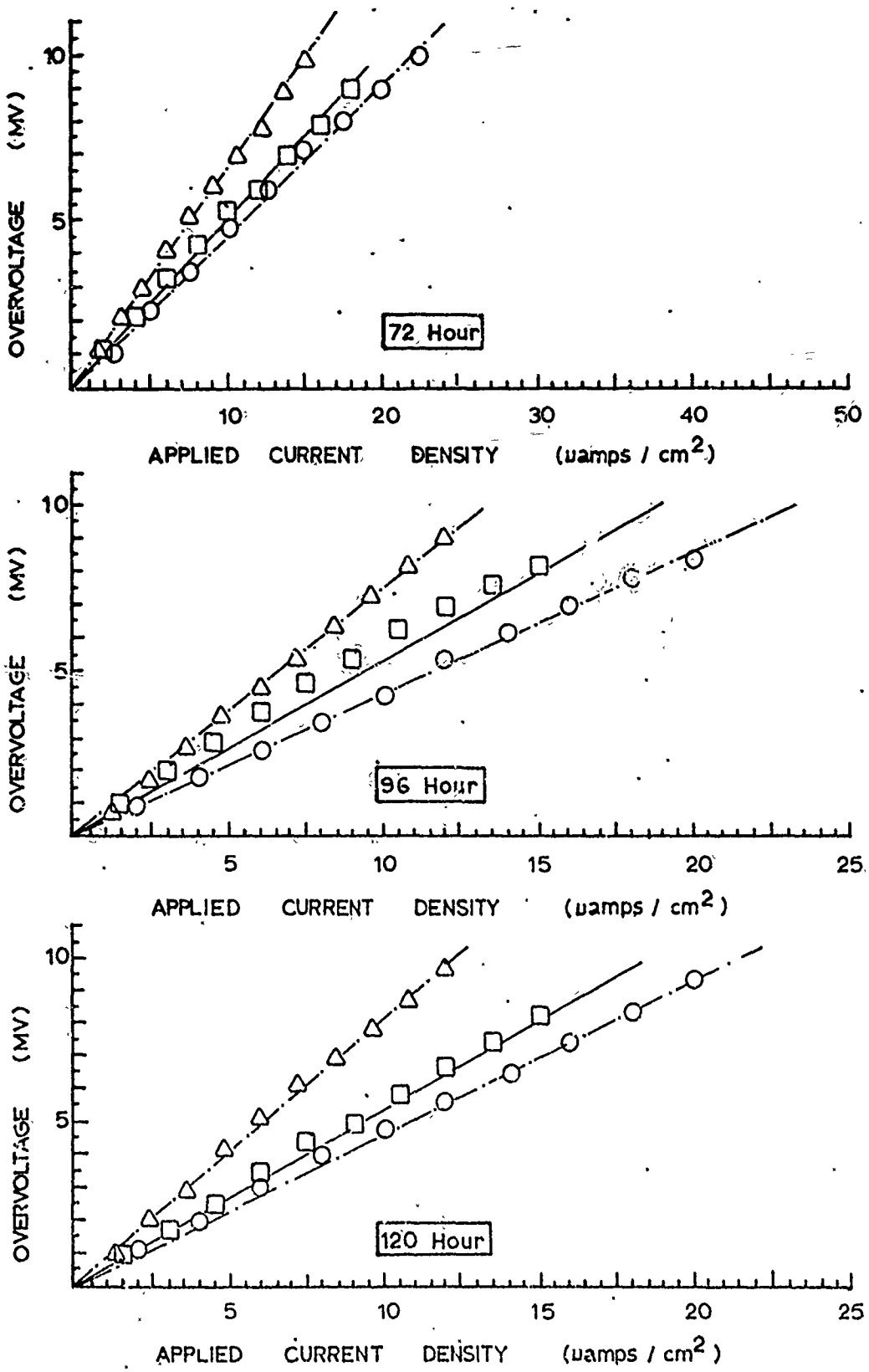

Figure 66: (Cont) Effect of Time on Galvanostatic Anodic Polarization Resistance of High Purity Iron with C/A Ratio = .5 in Hydrogen Saturated .1N Sulfuric Acid Determined Using an Experimental Probe.

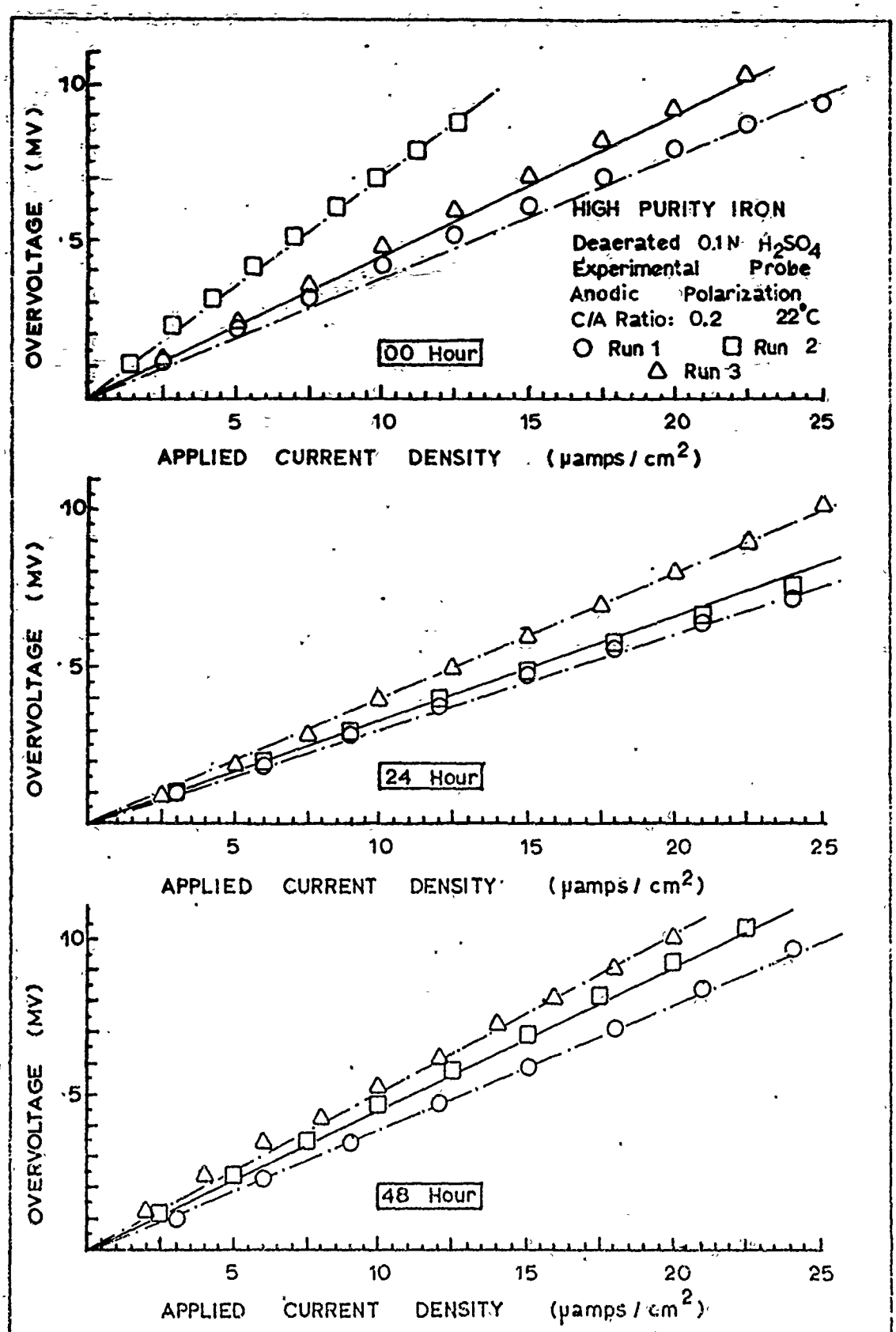

Figure 67: Effect of Time on Galvanostatic Anodic Polarization Resistance of High Purity Iron with C/A Ratio = .2 in Hydrogen Saturated .1N Sulfuric Acid Determined Using an Experimental Probe. (Cont)

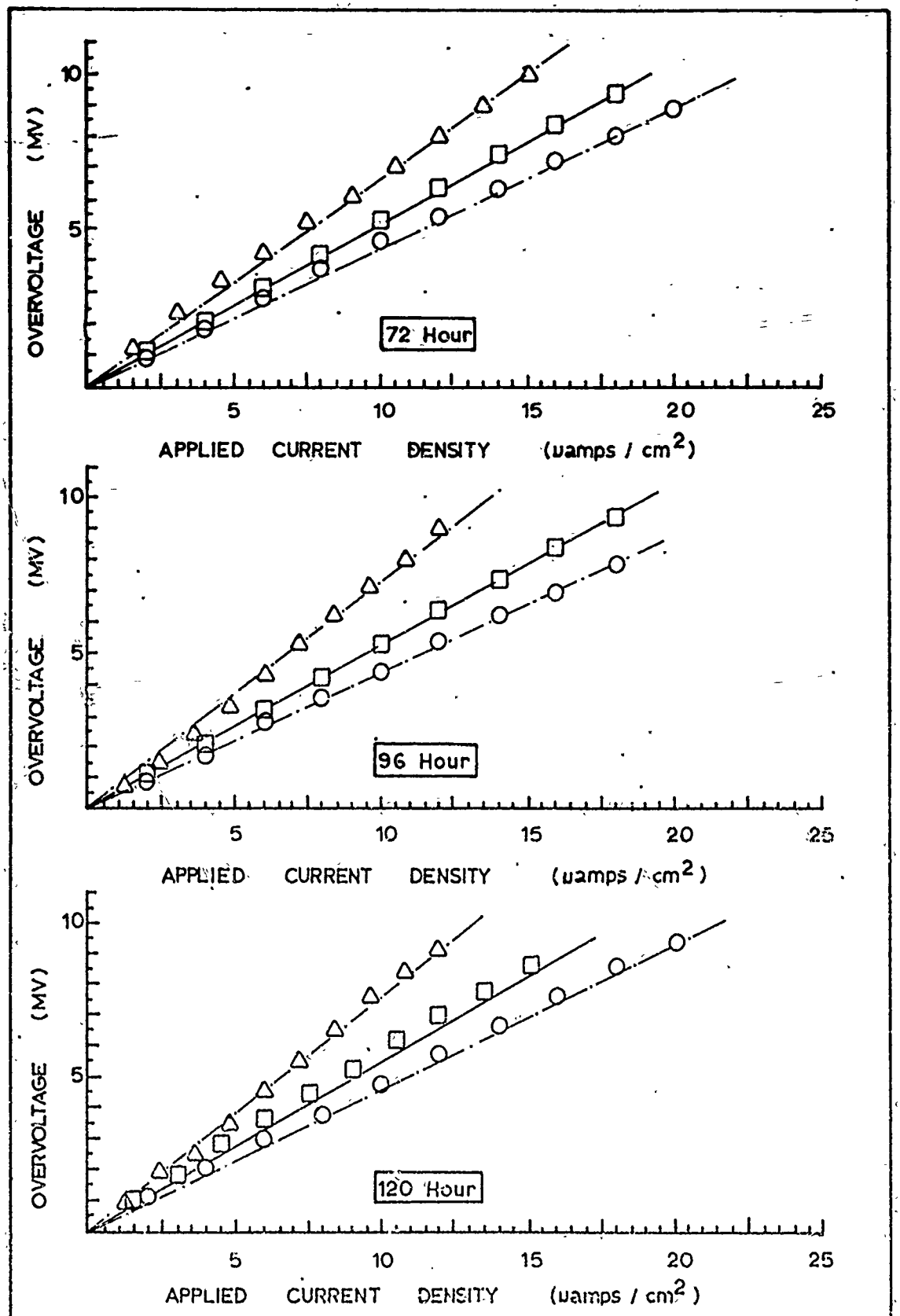

Figure 67: (Cont) Effect of Time on Galvanostatic Anodic Polarization Resistance of High Purity Iron with C/A Ratio = .2 in Hydrogen Saturated .1N Sulfuric Acid Determined Using an Experimental Probe.

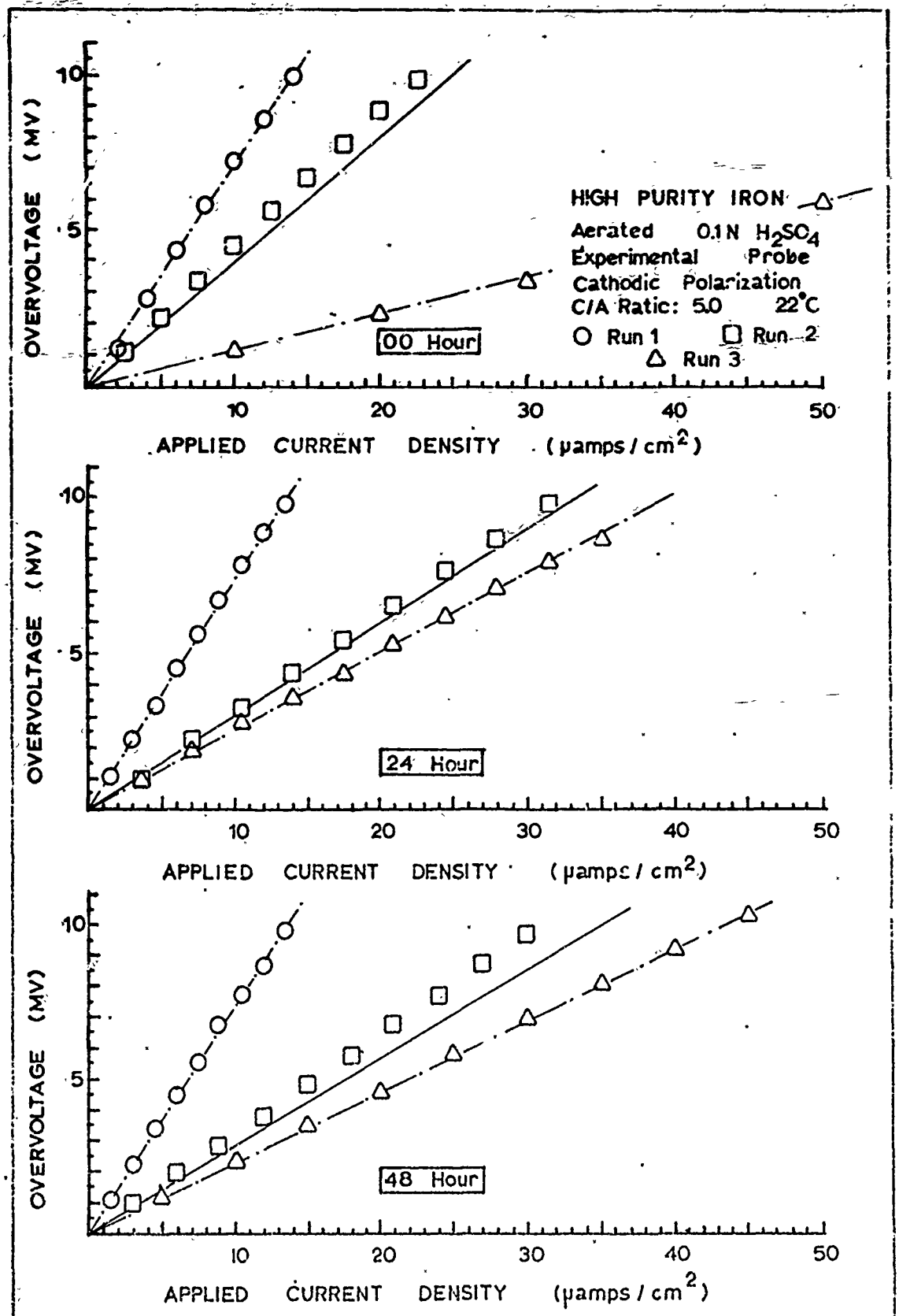

Figure 68: Effect of Time on Galvanostatic Cathodic Polarization Resistance of High Purity Iron with C/A Ratio = 5 in Aerated .1N Sulfuric Acid Determined Using an Experimental Probe. (Cont)

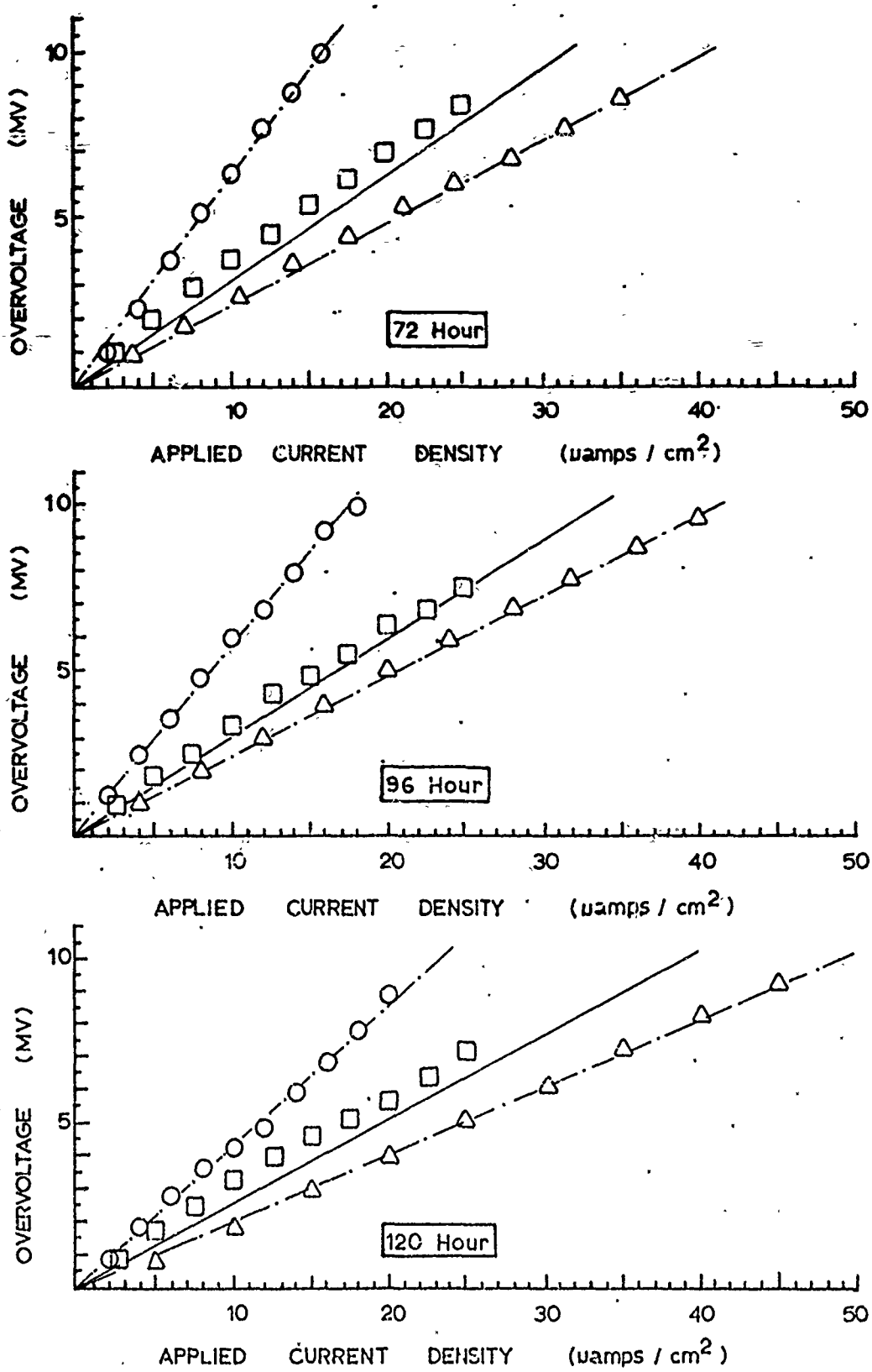

Figure 68: (Cont) Effect of Time on Galvanostatic Cathodic Polarization Resistance of High Purity Iron with C/A Ratio = 5 in Aerated .1N Sulfuric Acid Determined Using an Experimental Probe.

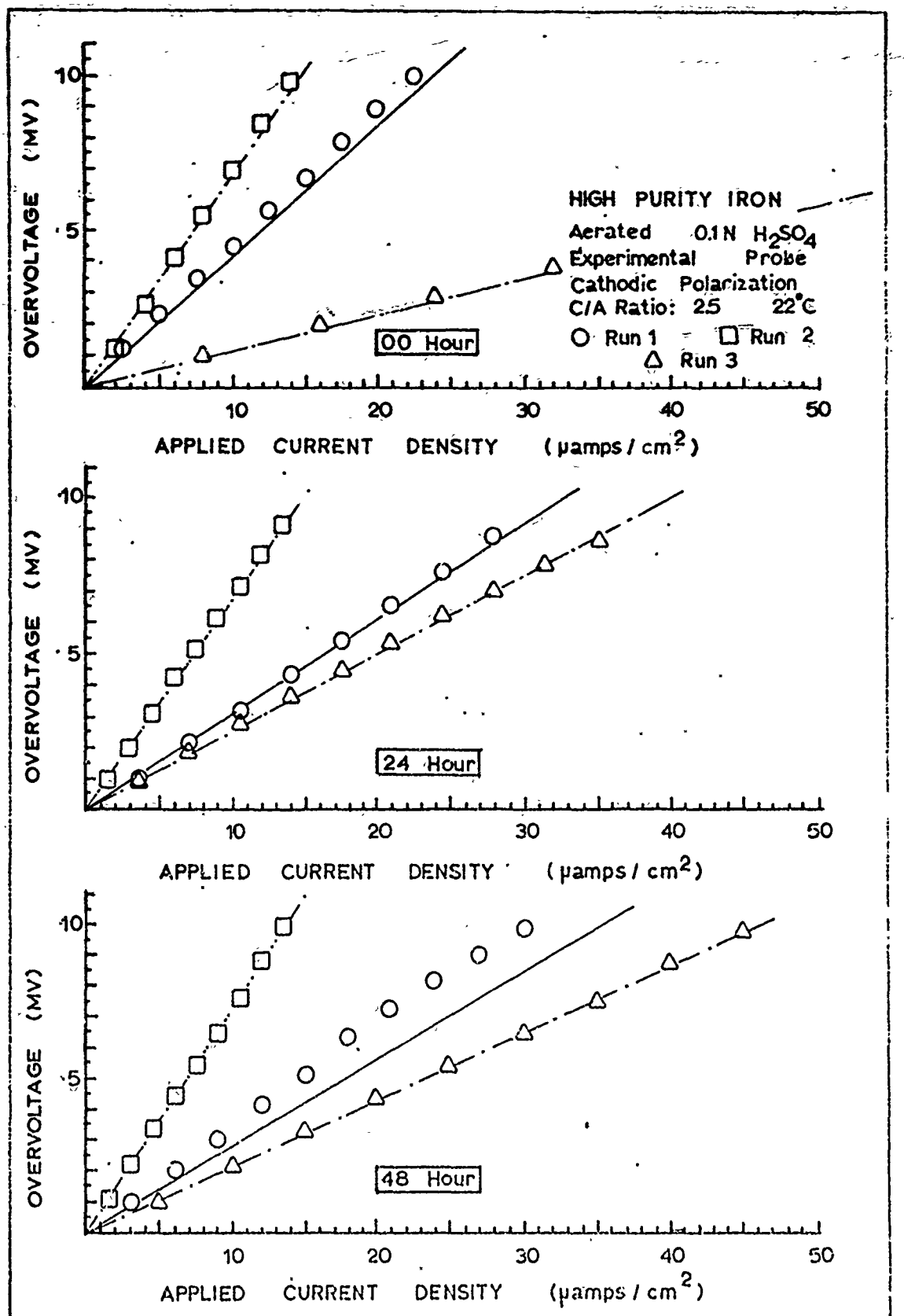

Figure 69: Effect of Time on Galvanostatic Cathodic Polarization Resistance of High Purity Iron with C/A Ratio = 2.5 in Aerated .1N Sulfuric Acid Determined Using an Experimental Probe. (Cont)

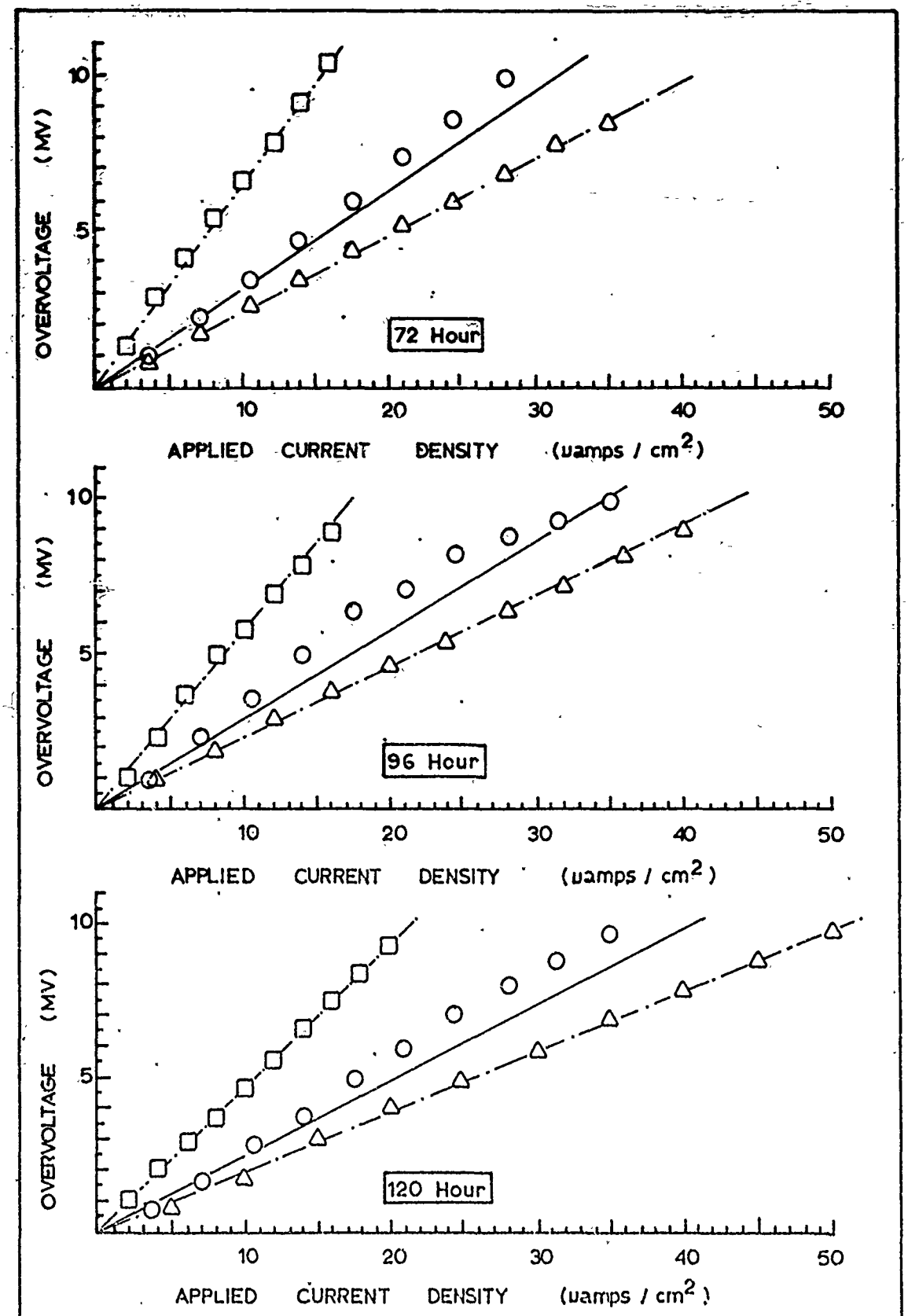

Figure 69: (Cont) Effect of Time on Galvanostatic Cathodic Polarization Resistance of High Purity Iron with C/A Ratio = 2.5 in Aerated .1N Sulfuric Acid Determined Using an Experimental Probe.

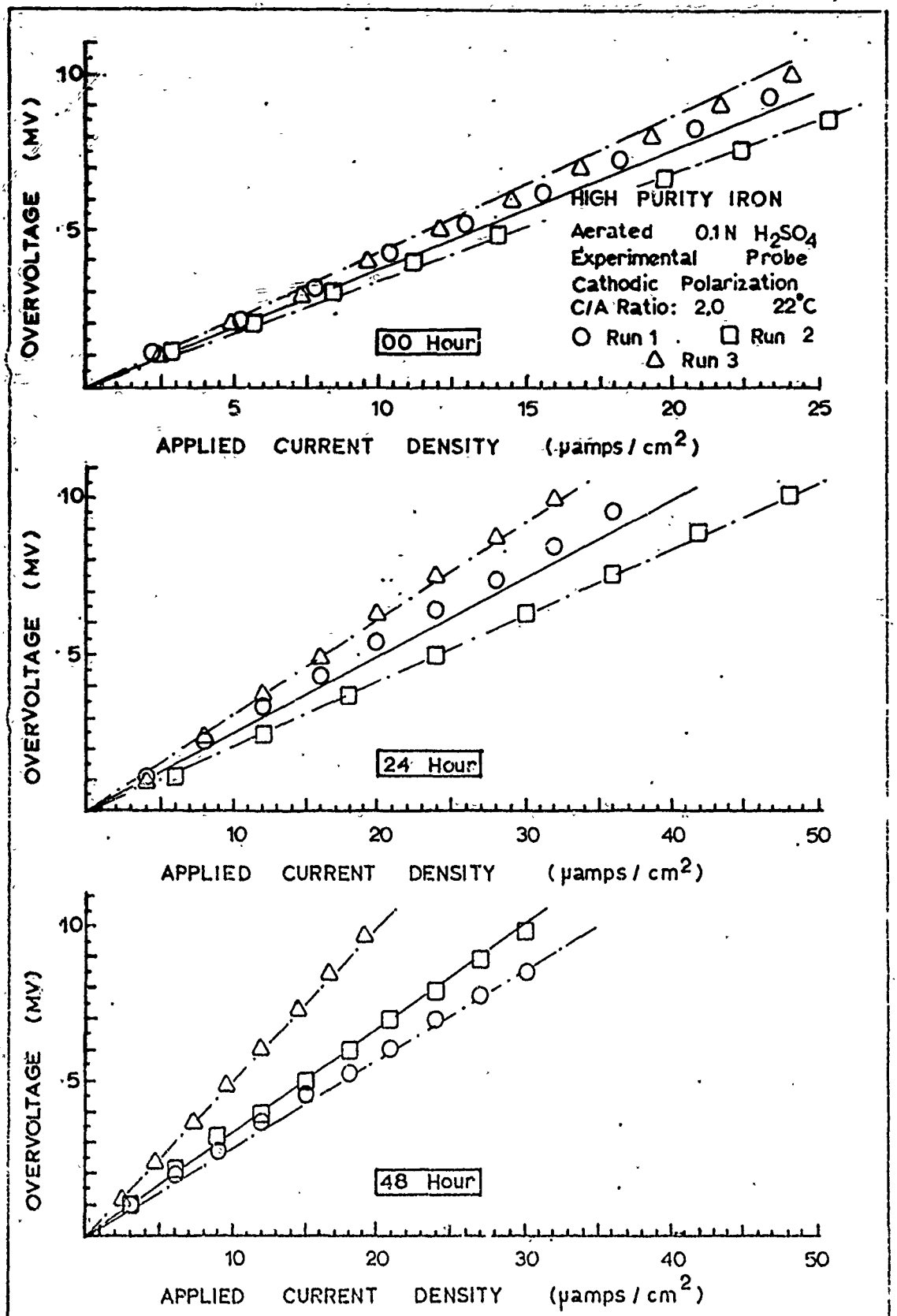

Figure 70: Effect of Time on Galvanostatic Cathodic Polarization Resistance of High Purity Iron with C/A Ratio = 2 in Aerated .1N Sulfuric Acid Determined Using an Experimental Probe. (Cont)

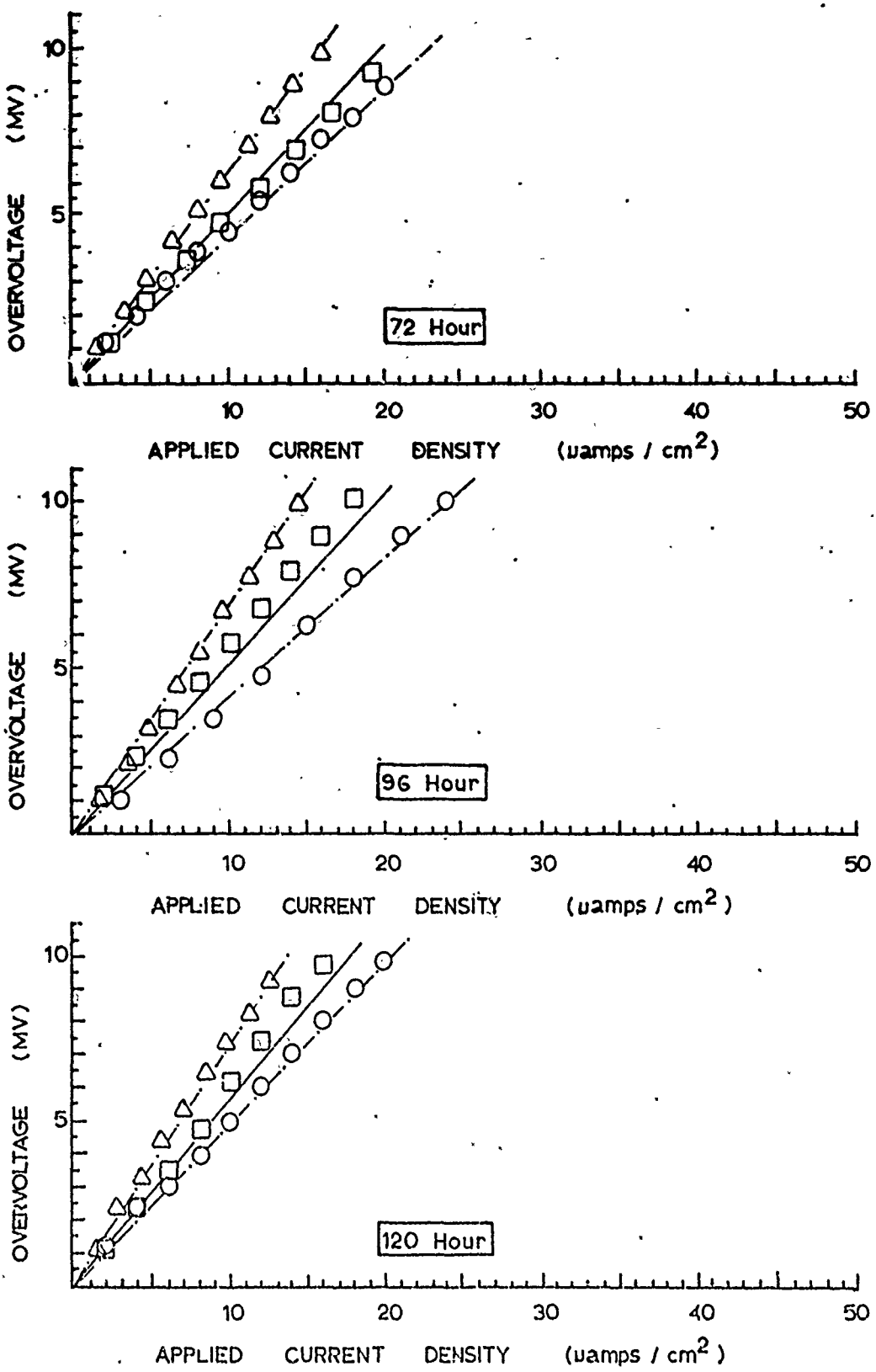

Figure 70: (Cont) Effect of Time on Galvanostatic Cathodic Polarization Resistance of High Purity Iron with C/A Ratio = 2 in Aerated .1N Sulfuric Acid Determined Using an Experimental Probe.

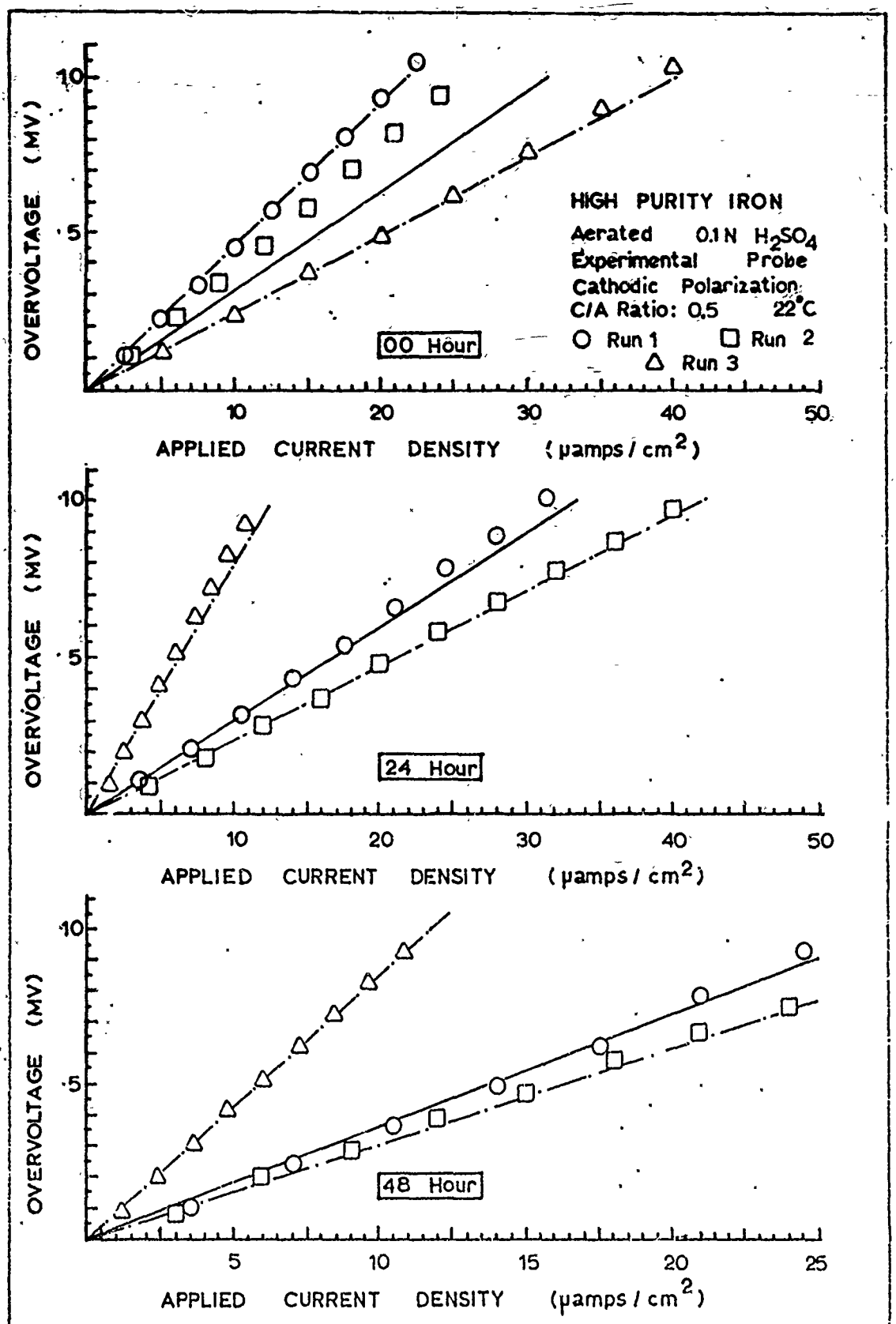

Figure 71: Effect of Time on Galvanostatic Cathodic Polarization Resistance of High Purity Iron with C/A Ratio = .5 in Aerated .1N Sulfuric Acid Determined Using an Experimental Probe. (Cont)

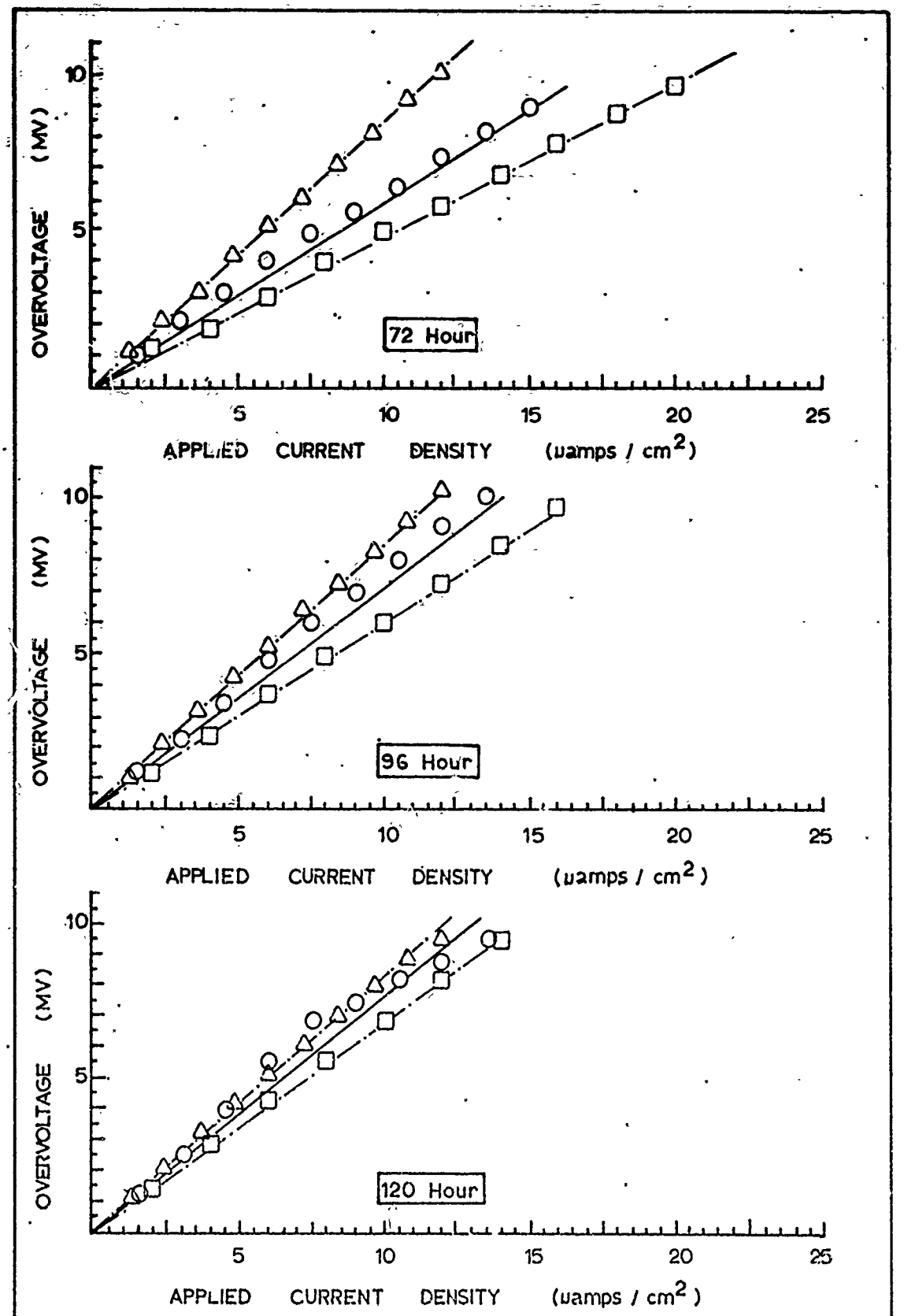

Figure 71: (Cont) Effect of Time on Galvanostatic Cathodic Polarization Resistance of High Purity Iron with C/A Ratio = .5 in Aerated .1N Sulfuric Acid Determined Using an Experimental Probe.

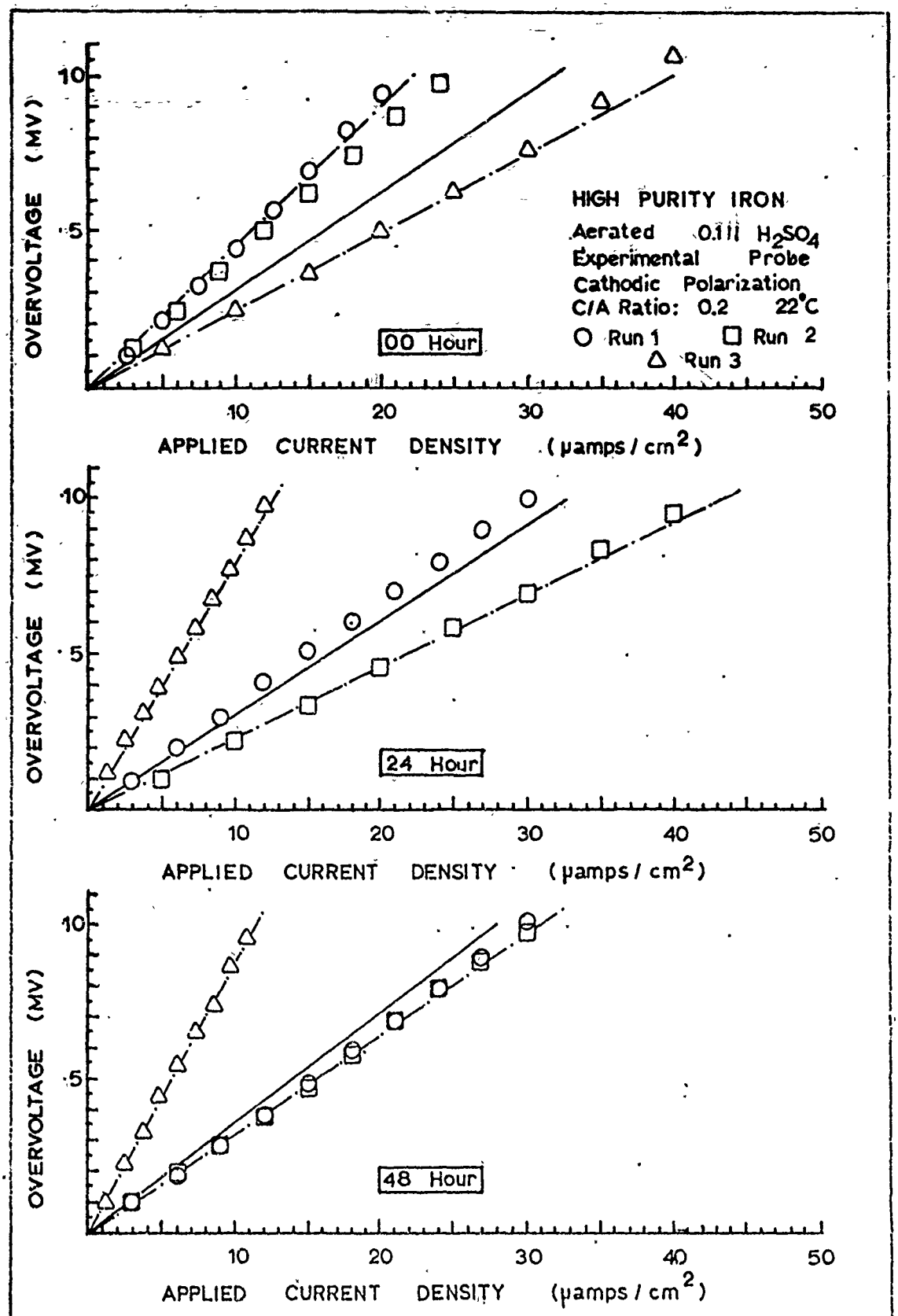

Figure 72: Effect of Time on Galvanostatic Cathodic Polarization Resistance of High Purity Iron with C/A Ratio = .2 in Aerated .1N Sulfuric Acid Determined Using an Experimental Probe. (Cont)

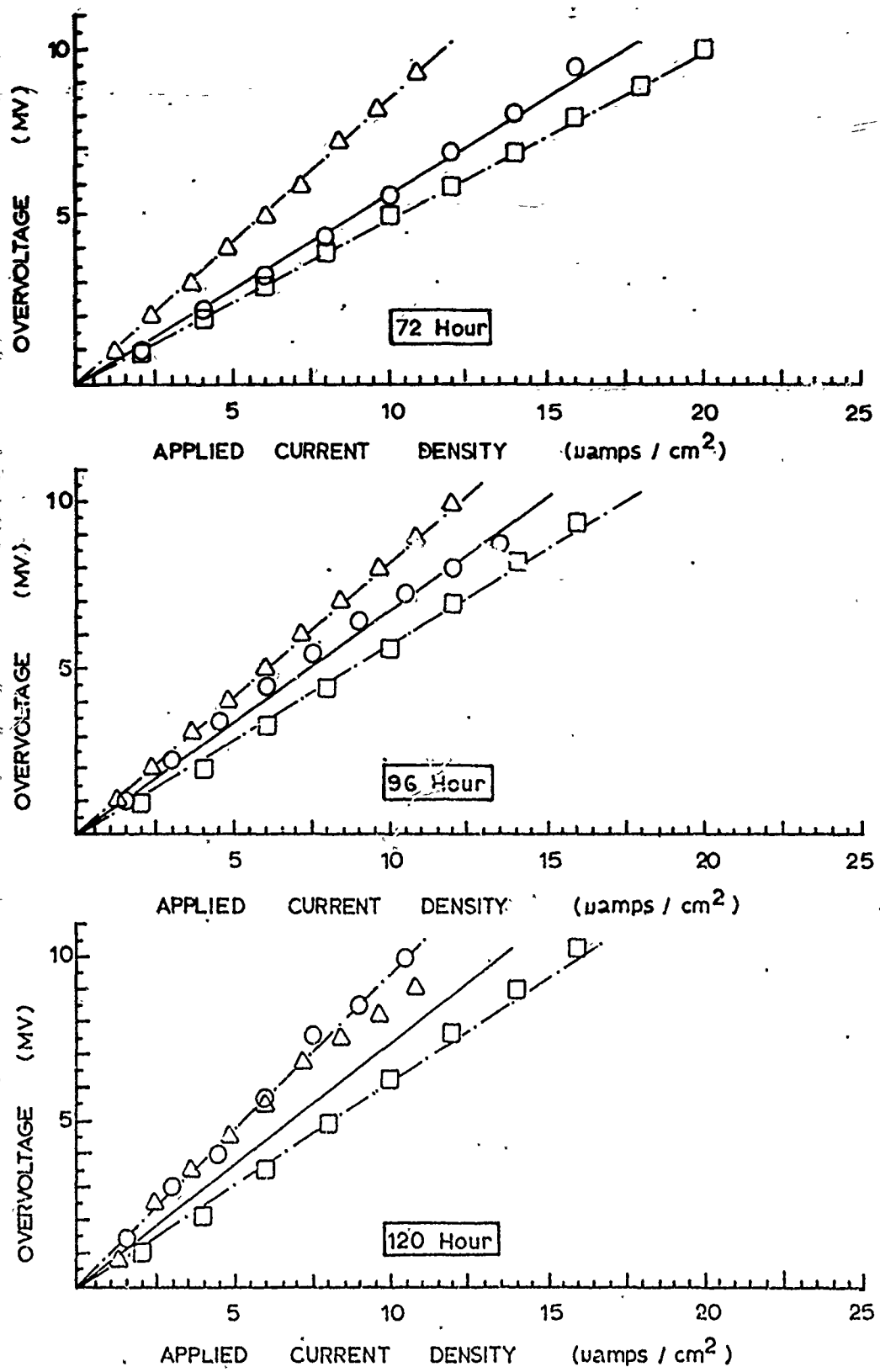

Figure 72: (Cont) Effect of Time on Galvanostatic Cathodic Polarization Resistance of High Purity Iron with C/A Ratio = .2 in Aerated .1N Sulfuric Acid Determined Using an Experimental Probe.

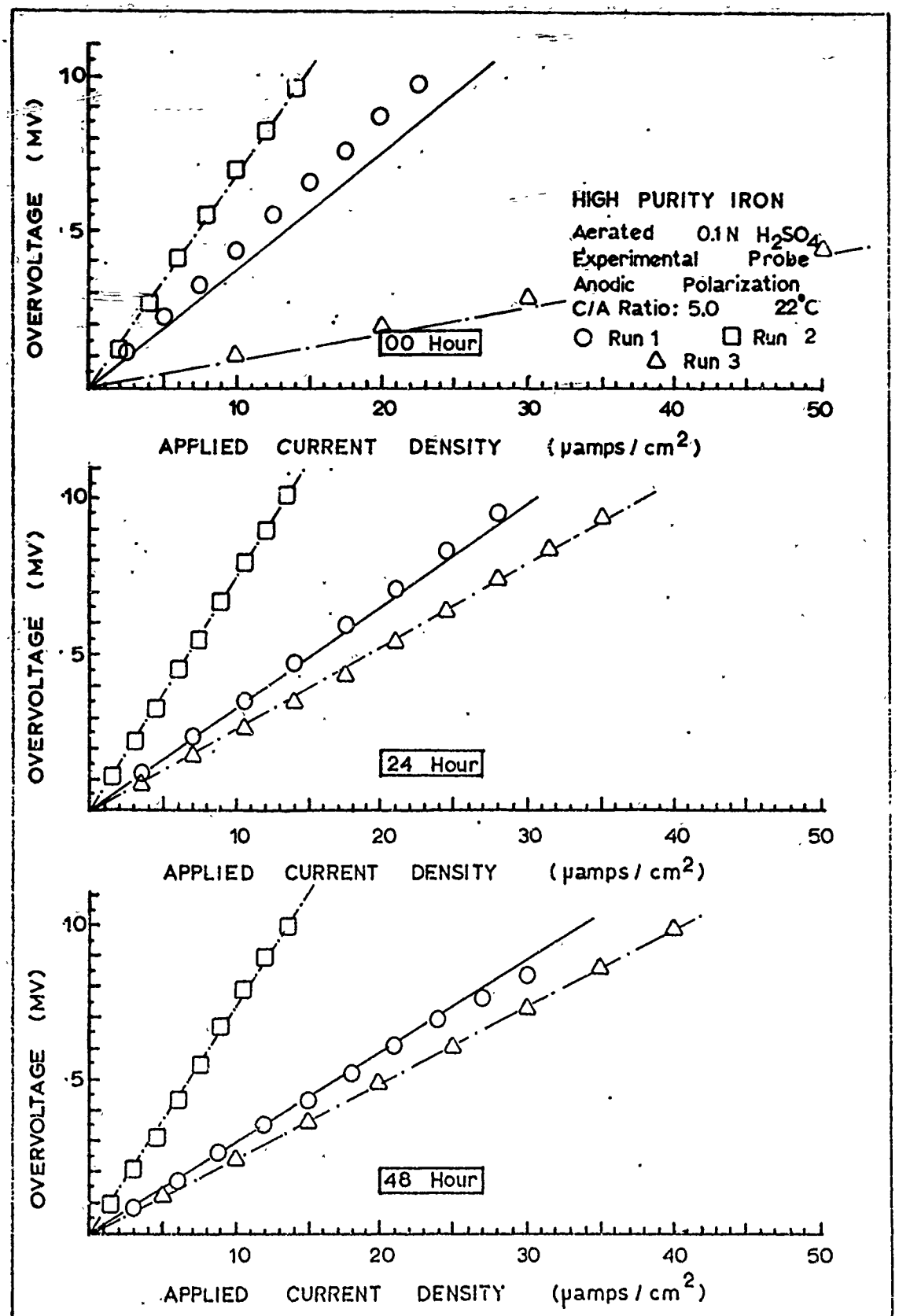

Figure 73: Effect of Time on Galvanostatic Anodic Polarization Resistance of High Purity Iron with C/A Ratio = 5 in Aerated .1N Sulfuric Acid Determined Using an Experimental Probe. (Cont)

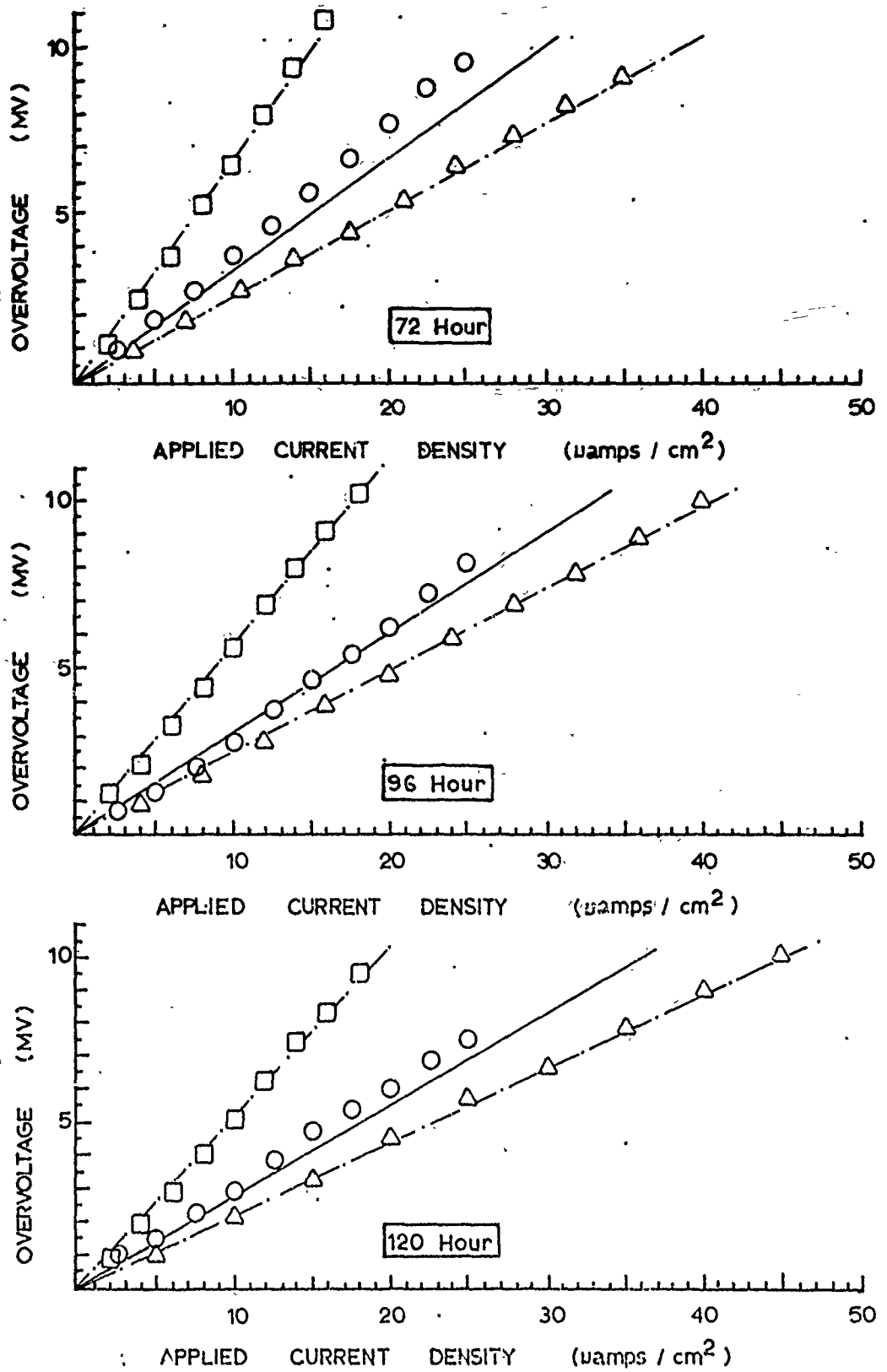

Figure 73: (Cont) Effect of Time on Galvanostatic Anodic Polarization Resistance of High Purity Iron with C/A Ratio = 5 in Aerated .1N Sulfuric Acid Determined Using an Experimental Probe.

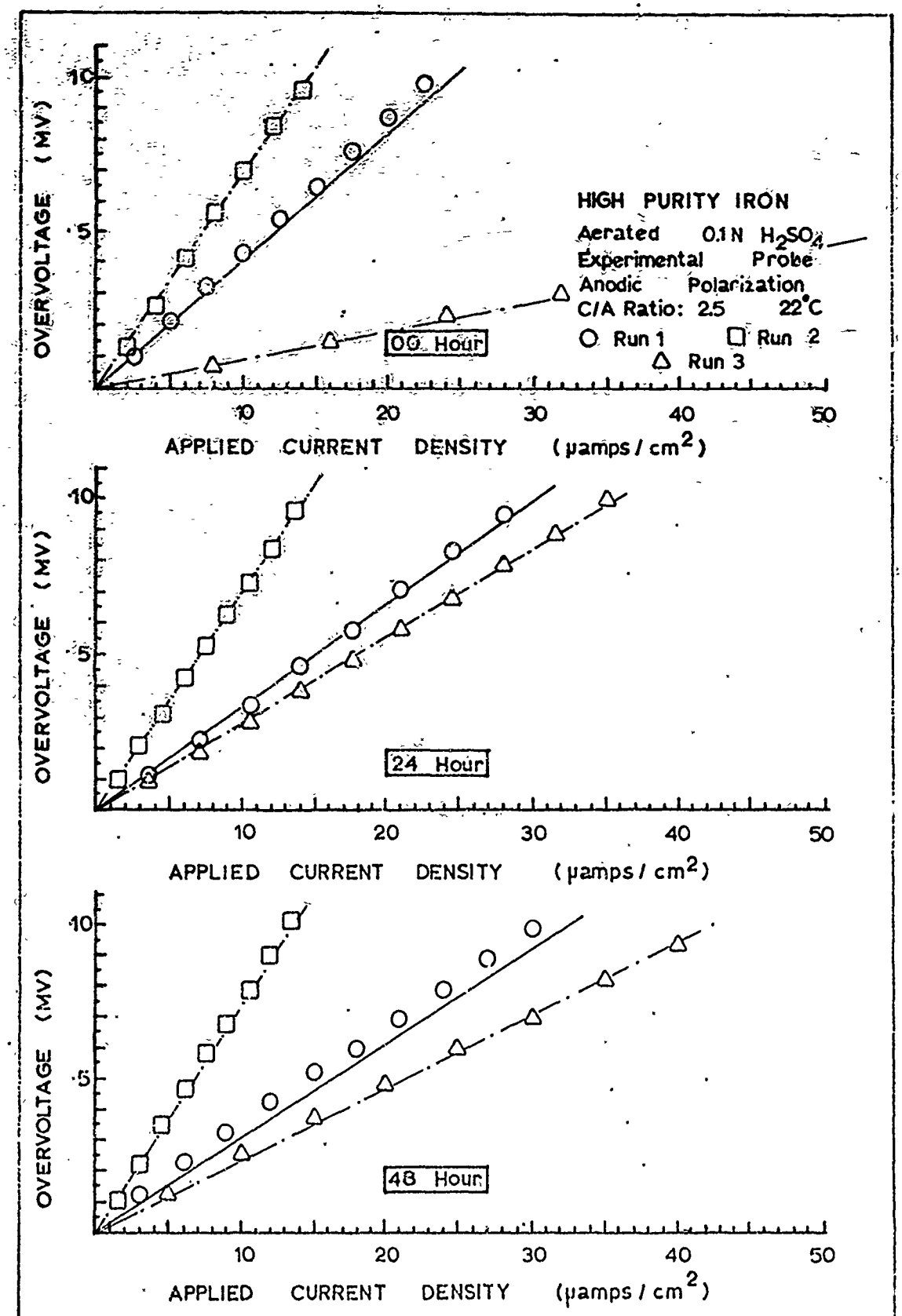

Figure 74: Effect of Time on Galvanostatic Anodic Polarization Resistance of High Purity Iron with C/A Ratio = 2.5 in Aerated .1N Sulfuric Acid Determined Using an Experimental Probe. (Cont)

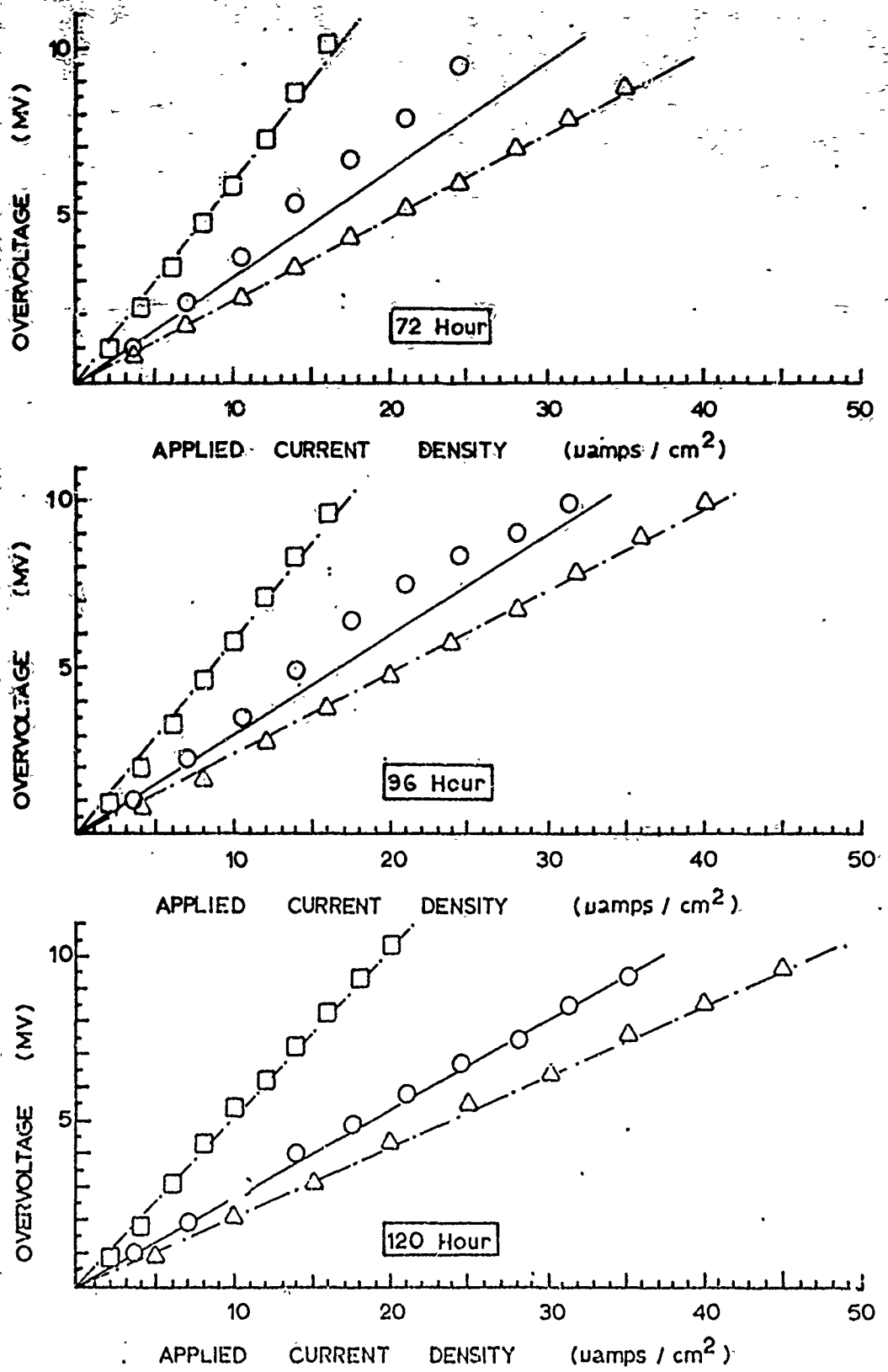

Figure 74: (Cont) Effect of Time on Galvanostatic Anodic Polarization Resistance of High Purity Iron with C/A Ratio = 2.5 in Aerated .1N Sulfuric Acid Determined Using an Experimental Probe.

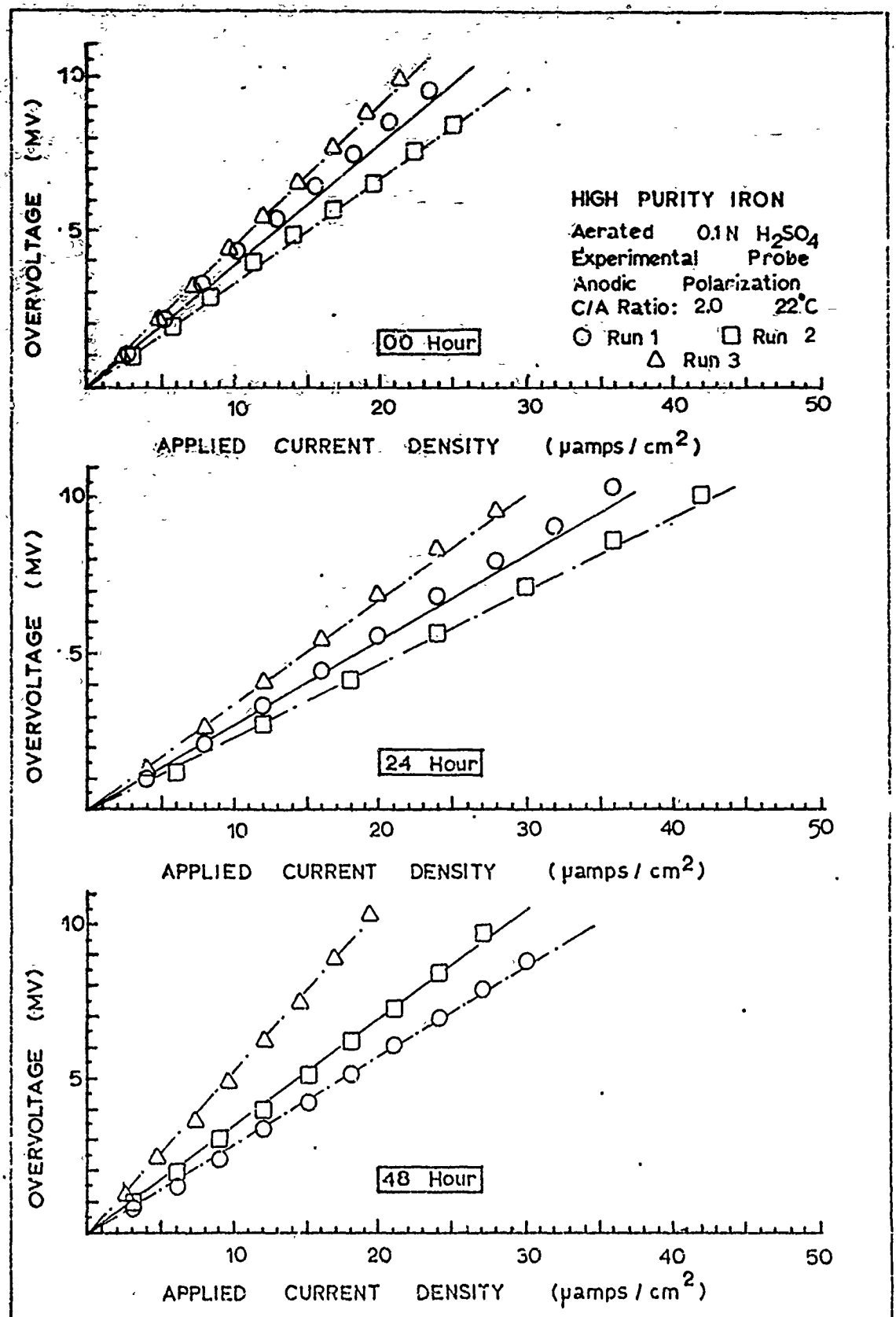

Figure 75: Effect of Time on Galvanostatic Anodic Polarization Resistance of High Purity Iron with C/A Ratio = 2 in Aerated .1N Sulfuric Acid Determined Using an Experimental Probe. (Cont)

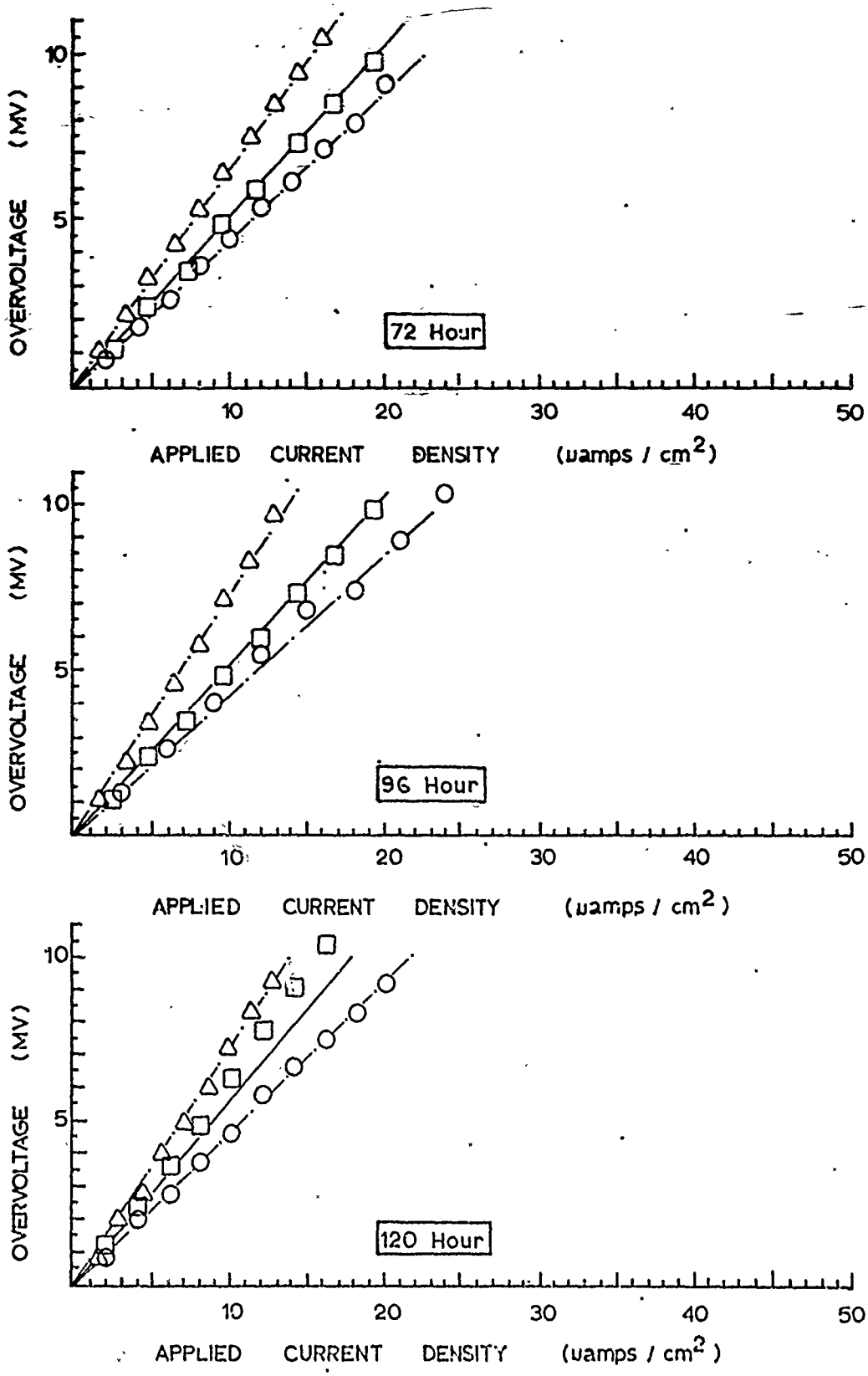

Figure 75: (Cont) Effect of Time on Galvanostatic Anodic Polarization Resistance of High Purity Iron with C/A Ratio = 2 in Aerated .1N Sulfuric Acid Determined Using an Experimental Probe.

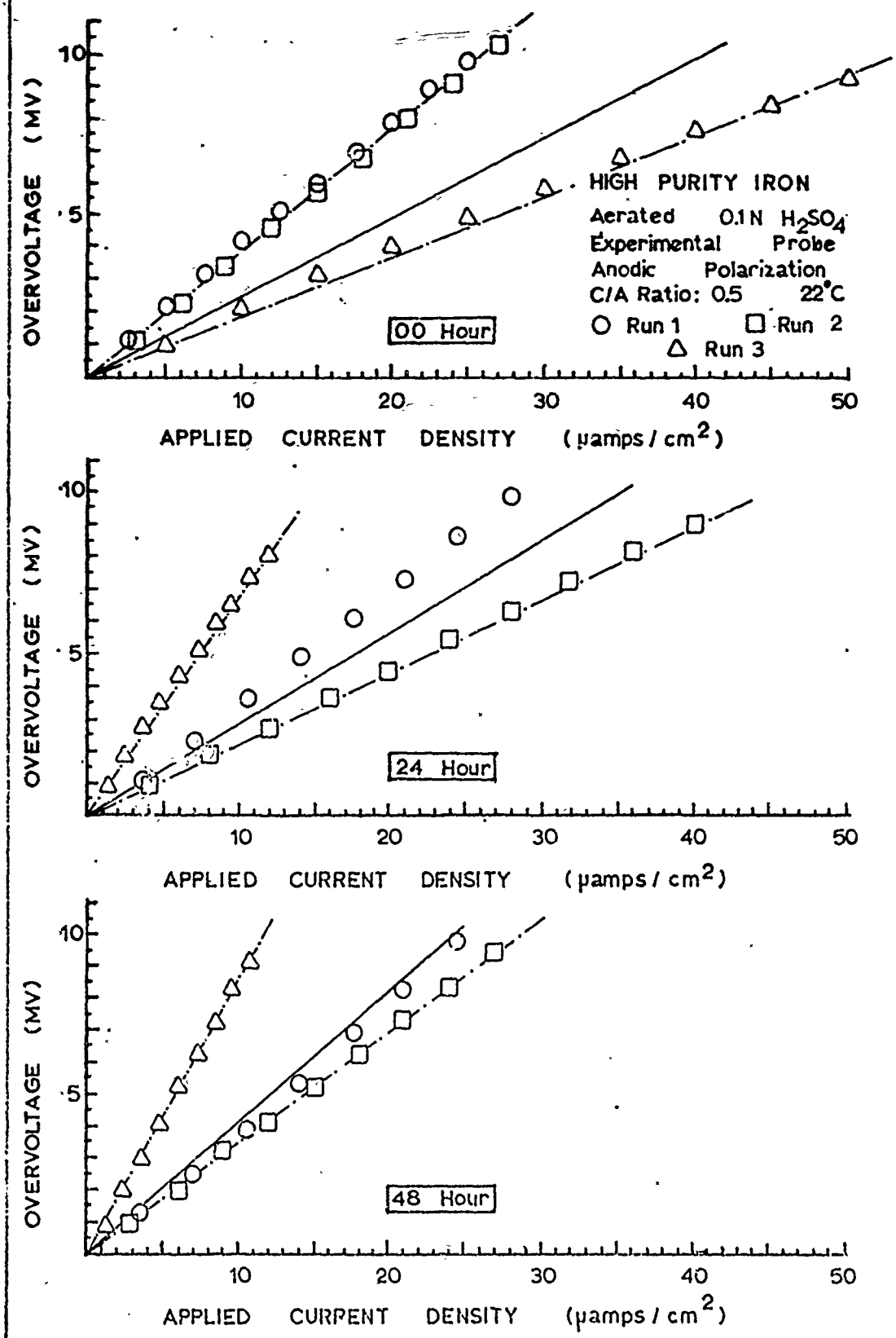

Figure 76: Effect of Time on Galvanostatic Anodic Polarization Resistance of High Purity Iron with C/A Ratio = .5 in Aerated .1N Sulfuric Acid Determined Using an Experimental Probe. (Cont)

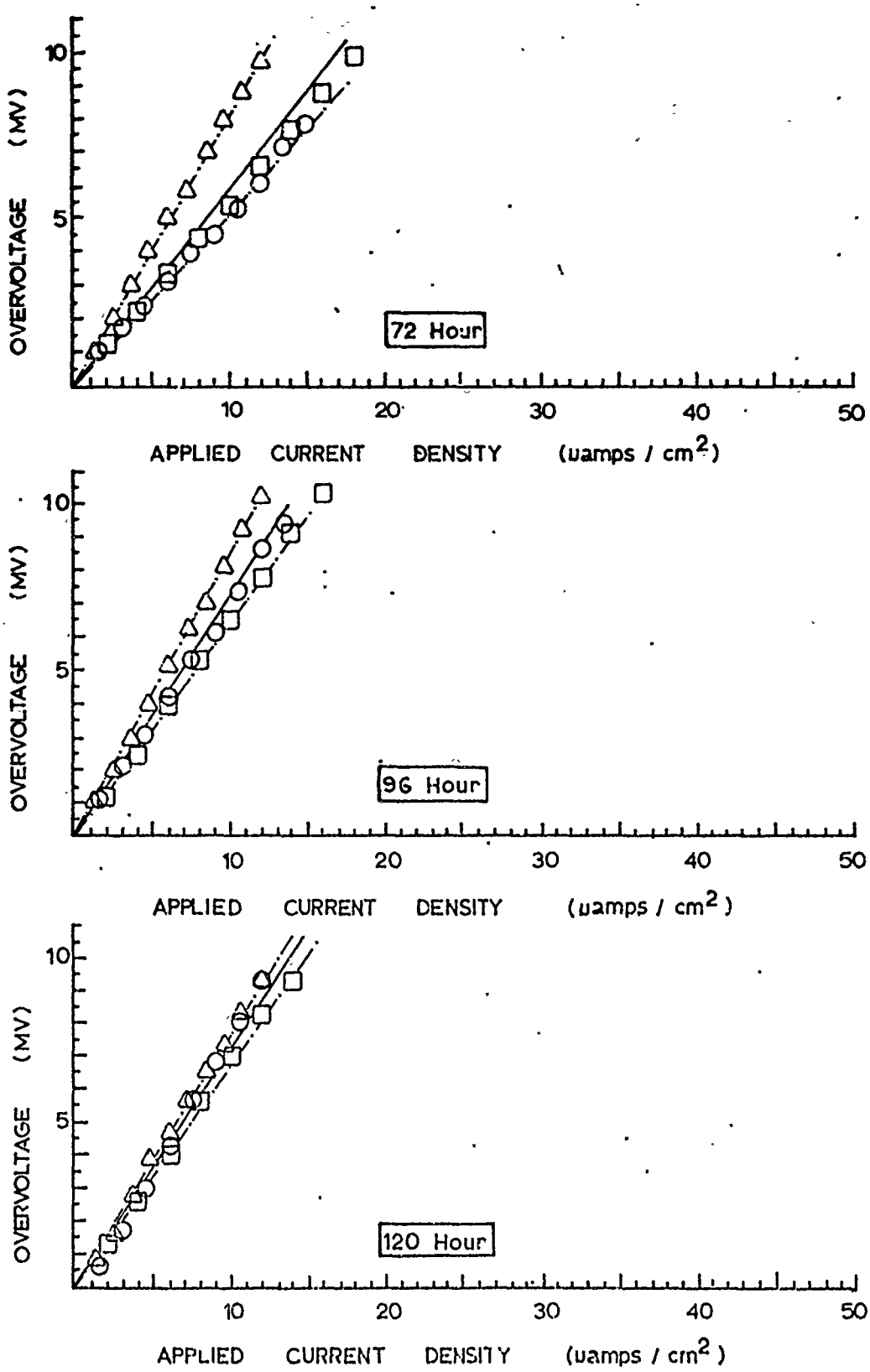

Figure 76: (Cont) Effect of Time on Galvanostatic Anodic Polarization Resistance of High Purity Iron with C/A Ratio = .5 in Aerated .1N Sulfuric Acid Determined Using an Experimental Probe.

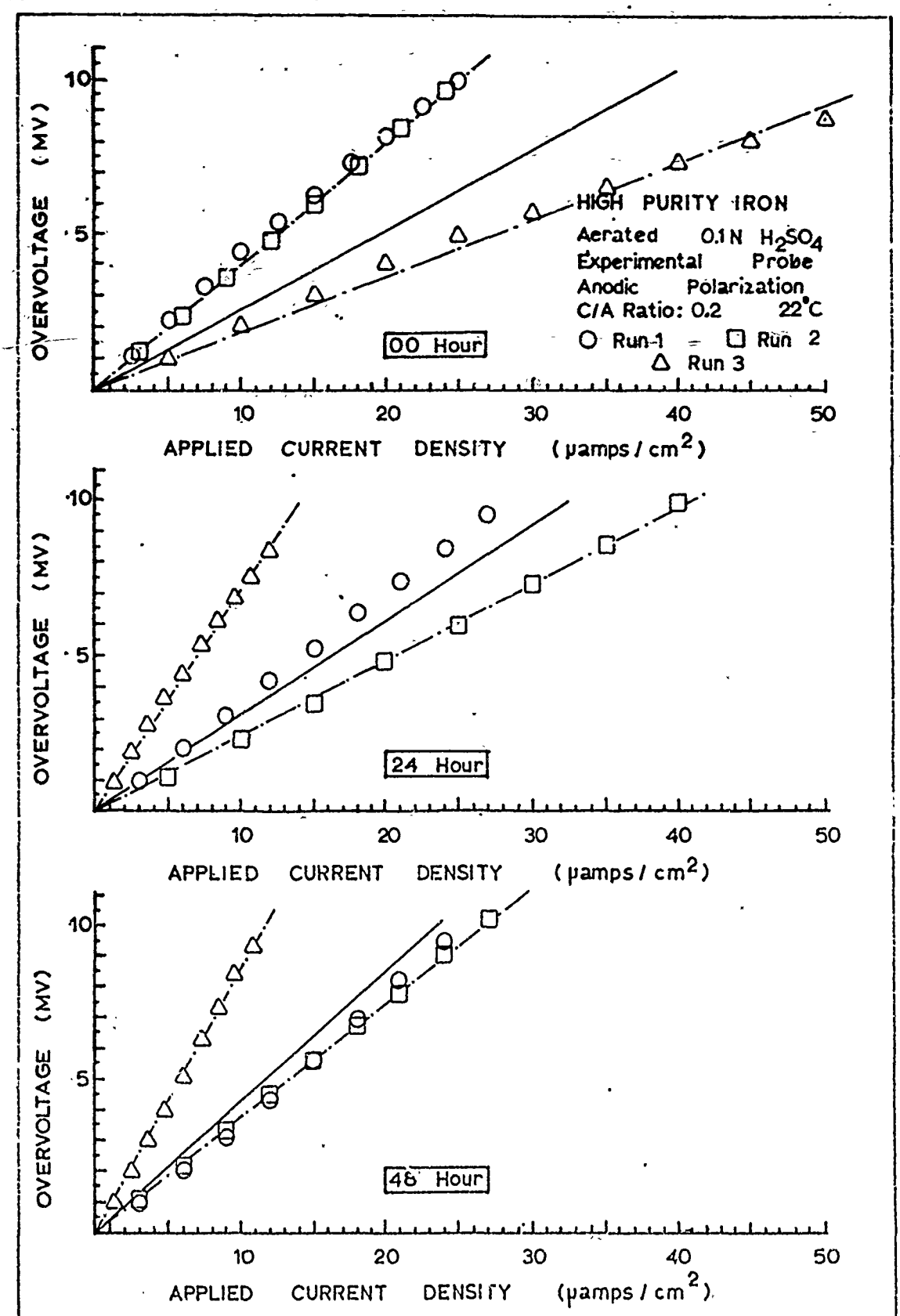

Figure 77: Effect of Time on Galvanostatic Anodic Polarization Resistance of High Purity Iron with C/A Ratio = .2 in Aerated .1N Sulfuric Acid Determined Using an Experimental Probe. (Cont)

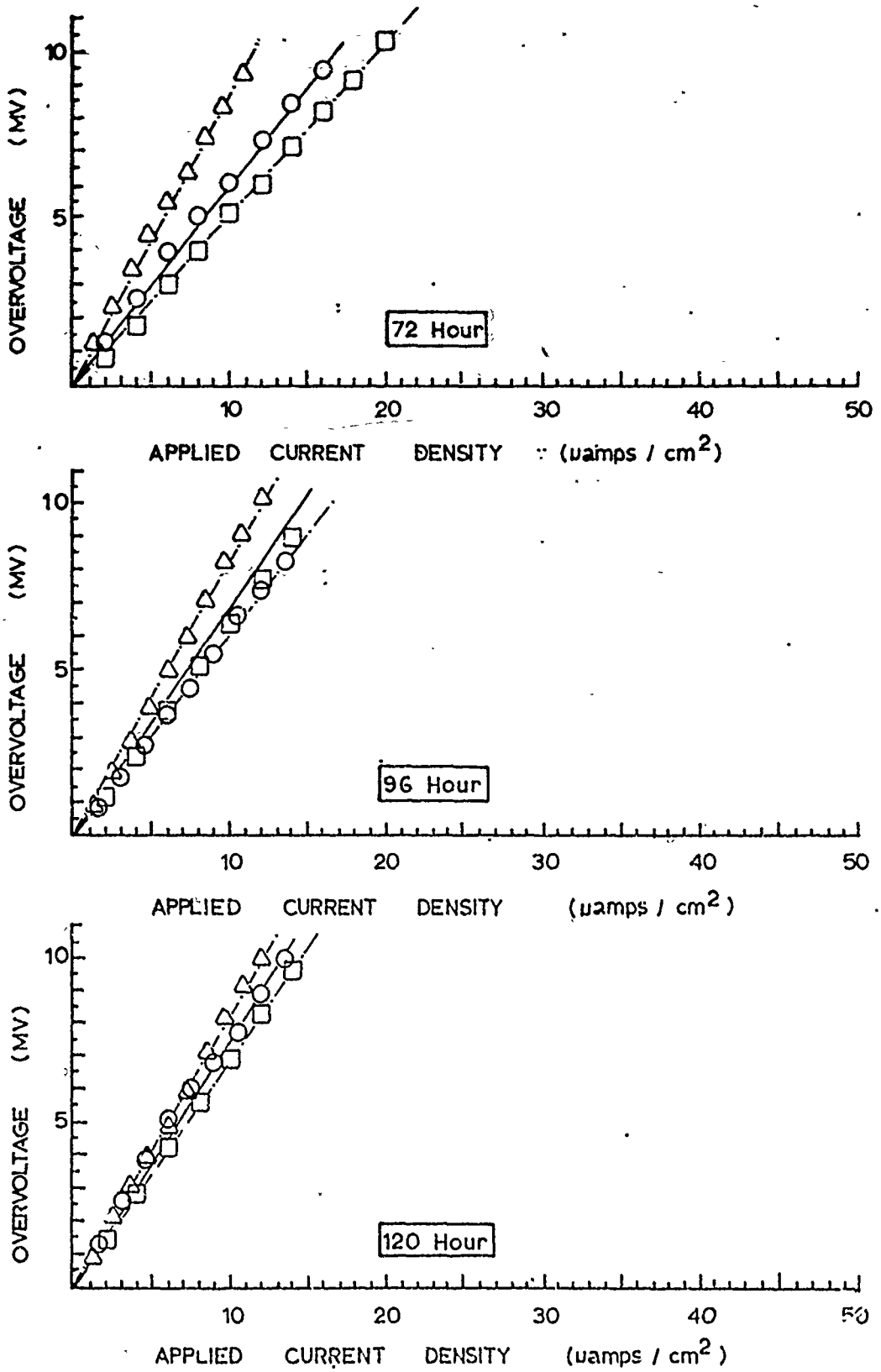

Figure 77: (Cont) Effect of Time on Galvanostatic Anodic Polarization Resistance of High Purity Iron with C/A Ratio = .2 in Aerated .1N Sulfuric Acid Determined Using an Experimental Probe.

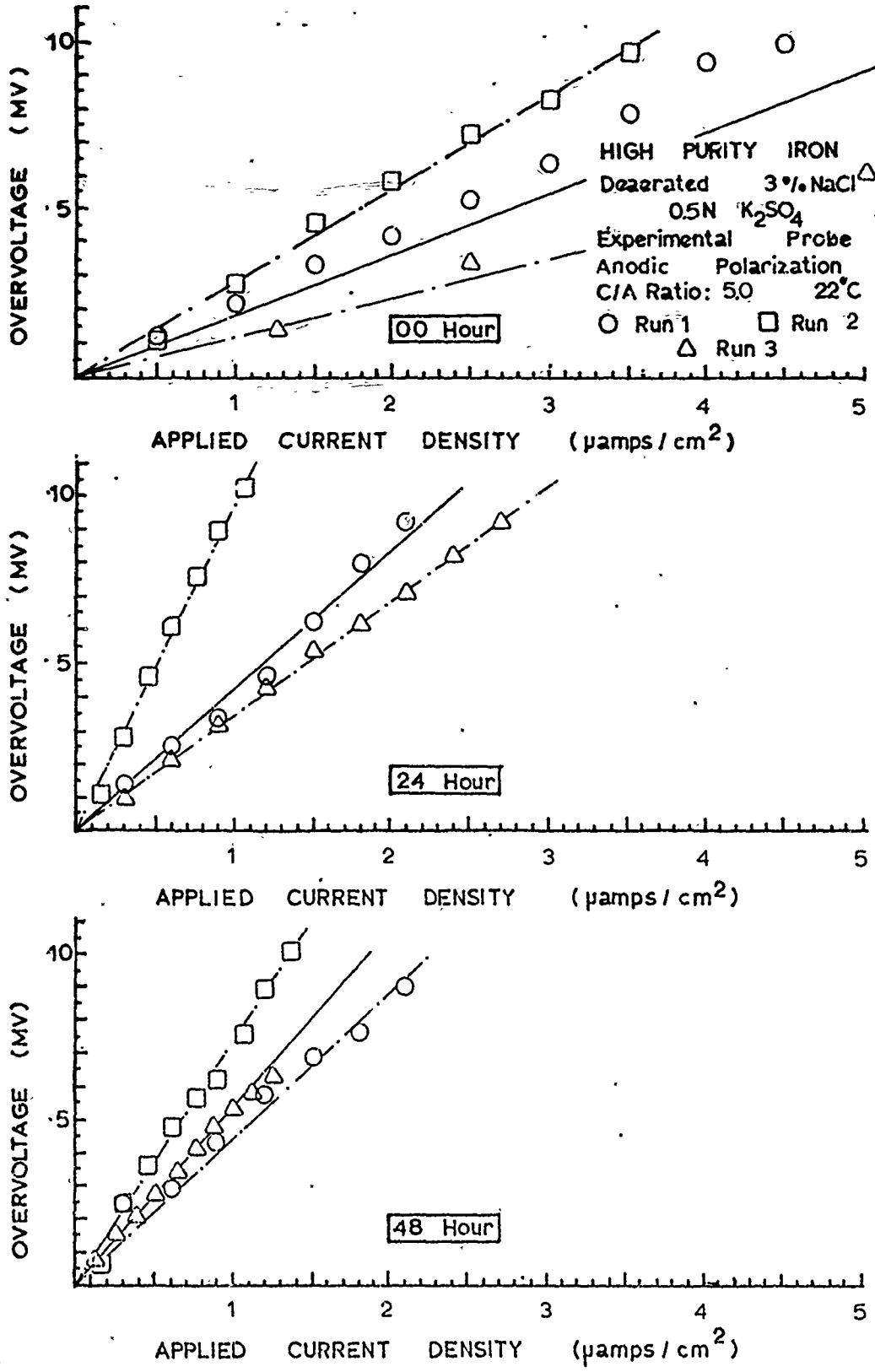

Figure 78: Effect of Time on Galvanostatic Anodic Polarization Resistance of High Purity Iron with C/A Ratio = 5 in Hydrogen Saturated 3% Sodium Chloride Determined Using an Experimental Probe. (Cont)

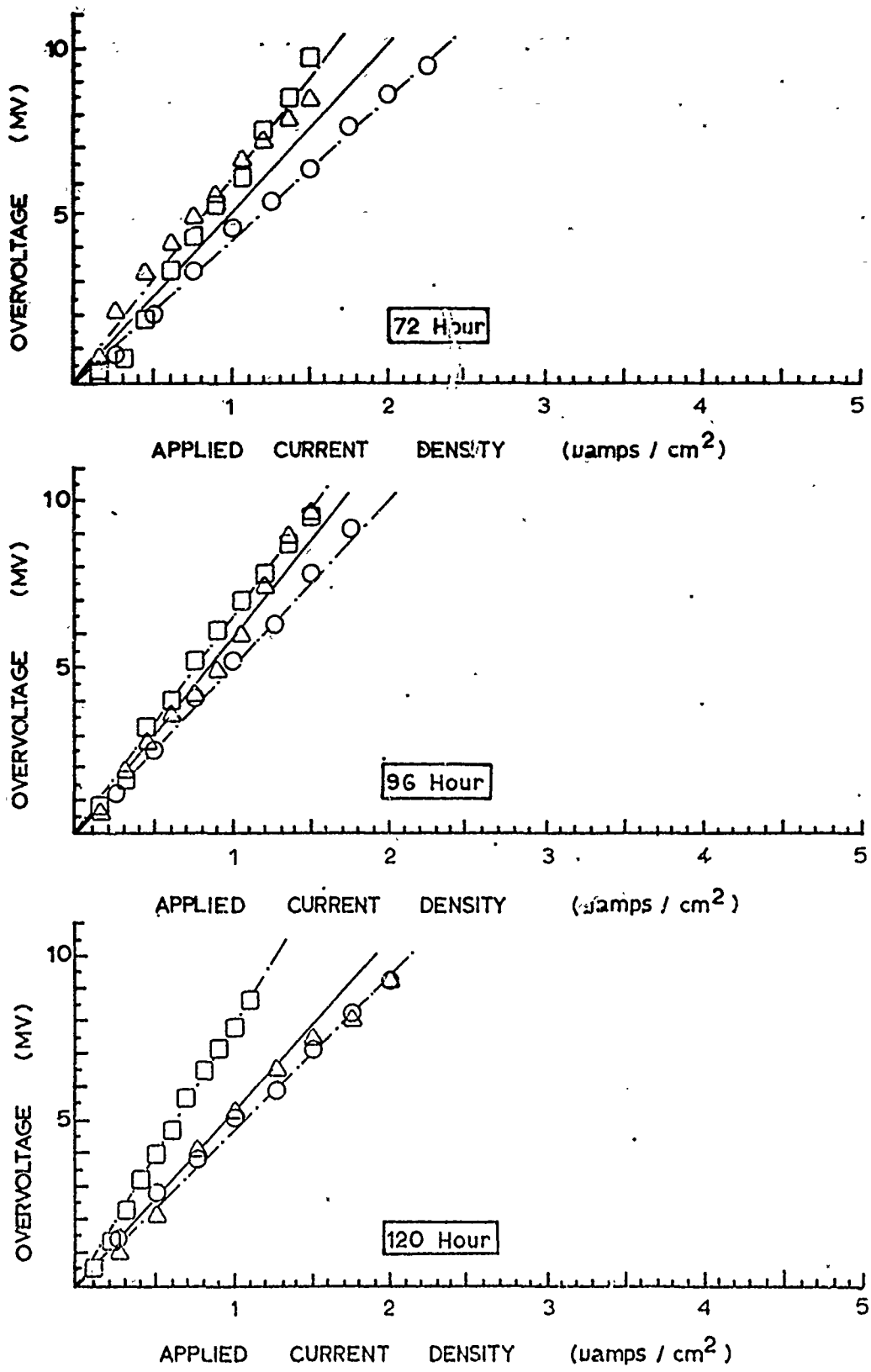

Figure 78: (Cont) Effect of Time on Galvanostatic Anodic Polarization Resistance of High Purity Iron with C/A Ratio = 5 in Hydrogen Saturated 3% Sodium Chloride Determined Using an Experimental Probe.

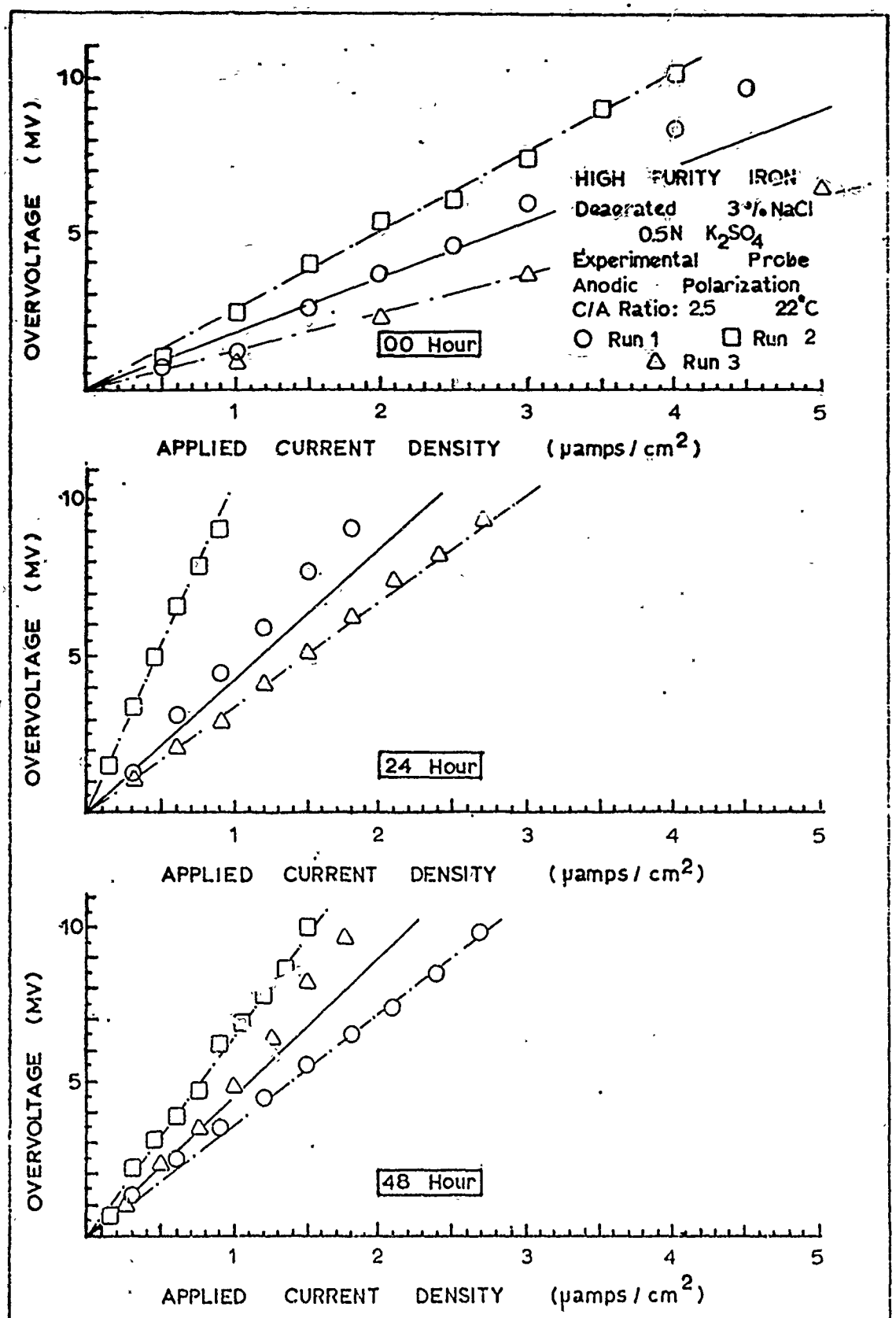

Figure 79: Effect of Time on Galvanostatic Anodic Polarization Resistance of High Purity Iron with C/A Ratio = 2.5 in Hydrogen Saturated 3% Sodium Chloride Determined Using an Experimental Probe. (Cont)

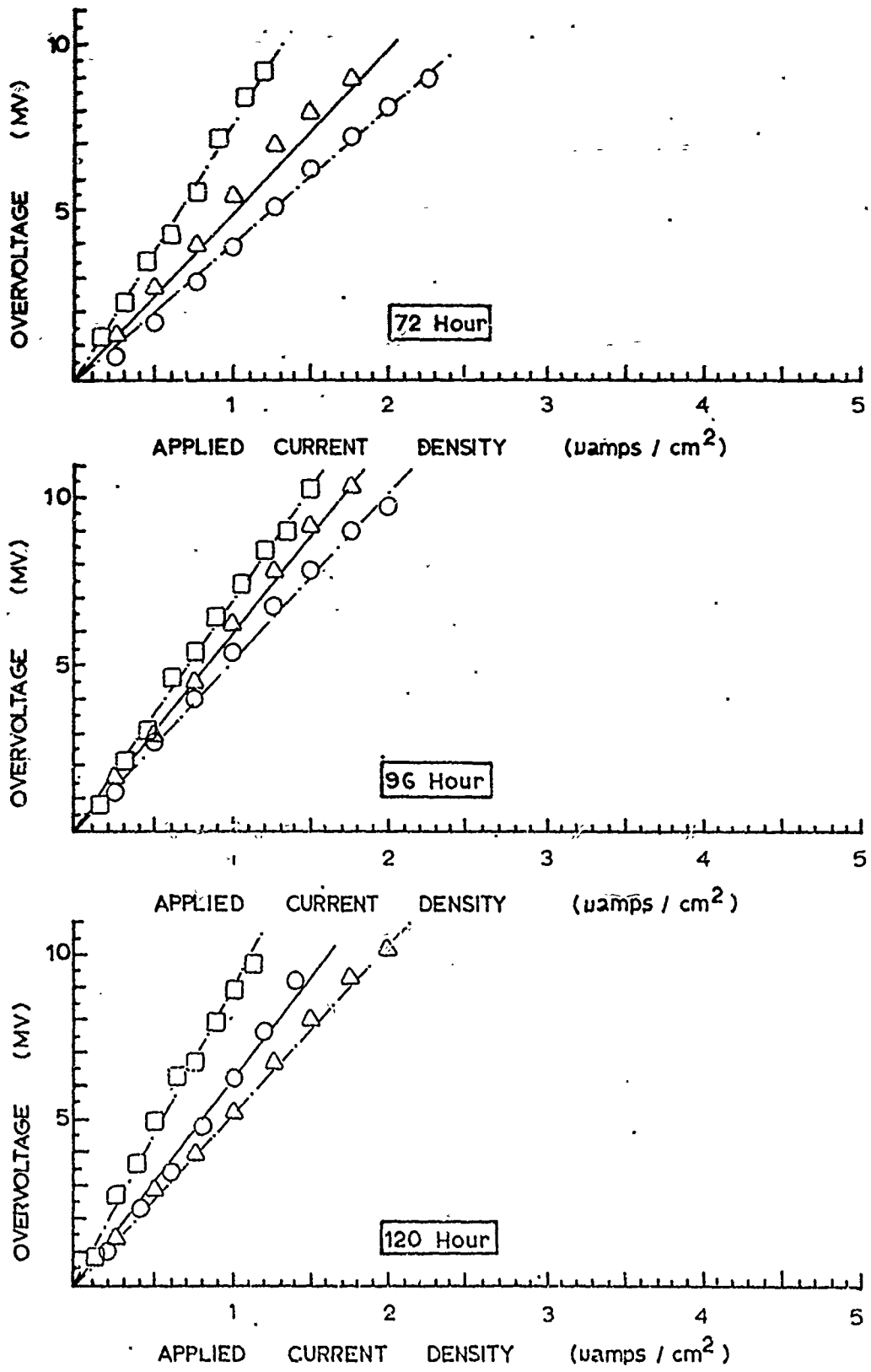

Figure 79: (Cont) Effect of Time on Galvanostatic Anodic Polarization Resistance of High Purity Iron with C/A Ratio = 2.5 in Hydrogen Saturated 3% Sodium Chloride Determined Using an Experimental Probe.

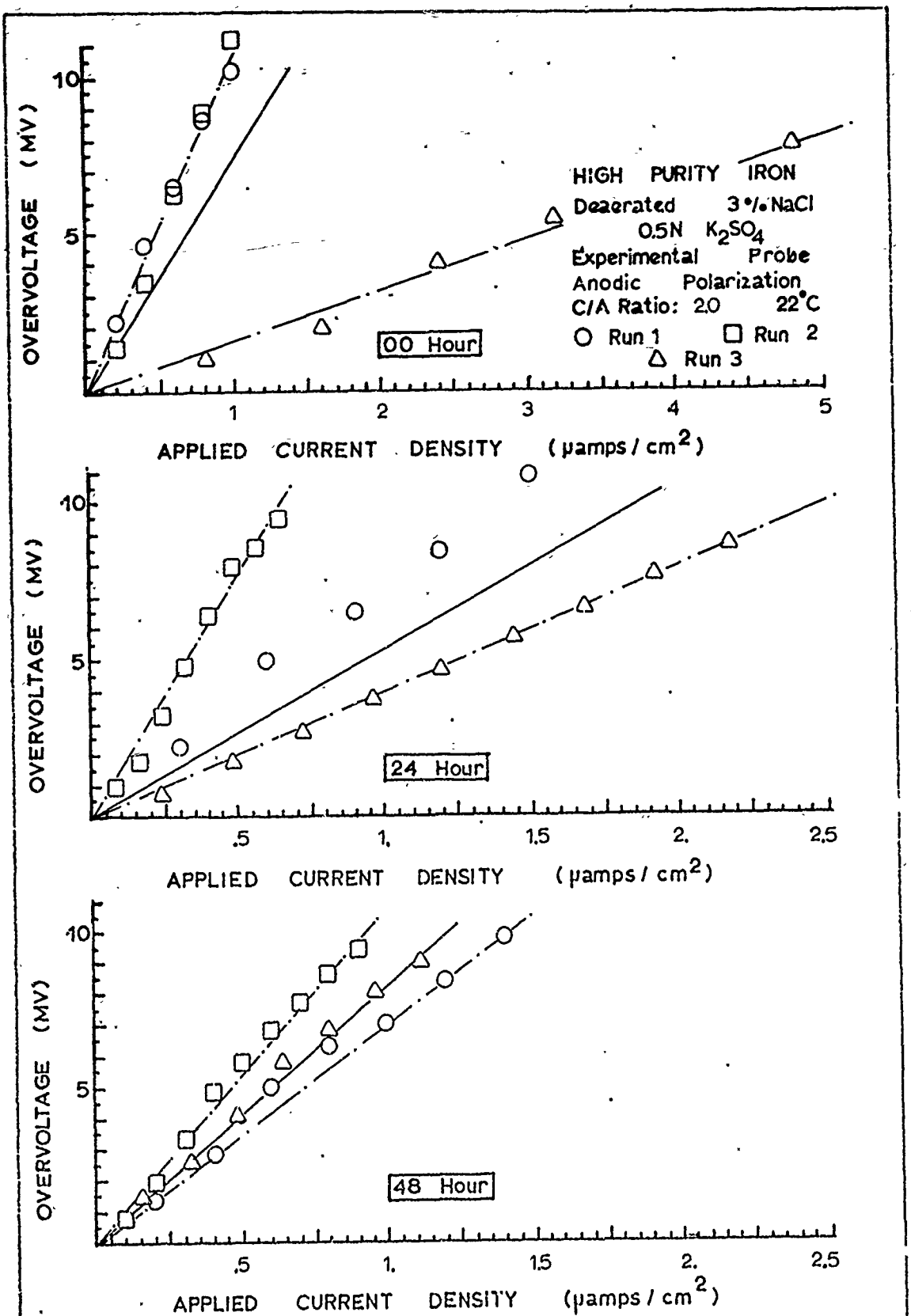

Figure 80: Effect of Time on Galvanostatic Anodic Polarization Resistance of High Purity Iron with C/A Ratio = 2 in Hydrogen Saturated 3% Sodium Chloride Determined Using an Experimental Probe. (Cont)

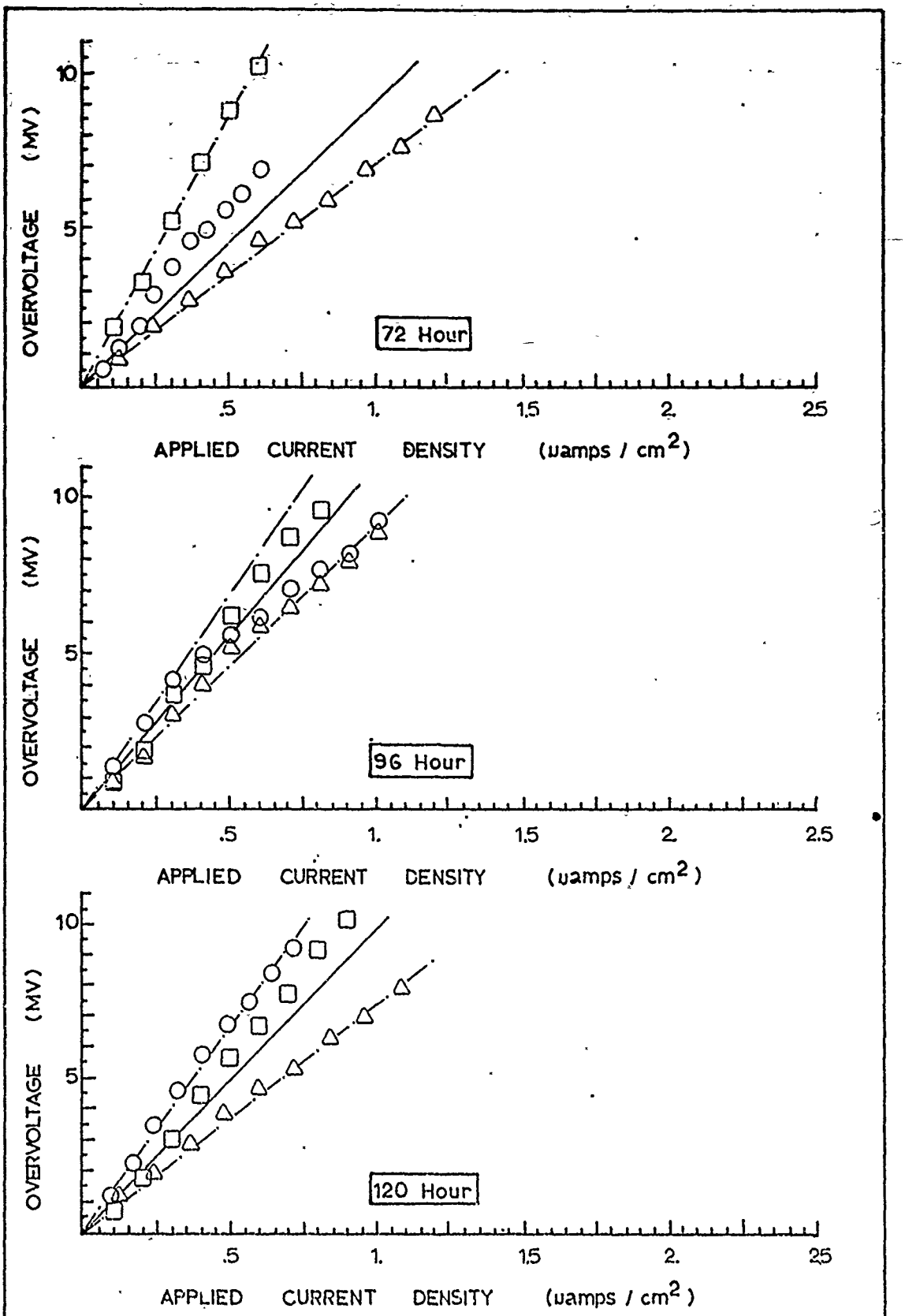

Figure 80: (Cont) Effect of Time on Galvanostatic Anodic Polarization Resistance of High Purity Iron with C/A Ratio = 2 in Hydrogen Saturated 3% Sodium Chloride Determined Using an Experimental Probe.

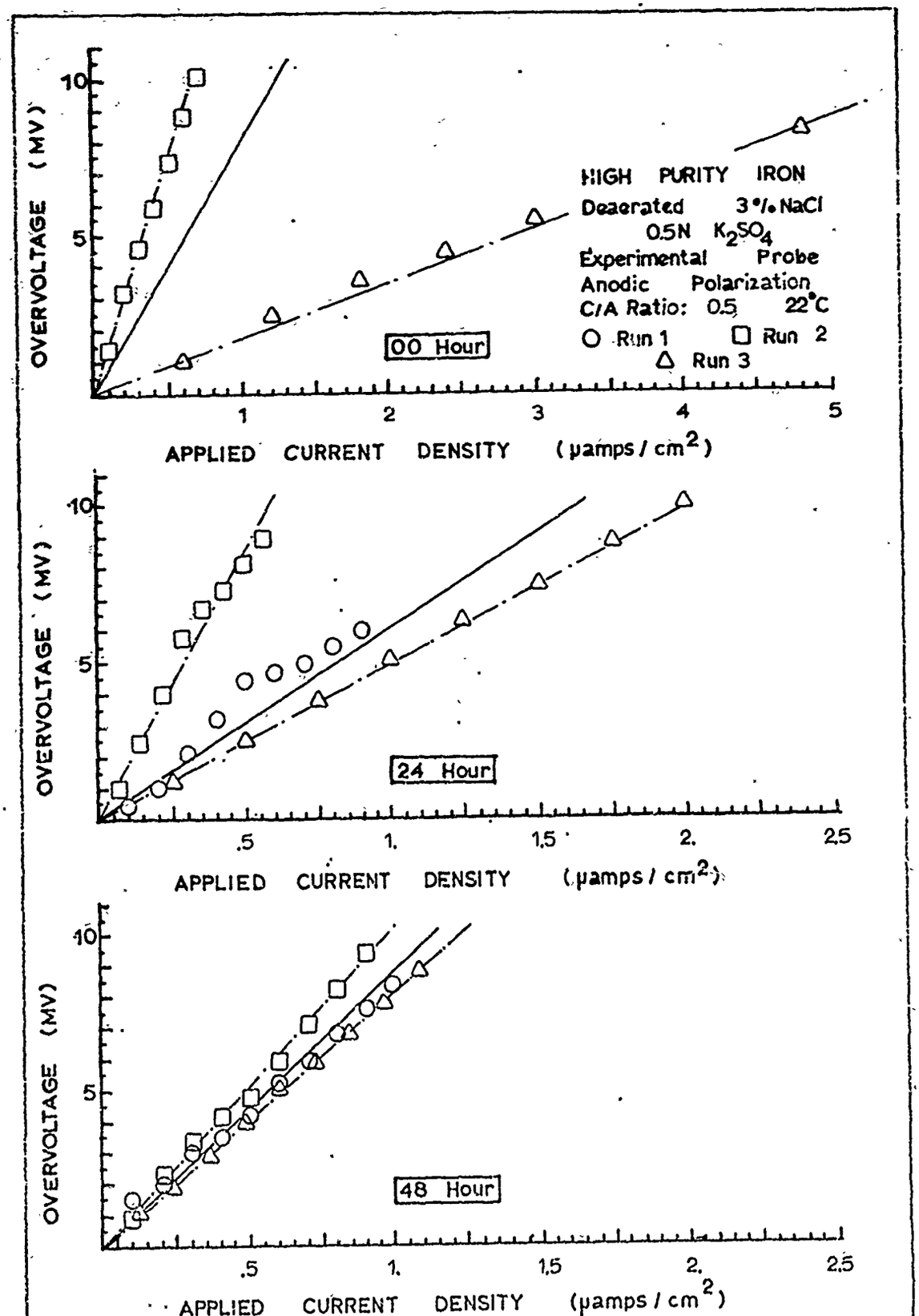

Figure 81: Effect of Time on Galvanostatic Anodic Polarization Resistance of High Purity Iron with C/A Ratio = .5 in Hydrogen Saturated 3% Sodium Chloride Determined Using an Experimental Probe. (Cont)

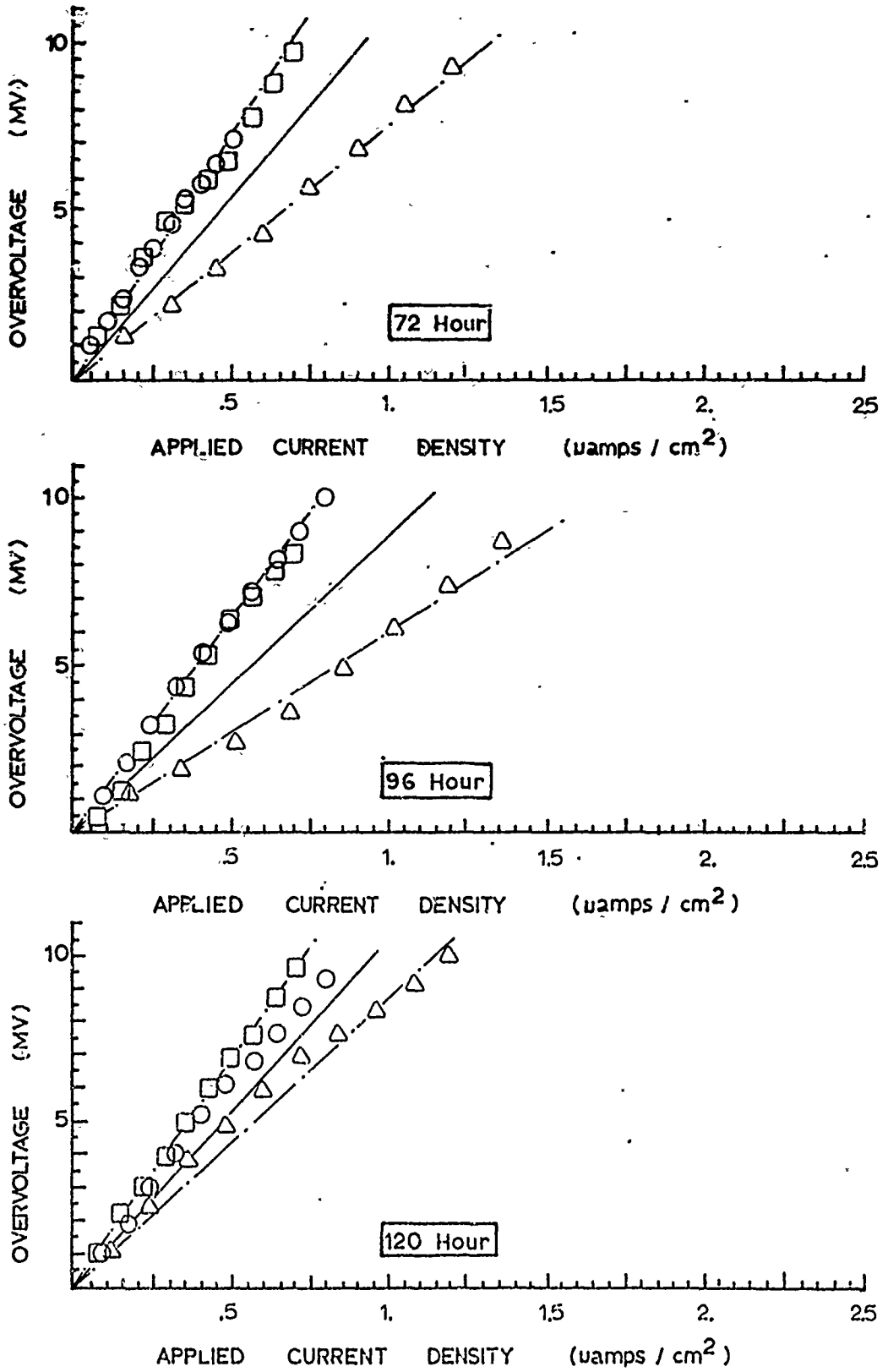

Figure 81: (Cont) Effect of Time on Galvanostatic Anodic Polarization I istance of High Purity Iron with C/A Ratio = .5 in Hydrogen Saturated 3% Sodium Chloride Determined Using an Experimental Probe.

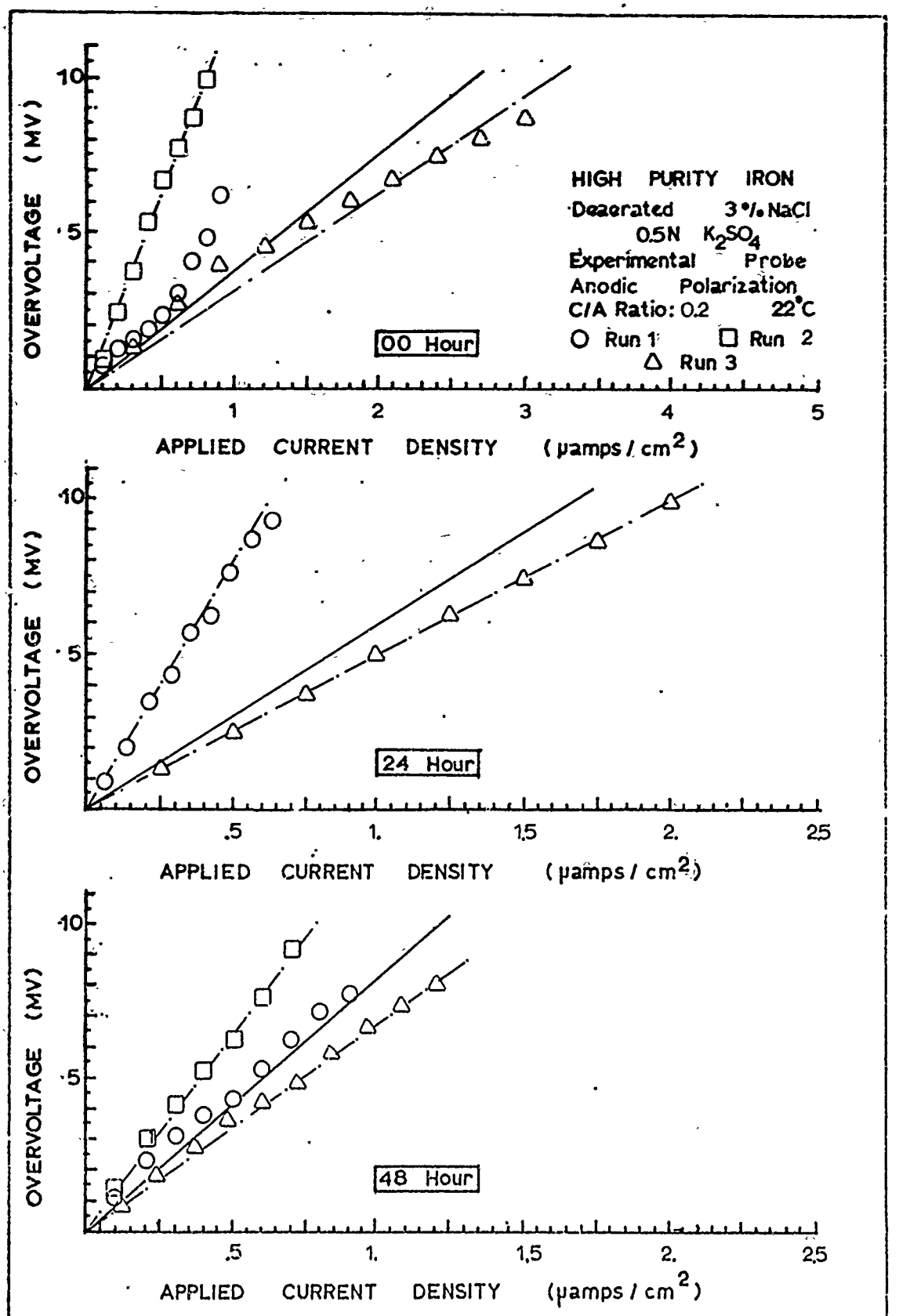

Figure 82: Effect of Time on Galvanostatic Anodic Polarization Resistance of High Purity Iron with C/A Ratio = .2 in Hydrogen Saturated 3% Sodium Chloride Determined Using an Experimental Probe. (Cont)

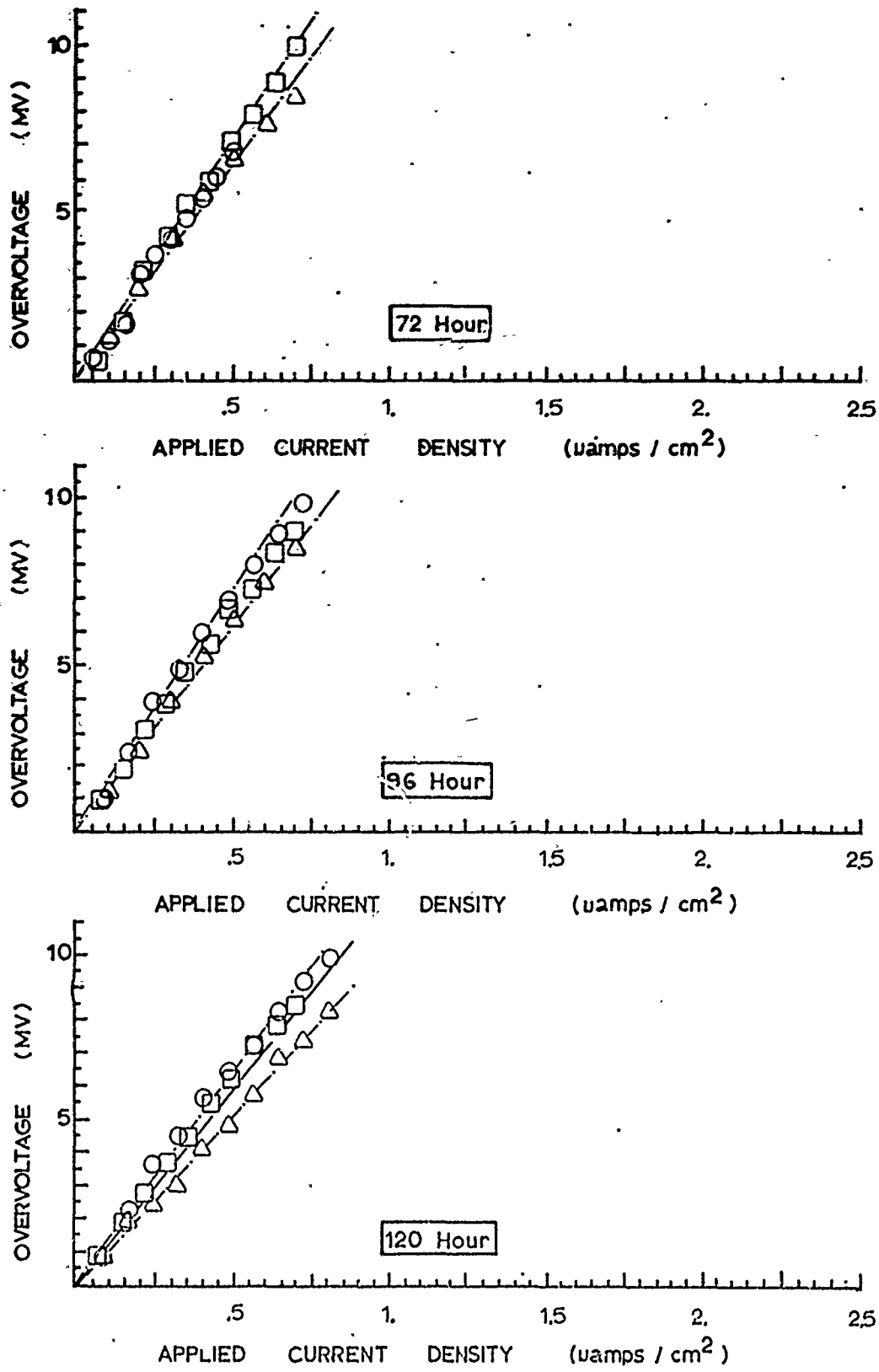

Figure 82: (Cont) Effect of Time on Galvanostatic Anodic Polarization Resistance of High Purity Iron with C/A Ratio = .2 in Hydrogen Saturated 3% Sodium Chloride Determined Using an Experimental Probe.

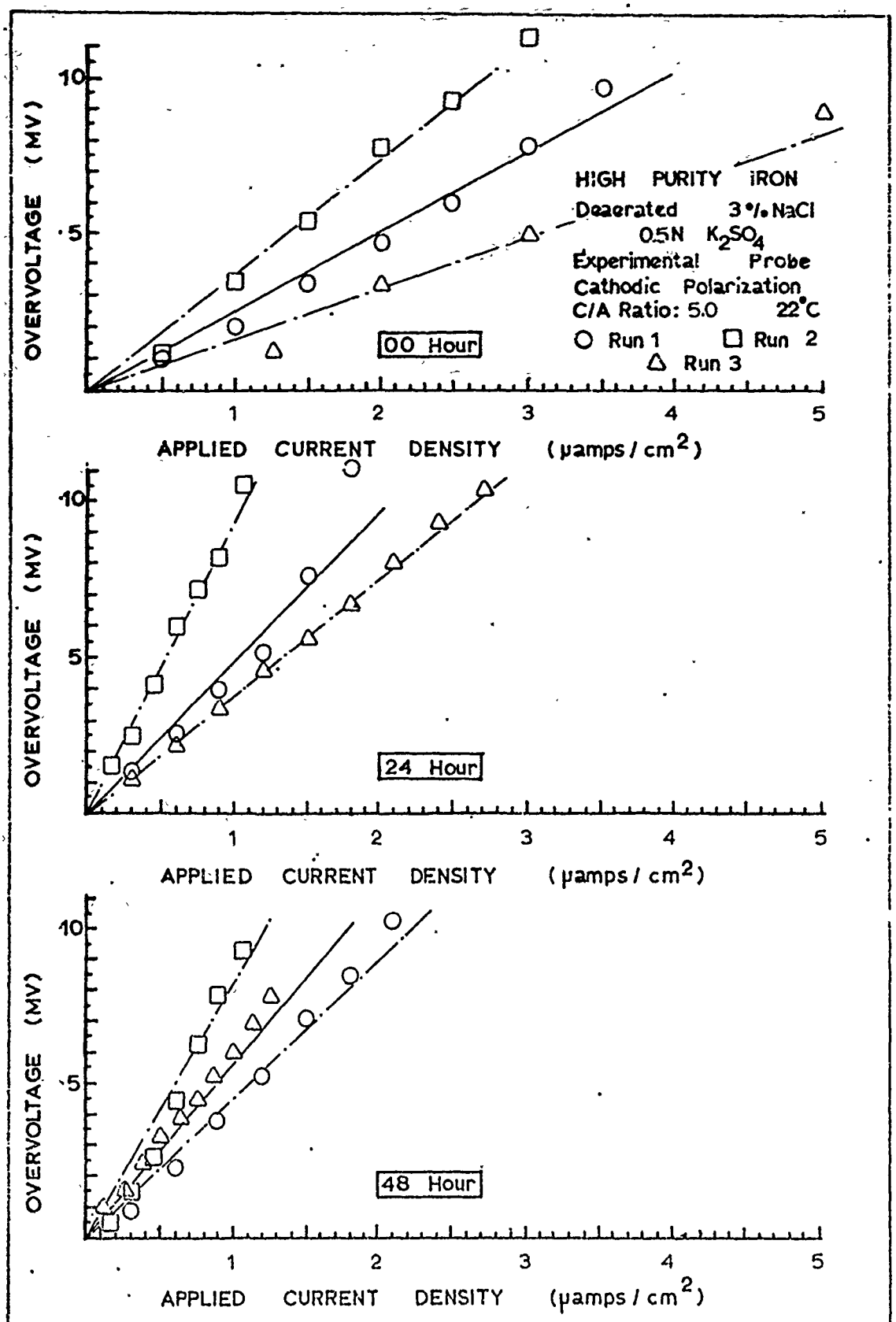

Figure 83: Effect of Time on Galvanostatic Cathodic Polarization Resistance of High Purity Iron with C/A Ratio = 5 in Hydrogen Saturated 3% Sodium Chloride Determined Using an Experimental Probe. (Cont)

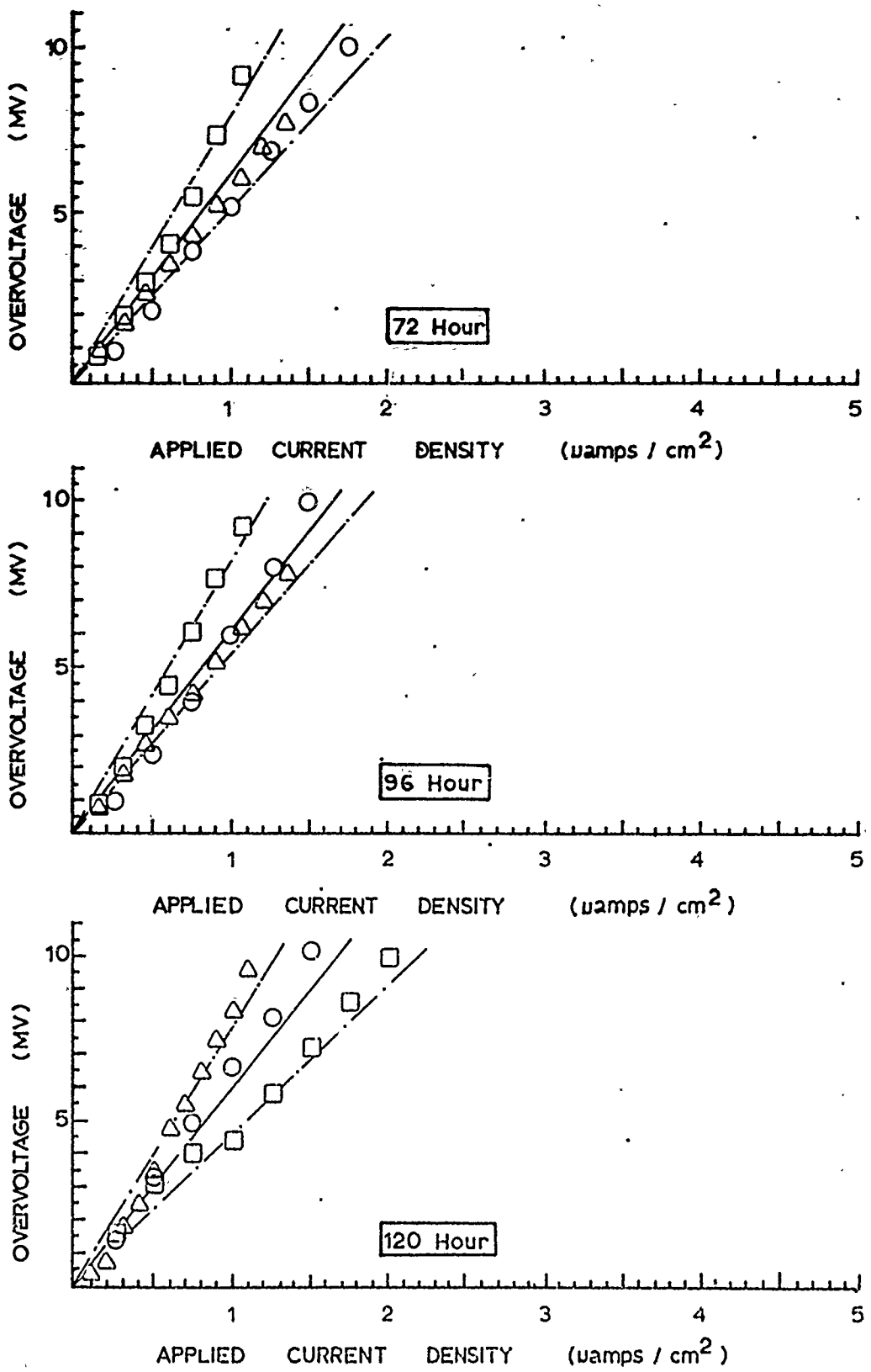

Figure 83: (Cont) Effect of Time on Galvanostatic Cathodic Polarization Resistance of High Purity Iron with C/A Ratio = 5 in Hydrogen Saturated 3% Sodium Chloride Determined Using an Experimental Probe.

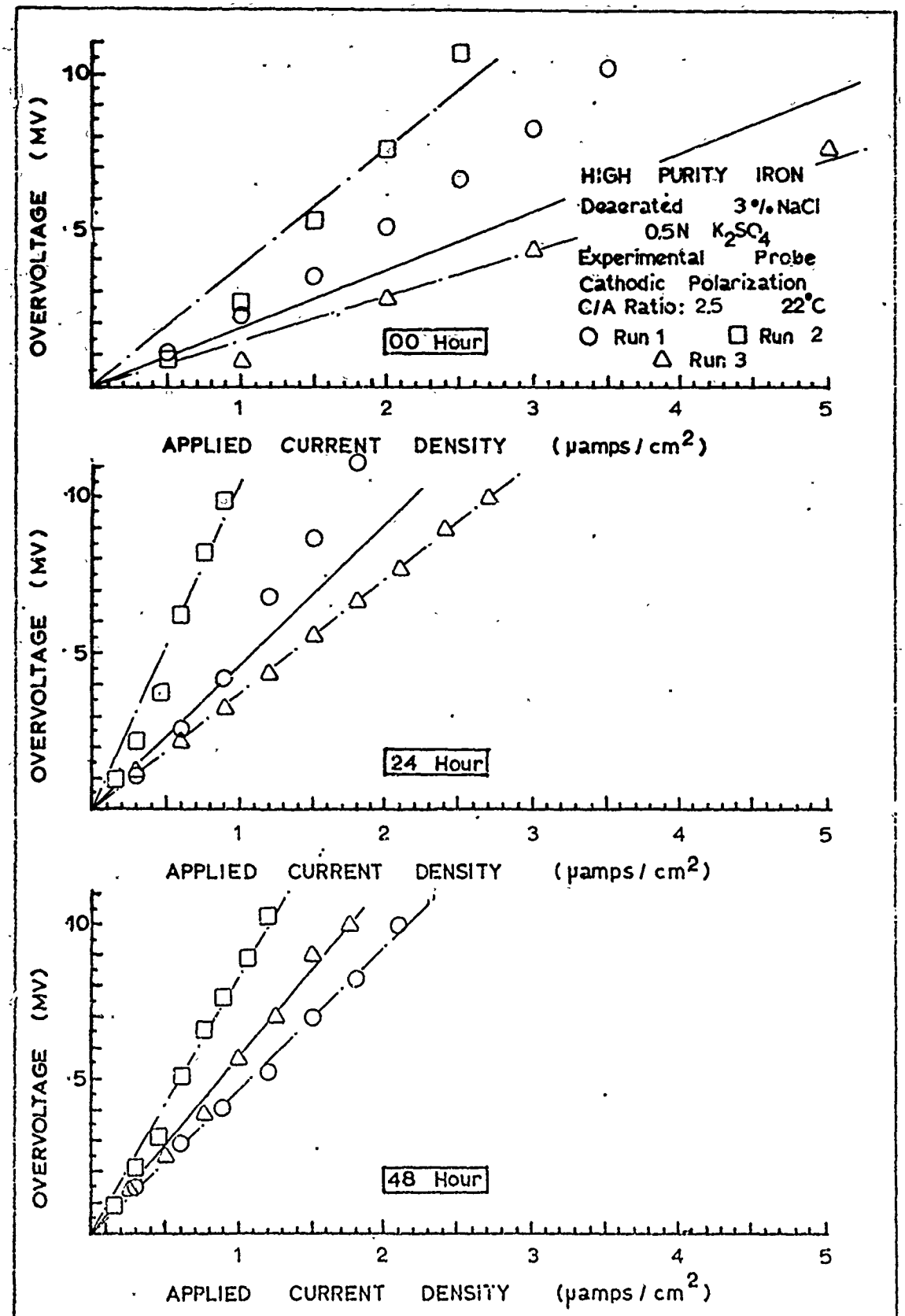

Figure 84: Effect of Time on Galvanostatic Cathodic Polarization Resistance of High Purity Iron with C/A Ratio = 2.5 in Hydrogen Saturated 3% Sodium Chloride Determined Using an Experimental Probe. (Cont)

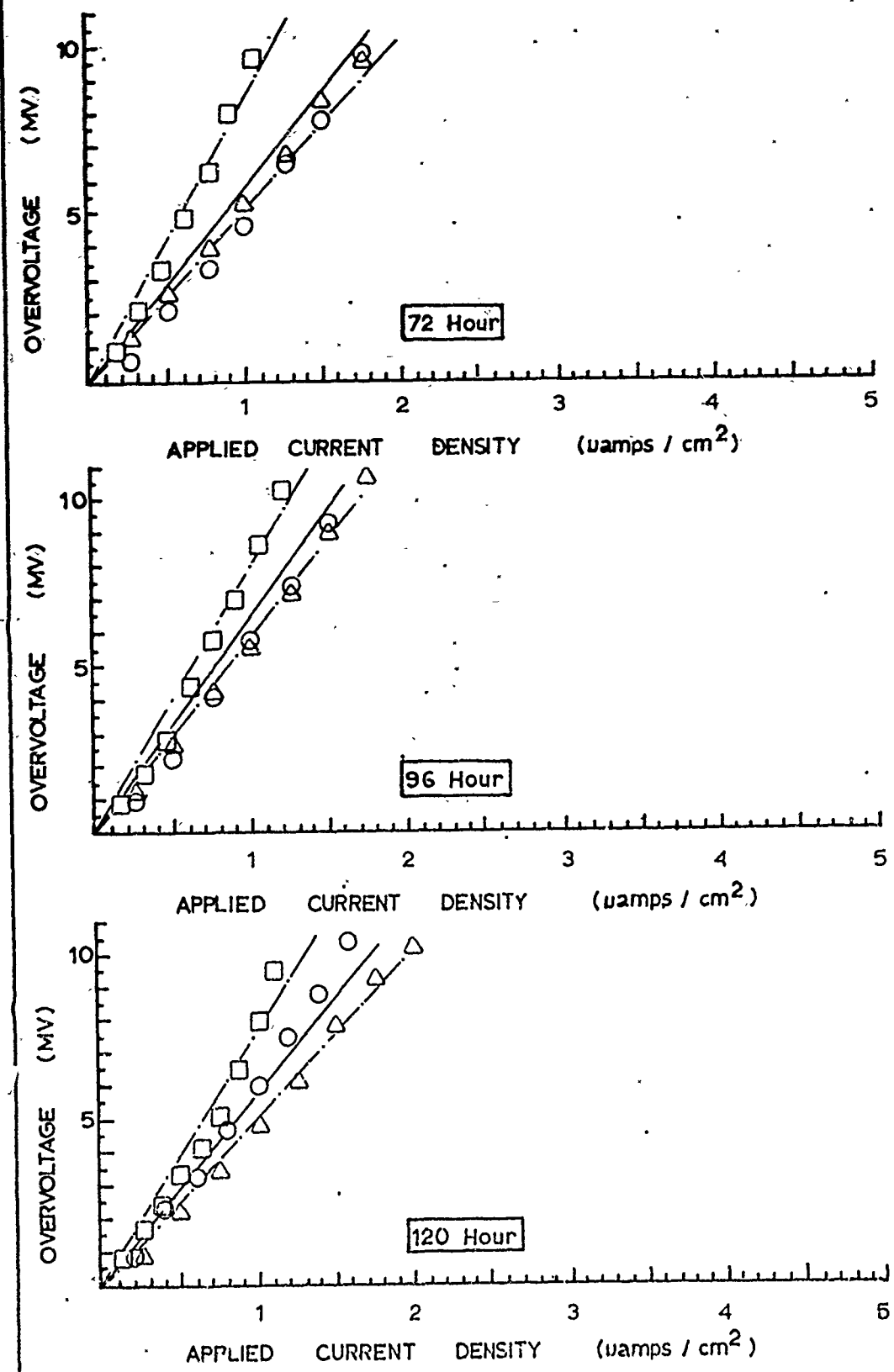

Figure 84: (Cont) Effect of Time on Galvanostatic Cathodic Polarization Resistance of High Purity Iron with C/A Ratio = 2.5 in Hydrogen Saturated 3% Sodium Chloride Determined Using an Experimental Probe.

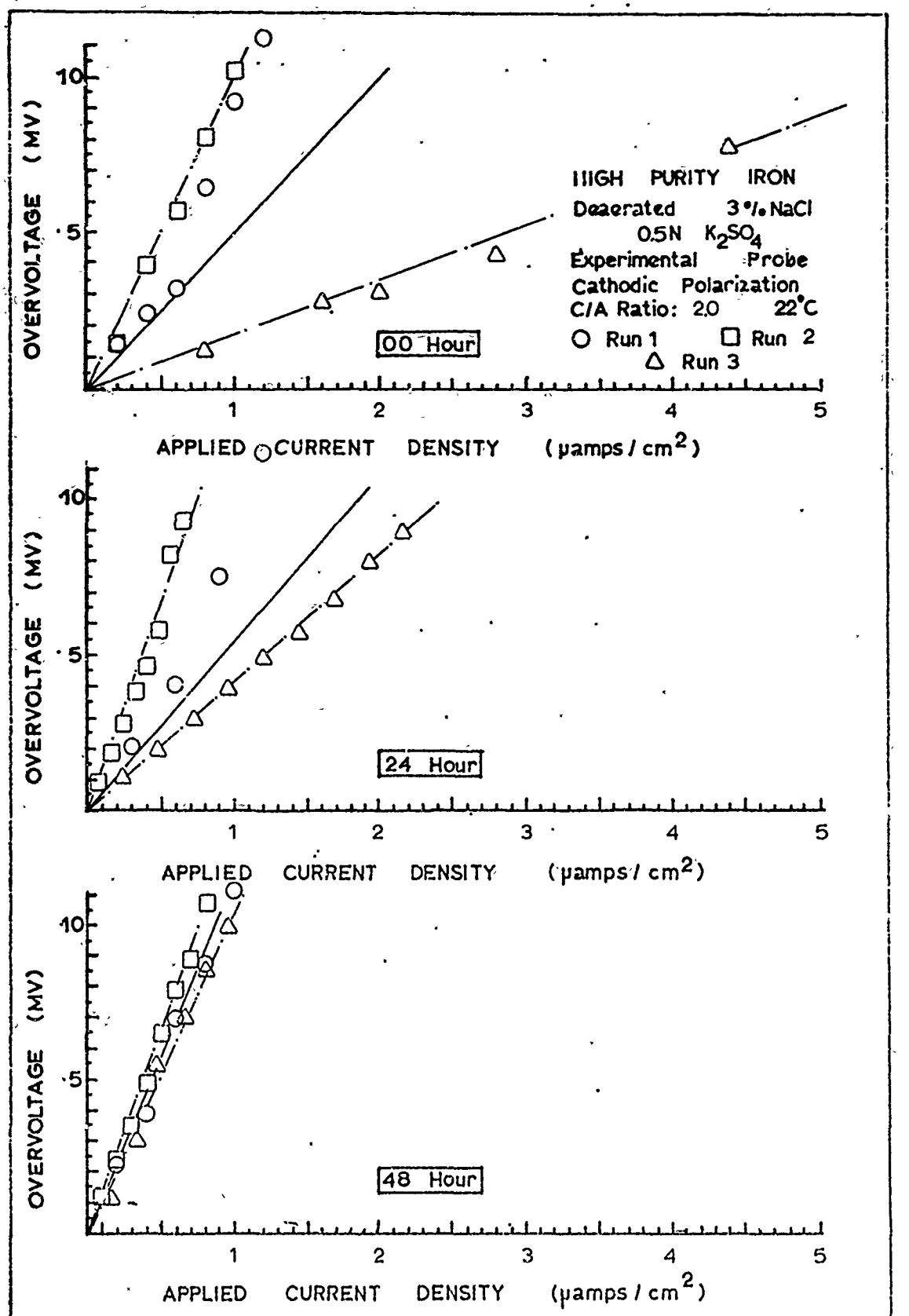

Figure 65: Effect of Time on Galvanostatic Cathodic Polarization Resistance of High Purity Iron with C/A Ratio = 2 in Hydrogen Saturated 3% Sodium Chloride Determined Using an Experimental Probe. (Cont)

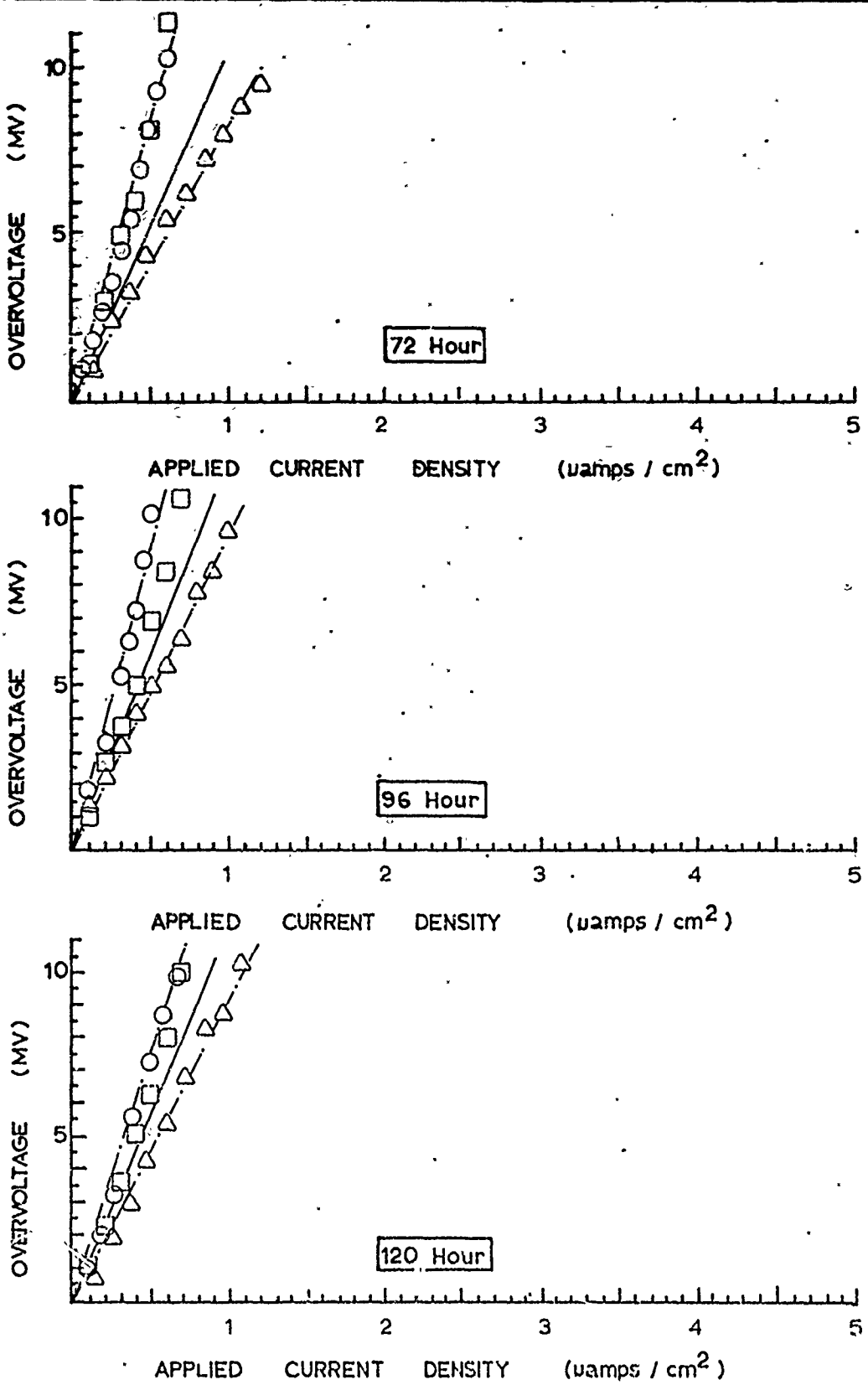

Figure 85: (Cont) Effect of Time on Galvanostatic Cathodic Polarization Resistance of High Purity Iron with C/A Ratio = 2 in Hydrogen Saturated 3% Sodium Chloride Determined Using an Experimental Probe.

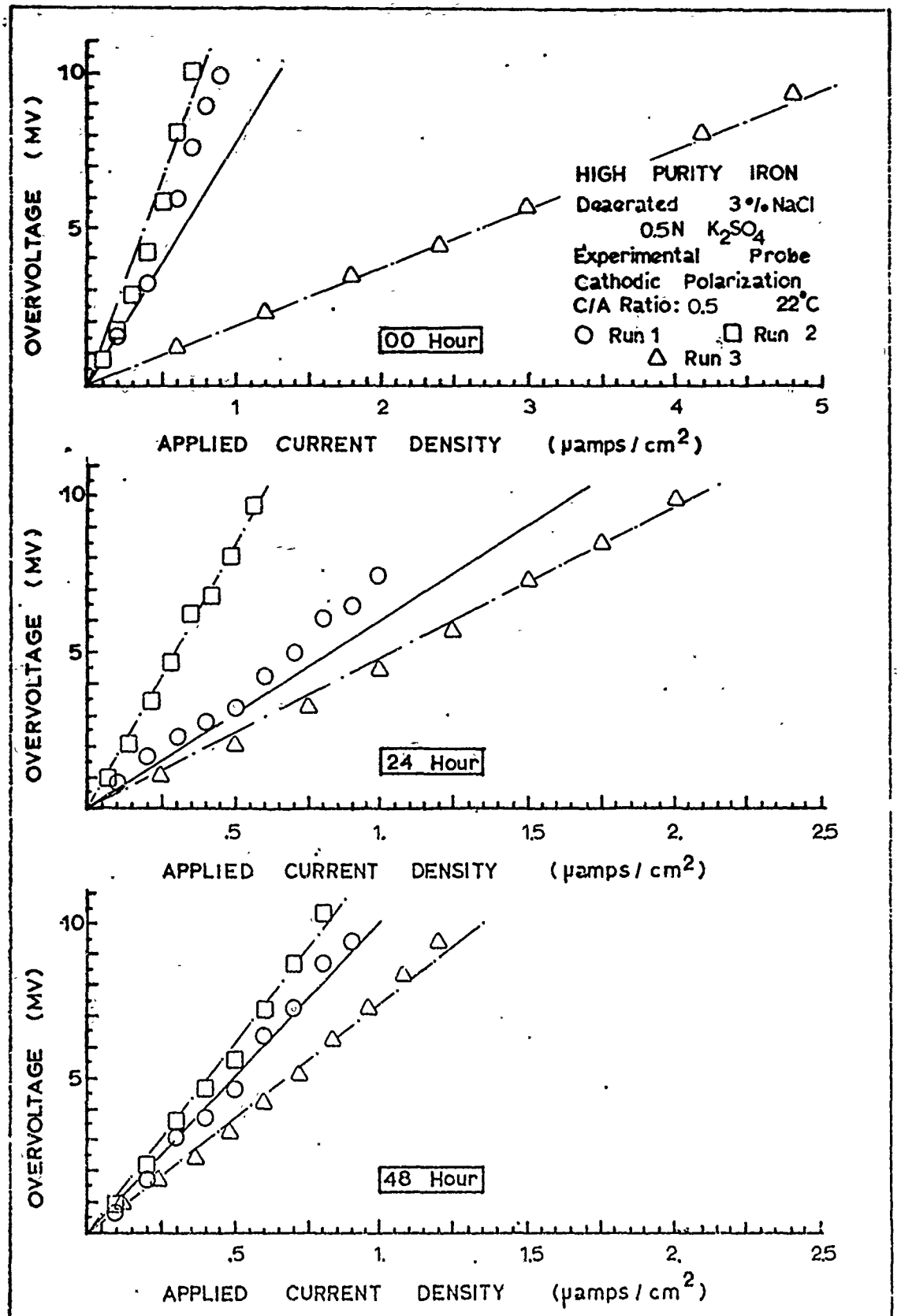

Figure 86: Effect of Time on Galvanostatic Cathodic Polarization Resistance of High Purity Iron with C/A Ratio = .5 in Hydrogen Saturated 3% Sodium Chloride Determined Using an Experimental Probe. (Cont)

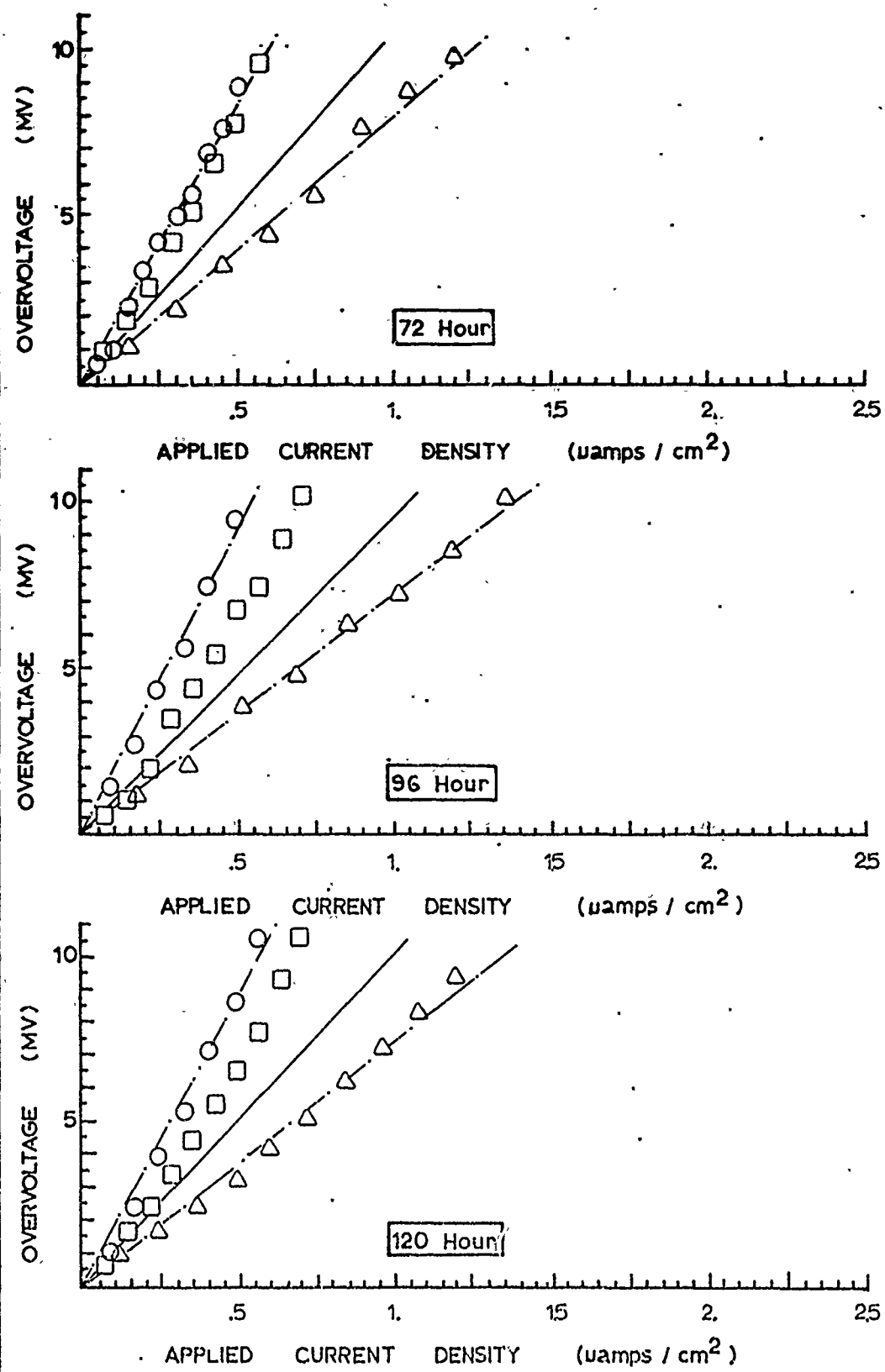

Figure 86: (Cont) Effect of Time on Galvanostatic Cathodic Polarization Resistance of High Purity Iron with C/A Ratio = .5 in Hydrogen Saturated 3% Sodium Chloride Determined Using an Experimental Probe.

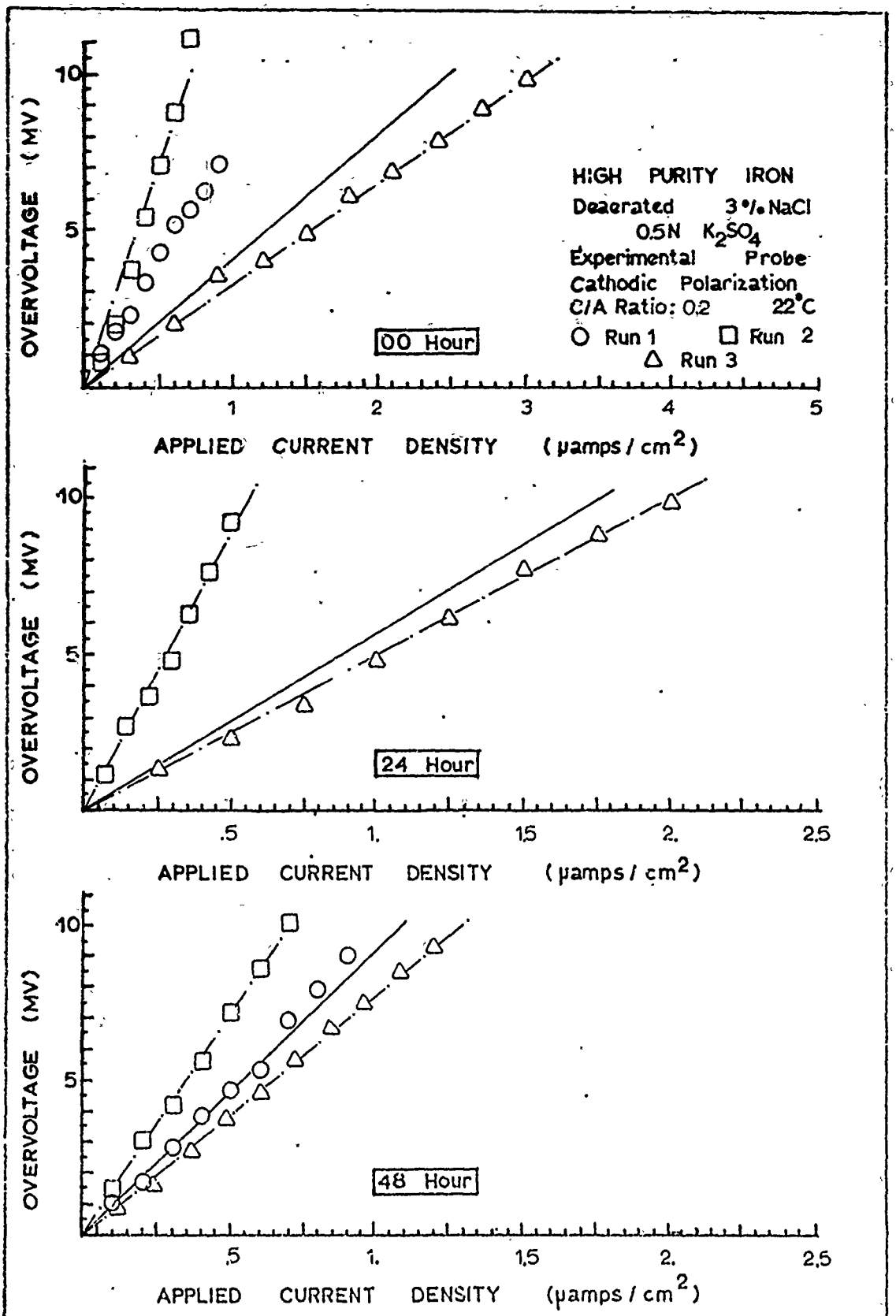

Figure 87: Effect of Time on Galvanostatic Cathodic Polarization Resistance of High Purity Iron with C/A Ratio = .2 in Hydrogen Saturated 3% Sodium Chloride Determined Using an Experimental Probe. (Cont)

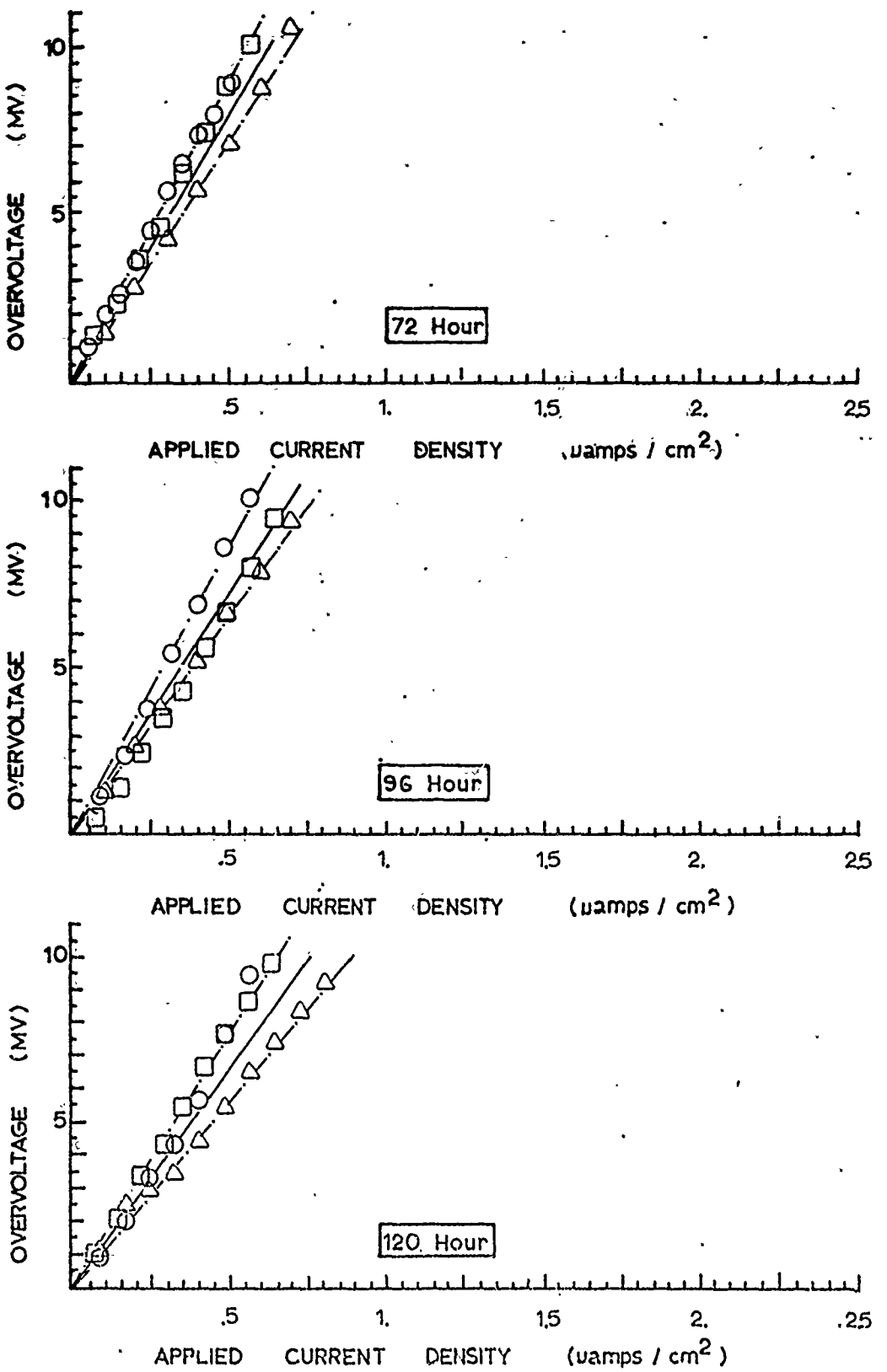

Figure 87: (Cont) Effect of Time on Galvanostatic Cathodic Polarization Resistance of High Purity Iron with C/A Ratio = .2 in Hydrogen Saturated 3% Sodium Chloride Determined Using an Experimental Probe.

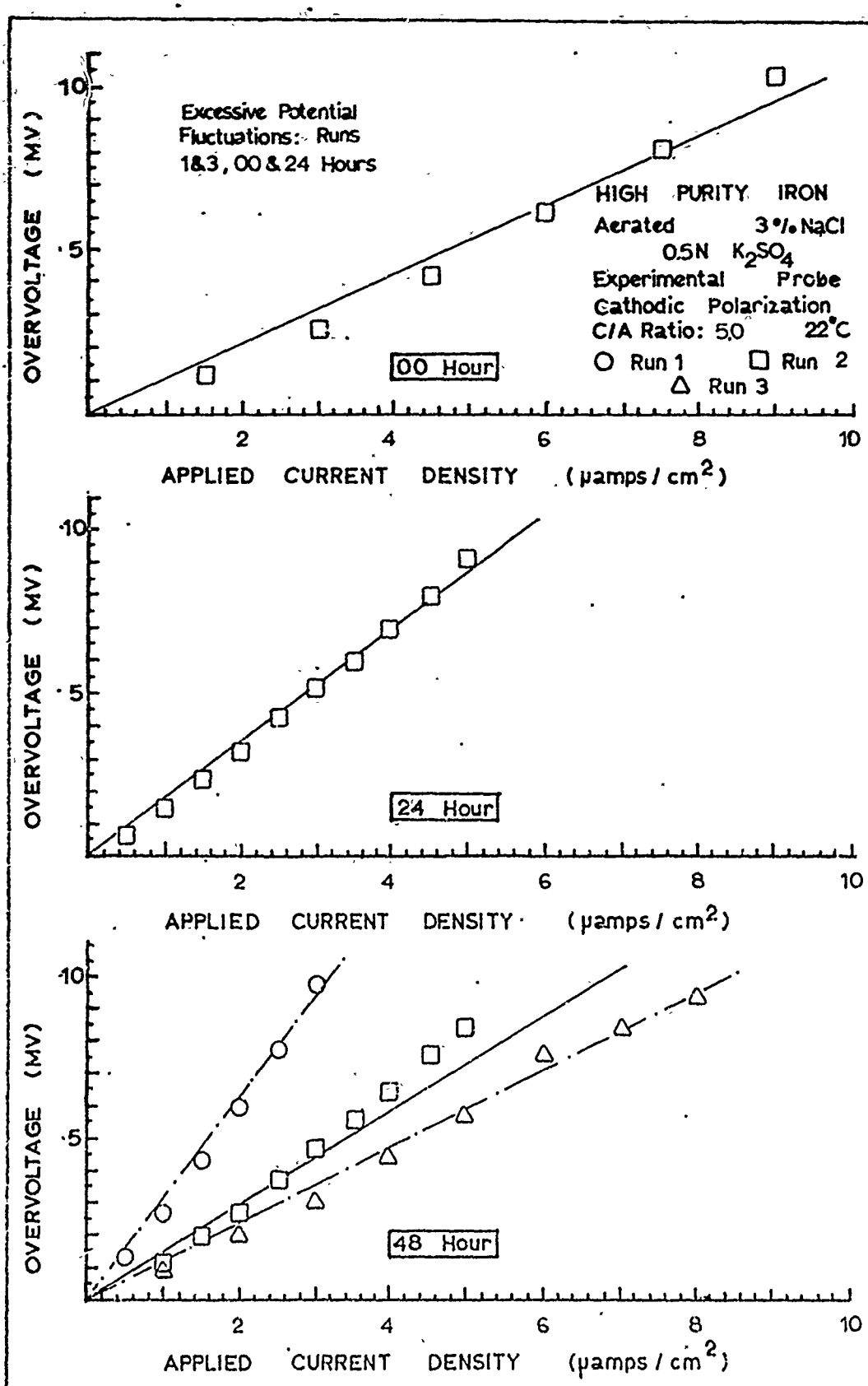

Figure 88: Effect of Time on Galvanostatic Cathodic Polarization Resistance of High Purity Iron with C/A Ratio = 5 in Aerated 3% Sodium Chloride Determined Using an Experimental Probe. (Cont)

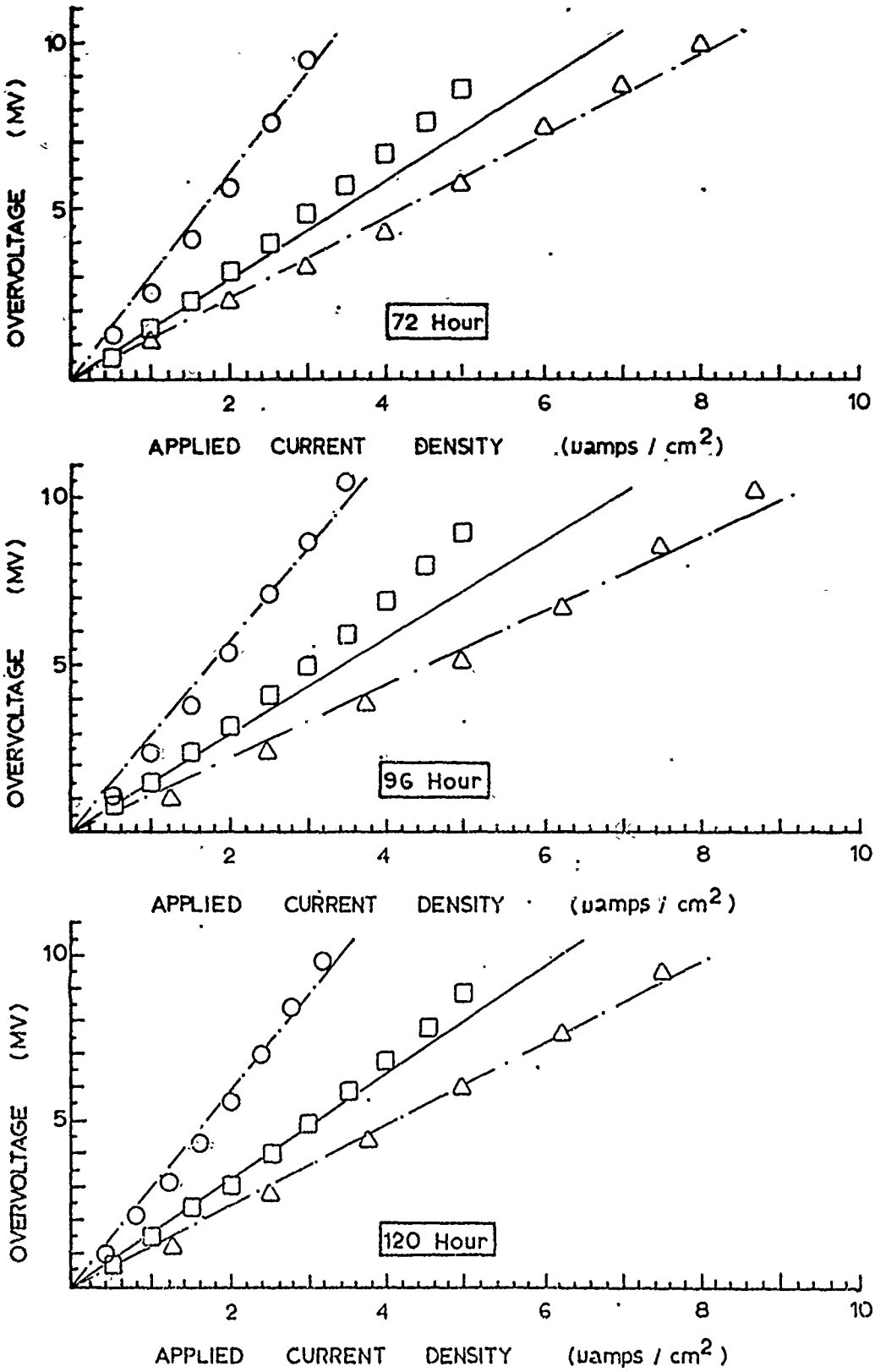

Figure 88: (Cont) Effect of Time on Galvanostatic Cathodic Polarization Resistance of High Purity Iron with C/A Ratio = 5 in Aerated 3% Sodium Chloride Determined Using an Experimental Probe.

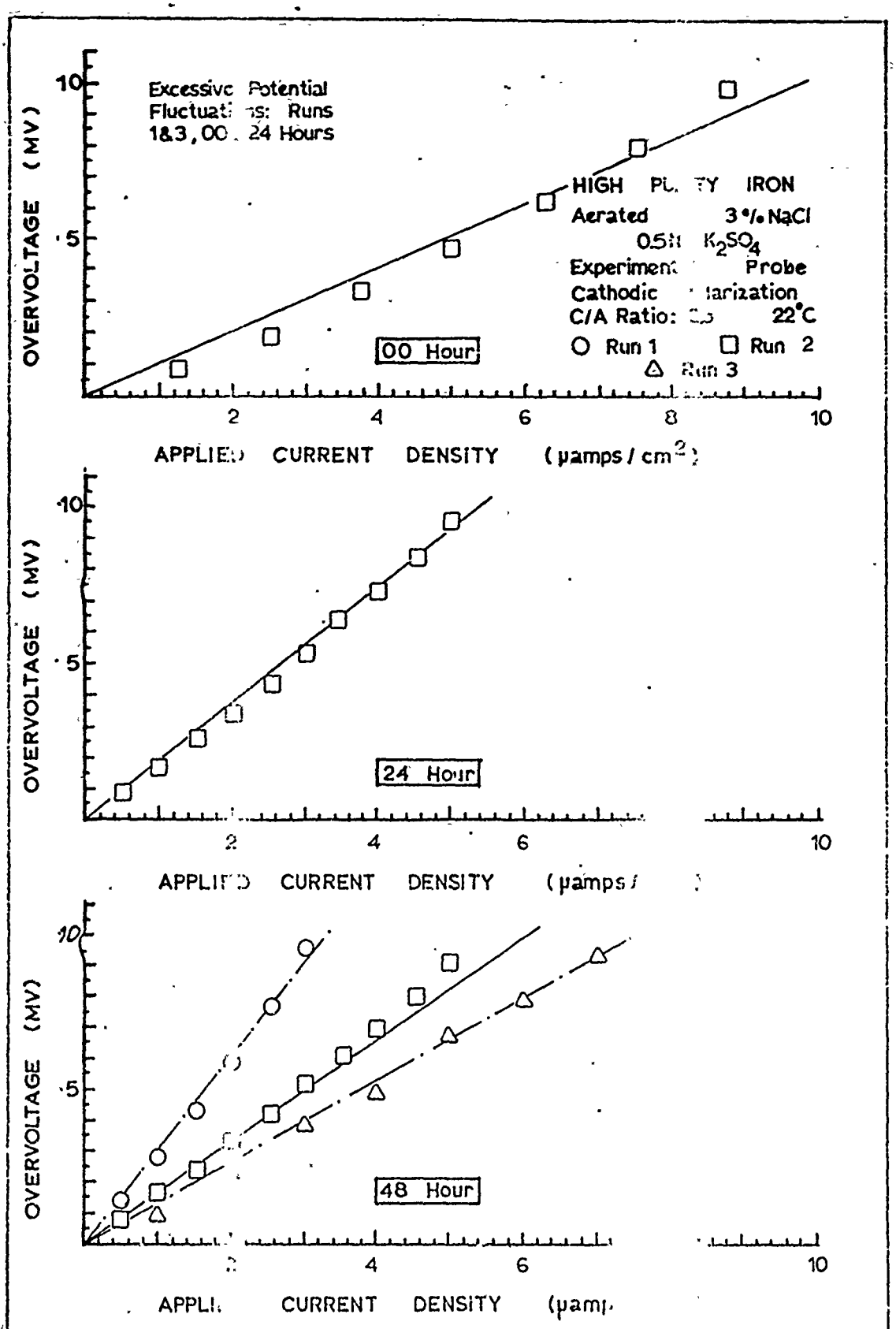

Figure 89: Effect of Time on Galvanostatic Cathodic Polarization of High Purity Iron with C/A Ratio = 2.5 in Aerated 3% Sodium Chloride Determined Using an Experimental Probe. (Cont)

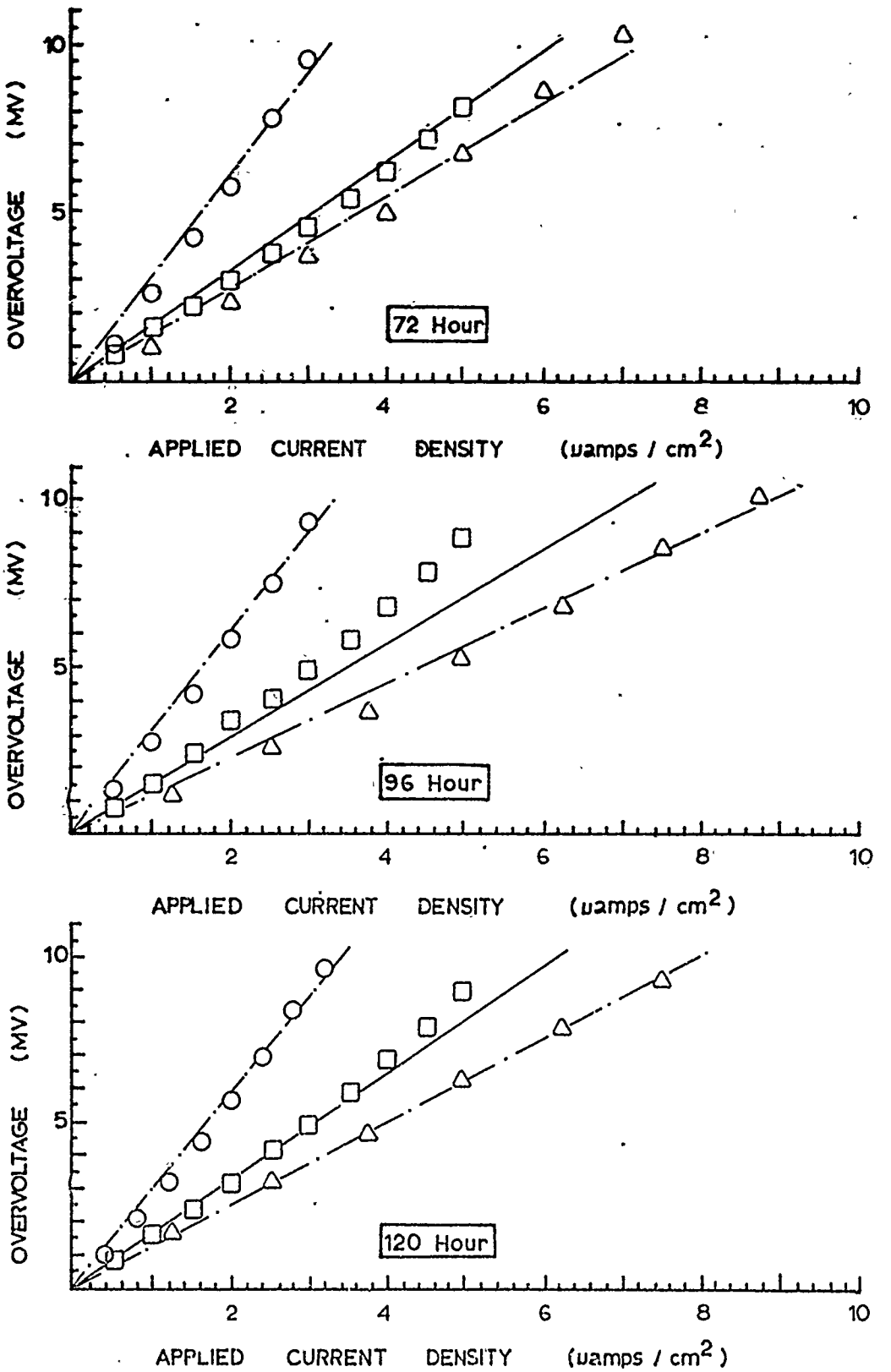

Figure 89: (Cont) Effect of Time on Galvanostatic Cathodic Polarization Resistance of High Purity Iron with C/A Ratio = 2.5 in Aerated 3% Sodium Chloride Determined Using an Experimental Probe.

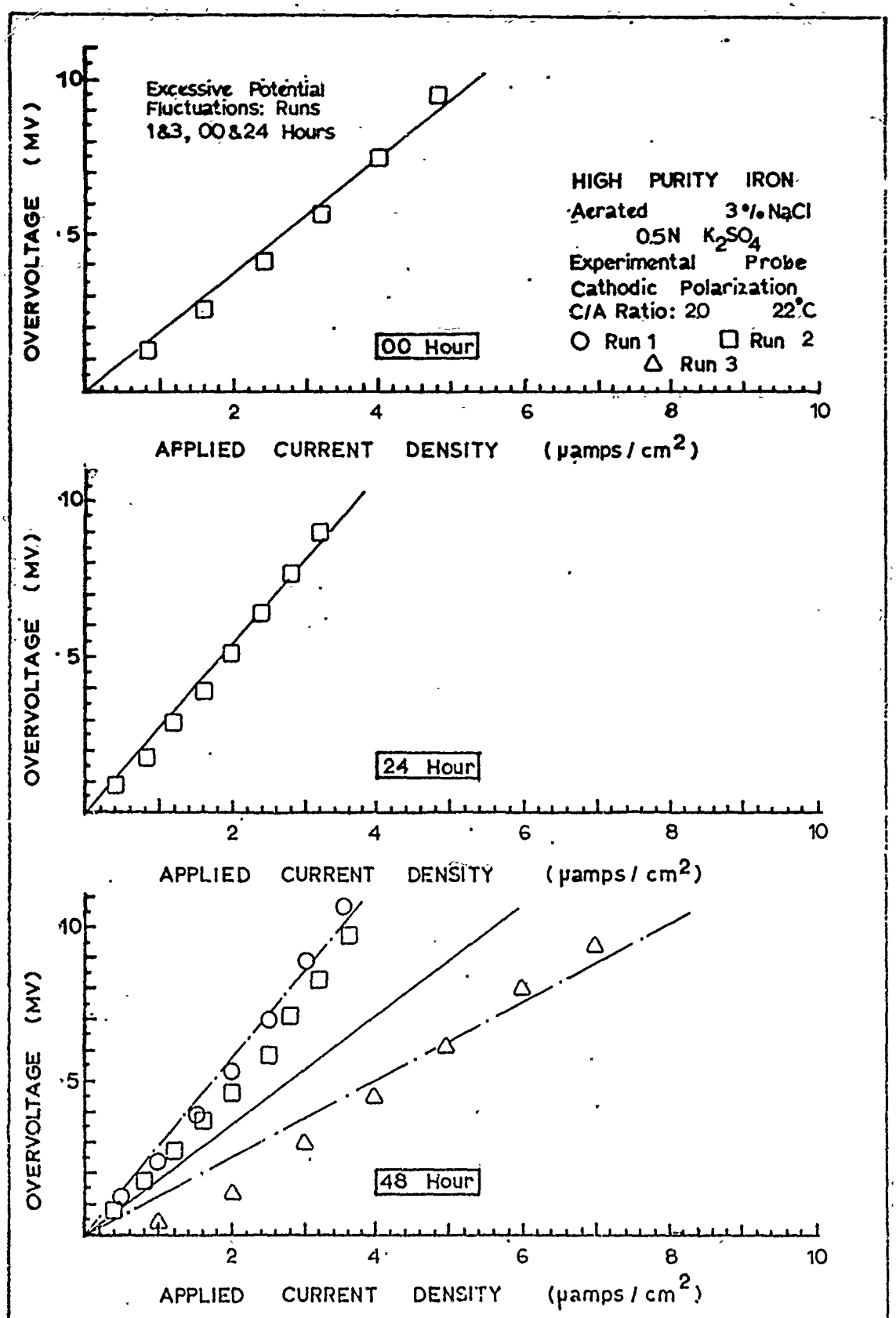

Figure 90: Effect of Time on Galvanostatic Cathodic Polarization Resistance of High Purity Iron with C/A Ratio = 2 in Aerated 3% Sodium Chloride Determined Using an Experimental Probe. (Cont)

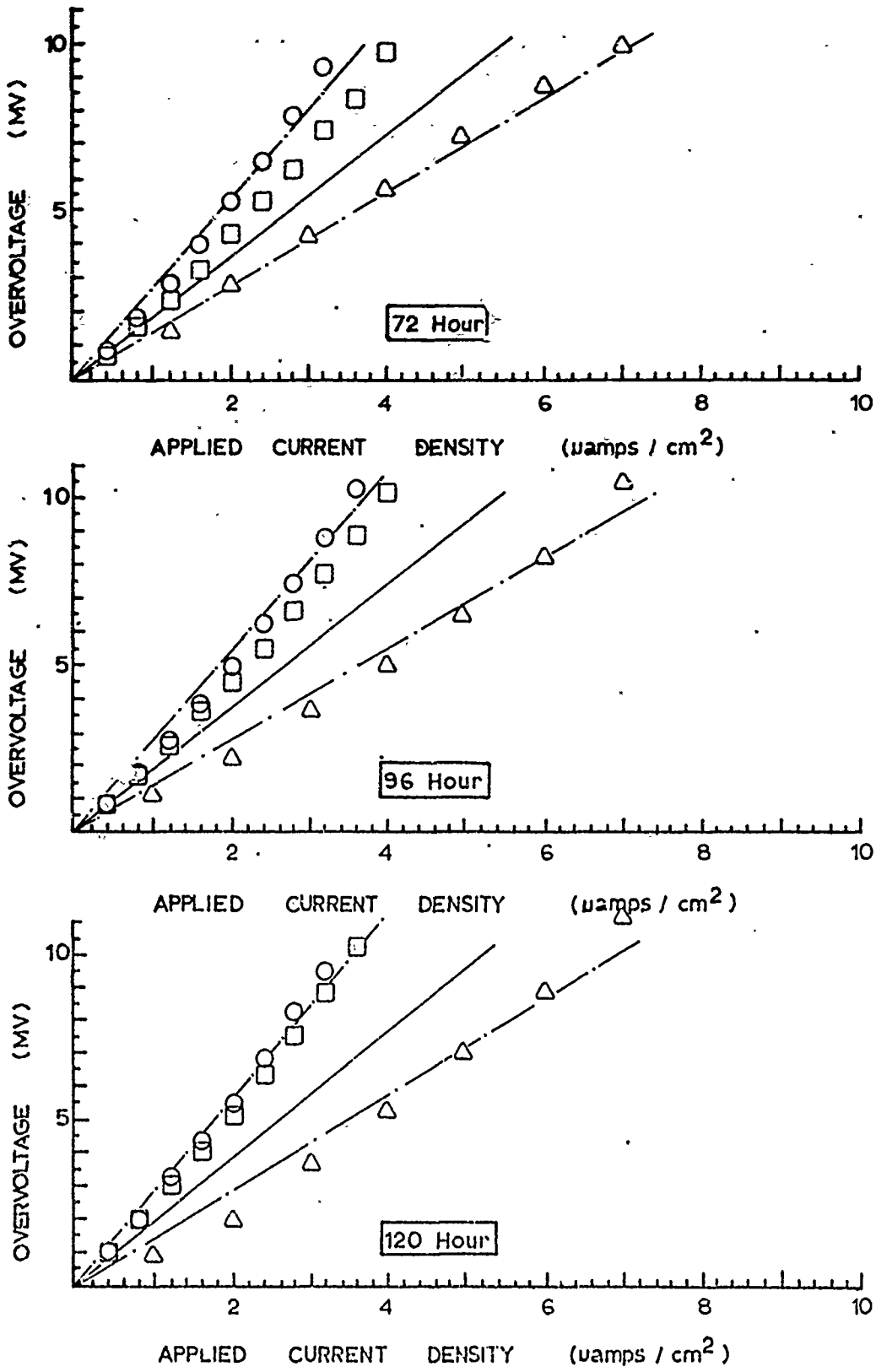

Figure 90: (Cont) Effect of Time on Galvanostatic Cathodic Polarization Resistance of High Purity Iron with C/A Ratio = 2 in Aerated 3% Sodium Chloride Determined Using an Experimental Probe.

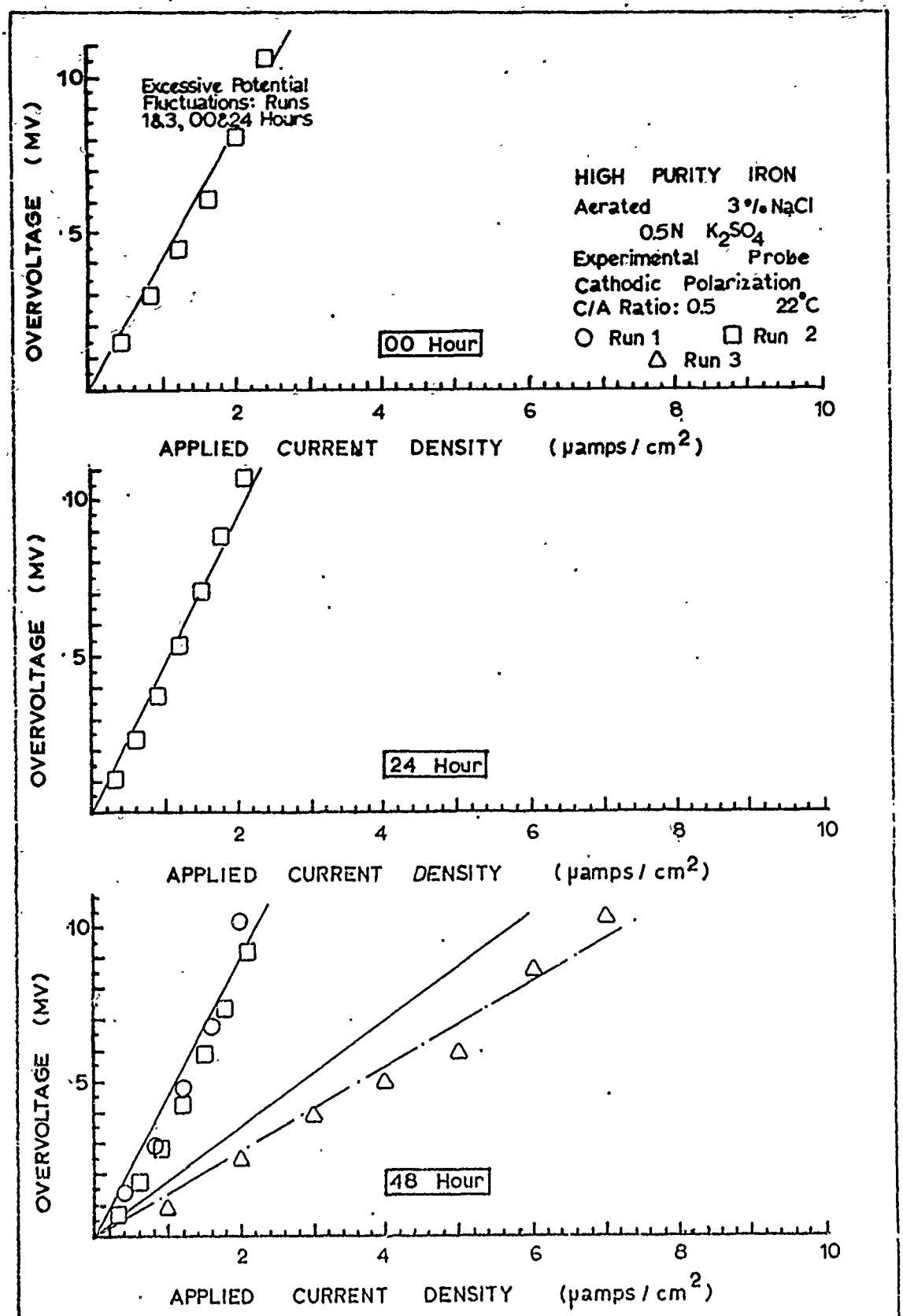

Figure 91: Effect of Time on Galvanostatic Cathodic Polarization Resistance of High Purity Iron with C/A Ratio = .5 in Aerated 3% Sodium Chloride Determined Using an Experimental Probe. (Cont)

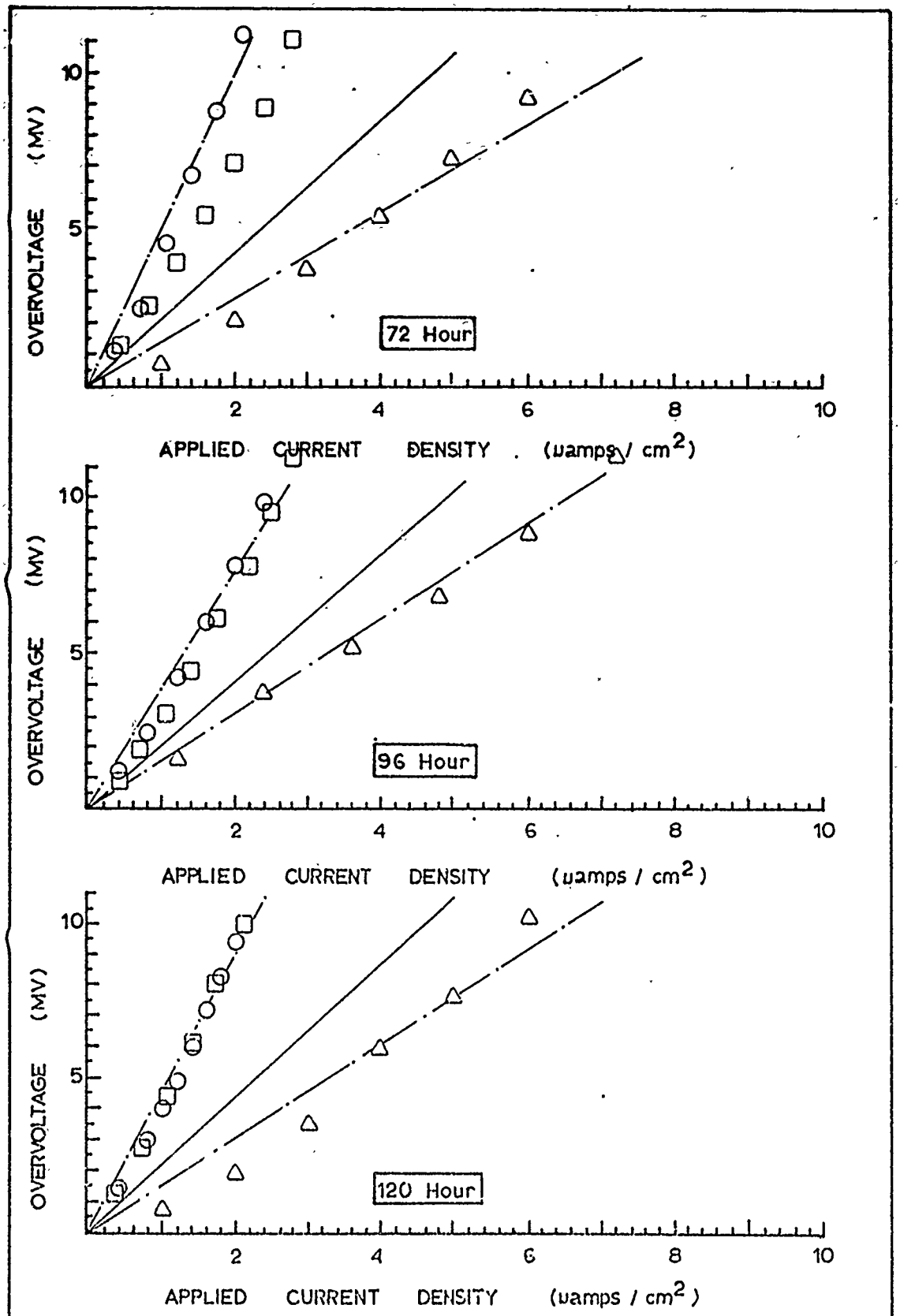

Figure 91: (Cont) Effect of Time on Galvanostatic Cathodic Polarization Resistance of High Purity Iron with C/A Ratio = .5 in Aerated 3% Sodium Chloride Determined Using an Experimental Probe.

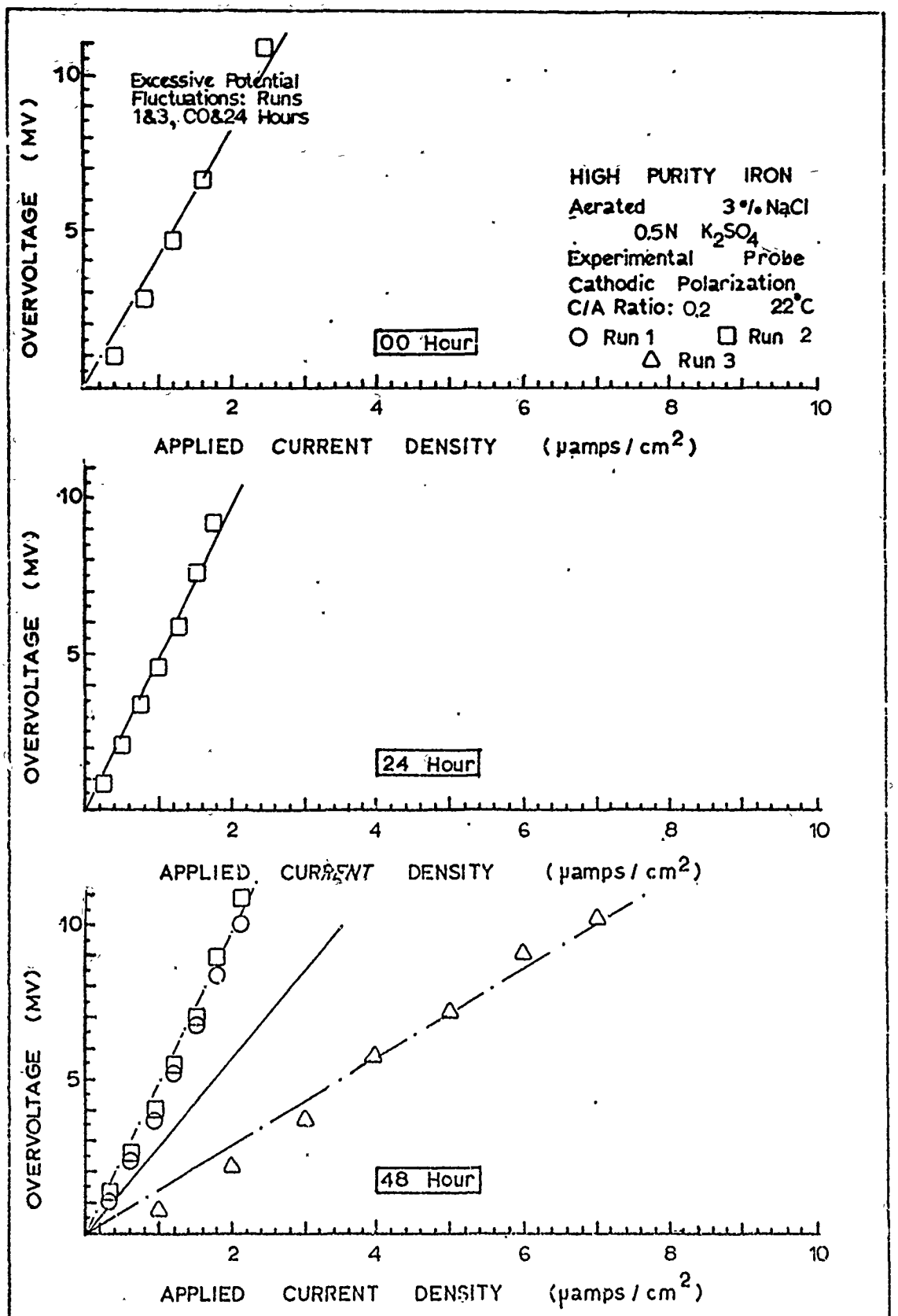

Figure 92: Effect of Time on Galvanostatic Cathodic Polarization Resistance of High Purity Iron with C/A Ratio = .2 in Aerated 3% Sodium Chloride Determined Using an Experimental Probe. (Cont)

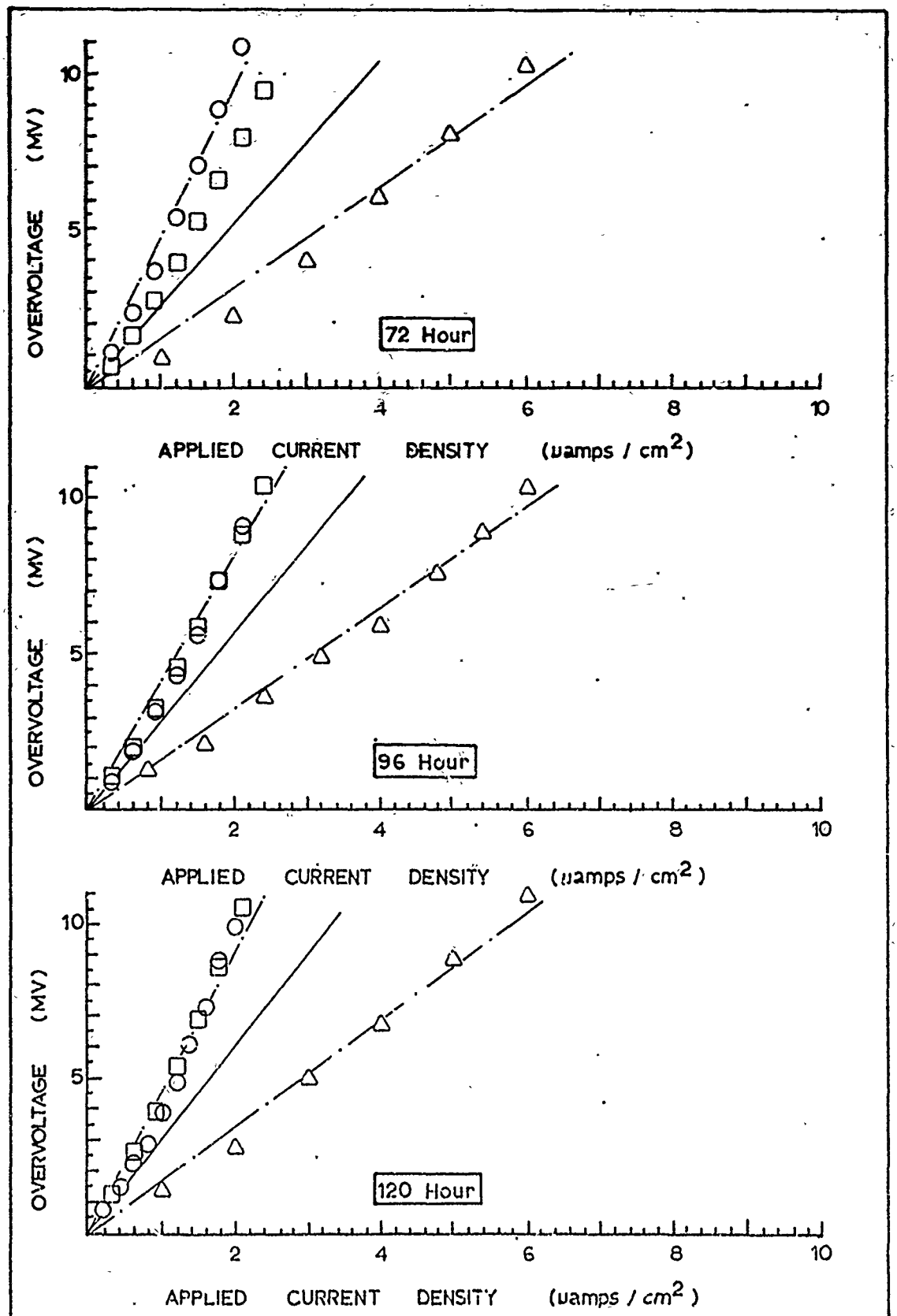

Figure 92: (Cont) Effect of Time on Galvanostatic Cathodic Polarization Resistance of High Purity Iron with C/A Ratio = .2 in Aerated 3% Sodium Chloride Determined Using an Experimental Probe.

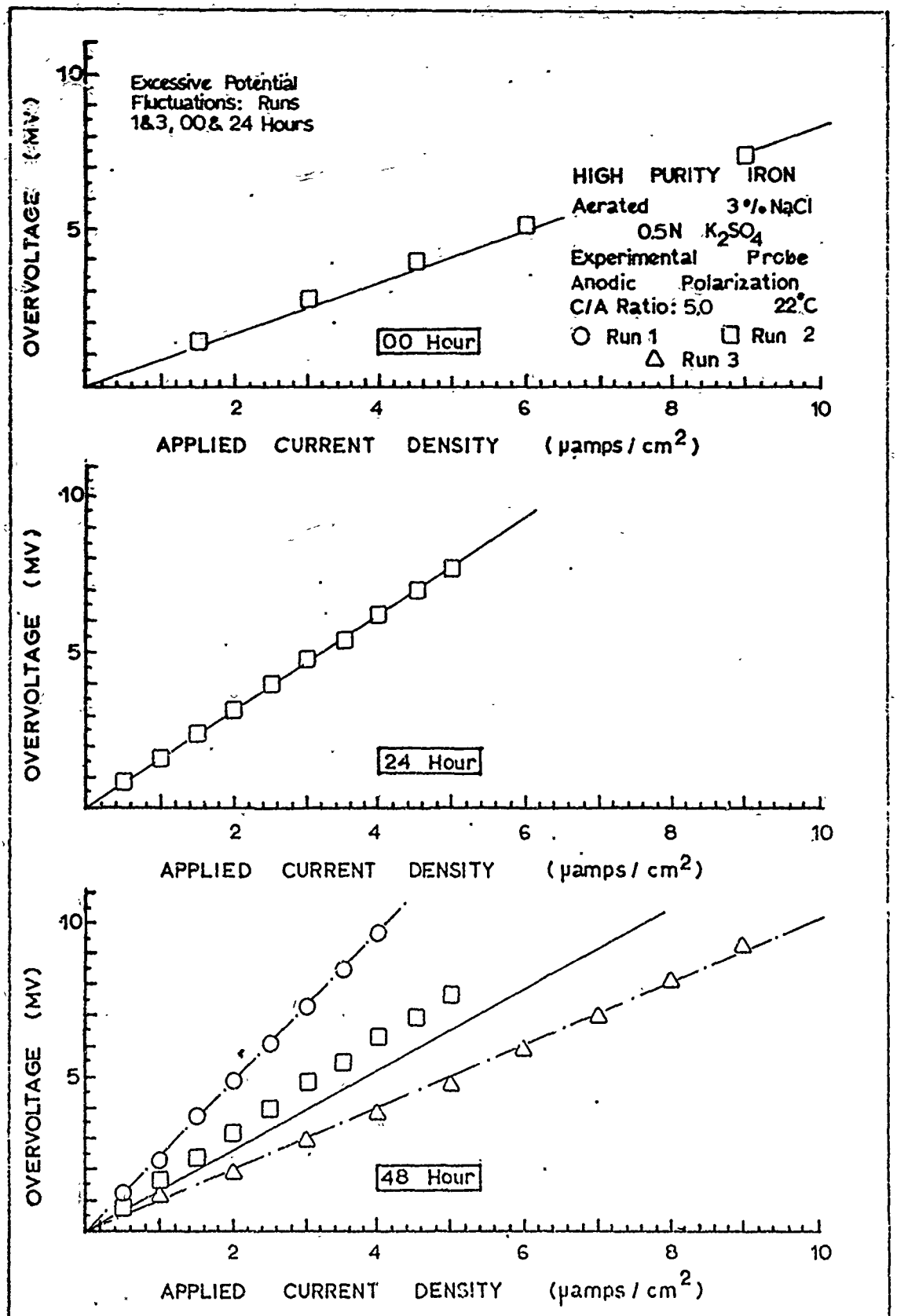

Figure 93: Effect of Time on Galvanostatic Anodic Polarization Resistance of High Purity Iron with C/A Ratio = 5 in Aerated 3% Sodium Chloride Determined Using an Experimental Probe. (Cont)

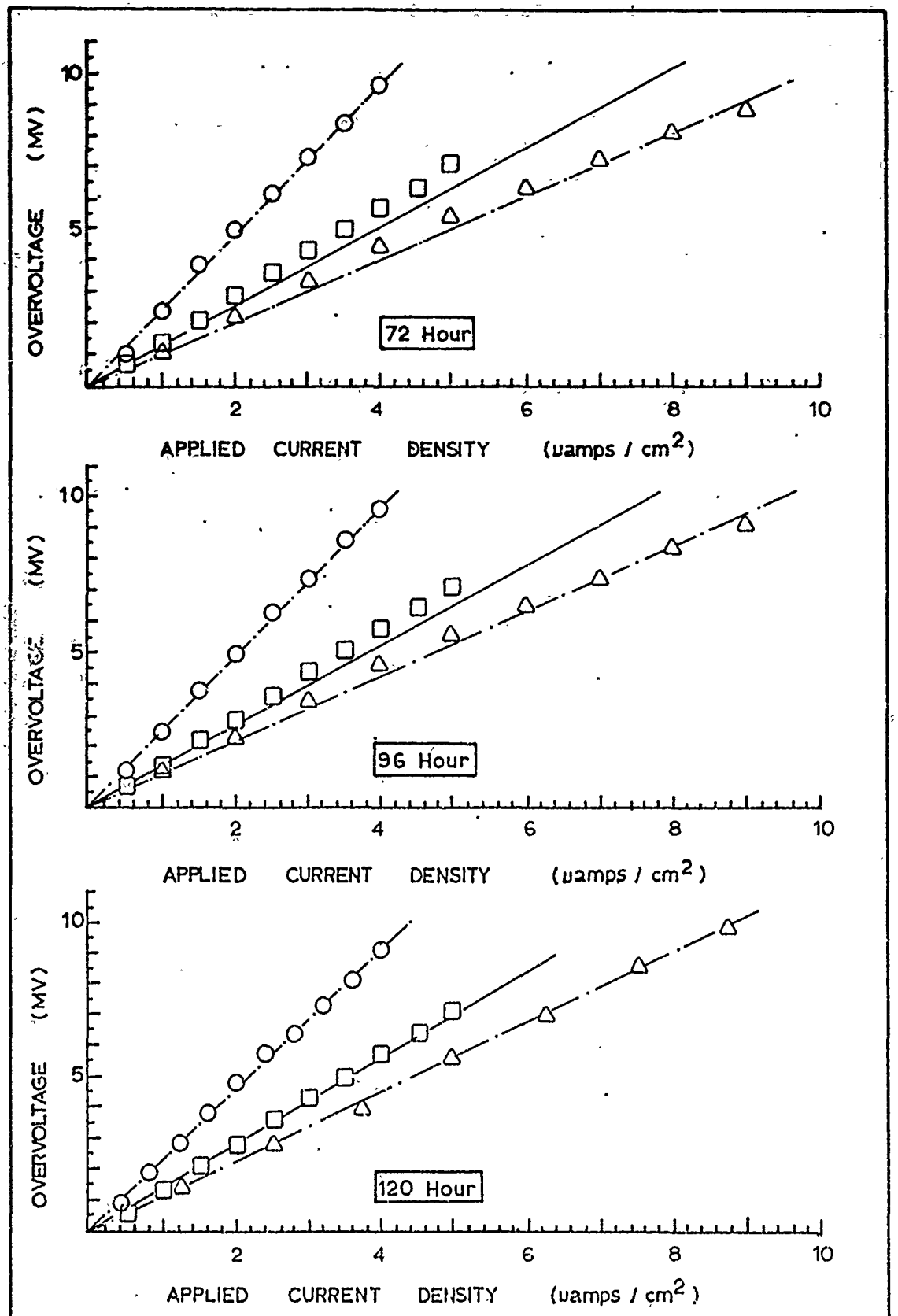

Figure 93: (Cont) Effect of Time on Galvanostatic Anodic Polarization Resistance of High Purity Iron with C/A Ratio = 5 in Aerated 3% Sodium Chloride Determined Using an Experimental Probe.

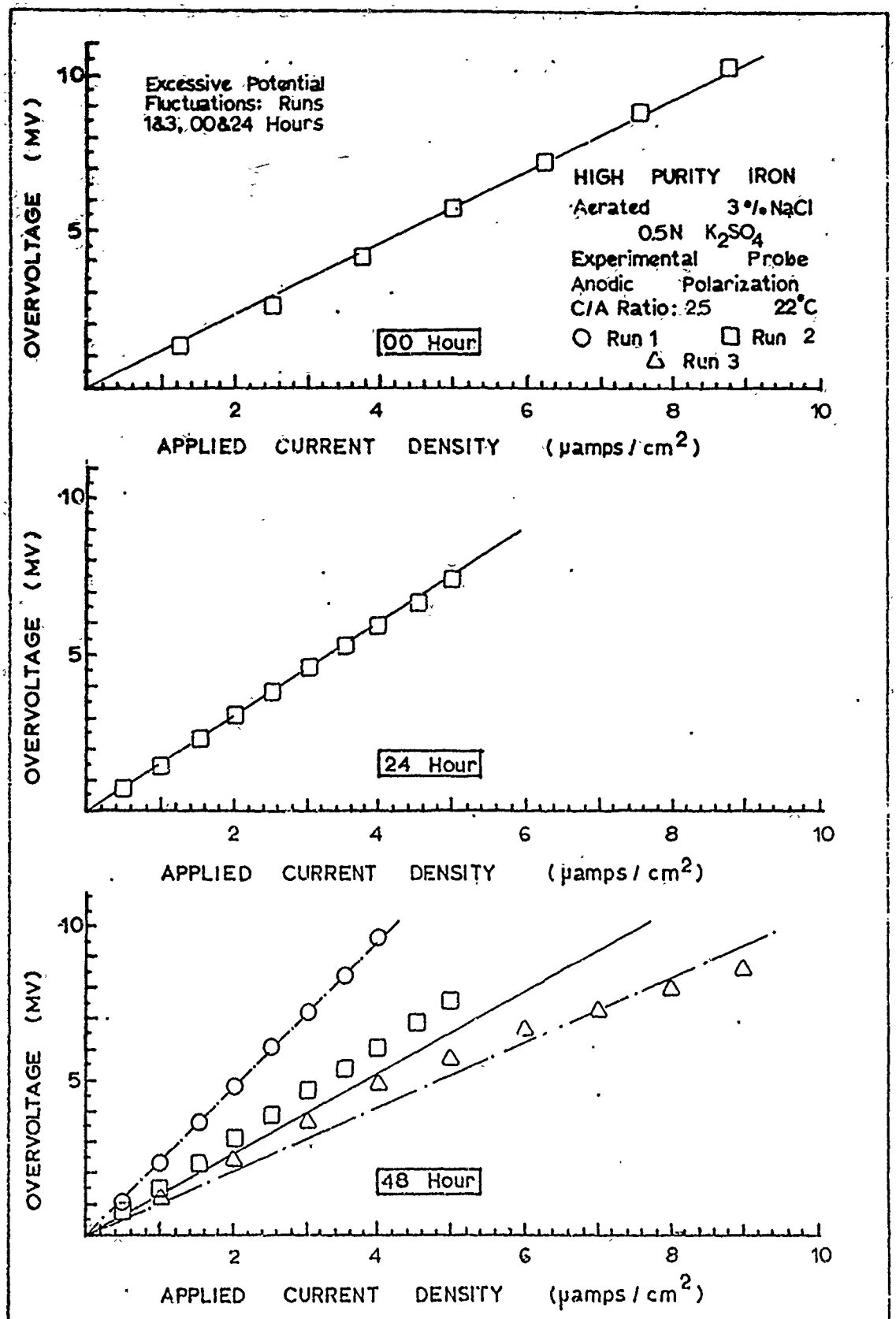

Figure 94: Effect of Time on Galvanostatic Anodic Polarization Resistance of High Purity Iron with C/A Ratio = 2.5 in Aerated 3% Sodium Chloride Determined Using an Experimental Probe. (Cont)

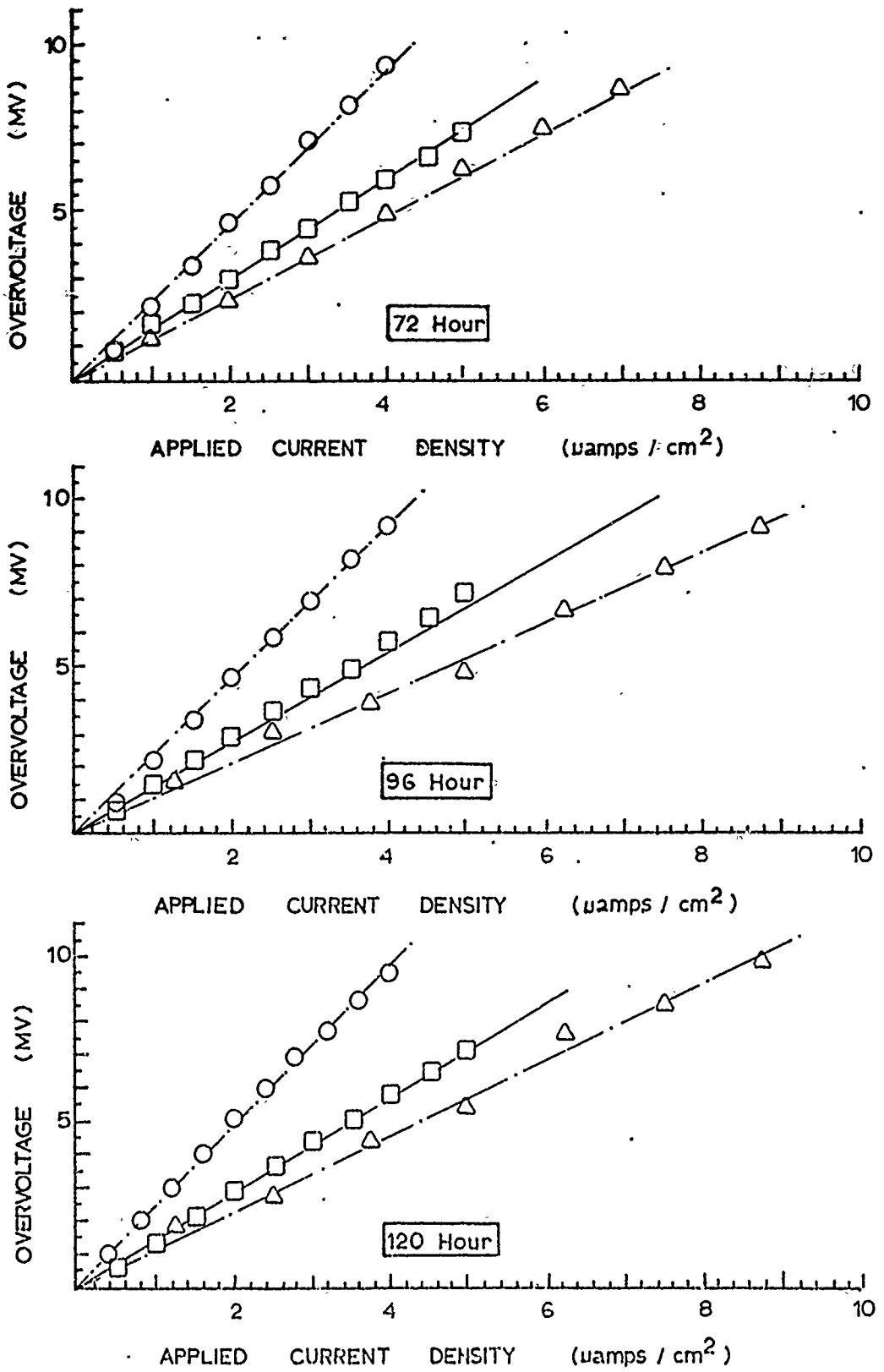

Figure 94: (Cont) Effect of Time on Galvanostatic Anodic Polarization Resistance of High Purity Iron with C/A Ratio = 2.5 in Aerated 3% Sodium Chloride Determined Using an Experimental Probe.

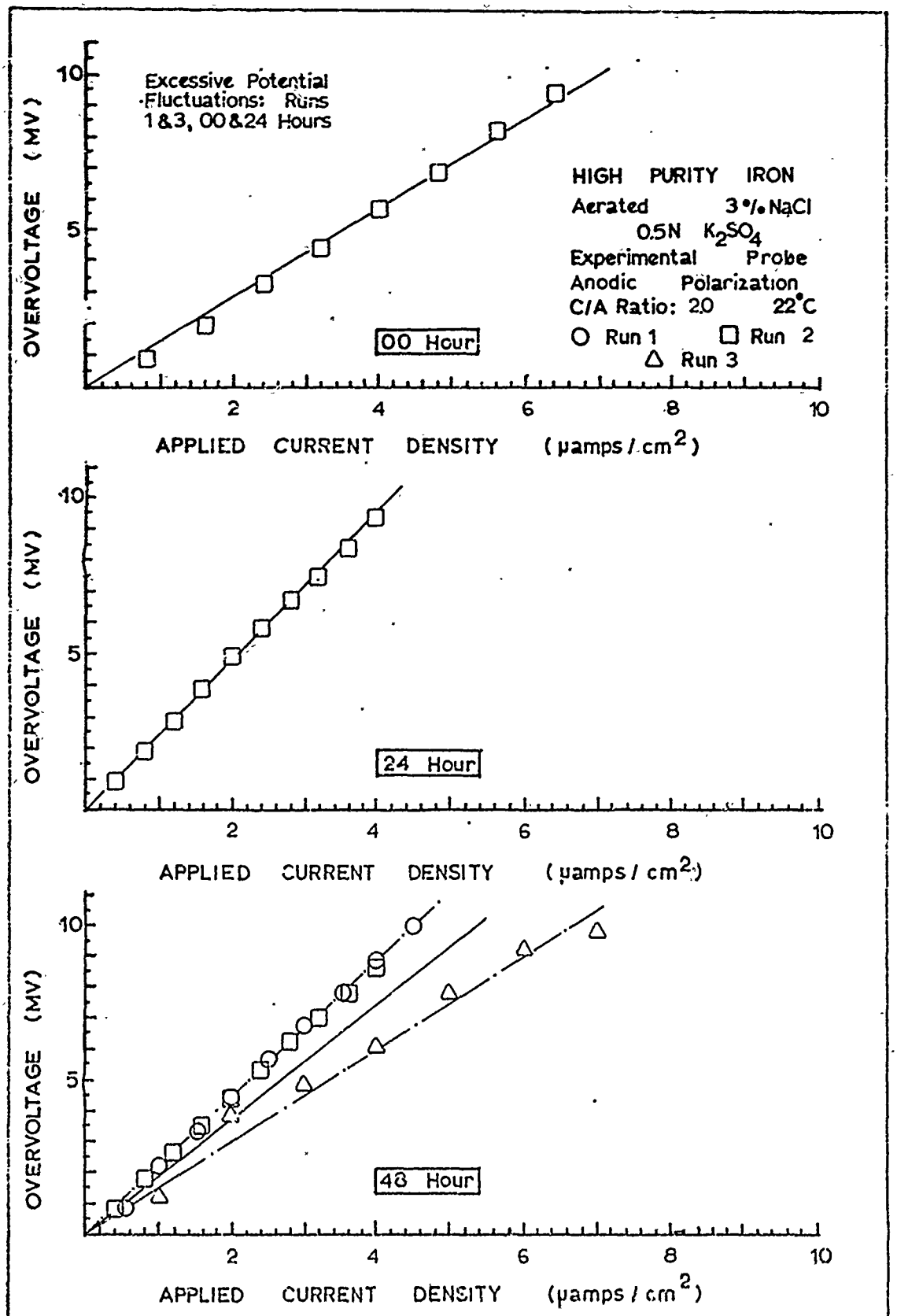

Figure 95: Effect of Time on Galvanostatic Anodic Polarization Resistance of High Purity Iron with C/A Ratio = 2 in Aerated 3% Sodium Chloride Determined Using an Experimental Probe. (Cont)

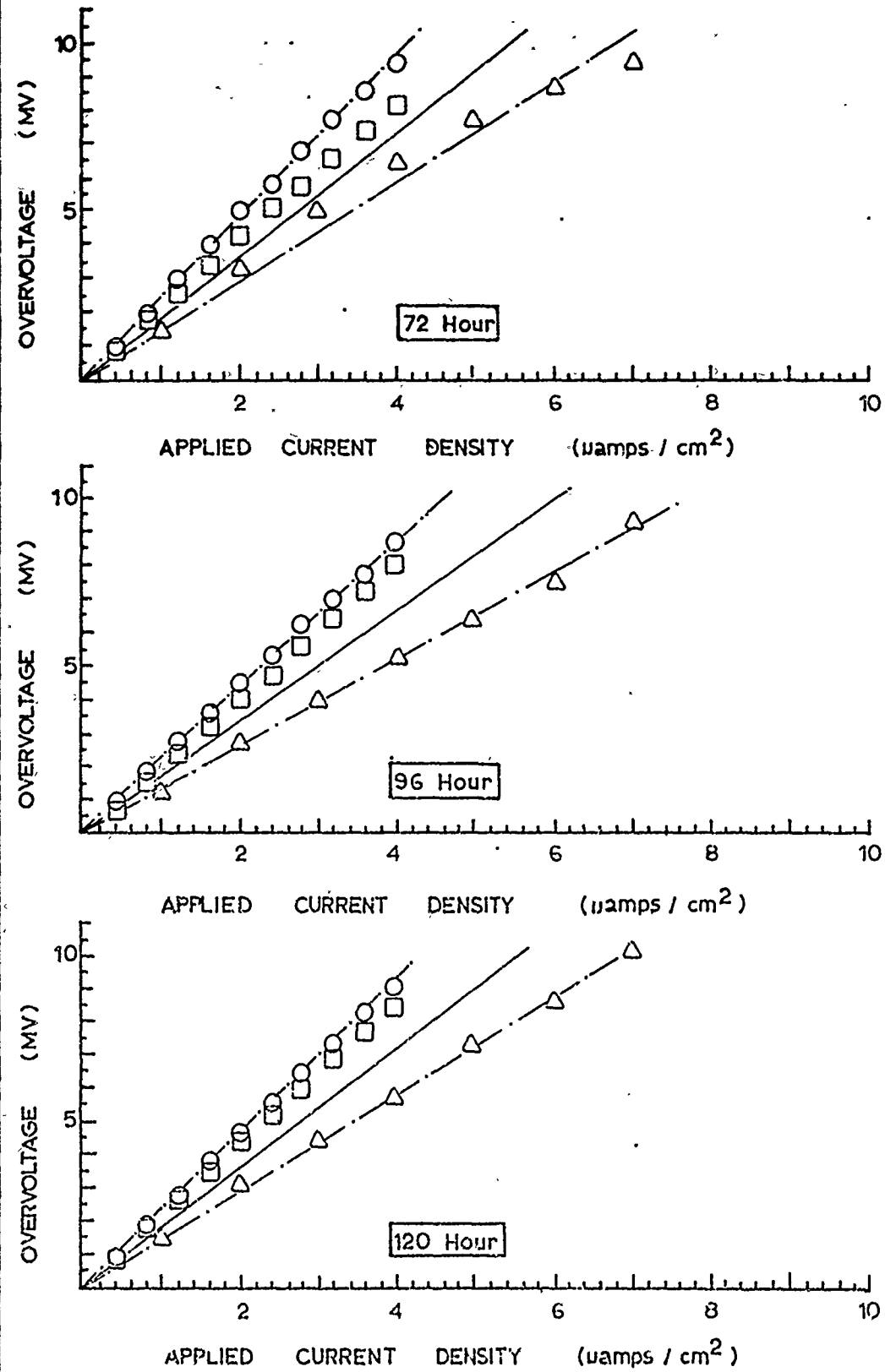

Figure 95: (Cont) Effect of Time on Galvanostatic Anodic Polarization Resistance of High Purity Iron with C/A Ratio = 2 in Aerated 3% Sodium Chloride Determined Using an Experimental Probe.

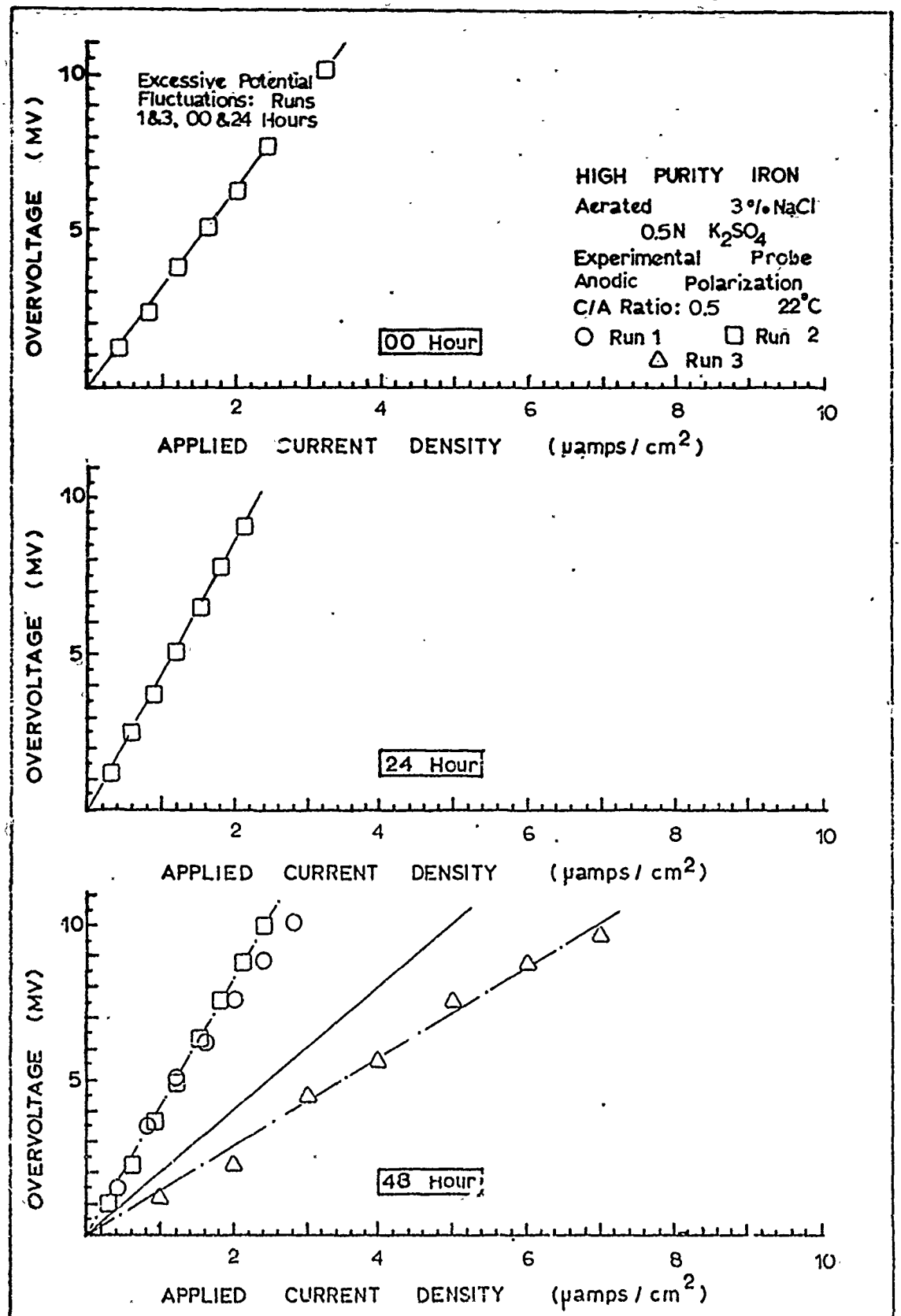

Figure 96: Effect of Time on Galvanostatic Anodic Polarization Resistance of High Purity Iron with C/A Ratio = .5 in Aerated 3% Sodium Chloride Determined Using an Experimental Probe. (Cont).

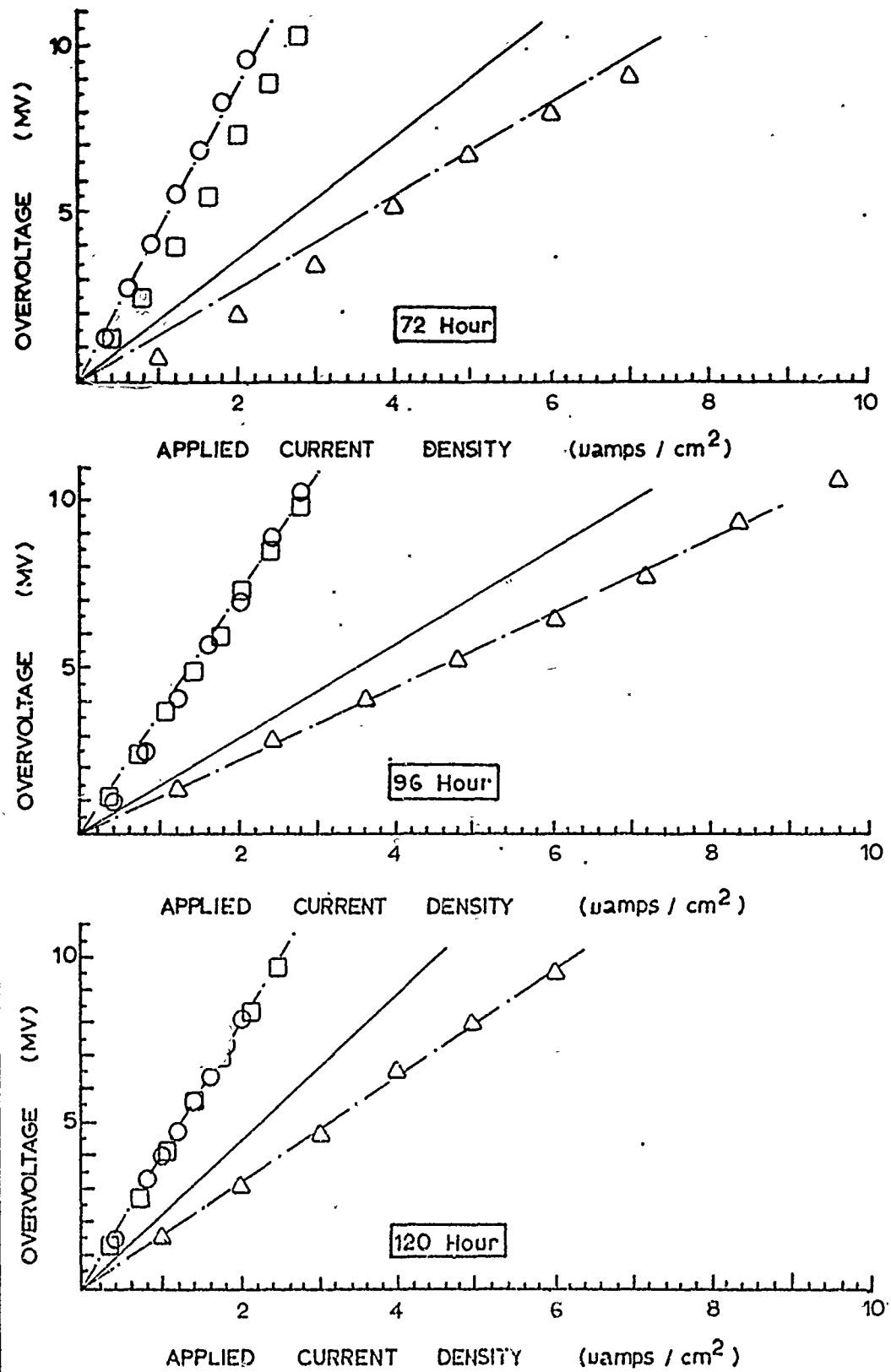

Figure 96: (Cont) Effect of Time on Galvanostatic Anodic Polarization Resistance of High Purity Iron with C/A Ratio = .5 in Aerated 3% Sodium Chloride Determined Using an Experimental Probe.

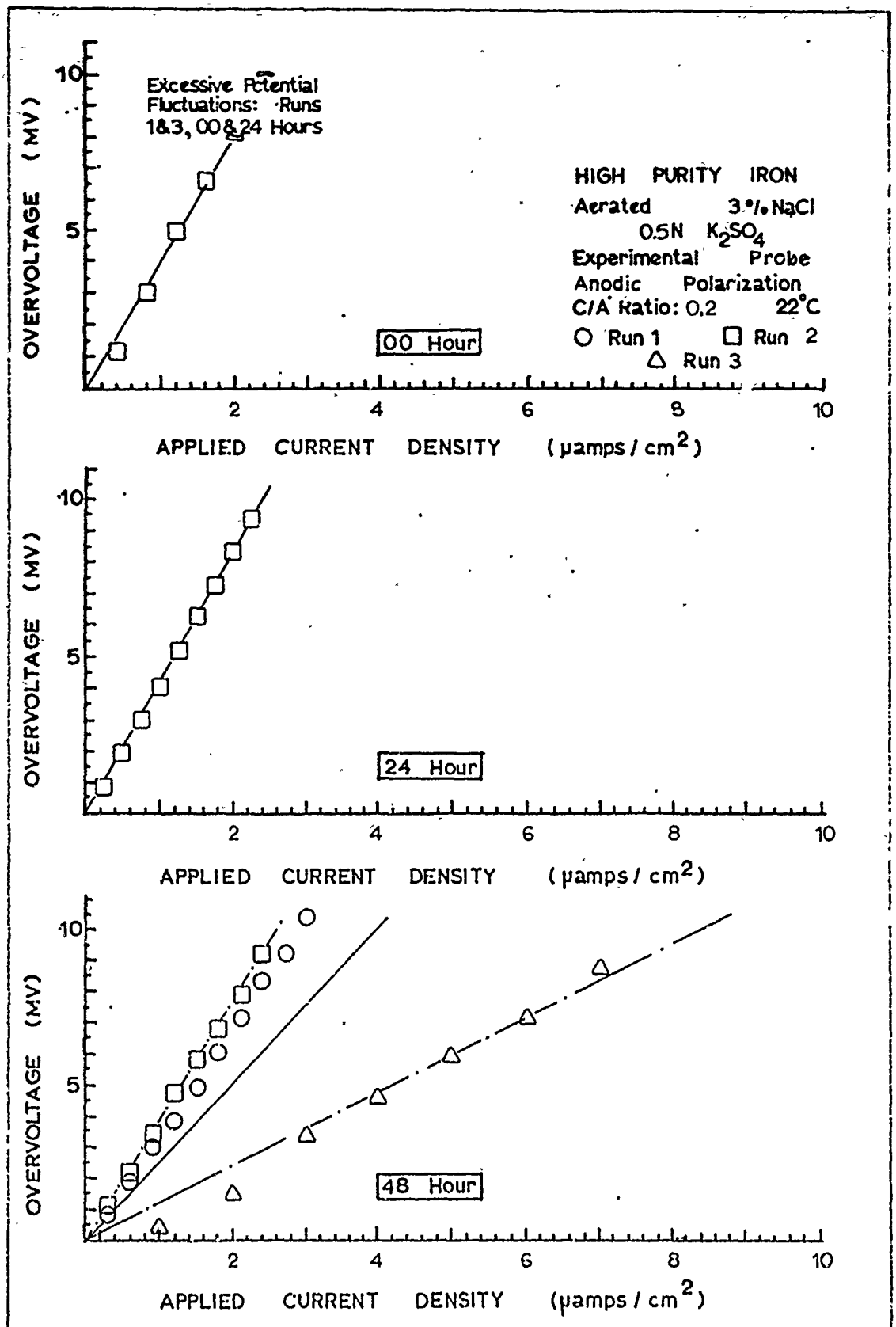

Figure 97: Effect of Time on Galvanostatic Anodic Polarization Resistance of High Purity Iron with C/A Ratio = .2 in Aerated 3% Sodium Chloride Determined Using an Experimental Probe. (Cont)

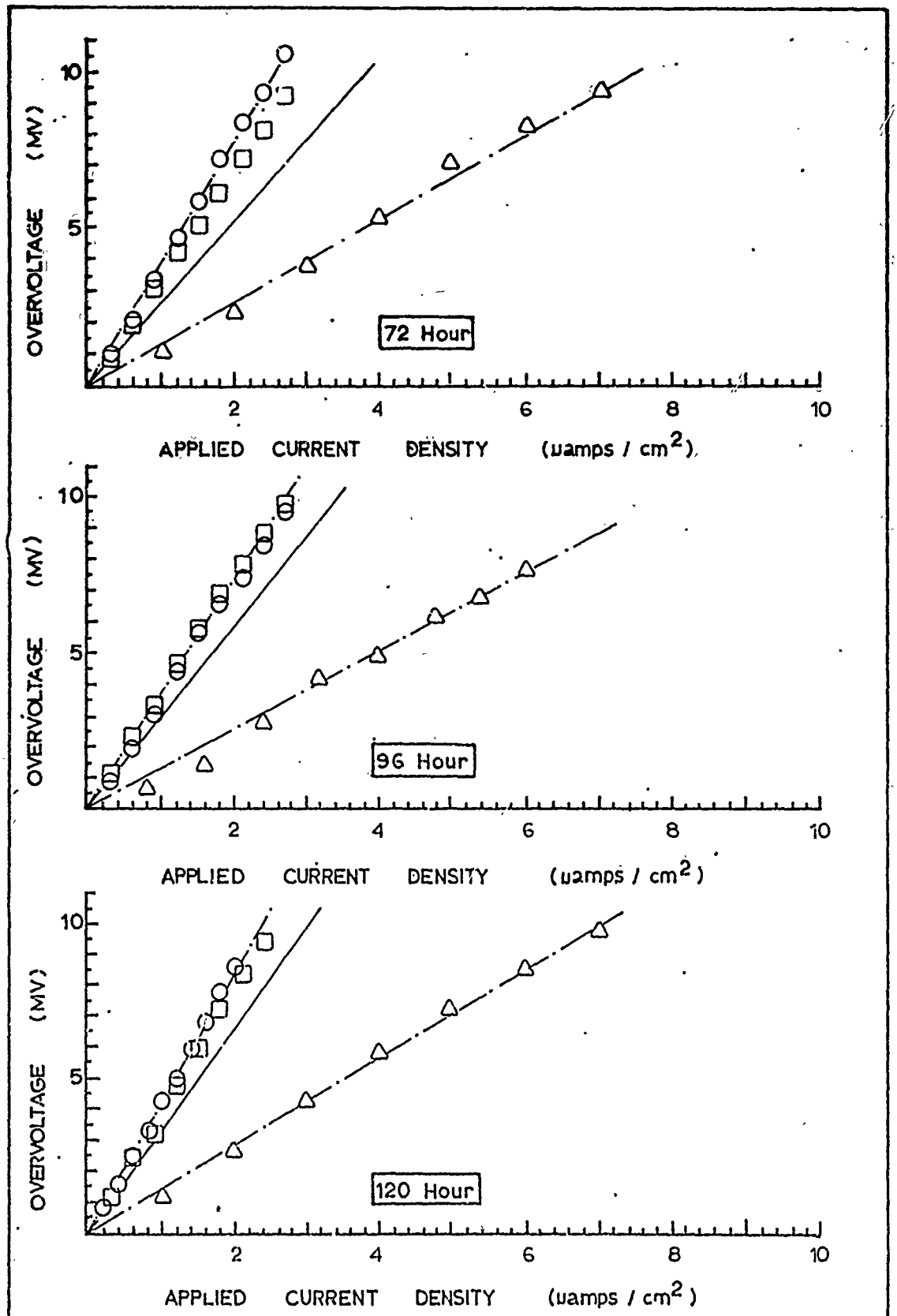

Figure 97: (Cont) Effect of Time on Galvanostatic Anodic Polarization Resistance of High Purity Iron with C/A Ratio = .2 in Aerated 3% Sodium Chloride Determined Using an Experimental Probe.

Appendix E

Supplementary Investigation - Effect of Time on Polarization Resistance and Corrosion Rate in Deaerated 0.01N Sulfuric Acid

The effect of time on polarization resistance and instantaneous corrosion rate for high purity iron I in deaerated 0.01N sulfuric acid are shown in this appendix. Anodic techniques were used to obtain laboratory test cell data. Cathodic techniques, which were unuseable for laboratory test cell observations, were used to obtain experimental test cell data. Note that the abscissa scales of Figures 98 and 99 are different.

Table X

Electrolyte pH Data for 0.01N Sulfuric Acid

Observations	2
pH Data	
Maximum	1.80
Minimum	1.71
Mean	1.76

Table XI

Effect of Time on High Purity Iron I Steady-State Corrosion Potential in 0.01N Sulfuric Acid

	CORROSION POTENTIAL (V) VS. S.C.E.					
RUN \ HOURS	00	24	48	72	96	120
1	-.5310	-.5260	-.5210	-.5160	-.5190	–
2	–	-.5540	-.5460	-.5310	-.5340	-.5330

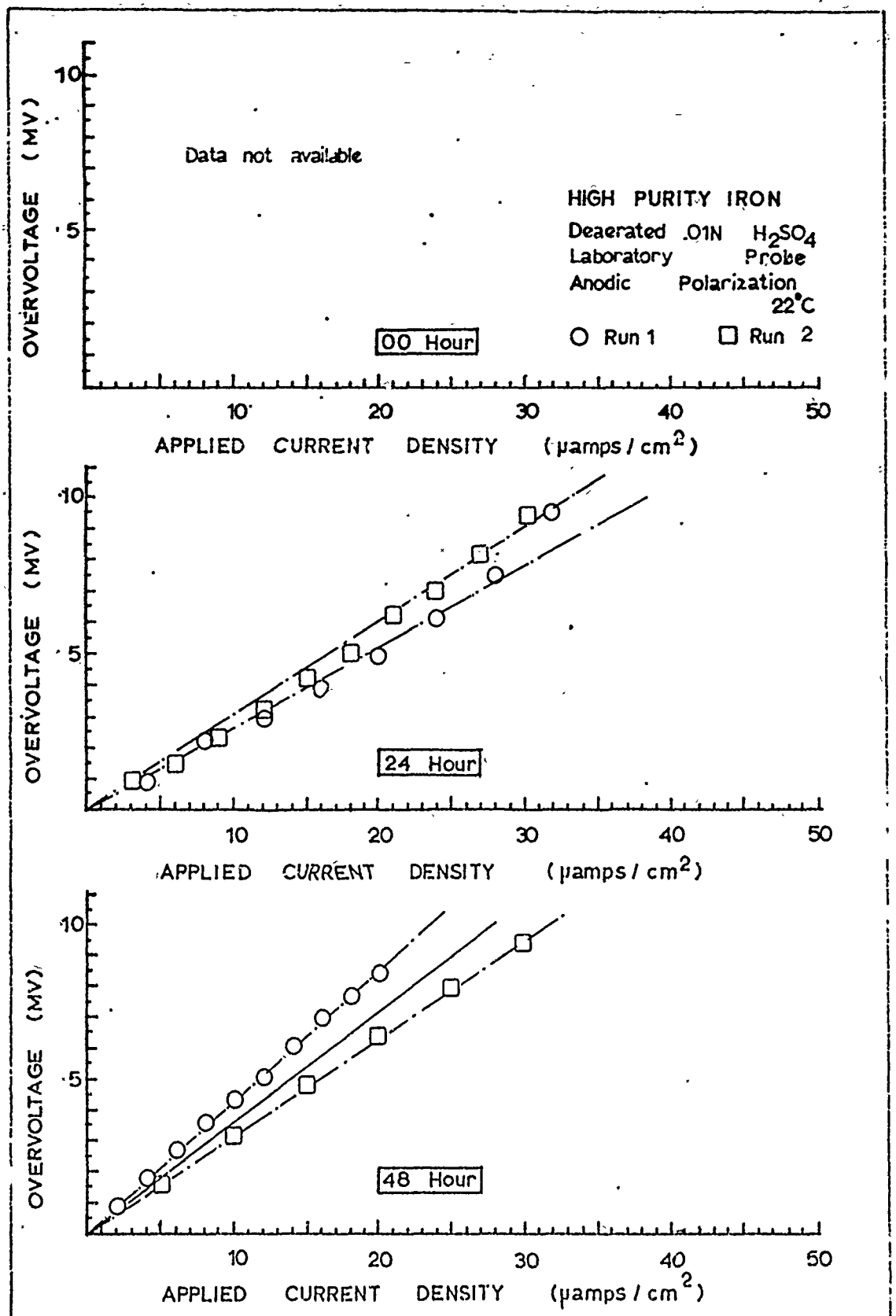

Figure 98: Effect of Time on Galvanostatic Anodic Polarization Resistance of High Purity Iron in Hydrogen Saturated .01N Sulfuric Acid Determined Using a Laboratory Probe. (Cont)

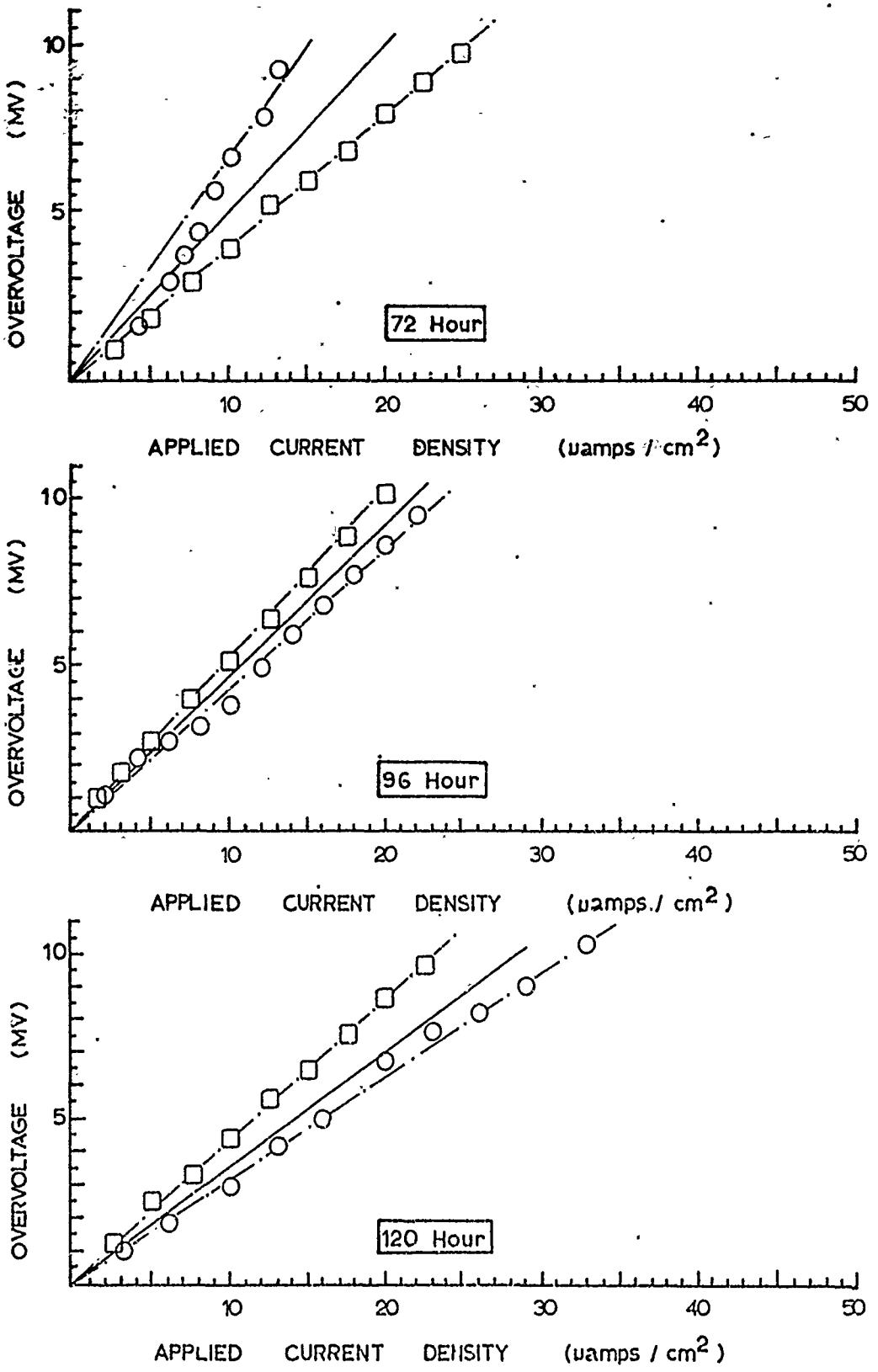

Figure 98: (Cont) Effect of Time on Galvanostatic Anodic Polarization Resistance of High Purity Iron in Hydrogen Saturated .01N Sulfuric Acid Determined Using a Laboratory Probe.

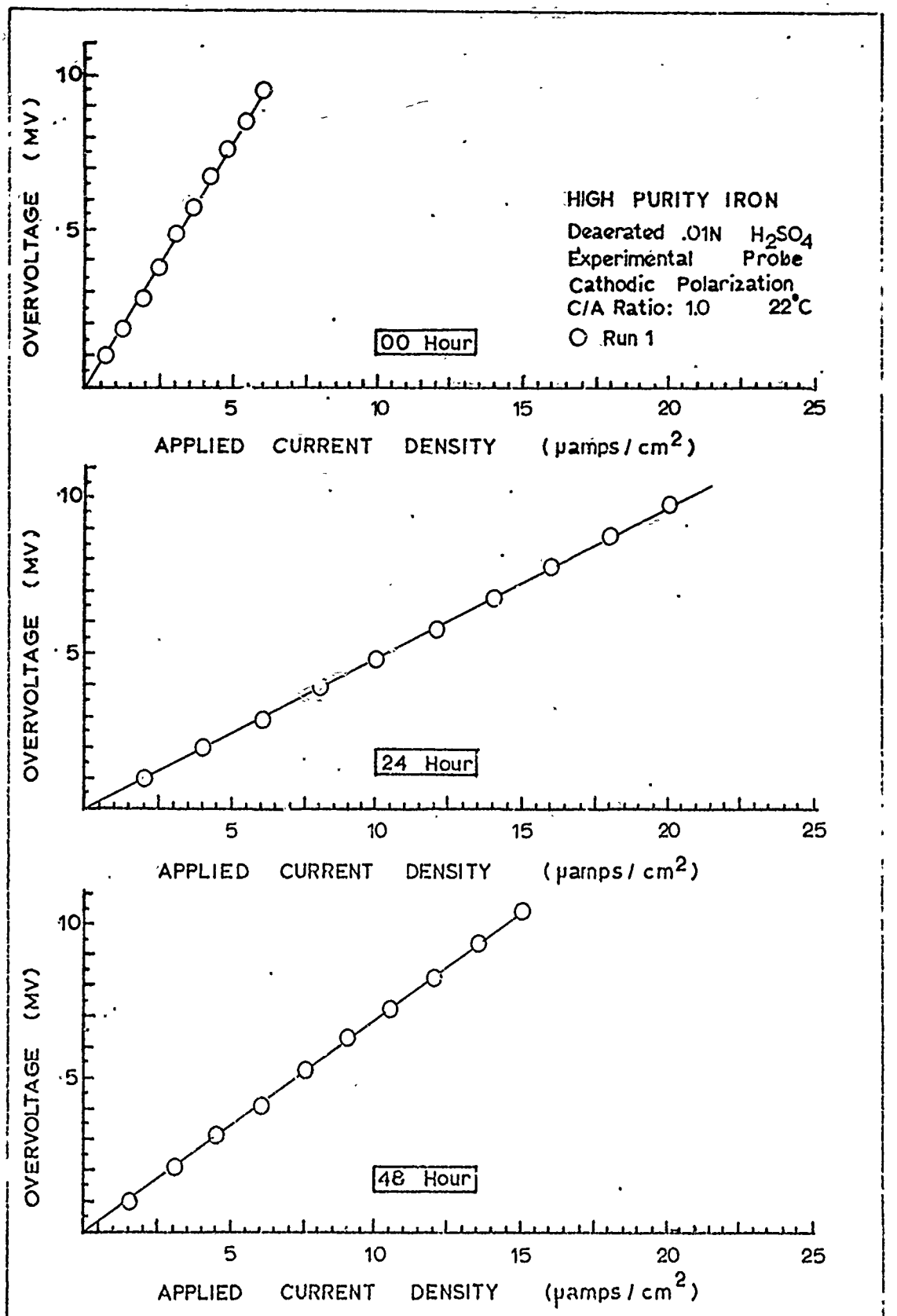

Figure 99: Effect of Time on Galvanostatic Cathodic Polarization Resistance of High Purity Iron with C/A Ratio = 1 in Hydrogen Saturated .01N Sulfuric Acid Determined Using an Experimental Probe. (Cont)

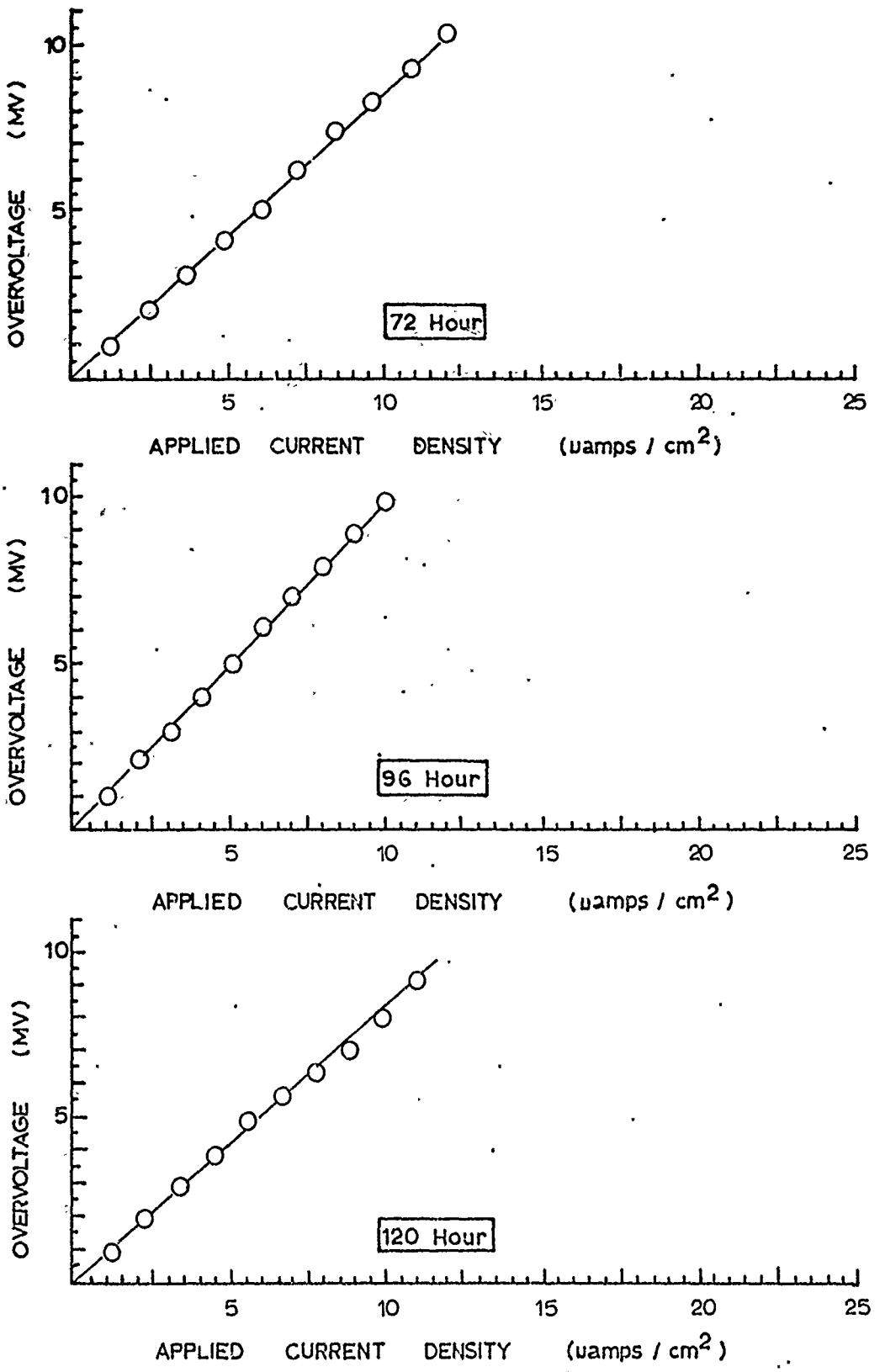

Figure 99: (Cont) Effect of Time on Galvanostatic Cathodic Polarization Resistance of High Purity Iron with C/A Ratio = 1 in Hydrogen Saturated .01N Sulfuric Acid Determined Using an Experimental Probe.

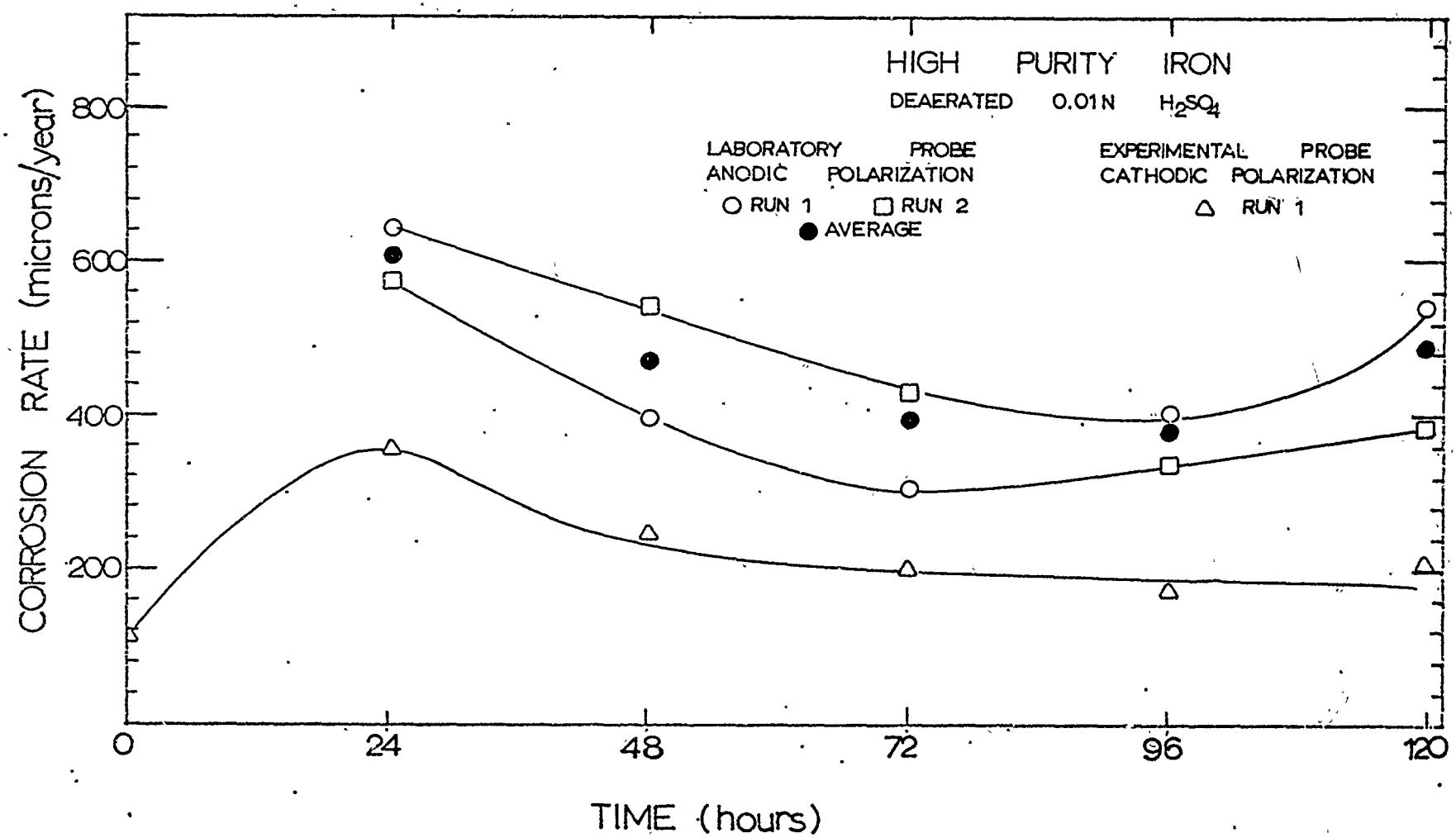

Figure 100: Effect of Time on the Instantaneous Corrosion Rate of High Purity Iron I in Hydrogen Saturated .01N Sulfuric Acid.

Appendix F

The Effect of Time on the Instantaneous Corrosion Rate of High Purity Iron I as Indicated Using Resistance Polarization Techniques and a Laboratory Probe

The effects of time on the indicated instantaneous corrosion rate of high purity iron (specimen I) in aerated and deaerated (hydrogen saturated) 1N and 0.1N sulfuric acids and 3% sodium chloride environments are shown in this appendix. The results obtained by both cathodic and anodic resistance polarization techniques using the laboratory test cell described in Chapter III are shown. The corrosion rates plotted were calculated using by run, by day and combined daily data determinated polarization resistance values. (See "Polarization Resistance Determination" in Chapter IV for terminology definitions). The envelopes shown are intended to display the approximate ranges of observed corrosion rate data. Note that ordinate scales may vary amongst the figures.

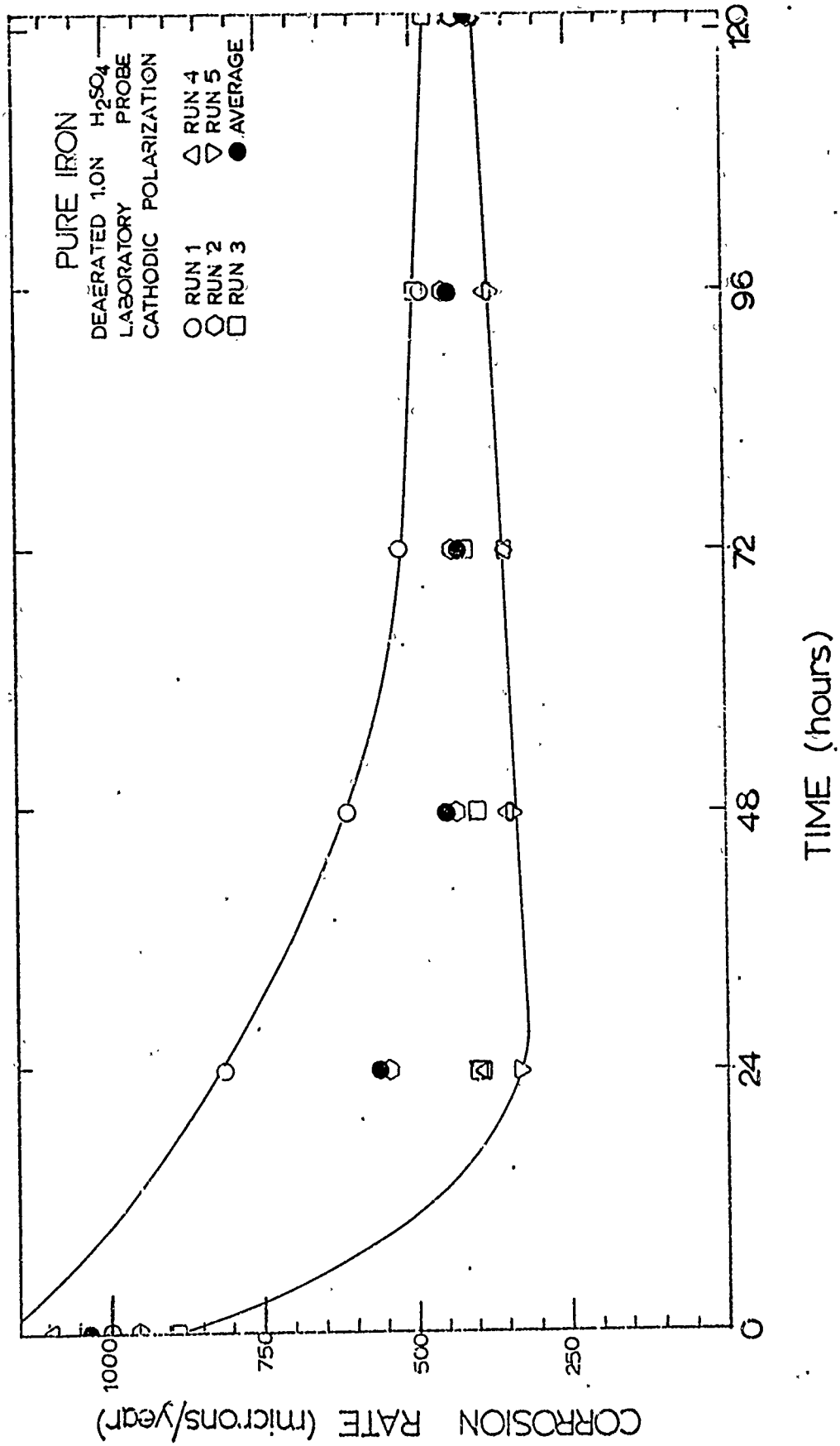

Figure 101: Effect of Time on the Corrosion Rate of High Purity Iron in Hydrogen Saturated 1N Sulfuric Acid Determined by Cathodic Polarization Using a Laboratory Probe.

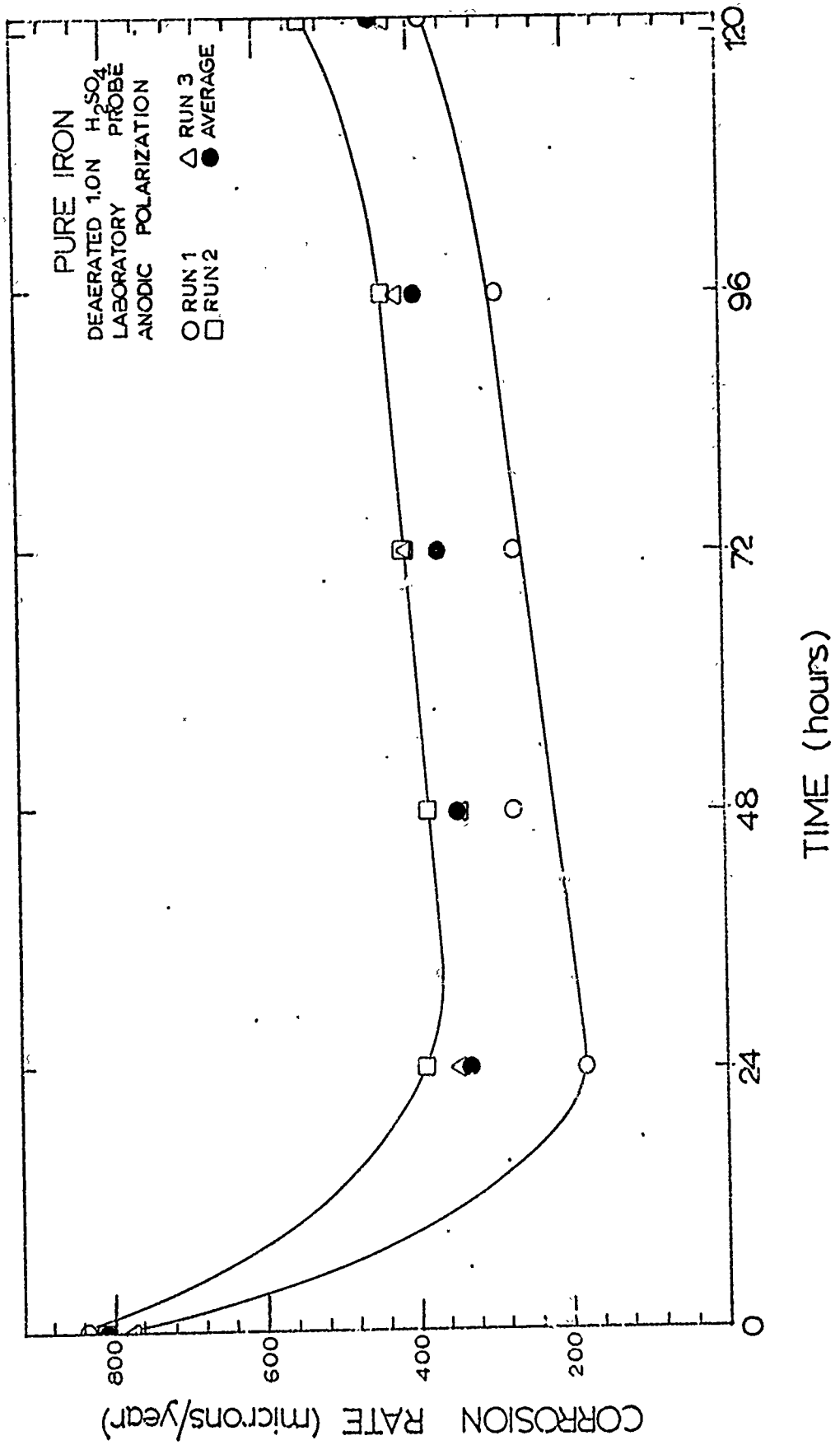

Figure 102 Effect of Time on the Corrosion Rate of High Purity Iron in Hydrogen Saturated 1N Sulfuric Acid Determined by Anodic Polarization Using a Laboratory Probe.

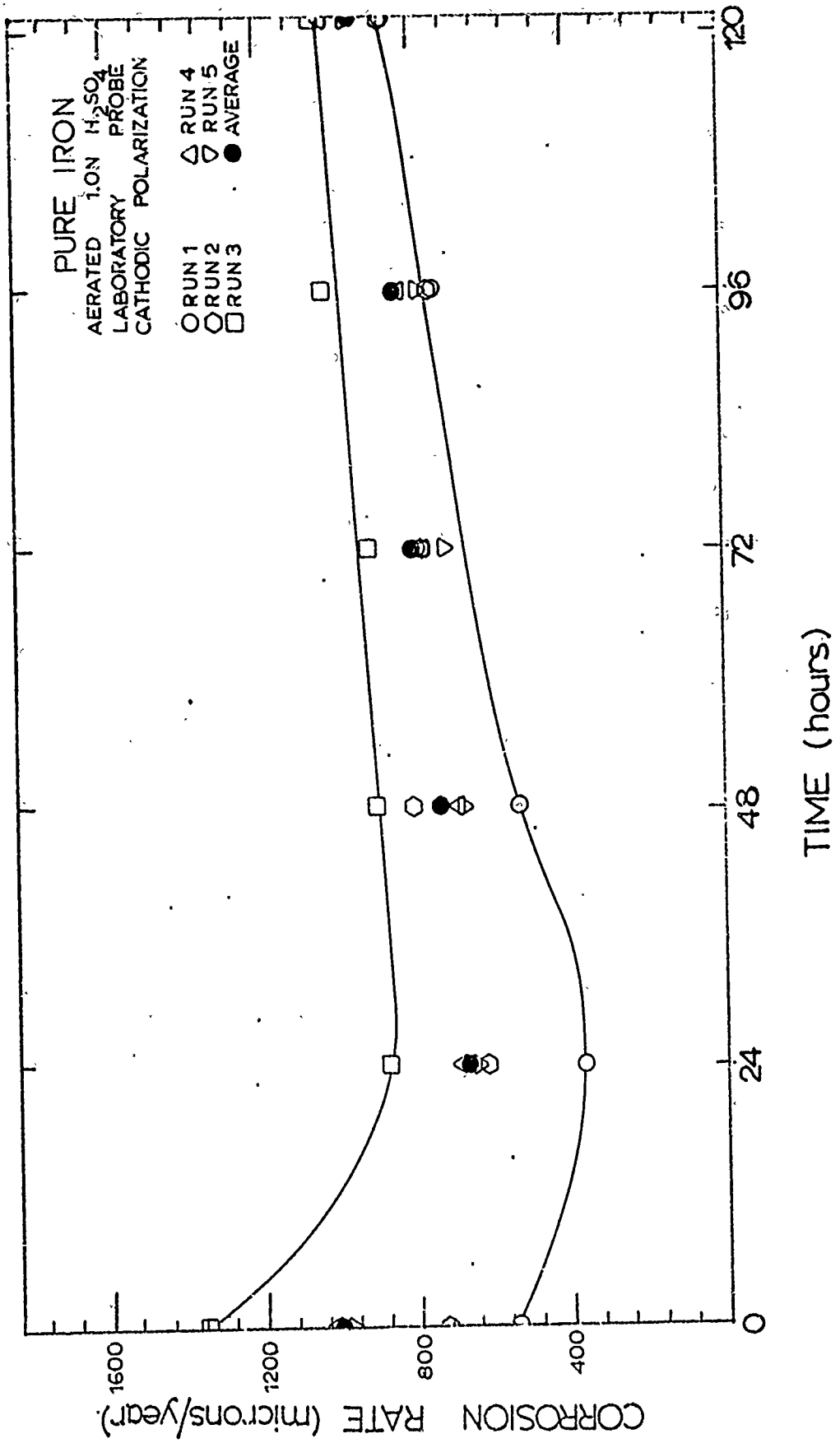

Figure 103: Effect of Time on the Corrosion Rate of High Purity Iron in Aerated 1N Sulfuric Acid Determined by Cathodic Polarization Using a Laboratory Probe.

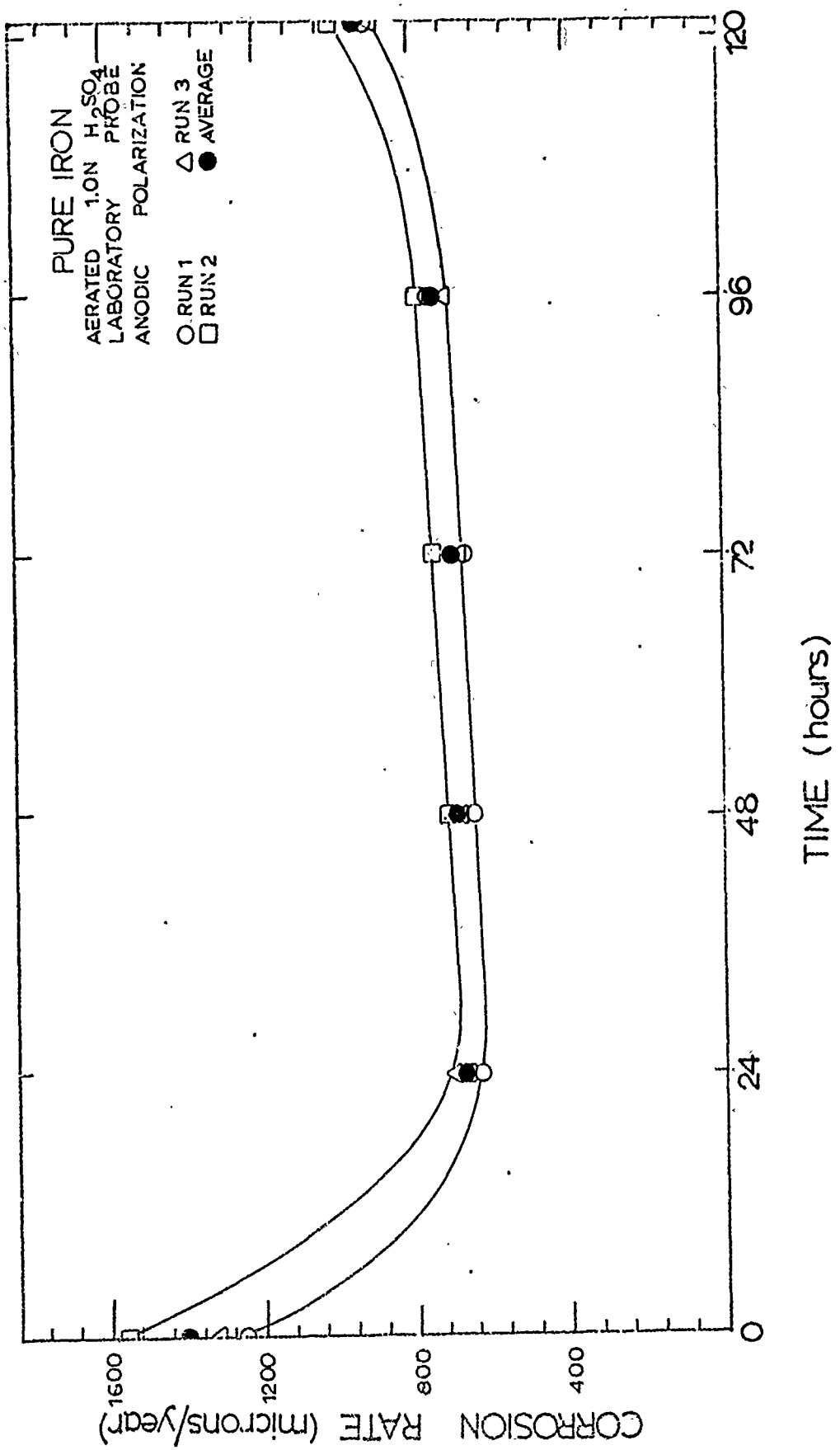

Figure 104: Effect of Time on the Corrosion Rate of High Purity Iron in Aerated 1N Sulfuric Acid Determined by Anodic Polarization Using a Laboratory Probe.

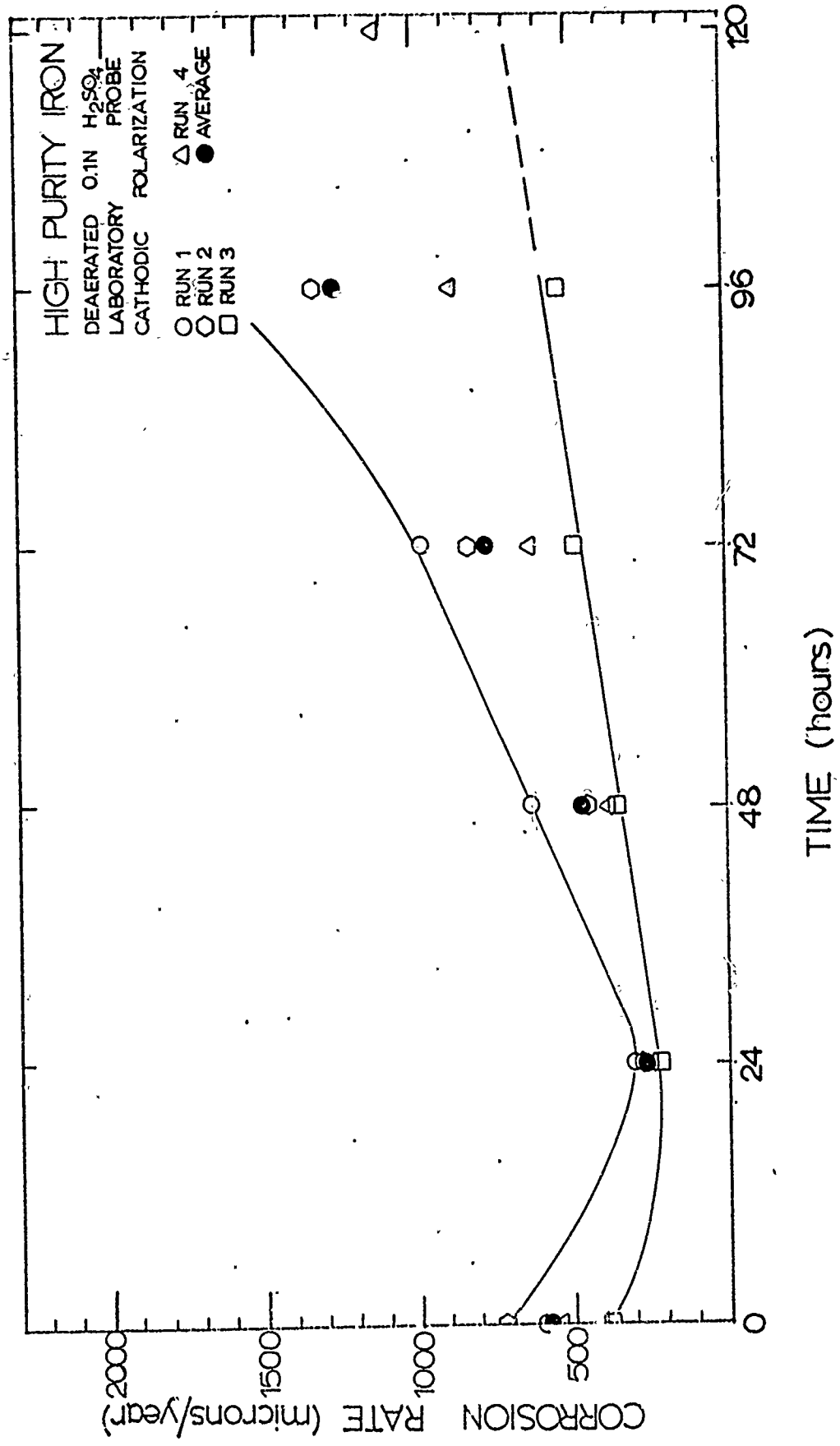

Figure 105: Effect of Time on the Corrosion Rate of High Purity Iron in Hydrogen Saturated .1N Sulfuric Acid Determined by Cathodic Polarization Using a Laboratory Probe.

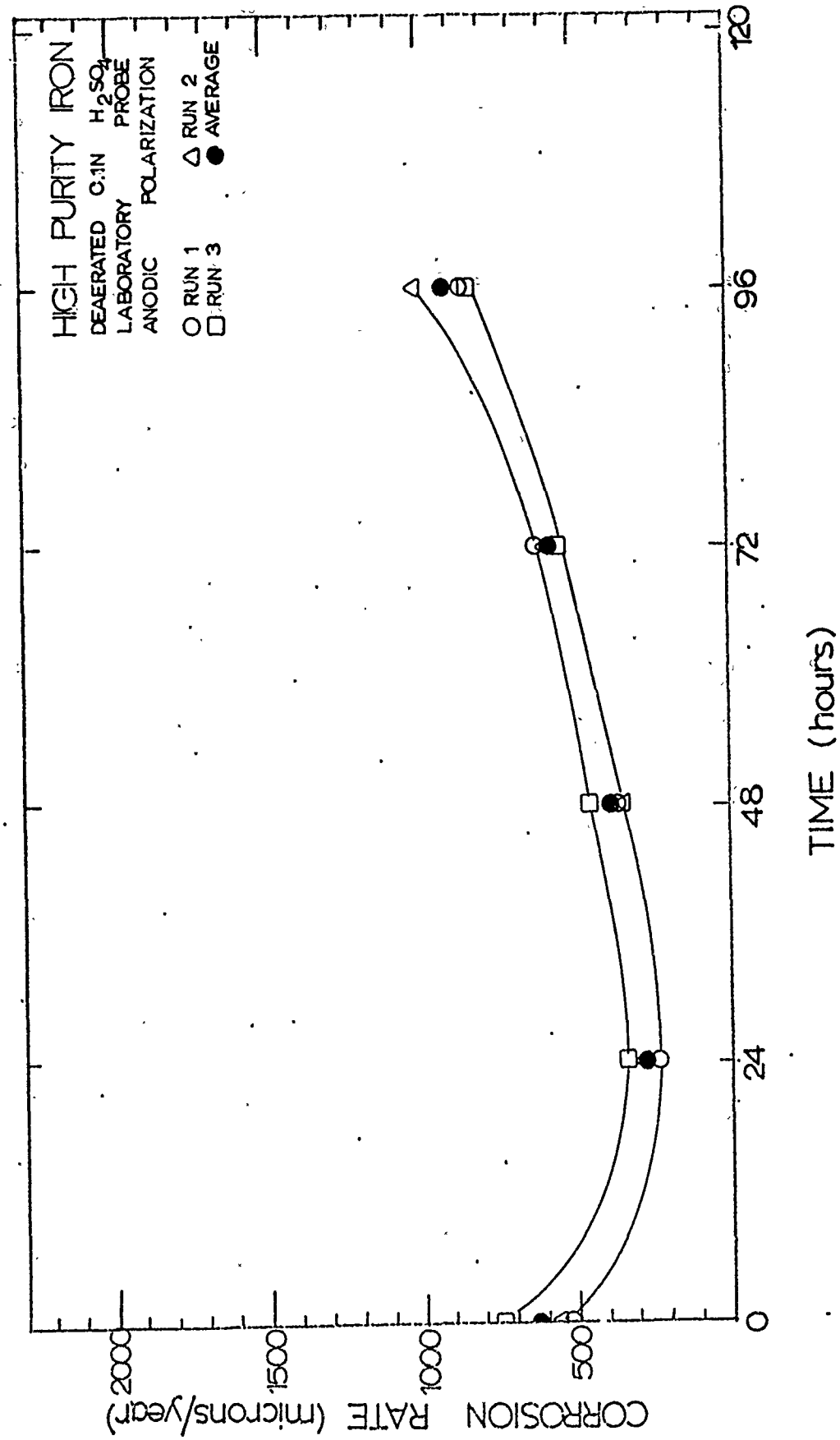

Figure 106: Effect of Time on the Corrosion Rate of High Purity Iron in Hydrogen Saturated .1N Sulfuric Acid Determined by Anodic Polarization Using a Laboratory Probe.

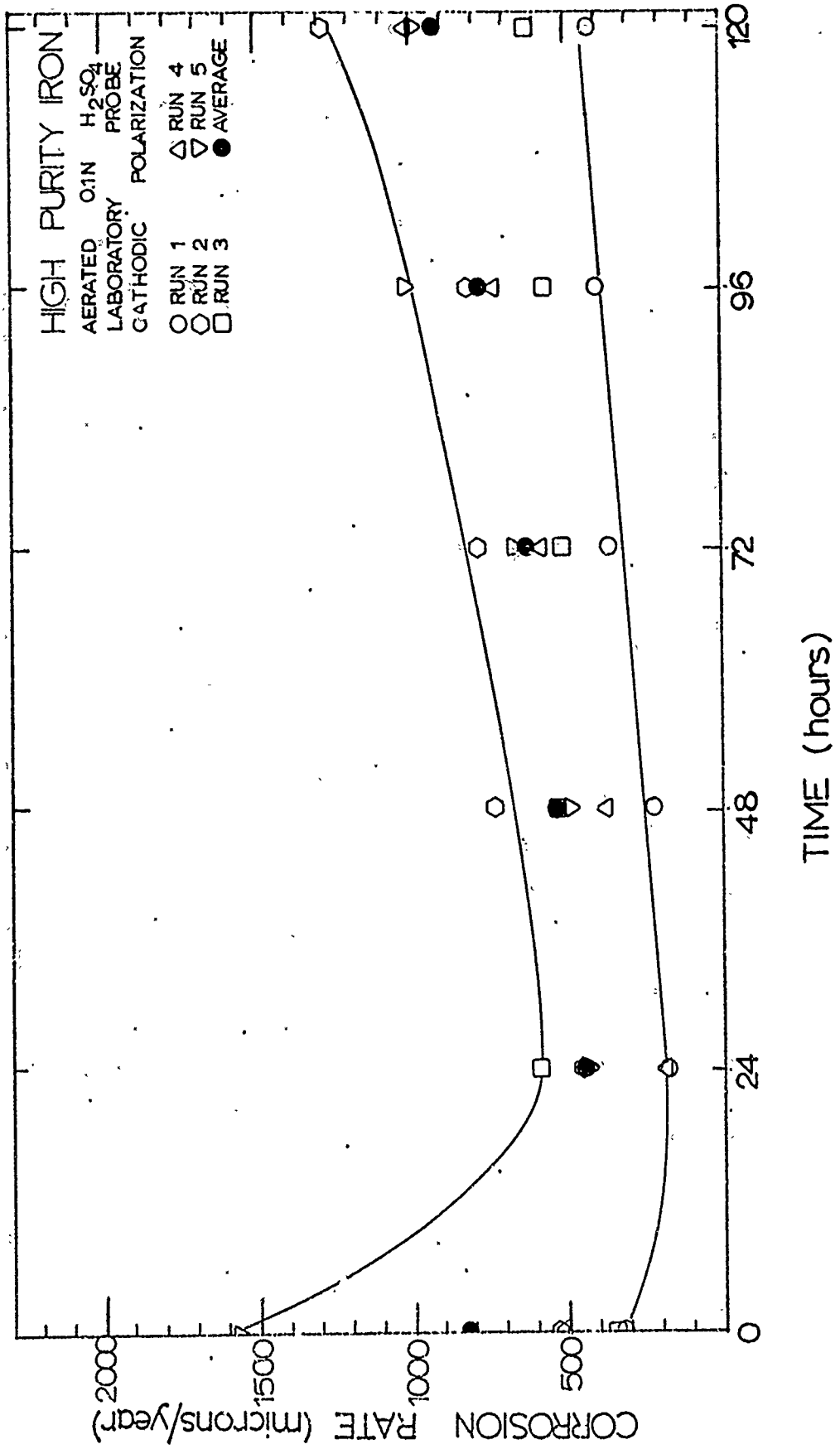

Figure 107: Effect of Time on the Corrosion Rate of High Purity Iron in Aerated .1N Sulfuric Acid Determined by Cathodic Polarization Using a Laboratory Probe.

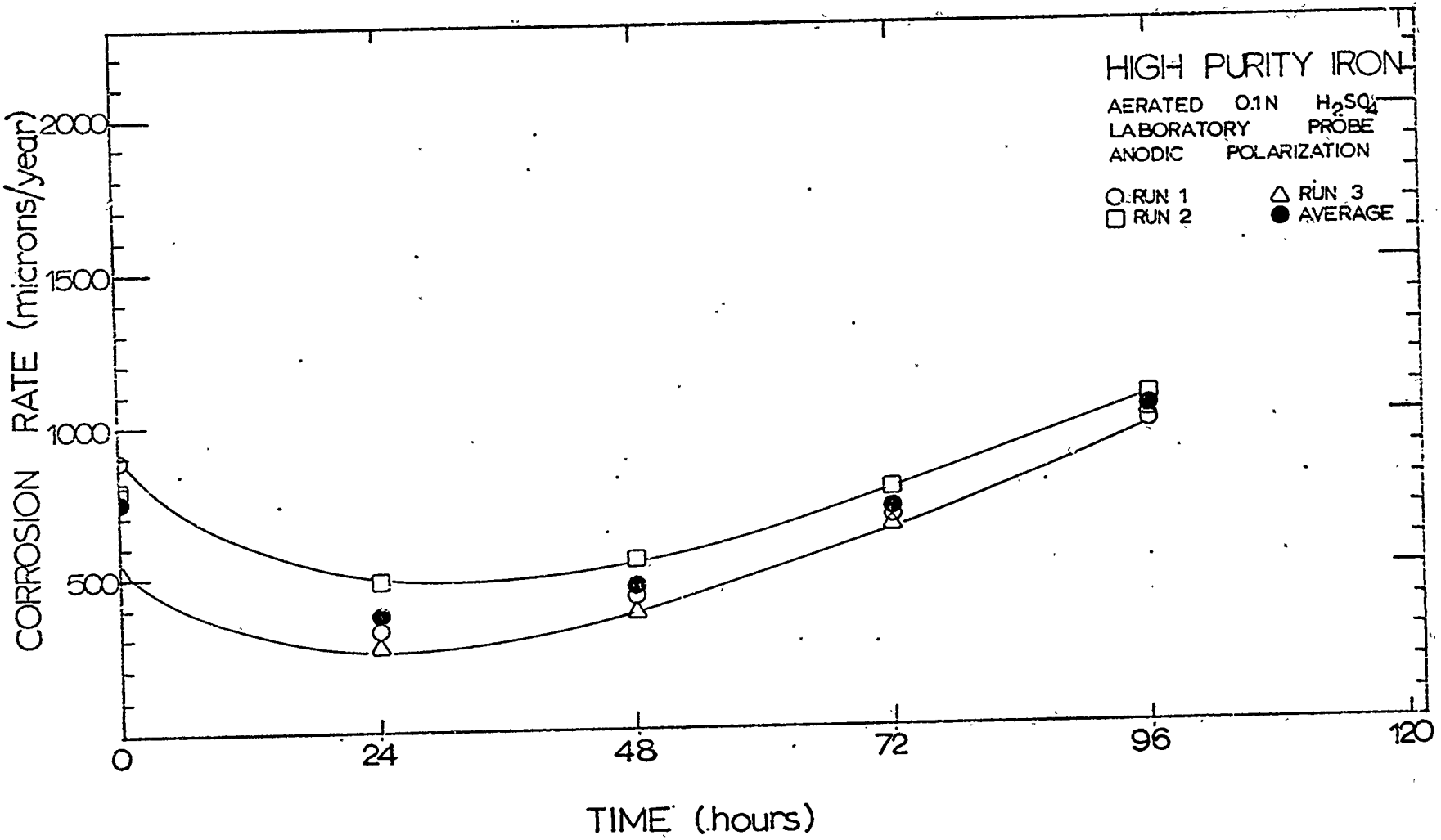

Figure 108: Effect of Time of the Corrosion Rate of High Purity Iron in Aerated .1N Sulfuric Acid Determined by Anodic Polarization Using a Laboratory Probe.

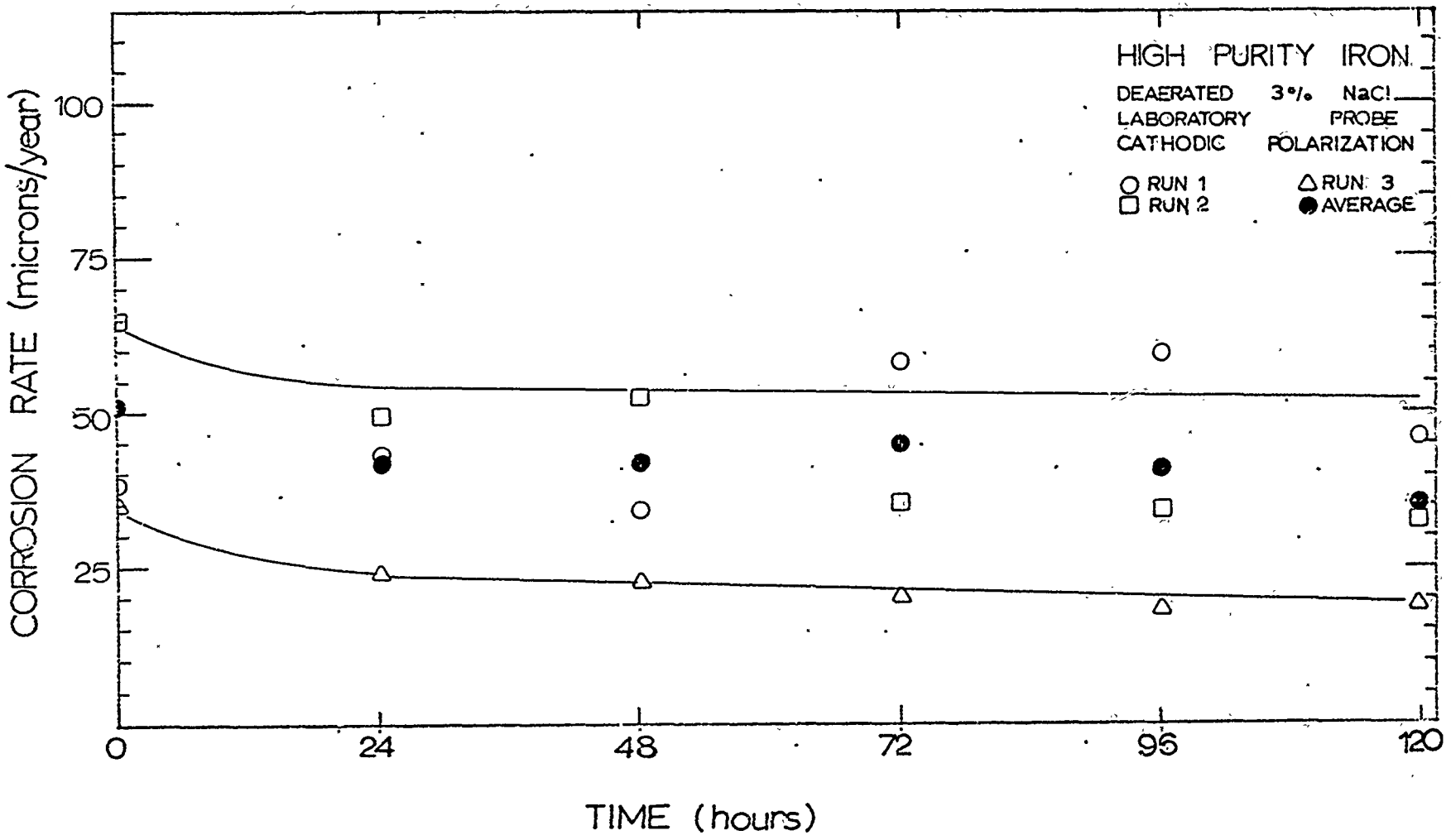

Figure 109: Effect of Time on the Corrosion Rate of High Purity Iron in Hydrogen Saturated 3% Sodium Chloride Determined by Cathodic Polarization Using a Laboratory Probe.

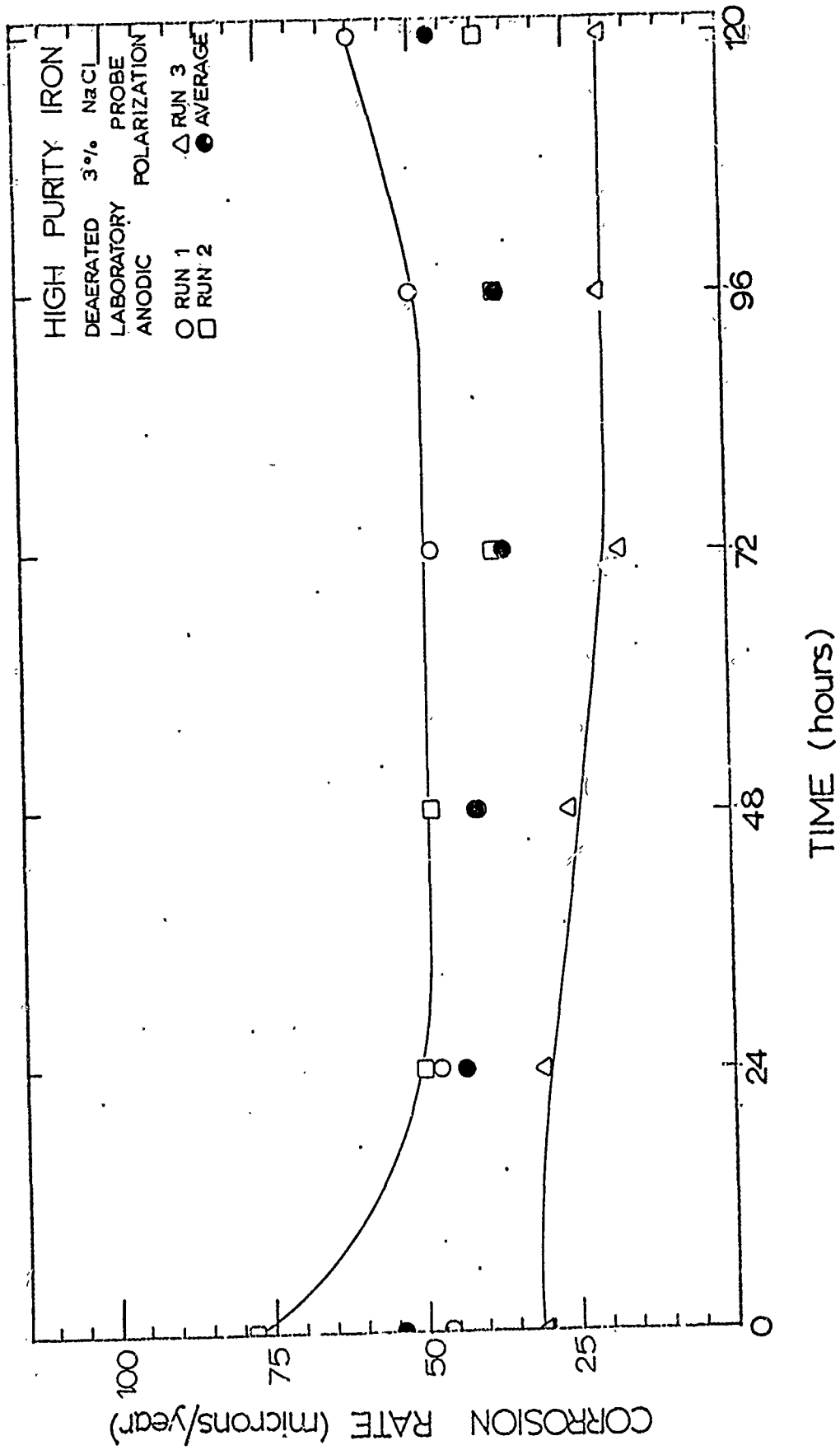

Figure 110: Effect of Time on the Corrosion Rate of High Purity Iron in Hydrogen Saturated 3% Sodium Chloride Determined by Anodic Polarization Using a Laboratory Probe.

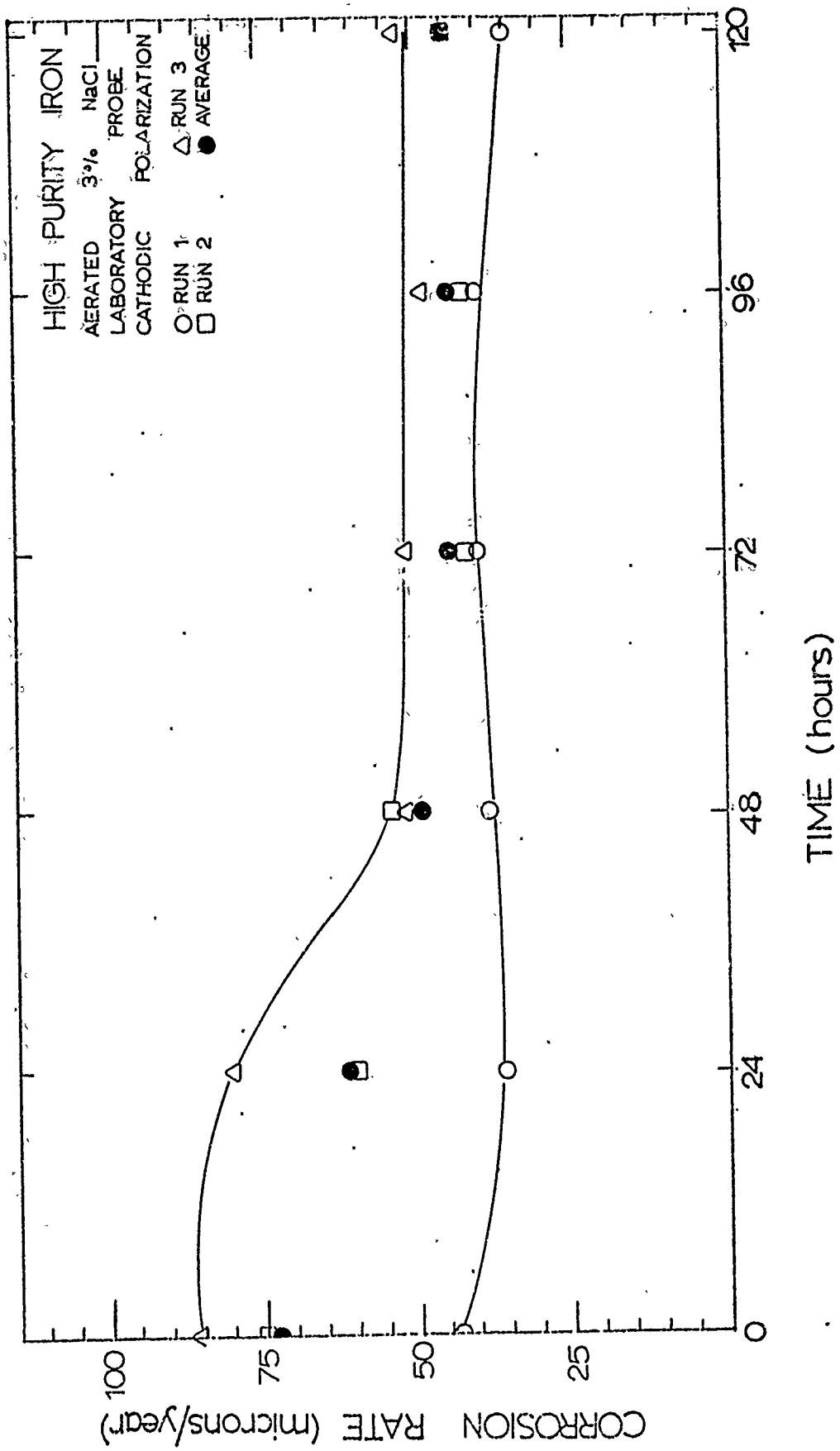

Figure 111: Effect of Time on the Corrosion Rate of High Purity Iron in Aerated 3% Sodium Chloride Determined by Cathodic Polarization Using a Laboratory Probe.

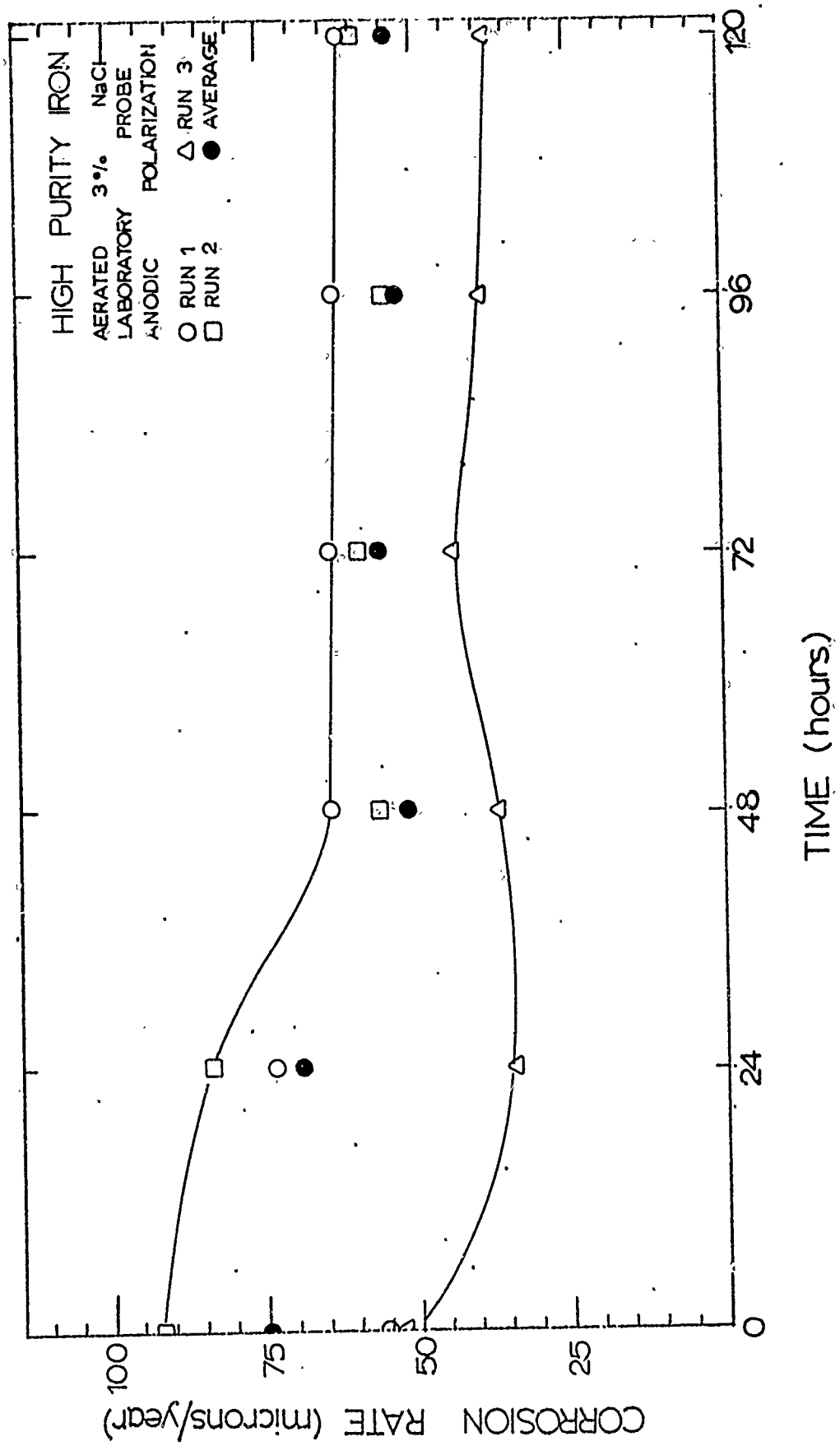

Figure 112: Effect of Time on the Corrosion Rate of High Purity Iron in Aerated 3% Sodium Chloride Determined by Anodic Polarization Using a Laboratory Probe.

Appendix G

The Effect of Time on the Instantaneous Corrosion Rate of High Purity Iron I as Indicated Using Resistance Polarization Techniques and an Experimental Probe

The effects of time on the indicated instantaneous corrosion rate of high purity iron (specimen I) in aerated and deaerated (hydrogen saturated) 1N and 0.1N sulfuric acids and 3% sodium chloride environments are shown in this appendix. The results obtained by both cathodic and anodic resistance polarization techniques using the experimental test cell described in Chapter III are shown. The corrosion rates plotted were calculated using by run, by day and combined daily data determined polarization resistance values. (See "Polarization Resistance Determination" in Chapter IV for terminology definitions). The envelopes shown are intended to display the approximate ranges of observed corrosion rate data. Note that ordinate scales may vary amongst the figures.

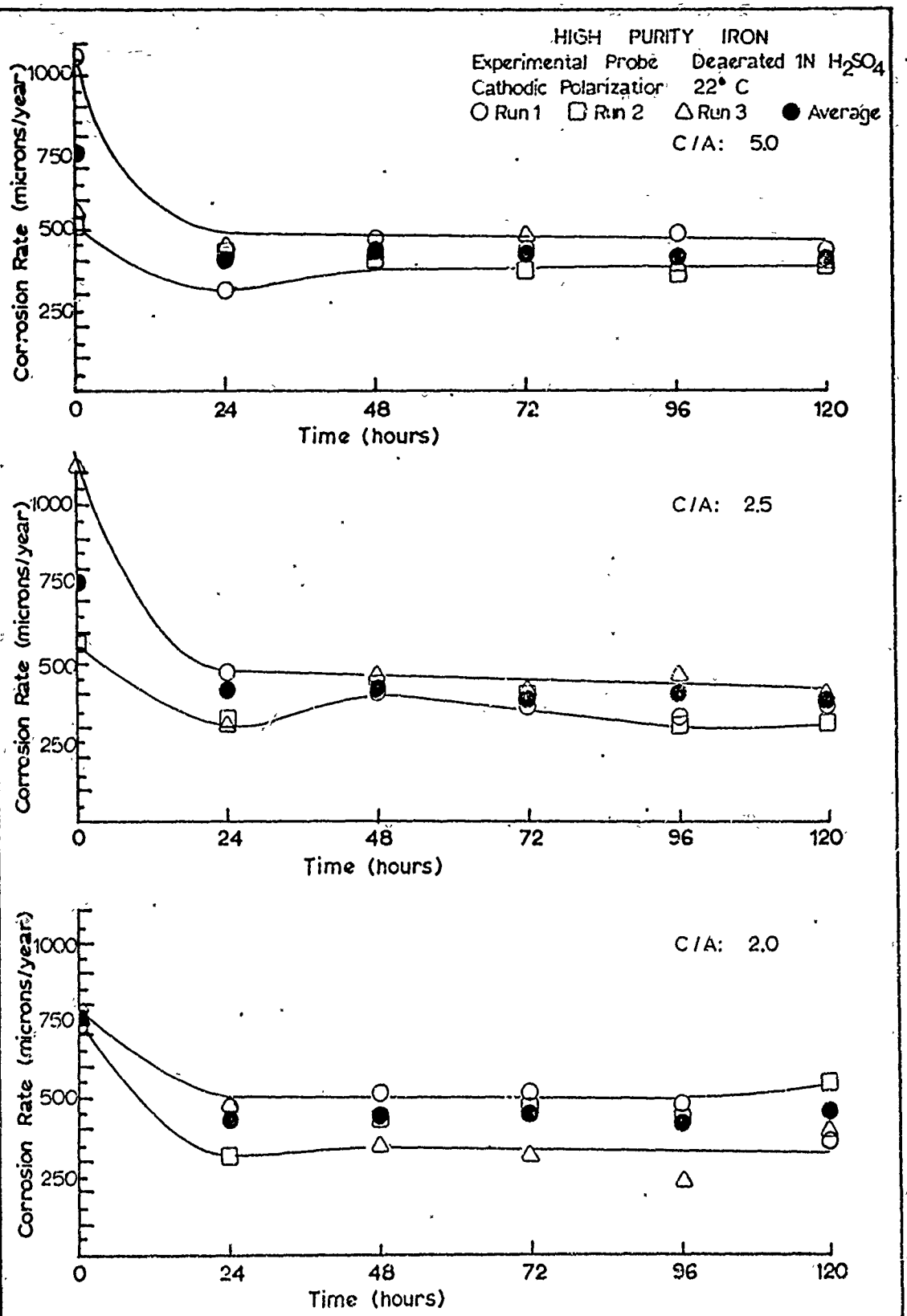

Figure 113: Effect of Time on the Corrosion Rate of High Purity Iron at Various C/A Ratios in Hydrogen Saturated 1N Sulfuric Acid Determined by Cathodic Polarization Using an Experimental Probe. (Cont)

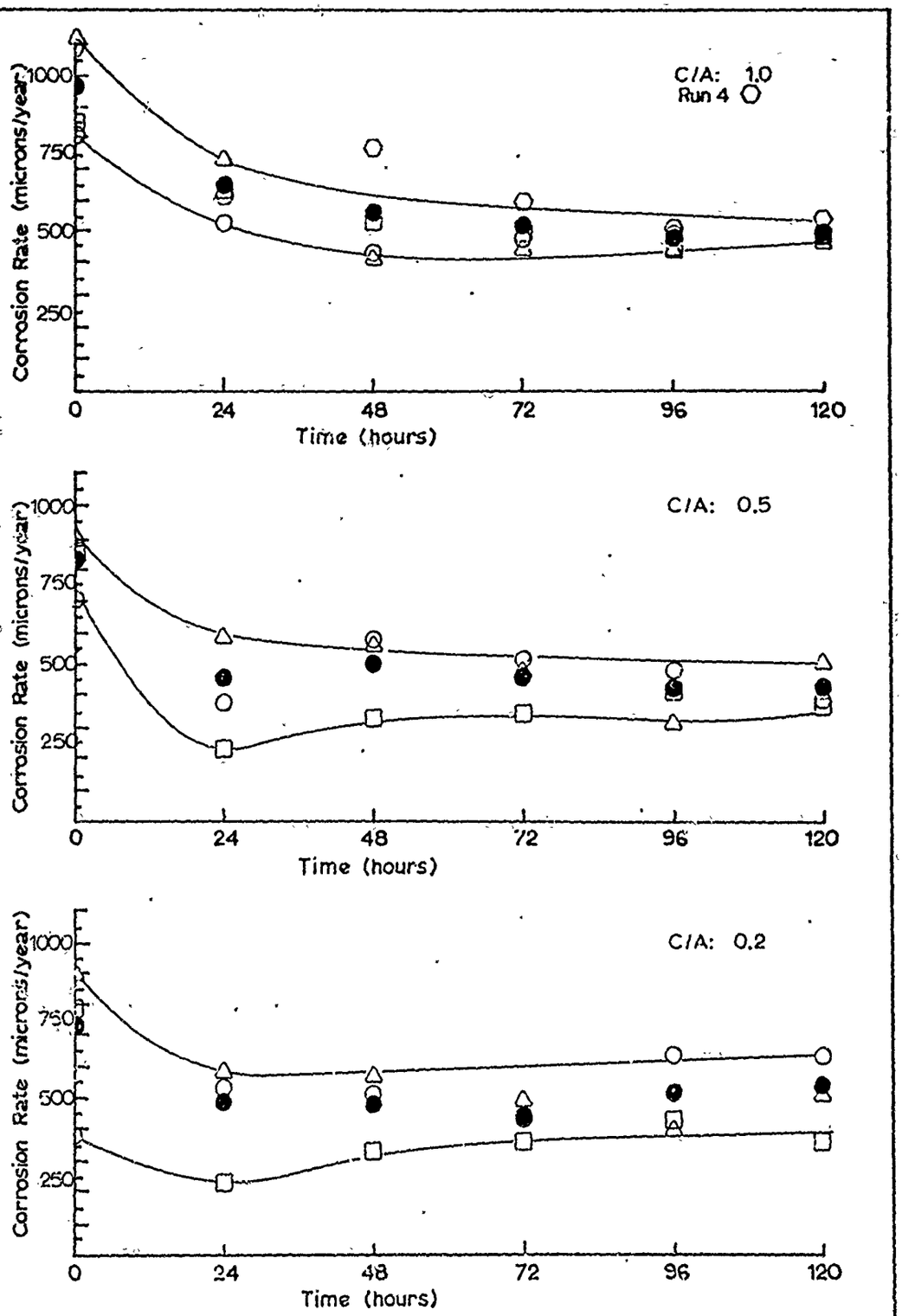

Figure 113: (Cont) Effect of Time on the Corrosion Rate of High Purity Iron at Various C/A Ratios in Hydrogen Saturated 1N Sulfuric Acid Determined by Cathodic Polarization Using an Experimental Probe.

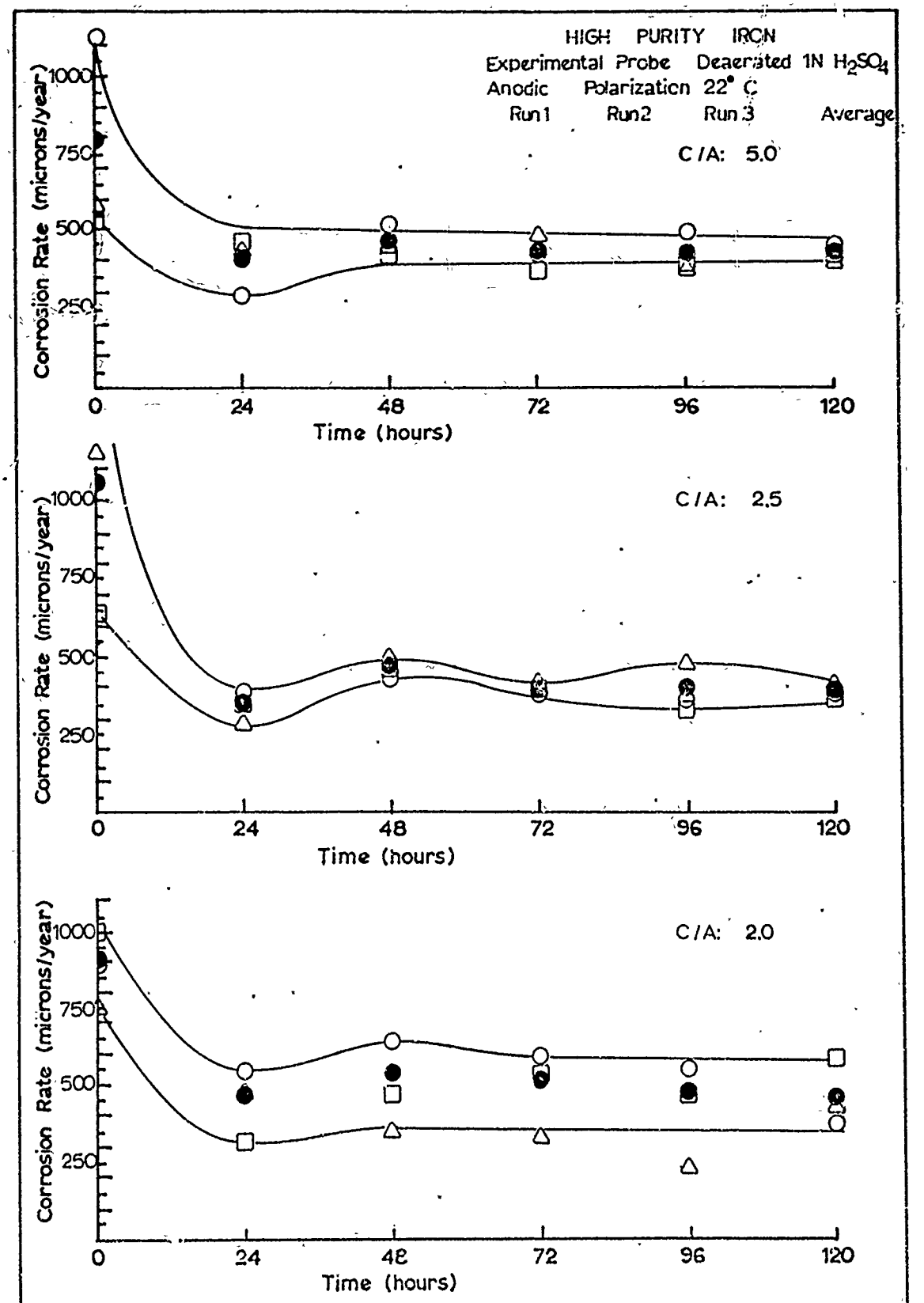

Figure 114: Effect of Time on the Corrosion Rate of High Purity Iron of Various C/A Ratios in Hydrogen Saturated 1N Sulfuric Acid Determined by Anodic Polarization Using an Experimental Probe. (Cont)

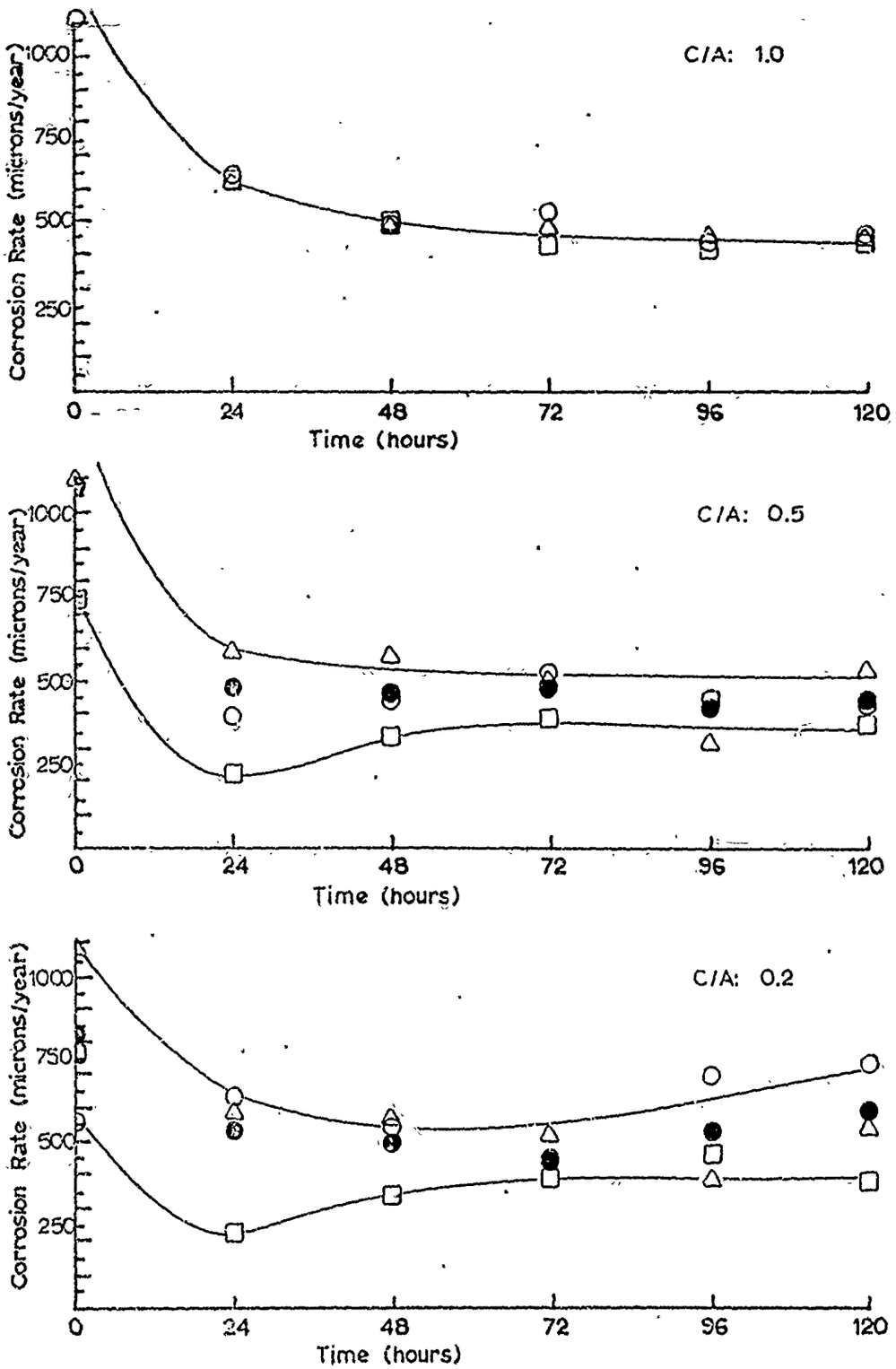

Figure 114: (Cont) Effect of Time on the Corrosion Rate of High Purity Iron of Various C/A Ratios in Hydrogen Saturated 1N Sulfuric Acid Determined by Anodic Polarization Using an Experimental Probe.

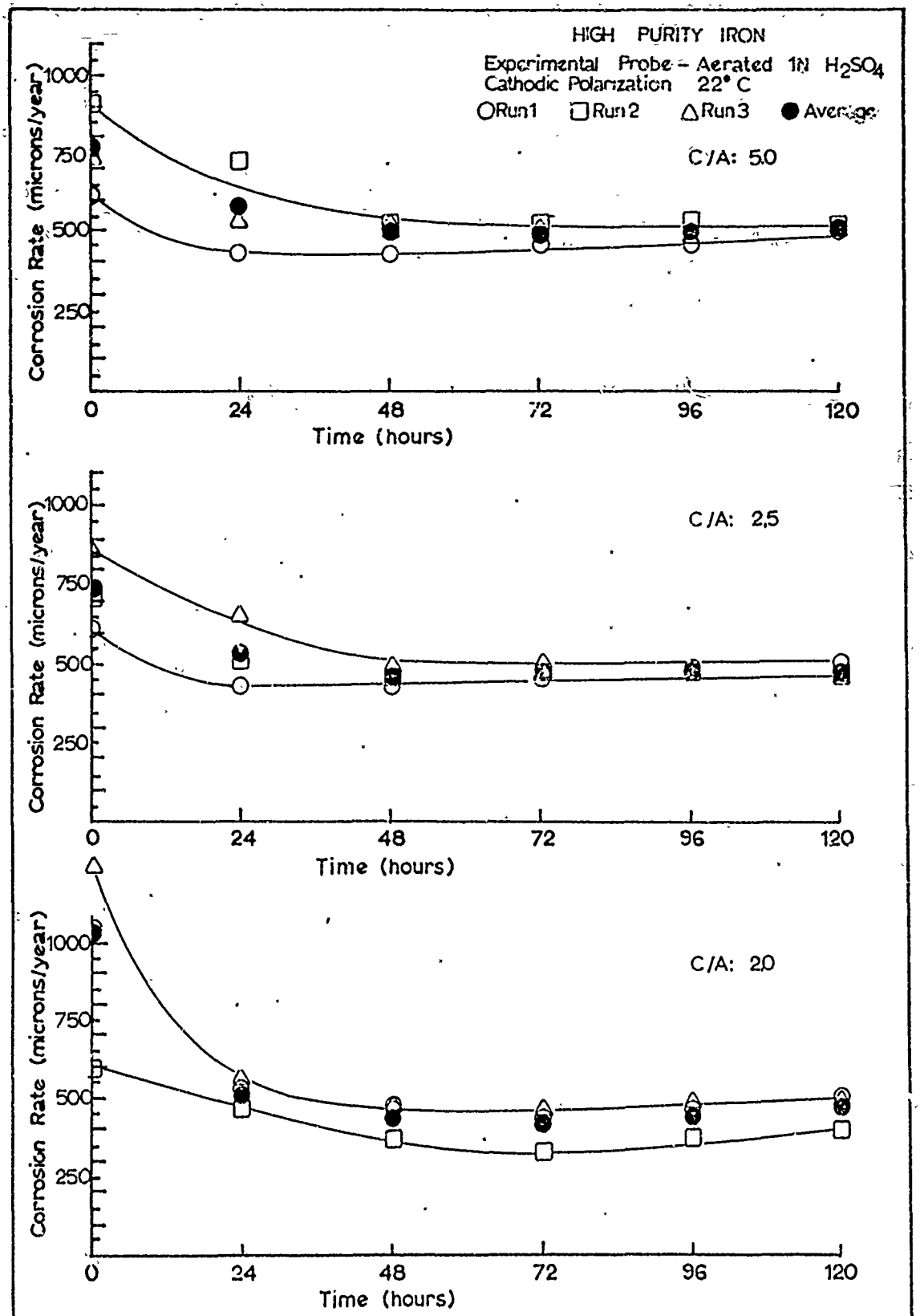

Figure 115: Effect of Time on the Corrosion Rate of High Purity Iron at Various C/A Ratios in Aerated 1N Sulfuric Acid Determined by Cathodic Polarization Using an Experimental Probe. (Cont)

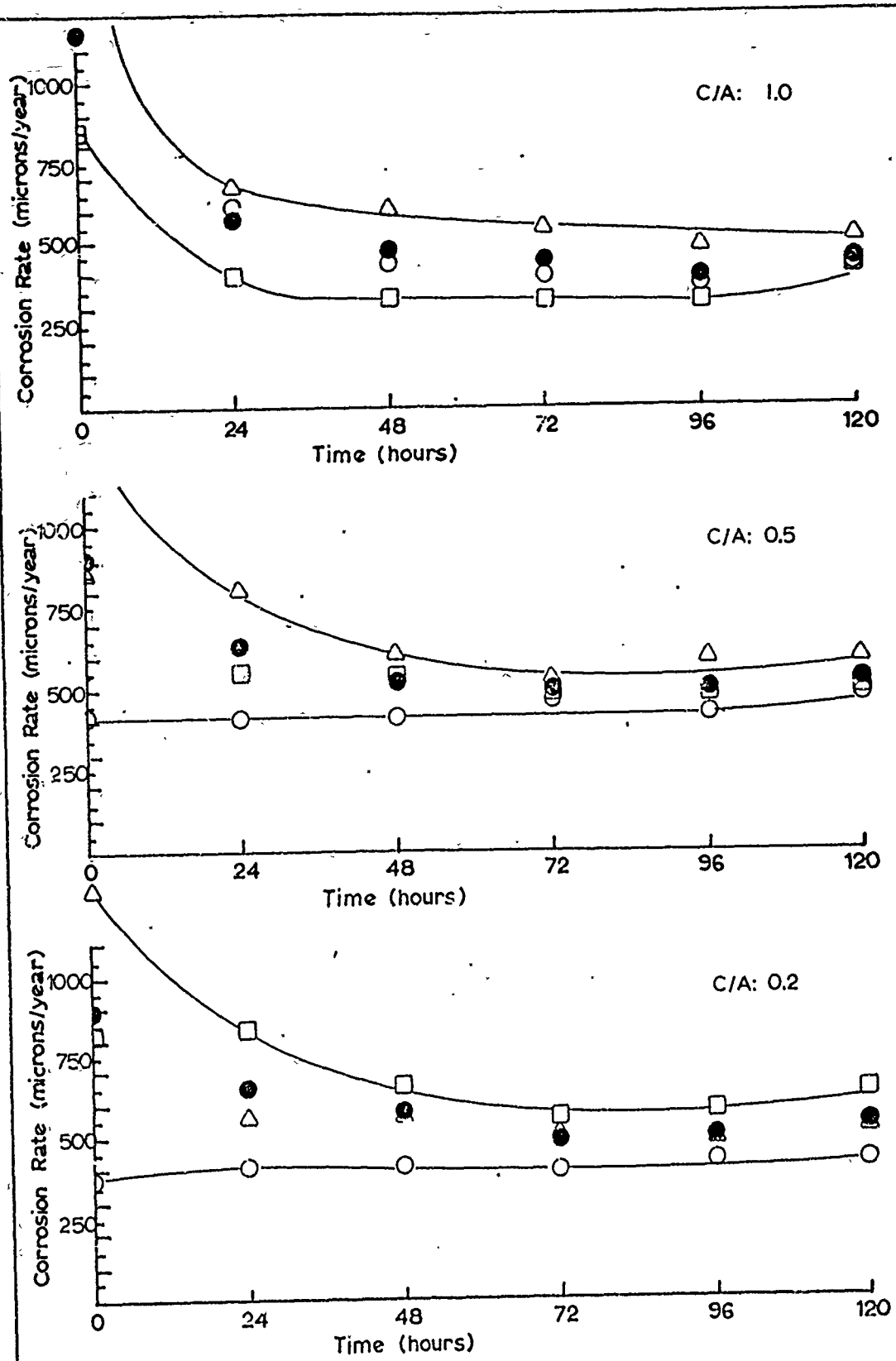

Figure 115 (Cont) Effect of Time on the Corrosion Rate of High Purity Iron at Various C/A Ratios in Aerated 1N Sulfuric Acid Determined by Cathodic Polarization Using an Experimental Probe.

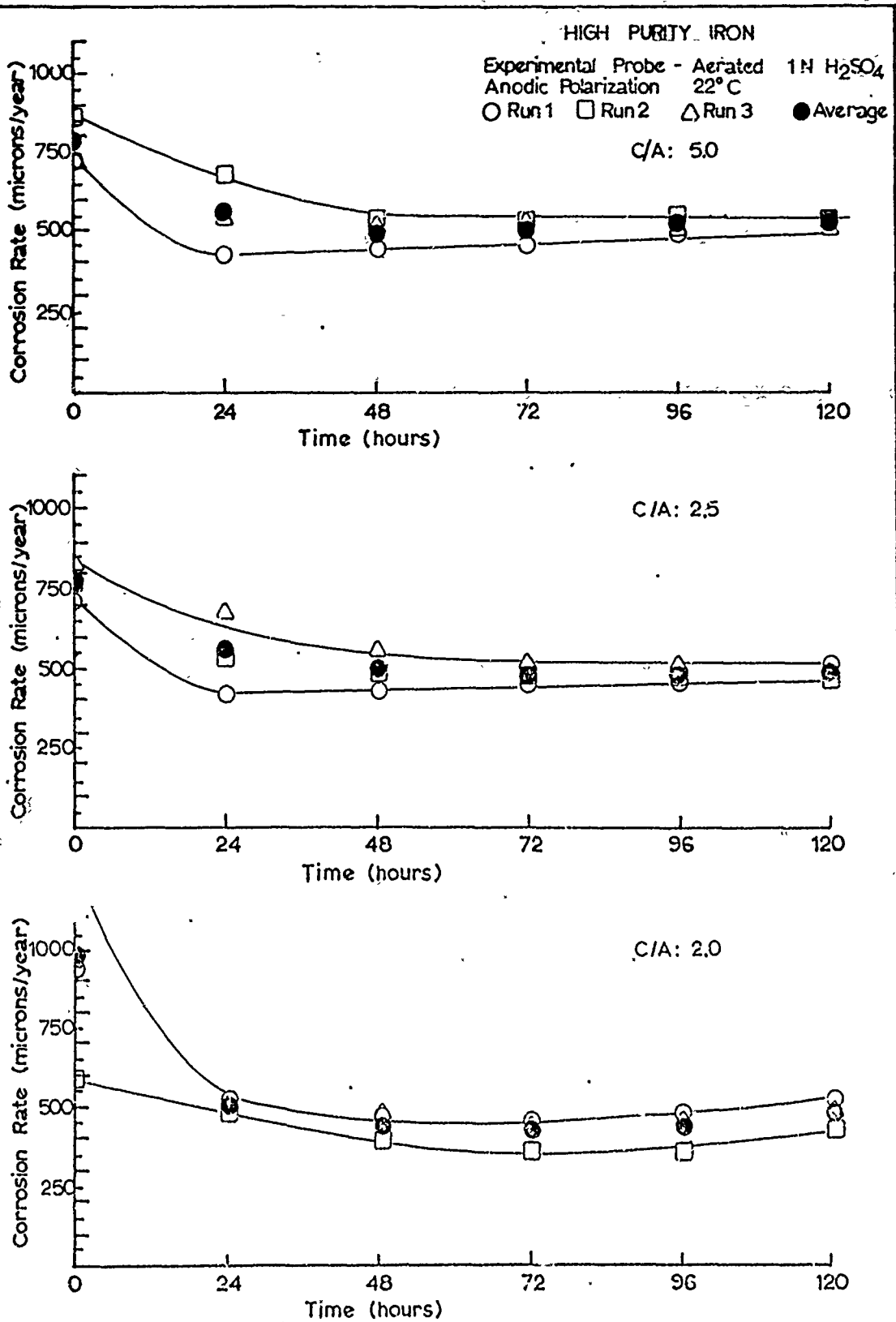

Figure 116: Effect of Time on the Corrosion Rate of High Purity Iron at Various C/A Ratios in Aerated 1N Sulfuric Acid Determined by Anodic Polarization Using an Experimental Probe. (Cont)

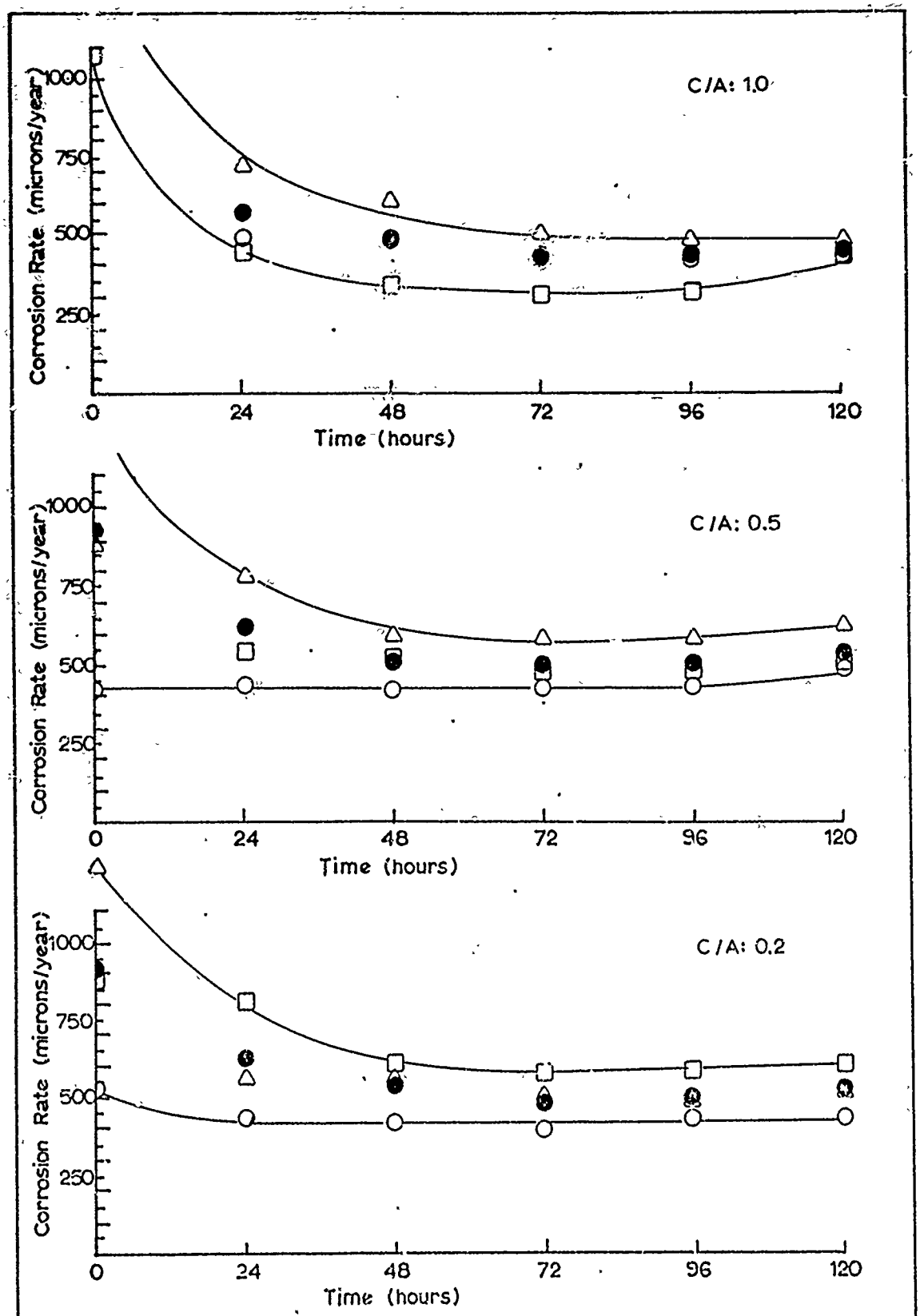

Figure 116: (Cont) Effect of Time on the Corrosion Rate of High Purity Iron at Various C/A Ratios in Aerated 1N Sulfuric Acid Determined by Anodic Polarization Using an Experimental Probe.

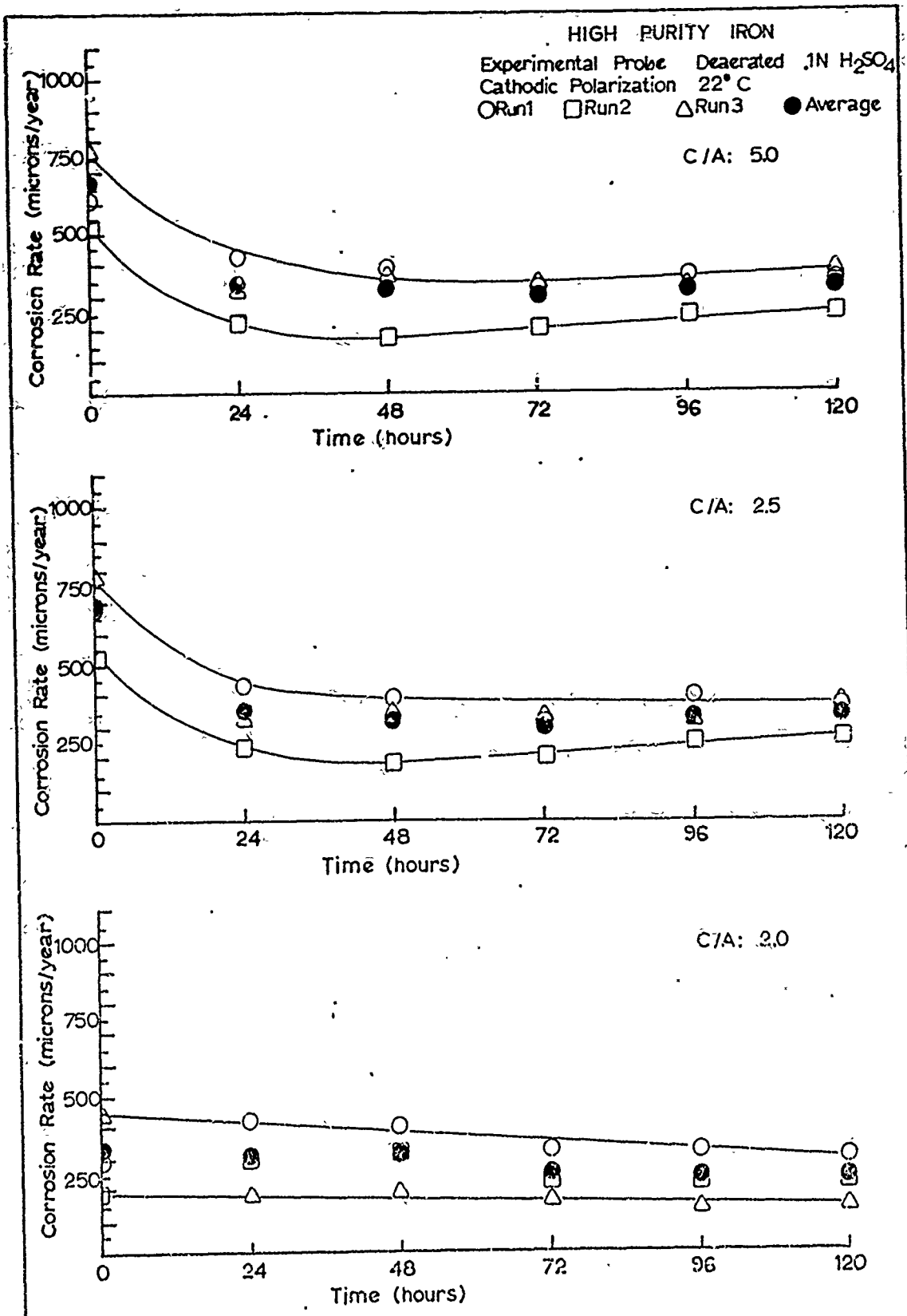

Figure 117: Effect of Time on the Corrosion Rate of High Purity Iron at Various C/A Ratios in Hydrogen Saturated .1N Sulfuric Acid Determined by Cathodic Polarization Using an Experimental Probe. (Cont)

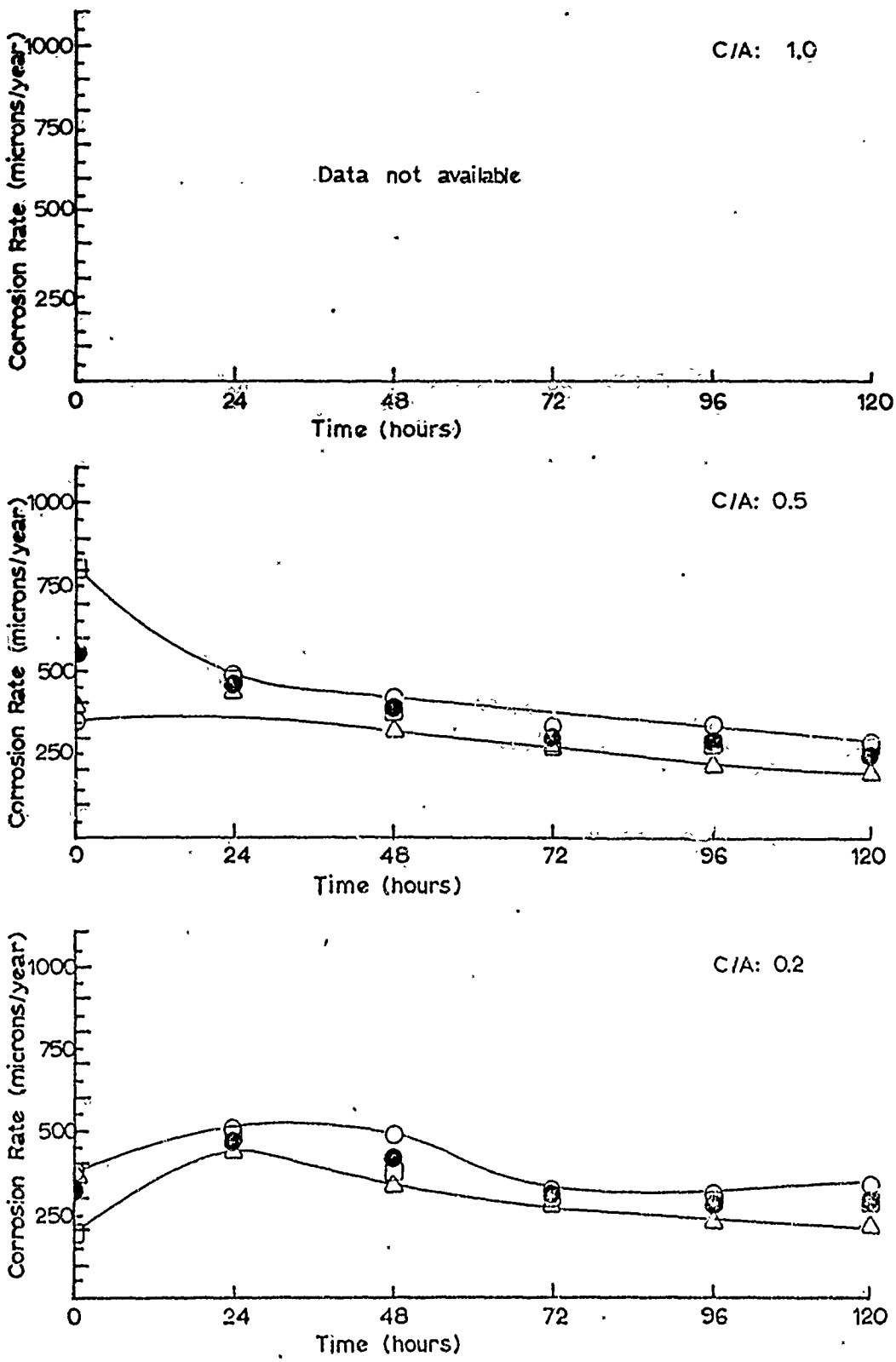

Figure 117: (Cont) Effect of Time on the Corrosion Rate of High Purity Iron at Various C/A Ratios in Hydrogen Saturated .1N Sulfuric Acid Determined by Cathodic Polarization Using an Experimental Probe.

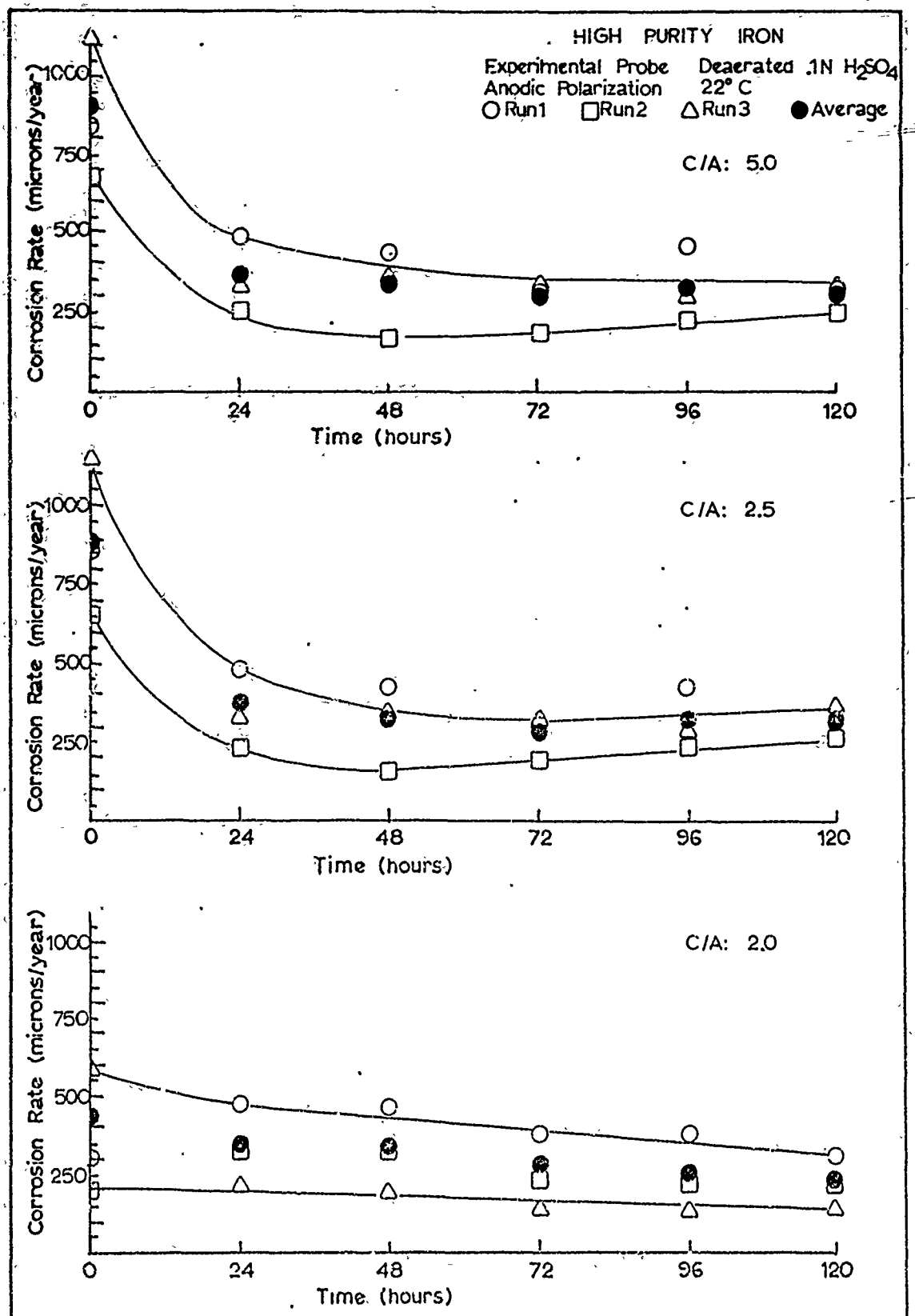

Figure 118 : Effect of Time on the Corrosion Rate of High Purity Iron at Various C/A Ratios in Hydrogen Saturated .1N Sulfuric Acid Determined by Anodic Polarization Using an Experimental Probe. (Cont)

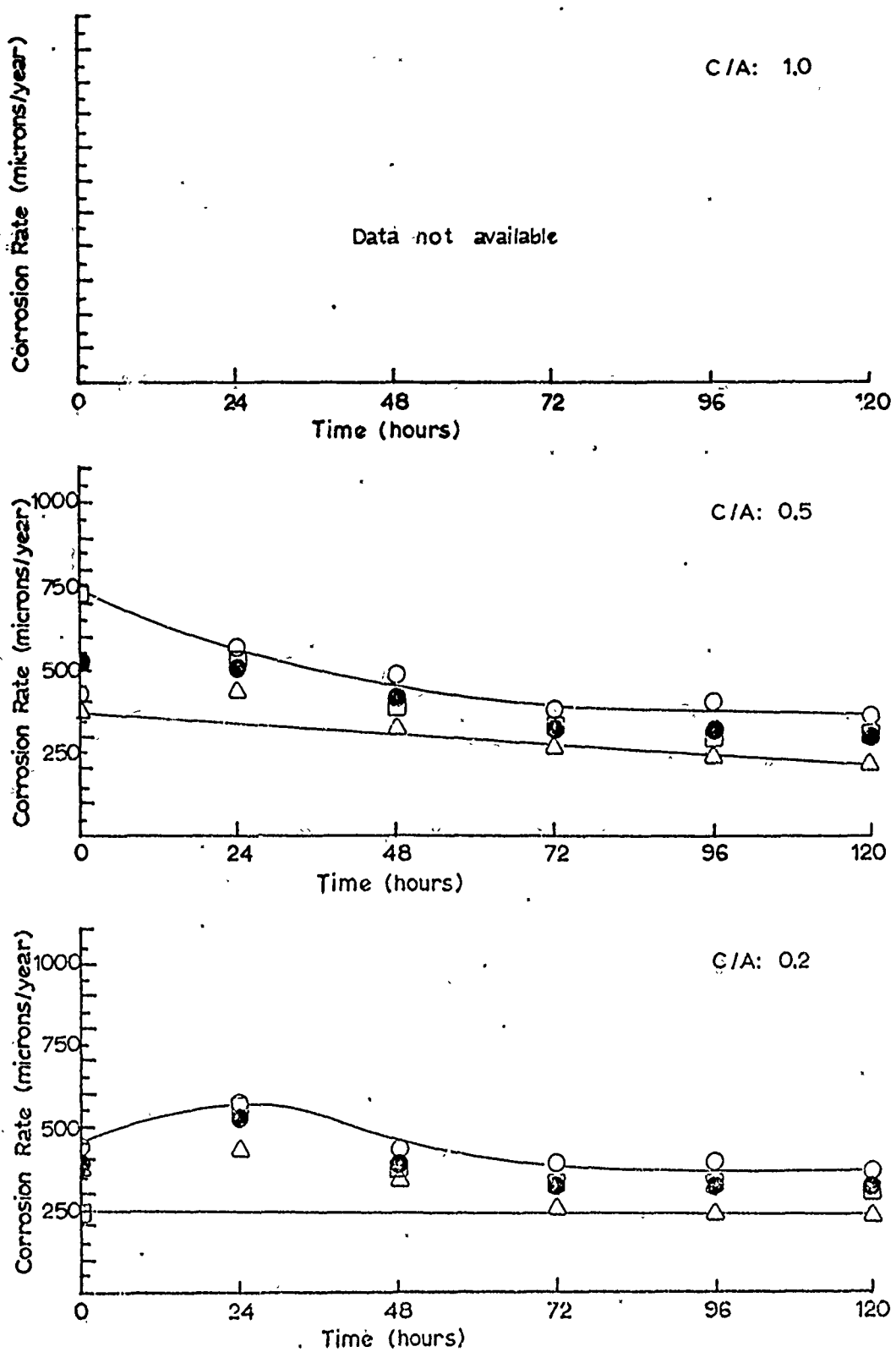

Figure 118 : (Cont) Effect of Time on the Corrosion Rate of High Purity Iron at Various C/A Ratios in Hydrogen Saturated .1N Sulfuric Acid Determined by Anodic Polarization Using an Experimental Probe.

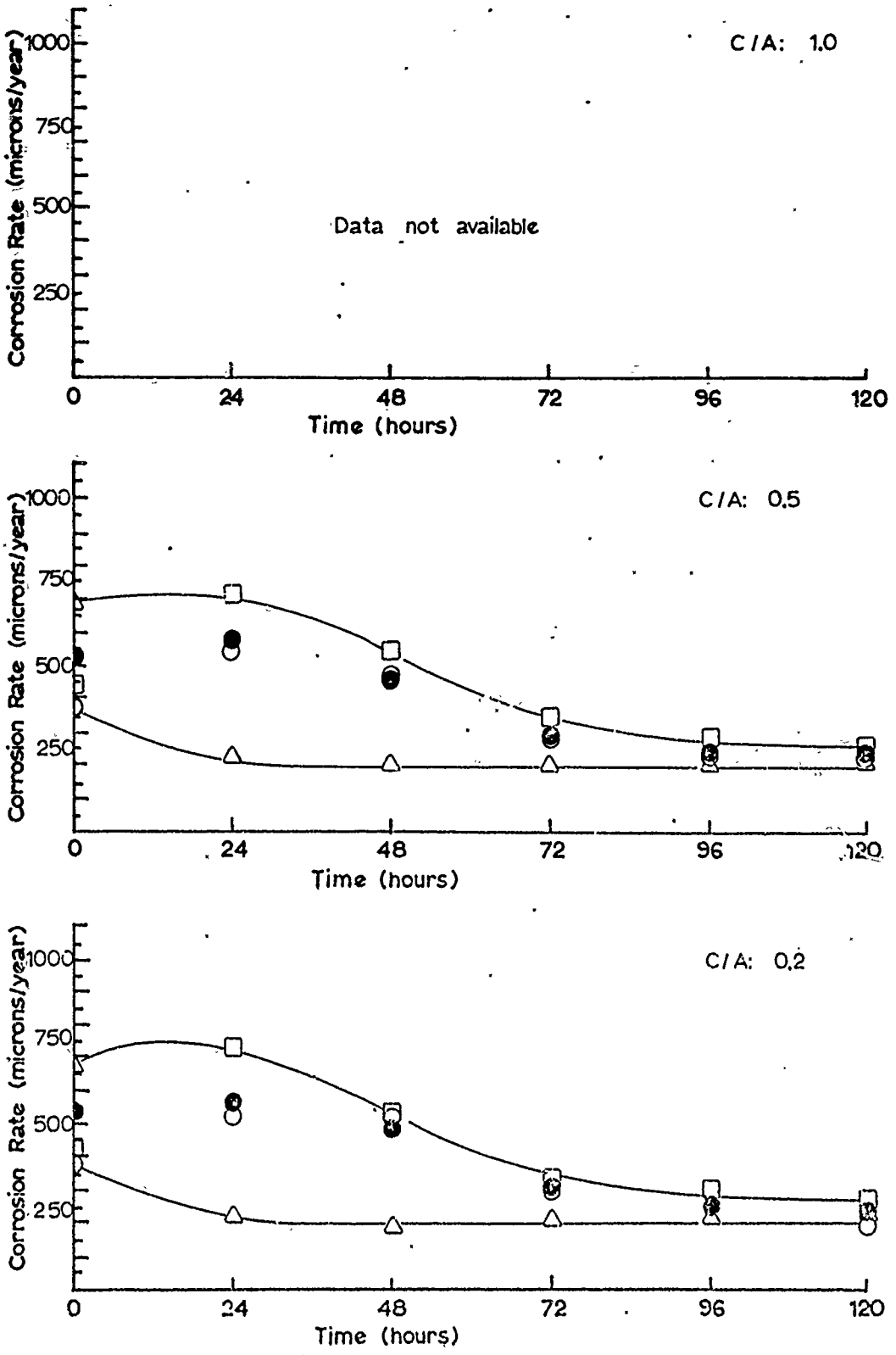

Figure 119: (Cont) Effect of Time on the Corrosion Rate of High Purity Iron at Various C/A Ratios in Aerated .1N Sulfuric Acid Determined by Cathodic Polarization Using an Experimental Probe.

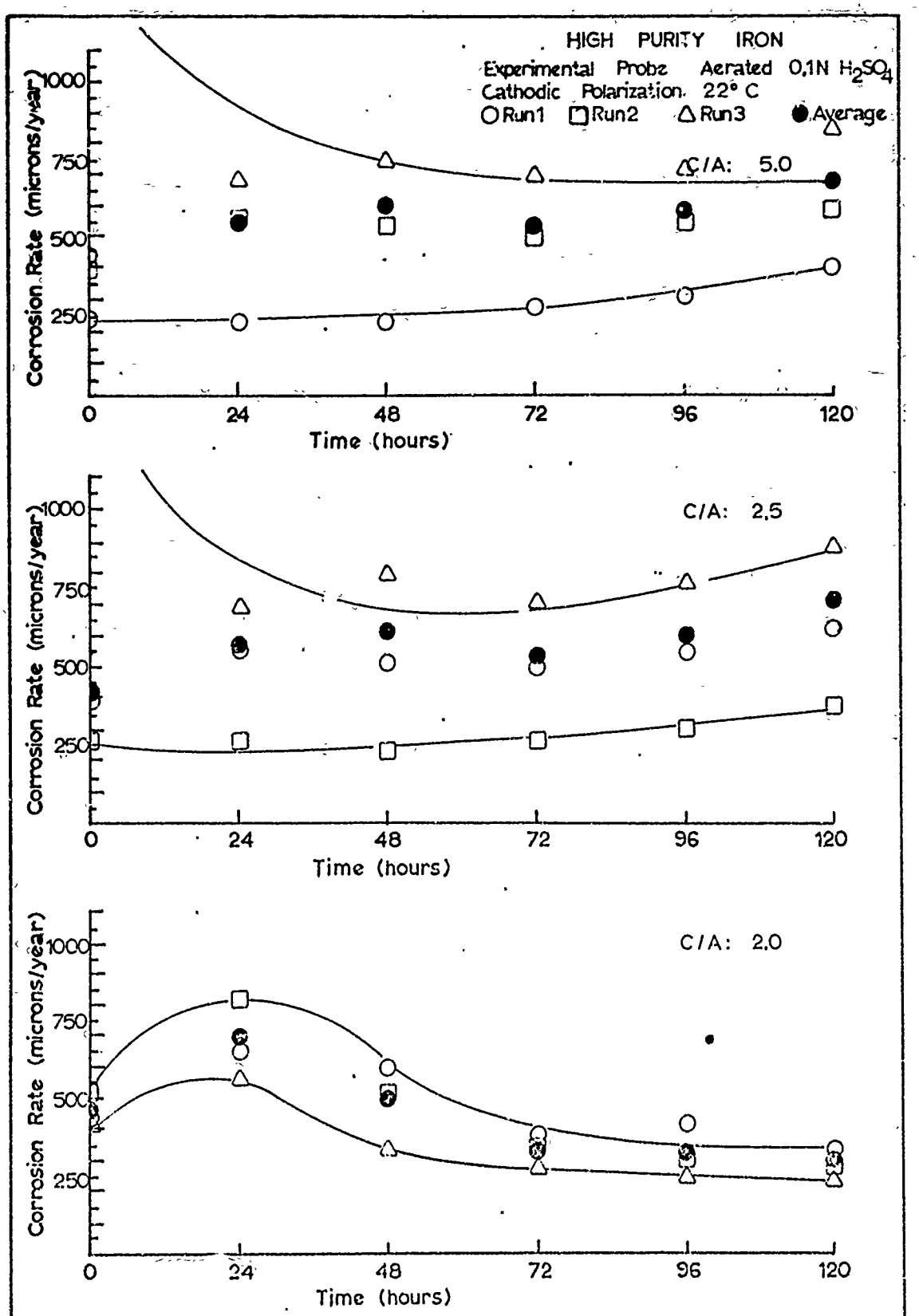

Figure 119: Effect of Time on the Corrosion Rate of High Purity Iron at Various C/A Ratios in Aerated .1N Sulfuric Acid Determined by Cathodic Polarization Using an Experimental Probe. (Cont)

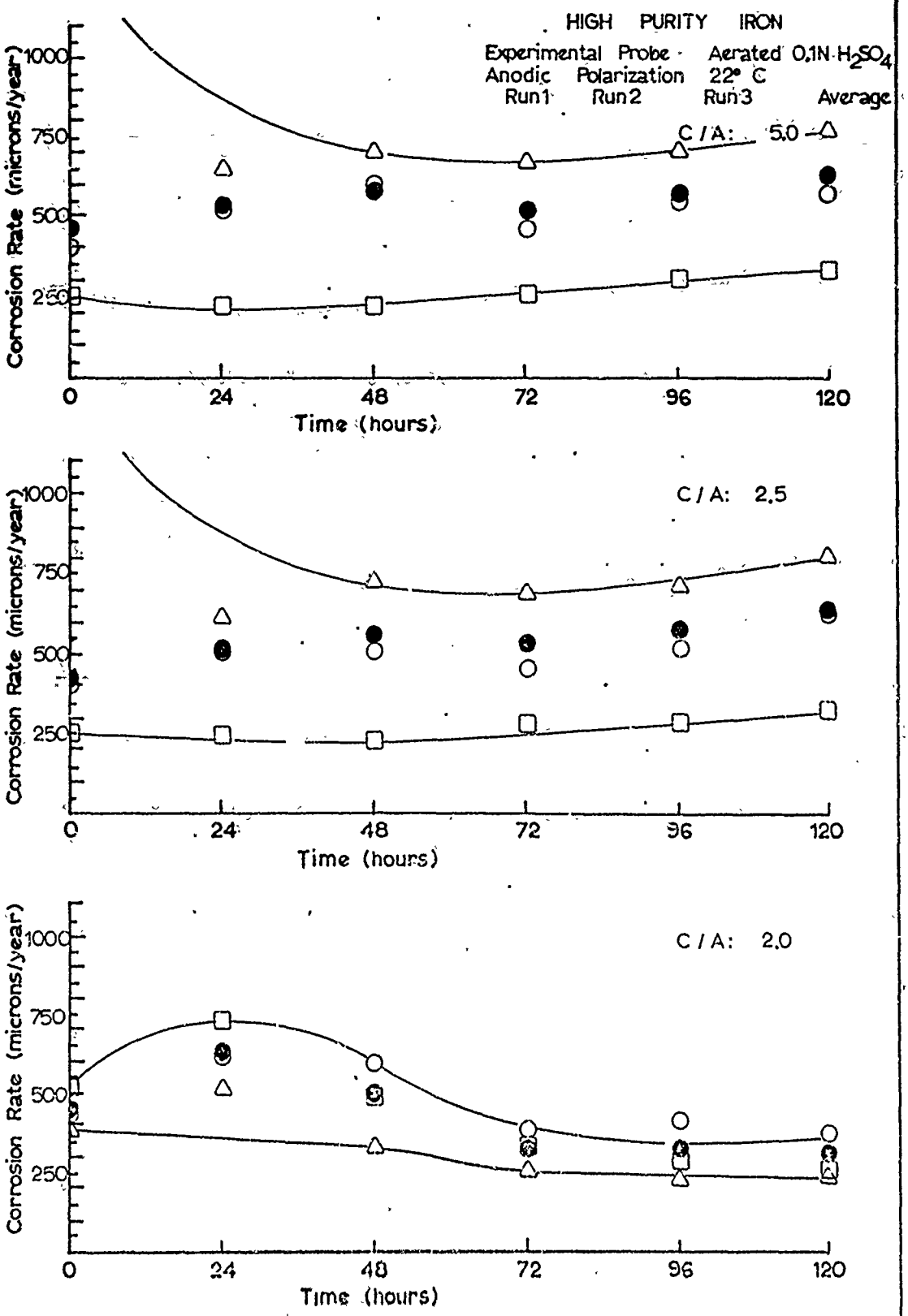

Figure 120: Effect of Time on the Corrosion Rate of High Purity Iron at Various C/A Ratios in Aerated .1N Sulfuric Acid Determined by Anodic Polarization Using an Experimental Probe. (Cont)

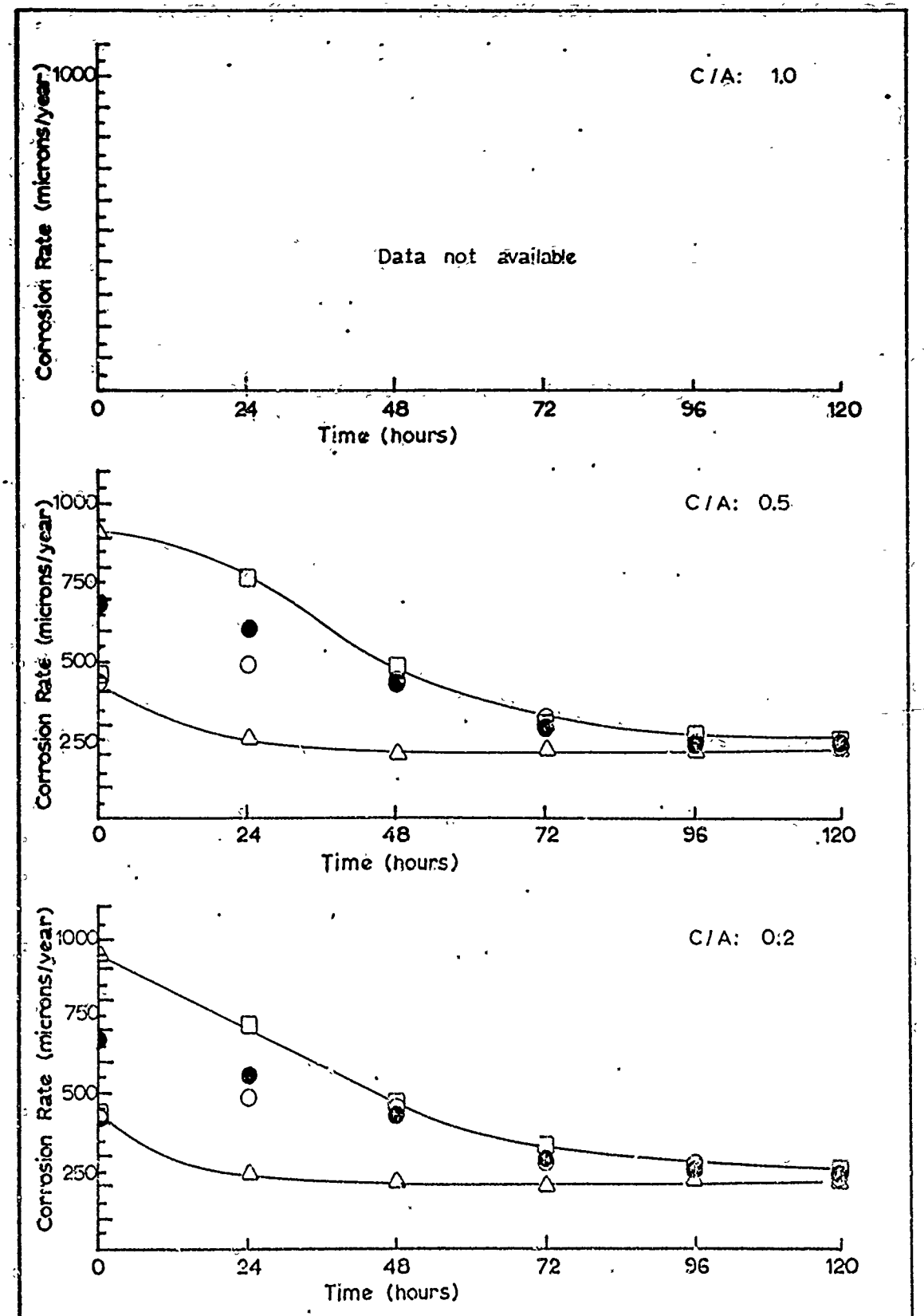

Figure 120: (Cont) Effect of Time on the Corrosion Rate of High Purity Iron at Various C/A Ratios in Aerated .1N Sulfuric Acid Determined by Anodic Polarization Using an Experimental Probe.

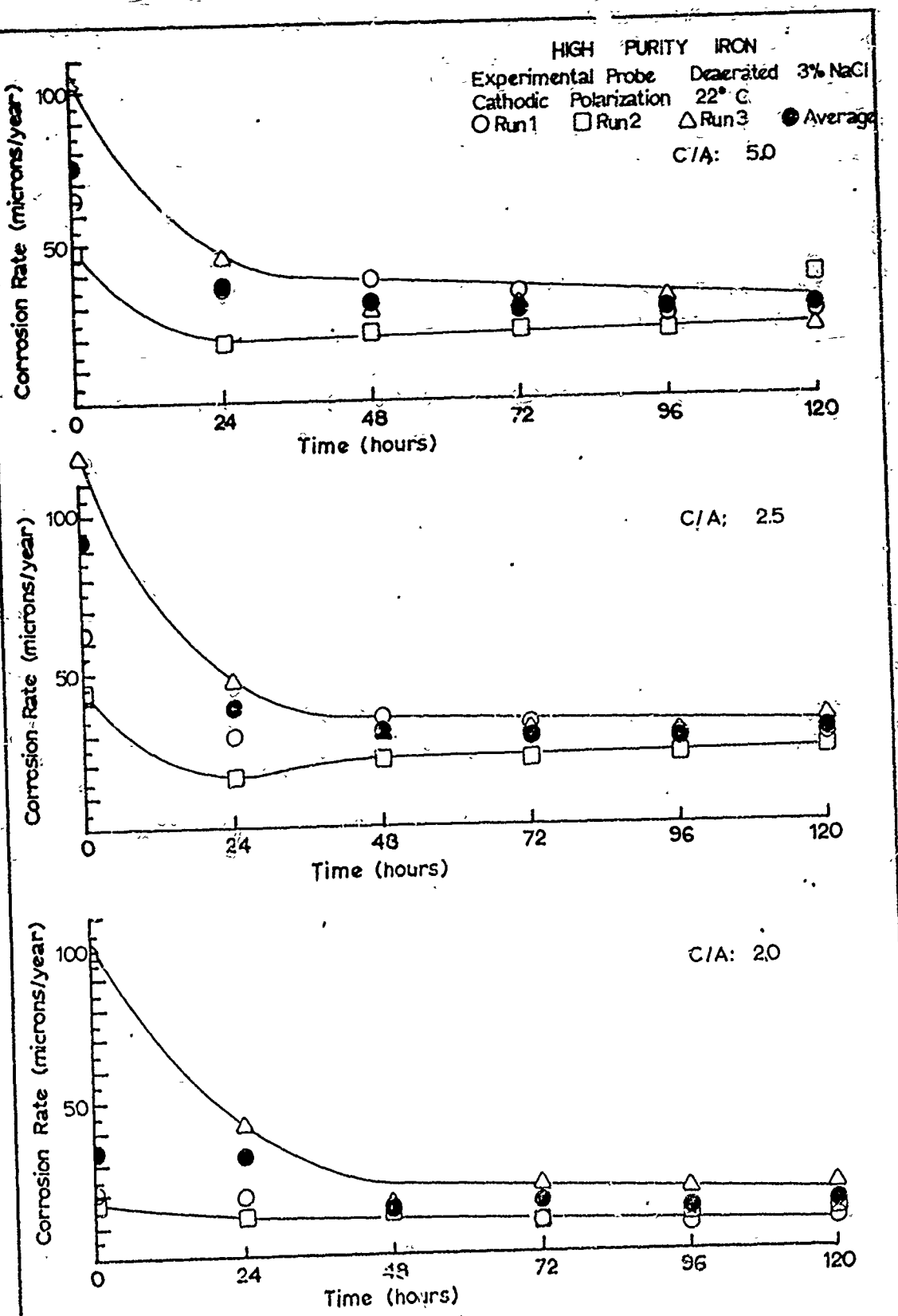

Figure 121: Effect of Time on the Corrosion Rate of High Purity Iron at Various C/A Ratios in Hydrogen Saturated 3% Sodium Chloride Solution Determined by Cathodic Polarization Using an Experimental Probe. (Cont)

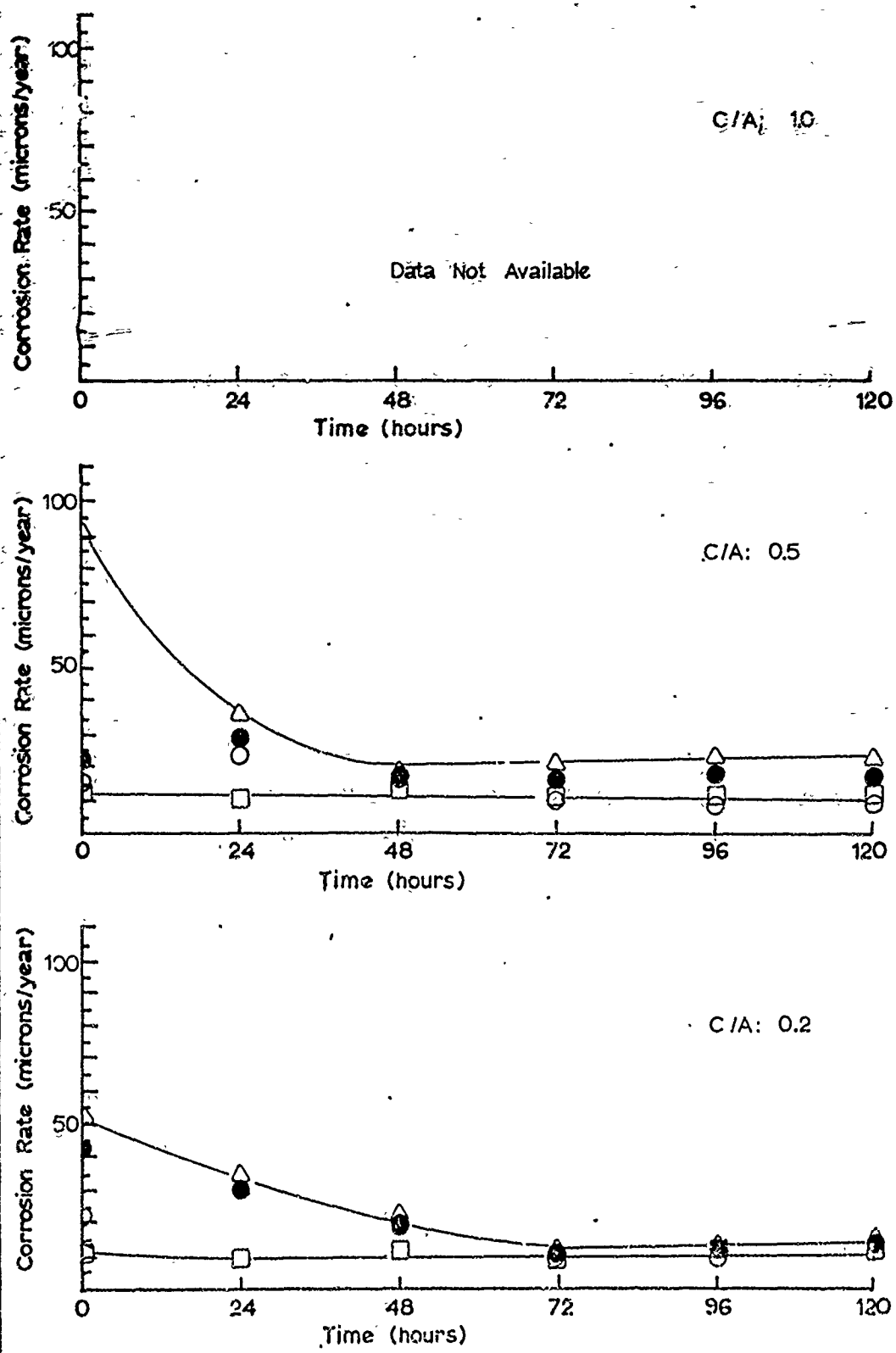

Figure 121: (Cont) Effect of Time on the Corrosion Rate of High Purity Iron at Various C/A Ratios in Hydrogen Saturated 3% Sodium Chloride Solution Determined by Cathodic Polarization Using an Experimental Probe.

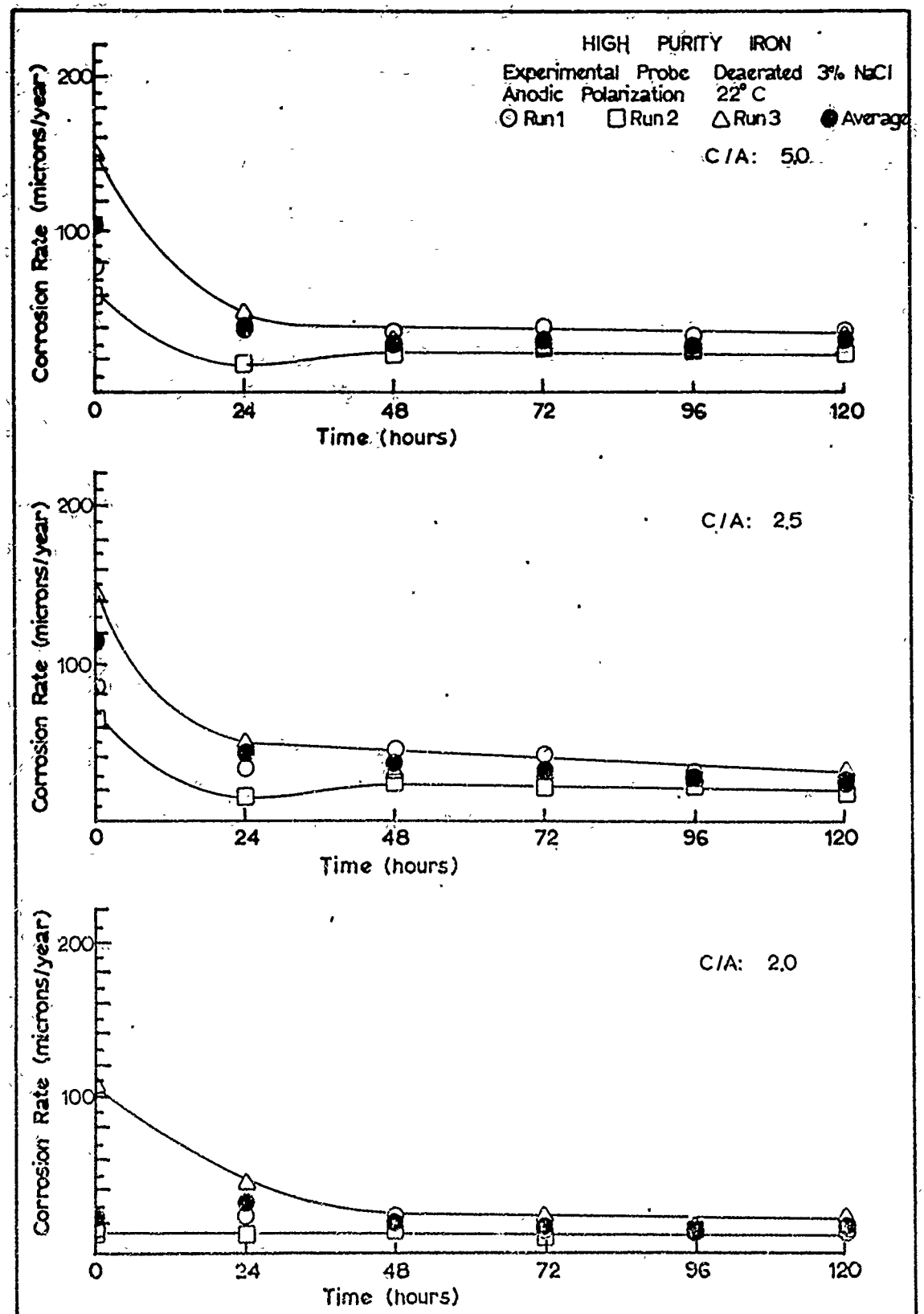

Figure 122: Effect of Time on the Corrosion Rate of High Purity Iron at Various C/A Ratios in Hydrogen Saturated 3% Sodium Chloride Solution Determined by Anodic Polarization Using an Experimental Probe. (Cont)

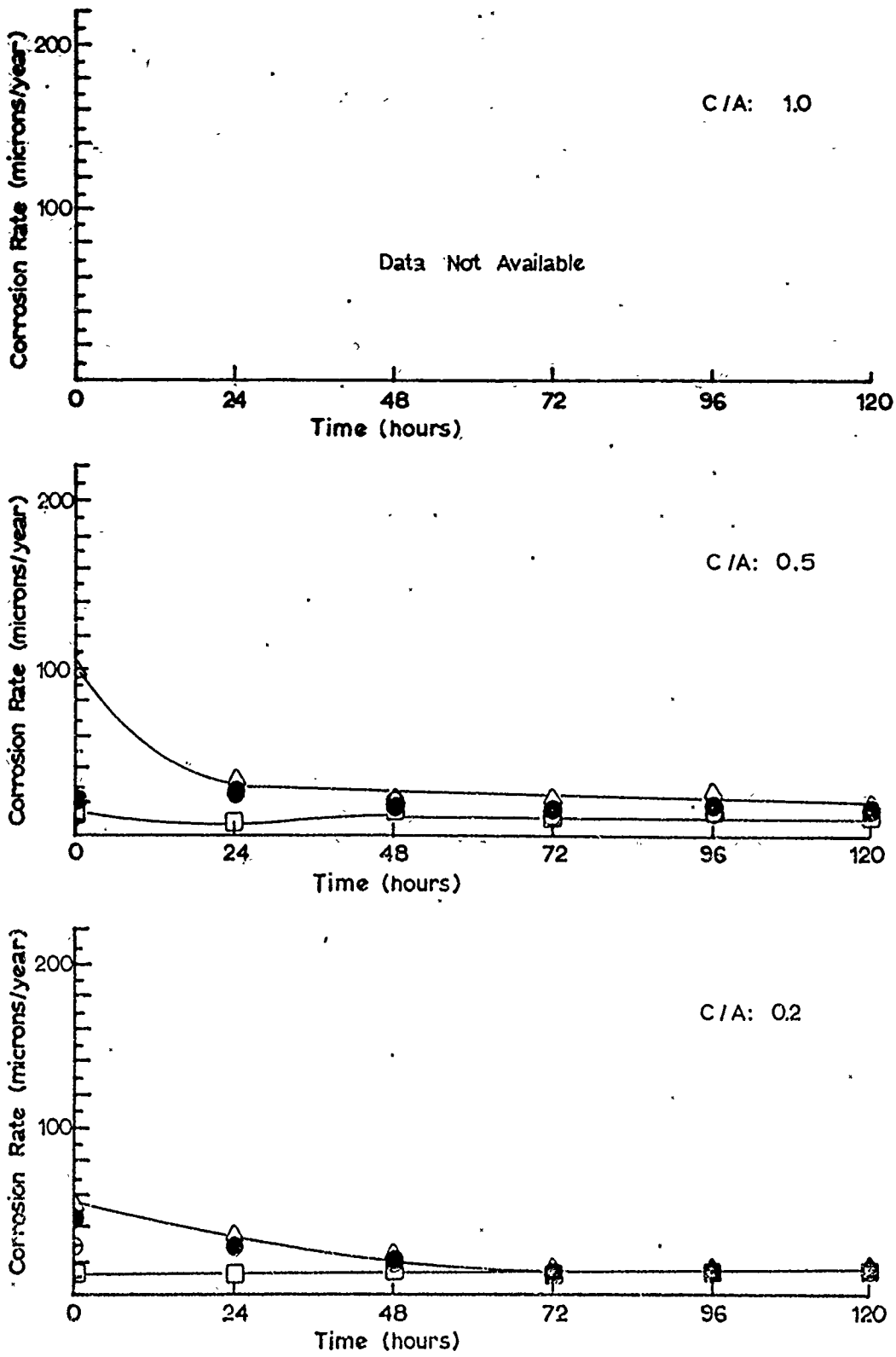

Figure 122: (Cont) Effect of Time on the Corrosion Rate of High Purity Iron at Various C/A Ratios in Hydrogen Saturated 3% Sodium Chloride Solution Determined by Anodic Polarization Using an Experimental Probe.

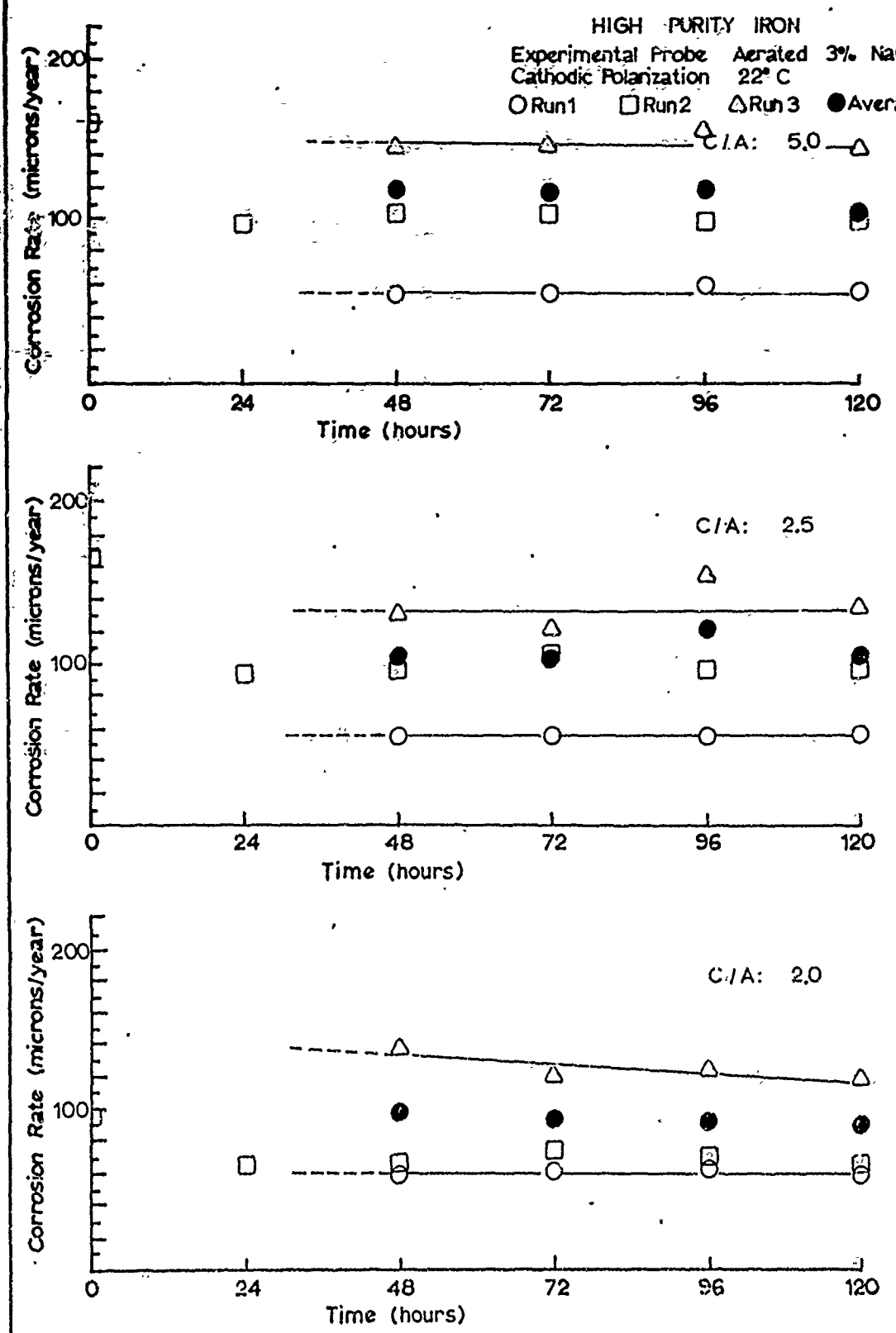

Figure 123: Effect of Time on the Corrosion Rate of High Purity Iron at Various C/A Ratios in Aerated 3% Sodium Chloride Solution Determined by Cathodic Polarization Using an Experimental Probe. (Cont)

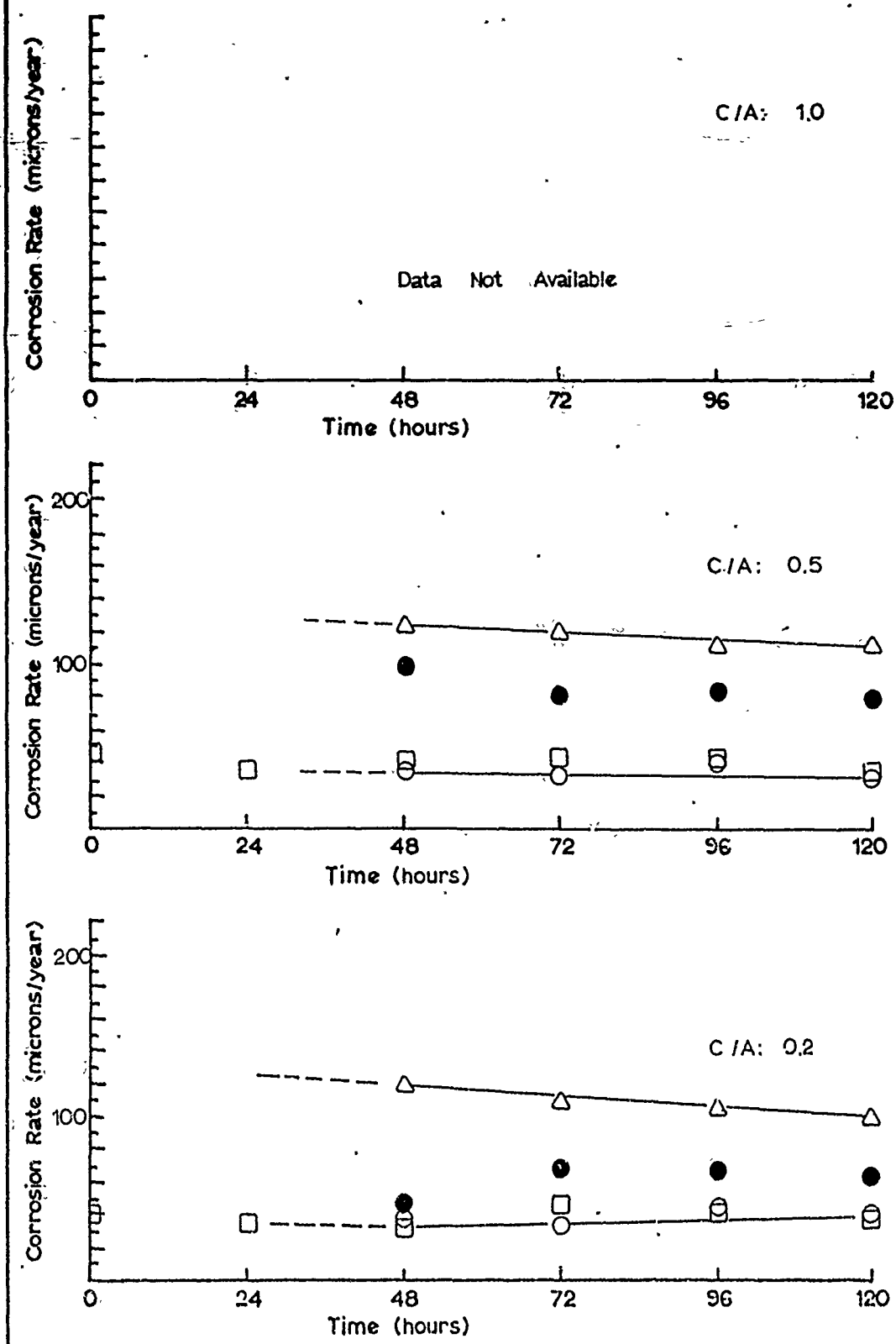

Figure 123: (Cont) Effect of Time on the Corrosion Rate of High Purity Iron at Various C/A Ratios in Aerated 3% Sodium Chloride Solution Determined by Cathodic Polarization Using an Experimental Probe.

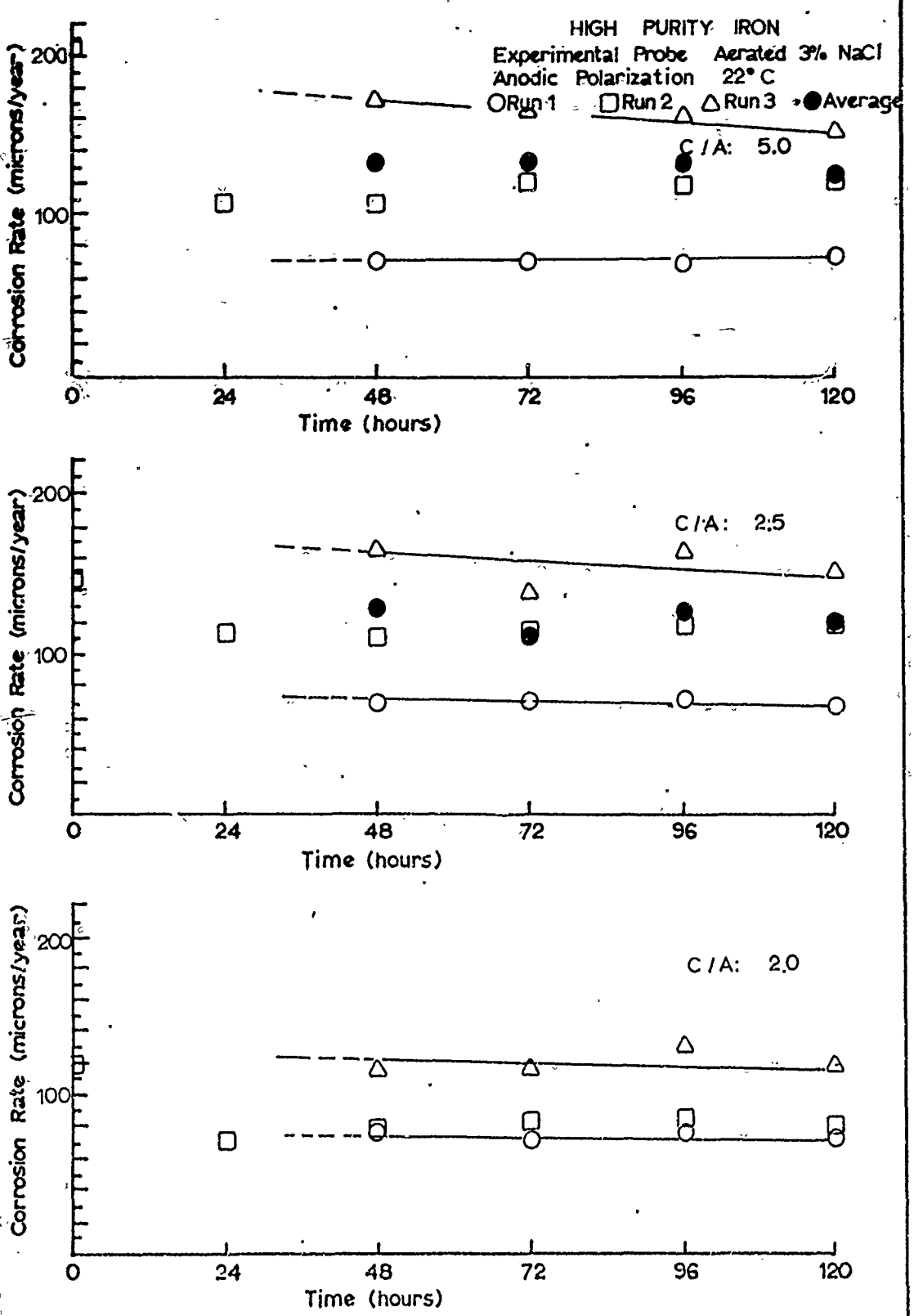

Figure 124: Effect of Time on the Corrosion Rate of High Purity Iron at Various C/A Ratios in Aerated 3% Sodium Chloride Solution Determined by Anodic Polarization Using an Experimental Probe. (Cont)

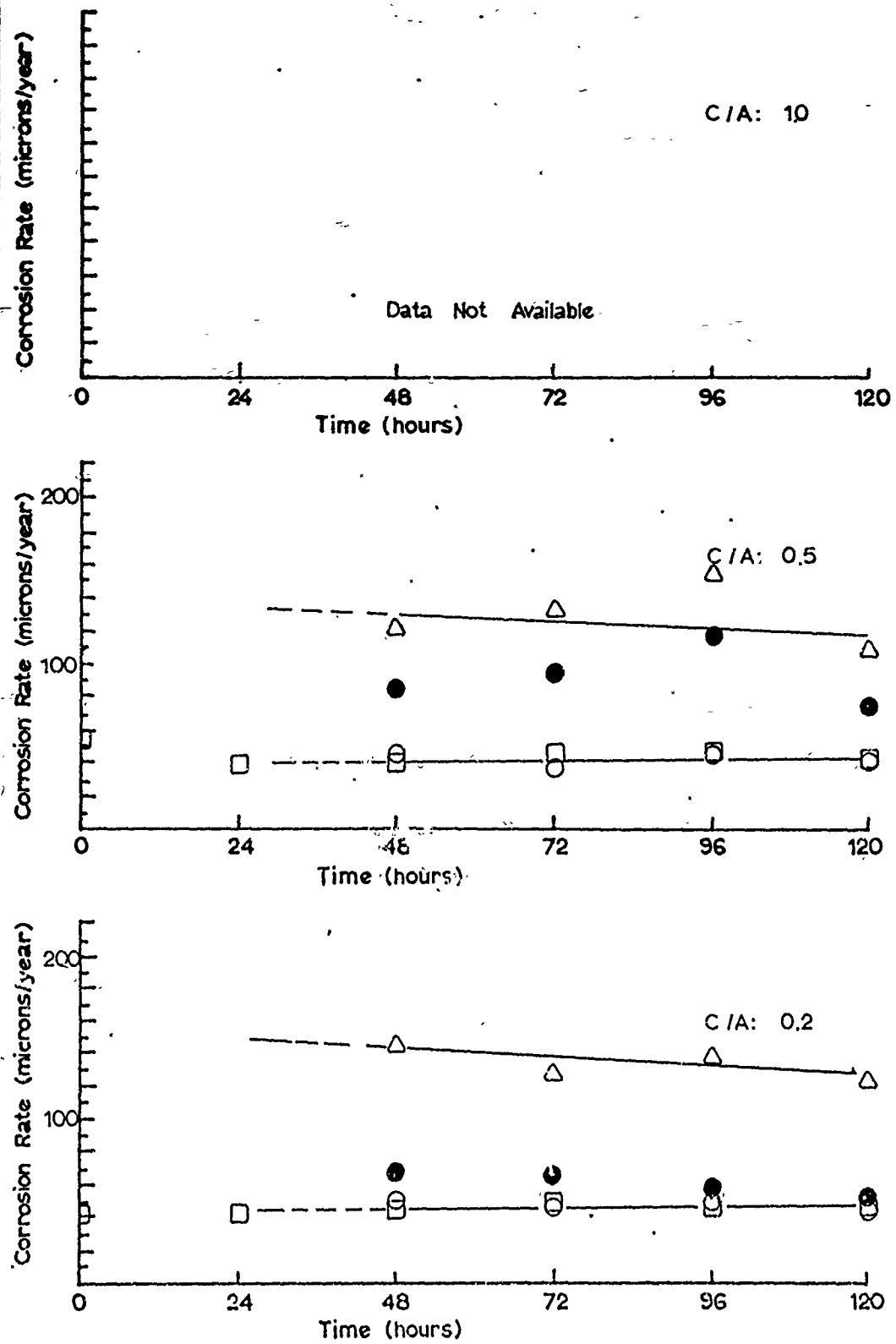

Figure 124: (Cont) Effect of Time on the Corrosion Rate of High Purity Iron at Various C/A Ratios in Aerated 3% Sodium Chloride Solution Determined by Anodic Polarization Using an Experimental Probe.

Appendix H

Indicated Steady-State Corrosion Rates of High Purity Iron I in a Laboratory Test Cell

The indicated steady-state corrosion rate ranges for high purity iron I in a laboratory test cell are shown in this appendix. Results were obtained using graphical techniques for each of the environments and test techniques used during this investigation. Each test cell configuration was coded according to Table XIX of Appendix K . The letter C or A following the configuration classification number indicates that cathodic or anodic galvanostatic resistance polarization techniques were used.

Table XII

Laboratory Test Cell Indicated Steady-State Corrosion Rate Range

Test Cell Configuration	Corrosion Rate (microns/year)		
	Minimum	Maximum	Range
1C	350	480	130
1A	270	410	140
3C	500	960	460
3A	640	750	110
5C*	230	300	70
5A*	225	330	105
7C*	175	575	400
7A*	250	475	225
11C	19	55	33
11A	21	46	25
13C	40	53	13
13A	38	62	24

*data convergence and stabilization with time were not observed.

Appendix I

The Effect of Experimental Probe C/A Ratio on the Indicated Steady-State Corrosion Rate of High Purity Iron I

The effect of varying experimental probe cathode-to-anode (C/A) surface area ratio on the "steady-state" corrosion rate obtained using resistance polarization techniques is shown in this appendix. The investigation was done using high purity iron I in each of the selected environments - 1N and 0.1N sulfuric acid and 3% sodium chloride/0.5N potassium sulfate. Computed steady-state corrosion rates were obtained using linear regression techniques (See "Steady-State Corrosion Rate Determination" in Chapter IV). These "computed steady-state rates" are also shown in Tables XIII-XV . "Graphic rate range" data were obtained by analyzing the figures of Appendix F. Note that a computed rate is not shown if this rate falls outside the graphic rate range. In addition, note that ordinate scales may vary amongst figures. The configuration classifications are coded according to Table XIX of Appendix K . The letter C or A following the configuration classification indicates that cathodic or anodic galvanostatic resistance polarization techniques were used.

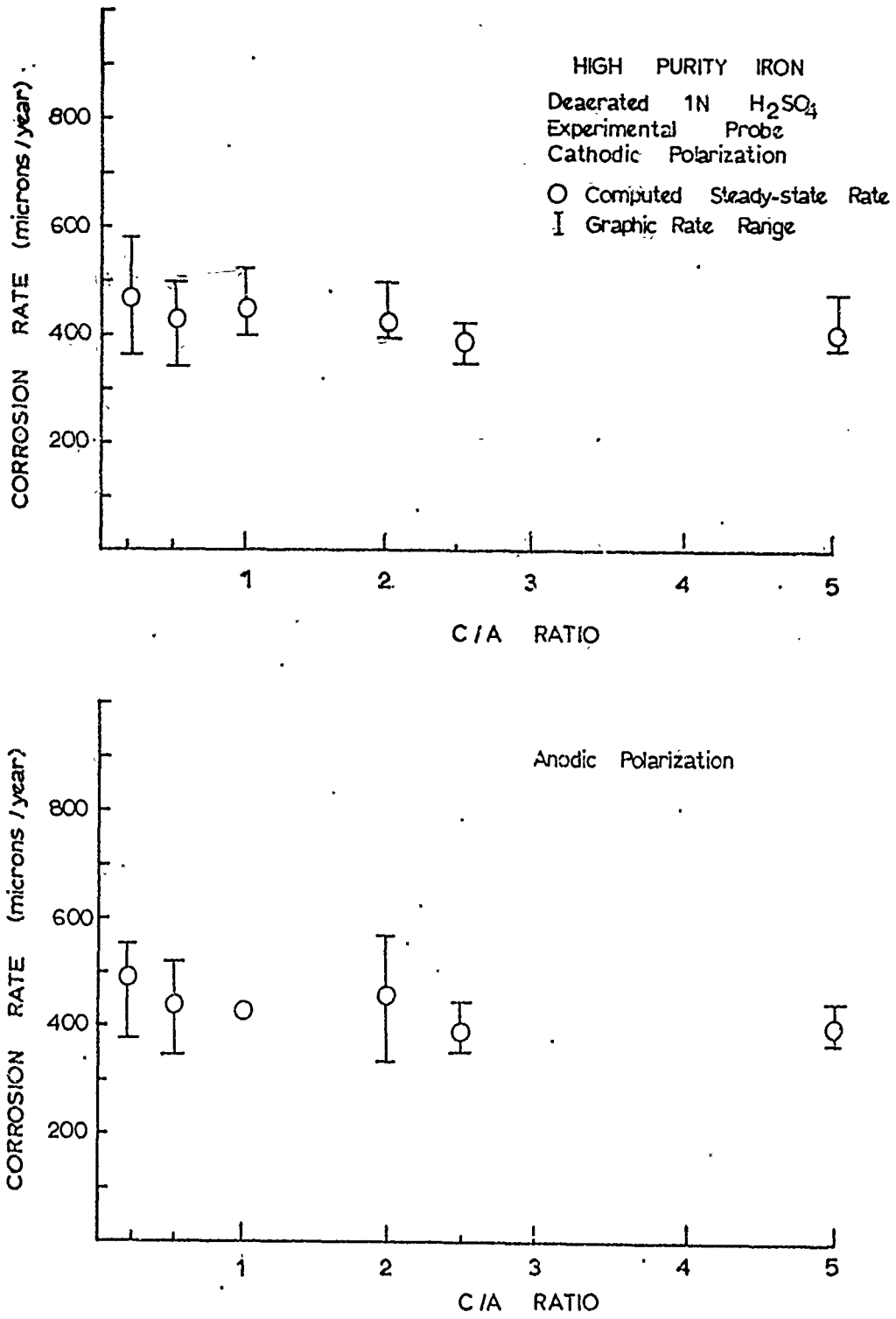

Figure 125: Effect of C/A Ratio on the Steady-State Corrosion Rate of High Purity Iron in Hydrogen Saturated 1N Sulfuric Acid Determined by Cathodic Polarization Using an Experimental Probe.

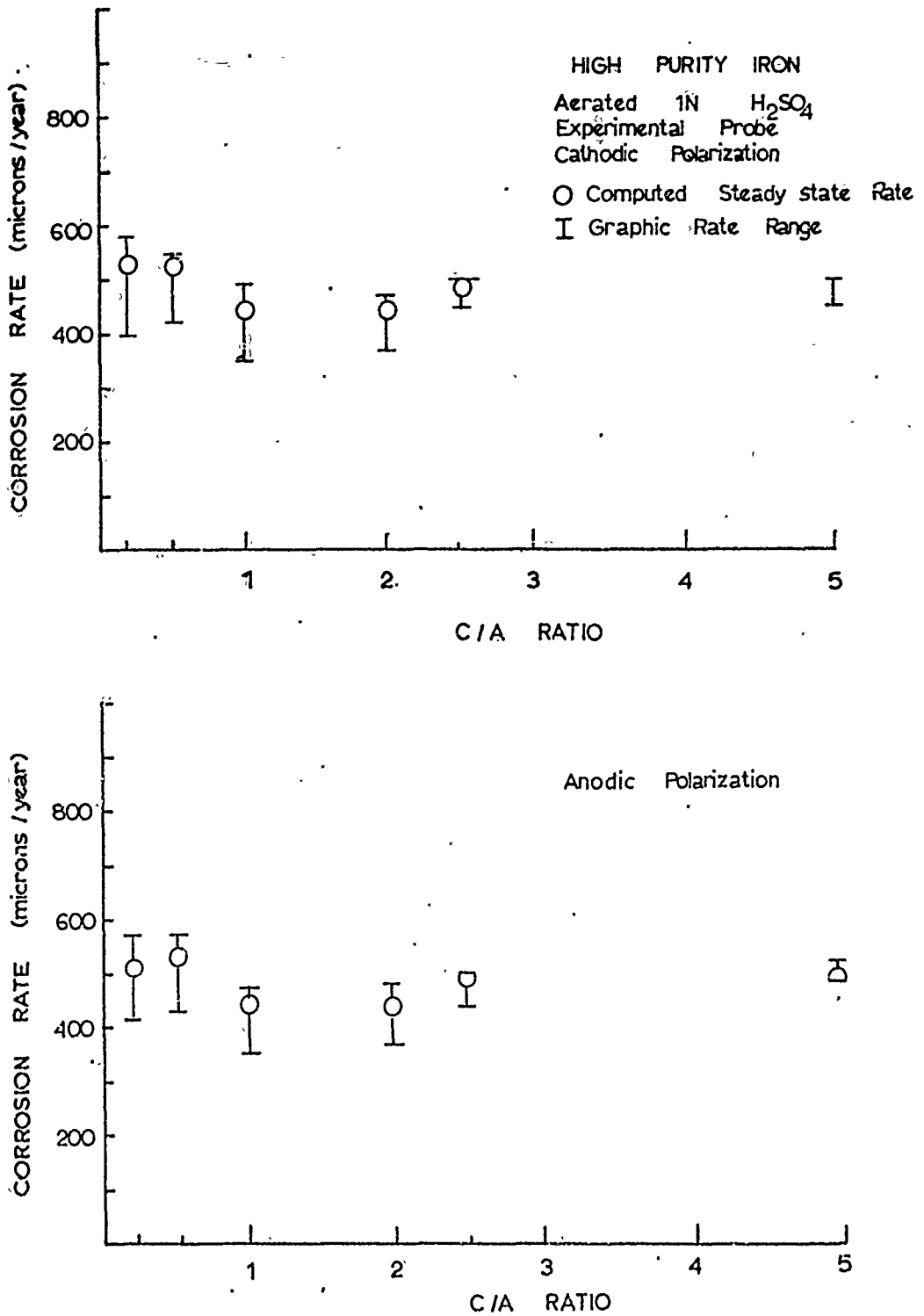

Figure 126: Effect of C/A Ratio on the Steady-State Corrosion Rate of High Purity Iron in Aerated 1N Sulfuric Acid Determined by Cathodic Polarization Using an Experimental Probe.

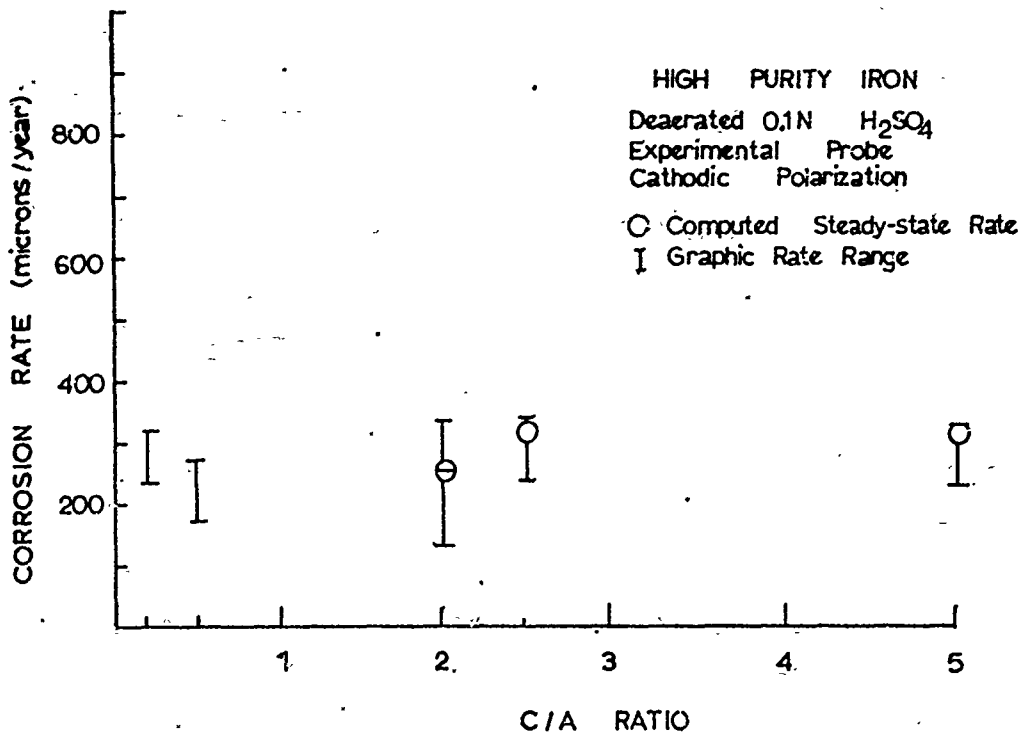

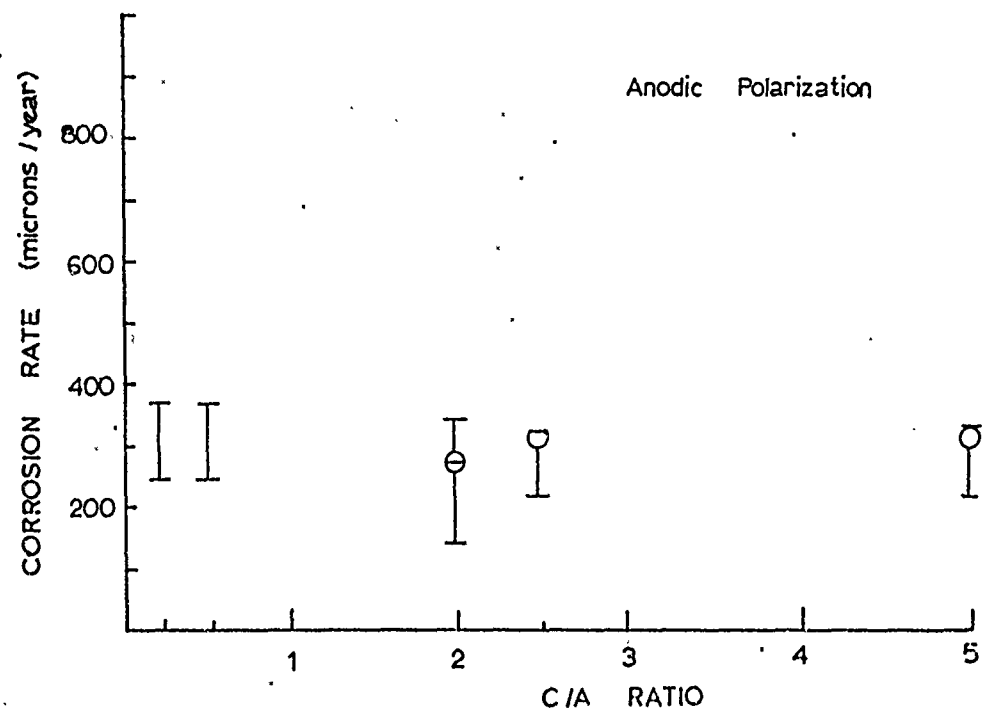

Figure 127: Effect of C/A Ratio on the Steady-State Corrosion Rate of High Purity Iron in Hydrogen Saturated .1N Sulfuric Acid Determined by Cathodic Polarization Using an Experimental Probe.

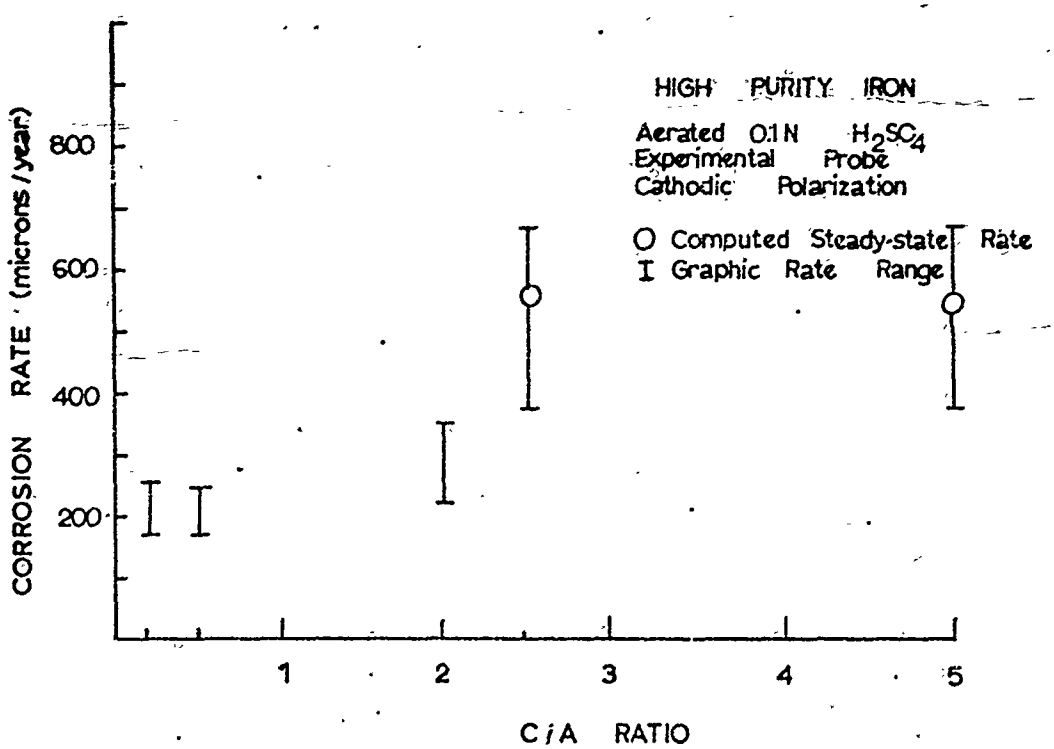

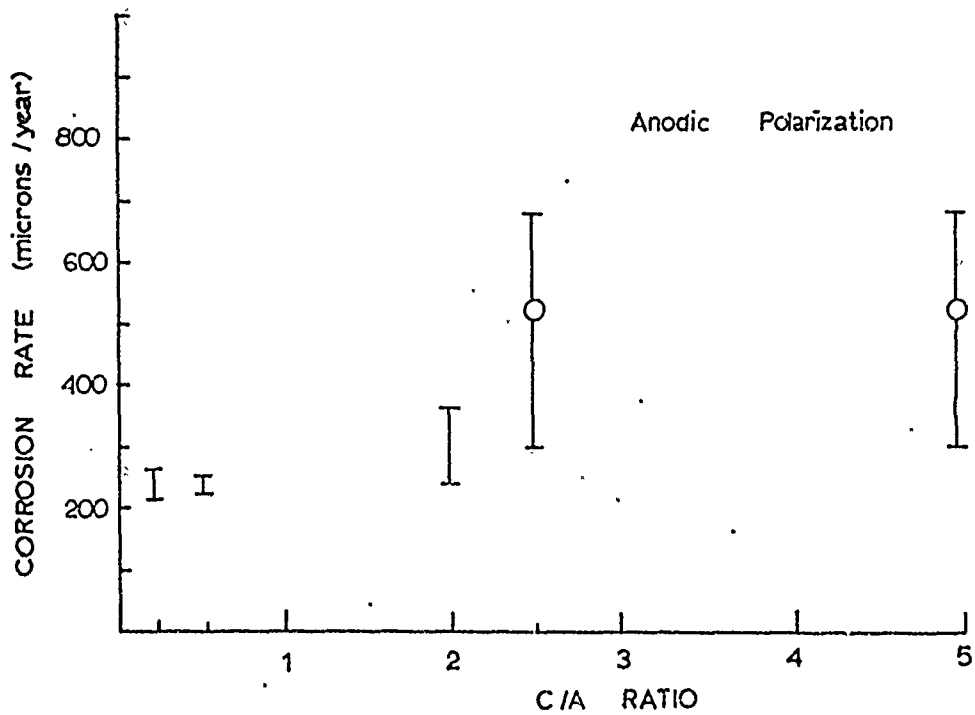

Figure 128: Effect of C/A Ratio on the Steady-state Corrosion Rate of High Purity Iron in Aerated .1N Sulfuric Acid Determined by Cathodic Polarization Using an Experimental Probe.

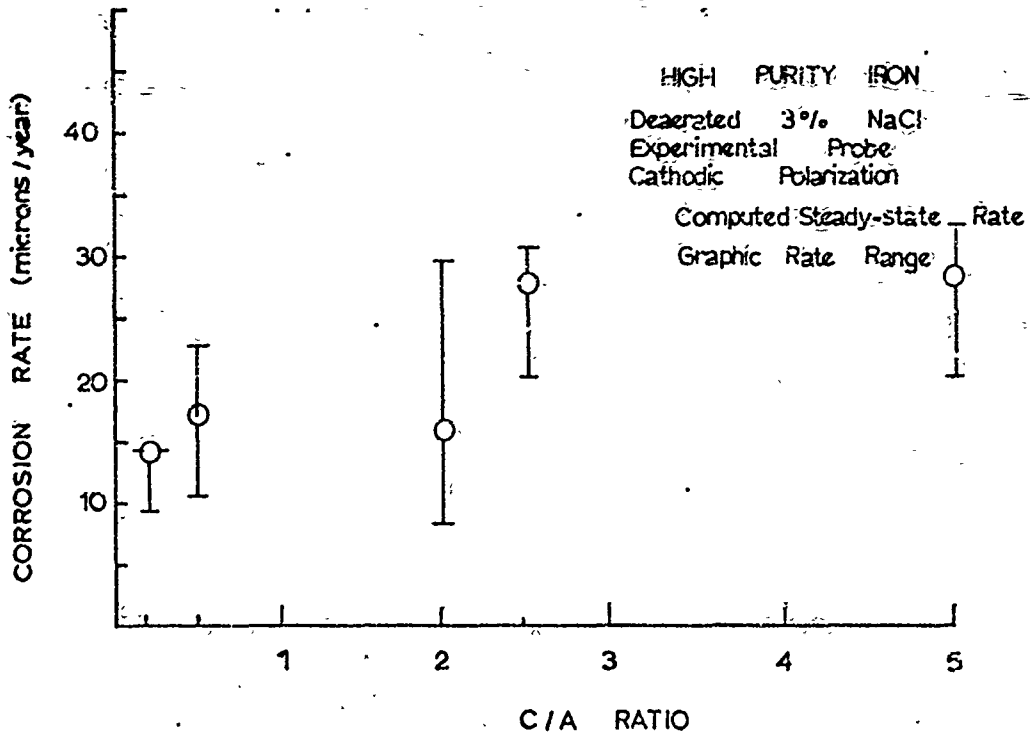

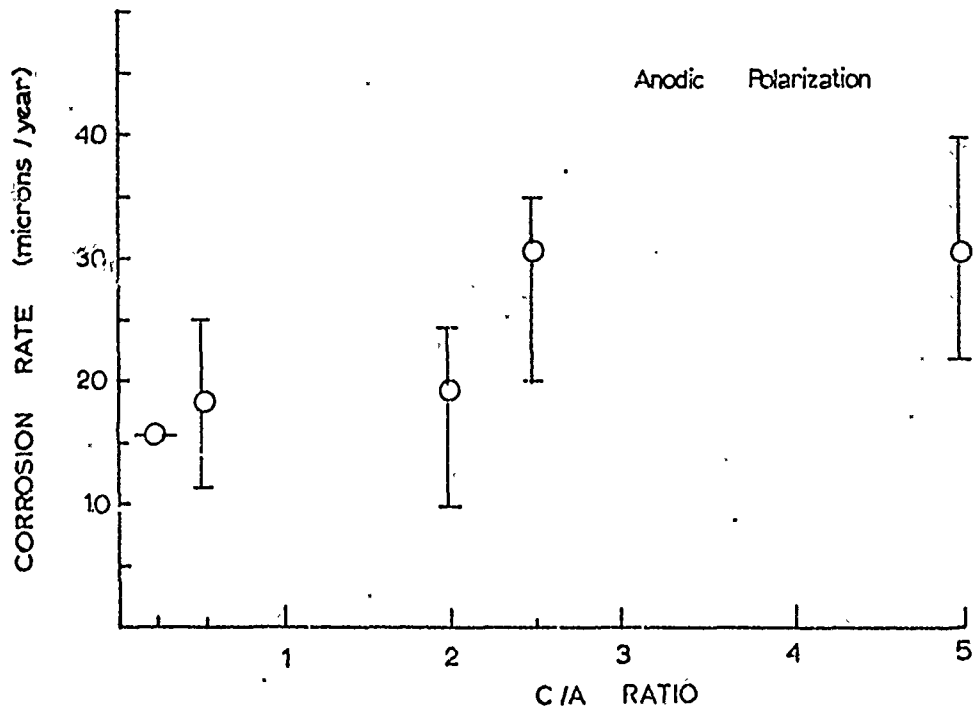

Figure 129: Effect of C/A Ratio on the Steady-state Corrosion Rate of High Purity Iron in Hydrogen Saturated 3% Sodium Chloride Solution Determined by Cathodic Polarization Using an Experimental Probe.

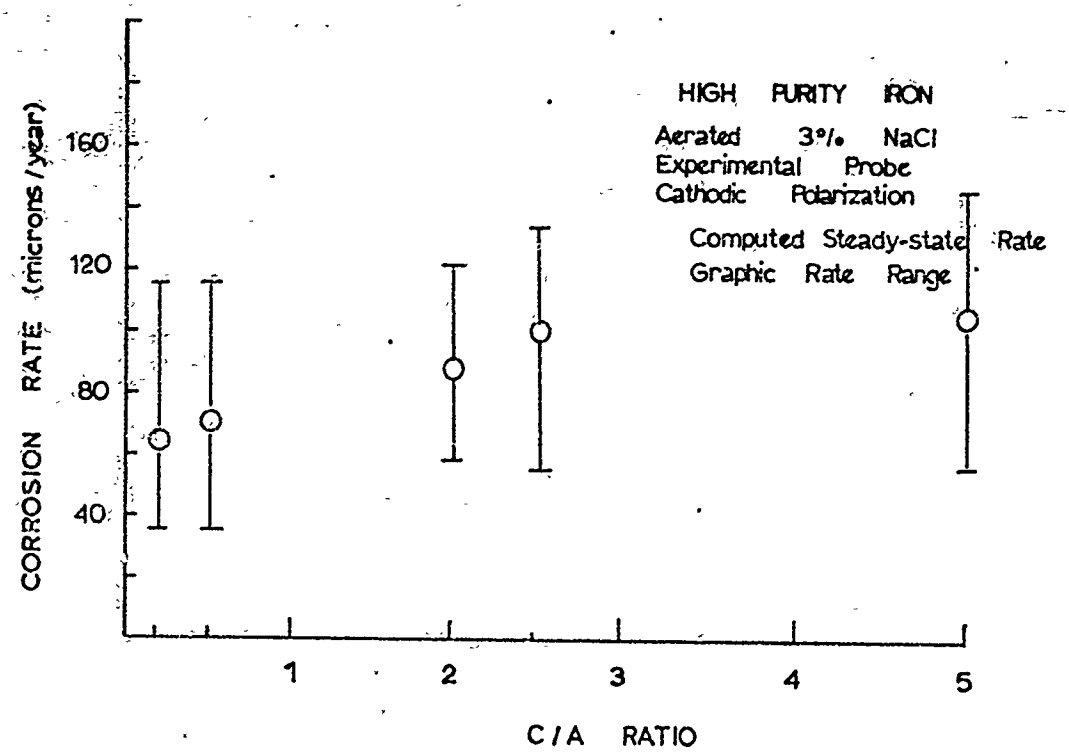

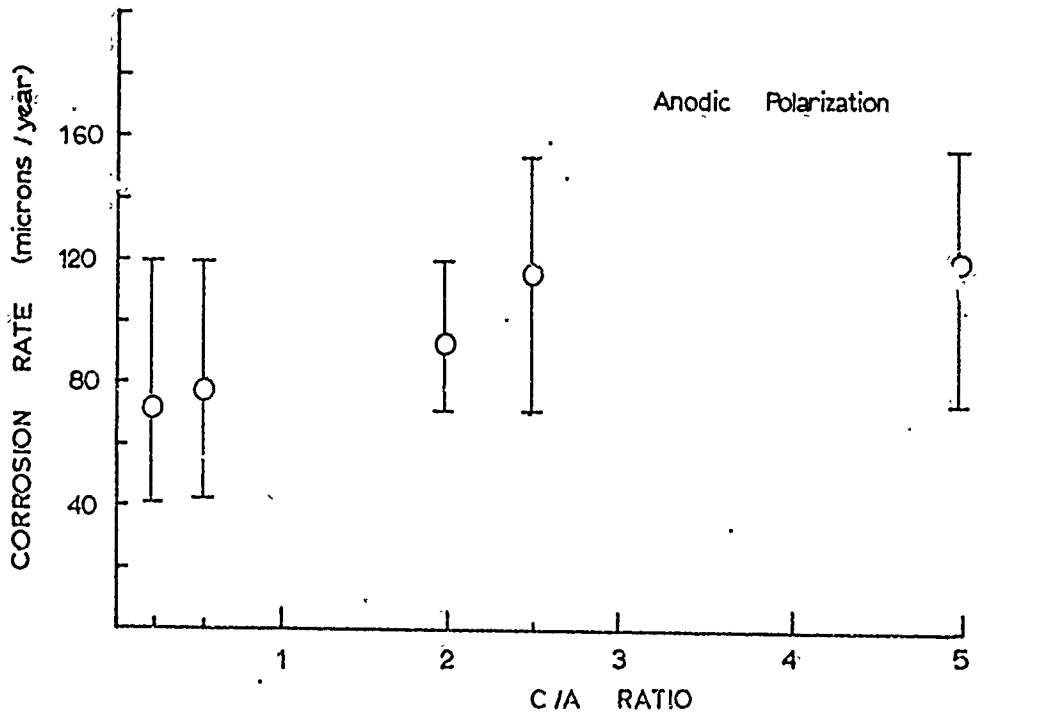

Figure 130: Effect of C/A Ratio on the Steady-state Corrosion Rate of High Purity Iron in Aerated 3% Sodium Chloride Solution Determined by Cathodic Polarization Using an Experimental Probe.

Table XIII

Computed Steady-State Corrosion Rates in 1N Sulfuric Acid Using an Experimental Probe

Test Cell Configuration	C/A Ratio	Steady-State Rate (microns/year)	Standard Deviation	t-test
2C	5	408	56	5.7
	2.5	387	74	7.5
	2	418	41	8.2
	1	521	49	9.2
	0.5	431	52	7.5
	0.2	471	80	2.4
2A	5	413	63	5.6
	2.5	390	60	10.4
	2	458	59	7.2
	1	476	63	15.4
	0.5	429	88	8
	0.2	495	78	4
4C	5	498	31	8.3
	2.5	488	32	7.7
	2	448	65	8.4
	1	446	71	10.3
	0.5	527	85	3.9
	0.2	529	94	3.3
4A	5	502	31	8.6
	2.5	494	30	9.3
	2	447	59	8.4
	1	444	59	14.7
	0.5	526	81	4.2
	0.2	513	76	2.8

Table XIV

Computed Steady-State Corrosion Rates in 0.1N Sulfuric Acid Using an Experimental Probe

Test Cell Configuration	C/A Ratio	Steady-State Rate (microns/year)	Standard Deviation	t-test
6C	5	310	39	8.7
	2.5	317	42	8.6
	2	259	48	1.3
	0.5	334	61	3.3
	0.2	347	50	0.6
6A	5	313	55	10.4
	2.5	312	58	10.1
	2	278	61	1.7
	0.5	368	59	2.5
	0.2	370	53	0.1
8C	5	542	147	0.6
	2.5	553	151	0.5
	2	425	86	0.4
	0.5	332	86	2.9
	0.2	339	96	2
8A	5	516	193	1.4
	2.5	518	186	1.2
	2	407	77	0.6
	0.5	330	91	3.3
	0.2	322	88	3.4

Table XV

Computed Steady-State Corrosion Rates in 3% Sodium Chloride Using an Experimental Probe

Test Cell Configuration	C/A Ratio	Steady-State Rate (microns/year)	Standard Deviation	t-test
12C	5	30	7	5.8
	2.5	28	7	6.8
	2	16	9	3.2
	0.5	17	8	2.2
	0.2	15	5	3.3
12A	5	31	9	7.7
	2.5	31	8	8.7
	2	19	10	2.2
	0.5	18	10	2.6
	0.2	16	5	4
14C	5	105	34	1.7
	2.5	100	31	2.1
	2	87	27	0.2
	0.5	70	36	0.8
	0.2	65	31	0.7
14A	5	119	35	2.5
	2.5	117	31	1.1
	2	92	19	1.4
	0.5	77	14	0.6
	0.2	72	17	0.6

Appendix J

The Effect of Time on Polarization Resistance and Instantaneous Corrosion Rate of High Purity Iron II

The effects of time on polarization resistance and indicated instantaneous corrosion rate of high purity iron II in deaerated (hydrogen saturated) 1N sulfuric acid are shown. Only cathodic polarization techniques were used.

Table XVI

Electrolyte pH Data for 1N Sulfuric Acid

Observations	2
pH Data	
Maximum	0.39
Minimum	0.38
Mean	0.385

Table XVII

Effect of Time on Steady-State Corrosion Potential of High Purity Iron II in Deaerated 1N Sulfuric Acid

	CORROSION POTENTIAL (V) VS. S.C.E.					
HOURS / RUN	00	24	48	72	96	120
1	-.4620	-.4280	-.4260	-.4270	-.4270	—
2	-.4910	-.4730	-.4690	-.4700	-.4720	—

Table XVIII

Weight-Loss Test Results
for High Purity Iron II

Test Cell Configuration	Observations	Weight-Loss Test Corrosion Rates		
		Maximum	Mean	Minimum
2C	2	13400	12000	10750

See Table XIX Appendix K for configuration classification

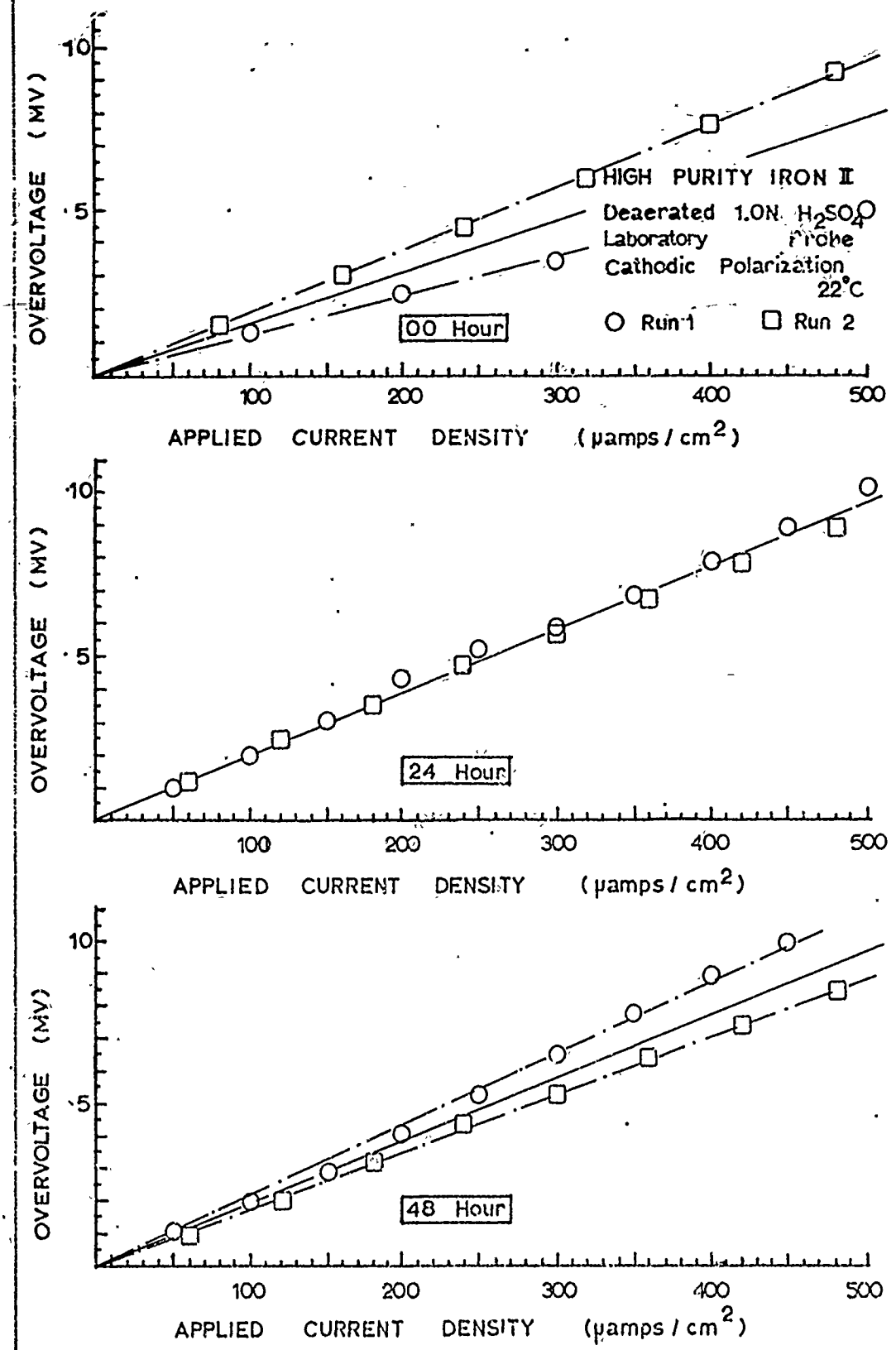

Figure 131: Effect of Time on Galvanostatic Cathodic Polarization Resistance of High Purity Iron II in Hydrogen Saturated 1N Sulfuric Acid Determined Using a Laboratory Probe. (Cont)

131

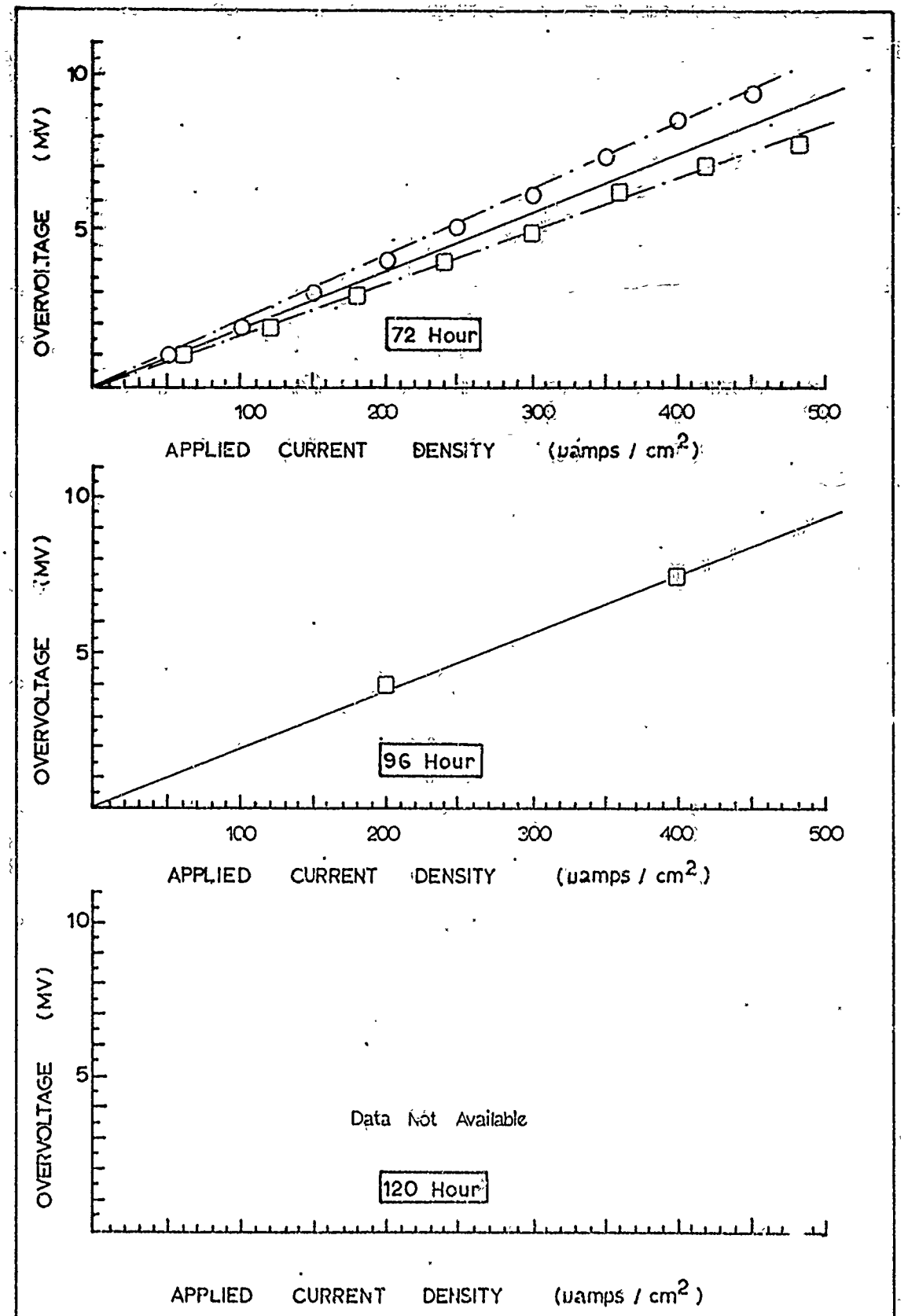

Figure 131: (Cont) Effect of Time on Galvanostatic Cathodic Polarization Resistance of High Purity Iron II in Hydrogen Saturated 1N Sulfuric Acid Determined Using a Laboratory Probe.

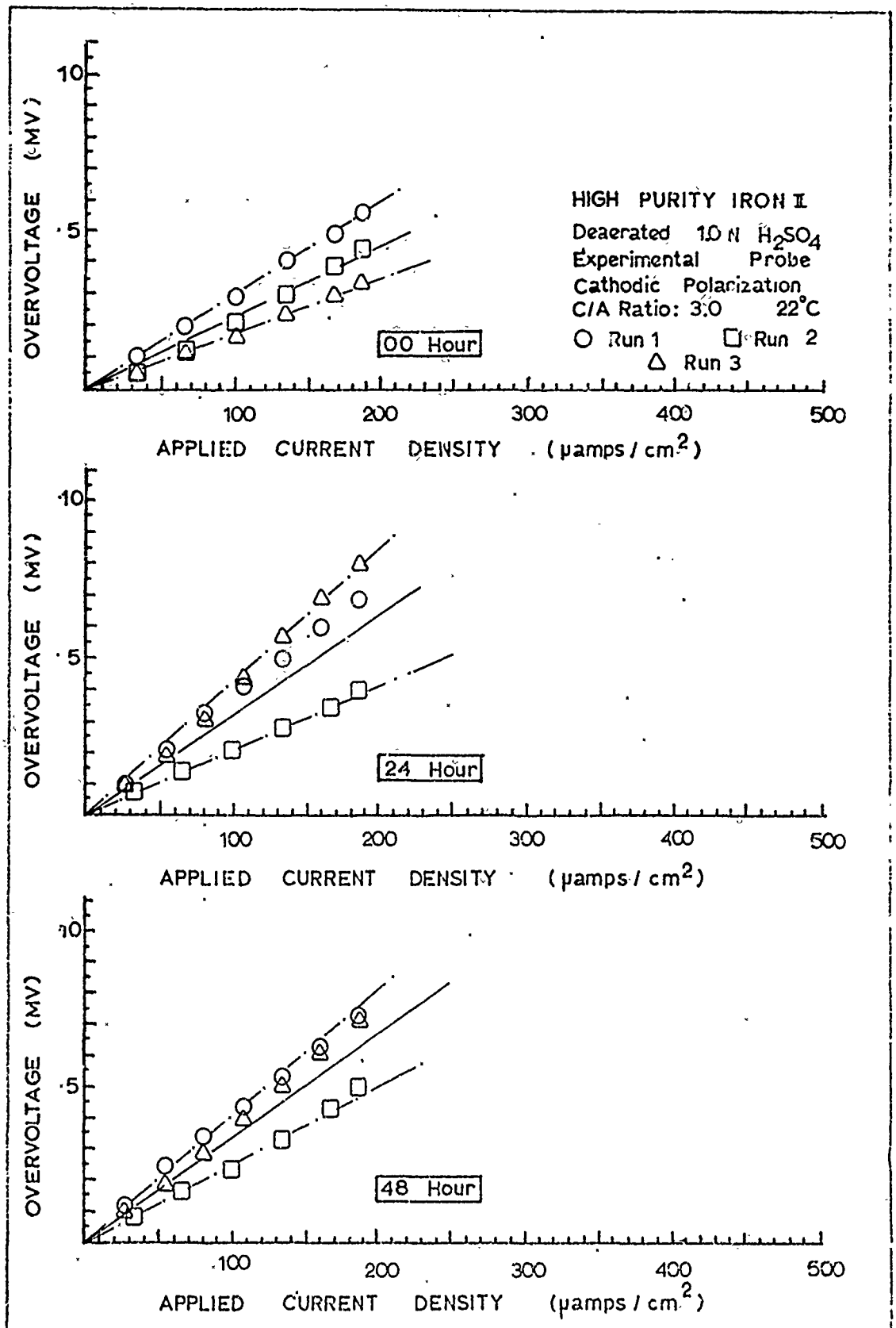

Figure 132: Effect of Time on Galvanostatic Cathodic Polarization Resistance of High Purity Iron II with C/A Ratio = 3 in Hydrogen Saturated 1N Sulfuric Acid Using an Experimental Probe. (Cont)

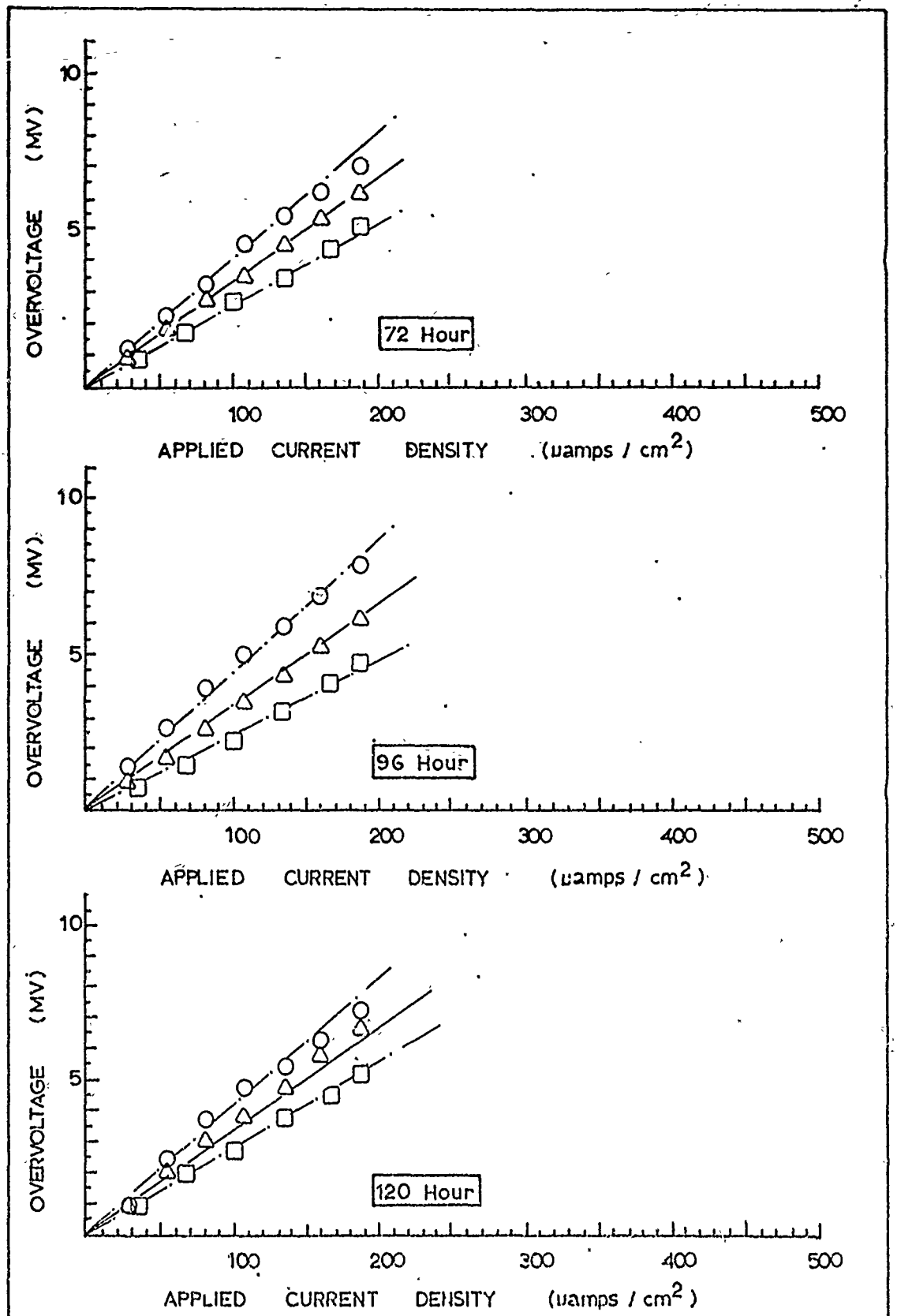

Figure 132: (Cont) Effect of Time on Galvanostatic Cathodic Polarization Resistance of High Purity Iron II with C/A Ratio = 3 in Hydrogen Saturated 1N Sulfuric Acid Using an Experimental Probe.

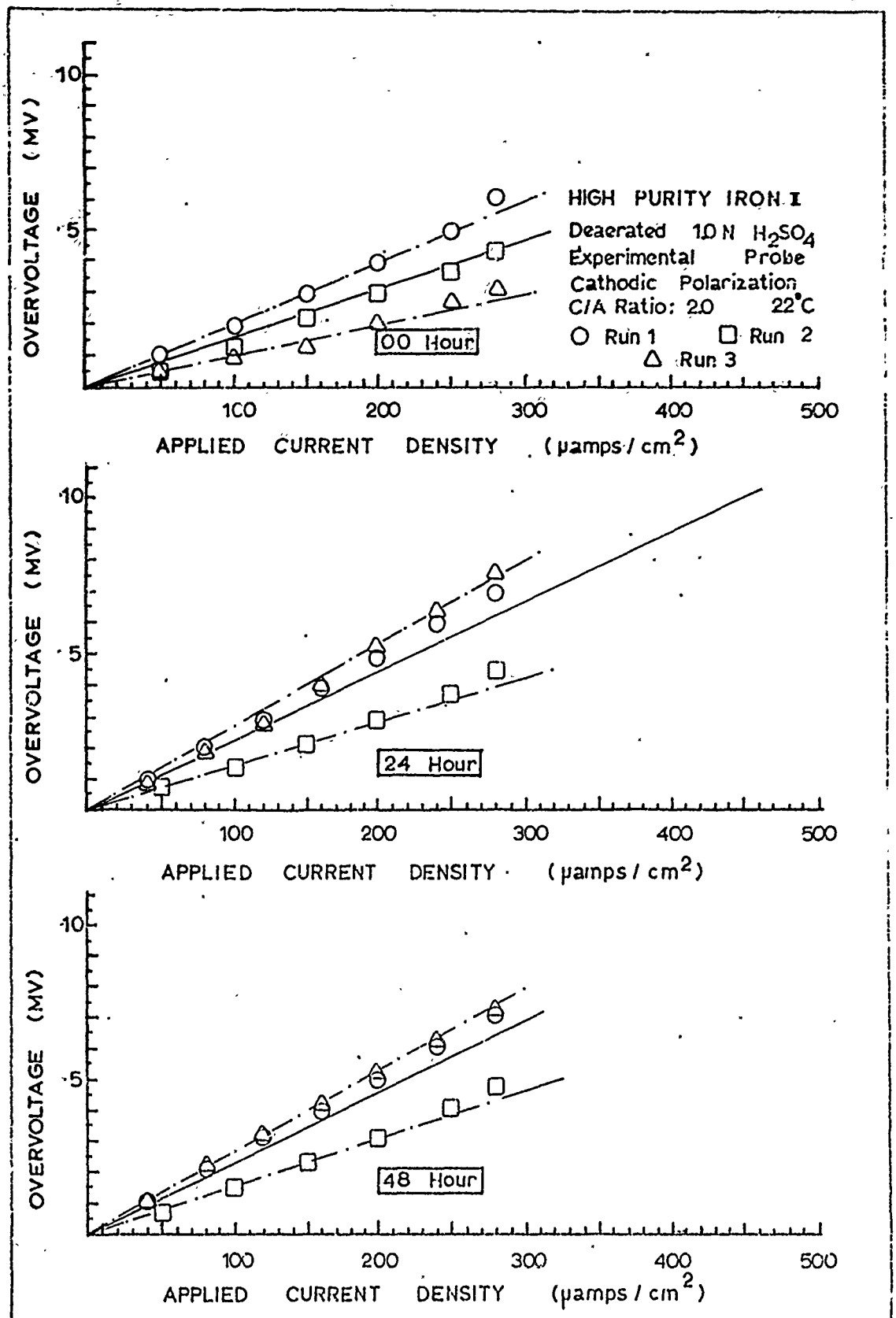

Figure 133: Effect of Time on Galvanostatic Cathodic Polarization Resistance of High Purity Iron II with C/A Ratio = 2 in Hydrogen Saturated 1N Sulfuric Acid Using an Experimental Probe. (Cont)

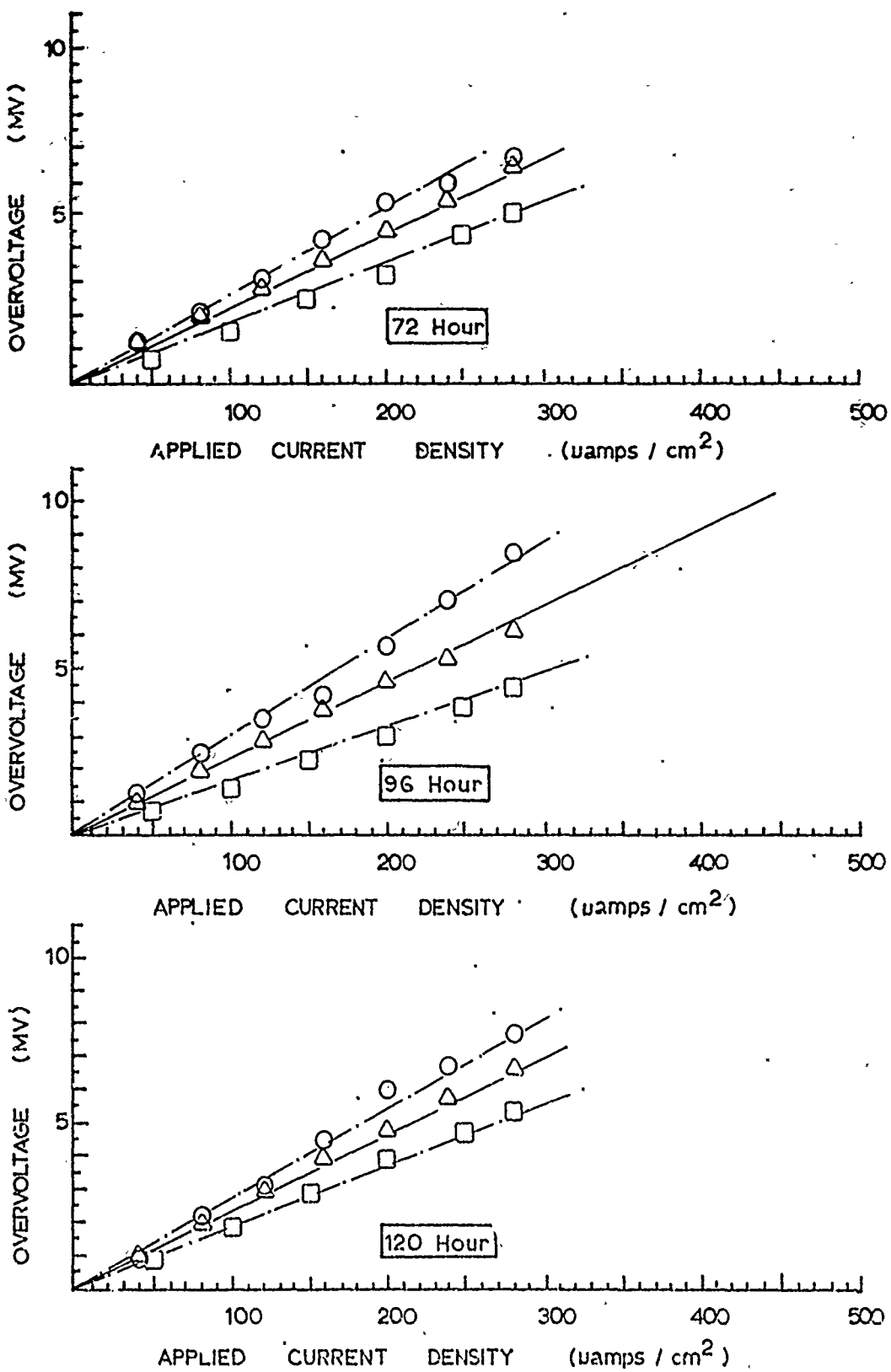

Figure 133: (Cont) Effect of Time on Galvanostatic Polarization Resistance of High Purity Iron II with C/A Ratio = 2 in Hydrogen Saturated 1N Sulfuric Acid Using an Experimental Probe.

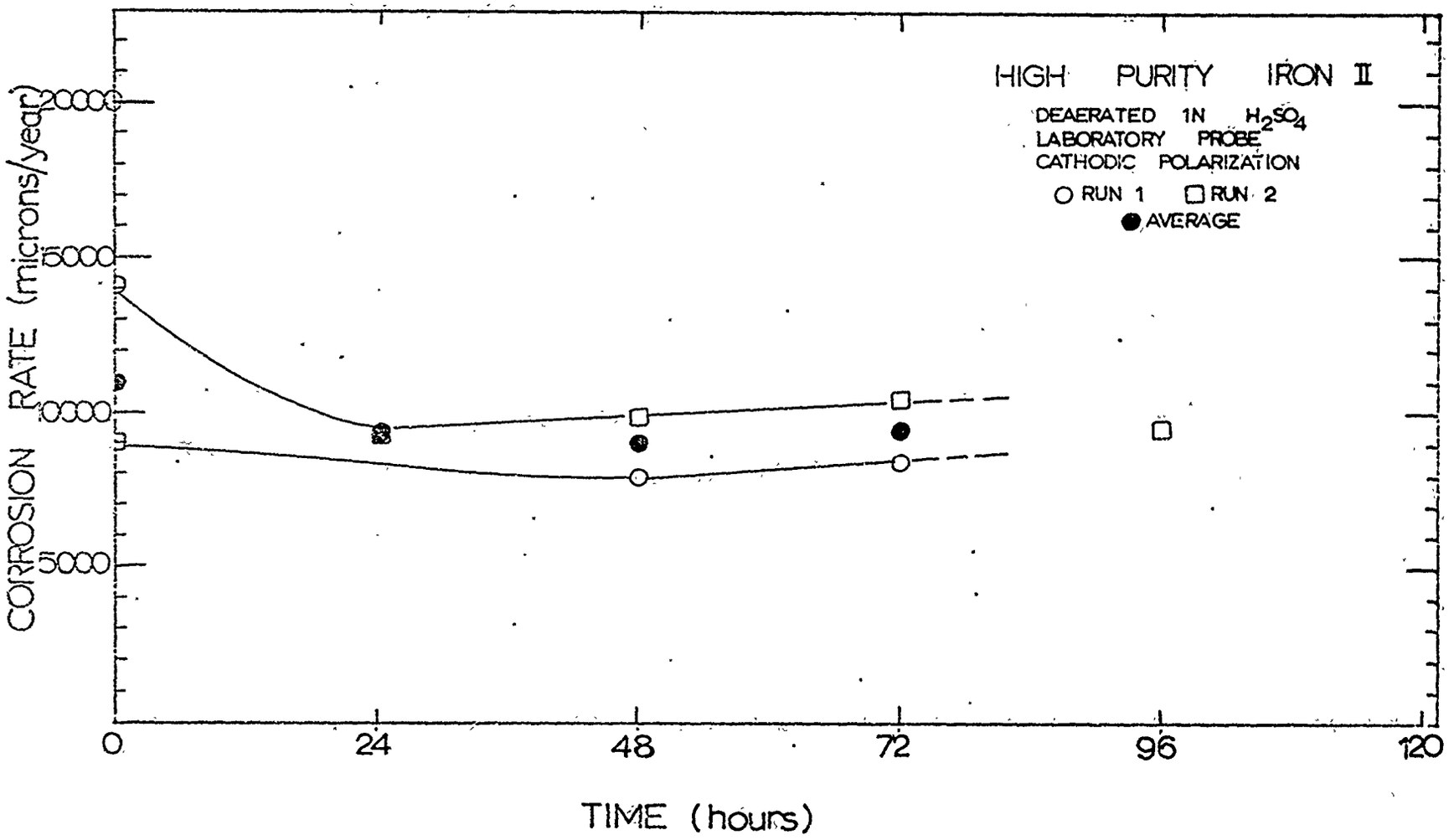

Figure 134: Effect of Time on the Corrosion Rate of High Purity Iron II in Hydrogen Saturated 1N Sulfuric Acid Determined by Cathodic Polarization Using a Laboratory Probe.

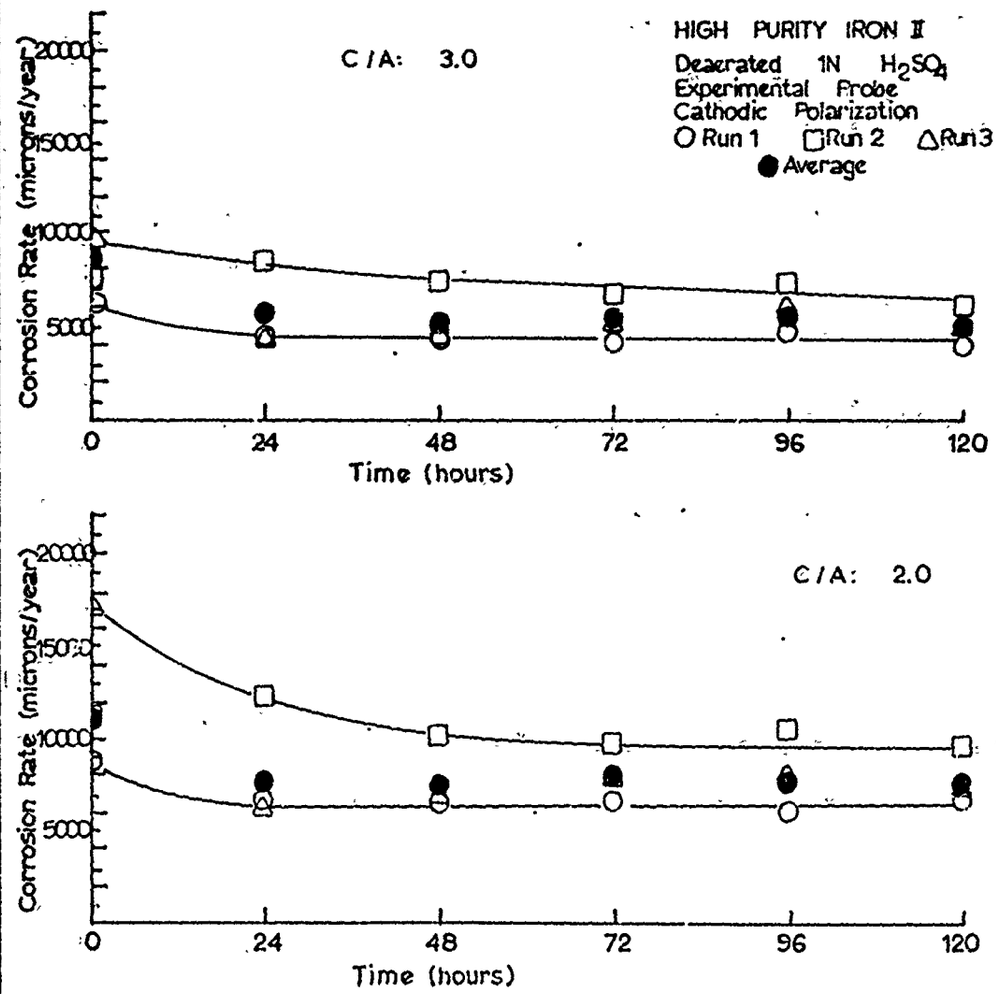

Figure 135: Effect of Time on the Corrosion Rate of High Purity Iron II at various C/A Ratios in Hydrogen Saturated 1N Sulfuric Acid Determined by Cathodic Polarization Using an Experimental Probe.

Appendix K

Weight-Loss Testing Results

Weight loss tests were conducted concurrently with resistance polarization tests. Data collected were classified by the electrolyte, electrolyte concentration, degree of aeration, and probe type used during testing. These classifications are shown in Table XIX. The number of observations, highest and lowest observed corrosion rates, and the calculated mean corrosion rate are shown by class in Table XX . Corrosion rate data are shown in units of microns/year and mils/year to facilitate comparison with data from other sources.

Class	Electrolyte	Concentration	Degree of Aeration	Probe Configuration
1	Sulfuric Acid	1N	Hydrogen Saturated	Laboratory
2				Experimental
3			Aerated	Laboratory
4				Experimental
5		0.1N	Hydrogen Saturated	Laboratory
6				Experimental
7			Aerated	Laboratory
8				Experimental
9		0.01N	Hydrogen Saturated	Laboratory
10				Experimental
11	Sodium Chloride	3%	Hydrogen Saturated	Laboratory
12				Experimental
13			Aerated	Laboratory
14				Experimental

Table XIX: Test Cell Configuration Classifications

Table XX

Corrosion Rates Determined from Weight-Loss Tests

Class	Observations	Weight Loss Test Corrosion Rates		
		Highest	Mean	Lowest
1	6	1223/49	989/39	648/26
2	8	1122/45	859/34	674/27
3	6	2150/86	1342/53	1019/41
4	12	1482/58	787/31	613/24
5	4	1858/74	1556/61	1175/47
6	12	633/25	537/21	434/17
7	8	1958/78	1564/62	1015/40
8	9	945/38	732/29	550/22
9	2	720/29	640/25.5	560/22
10	3	678/27	567/23	475/19
11	3	93/3.7	59/2.3	39/1.5
12	6	93/3.7	90/3.6	83/3.3
13	3	185/7.4	149/5.9	111/4.4
14	9	342/13.4	247/9.7	167/6.7

Appendix L

Photomicrographs of Specimens From Various Test Configurations and Environments

This appendix contains photomicrographs made of various specimens used during this investigation. The specimens of which the photomicrographs were taken were used in various environments throughout the investigation. Specimen conditions emphasized by the photomicrographs were characteristic of conditions noted throughout the investigation.

Figure 136: Approximate Center of the Exposed Surface of a 1 cm^2 Laboratory Specimen of High Purity Iron I After 120 Hour Immersion in Aerated 1N Sulfuric Acid (20X)

Figure 137: Approximate Center of the Exposed Surface of a 1 cm^2 Laboratory Specimen of High Purity Iron I After 120 Hour Immersion in Aerated 1N Sulfuric Acid (100X)

Reproduced from best available copy.

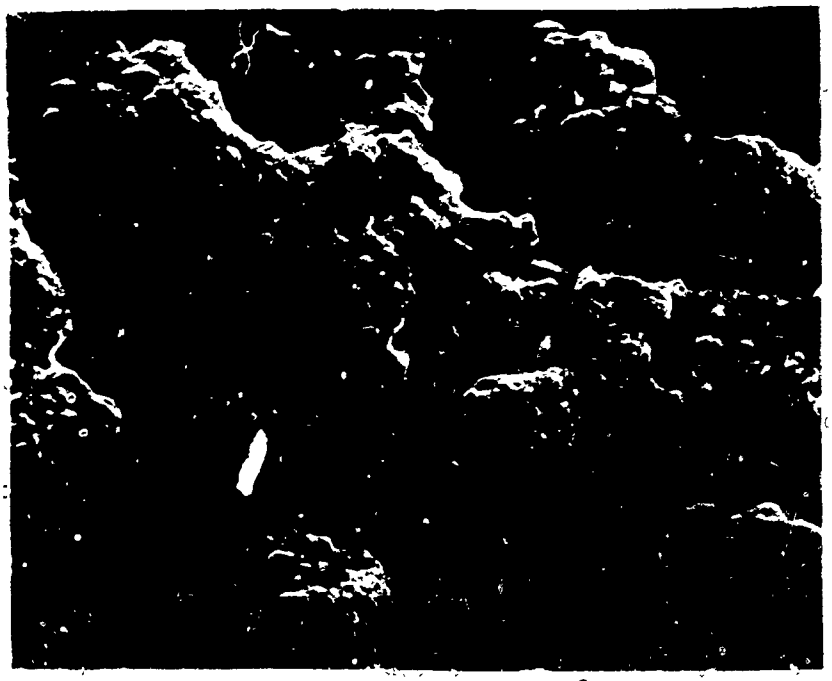

Figure 138: Approximate Center of the Exposed Surface of a 1 cm^2 Laboratory Specimen of High Purity Iron I After 120 Hour Immersion in Aerated 1N Sulfuric Acid (1000X)

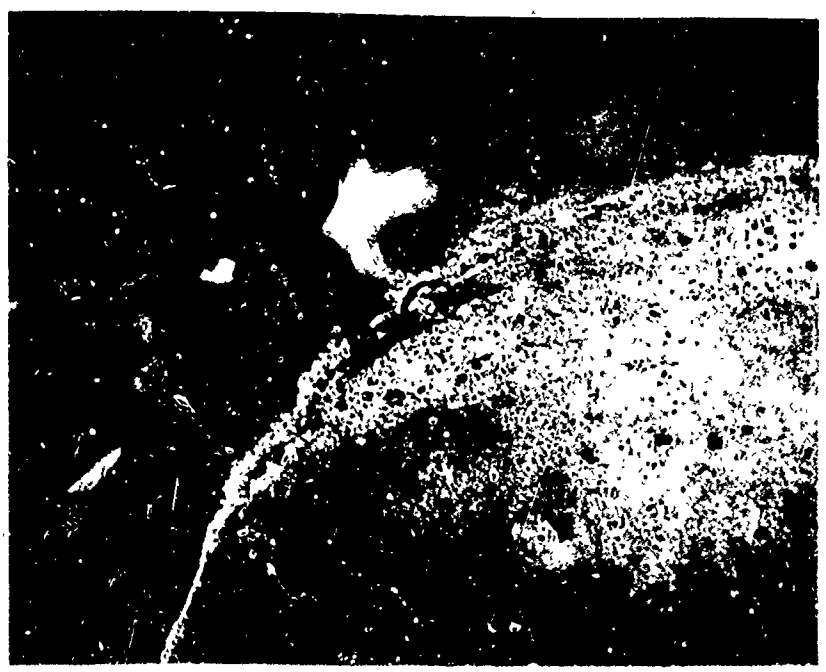

Figure 139 Approximate Center to Circumference of Exposed Surface and Unexposed Surface of 1 cm^2 Laboratory Specimen of High Purity Iron I After 120 Hour Immersion in Deaerated 0.1N Sulfuric Acid (20X)

Reproduced from best available copy.

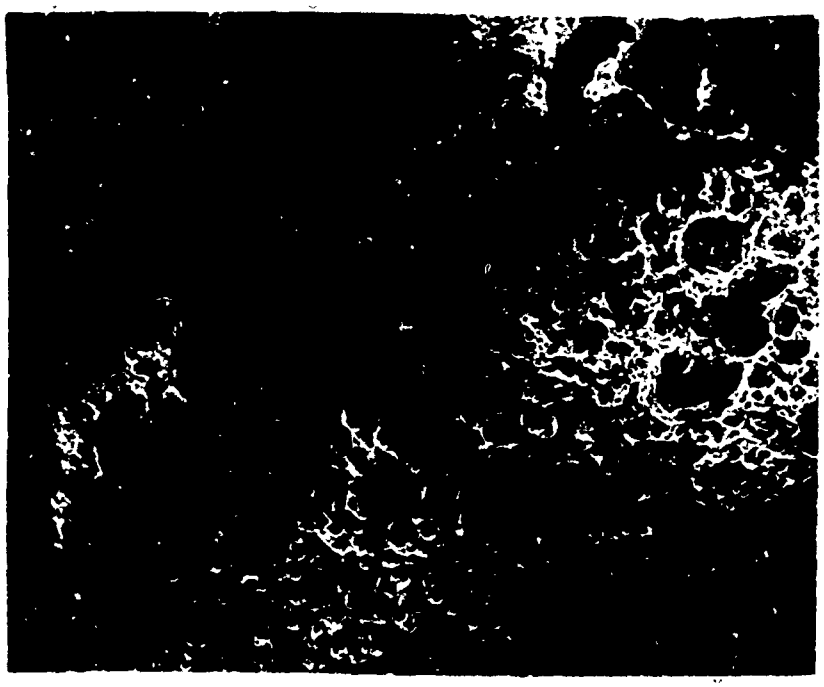

Figure 140: Circumference of Exposed Surface Area of 1 cm^2 Laboratory Specimen (Figure 139) of High Purity Iron I After 120 Hour Immersion in Deaerated 0.1N Sulfuric Acid (100X)

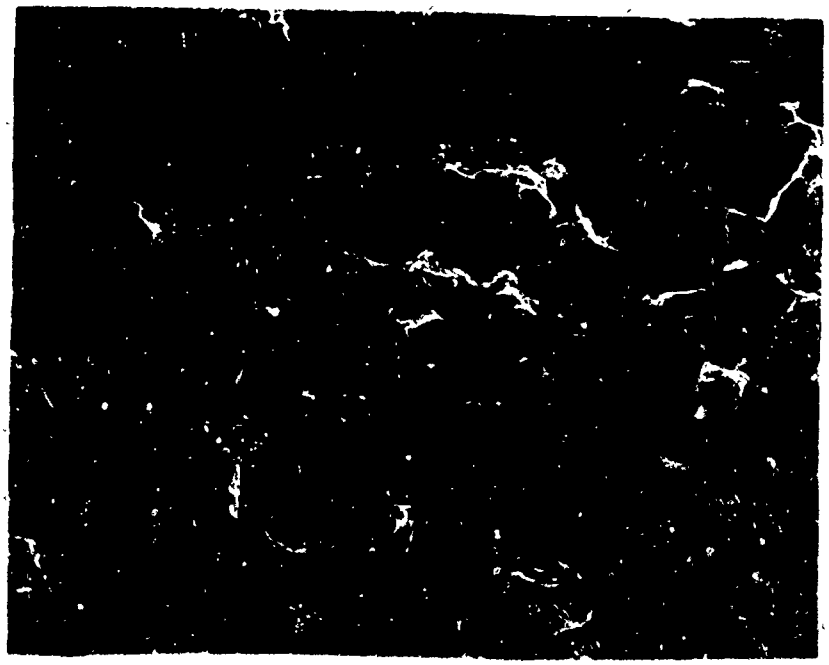

Figure 141: Area Approximately 0.3 cm Toward Center From Exposed Surface Circumference of 1 cm^2 Laboratory Specimen (Figure 140) of High Purity Iron I After 120 Hour Immersion in Deaerated 0.1N Sulfuric Acid (500X)

Figure 142: Approximate Center of Exposed Surface Area of 1 cm^2 Laboratory Specimen (Figure 139) of High Purity Iron I After 120 Hour Immersion in Deaerated 0.1N Sulfuric Acid (200X)

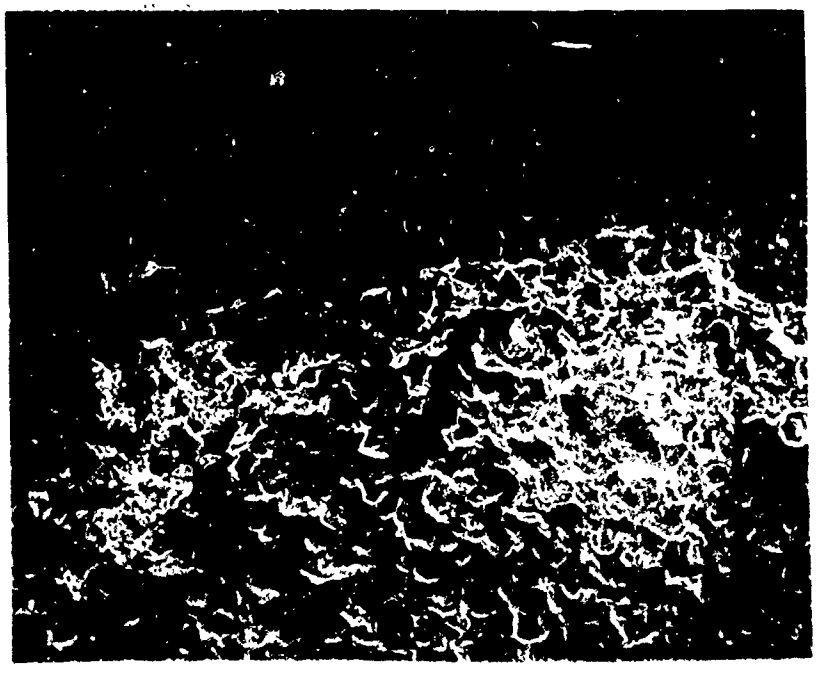

Figure 143 Approximate Center to Circumference of Exposed Surface and Unexposed Surface of 1 cm^2 Laboratory Specimen of High Purity Iron II After 120 Hour Immersion in Deaerated 1N Sulfuric Acid (20X)

Reproduced from best available copy.

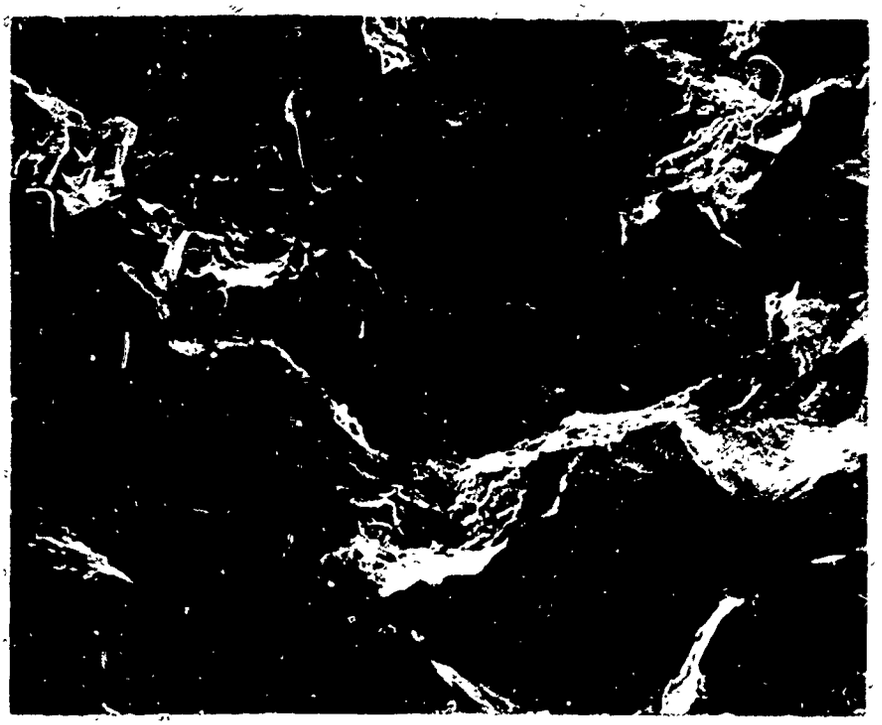

Figure 144: Approximate Center of Exposed Surface of 1 cm^2 Laboratory Specimen (Figure 143) of High Purity Iron II After 120 Hour Immersion in Deaerated 1N Sulfuric Acid (200X)

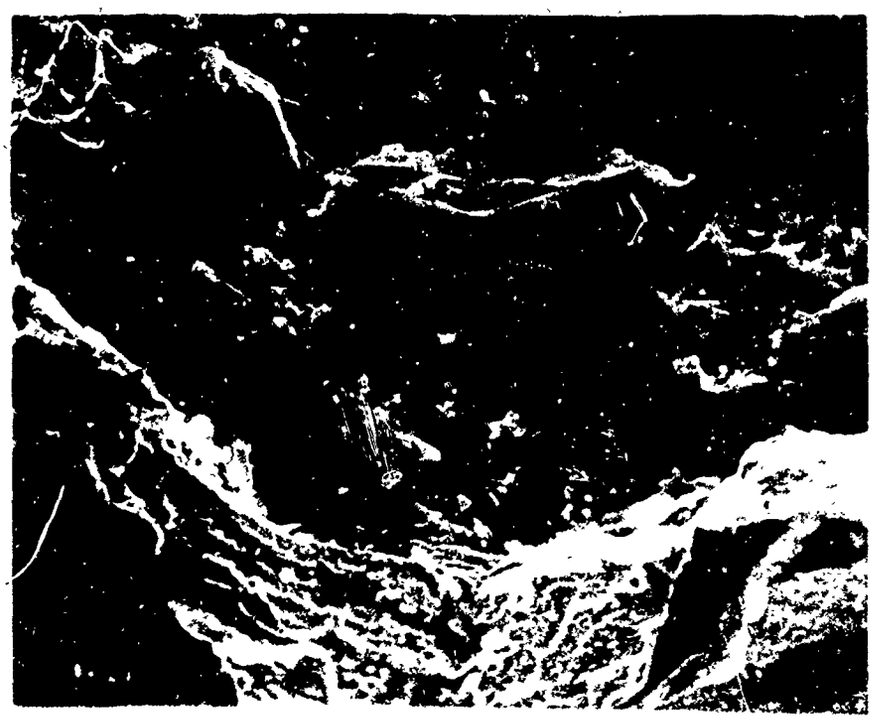

Figure 145 Approximate Center of Exposed Surface of 1 cm^2 Laboratory Specimen (Figure 143) of High Purity Iron II After 120 Hour Immersion in Deaerated 1N Sulfuric Acid (500X)

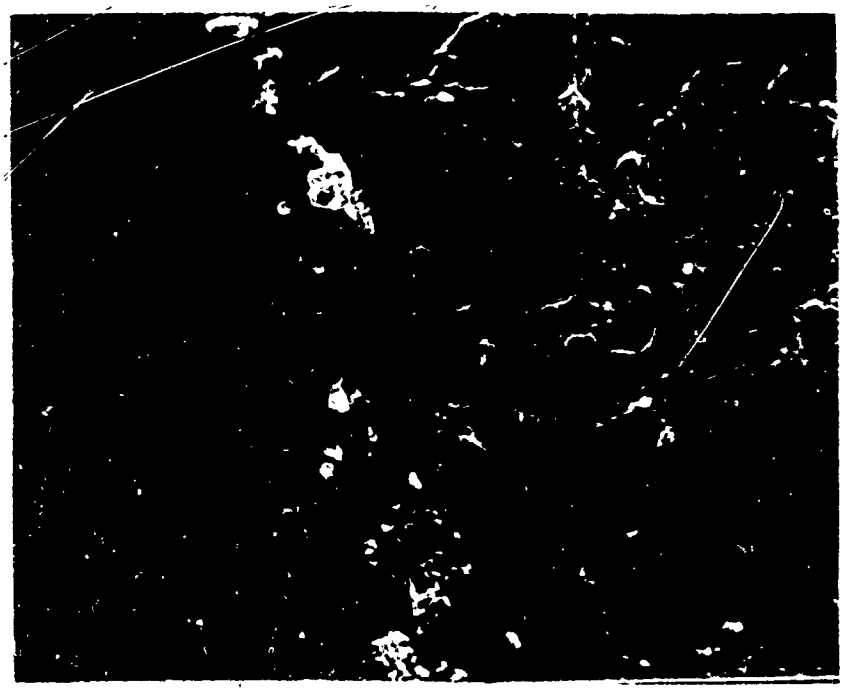

Figure 146 Approximate Center of Exposed Surface of 1 cm^2 Laboratory Specimen of High Purity Iron I After 120 Hour Immersion in Aerated 3% Sodium Chloride/0.5N Potassium Sulfate (500X)

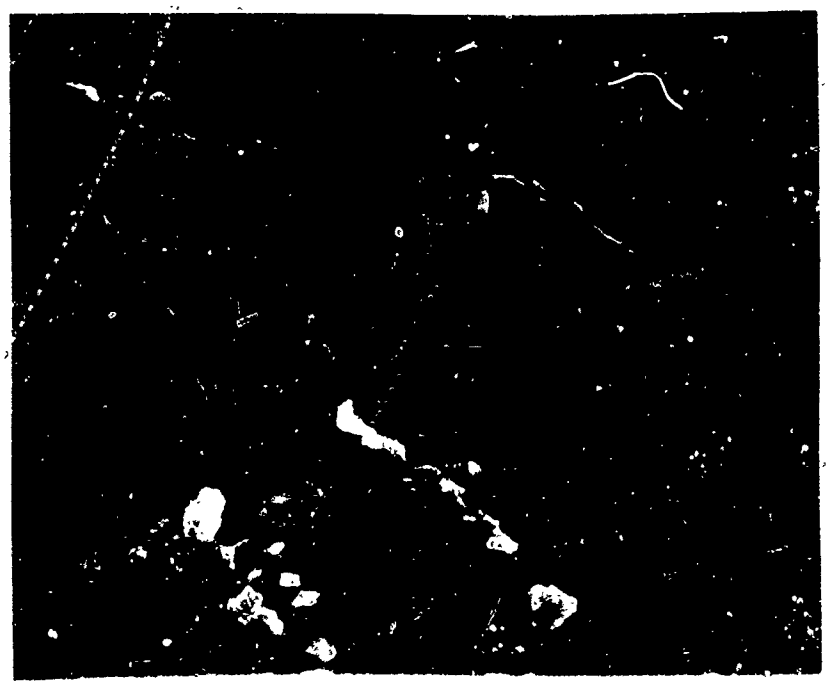

Figure 147 Approximate Center of Exposed Surface of 1 cm^2 Laboratory Specimen of High Purity Iron I After 120 Hour Immersion in Aerated 3% Sodium Chloride/0.5N Potassium Sulfate (1000X)

Reproduced from best available copy.

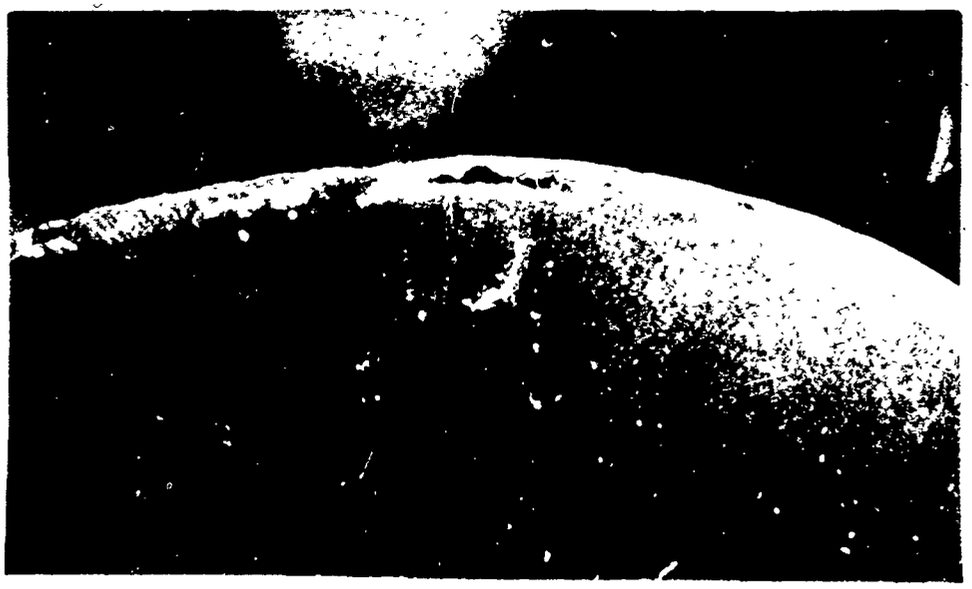

Figure 148: Unexposed (bottom) Surface of 10 cm^2 Experimental Specimen of High Purity Iron I After 120 Hour Immersion in 1N Deaerated Sulfuric Acid (20X)

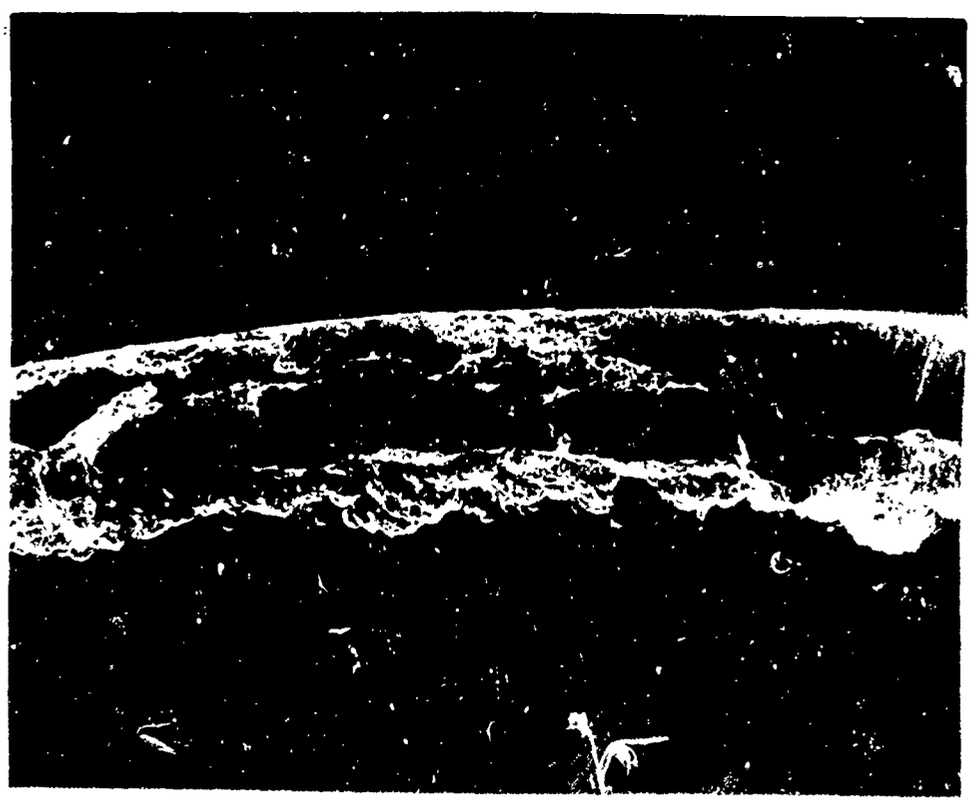

Figure 149. Increased Magnification of Unexposed Surface (Figure 148) of High Purity Iron I After 120 Hour Immersion in 1N Deaerated Sulfuric Acid (100X)

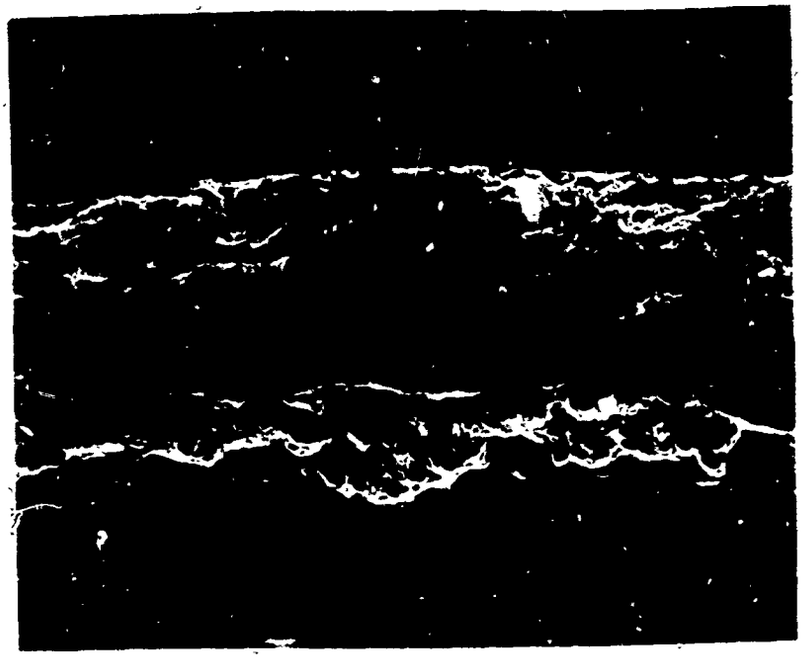

Figure 150 Further Increased Magnification of Unexposed Surface (Figure 148) of High Purity Iron I After 120 Hour Immersion in 1N Deaerated Sulfuric Acid (200X)

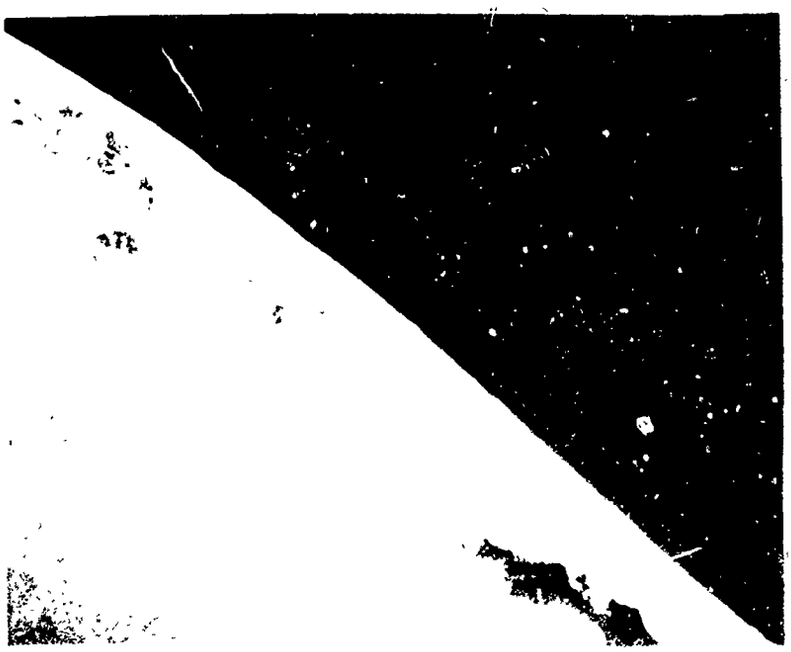

Figure 151 Unexposed Surface of 10 cm^2 Experimental Specimen of High Purity Iron I After 120 Hour Immersion in 1N Deaerated Sulfuric Acid (200X)

Figure 152: Exposed Circumferential Surface of 5 cm^2 Experimental Specimen of High Purity Iron I After 120 Hour Immersion in Deaerated 3% Sodium Chloride/0.5N Potassium Sulfate (20X)

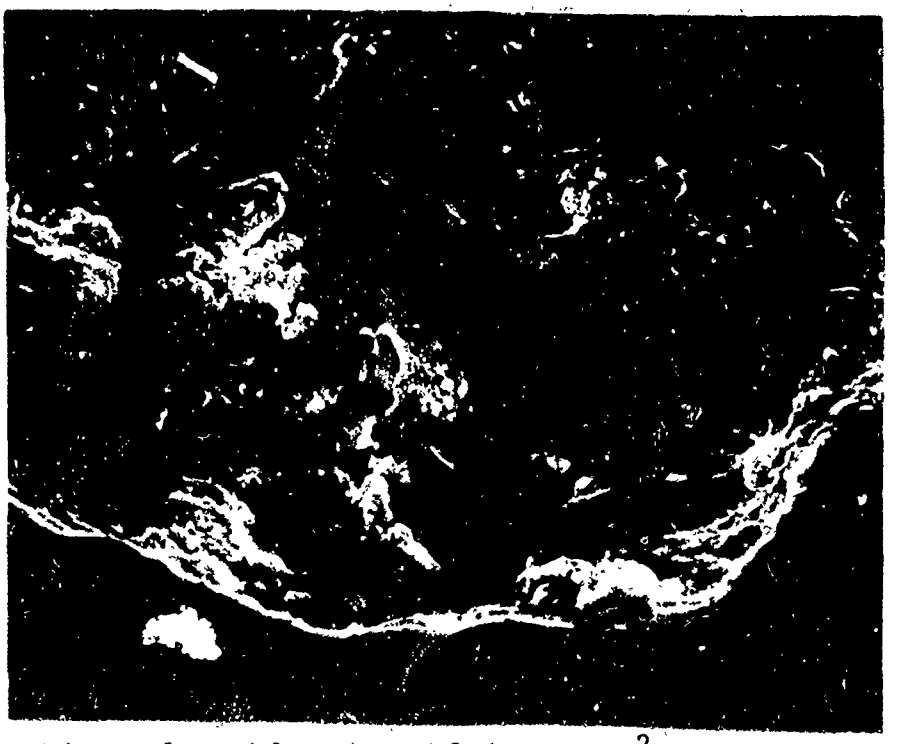

Figure 153 Pitted Area on Exposed Circumferential Surface of 5 cm^2 Experimental Specimen (Figure 152) of High Purity Iron I After 120 Hour Immersion in Deaerated 3% Sodium Chloride 0.5N Potassium Sulfate (500X)

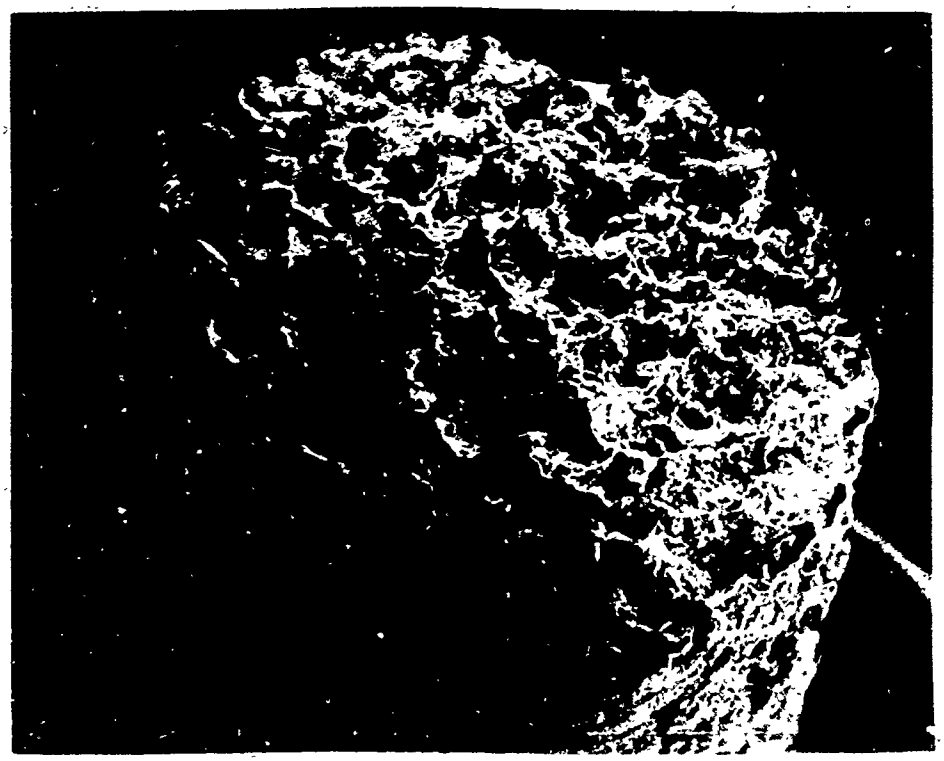

Figure 154: Exposed End of 2 cm^2 Experimental Specimen of High Purity Iron II After 120 Hour Immersion in Deaerated 1N Sulfuric Acid (20X)

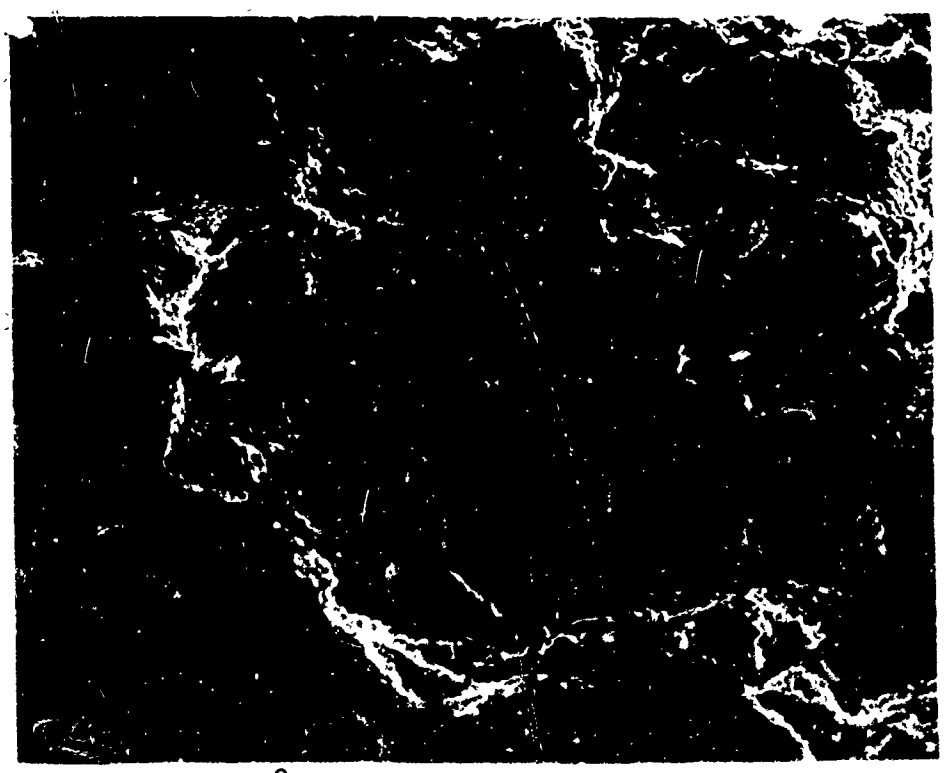

Figure 155. Exposed End of 2 cm^2 Experimental Specimen of High Purity Iron II After 120 Hour Immersion in Deaerated 1N Sulfuric Acid (100X)

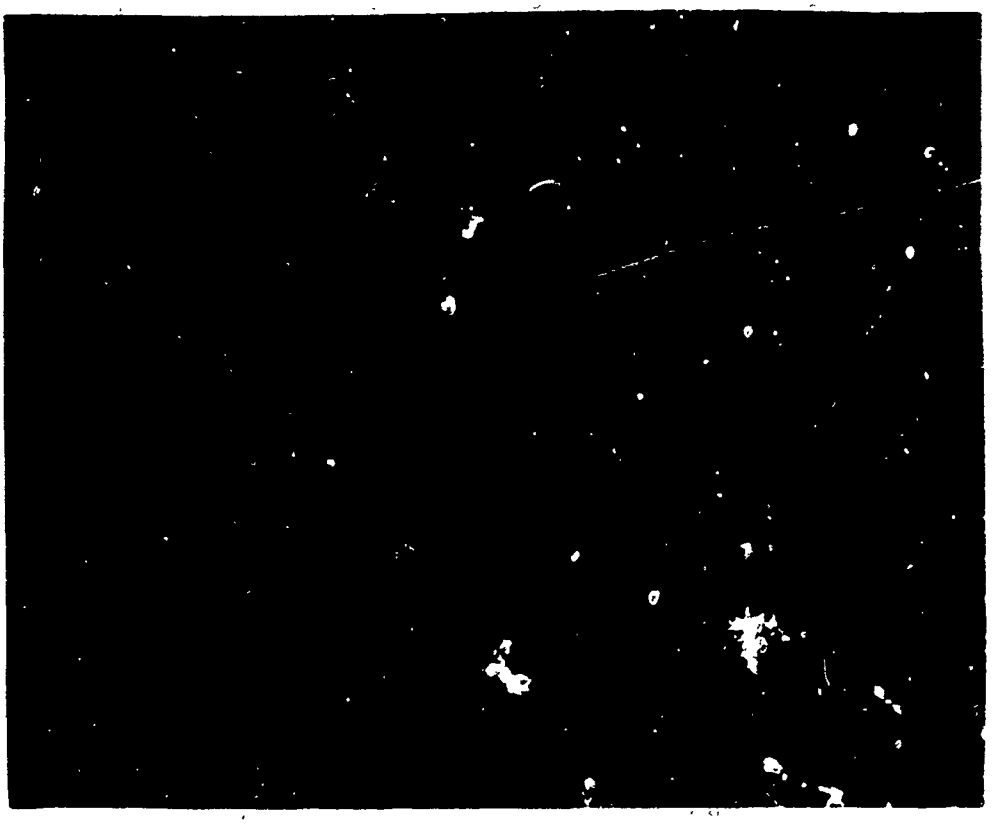

Figure 156: Grain Structure of Polished and Etched High Purity Iron II Specimen (2000X)

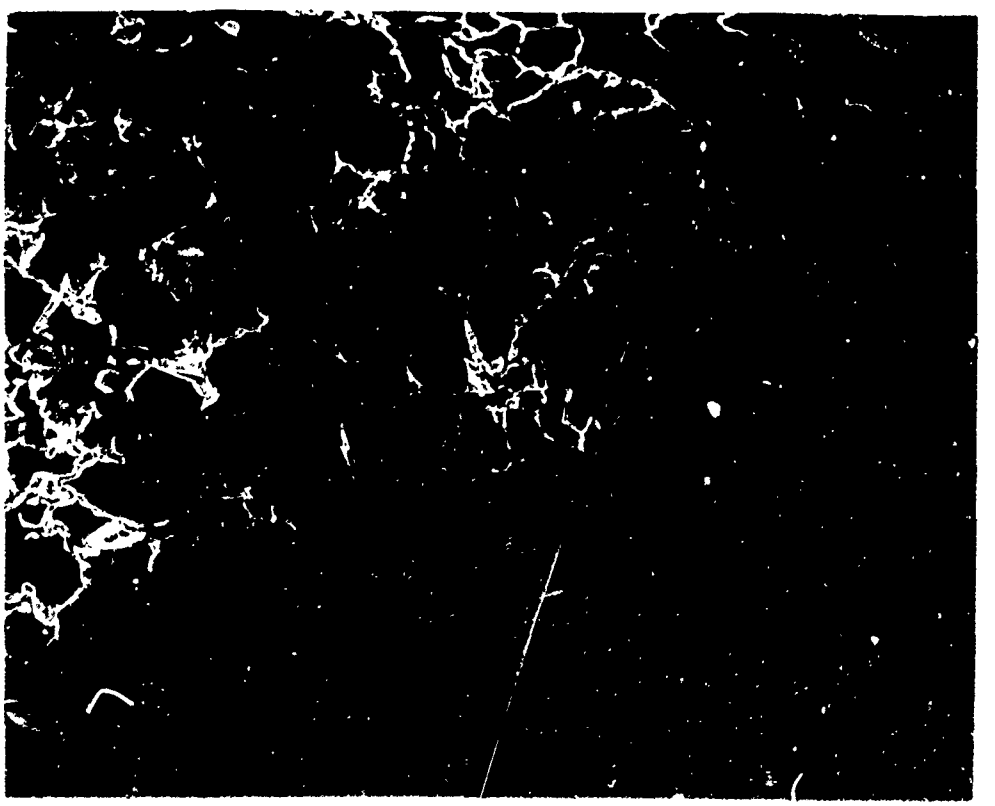

Figure 157 Polished Surface of a Laboratory Specimen (Figure 136) After 120 Hour Immersion in Aerated 1N Sulfuric Acid

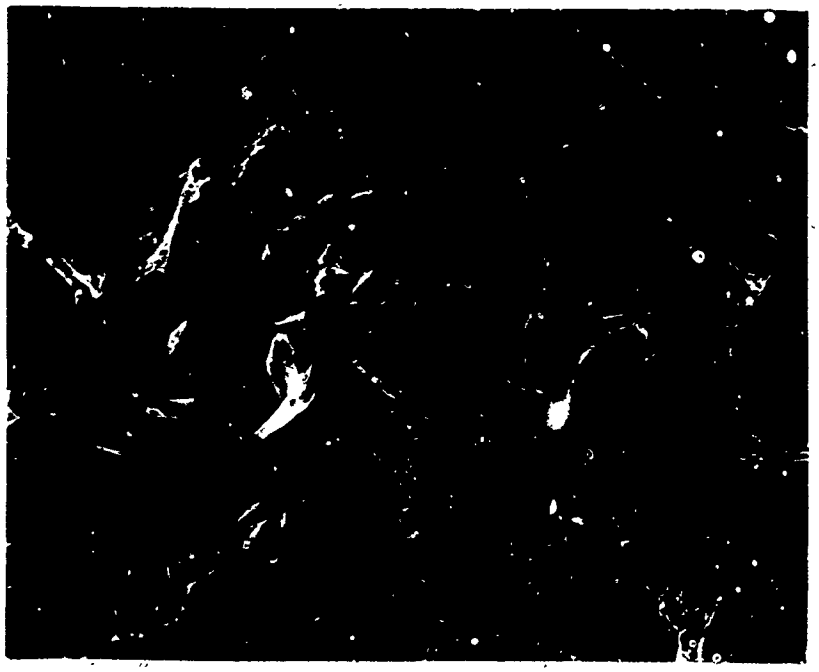

Figure 158 Polished Surface of a Laboratory Specimen (Figure 136) After 120 Hour Immersion in Aerated 1N Sulfuric Acid (180X)

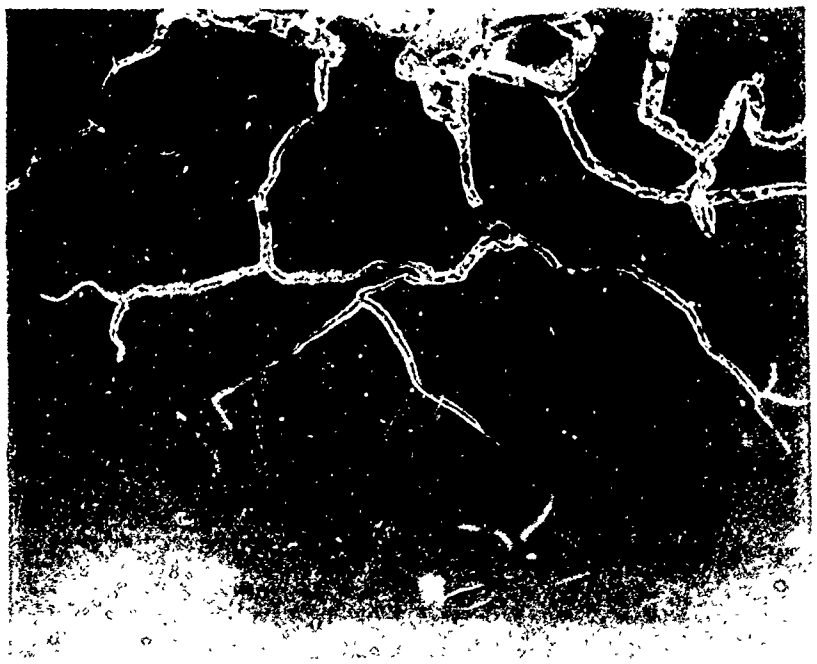

Figure 159 Polished Surface of a Laboratory Specimen (Figure 136) After 120 Hour Immersion in Aerated 1N Sulfuric Acid (200X)

Reproduced from best available copy.

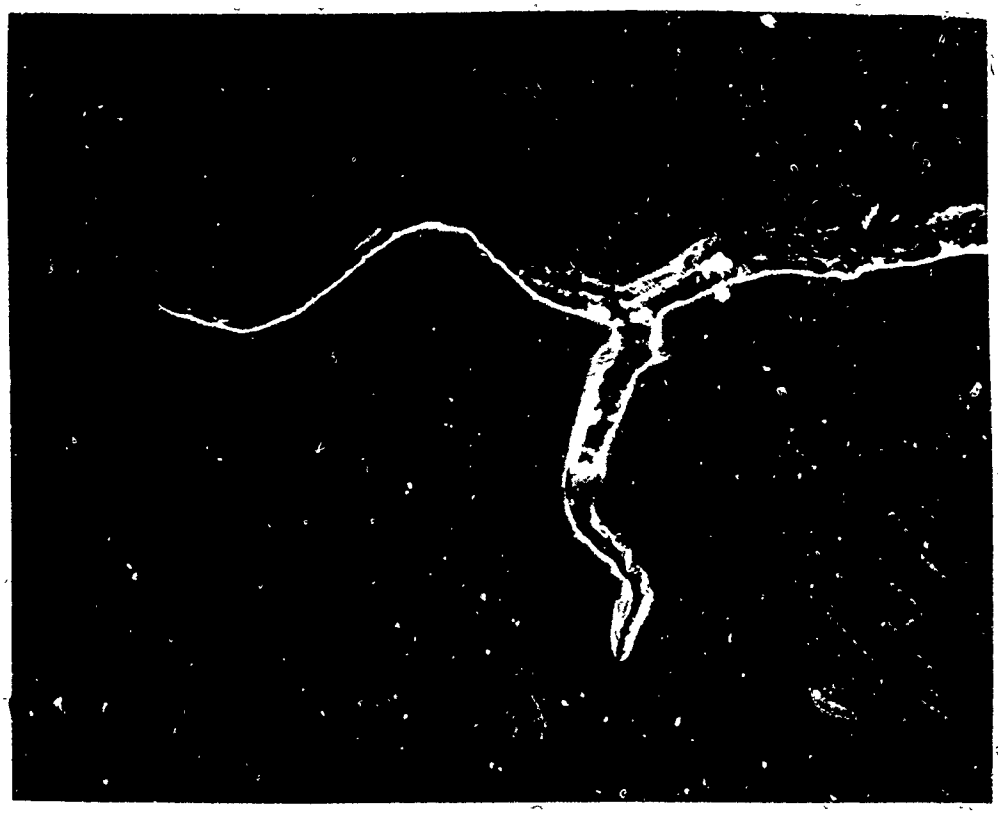

Figure 160: Polished Surface of a Laboratory Specimen (Figure 136) After 120 Hour Immersion in Aerated 1N Sulfuric Acid (1000X)

Appendix M

Linear Regression Program Instructions

The procedures followed to obtain general information about and operating instructions for the linear regression program used in this investigation are contained in this appendix.

```
USER ID -ENST
PASSWORD--
[illegible]
PROBLEM NO.--
[illegible]
SYSTEM ?CARD
OLD OR NEW-O ENSLIB/FORTRAN/IREGRESS,R
READY
*LIST
```

THIS IS A DOUBLE PRECISION REGRESSION PROGRAM. IT ALLOWS YOU TO RUN A NUMBER OF DATA SETS AND NUMEROUS PROBLEMS ON EACH SET IN ONE SET-UP.
VARIOUS TRANSFORMATIONS OF THE DATA ARE ALLOWED.
IF YOU DESIRE TO OBTAIN A LISTING OF THE SET UP INSTRUCTION ENTER FOLLOWING STREAM OF COMMMANDS:

```
SYSTEM?CARD
OLD OR NEW?O ENSLIB/CARDIN/REGRESSP,R
READY
*RUN
  SNUMB # PØ11T
CARD FORMAT, DISPOSITION?
ASIS
TAB CHARACTERS AND SETTINGS?
(HIT THE RETURN KEY)
```

THE SET-UP INSTRUCTIONS WILL BE PRINTED AT THE CE PRINTER.
IF YOU DESIRE TO LIST THE INSTRUCTIONS AT YOUR TERMINAL YOU MAY ENTER THE FOLLOWING:

```
SYSTEM?CARD
OLD OR NEW?O ENSLIB/FORTRAN/RSETUP,R
READY
*LIST
```

IT WILL NORMALLY TAKE 5 TO 10 MINUTES TO PRINT THE ENTIRE LIST OF INSTRUCTIONS SO THIS PROCEDURE SHOULD NOT BE USED IF PEOPLE ARE WAITING FOR THE TERMINAL.
SINCE THE SET UP INSTRUCTIONS SHOW YOU HOW TO SET-UP AND RUN THE OBJECT DECK YOU WILL NOT GET A PRINT OUT OF THE FORTRAN VERSION OF THE PROGRAM. IF YOU DESIRE TO OBTAIN A COPY OF THE FORTRAN PROGRAM IN ORDER TO CHAGE THE PROGRAM, IT CAN BE ATTACHED FROM THE CARDIN OR EDITOR SYSTEMS BY THE FOLLOWING COMMAND:

```
OLD OR NEW? O ENSLIB/FORTRAN/REGRESS,R
```

Appendix N

Data Treatment Computer Program

This appendix contains a listing of the computer program used to compute and tabulate resistance polarization and corrosion rate data. This program was compatible with the AFLC CREATE System. Previous investigators[3, 10] used a similar program which was compatible with the CDC 6600 computer. The specific uses of the program used during this investigation are listed in "Daily Corrosion Rate Determination" of Chapter IV. The program and all computer output from this investigation are available from the Department of Mechanics, School of Engineering, Air Force Institute of Technology.

```
C
C     PROGRAM RUST (INPUT, OUTPUT)
C
C
C
      DIMENSION EPT(6), PH(6), ECORR(6,6), S(6,6), R(6), ICORR(6,6),IPY(
     16,6), MDD(6,6), MPY(6,6), CICORR(6), CIPY(6), CMDD(6), CMPY(6), A(
     26,6,20), B(6,6,20)
      REAL ICORR, IPY, MDD, MPY
C
C
C     BETA A AND BETA C ARE TAFEL SLOPES
C
C     RHO IS MATERIAL DENSITY
C
C     EQVWT IS EQUIVALENT WEIGHT >  ATOMIC WT / VALENCE
      READ (05,300)  BETAA, BETAC, RHO, EQVWT                           114
  300 FORMAT (2X, 4F12.6)                                               008
      PRINT 10
   10 FORMAT (1H1, //////////, 30X, :CORROSION RATE DATA: //)
      PRINT 11
   11 FORMAT (30X, :CATHODIC POLARIZATION: /////)
   15 READ (05,16) AREA                                                 9B
   16 FORMAT (1X, F10.2)                                                10
      PRINT 20, AREA
   20 FORMAT (20X, :ANODE[  :, F5.0, : SQ CM HIGH PURITY IRON: ///)
      PRINT 30                                                          012
   30 FORMAT (20X, :CATHODE    25.00 SQ CM PLATINUM MESH: ///)
      READ (05,31) CONC
   31 FORMAT (1X, F10.3)                                                13B
      PRINT 40, CONC                                                    14
   40 FORMAT (20X, :ELECTROLYTE[  :, F5.1, :N SULFURIC ACID (H2SO4):///)  15
      PRINT 41                                                          15A
   41 FORMAT (20X, :ENVIRONMENT[  HYDROGEN SATURATED: ///)
      PRINT 50                                                          017
   50 FORMAT (20X, :ELECTROLYTE PH DATA[  : ///)
C
```

```
C
C     PH IS ELECTROLYTE PH
C
C     EPT IS CATHODIC POTENTIAL (V.)  VS  SATURATED CALOMEL ELECTRODE
C
C     (I) IS THE RUN NUMBER OF (IMAX) RUNS
C
C     (J) IS THE DAY NUMBER OF (JMAX) DAYS
C
C
      READ (05,51)  IMAX, JMAX
   51 FORMAT (2X, 2I2)                                                  18B
      READ (05,70)  (EPT(I), I > 1, IMAX)
   70 FORMAT (2X, 6E10.4)                                               21
      DO 60  I > 1, IMAX                                                21
      IF (EPT(1) .GE. 1 .) GO TO 85
      EPT(I) > - EPT(1)
      PH(I) > -(EPT(I) < 0.242) / .059                                  23
   60 PRINT 80, I, PH(I), EPT (I)                                       024
   80 FORMAT (30X, :RUN :,I3, :[  :, F6.4, 5X, :( :, F7.4, : V): , /)   25
      GO TO 105                                                         026
   85 PRINT 95                                                          027
   95 FORMAT (30X, :PH DATA NOT AVAILABLE:, //////////)
  105 PRINT 90                                                          029
   90 FORMAT (1H1, //////////, 37X, :CORROSION POTENTIAL (V) VS.  S.C.E.
     1:, ///)                                                           13A
      PRINT 100                                                         031
  100 FORMAT (20X, :RUN//DRS:, 4X, :00:, 9X, :24:, 9X, :48:, 9X, :72:,  032
     1 9X, :96:, 9X, :120:, //)                                         033
      I > 1                                                             034
  130 READ (05,110)  (ECORR(I,J), J > 1, JMAX)
  110 FORMAT (2X, 7F10.4)                                               36
      IF (ECORR (1,1) .GE. 1.) GO TO 101
      PRINT 120,  I, (ECORR(I,J), J>1, JMAX)                            37
  120 FORMAT (//,21X, I1, 4X, F10.4, 7F11.4)
      I > I < 1                                                         039
```

```
      IF (I - IMAX) 130, 130, 179
  101 PRINT 102
  102 FORMAT (20X,:EQUILIBRIUM CORROSION POTENTIAL NOT AVAILABLE FROM EX
     CPERIMENTAL CONFIGURATION USED:, ////)
  179 PRINT 180
  180 FORMAT (1H1,          //, 30X, :POLARIZATION RESISTANCE DATA: )
  184 READ (05,185) KMAX, M, N
  185 FORMAT (2X, 3I2)                                                  70
      IF (KMAX .EQ. 0) GO TO 241
C                                                                       70A
C     KMAX IS THE NUMBER OF DATA POINTS ON DAY (N) OF RUN (M)           70B
C                                                                       70C
      KMAX > KMAX < 1                                                   71
      IF (M .GT. 1) GO TO 189
      GO TO 188
  189 IF (N .EQ. 1)  GO TO 186
      GO TO 186
  186 PRINT 187
  187 FORMAT (1H1)
  188 PRINT 215, M, N                                                   72
  215 FORMAT (///  , 30X, :RUN   :  , I1,10X, :DAY   :  , I1, //)       73
      DO 195 K > 1, KMAX
C
C
C     DELTA E IS THE ANODE POTENTIAL CHANGE RESULTING FROM AN IMPRESSED
C     CATHODIC POLARIZATION CURRENT DENSITY OF DELTA I (MICROAMPS/SQ CM)
C
C
C     S >  POLARIZATION RESISTANCE DETERMINED FROM LEAST SQUARES ESTIMA-
C     TIONS FOR RUN AND DAY IN QUESTION
      READ (05,196)  A(M,N,K), B(M,N,K)
  196 FORMAT (2X, 2F10.1)                                               76
  195 B(M,N,K) > B(M,N,K) / AREA
      READ (05,240)  S(M,N)
  240 FORMAT (2X, F12.6)                                                82
      S(M,N) > S(M,N) * AREA
```

```
      GO TO 221
  241 PRINT 222
  222 FORMAT (30X, :DATA NOT AVAILABLE:)
      GO TO 251
 221  PRINT 220, (A(M,N,K), K > 1, KMAX)                                77
  220 FORMAT (2X, :DELTA E (MV)        :, 15F7.1)                      78
      PRINT 230, (B(M,N,K), K>  1, KMAX)                               79
  230 FORMAT (2X, :DELTA I (MUA/SQ CM):, 15F7.1)                       80
      PRINT 250, S(M,N)                                                83
 250  FORMAT (/,20X:POLARIZATION RESISTANCE >    :, F12.6:  KOHMS:)    84
  251 IF (M .LT. IMAX) GO TO 184                                       85
      IF (N .LT. JMAX) GO TO 184                                       86
C
C
C     R IS POLARIZATION RESISTANCE FOR ALL DATA BY DAY FOR ALL RUNS
C     TAKEN TOGETHER. J CORRESPONDS TO DAYNR.
C
C
      DO 280  J > 1, JMAX                                             111
      READ (05,281)  R(J)
  281 FORMAT (2X,F12.6)                                              112A
  280 R(J) > P(J) * AREA
C
C
C     CORROSION RATE CALCULATIONS
C
C     I CORR IS CORROSION CURRENT DENSITY IN MA / SQ CM
C
C     MDD (MG/SQ DM/DAY), IPY (IN/YR), MPY (MICRONS/YR) ARE  MEASURES OF
C    1CORROSION RATE
C
C
      DO 310  I > 1, IMAX
      DO 310  J > 1, JMAX
      ICORR (I,J) > (BETAA * BETAC) / (2.3* S(I,J) * (BETAA < BETAC))  117
      IPY (I,J) > (ICORR (I,J) *EQVWT *3600.*24.*365.)/(RHO*2.54*96500.)  118
```

```
      IPY (I,J) > IPY (I,J) / 1000.
      MPY (I,J) > 3268.* ICORR (I,J) * EQVWT / RHO
  310 MDD (I,J) > IPY (I,J) * RHO * 254. / 0.365
      DO 360 I > 1, IMAX
      PRINT 320
  320 FORMAT (1H1, //////////, 30X, :CORROSION RATE DATA BY RUN BY DAY:
     1/////)
  369 PRINT 370, I
  370 FORMAT (37X, :RUN  :, I1, /////)
      PRINT 371
  371 FORMAT (10X, :DAY:, 23X, :00:, 9X, :24:, 9X, :48:, 9X, :72:, 9X,
     1:96:, 9X, :120:, ///)
      PRINT 330,(ICORR(I,J), J>1, JMAX)
  330 FORMAT (10X, :I CORR (MA/SQ CM)     :, 8F11.5)
      PRINT 340,(IPY(I,J), J>1, JMAX)
  340 FORMAT (///, 10X, :IPY (INCHES/YEAR)     :, 8F11.5)
      PRINT 350, (MDD(I,J), J>1,JMAX)
  350 FORMAT (///, 10X, :MDD (MG/SQ DM/DAY)    :, 8F11.3)
  360 PRINT 365, (MPY(I,J), J>1,JMAX)
  365 FORMAT (///, 10X, :MPY (MICRONS/YEAR)    :, 8F11.3)
C
C
C     CICORR IS COMBINED CURRENT DENSITY IN MA/SQ CM
C
C     CIPY IS COMBINED CORROSION RATE IN INCHES/YEAR
C
C     CMPY IS COMBINED CORROSION RATE IN MICRONS/YEAR
C
C     CMDD IS COMBINED CORROSION RATE IN MG/SQ DM/DAY
C
      DO 390 J>1, JMAX
      CICORR(J) > (BETAA*BETAC)/(2.3*R(J)*(BETAA<BETAC))
      CIPY (J)> (CICORR(J)*EQVWT*3600.*24.*365.)/(RHO*2.54*96500.)
      CIPY(  J) > CIPY(  J) / 1000.
      CMPY (J)> 3268.* CICORR (J)*EQVWT / RHO
  390 CMDD (J) > CIPY (J) * RHO * 254. / .365
```

```
      PRINT 380                                                         134
  380 FORMAT (1H1, ////////////, 20X, :CORROSION RATES FROM COMBINED DAILY
     1 DATA:, /////)
      PRINT 381
  381 FORMAT (10X, :DAY.  23X, :00:, 9X, :24:, 9X, :48:, 9X, :72:, 9X,
     1:96:, 9X, :120:, ///)
      PRINT 399, (R(J), J>1, JMAX)                                      139D
  399 FORMAT (10X, :POL. RESIS. (KOHMS) :  8F11.6)
      PRINT 400, (CICORR(J), J > 1, JMAX)                               140A
  400 FORMAT (///, 10X, :ICORR (MA/SQ CM)    :, 8F11.5)
      PRINT 410, (CIPY(J), J > 1, JMAX)                                 142
  410 FORMAT (///, 10X, :IPY (INCHES/YEAR)   :, 8F11.5)
      PRINT 415, (CMDP(J), J > 1, JMAX)                                 144
  415 FORMAT (///, 10X, :MDD (MG/SQ DM/DAY)  :, 8F11.3)
      PRINT 420, (CMPY(J), J > 1, JMAX)                                 146
  420 FORMAT (///, 10X, :MPY (MICRONS/YEAR)  :, 8F11.3)
      PRINT 421
  421 FORMAT (////////)
      PRINT 430 , BETAA, BETAC, RHO                                     148
  430 FORMAT (10X, :BETA A > :,F6.4,4X :BETA C > :,F6.4,4X :DENSITY > :,
     1F10.5, : GM/CU CM :, //)                                          150
      PRINT 440
  440 FORMAT (1H1, /////, 30X, :SUMMARIZED POLARIZATION RESISTANCE DATA:
     1, //)
      PRINT 445
  445 FORMAT (45X, :KOHMS:, //)
      PRINT 450
  450 FORMAT (10X, :RUN//HOUR:, 14X, :00:, 9X, :24:, 9X :48:, 9X, :72:,
     19X, :96:, 9X, :120:, /)
      DO 460  M > 1, IMAX
  460 PRINT 470, M, (S(M,N), N > 1, JMAX)
  470 FORMAT (//, 11X, I1, 16X, 8F11.6)
      PRINT 480, (R(N), N > 1, JMAX)
  480 FORMAT (//, 10X, :AVE:, 15X. 8F11.6)
      PRINT 490
  490 FORMAT (1H1, /////, 30X, :SUMMARIZED CORROSION CURRENT DENSITY DAT
```

```
     1A:, //)
      PRINT 495
  495 FORMAT (45X, :MA/SQ CM:, //)
      PRINT 500
  500 FORMAT (10X, :RUN//HOUR:, 14X, :00:, 9X, :24:, 9X :48:, 9X, :72:,
     19X, :96:, 9X, :120:, /)
      DO 510 M > 1, IMAX
  510 PRINT 520 , M, :ICORR(M,N), N > 1, JMAX)
  520 FORMAT (// 11X, I1, 16X, 8F11.5)
      PRINT 530, (CICORR(N), N > 1, JMAX)
  530 FORMAT (//, 10X, :AVE:, 15X, 8F11.5)
      PRINT 540
  540 FORMAT (1H1, /////, 30X, :SUMMARIZED CORROSION RATE DATA:, //)
      PRINT 545
  545 FORMAT (40X, :MICRONS/YEAR:, //)
      PRINT 550
  550 FORMAT (10X, :RUN//HOUR:, 17X, :00:, 9X, :24:, 9X :48:, 9X, :72:,
     19X, :96:, 9X, :120:, /)
      DO 560  M > 1, IMAX
  560 PRINT 570, M, (MPY(M,N), N > 1, JMAX)
  570 FORMAT (//, 11X, I1, 16X, 8F11.2)
      PRINT 580, ( CMPY(N), N > 1, JMAX)
  580 FORMAT (//, 10X, :AVE:, 15X, 8F11.2)
      STOP
      END
$      EXECUTE
```

Special Data Preparation Instructions

Data Card Number	Format Card Number	Card Contents
1	300	β_a, β_c, density, equivalent weight
2	16	Anode surface area
3	31	Electrolyte concentration
	40	Must be changed if other than sulfuric acid is used
4	51	Number of runs (IMAX) Number of days/run (JMAX)
5	70	Electrolyte pH data. Enter potential as absolute quantity. If no data available, set EPT(1) ≥ 1
IMAX	130	Steady-state corrosion potential, ECORR (I,J). If no data available set ECORR (1,1) ≥ 1.
Test Data	185	Top card: KMAX, M, N
	196	Data card: KMAX + 1 cards
	240	Slope card: S(M,N)
		Top card:
		.
		.
		.
		.
		Slope card: S (IMAX, JMAX)
	281	Slope cards: R(J)

Vita

Robert Leroy Kuhnle was born on 9 November 1941 in Baltimore, Maryland, the son of Joseph Robert and Audrey Mitchell Kuhnle. After graduation from Milford Mill High School, Baltimore, Maryland in 1959, he entered the U. S. Coast Guard Academy at New London, Connecticut. In June 1963, he graduated with a Bachelor of Science degree in Engineering and received a commission as an Ensign in the U. S. Coast Guard. After graduation, he served aboard the CGC Pontchartrain (WHEC-70) and commanded the CGC Cape Higgon (WPB 95302) before entering flight training at NAS Pensacola, Florida in 1965. Upon completion of flight training in 1966, he was assigned to the CG Air Station, St. Petersburg, Florida, as a search and rescue pilot of the HU-16E amphibian and the HH 52A Helicopter. After attending the Aircraft Maintenance Officer course at Chanute AFB, Illinois in 1968-1969, he was assigned as the Chief of Maintenance at the CG Air Station, San Diego, California. In June 1971, he was assigned to the Air Force Institute of Technology to undertake studies leading to Master of Science degrees in Aerospace-Mechanical Engineering and Systems Management.

Address: 3637 Sussex Road
Baltimore, Maryland

This thesis was typed by Miss Donna J. Schuh.